1-1-2018

Variability of the Be Star Population

Jonathan M. Labadie-Bartz
Lehigh University, jon.m.bartz@gmail.com

Variability of the Be Star Population

by

Jonathan Labadie-Bartz

A Dissertation
Presented to the Graduate Committee
of Lehigh University
in Candidacy for the Degree of
Doctor of Philosophy
in
Physics

Lehigh University
January 2018

Approved and recommended for acceptance as a dissertation in partial fulfillment of the requirements for the degree of Doctor of Philosophy.

Jonathan Labadie-Bartz
Variability of the Be Star Population

Date

Joshua Pepper, Dissertation Director, Chair
(Must Sign with Blue Ink)

Accepted Date

Committee Members

M. Virginia McSwain

W. Beall Fowler

Gary G. DeLeo

Jon E. Bjorkman

Contents

Acknowledgements

I am immensely fortunate for the friendship, support, and mentoring that I have received in my time spent as a graduate student at Lehigh. This holds true in my studies, and likewise in other aspects of my life. The completion of this work is an accomplishment that is not mine alone.

First, I acknowledge the ever-present support of my family and friends. My parents and grandparents have nurtured curiosity and determination from a young age, and continue to support me in all of my endeavors. Both of my sisters have been full of encouragement, and inspire me with their love and humanity. My partner in life, Lindsay, has been a constant source of structure and support, helping to navigate through any challenges that arise. My friends, both in graduate school and otherwise, have greatly lightened the load, making this whole process bearable.

I thank the members of my thesis committee. Dr. Joshua Pepper, in addition to your advisement in science and writing, I have learned the importance of networking, and developing an interest in a variety of topics. Dr. M. Virginia McSwain, your discerning eye has helped me to improve the quality of my own work, and encourages me to critically approach problems and results in scientific literature. From Dr. Jon. E. Bjorkman, I am learning to appreciate the fundamentals and to consider scientific problems in a larger scope, something that is aided by thinking about making progress on long timescales, and not just focusing on short-term results. For Dr. W. Beall Fowler, your interest in a variety of science topics is refreshing, and reminds me to appreciate the innumerable avenues that are being explored in the name of science. Dr. Gary G. DeLeo, I thank you especially for your mentorship during the first few years of graduate school, and your efforts to cultivate a positive attitude in learning, teaching, and life in general.

List of Tables

List of Figures

List of Abbreviations

ABE .... APOGEE Be star sample

AK .... APOGEE-KELT

AO .... Adams Observatory

APO .... Apache Point Observatory

APOGEE .... Apache Point Observatory Galactic Evolution Experiment

ARCES ...... Astrophysical Research Consortium Echelle Spectrograph

BeSS .... Be Star Spectra Database

BK .... BeSS-KELT

Br11 .... The hydrogen Brackett series transition between n = 4 – 11

EB .... Eclipsing Binary

EW .... Equivalent Width

FAP .... False Alarm Probability

H .... Hydrogen

Hα .... The hydrogen Balmer series transition between n = 2 – 3

i .... Inclination Angle

IP .... Intermediate Periodicity (P > 2 days)

KELT .... Kilodegree Extremely Little Telescope

LS .... Lomb-Scargle

LSP .... Lomb-Scargle Periodogram

LTV .... Long-Term Variation

MAD .... Median Absolute Deviation

MiMeS .... Magnetism in Massive Stars

MS .... Main Sequence

NIR .... Near-Infrared

NRP .... Non-Radial Pulsation

OTB .... Outburst

P .... Period

RV .... Radial Velocity

SDSS .... Sloan Digital Sky Survey

SNR .... Signal-to-Noise Ratio

TESS .... Transiting Exoplanet Survey Satellite

TFA .... Trend Filtering Algorithm

VDD .... Viscous Decretion Disk

Δv_p .... Peak separation (in velocity) between the violet and read peaks

V/R .... Violet to Red emission peak ratio for emission lines

Abstract

The goal of this dissertation is to describe the behavior of the Be star population. To do this, we have studied large samples with high precision and long time baselines. The primary data type used is optical time-series photometry, but infrared and optical spectroscopy are also important. In the process of studying many hundreds of Be stars, we have characterized their diverse photometric variability, identified systems of particular interest, and established links between photometric and spectroscopic variations.

Be stars and their disks have generally been characterized by the emission lines in their spectra, and especially the time variability of those spectroscopic features. They are known to also exhibit photometric variability at multiple timescales, but have not been broadly compared and analyzed by that behavior. We have taken advantage of the advent of wide-field, long-baseline, and high-cadence photometric surveys that search for transiting exoplanets to perform an analysis of brightness variations among a large number of known Be stars. The photometric data comes from the KELT transit survey, with a typical cadence of 30 minutes, baseline of up to ten years, photometric precision of about 1%, and coverage of about 70% of the sky. We analyze KELT light curves of 610 known Be stars in both the Northern and Southern hemispheres in an effort to study their variability in a comprehensive way. Consistent with other studies of Be star variability, we find most of the systems to be variable. We derive lower limits on the fraction of stars in our sample that exhibit features consistent with non-radial pulsation (25%), disk-building events ('outbursts'; 36%), and long-term trends in the circumstellar disk (37%), and show how these are correlated with spectral sub-type. Other types of variability,

such as those owing to binarity, are also explored. Simultaneous spectroscopy for some of these systems from the Be Star Spectra (BeSS) database allow us to better understand the physical causes for the observed variability, especially in cases of outbursts and changes in the disk. This sample is referred to as the “BK sample” (for BeSS-KELT).

In order to study the growth and evolution of circumstellar disks around classical Be stars, we analyze optical time-series photometry from the KELT survey with simultaneous infrared and visible spectroscopy from the APOGEE survey and BeSS database for a sample of 160 Galactic classical Be stars. This sample is referred to as the “AK sample” (for APOGEE-KELT, since all systems have both APOGEE and KELT data). The systems studied here show variability including transitions from a disk-less to disk-possessing state (and vice versa), and persistent disks that vary in strength, being replenished at either regularly or irregularly occurring intervals. We detect disk-building events (outbursts) in the light curves of 28% of this sample. Outbursts are more commonly observed in early- (57%), compared to mid- (27%) and late-type (8%) systems. A given system may show anywhere between 0 – 40 individual outbursts in its light curve, with amplitudes ranging up to $\sim$0.5 mag and timescales between $\sim$2 – 1000 days. We study how both the photometry and spectroscopy change together during active episodes of disk growth or dissipation, revealing details about the evolution of the circumstellar environment. We demonstrate that photometric activity is linked to changes in the inner disk, and show that, at least in some cases, the disk growth process is asymmetrical. Observational evidence of Be star disks both growing and clearing from the inside out is presented. The duration of disk build-up and dissipation phases are measured for 70 outbursts, and we find that the average outburst takes about twice as long to dissipate as it does to build up in optical photometry. Our analysis hints that dissipation of the inner disk proceeds relatively slowly for late-type Be stars.

Although both the BK and AK samples are comprised of Be stars, there are some minor differences. For each system in the AK sample, we have multiple high-resolution, infrared spectroscopic measurements, as well as optical light curves, and, in about a quarter of the sample, optical spectroscopy. Our analysis of the AK sample is mainly focused on studying disk creation, growth, and dissipation. Significant attention is given to systems with spectroscopic measurements that are near-contemporaneous with light curve variability. Each system in the BK sample has an optical light curve, but only about half of the sample has any spectroscopic data. Analysis of the BK sample emphasizes all types of photometric variability on all timescales, from hours to many years. The primary goal of our work with the BK sample is to generally classify photometric variability in Be stars as a population. Spectroscopic data is sometimes incorporated into the analysis of certain members of the BK sample, but is secondary to the photometric data. For these reasons, these two samples are kept separate in the text.

Chapter 1

Introduction

The field of astronomy is generally concerned with furthering our understanding of the universe and the celestial objects contained within it. Observations of solar system bodies, stars, galaxies, and other objects are taken, and theoretical frameworks are created in an attempt to describe the available data and to make predictions. Despite tremendous advancements in the field, there remain many unanswered questions. New telescopes and instruments are being designed and built, and as more data continue to be collected, more advanced models are developed to better match observations.

Stars are celestial bodies that spend the majority of their life existing in an approximate balance between the forces of gravity (pulling material inward) and of radiation pressure (pushing material outward). The gravitational force arises from the accumulated mass of the system, while the radiation pressure has its origins in energy generated in the core of a star. The source of this outwardly-diffusing energy comes from nuclear fusion. A given star will spend a large fraction of its total life fusing hydrogen into helium. This nuclear reaction releases energy. Hydrogen therefore acts as the primary source of fuel for stars. During this hydrogen fusing phase, a star is said to be on the "Main Sequence" (MS), and is generally stable. After exhausting its hydrogen fuel, a star will leave the MS and undergo rapid and profound changes, the details of which depend on the mass, composition, and history of the star. From these late phases of stellar evolution arise giants, supergiants, planetary nebulae, supernovae, white dwarfs, neutron stars, black holes, and other exotic systems.

All stars are assigned a spectral class, which is generally based on the appearance of their spectrum. These standard spectral classifications are denoted by the following letters: O, B, A, F, G, K, and M. This sequence is ordered according to temperature, where O- and B-type stars are the hottest, and K- and M-type stars are coolest. There are also L, T, and Y classifications, which characterize the coolest low-mass stars. The reasoning behind these labels is historical. For reference, our Sun is a G-type star, having an intermediate mass and temperature. Each spectral class is further divided and assigned numbers ranging from 0 – 9, going from hotter to cooler. For example, O8, O9, B0, B1, B2 describe a series that is decreasing in temperature. The adopted nomenclature describes "early-type" stars as being hot relative to "mid-" and "late-type" stars (that is, an early-type star is hotter than a mid-type star, which is hotter than a late-type star).

1.1 Massive Stars

Stars exist on a spectrum of mass, ranging from between approximately 0.1 – 100 $M_\odot$ (where the mass of our sun = 1 $M_\odot$). Mass is the most important initial condition that determines the properties of a given star, dictating its temperature, density, luminosity, lifetime, evolution, and ultimately its death. Although the vast majority of stars are of relatively low mass, their high-mass counterparts have a profound effect on the interstellar environment. Massive stars emit high-energy radiation that ionizes nearby interstellar gas, altering its chemistry. Heavy elements are created by massive stars, which are then introduced into the environment through strong stellar winds or by supernovae. Supernovae arise from only high-mass stars, and can even cause new episodes of star formation. As the shockwave from a supernova exerts mechanical forces on the interstellar medium, this sometimes triggers clouds of gas to collapse. Nearly all massive stars are found in binary pairs, where the two stars are likely to interact as they evolve, sometimes exchanging mass or interacting through strong stellar winds.

As mentioned in the previous section, all stars can be assigned a spectral class. This designation is largely based on temperature, which is the primary factor (along with composition) that shapes a stellar spectrum. Because the temperature of a star is determined mainly by its mass (while on the main sequence), the spectral class of a star is also a proxy for mass. So, hot stars on the MS are massive, while cool stars on the MS are low mass. This work is primarily focused on hot, massive, B-type stars.

1.2 Be Stars

Classical Be stars are a sub-set of B-type stars that are on, or near the MS (that is, they are still fusing hydrogen in their core, and are not evolved giant stars). All B-type stars have absorption lines in their spectrum, but Be stars also exhibit emission features (hence the 'e' in Be). This 'extra' emission implies that there is line-emitting material in the circumstellar environment. Progress over the last many decades has lead to a consensus that this line-emitting circumstellar material exists in a viscous disk that orbits the star approximately in accordance to Kepler's laws (a "Keplerian disk"). Be stars span the entire range of spectral sub-types of B-type stars, with the "Be phenomenon" even extending to late O- and early A-type stars.

Disks are not uncommon in astrophysical systems, and exist in many different situations, including protostellar and protoplanetary disks, active galactic nuclei, accretion disks around stars and more compact objects, and Be stars. The disks of Be stars are unique, however, because they are "decretion" disks, forming from material shed from the star itself, with the disk growing outward over time, as opposed to the more common accretion disk, which is fed from some external source.

Largely because Be stars are bright and numerous, their disks are well-suited for studying the effects of viscosity in a large number of systems across a range of parameters. Although viscosity is pervasive in astrophysical disks, it is notoriously difficult to describe on a microscopic level. It is then convenient to parameterize the effects of viscosity, which essentially describes the degree to which material is coupled. In the case of viscous disks, viscosity is responsible for modifying the angular momentum of particles in the disk, allowing material to flow either radially inward (losing angular momentum) or radially outward (gaining angular momentum). The strength of viscosity is parameterized as α, according to the α-disk model (Shakura and Sunyaev 1973), which dictates the timescales over which Be star decretion disks evolve and dissipate (*e.g.* a disk with a high value of α will dissipate relatively quickly). The α-disk model is relevant to not only Be stars, but also to other viscous astrophysical disks. Therefore, progress made in understanding the viscous disks of Be stars can then be applied to other systems with viscous disks, which, in most cases, are notoriously difficult systems to describe the physics of. The viscous decretion disk model (VDD; Carciofi 2011; Lee et al. 1991) is currently the best theoretical framework describing the evolution of Be star disks once formed. According to the VDD model (and corroborated by observational evidence; Carciofi et al. 2012), gas placed in the immediate circumstellar environment will self-interact through viscous forces. This causes a shuffling of angular momentum. A small fraction ($\sim$1%) of this mass will acquire enough angular momentum to migrate outwards, but the majority of the gas ultimately falls back onto the star. As the disk grows, it becomes more diffuse and less massive. In order for a Be star disk to approach a steady state, it must be fed at a near-constant rate via stellar mass loss for a long time (effectively a few to tens of years or more, although a true steady state in a decretion disk state requires infinite time; Haubois et al. 2012a). However, this is often not the case, as mass loss from a given Be star tends to vary over time. Their disks then also vary in total mass, and the distribution of this mass. Be star disks can even disappear completely, only to return at some later time (McSwain et al. 2009). Even if a disk approaches a steady state (*i.e.* has a near constant radial distribution of mass), it may still be variable. Azimuthal density structures in the form of a one-armed spiral wave are well known features that sometimes exist in otherwise steady disks. These global oscillation modes in the disk have typical periods of $\sim$7 – 10 years, which is hundreds of times longer than the orbital timescales at the locations in the disk where these density enhancements are observed (Okazaki 1991; Papaloizou et al. 1992).

Besides their remarkable disks, Be stars themselves have many interesting properties. All Be stars are very rapid rotators. In fact, Be stars are the most rapidly rotating non-degenerate class of stars known (Townsend et al. 2004). The average Be star rotates at around 80% of its critical velocity (v_c, defined to be the rotational velocity where the centrifugal forces at the stellar equator balance Newtonian gravity, resulting in zero effective gravity), although the exact rotational velocity varies from star to star (Rivinius et al. 2013, and references therein). Be stars are also pulsators. All Be stars observed with data of sufficient quality are found to exhibit multiple modes of non-radial pulsation (NRP). Having both rapid rotation and multi-mode NRP, Be stars serve as excellent laboratories by which to test theories regarding rapid rotation and its role in stellar evolution and structure, the relationship between rapid rotation and pulsation, and also theories addressing the transport of angular momentum from the stellar interior outward.

One of the most significant open questions in Be star science asks: how is material launched from the stellar surface with sufficient velocity and angular momentum to form a disk, and what governs this (often variable) mass-loss behavior? It is clear that Be stars create disks by ejecting mass from their surface, but the relevant mechanism(s) responsible are poorly understood. Rapid rotation is a necessary ingredient in the mass-loss mechanism of Be stars, since near-critical rotation significantly lowers the gravitational barrier for achieving orbit. However, unless the star is rotating above v_c, rapid rotation in itself cannot be the sole mechanism by which mass is ejected. Some additional mechanisms(s) must act to trigger mass loss episodes. Pulsation is a natural candidate for this additional mechanism.

The disturbance caused by a single NRP mode can perhaps provide a sufficient 'kick' to a localized region of the stellar surface to launch some material into orbit (Kee et al. 2014; McSwain et al. 2008). However, the scenarios considered where a single NRP mode can create a disk require the star to be rotating at $\gtrsim 95\%$ of v_c. While some Be stars may rotate this rapidly, most (or at least some) do not, and are thus unable to form a disk this way. The observational fact that all Be stars observed with high quality data are found to be *multi-mode* pulsators then becomes relevant. A suggestion for the mechanism acting to drive mass loss is the coupling of two (or more) non-radial pulsation modes, which interact (Kurtz et al. 2015), occasionally resulting in a high-amplitude disturbance capable of launching surface material into orbit (Baade et al. 2017; Rivinius et al. 2016). This idea is promising, but requires further study.

To summarize, Be stars are rapidly rotating, non-radially pulsating B-type stars that build orbiting equatorial disks from mass ejected from the stellar surface. Rapid rotation sets the stage on which some additional mechanism, possibly pulsation, acts to drive mass loss. Once ejected, material is circularized through viscous forces and orbital phase mixing (*i.e.* a parcel of gas, with some finite radial extent, will become circularized since the orbital period depends on radius). Viscosity redistributes angular momentum, allowing a small fraction of mass to attain progressively wider orbits, at the cost of the majority of material falling back onto the star. In this way an outwardly diffusing disk is formed.

The aim of this dissertation is to analyze observational data for hundreds of Be stars to describe their behavior as a population. This includes measuring properties of both the star and its disk. In pursuit of this goal, I have analyzed different (and often complementary) types of observational data, and have arrived at statistics that describe the diverse variability seen in the Be star population. These statistics are necessary to inform population synthesis models that predict the behavior of Be stars at large, over the wide range of timescales and stellar spectral types observed, as well as models that describe the physics of Be star disks. Many systems of particular interest are identified, which may prove useful in addressing some of the mysteries that still surround Be stars, such as the mechanism by which they eject material. A number of systems have complementary types of observational data that coincide in time, from which we infer details about the disk build-up and dissipation process. The different types of behavior that Be stars and their disks exhibit are discussed further in the following chapters. Most of the results presented in this manuscript have been published in Labadie-Bartz et al. (2017a,b).

1.3 Organization

Chapter 2 introduces the data that is used throughout this work, describing its origins, properties, and how it is analyzed and interpreted. Chapter 3 discusses the different types of periodic signals that are exhibited in Be stars, describes how they are recovered from the data, and shows the corresponding results. This is followed by Chapter 4, which is concerned with measuring discrete episodes of mass loss through analysis of both photometric and spectroscopic data. The behavior of Be stars in regards to outbursts is described through distributions of outburst properties, and many individual systems are examined in further detail. This chapter comprises a substantial portion of this work. Chapter 5 considers changes in Be star systems that occur slowly, over the course of years. These slow changes are generally attributed to disk variability. Chapter 6 introduces systems that are similar to classical Be stars in many ways, but also have important differences. These include massive magnetic stars, β Cephei pulsators, and eclipsing binaries. This work concludes with Chapter 7, which provides a summary and a brief description of further projects that can enhance our understanding of Be stars (some of which are already in progress).

Chapter 2

Observational Techniques and Data

2.1 Photometry

Most of what we know about our universe is derived from information carried by light. All stars shine, and much can be learned about stars by studying their emitted light. Perhaps the most simple way to begin to understand the properties of an astronomical object is by measuring the intensity of light received by some observer on (or near) Earth. At its core, the technique of photometry involves measuring the brightness of some object. If the brightness of a star is changing over time, this can be measured by taking multiple photometric measurements across time. A series of such measurements over a span of time is called a 'light curve,' and is an important and useful tool in astronomy. A few examples of light curve utility include discovering and studying exoplanets, comets, and asteroids, and learning about the birth, life, and death of stars. In this work, light curves are used to monitor changes in Be stars and their disks.

2.1.1 *KELT photometry*

The Kilodegree Extremely Little Telescope (KELT) is a photometric survey using two small-aperture (42 mm) wide-field (26° x 26°) telescopes, with a northern location at Winer Observatory in Arizona in the United States, and a southern location at the South African Astronomical Observatory near Sutherland, South Africa. The KELT survey covers over 70% of the sky and is designed to detect transiting exoplanets around stars in the magnitude range $8 < V < 10$, but obtains photometry for stars between $7 < V < 13$. See Figure 2.1 for a map showing the location of KELT fields on the sky. Northern fields are designated as "KN##" (where ## is a two digit number corresponding to a single field), southern fields are labeled like "KS##", and joint fields (observed by both the northern and southern KELT telescopes) are labeled like "KJ##". Designed for high photometric precision of better than 1%, KELT's observing strategy involves long baselines of up to 10 years, with light curves for ∼4.4 million objects at the time of this writing[1]. The effective passband of KELT is roughly equivalent to a broad R-band filter (centered at 691 nm, with an effective width of 318 nm). The long baseline combined with a typical cadence of 30 minutes and high photometric precision makes the KELT dataset a valuable resource for studying variable stars across a range of timescales and magnitudes. KELT uses a German Equatorial Mount, requiring data acquired in the eastern orientation and western orientation to be reduced separately (Pepper et al. 2007, 2012). For most objects observed by KELT, there are both raw and detrended versions of the light curves available. The detrending process is built into the KELT pipeline, and uses the Trend Filtering Algorithm (TFA; Kovács et al. 2005) as implemented in the Vartools package (Hartman 2012). The nearest 150 stars within two instrumental magnitudes of the target star (outside of a 20 pixel exclusion zone centered on the target star) provide the photometric reference for the detrending. Additionally, outliers are removed and long-term trends are subtracted out.

The per-point photometric errors for KELT observations are small, typically a few mmag for brighter sources, and up to a few percent for the faintest targets. The

[1] November, 2017

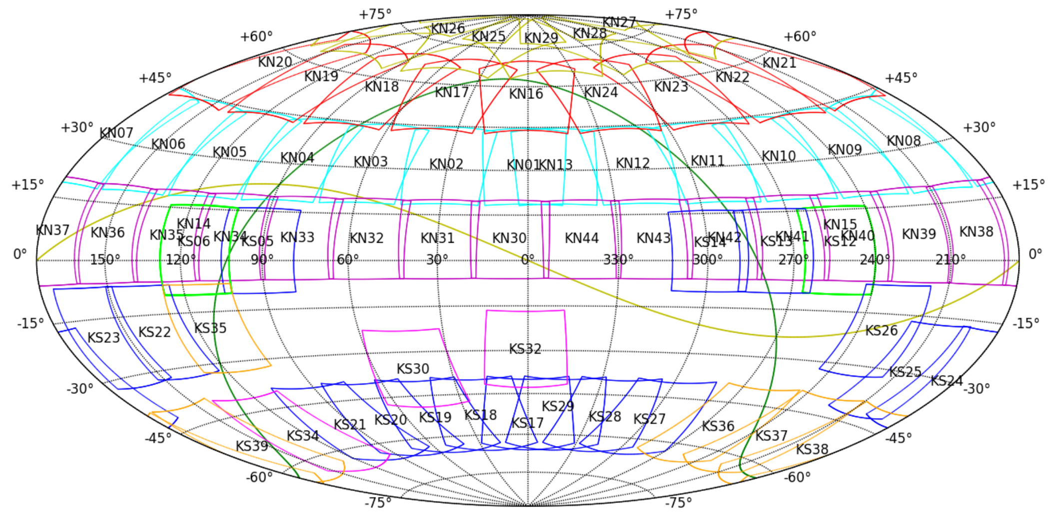

Figure 2.1: A map of all KELT fields projected onto the sky. The yellow curve is the ecliptic, and the green curve is the Galactic plane. Most Be stars are found in the vicinity of the Galactic plane.

typical photometric error for the KELT data in this analysis is 7 mmag. We find that our photometric errors are dominated by a complex combination of systematic noise sources (which are generally larger than our photon errors), so the typical errors quoted above are based on the empirical scatter of KELT light curves that do not display obvious variability. With each light curve having thousands of data points, plots can quickly become very cluttered with the inclusion of error bars. Or, depending on the scaling of the figure, the sizes of the error bars can be comparable to or smaller than the plotted data points themselves. For these reasons, we choose not to display error bars in any light curve plots.

High cadence, long baselines, and high photometric precision are integral to the KELT observing strategy. With the ability to recover periodic signals on timescales of tenths of a day, to the detection of slow, long-term changes in flux occurring over thousands of days, KELT light curves are an excellent tool for studying the wide range of Be star variability. These points are amplified by the large number of objects observed by the survey, making the KELT dataset a valuable resource for studying the population of Galactic Be stars. An example light curve is shown in Figure 2.2.

Because of the large pixel scale of KELT (23″) and the relatively crowded fields lying in or near the Galactic plane where most Be stars are found, light from other sources is often blended with the target star in KELT. Put another way, the aperture used to extract the light curve of the target star may include light from other nearby sources. If a neighboring star is blended with the target star and is variable, then this variability can appear in the light curve for the target. This contamination is addressed by analyzing difference images of the pixels in the vicinity of the target to determine precisely which pixels are the source of variability. Inspecting the density of background sources in the vicinity of the target star is an important step in this process. This analysis was done for all stars showing any type of photometric variability. This process can robustly identify contaminating sources further than two KELT pixels away from the target. Another consequence of blending is that the amplitude of variability in the target star will be diluted depending on how much flux from neighboring sources leaks into the target star's aperture. Therefore, all photometric amplitudes quoted here should be understood as a lower limit, although this effect is small in practice for the majority of stars in our samples.

2.1.2 Time-series analysis of KELT photometry

Time-series data has become an invaluable tool in virtually all areas of astronomy. Extracting meaningful information out of time-series data requires the application of the appropriate type of signal processing. There is no single 'best' processing method, as the most appropriate method depends on many factors, including the timing of the observing pattern, the number of measurements, the baseline over which the target is observed, the precision of the measurements, various systematic effects, and, importantly, the type of signal being searched for. With the primary data source used in this work (light curves, or time-series measurements of brightness), a common desire is to recover periodic signals with timescales much shorter than the observational baseline. In the most ideal situation, this can be achieved by

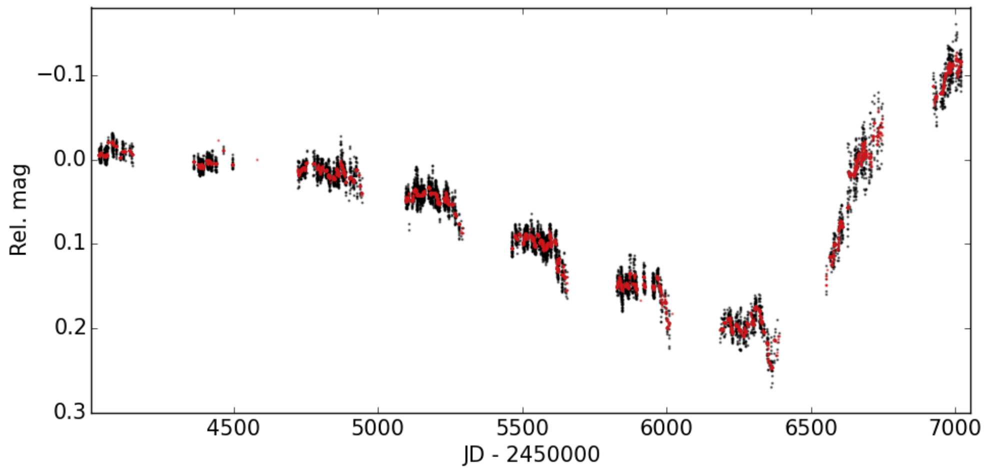

Figure 2.2: An example KELT light curve of a variable Be star. Black points depict raw photometric measurements, with red points showing the data after applying a low-pass filter.

a simple Fourier transform of the data. However, a number of complications arise, and a modified approach is required. The most relevant of these complications is that the astronomical data that we are dealing with is discretely sampled at irregular intervals over a finite baseline, with many large observing gaps. While there are multiple techniques available, an appropriate and popular choice for recovering periodic signals in this type of data is the generalized "Lomb-Scargle Periodogram" (LSP; Press et al. 1992; Zechmeister and Kürster 2009), as implemented in the Vartools light curve analysis package (Hartman 2012). This method allows for an efficient computation of a Fourier-like power spectrum estimator from the time-series data, by which we can determine the frequency (or multiple frequencies) that exist in the data. In the case where multiple, independent periodic signals exist in a dataset, these can be recovered in an iterative way. First, the LSP is calculated and the strongest peak identified. This signal is then removed from the data (with knowledge of its frequency, amplitude, and phase) in a method referred to as "pre-whitening." The LSP is then re-calculated from the pre-whitened data, which now has no trace of the original signal, allowing the next strongest peak to be detected.

An added advantage of this is that aliases of a given signal will be removed upon pre-whitening.

The LSP must be used carefully, as there are many ways a naive user can be misled into erroneous conclusions. Potential pitfalls and complications include aliases of a real signal with some feature of the observing pattern (*e.g.* daily aliases), spurious signals that result from various systematic effects (on different timescales; *e.g.* the Lunar cycle), non-sinusoidal signals, harmonics, and aperiodic variability (and aliases of this). Encounters with, and solutions to these difficulties are explained in more detail in further sections where this method is used to recover various types of signals. See VanderPlas (2017) for an introduction and a practical guide to using this method.

2.2 Spectroscopy

Spectroscopy is another technique by which light is used to study celestial objects, and relies on using instruments that spread out light, so that its constituent colors (or wavelengths) can be analyzed. Where photometry relies on measuring the total flux received from some source, spectroscopy is more sophisticated – the incident flux is measured as a function of wavelength. Spectroscopy is an invaluable tool in astronomy, directly informing us about the composition, temperature, and motion of objects.

The vast majority of stellar spectral features exist as a result of relatively cool gas in the outer layers of a star absorbing and scattering light radiated outward from the hot internal layers. This results in a decrement of flux at certain wavelengths, which depends on the temperature and composition of the gas. These absorption lines are not unique to astronomy, and exist wherever a relatively cool diffuse gas lies between a radiation source and an observer. Conversely, hot, unobscured gas creates emission lines, apparent as an increase in flux at certain wavelengths. Absorption lines generally arise in the atmosphere of the central Be star, while emission lines originate in the circumstellar disk.

An impressive amount of information is encoded in the spectrum of a Be star system, but both the Be star and its disk contribute to the spectrum in different ways, complicating matters. Therefore, a great amount of caution is required when analyzing spectroscopic data for Be stars. By using spectral lines that are not contaminated by the disk, the projected rotational velocity of the star (*i.e.* how rapidly it is spinning along our line of sight) and its spectral type and composition can be estimated by measuring the line profiles and relative strengths of lines in the spectrum. Time-series spectroscopic measurements can be used to measure stellar pulsation. Emission features trace the circumstellar disk, revealing information about its kinematic properties and density profile. Different lines probe different regions of the disk, giving a more complete picture to its overall structure. Measurements of emission lines over time can reveal episodes of disk formation, growth, and decay, as well as density oscillations.

Except when viewed pole-on, observations of any rotating structure (including Be stars and also their disks) reveal that half of the emitting material is moving towards the observer (imparting a Doppler shift towards blue wavelengths), while the other half is moving away from the observer (imparting a red-shift). Therefore, disk emission features typically have two peaks on either side of the line center, one being blue-shifted (the violet peak), and the other red-shifted (the red peak). The line profile, in particular the two peaks, encodes information about the kinematic properties of the emitting disk material. Useful measurements include the peak separation, Δv_p (the separation between the violet and red peaks in terms of velocity, usually expressed in km s^{-1}), and the ratio of the intensity of the violet peak to the red peak (V/R ratio).

2.2.1 Interpreting emission features

The appearance of a spectral line can tell us about the status and properties of the disk, and can also give some information about the inclination angle of the system. Figure 2.3 demonstrates the Hα line profile of a Be star disk viewed at different

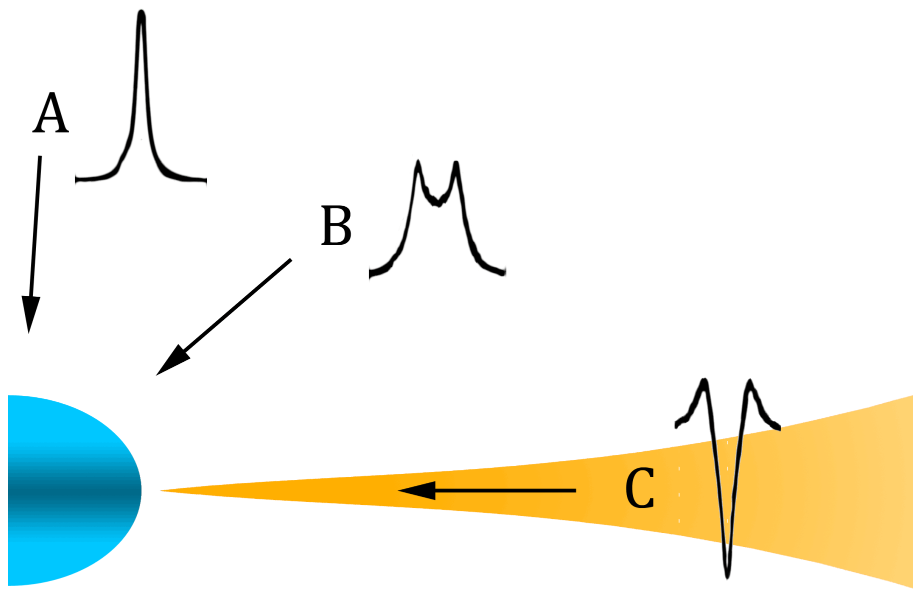

Figure 2.3: This schematic shows the effect that inclination angle has on the perceived emission line profile arising from a Be star disk. In particular, this shows the Br11 lines of ABE-A26 (A; low i), ABE-082 (B; intermediate i), and ABE-026 (C; high i).

inclination angles. This figure highlights the double-peaked emission feature characteristic of Be star disks (except for the single-peaked case of line-of-sight 'A', where the system is viewed pole-on). Disk kinematics can be inferred by measuring the separation between the violet and red emission peaks, and by analyzing the shape of the line profile. It is important to note that Be star disks are variable, which is reflected in changes in their line profiles.

2.2.2 BeSS spectroscopy

The Be Star Spectra (BeSS) database[2] is a continually updated catalog that attempts to include all known Be stars and their stellar parameters. This catalog is

[2]http://basebe.obspm.fr

based primarily on the catalog of classical Be stars published by Jaschek and Egret (1982), but also includes more recently discovered Be stars from a variety of sources (e.g. Martayan et al. 2006; Neiner et al. 2005). The BeSS database is updated regularly as new Be stars are discovered, confirmed, or dismissed in the literature (Neiner et al. 2011). Dozens of observers, both professional and amateur, have collectively submitted over 100,000 spectra to the BeSS database. These data come from a large variety of telescopes and instruments, and are therefore of inhomogeneous quality, depending on the expertise of the observer and the equipment used. However, each spectrum is subject to a quality check for format and scientific validity by the BeSS administrators before being incorporated into the database. Although any wavelength regime is allowed, optical spectra are by far the most common type of submission. In particular, we focus on the Hα line, which is a popular observable of Be stars, and is covered in a majority of BeSS spectra. An example Hα spectrum is shown in Figure 2.4. This spectroscopic feature informs us about the status of these disks. Spectra are available for many of the Be stars under consideration here, providing a valuable complement to the photometric data, especially in cases where there are time-series spectroscopic measurements simultaneous with the KELT light curve. We have selected a few particularly illustrative cases for which we present both the photometric and spectroscopic data.

2.2.3 APOGEE spectroscopy

The Apache Point Observatory Galactic Evolution Experiment (APOGEE) employs a 300 fiber spectroscopic instrument characterized by high resolution ($R \sim$ 22,500), high S/N (> 100), and H-band near-infrared (NIR) coverage (1.51 - 1.70 μm; Majewski et al. 2015). APOGEE-I, a program in the Sloan Digital Sky Survey III (SDSS-III), has observed 238 classical Be stars, 128 of which are new discoveries (Chojnowski et al. 2015). The APOGEE Be (ABE) sample includes other types of B-type, emission-line stars (namely Herbig Ae/Be and B[e] objects), which are not discussed here. We limit our discussion in this paper to only the classical Be stars, hereafter referred to as “Be stars.” The APOGEE data presented here is from the

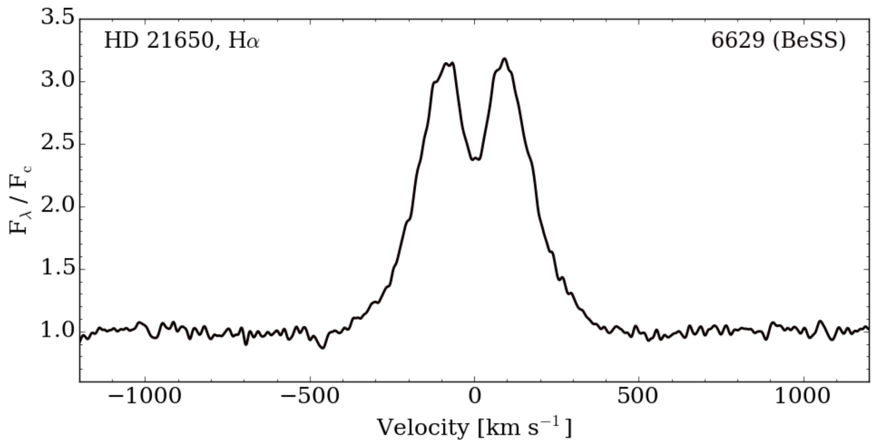

Figure 2.4: An example Hα spectrum from the BeSS database. The x-axis is given in units of velocity, according to the Doppler shift relative to the line center (at 6562.8 Å).

twelfth data release of SDSS-III (Alam et al. 2015).

Whenever possible, the velocity separation of the violet and red emission peaks (Δv_p) were measured interactively (visually) for all Be star spectra with well-defined Brackett (Br) series line profiles. In interpreting the profiles of the H-Br lines, the models of optically thin lines from Hummel and Dachs (1992) were largely relied on. In the case of Be stars with Keplerian disks, measuring the peak separations for optically thin lines gives a lower limit to twice the projected rotational velocity ($2\ v \sin i$) of the stars (Hummel 1994). For systems with double-peaked line profiles, the systemic radial velocities (RVs) were estimated by measuring the position of both the violet and red peak, and then taking the average of the two peaks as the line center. This was done for each H-Br line in a given spectrum, and the individual H-Br RVs were averaged to get a single RV for each spectrum. In addition, the equivalent width (EW; defined to be positive in absorption, and negative in emission) of the Br11 line ($W_{\rm Br11}$) was measured via direct summation of a 100 Å window centered on Br11, with typical errors of $\sim$0.32 Å. All of these measurements, and more detailed explanations of the methods used, are provided in Chojnowski et al. (2017), including both star-averaged and individual spectrum quantities. In

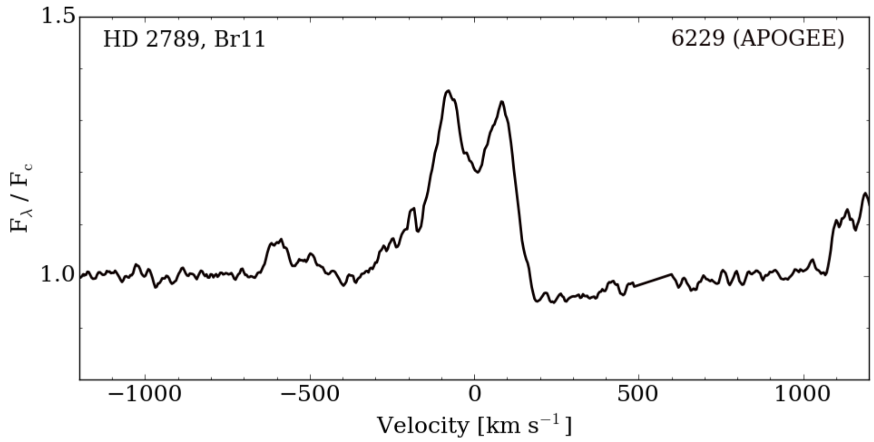

Figure 2.5: An example Br11 spectrum for an APOGEE-observed Be star. The x-axis is given in units of velocity, according to the Doppler shift relative to the line center (at 16811 Å).

this paper, we focus mainly on the Br11 line (centered at 16811 Å), since it tends to be the strongest in the series, but similar trends are seen in the other Br lines. An example Br11 line for a Be star observed by APOGEE is shown in Figure 2.5.

2.2.4 AO and APO spectroscopy

Because a large fraction of the ABE star sample lacks spectral type information in the literature, we obtained high-resolution optical spectra of stars of interest using the Apache Point Observatory (APO) 3.5m telescope and the Astrophysical Research Consortium Echelle spectrograph (ARCES; Wang et al. 2003). In each exposure, the ARCES instrument covers the full optical spectrum (3,500–10,000 Å) at a resolution of R∼31,500, recording the light in 107 orders on a 2048x2048 SITe CCD. We used standard echelle data reduction techniques in IRAF[3], including bias subtraction, scattered light and cosmic ray removal, flat-field correction, and wavelength calibration via Thorium-Argon lamp exposures. The orders were then

[3]IRAF is distributed by the National Optical Astronomy Observatories, which are operated by the Association of Universities for Research in Astronomy, Inc., under cooperative agreement with the National Science Foundation.

continuum normalized, trimmed so as to allow a 10 Å overlap between orders, and merged into a single one-dimensional spectrum. Exposure times were estimated with the goal of achieving signal-to-noise ratio (SNR) of at least 50 at 4500 Å. The OB spectral atlas of Walborn and Fitzpatrick (1990) provides an appropriate set of standard stars to which ARCES spectra were compared visually.

A number of our stars were also targeted using a low-resolution long-slit spectrograph at Adams Observatory (AO), Austin College. We used a grating with 1200 grooves per millimeter that disperses the light to 0.54 Å per pixel in the wavelength range 3850 - 4950 Å. The slit size is matched to a two pixel width, and the resolution ($\lambda/\Delta\lambda$) varies between 3000 - 4500 across the spectrum. Data reduction procedures were written in Python, and are explained in depth in Whelan and Baker (2017).

2.2.5 Estimating Spectral Types

With the exception of B and Be stars hotter than B1, for which the presence and strength of He II λ 4685 and ratios of Si III / Si IV are used for spectral typing, spectral classification of the majority of B and Be stars relies on the relative strengths of the He I lines versus those of Mg II λ 4481 and Si II λ 4128-4130. For instance, the relative strengths of the He I λ 4471 Å and Mg II λ 4481 Å lines offer a relatively good proxy for temperature, although rotation is known to play a role in interpreting their relative strengths (*e.g.*, Gray and Corbally 2009, and references therein). Luminosity class is largely determined by the widths of the hydrogen Balmer and metallic absorption lines.

Spectral classifications of stars are historically done by comparison to a set of spectra of known spectroscopic standard stars. Morgan and Keenan (1973), for example, provides one of the most complete sets of spectroscopic standard stars. A number of complications arise when assigning spectral classifications to Be stars. They are very rapidly rotating and therefore have broad spectral features. This introduces difficulties, especially since rapid rotation can alter the relative depths of lines with different intrinsic widths (Gray and Corbally 2009). Rapid rotation adds further complications besides line broadening. Be stars bulge outward near the equator (due to their rapid rotation), and therefore have a substantially higher surface gravity and temperature at the poles compared to the equatorial region. The inclination angle of the star then influences perceived line strengths. Line damping is yet another issue adding to the difficulty of classifying Be star spectral types. This effect arises from the filling in of absorption lines due to flux from the circumstellar disk, making the absorption lines appear weaker than they actually are. Furthermore, photospheric lines can have significant contributions from the disk, in addition to the continuum line damping). As the amount of material in the disk is often varying, so too do these effects change over time.

Because of these difficulties, spectral types for Be stars must be considered carefully. All stars for which we present new spectral classifications with temperature hotter than B1 have clear He II λ 4685 absorption line detection, as well as luminosity-sensitive lines like O II. We expect our new classifications to be accurate to within ±0.5 in temperature class for stars earlier than and including B2, thanks in part to features such as the Si III lines at 4552, 4567, 4571 Å. For stars later than B2, an uncertainty of ±1 in spectral type is typical, but some cases (*e.g.* shell stars) have larger uncertainties of ±2. These uncertainties are appropriate for the newly reported spectral types presented here, but it is also prudent to apply similar levels of caution to spectral types reported in the literature for Be stars, especially when these are determined in any sort of automated way.

Considering the uncertainties in the reported spectral types, it is useful to adopt coarse bins in stellar temperature. For stars that have not yet been spectral typed in this work, a designation from the literature is adopted. Following the convention of Labadie-Bartz et al. (2017b, hereafter "LB17"), we consider "early-type" Be stars as those with spectral types earlier than B4, "mid-type" Be stars have spectral types including B4, B5, and B6, and "late-type" Be stars have spectral types including B7 and later. Stars without a specific spectral type (e.g. a spectral type of "Be") are considered "unclassified." Despite the difficulties in assigning a specific temperature class to Be stars, they are still reliably cast into these 'early-', 'mid-', and 'late-type' designations (although we can only be certain of this for stars newly spectral typed in this work).

2.3 Relevant Be star observables

The features and behavior of Be stars leave characteristic imprints in various modes of observation. Pulsation is the main feature that causes light originating from the stellar photosphere to vary, while changes in the circumstellar environment are generally the cause of most other signals. The imprint left by pulsation in photometry is an oscillating brightness, according to the period and amplitude of the pulsation mode. Pulsation can also be detected in spectroscopy by measuring the distortion in certain absorption features that originate in the stellar photosphere.

The intensity and shape of an emission feature in the spectrum of a Be star encodes information about the disk, including the total amount of emitting material and its distribution and kinematics, and the inclination angle of the system. An axisymmetric Be star disk viewed at an intermediate inclination angle will show double-peaked line emission, with the violet and red peaks having equal heights (V/R = 1). If viewing this structure at a very low inclination angle (near pole-on), the line profile will have only a single peak at the line center, since the projected rotational velocity of the disk is near zero. At very high inclination angles (near edge-on), a deep central absorption core exists, as the disk absorbs more line photons than it emits. This is sometimes accompanied by emission wings. These edge-on systems are referred to as "shell stars." Asymmetries in the disk translate to asymmetries in the line profile. In photometry, the presence of a disk will increase the net brightness of the system, except at high inclination angles, where a disk will partially obscure the star and cause a dimming. Monitoring changes in these observables over time traces the evolution of the disk.

A binary system that includes a Be star may reveal itself in spectroscopy through a periodic radial velocity signal (in the Be star lines, and also those of the companion if the system is double-lined), according to the binary orbital period. However, the very broad spectral lines caused by the rapid rotation of the Be star, and also the presence of a (variable) disk make such detections difficult. The Be star disk may become elliptical and precess with the orbital period, due to the tidal influence of a companion (Panoglou et al. 2016). This effect can modulate the brightness of the system, and also certain spectral features. Other possible consequences of binarity are discussed in Section 3.3.

2.4 Formation Loci of Observables

Throughout this work, we deal mainly with three different observables – visible continuum photometry (KELT), the Brackett series in the NIR (APOGEE), and visible spectroscopy (mainly the Hα line; ARCES, AO, and BeSS). These three observables are sensitive to different parts of a Be star disk. This idea, and relevant model predictions, are presented and discussed in Carciofi (2011), which serves as a useful reference for estimating the disk regions probed by the observables used in this work. KELT photometry primarily probes the inner $\sim$1 – 2 R_* of the disk, as measured out from the stellar equator. The NIR Br11 line probes the disk at larger radii, out to $\sim$2 – 6 R_* (Chojnowski et al. 2015). Hα traces an even larger area of the disk, out to $\sim$5 – 15 R_* (Rivinius et al. 2013), or greater. Slettebak et al. (1992) find that Hα emission arises in the range of 7 – 19 R_*, on average. Observations of Be stars at longer wavelengths (*e.g.* millimeter or radio) reveal disks that extend out to many tens or hundreds of stellar radii (*e.g.* Klement et al. 2017). These more extended regions of the disk are largely inaccessible to the modes of observation used in this work. The exact extent that our observables probe depends on many factors, including the stellar flux, inclination angle, and the distribution of material in the disk (which varies with time). Despite these complications, it remains generally true that the KELT, Br11, and Hα observations probe what we refer to as the 'inner,' 'mid,' and 'outer' disk areas. We stress that these regions are not rigidly defined, as applied in this work. However, they are useful constructs when considering different types of data taken at similar times for a given system. This scheme is qualitatively illustrated in Figure 2.6.

For all non-shell systems with both optical and NIR spectra, there is a greater separation between the violet and red peaks in the Br11 line, compared to Hα. Multiple factors contribute to this. When part of a disk is optically thick in some

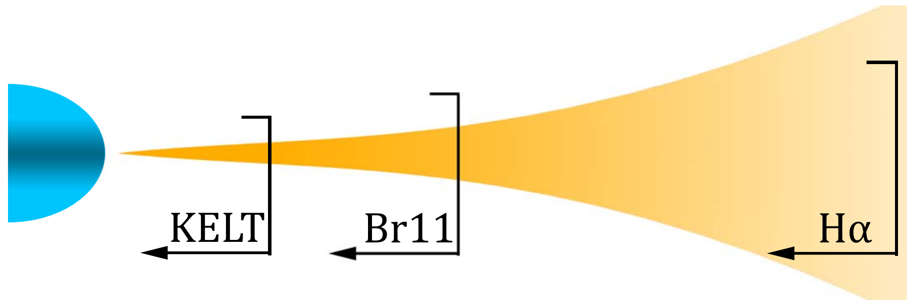

Figure 2.6: A schematic view of a Be star with a flared disk. The approximate extent of the regions from which our three main observables arise are marked.

line (which is not uncommon for Hα), non-coherent scattering broadening can act to decrease the peak separation (Hummel 1994). This effect influences both the peak separation and the emission line profile. Orbital velocity of particles in the disk decrease with distance ($v_{orb} \propto r^{-1/2}$), so emission originating at larger disk radii will also contribute to a smaller peak separation.

Variability in the disk tends to occur most rapidly in the inner-most regions, with timescales increasing with radius. In part because Hα probes a much greater area of the disk relative to the other observables, the Hα line often exhibits the most dramatic disk signatures, with emission features sometimes exceeding ten times the continuum level.

2.5 Samples

This work primarily deals with two different samples of Be stars. The "BeSS-KELT" (BK) sample, and the "APOGEE-KELT" (AK) sample. Analysis was performed separately for these two samples, with slightly different goals in mind. Although these sets are mostly unique, there are a small number of systems that exist in both. Table 2.1 shows the percentage of early, mid, late, and unclassified stars for both samples. The BK sample has a higher fraction of early-type stars, which tend to show higher levels of activity relative to their cooler counterparts.

The BK sample begins with the catalog of classical Be stars listed on the BeSS database. All Be stars with V-band magnitudes between $6-13$ (1362 unique objects) were cross-matched to the KELT catalog. This magnitude range was chosen to align with KELT's bright and faint limits. A total of 610 of these Be stars were found to have KELT light curves. Unique, short identifiers are assigned to each object for convenience (the "BK number"), beginning at BK-000 and incrementing up to BK-609. However, 100 of these are saturated in the KELT photometry, and are not analyzed at present. This effectively leaves 510 Be stars in the BeSS-KELT sample. Approximately half of these have at least one spectrum archived in the BeSS database. This sample has been analyzed for all types of variability that manifest in light curve data, including pulsation, other periodic variability (possibly attributed to binarity in some cases), episodes of disk creation and growth, disk dissipation, and long-term (years) variability in the inner disk. Spectroscopic data are occasionally incorporated into the analysis of these systems, but the main focus is characterizing light curve variability.

The APOGEE-KELT sample starts with the 238 Be stars observed in the APOGEE-I program. These APOGEE-observed Be stars are numbered starting with ABE-001, as in Chojnowski et al. (2015). Some Be stars were specifically targeted, and these are numbered starting with ABE-A01. Of all APOGEE-I Be stars, there are 160 classical Be stars with non-saturated KELT light curves, of which 120 are observed by KELT-North, 33 are observed by KELT-South, and 7 are observed by both KELT-North and KELT-South (the joint field J06). Every star in this sample has multiple infrared APOGEE spectra, nearly all of which are simultaneous with the KELT photometry. Analysis of this sample mainly focuses on the details of disk build-up and dissipation, and how these properties are distributed among the population. Spectroscopic data (mainly APOGEE, but also from BeSS) are given additional context by the photometric data, and contribute significantly to the analysis. There are 32 Be stars that are common to both the AK and BK samples. However, we still consider the AK and BK samples separately, since the two samples were analyzed in slightly different ways.

Table 2.1: Demographics for the AK and BK samples

	Early	Mid	Late	Unclassified	Total number
AK	33.8%	13.8%	38.1%	14.4%	160
BK	56.3%	14.1%	16.3%	13.3%	510

Chapter 3

Periodic Variability

Certain types of behavior in astrophysical sources necessarily repeat at a regular rate. Some examples include the revolution of the Earth around the Sun, the orbit of a binary star system, and stellar pulsations. When a periodic signal is detected in some system, the frequency of the variability can give important clues as to the physical origin of the changes. In this section, we first describe the methods used to recover periodic signals, and then discuss the results of our frequency analysis.

3.1 Recovering periodic signals

Light curves for all Be stars in the BK sample were analyzed for periodic variability between 0.05 - 300 days using a generalized LS search, as implemented in the VARTOOLS light curve analysis package. The LS method essentially involves a fourier transform of time-series data, optimized for non-uniform time sampling (which is the case with KELT light curves). With the wide range of variability seen in Be stars, this had to be done very carefully. A given light curve may have, for example, a high frequency periodic signal, a low frequency periodic signal, and long-term monotonic variability. In order to successfully recover each unique signal in a given system, four different versions of its light curve were analyzed simultaneously: TFA detrended (described in Section 2.1.1), raw, and the raw data after applying two different high-pass median filter and outlier removal, using windows sizes of both 20 and 100 days. There is no single version of the light curve (raw, TFA, or median smoothed at 100 or 20 days) that is best suited for recovering periodic signals globally in our sample, since this depends on the presence of other types of aperiodic variability and the associated timescales, which differ greatly between objects.

Periodic signals associated with astrophysical variability may be detectable in the raw data for a given system. However, the presence of any high amplitude aperiodic variation will alias strongly with KELT's diurnal sampling, dominating the LS periodogram (LSP) for such systems and rendering the detection of relatively low-amplitude periodic signals intractable. The high-pass median filtered raw data is appropriate for the recovery of periodic signals in light curves that also exhibit aperiodic variation, as long as the filtering window timescale is longer than the period being searched for, and comparable to or shorter than the timescales associated with the aperiodic variability that is to be filtered out. A window size of 20 days preserves high frequency signals, and smooths out variability on timescales longward of 20 days, while a window size of 100 days smooths out only the variability occurring on timescales of 100 days and longer. In cases where there is little to no high-amplitude aperiodic variability, the TFA detrended light curve is also a reliable version for the recovery of periodic signals. Since the TFA detrended light curve is a product of KELT's automated data reduction pipeline and is optimized for exoplanet detection around otherwise photometrically stable stars, it is not as well suited for the recovery of periodic signals for sources that have intrinsic aperiodic variability, which is the case with a large fraction of our Be star sample. For example, the TFA algorithm handles outbursts poorly, and distorts the data before, during, and after the outburst.

LSPs were generated for all objects. For each of the four light curve versions associated with a single object, the top LSP peak was identified. Each light curve was then prewhitened to its top period, and a new LSP was re-calculated on the prewhitened light curve. This process was iteratively repeated a total of six times. The process of prewhitening light curves is necessary to identify which peaks are associated with a single frequency. A single real signal at a given frequency will create several associated spikes in a periodogram through aliasing (most prominently with the diurnal observing pattern of KELT). By using prewhitened periodograms, we diminish the chances of erroneously interpreting such aliases as real signals.

The top peak for each iteratively whitened version of the LSP was used to phase the photometric data. Extra caution was exercised for periods near integer fractions of one day. As a first-pass cut to separate spurious signals from those that may be real, a sinusoid was fit to each phased light curve, and its amplitude (peak-to-trough) and the median absolute deviation (MAD) of the residuals to the sinusoidal fit were calculated. The ratio of the signal amplitude to the MAD of the residuals was used to parametrize the strength of the signal relative to the scatter in the data, serving as a metric for the reliability of the recovered signal. Cases where this ratio is less than 0.75 are deemed to be non-detections. When this ratio is greater than 0.75, periodograms (both whitened and non-whitened) and photometric data phased to the recovered period for each of the four light curve flavors are inspected for consistency. In practice, the ratio for most spurious signals had values less than 0.5, while the ratio value for real signals was typically greater than one. In most systems with periodicity, the same signal is unambiguously identified as the top peak in the LSP of multiple versions of the light curve. However, there are still a substantial number of more complicated cases where this more thorough approach is required, especially when there are other high-amplitude trends in the light curve. Although this technique is somewhat subjective, it was empirically found to be more reliable than automatic methods that identify top LSP peaks and judge their authenticity based on the associated Lomb-Scargle power and a calculated false alarm probability (these quantities are automatically output in the VARTOOLS implementation of the LS routine) . Such automatic methods generate a large number of false-positive detections, where, although the signal may exist in a given light curve, the signal is not the result of true periodicity, but is rather the aliasing of longer term variation with the diurnal sampling. The same difficulties often prevent automatic methods from identifying real periodic signals when there is other variability present.

3.2 Stellar pulsation

Be stars are a pulsating class of stars, and exist in a region of the Hertzsprung-Russel diagram that overlaps other near-MS B-type pulsators, namely β Cephei stars and Slowly Pulsating B (SPB) stars. β Cephei stars tend to be early B-type stars (roughly B0 – B2.5), that primarily oscillate in high-frequency ($\sim 3.5 - 15$ d^{-1}) g-mode (where the restoring force is gravity) pulsations (*e.g.* Stankov and Handler 2005). SPB stars have relatively later spectral types (roughly B2 – B9), and pulsate in lower-frequency ($\lesssim 3.0$ d^{-1}) g-modes (*e.g.* De Cat 2002). Be stars are pulsators, and span a range of spectral types from late O to early A. In these ways, Be stars are similar to β Cephei and SPB stars. However, only Be stars rotate near their critical velocity and eject mass to form disks.

NRP are commonly observed in Be stars, with typical timescales between $\lesssim$0.1 day to 2 days. Cuypers et al. (1989) detect NRP in $\sim$82% of a sample of 17 Be stars. In a sample of 57 Be stars, Gutiérrez-Soto et al. (2007) detect short-term variability indicative of NRP in 74% of early-type Be stars, and in 31% of mid- and late-type Be stars. The photometric amplitudes associated with NRP in Be stars can be quite low, down to the sub-mmag level (Emilio et al. 2010; Saio et al. 2007; Walker et al. 2005a,b). When Be stars are actively ejecting mass during observations, frequency spectra become more complex and care must be taken to distinguish the stellar from the circumstellar variability (Rivinius et al. 2016). Although signatures of these stellar pulsations can be very difficult to detect, all Be stars that have been analyzed with high-cadence, long-duration space-based photometry have been reported to be multiperiodic and to pulsate, with amplitudes decreasing with later spectral subtypes (Rivinius et al. 2013). It therefore seems that, as a class of objects, Be stars are pulsators.

All values quoted in this section are for the BK sample only, which consists of 510 Be stars. We detect high-frequency periodic variability (having P $<$ 2 days), which we interpret as being indicative of NRP, in 25% of the sample. Incidence rates are similar for early- and mid-type Be stars (28% and 25%, respectively), and lower for late-types (17%). Figure 3.1 shows examples of phased light curves for three such systems, and Figure 3.2 shows the distribution of the recovered periods for all systems showing signs of NRP. It is important to note that the absence of a detectable periodic signal in a KELT light curve does not imply that the star is not pulsating, but rather suggests an upper limit to amplitudes of long lasting pulsational modes. Space-based photometry has shown that pulsations in Be stars with amplitudes less than 1 mmag are common (Gutiérrez-Soto et al. 2008), but this degree of precision is not realized in the ground-based KELT photometry. Additionally, Be stars are sometimes found to exhibit transient pulsational modes which last for a few days to months. These transient modes may precede an outburst, then disappear or diminish in amplitude following the outburst event (Gutiérrez-Soto et al. 2008; Huat et al. 2009; Rivinius et al. 2013). Even if these transient modes are of a large enough amplitude to be detectable in KELT photometry, they are unlikely to be detected if they are present for only a small fraction of the total baseline of observation. In this analysis, we look only for periodic variability present throughout the whole baseline of observation. For these reasons, it is not surprising that we detect NRP in a significantly smaller fraction of our sample when compared to other studies that were specifically designed to detect these signatures, such as those mentioned in the introduction.

3.3 Other periodic signals

There are numerous physical scenarios capable of giving rise to periodic variability longward of 2 days in Be stars. Single Be stars may experience low-frequency NRP modes, multiple NRP modes coupled at a difference frequency, Rossby modes, or circumstellar activity. The coupling of multiple NRP modes can cause periodic variability, with the period depending on how closely spaced in frequency the modes are. Single vibrational modes may be modulated by the rotation of the star, resulting in Rossby modes with periods longer than those typically attributed to NRP (Townsend 2003). Circumstellar activity owing to clumps of recently ejected material can cause observable variability. These clumps will have an orbital period that depends on their orbital radius, which may not be constant. Circumstellar processes of this nature are not expected to be strictly periodic. The shifting period and noise intrinsic in these processes will result in complicated frequency spectra, especially when considering aliases with both astrophysical and instrumental signals (e.g. Rivinius et al. 1998; Štefl et al. 1998, 2000). Interactions between a Be star and a binary companion can also induce periodic variability modulated by the orbital period of the binary pair. Ellipsoidal precession of a Be star disk, tidally locked density waves in the disk, tidally induced disk warping, heating of the outer region of the disk by a hot companion, or the deformation of the stellar surface of one or both components can arise from gravitational interactions between the two binary components. Reflection effects may also be present. Global oscillations (i.e. density waves) in the circumstellar disk can also cause long-term cyclic variability in effectively single Be star systems, but these are considered separately, as the timescale is much longer (typically on the order of 10 years). Binarity is common amongst massive stars, and Be stars are not exceptions to this. We therefore expect an appreciable fraction of our sample to be in a binary system. Oudmaijer and Parr (2010) use adaptive optics to probe the binary fractions of B and Be stars, with the sensitivity to detect binary companions separated by 20 - 1000 au. They find virtually the same binary fractions between B and Be stars (29 ± 8 % and 30 ± 8 %, respectively), with similar underlying distributions of mass ratios, binary separations, and cumulative distributions. Moe and Di Stefano (2016) perform a meta-analysis of about 30 separate surveys, asserting that "massive stars are dominated by interactions with binary companions." We expect this statement to apply to Be stars since they are a subset of the massive star population.

Simulations for coplanar binaries including a Be star and disk show that in nearly all cases, the disk will exhibit periodicity in its structure that would otherwise be absent in an isolated system. In circular orbits the density structure will rotate with the orbital phase, and in elliptical orbits the disk brightness will change over an orbital cycle (Panoglou et al. 2016). These signals are potentially detectable in photometry, and may be the cause of the intermediate periodicity detected in some cases.

A slightly different situation can arise if there is even a slight misalignment between the disk and the binary orbit. In these cases, tidally induced disk warping can occur, and will cause disk precession (Martin et al. 2011). Spectroscopic evidence for a warped disk can be seen in Be star systems that transition between a shell-absorption phase and an emission phase.

Many instances of periodic variability on timescales longer than two days have been detected in Be stars. Cyclical variability between 60 - 100 days was detected in the Be star δ Scorpii (Jones et al. 2013). Sterken et al. (1996) find periodic and quasi-periodic oscillations in brightness in 4 Be stars (from a sample of 15 Be stars earlier than B3) with periods ranging between 4 and 93 days. The authors suggest pulsations, rotation of an inhomogeneous stellar surface, and/or oscillations in the circumstellar envelope as plausible explanations for the shorter period case (HD 89890, P=4.656 days). For the three with longer periods (HD 173219, P=61.4 days; HD 48917, P=87.9 days; HD 58978, P=92.7 days), an elliptical precessing disk is suggested. One of these, HD 173219, has a confirmed radial velocity orbit within $\sim$5% of the photometric period (Hutchings and Redman 1973), which supports the idea that tidal forces acting on the circumstellar disk as a result of a binary companion can be responsible for the observed periodicity. In a similar analysis, Mennickent et al. (1994) detect QPO in two stars (27 CMa and 28 CMa) with periods between 10 and 20 days. Hubert and Floquet (1998) make use of Hipparcos photometry (van Leeuwen 1997) and find QPO with a period of 11.546 days in the Be star MX Pup. Such variability has many possible causes, including single NRP modes, the coupling of two or more NRP modes with closely spaced frequencies, circumstellar activity, and multiple scenarios involving binarity. This is an important topic of study, since it appears that the beating of multiple NRP modes can trigger outbursts (Rivinius et al. 2001, 2013).

Another scenario involving brightness modulated by binarity is the well known case of ellipsoidal variables, where one or both binary components are elongated according to the gravitational influence of the other component. The star HD 50123 (misclassified as a classical Be star in BeSS) was found by Sterken et al. (1994) to be an interacting binary consisting of a B6Ve primary and an early K giant secondary filling its Roche lobe, with each of the two components contributing roughly the same to the total flux in the V-band. This binary system is at an intermediate inclination angle (on the order of 60°), has a mass ratio of q≈0.3, an orbital period of 28.601 days, and shows a double-waved modulation of its light curve typical of ellipsoidal variables. In this configuration, gas from the K giant feeds the circumstellar shell around the primary component. No classical Be stars with a Roche lobe filling companion are known, since mass transferring binaries are excluded from the definition of classical Be stars (Rivinius et al. 2013). Although HD 50123 is not a classical Be star, the accretion onto the B-type star results in similar observable features, namely Hα emission and rapid rotation. It is therefore likely that some of the variables presented here are not classical Be stars, despite the possible presence of line emission and a B-type spectral designation. A more detailed analysis would be required to make any claims regarding the classical Be star status of these objects.

In the BK sample, 38% (194/510) of Be stars exhibit periodic behavior at intermediate timescales (having $2\ \mathrm{d} < \mathrm{P} \lesssim 100\ \mathrm{d}$), and are labeled as "IP variables" (for intermediate periodicity). Most of these are single-waved, and are well described by a single sinusoid. However, an appreciable fraction are double-waved, having unequal maxima and/or minima and requiring two or more sinusoids to describe their shape. Characteristic examples of these are shown in Figure 3.3, with the top panel showing a double-waved phased light curve, while the lower two are single-waved. With KELT photometry alone, we cannot further constrain the physical cause of this behavior like we do with the short period NRP candidates. Nonetheless, it is interesting to see such a large fraction of observed stars showing periodicity in this range. These objects are good candidates for continued investigation. One such example IP variable with a period of 61.253 days and a clear double-wave modulation is shown in the upper panel of Figure 3.4. This object (BK-050 = HD 33461) has eight BeSS spectra that are each spaced about a year apart and are simultaneous with the KELT light curve. When these spectra are phased to the photometric period, they show coherent variability. This seems to imply that the same mechanism is responsible for modulating both the brightness and spectroscopic line profile of the system. BK-050 is a good candidate for binarity. Cases like this, where spectroscopic data can be phased to a photometric period, can provide valuable clues for uncovering the underlying mechanism(s) causing the observed variability.

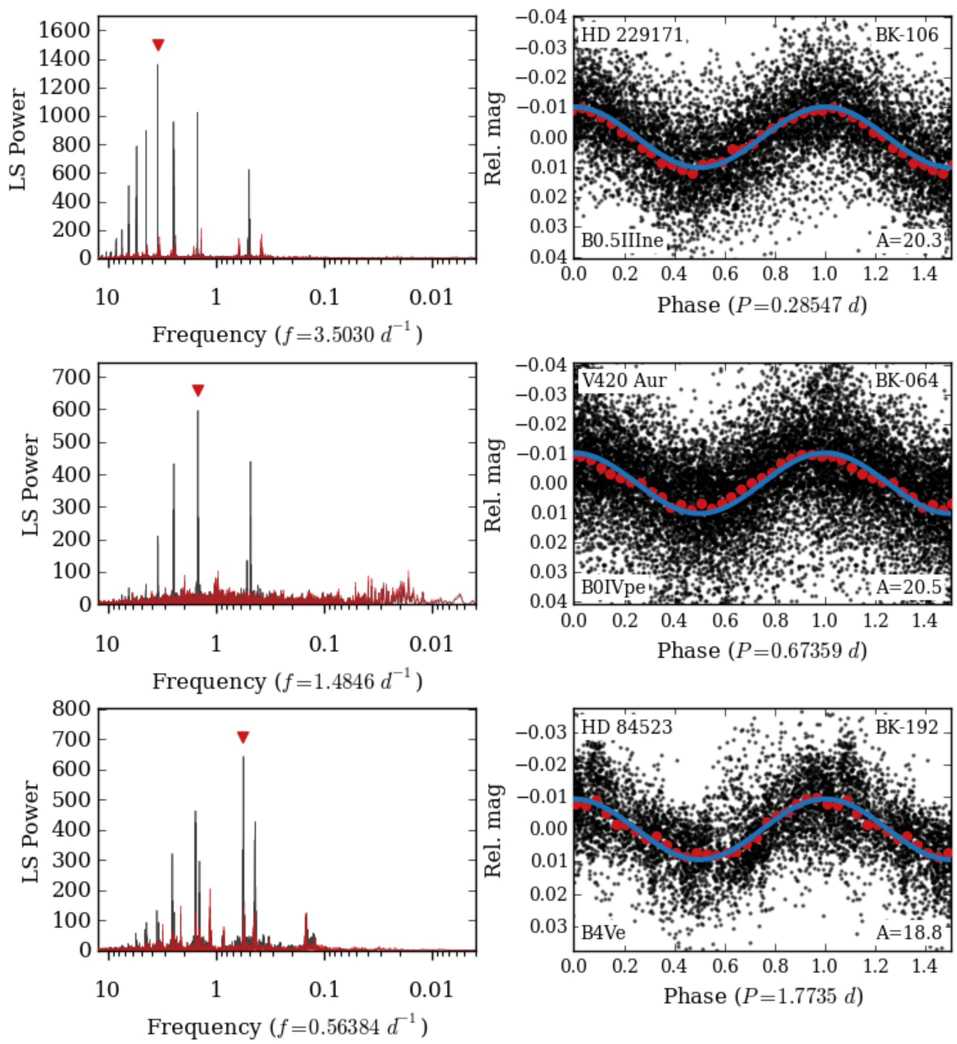

Figure 3.1: *Left:* Lomb-Scargle periodograms for three stars showing signals consistent with NRP. The black curve shows the original periodogram, and the red curve shows a periodogram after prewhitening against the top period. *Right:* Light curves for three different stars phased to their recovered period. Red points show the light curve binned in phase using a bin size of 0.04, and the blue curve is a sinusoidal fit. The amplitude, given in the bottom-right corner of each panel, is the difference between the maximum and minimum points of the sinusoidal fit in units of mmag. These phased light curves are typical of the signals we interpret as being caused by NRP.

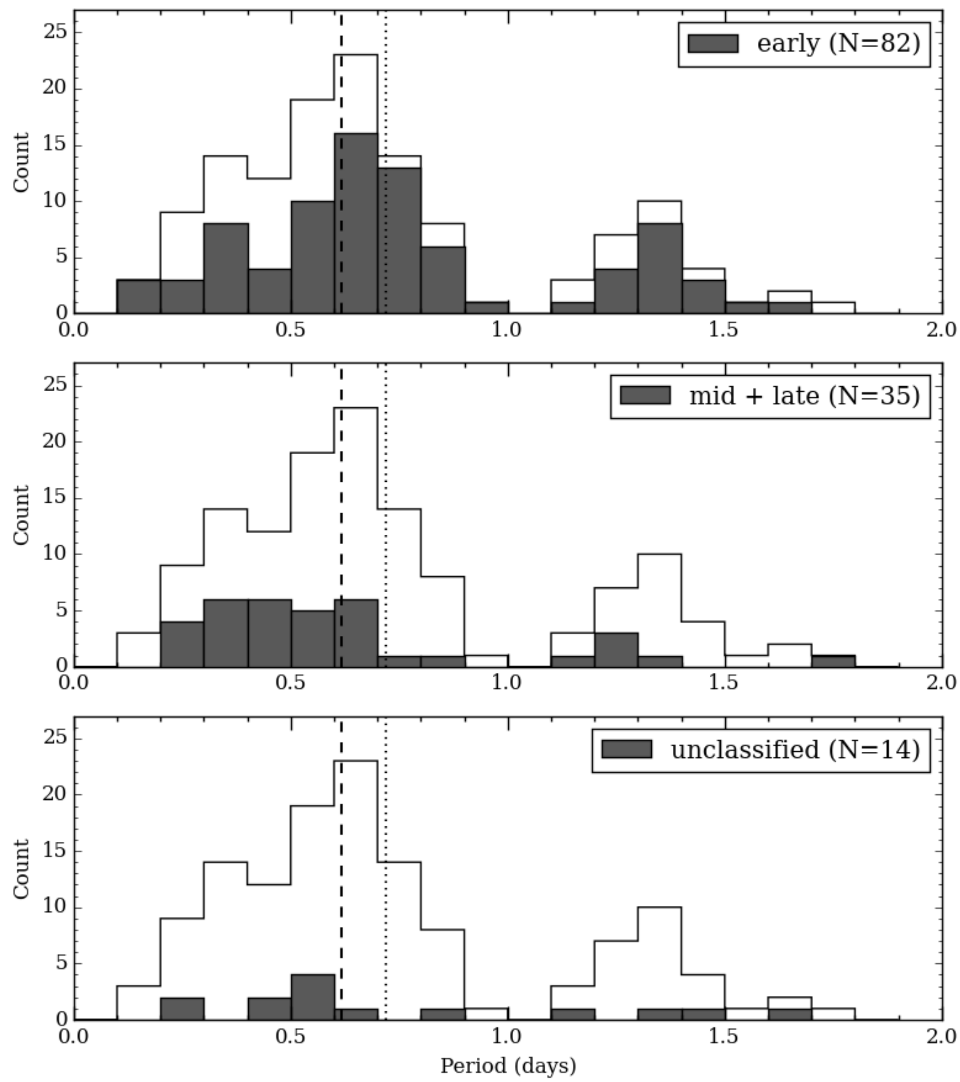

Figure 3.2: Histogram showing the distribution of high-frequency periodic signals detected in the BK sample, presented in the same manner as in Figure 4.13. The dearth of recovered periods close to one day is largely a consequence of the diurnal sampling of KELT, and should be interpreted as a systematic effect. In a small number of stars, we have detected more than one independent high-frequency signal. In such cases, all detected signals are included in this figure.

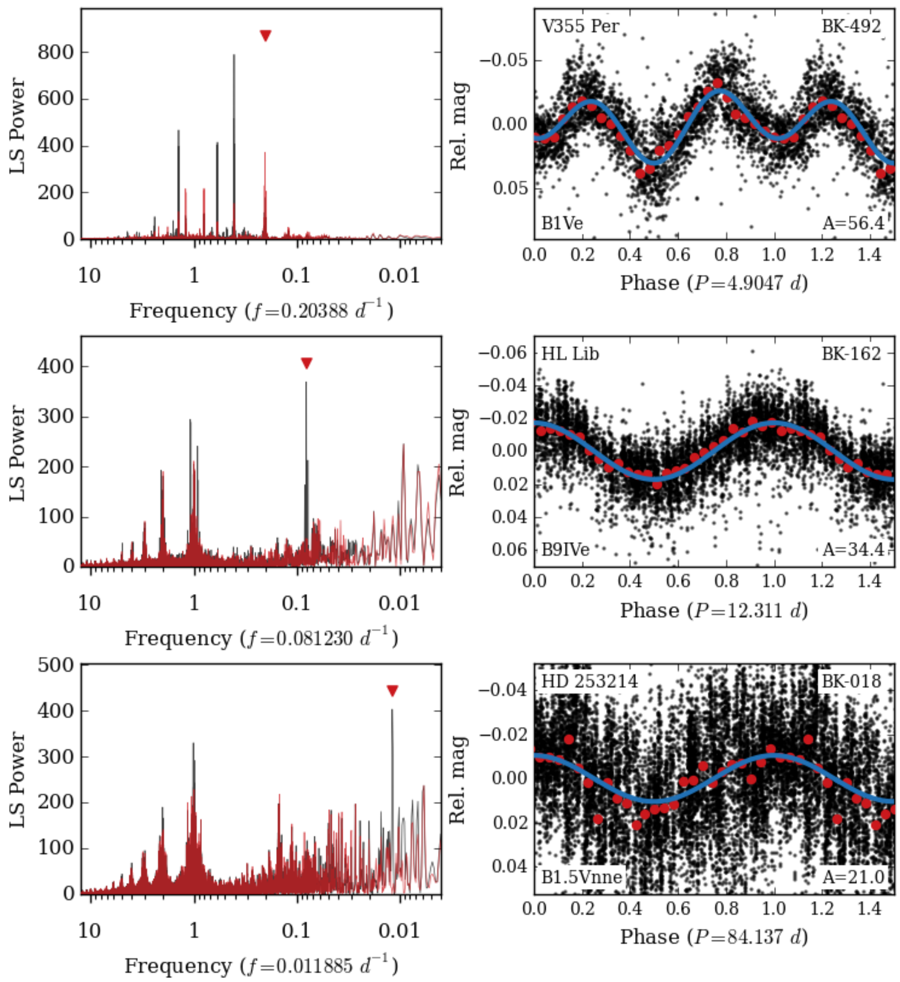

Figure 3.3: Same as Figure 3.3, but for longer periods. The top panel shows a double-waved signal, and is fit with a combination of two sinusoids.

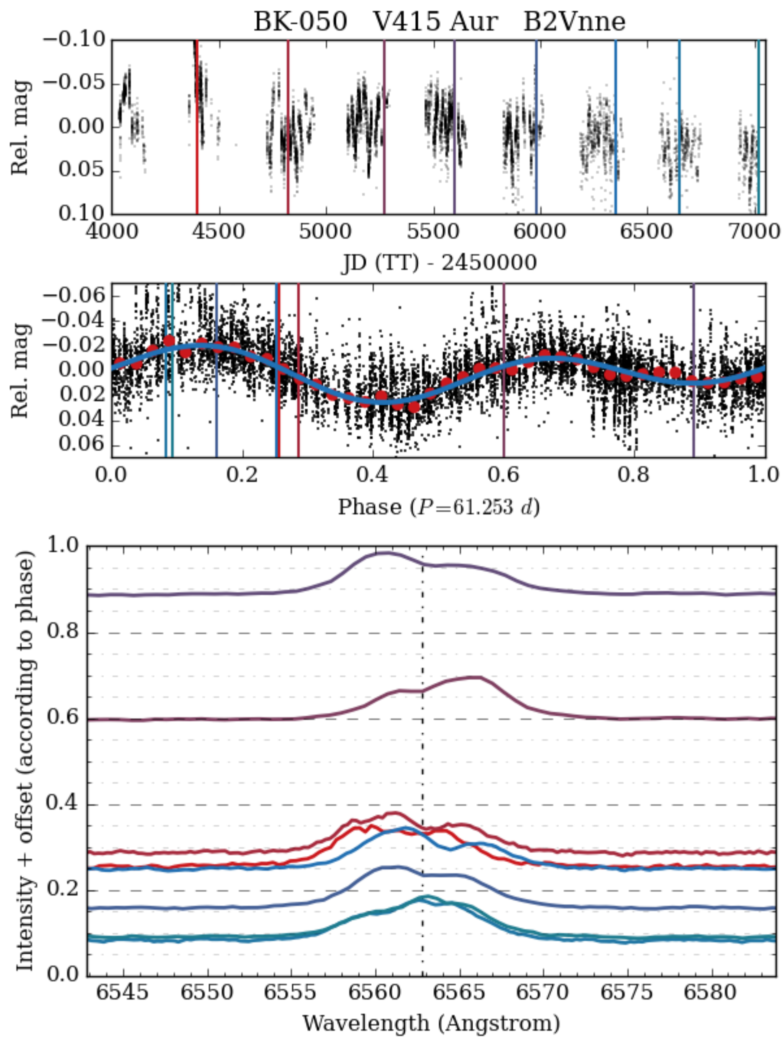

Figure 3.4: *Top:* Raw KELT light curve for BK-050 (HD 33461 = V415 Aur; B2Vnne), with vertical lines indicating dates of BeSS spectra. *Middle:* TFA detrended KELT data phased to a period of 61.253 days. The time-series spectra are then phased to this period, with the color corresponding to the epoch of observation as indicated in the top panel. *Bottom:* Shown are the normalized Hα profiles for each of the eight BeSS spectra offset by the photometric phase.

3.4 Confirming new Be star binaries - ABE-A15

The Be star ABE-A15 was noticed to be RV variable in Chojnowski et al. (2017). This fact prompted the authors to search for confirmation of binarity in this system, which is the topic of Chojnowski *et al.* (2017b, in prep.). Many high-quality spectra were taken, and this is found to be a double-lined binary with a clear RV orbit. This star also exists in the AK sample (*i.e.* has a KELT light curve). Independent analysis of the KELT data finds a significant periodic signal at P=46.793 d, as well as other high-frequency signals. This section describes the photometric analysis, results, and interpretation of these results. While this work is still underway, and therefore preliminary, it demonstrates that periodic photometric signals on intermediate timescales (tens to $\sim$100 days) can lead to the discovery of new Be star binaries.

3.4.1 Raw light curve analysis

The full KELT light curve of ABE-A15 includes four seasons of data, and is displayed in the upper panel of Figure 3.5. The median magnitude has been subtracted off. The histogram of magnitude values in the upper-right panel of Figure 3.5 shows a typical amount of scatter for a KELT light curve, which can be attributed to a combination of astrophysical variability and instrumental noise. Because the histogram is well fit by a Gaussian, this shows that the data is distributed normally about the median. The presence of eclipses would skew the histogram towards the fainter side, while outbursts or flare-type events would skew the histogram towards the brighter side. There are no obvious long-term trends in the data. The next three panels in Figure 3.5 show the light curve for the last three seasons of data, after applying a low-pass filter with a window size of four days. The brightness is varying in a somewhat cyclic way, but is not strictly periodic. A relative brightness maximum is often seen near conjunction, and brightness minima tend to occur near quadrature, although there are exceptions to this pattern. While this oscillatory behavior seems related to the systems orbit, the additional variability may be due to changes in the Be star disk. If the mass loss from the Be star is not constant, then so too will the amount of material (and its distribution) in the disk vary. A variable disk will typically influence the brightness of a given system (e.g. Haubois et al. 2012a; Labadie-Bartz et al. 2017a).

The lack of strong outbursts in the ABE-A15 light curve is somewhat surprising. Spectroscopic data show the disk is strongly detected in all observed epochs, with the equivalent widths of most lines showing little or no significant variability over the ∼15.5 year period between the first and final spectrum. This is in contrast to some Be stars whose disks appear and disappear, or substantially vary in strength (Chojnowski et al. 2017) over timescales from weeks to years. Persistent disks around Be stars require the transfer of mass from star to disk, since Be star disks necessarily dissipate in the absence of mass injection (Lee et al. 1991). Despite the non-detection of strong outbursts in the light curve of ABE-A15, the central Be star must be feeding its disk through mass loss. One possibility is that the inclination angle of the system is such that outbursts do not leave a detectable imprint in the brightness of the system. At an inclination angle of $\sim 70^{\circ}$, an outburst will have close to zero net effect on the brightness of the system, as any increase in flux is effectively cancelled out by the disk partially obscuring the star (Haubois et al. 2012a). Another is that episodic mass loss does occur, but in closely-spaced events with low amplitudes below the detection threshold of KELT. A third possibility is that the Be star loses mass in a more continuous, but still possibly variable, process.

3.4.2 Frequency analysis

A frequency analysis is performed to search for periodic signals between 0.002 – 1000 days. The results presented here are from analysis of the TFA detrended KELT light curve. This analysis was repeated with the raw KELT data, as well as the raw KELT data processed with custom detrending methods. Results are essentially the same for all versions of the light curve. A preliminary analysis suggests that periodic signals exist in three different regimes – low-frequency ($f \lesssim 0.3d^{-1}$), high-frequency ($1\ d^{-1} \lesssim f \lesssim 10\ d^{-1}$), and very high-frequency ($f \gtrsim 50d^{-1}$). The results of this analysis are summarized in Table 3.1. The recovered frequency, period, and amplitude are listed. The logarithm of the false alarm probability (FAP) is listed next. This quantity is output for each peak recovered in the LS periodogram, and measures the probability that a light curve without any periodic signal would result in a peak of the same height, just through coincidental arrangement of the data. The final column shows the spectroscopic signal to noise ratio (SNR), which is also output for each peak. Our requirement for a peak to be significant is that it have values for log(FAP) $\leq$ -2.0, and a SNR $\geq$ 10.0. The exception is f_7, with log(FAP) = -1.05. However, we still consider this a reliable detection for reasons explained below.

In order to interpret a LS periodogram, it is necessary to understand the "window function" associated with the light curve, which is determined by the patterns of the timing of each observational epoch. With KELT (and other ground-based surveys), there are strong daily, monthly, and yearly components inherent to the observing strategy, which leaves a characteristic imprint in periodograms calculated from ground-based data. If not treated cautiously, these signals, which are purely a result of the timing of observations, can be misinterpreted as real, astrophysical frequencies. Another consequence of this is that any true, single, periodic signal originating in the source will alias with the window function, causing multiple periodogram peaks. This problem can be mitigated by understanding the window function, and by applying the method of pre-whitening to remove a given signal. The window function can be visualized by fixing all magnitude values in a light curve to unity (while leaving the time values unchanged), and then computing the LS periodogram on this perfectly flat time series. Any peaks in the resultant periodogram are then solely due to the observing pattern.

Table 3.1: Periodic signals detected in photometry

	Frequency (d^{-1})	Period (d)	Amplitude (mmag)	Log(FAP)	SNR
f_0	0.02138	46.783	4.2	-23.19	29.56
f_1	2.54400	0.39308	5.4	-35.10	61.61
f_2	2.56031	0.39058	4.1	-25.38	46.80
f_3	4.25419	0.23506	3.3	-7.77	19.13
f_4	4.53087	0.22071	2.0	-4.56	14.26
f_5	7.35575	0.13595	2.4	-2.84	11.62
f_6	5.21677	0.19169	1.9	-2.05	10.48
f_7	93.7243	0.01067	2.7	-1.05	16.99

Table of frequencies detected in the light curve of HD 55606.

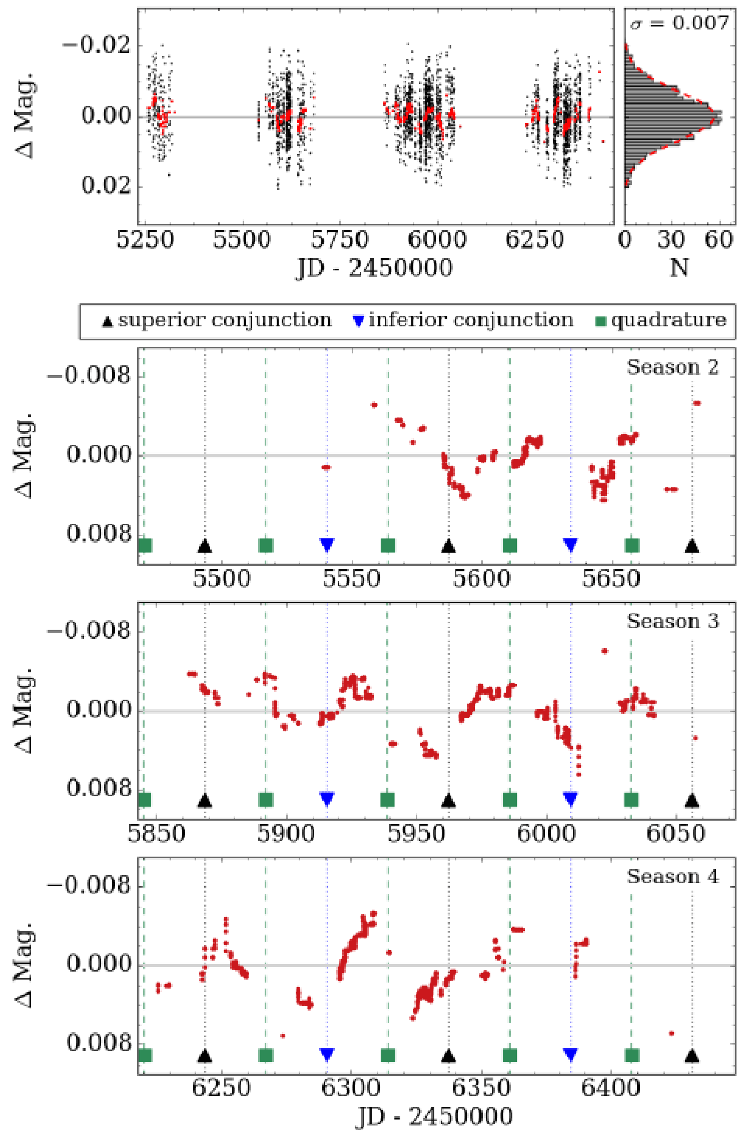

Figure 3.5: Full KELT light curve of ABE-A15 (black points). The red points show the data after applying a low-pass filter. The right panel shows a histogram of the relative magnitude values, with bin sizes of 0.001 mag (1 mmag). There are 42 bins in total, and a single Gaussian is fit to this distribution, having a standard deviation of 0.007 mag. The lower three panels show the latter three seasons of KELT data (after applying a low-pass filter). The first season is not highlighted, due to a relative dearth of observations. The orbital configuration, as computed from the spectroscopic orbit, is indicated by vertical dashed lines and triangles (squares) to indicate conjunction (quadrature).

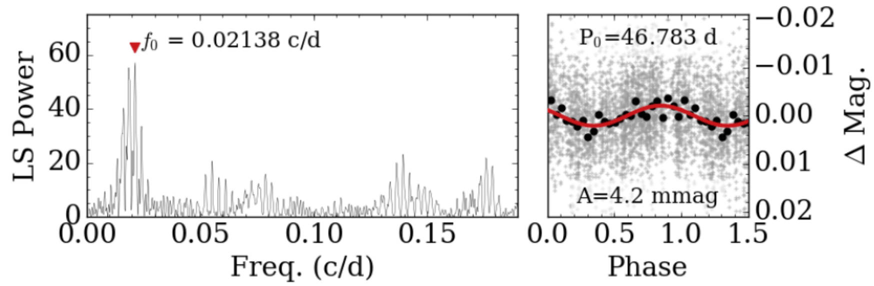

Figure 3.6: *Left :* Low-frequency region of the LS periodogram calculated from the light curve of ABE-A15. *Right :* KELT data phased to the recovered period, plotted as gray "+" signs. Large black points denote median-binned data, with 25 bins in phase (or, a bin size of 0.04 in phase). Each bin then contains approximately 100 photometric data points on average. A single sinusoid (red curve) is fit to the binned data. The peak-to-trough amplitude of this sinusoid is shown in units of mmag.

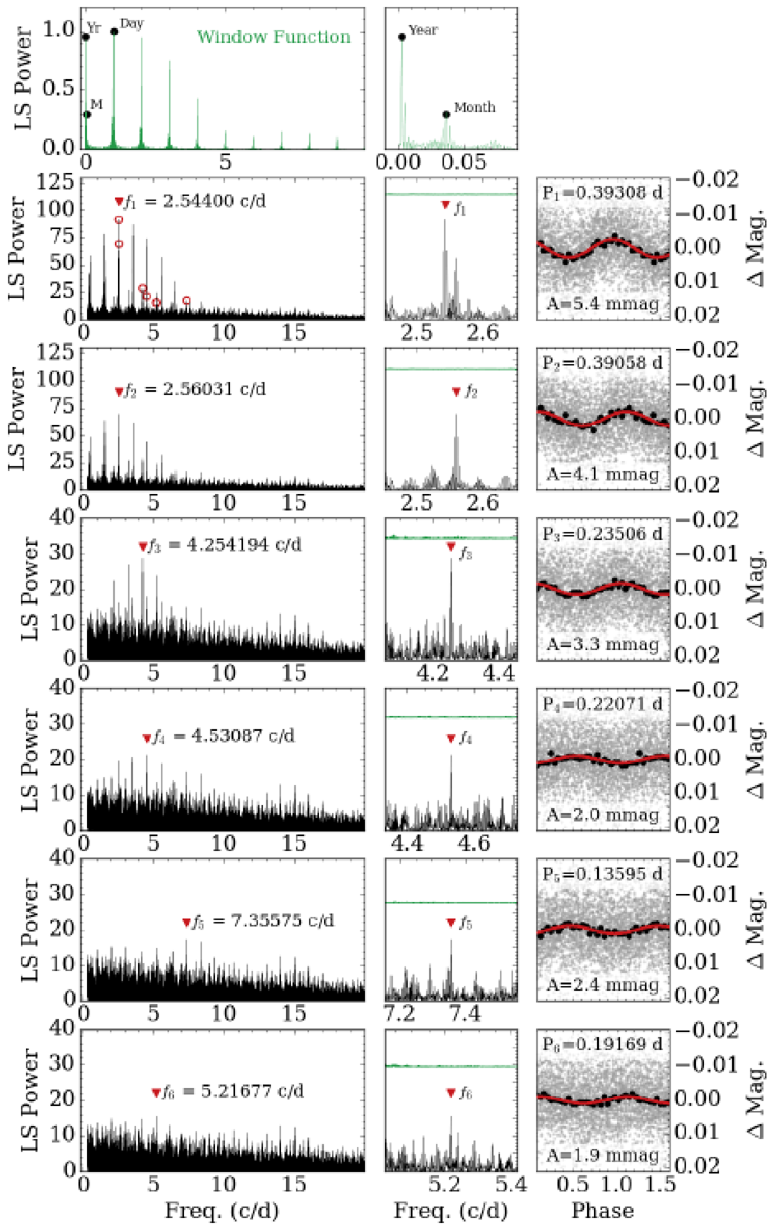

Figure 3.7: *Top :* Window function associated with the light curve, with the low-frequency regime highlighted on the right. The remaining six rows show, for $f_1 - f_6$, the LS periodogram, a zoom-in on the relevant peak, and phased KELT data, shown in the same manner as in Figure 3.6. These six frequencies are marked with red circles in the periodogram in the second row. The data is prewhitened against the top peak before the next periodogram is computed. In the middle column, the window function is shown near the top, scaled by a factor of 40. None of these peaks coincide with a peak in the window function.

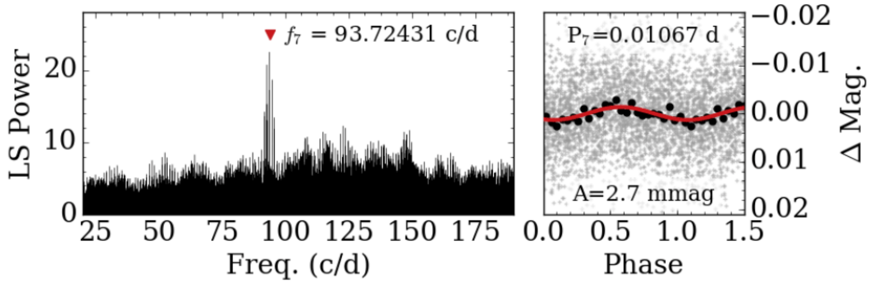

Figure 3.8: Same as in Figure 3.6, but for the very high frequency signal f_7. The window function is now shown, but is entirely featureless in this frequency regime.

First, we consider the low-frequency regime, where we might expect to see signals associated with disk variability or binarity. A strong signal is detected at P_0=46.783 days, with the corresponding section of the periodogram and the phase-folded light curve shown in Figure 3.6. There is no power in the window function near this frequency. No other independent significant peaks were found in this frequency regime.

In order to facilitate the search for high-frequency signals, all variability with timescales of 3 days or longer is first subtracted from the data. We then compute the LSP, searching for signals with frequencies up to 20 d^{-1}. Pulsation in Be stars is typically found within this frequency regime. Figure 3.7 shows the results of this step in our frequency analysis. The top row shows the window function (in green), where strong peaks are obvious at one day and integer fractions of one day. The panel immediately to the right zooms in on the low-frequency limit, highlighting the monthly and yearly peaks of the window function (note that $f_0 = 0.02138d^{-1}$ lies comfortably between the monthly and yearly peaks). The remaining rows show LSPs calculated from the light curve of ABE-A15 (left column), with a zoom-in around the frequency of the recovered signal (middle column), and the KELT light curve phase-folded to the recovered period (right column). In each row in the central column, the corresponding section of the window function is also displayed, scaled by a factor of 40, plus a vertical offset. We find six significant and independent peaks ($f_1 - f_6$), marked with red o's on the periodogram in the second row. The data is iteratively prewhitened against each recovered frequency, before being re-calculated.

We also searched for very high frequencies, between 20 – 480 d^{-1}. This upper limit was chosen because the maximum cadence of images in KELT is 3 minutes, corresponding to 480 d^{-1}. Before running our search, we prewhitened the light curve against the signals f_0 – f_6. We find one convincing signal in this regime at f_7 = 93.7243 d^{-1}. The light curve phased to P_7 = 0.01067 d, and the relevant section of the periodogram are shown in Figure 3.8. Although this signal has a FAP lower than our threshold, we still consider this a significant detection. This same procedure was applied to other stars of similar brightness from the same KELT field (and therefore of similar precision and at virtually the same cadence), and none showed any periodogram features in this regime. There is virtually no power in the window function at these high frequencies. The very long baseline of the light curve (relative to the signal) makes these peaks extremely narrow and well-defined. Nothing is found that suggests f_7 is caused by the observing cadence or any systematic effects.

3.4.3 Discussion

The longest periodic signal (P_0 = 46.783 days) is very close to half of the spectroscopic orbital period reported in (Chojnowski *et al.* 2017b, in prep.; within about 0.2%). This strongly suggests that the physical origin of this signal is related to the binary orbit of this system. Qualitatively similar signals (periodic brightness variability at half the orbital period) are seen in the familiar case of ellipsoidal variables, where the surface of one or both stars is deformed, and elongated along the line connecting the two. The system parameters of ABE-A15 do not allow for this – the two components are too far separated to gravitationally deform each other's surface in a significant way. However, the companion likely interacts with the Be star disk both gravitationally and radiatively. Panoglou et al. (2016) use three-dimensional smoothed particle hydrodynamics code to simulate systems comprised of a Be star and its disk, and a binary companion. The authors find that tidal forces from the secondary can cause many aspects of the Be star disk to acquire an azimuthal structure, including the truncation radius, the density profile in the inner and outer disk, and the disk base surface density. One notable prediction of these models is that the disk will become elongated both in the direction of 20° ahead of the companion, and also in the direction opposite this. This structure becomes phase-locked, and rotates with the binary orbit. Additionally, the hot companion illuminates the side of the Be star disk facing it. It is not clear precisely what mechanisms are responsible for modulating the brightness of ABE-A15 over its orbit.

Figure 3.5 shows that there is variation from orbit to orbit, in addition to the periodic signal. As mentioned in Section 3.4.1, this additional variability may be due to changes in the Be star disk. The KELT light curve has a baseline of 1165 days, over which ~12.4 orbits occur. Only about half of these are sampled at all, given the gaps in coverage. Photometric variability is both observed and predicted in certain Be star binary configurations. The Be+sdO binary ϕ Per exhibits complex light variability over its orbital period of ~126.7 days (Bozic et al. 1995), and the models of Panoglou et al. (2016) predict photometric variability caused by the co-rotating structure of the Be star disk. It is also possible that the effects of irradiation from the companion on the Be star disk can contribute to the observed net brightness.

Pulsation seems to be ubiquitous among Be stars– all Be stars observed with high-cadence, long duration space-based photometry are found to be multi-mode, non-radial pulsators (Rivinius et al. 2013, and references therein). The high-frequency signals $f_1 - f_6$ have timescales and amplitudes that are consistent with stellar non-radial pulsation in Be stars (e.g. Baade et al. 2016b; Huat et al. 2009). Some Be stars oscillate in modes with amplitudes in the sub-mmag regime (e.g. HD 49330 (B0.5IVe) Huat et al. 2009), so it is possible that additional frequencies exist in ABE-A15, but avoid detection in our data.

The very high-frequency signal, f_7, occurs on a much shorter timescale than is expected for oscillations in Be stars. This signal, with a period of $P_7 = 0.01067d = 15.36\ min$, possibly represents pulsation in the companion. Hot subdwarf stars are known to pulsate, often in multiple modes and with typical periods between $\sim 2 - 45$ minutes (e.g. Kawaler et al. 2010; Østensen et al. 2001a,b; Reed et al. 2010). Often these have low amplitudes on the order of $\sim 1 - 10$ mmag. However, in some cases the amplitudes can be much larger. For example, the sdO star PG 1605+072 shows over 55 modes, the strongest of which has a period of 8.03 minutes and an amplitude of over 50 mmag (Pereira and Lopes 2004). Given that the Be star component of ABE-A15 dominates the visible flux, we do not expect to detect any low-amplitude signals in the companion. However, a high-amplitude signal, like that observed in PG 1605+072, is potentially strong enough to detect, although the amplitude will be severely diminished because of contamination from the Be star component.

3.5 Summary of periodic variability

A histogram showing the distribution of all recovered periods is shown in Figure 3.9. This histogram includes all types of periodic variability, and is complicated by the fact that a single star can exhibit more than one period in its light curve. Because of the diurnal sampling of the KELT survey, periodic signals very close to one day are poorly sampled. The dearth of detected periods very near to one day is a result of this systematic effect.

Lomb-Scargle periodograms and phase-folded light curves are presented for each object in the BK sample where a periodic signal was recovered. Figure 3.10 shows systems with high-frequency signals, which are best explained by pulsation. Figure 3.11 shows those systems where low-frequency signals are recovered, ordered by increasing period.

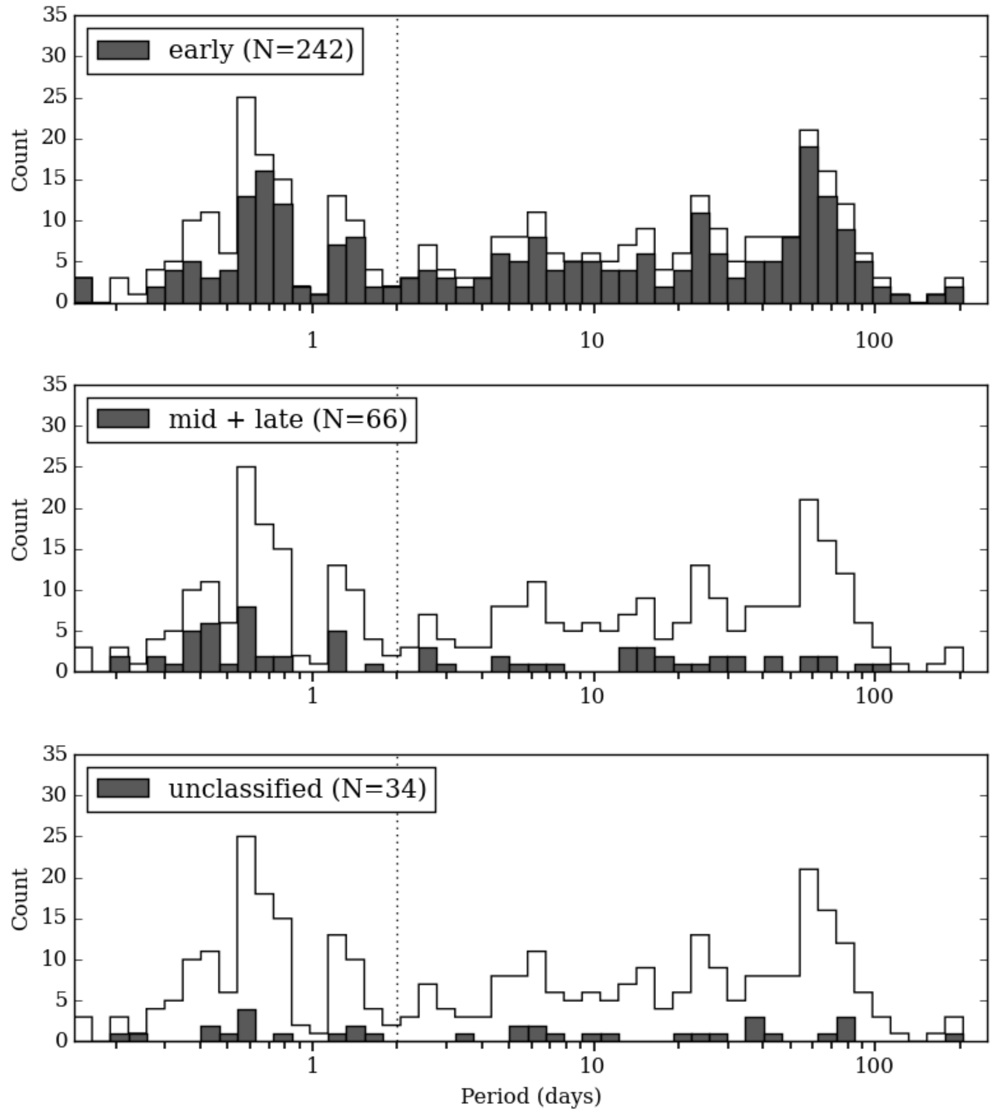

Figure 3.9: Histogram showing the distribution of all periodic signals found in objects within the BK sample on a logarithmic scale spanning between 0.1 - 200 days, displayed in the same manner as in Figure 4.13. The vertical dotted line at 2 days marks the cutoff between short periods and intermediate periods. The short-period variables are left of the dotted line, and are best explained by NRP modes in the star. All types of periodic variability are included in this histogram. A single star may have multiple periods at different timescales and thus may appear in up to three different bins, although the majority of periodically variable stars have a single dominant frequency.

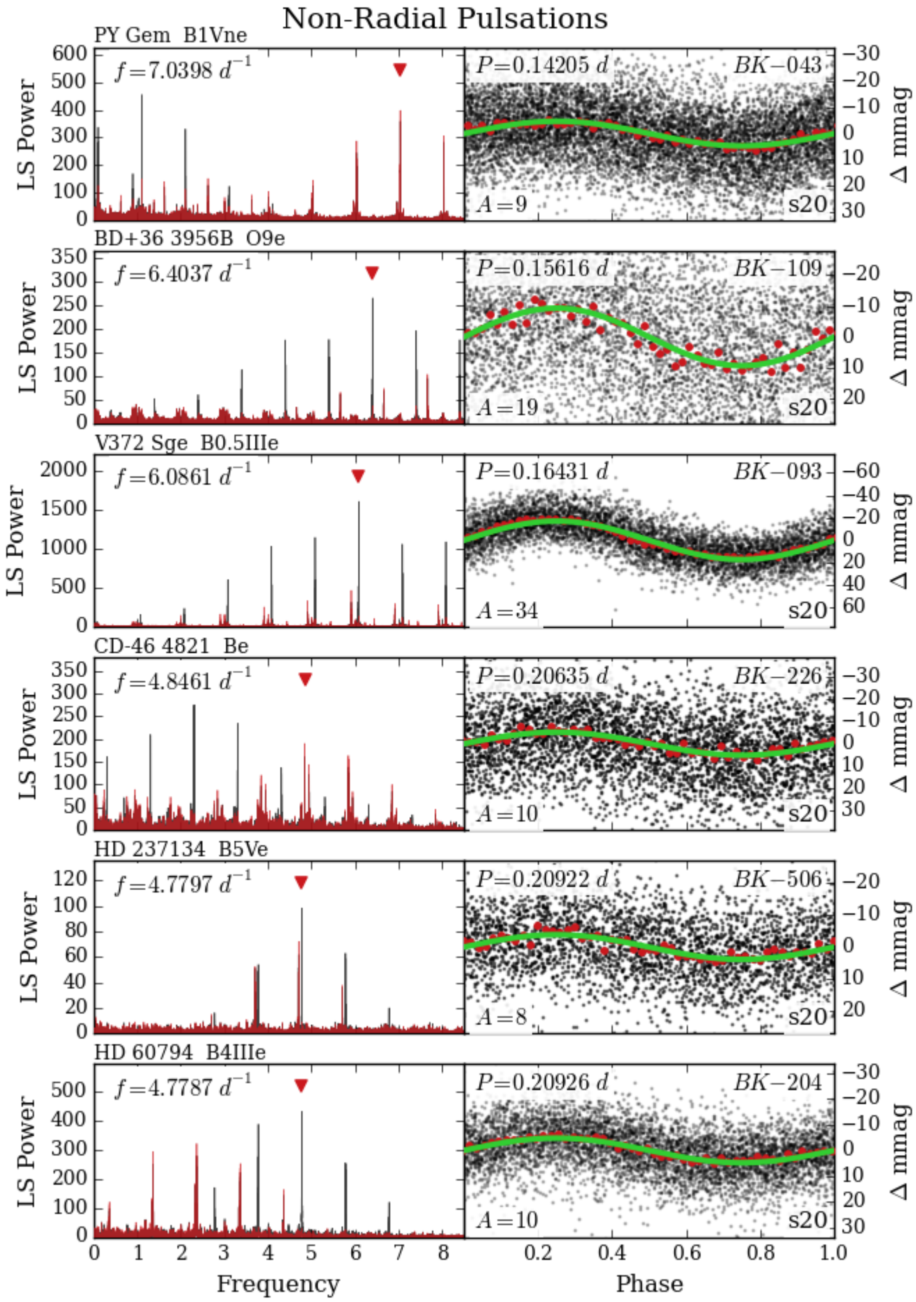

Figure 3.10: Panels showing phased light curves are similar to those in Figure 3.1. The green curve shows a fit using one sinusoid for single-wave signals, or two sinusoids for double-wave signals. The other panels show Lomb-Scargle periodograms in black, and whitened periodograms in red.

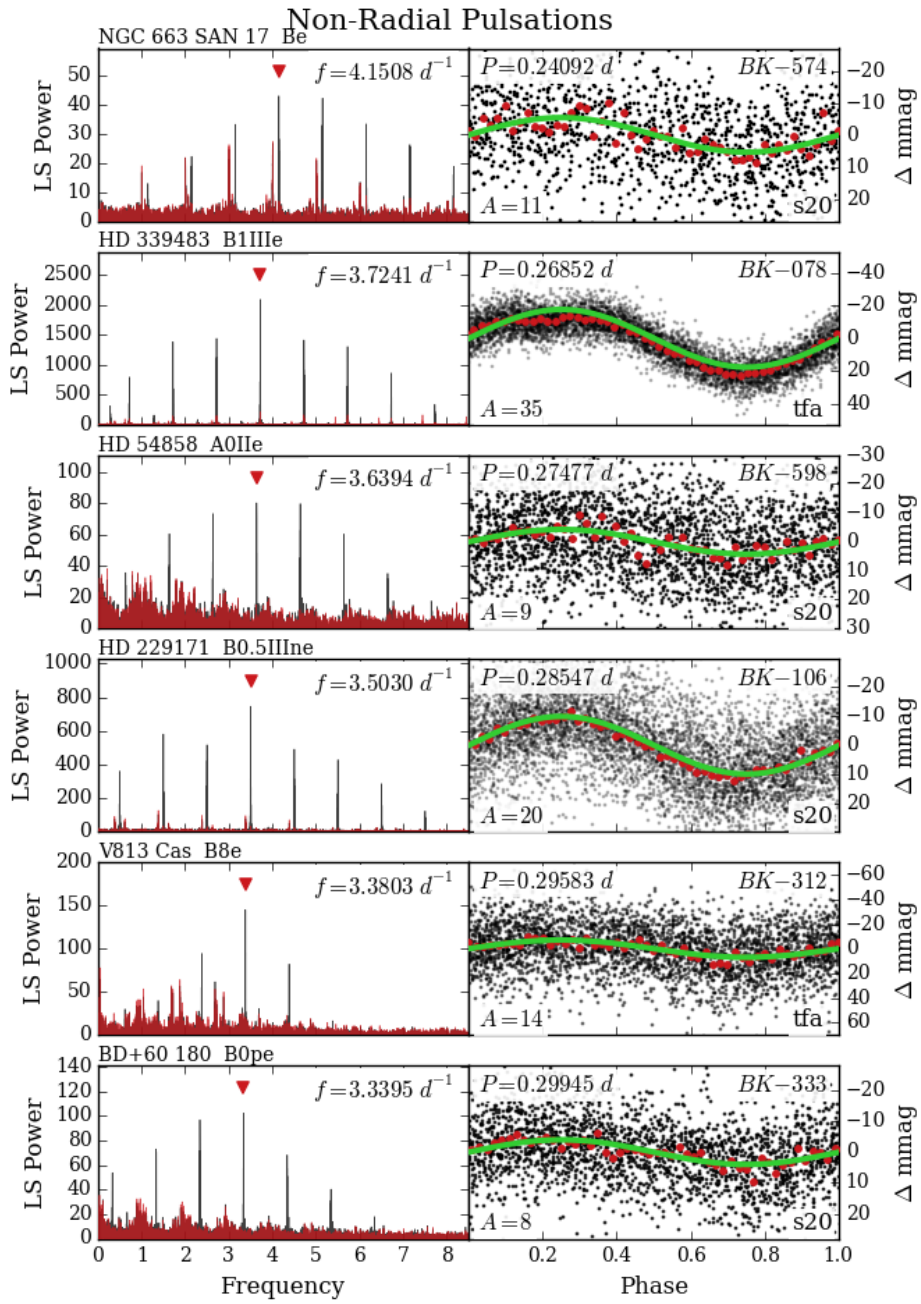
Non-Radial Pulsations
NGC 663 SAN 17 Be
f=4.1508 d^-1
P=0.24092 d
BK-574
A=11
s20
HD 339483 B1IIIe
f=3.7241 d^-1
P=0.26852 d
BK-078
A=35
tfa
HD 54858 A0IIe
f=3.6394 d^-1
P=0.27477 d
BK-598
A=9
s20
HD 229171 B0.5IIIne
f=3.5030 d^-1
P=0.28547 d
BK-106
A=20
s20
V813 Cas B8e
f=3.3803 d^-1
P=0.29583 d
BK-312
A=14
tfa
BD+60 180 B0pe
f=3.3395 d^-1
P=0.29945 d
BK-333
A=8
s20
LS Power
Δ mmag
Frequency
Phase

Figure 3.10: B

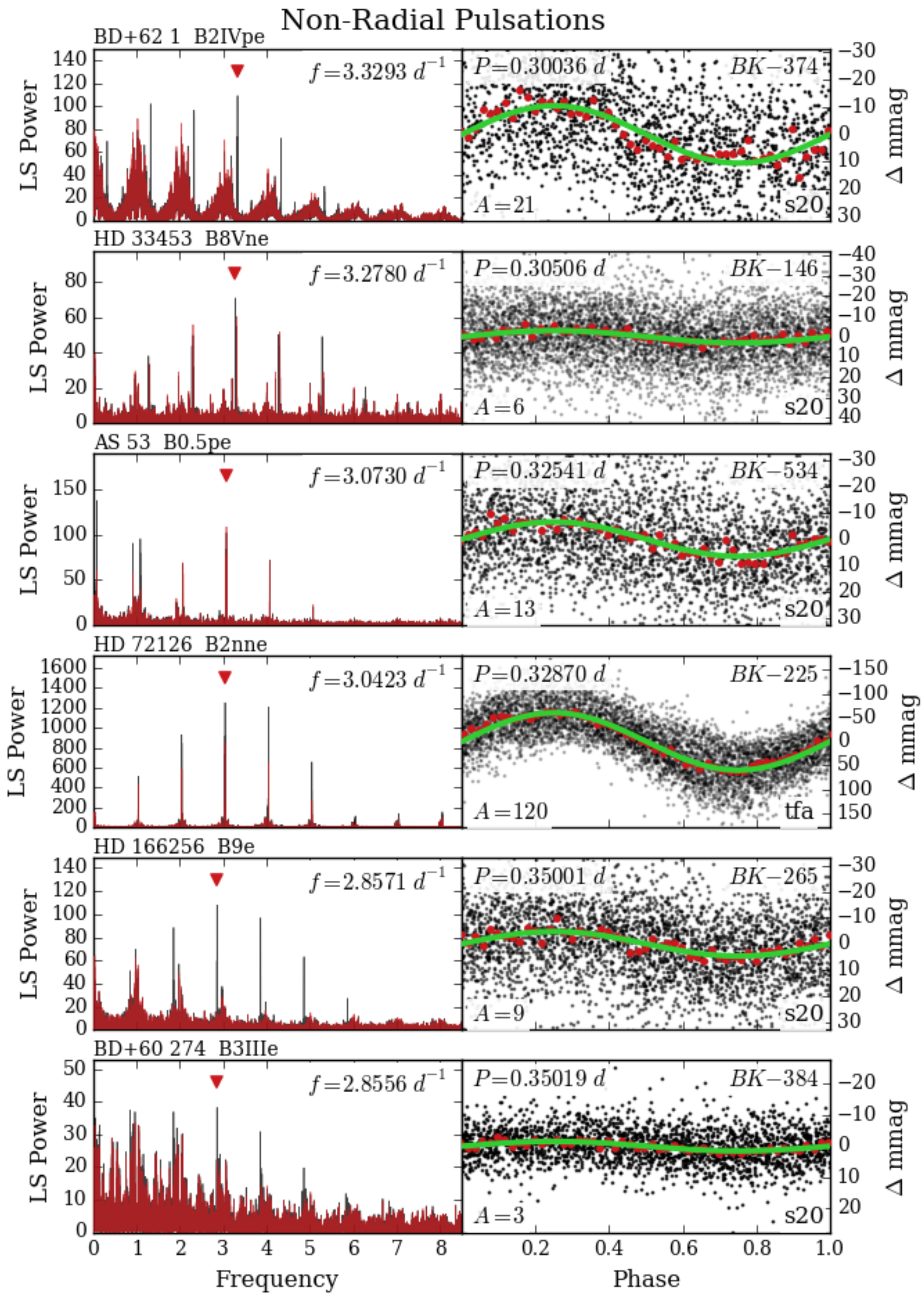
Non-Radial Pulsations
BD+62 1 B2IVpe
f = 3.3293 d^-1
P = 0.30036 d
BK−374
A = 21
s20
HD 33453 B8Vne
f = 3.2780 d^-1
P = 0.30506 d
BK−146
A = 6
s20
AS 53 B0.5pe
f = 3.0730 d^-1
P = 0.32541 d
BK−534
A = 13
s20
HD 72126 B2nne
f = 3.0423 d^-1
P = 0.32870 d
BK−225
A = 120
tfa
HD 166256 B9e
f = 2.8571 d^-1
P = 0.35001 d
BK−265
A = 9
s20
BD+60 274 B3IIIe
f = 2.8556 d^-1
P = 0.35019 d
BK−384
A = 3
s20
LS Power
Δ mmag
Frequency
Phase

Figure 3.10: C

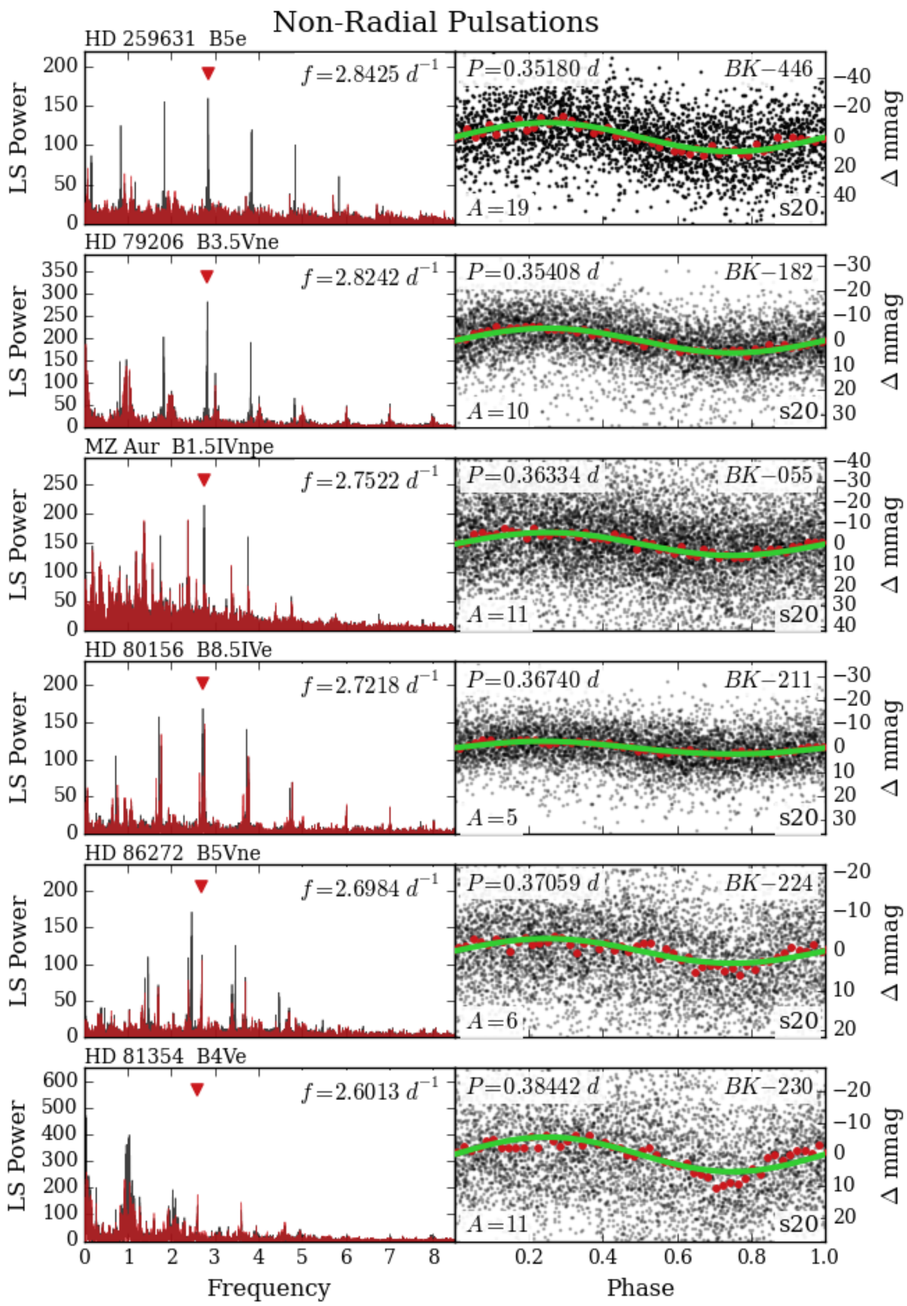

Non-Radial Pulsations
HD 259631 B5e
$f=2.8425\ d^{-1}$
$P=0.35180\ d$
$BK-446$
$A=19$
s20
HD 79206 B3.5Vne
$f=2.8242\ d^{-1}$
$P=0.35408\ d$
$BK-182$
$A=10$
s20
MZ Aur B1.5IVnpe
$f=2.7522\ d^{-1}$
$P=0.36334\ d$
$BK-055$
$A=11$
s20
HD 80156 B8.5IVe
$f=2.7218\ d^{-1}$
$P=0.36740\ d$
$BK-211$
$A=5$
s20
HD 86272 B5Vne
$f=2.6984\ d^{-1}$
$P=0.37059\ d$
$BK-224$
$A=6$
s20
HD 81354 B4Ve
$f=2.6013\ d^{-1}$
$P=0.38442\ d$
$BK-230$
$A=11$
s20
LS Power
Δ mmag
Frequency
Phase

Figure 3.10: D

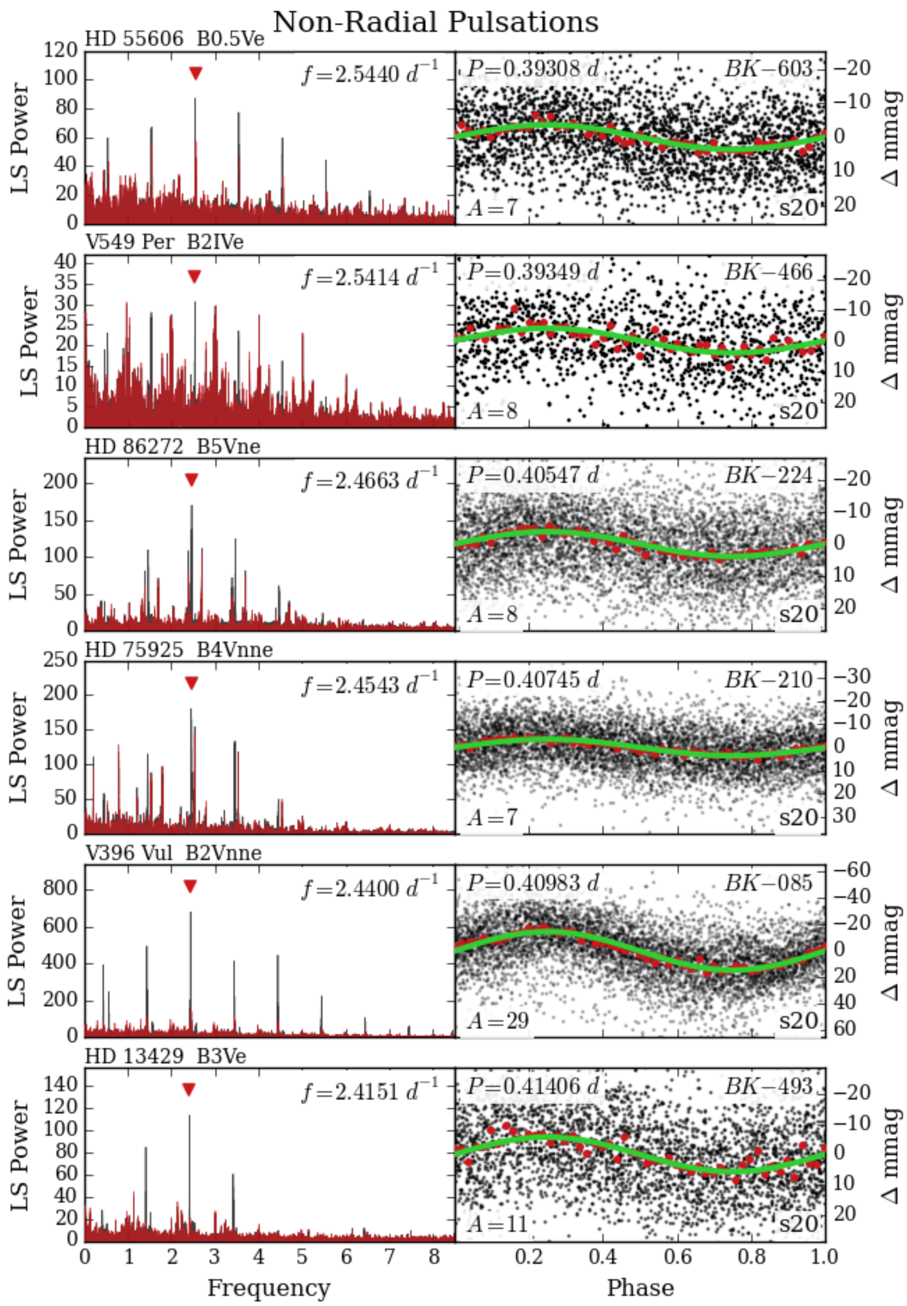

Non-Radial Pulsations
HD 55606 B0.5Ve
f=2.5440 d^-1
P=0.39308 d
BK−603
A=7
s20
V549 Per B2IVe
f=2.5414 d^-1
P=0.39349 d
BK−466
A=8
s20
HD 86272 B5Vne
f=2.4663 d^-1
P=0.40547 d
BK−224
A=8
s20
HD 75925 B4Vnne
f=2.4543 d^-1
P=0.40745 d
BK−210
A=7
s20
V396 Vul B2Vnne
f=2.4400 d^-1
P=0.40983 d
BK−085
A=29
s20
HD 13429 B3Ve
f=2.4151 d^-1
P=0.41406 d
BK−493
A=11
s20
LS Power
Δ mmag
Frequency
Phase

Figure 3.10: E

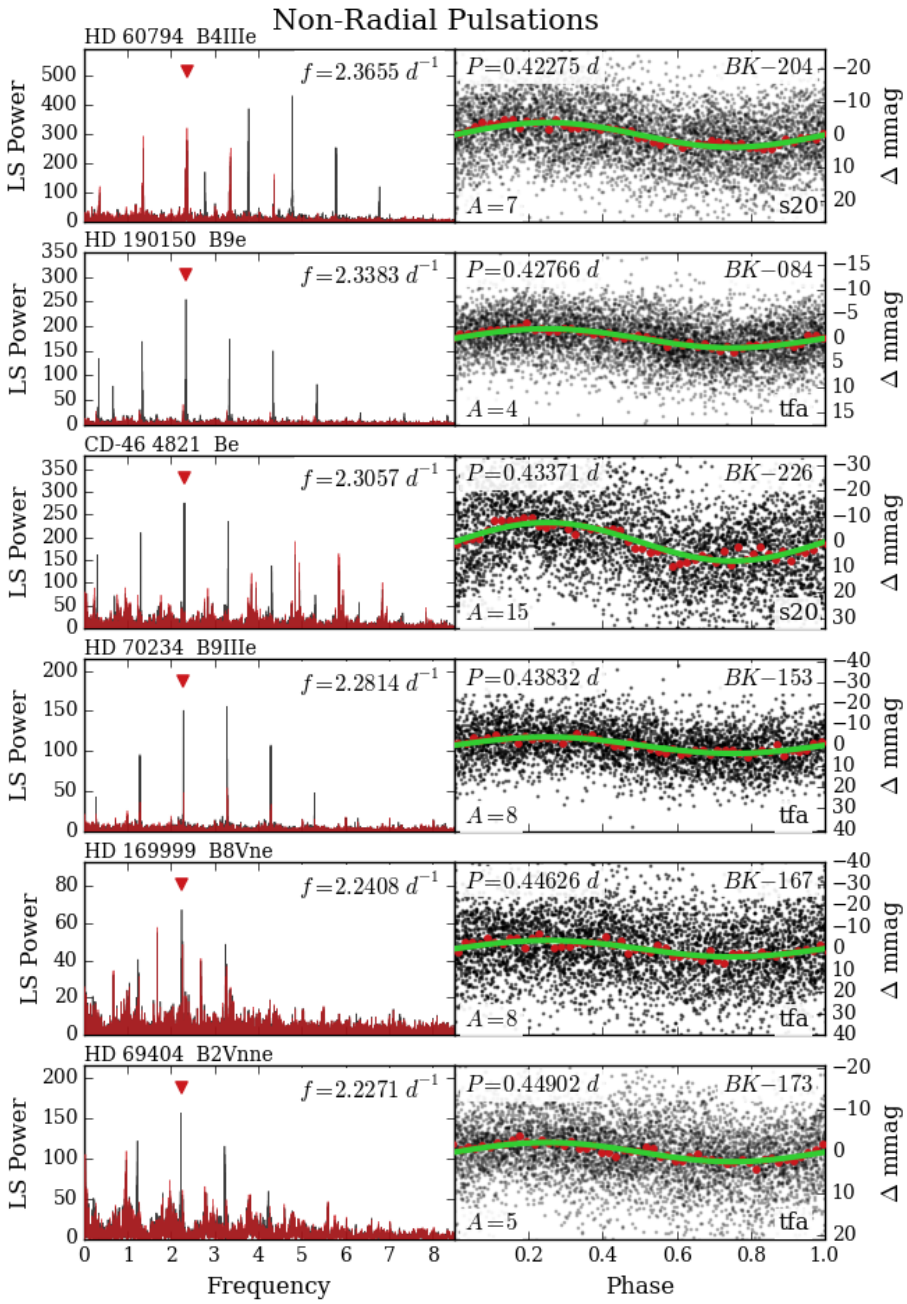
Non-Radial Pulsations
HD 60794 B4IIIe
$f=2.3655\ d^{-1}$
$P=0.42275\ d$
$BK-204$
$A=7$
s20
HD 190150 B9e
$f=2.3383\ d^{-1}$
$P=0.42766\ d$
$BK-084$
$A=4$
tfa
CD-46 4821 Be
$f=2.3057\ d^{-1}$
$P=0.43371\ d$
$BK-226$
$A=15$
s20
HD 70234 B9IIIe
$f=2.2814\ d^{-1}$
$P=0.43832\ d$
$BK-153$
$A=8$
tfa
HD 169999 B8Vne
$f=2.2408\ d^{-1}$
$P=0.44626\ d$
$BK-167$
$A=8$
tfa
HD 69404 B2Vnne
$f=2.2271\ d^{-1}$
$P=0.44902\ d$
$BK-173$
$A=5$
tfa
LS Power
Δ mmag
Frequency
Phase

Figure 3.10: F

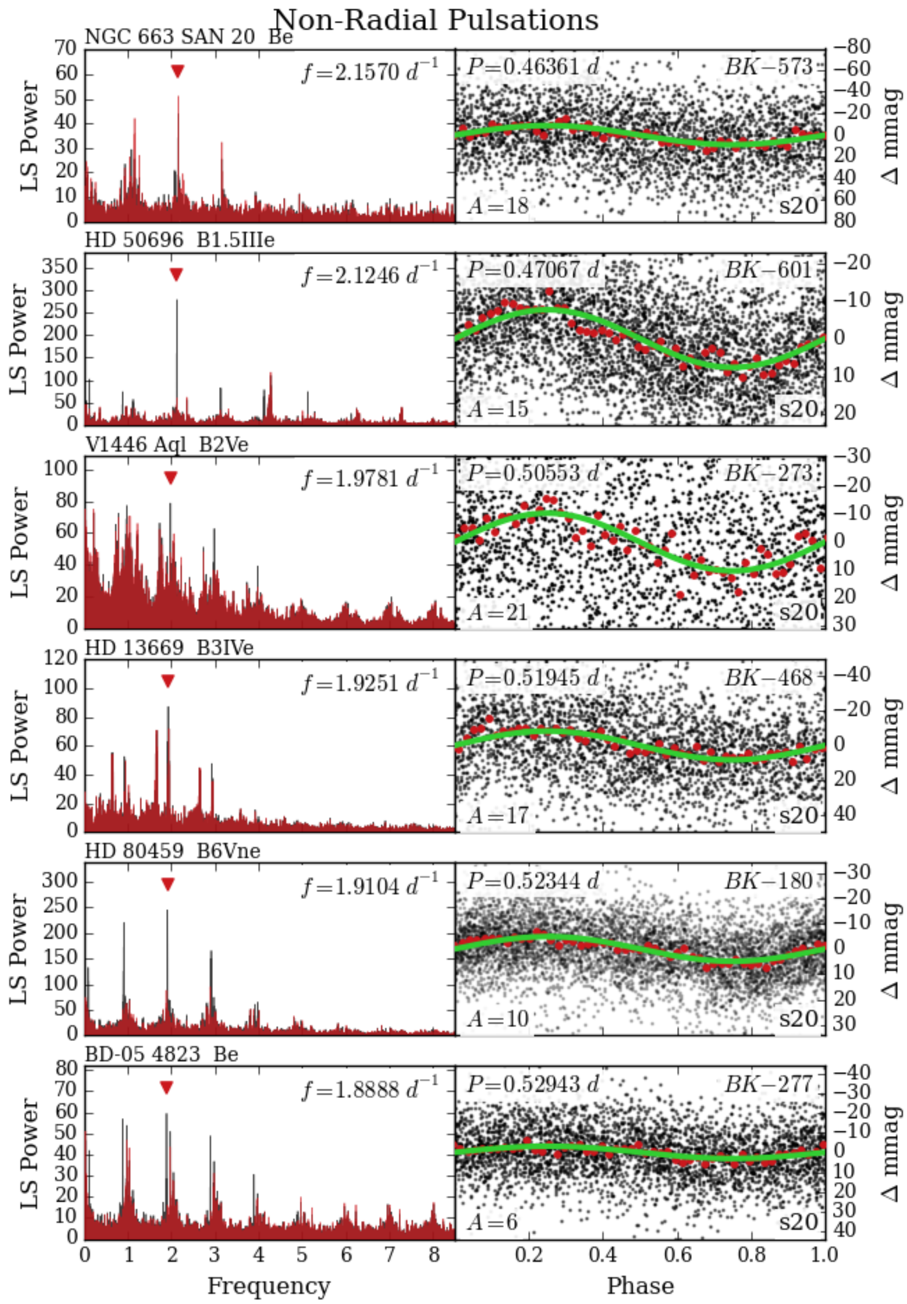
Non-Radial Pulsations
NGC 663 SAN 20 Be
f=2.1570 d^-1
P=0.46361 d
BK−573
A=18
s20
HD 50696 B1.5IIIe
f=2.1246 d^-1
P=0.47067 d
BK−601
A=15
s20
V1446 Aql B2Ve
f=1.9781 d^-1
P=0.50553 d
BK−273
A=21
s20
HD 13669 B3IVe
f=1.9251 d^-1
P=0.51945 d
BK−468
A=17
s20
HD 80459 B6Vne
f=1.9104 d^-1
P=0.52344 d
BK−180
A=10
s20
BD-05 4823 Be
f=1.8888 d^-1
P=0.52943 d
BK−277
A=6
s20
LS Power
Δ mmag
Frequency
Phase

Figure 3.10: G

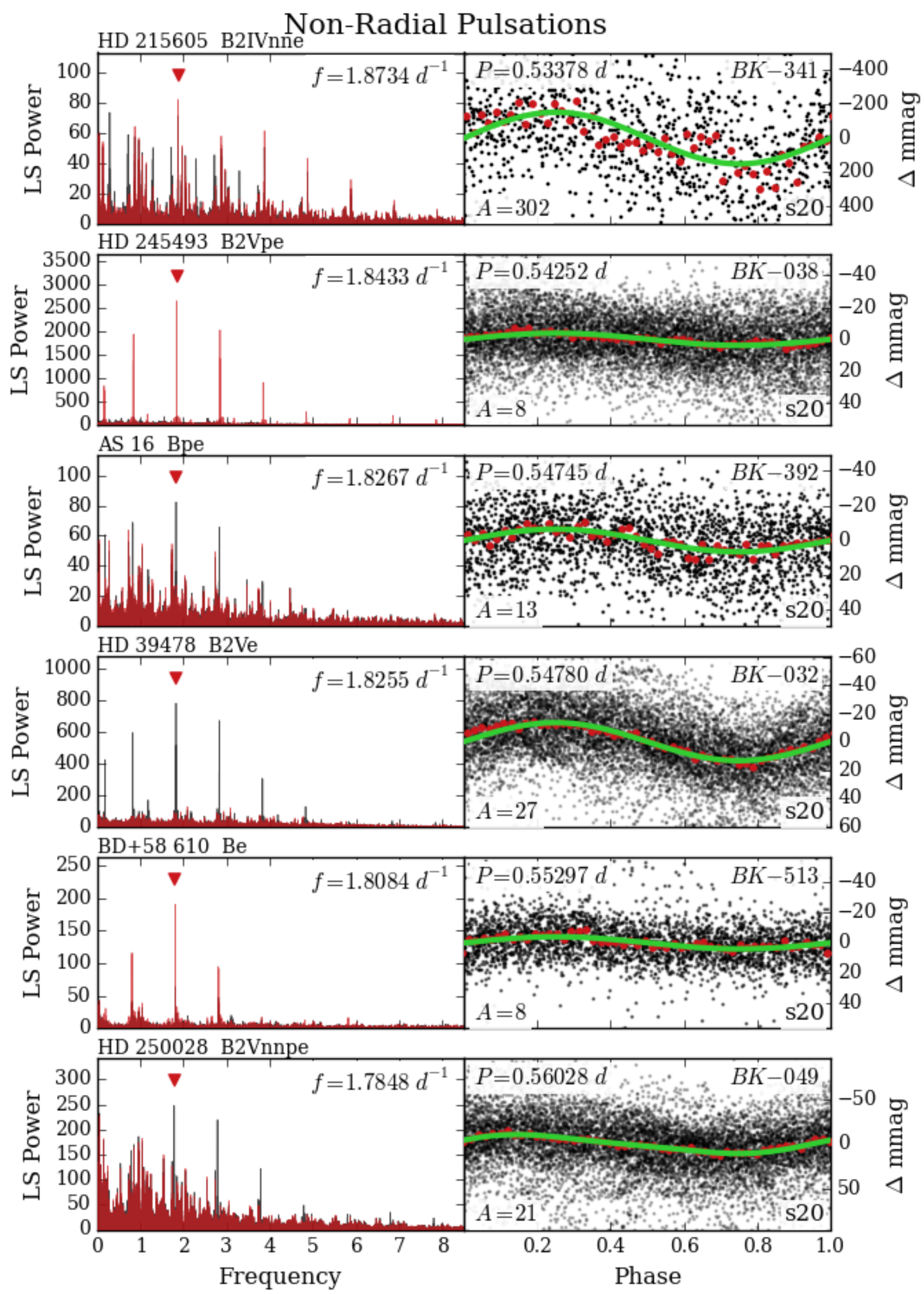

Non-Radial Pulsations
HD 215605 B2IVnne
f = 1.8734 d^-1
P = 0.53378 d
BK−341
A = 302
s20
HD 245493 B2Vpe
f = 1.8433 d^-1
P = 0.54252 d
BK−038
A = 8
s20
AS 16 Bpe
f = 1.8267 d^-1
P = 0.54745 d
BK−392
A = 13
s20
HD 39478 B2Ve
f = 1.8255 d^-1
P = 0.54780 d
BK−032
A = 27
s20
BD+58 610 Be
f = 1.8084 d^-1
P = 0.55297 d
BK−513
A = 8
s20
HD 250028 B2Vnnpe
f = 1.7848 d^-1
P = 0.56028 d
BK−049
A = 21
s20
LS Power
Δ mmag
Frequency
Phase

Figure 3.10: H

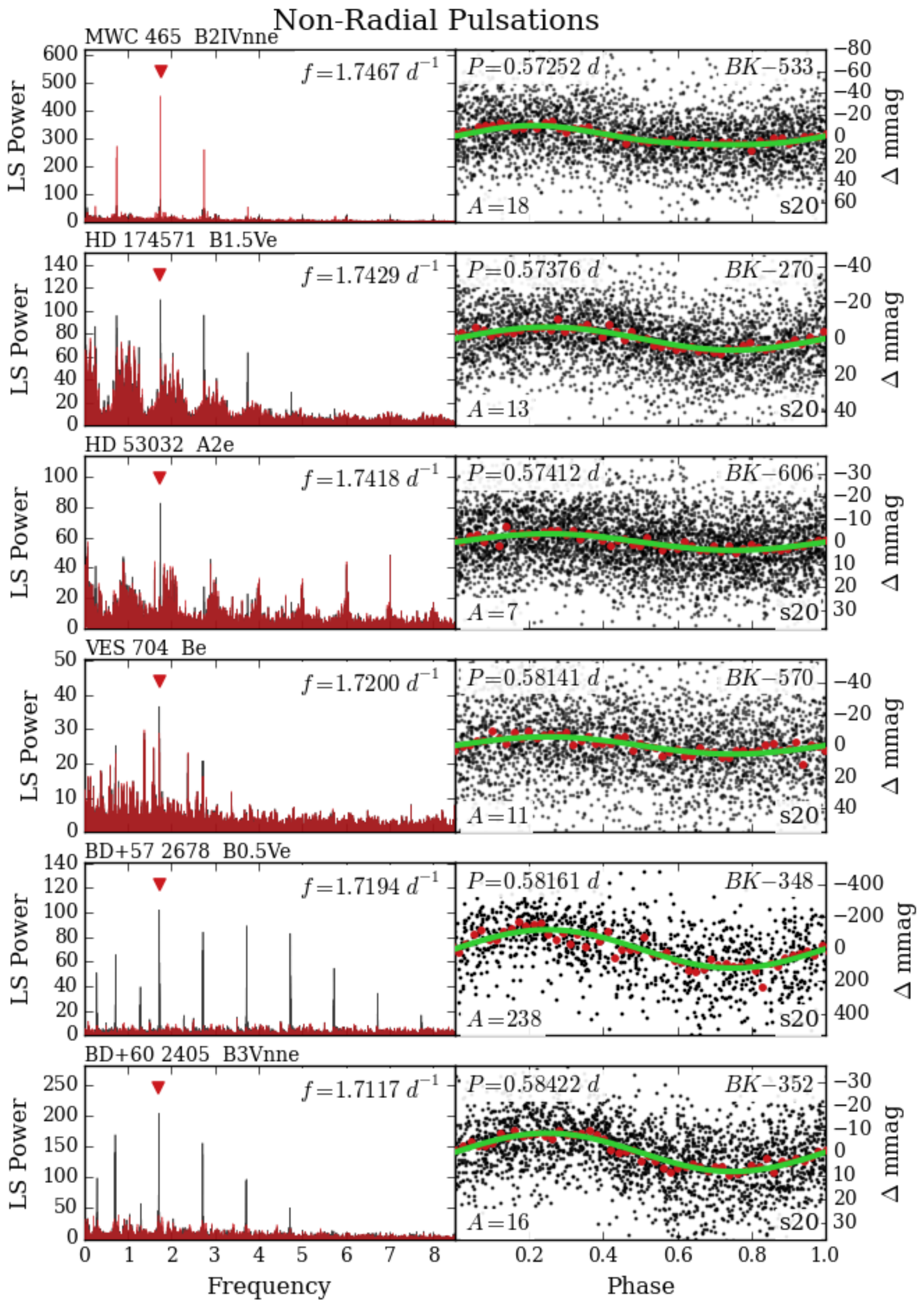
Non-Radial Pulsations
MWC 465 B2IVnne
f=1.7467 d^-1
P=0.57252 d
BK−533
A=18
s20
HD 174571 B1.5Ve
f=1.7429 d^-1
P=0.57376 d
BK−270
A=13
s20
HD 53032 A2e
f=1.7418 d^-1
P=0.57412 d
BK−606
A=7
s20
VES 704 Be
f=1.7200 d^-1
P=0.58141 d
BK−570
A=11
s20
BD+57 2678 B0.5Ve
f=1.7194 d^-1
P=0.58161 d
BK−348
A=238
s20
BD+60 2405 B3Vnne
f=1.7117 d^-1
P=0.58422 d
BK−352
A=16
s20
LS Power
Δ mmag
Frequency
Phase

Figure 3.10: I

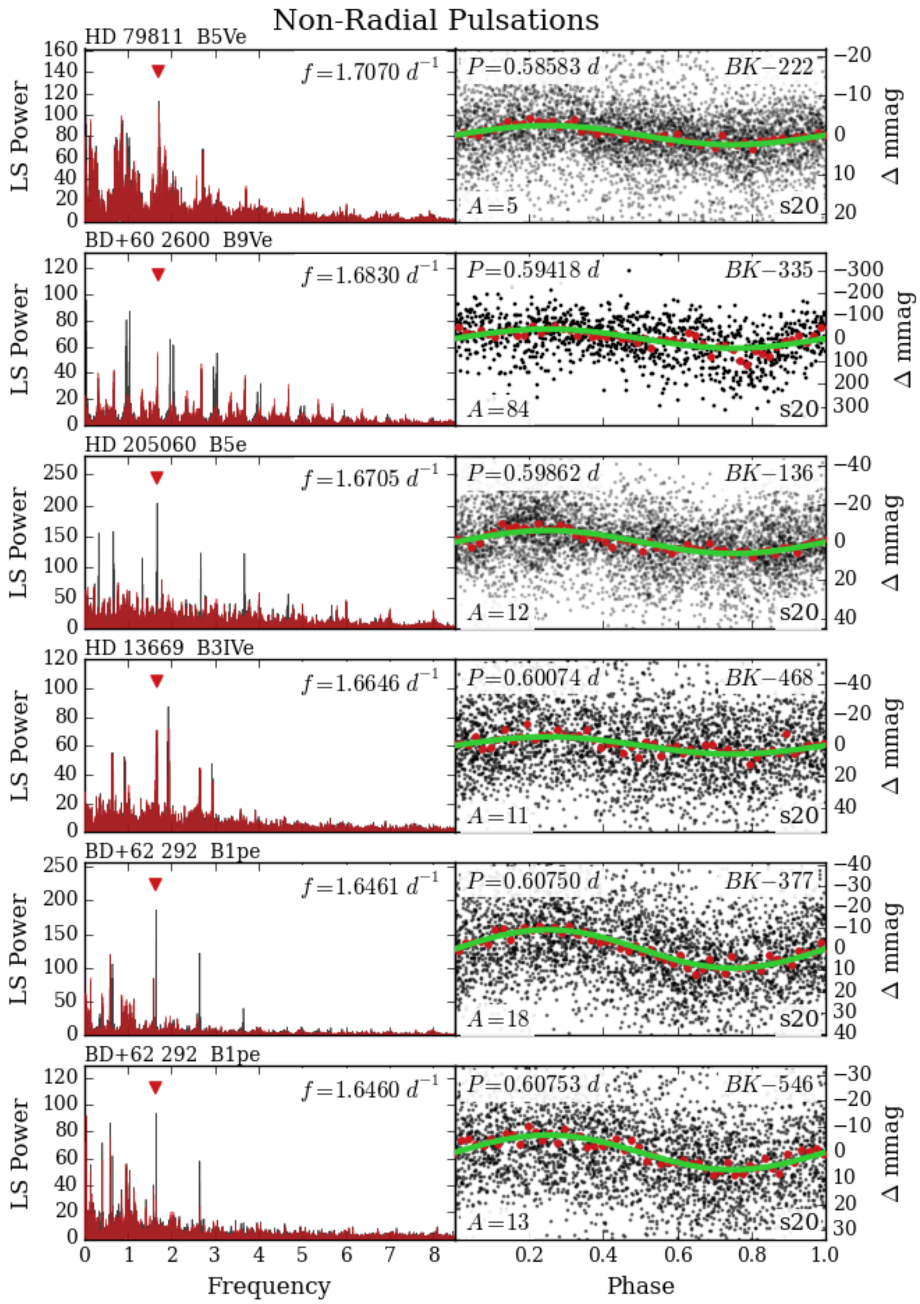
Non-Radial Pulsations
HD 79811 B5Ve
f=1.7070 d^-1
P=0.58583 d
BK−222
A=5
s20
BD+60 2600 B9Ve
f=1.6830 d^-1
P=0.59418 d
BK−335
A=84
s20
HD 205060 B5e
f=1.6705 d^-1
P=0.59862 d
BK−136
A=12
s20
HD 13669 B3IVe
f=1.6646 d^-1
P=0.60074 d
BK−468
A=11
s20
BD+62 292 B1pe
f=1.6461 d^-1
P=0.60750 d
BK−377
A=18
s20
BD+62 292 B1pe
f=1.6460 d^-1
P=0.60753 d
BK−546
A=13
s20
LS Power
Δ mmag
Frequency
Phase

Figure 3.10: J

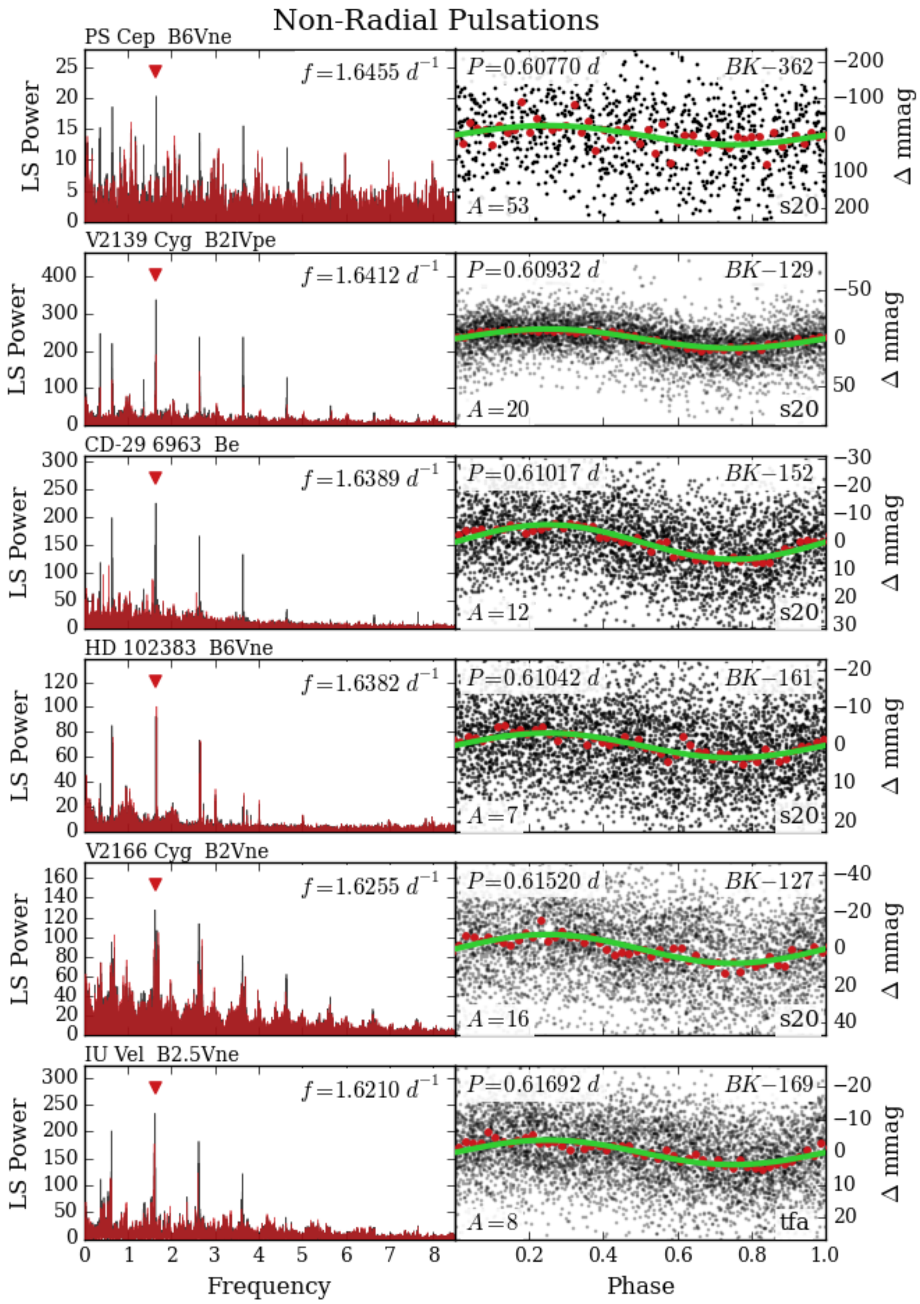

Non-Radial Pulsations
PS Cep B6Vne
f=1.6455 d^-1
P=0.60770 d
BK−362
A=53
s20
V2139 Cyg B2IVpe
f=1.6412 d^-1
P=0.60932 d
BK−129
A=20
s20
CD-29 6963 Be
f=1.6389 d^-1
P=0.61017 d
BK−152
A=12
s20
HD 102383 B6Vne
f=1.6382 d^-1
P=0.61042 d
BK−161
A=7
s20
V2166 Cyg B2Vne
f=1.6255 d^-1
P=0.61520 d
BK−127
A=16
s20
IU Vel B2.5Vne
f=1.6210 d^-1
P=0.61692 d
BK−169
A=8
tfa
LS Power
Δ mmag
Frequency
Phase

Figure 3.10: K

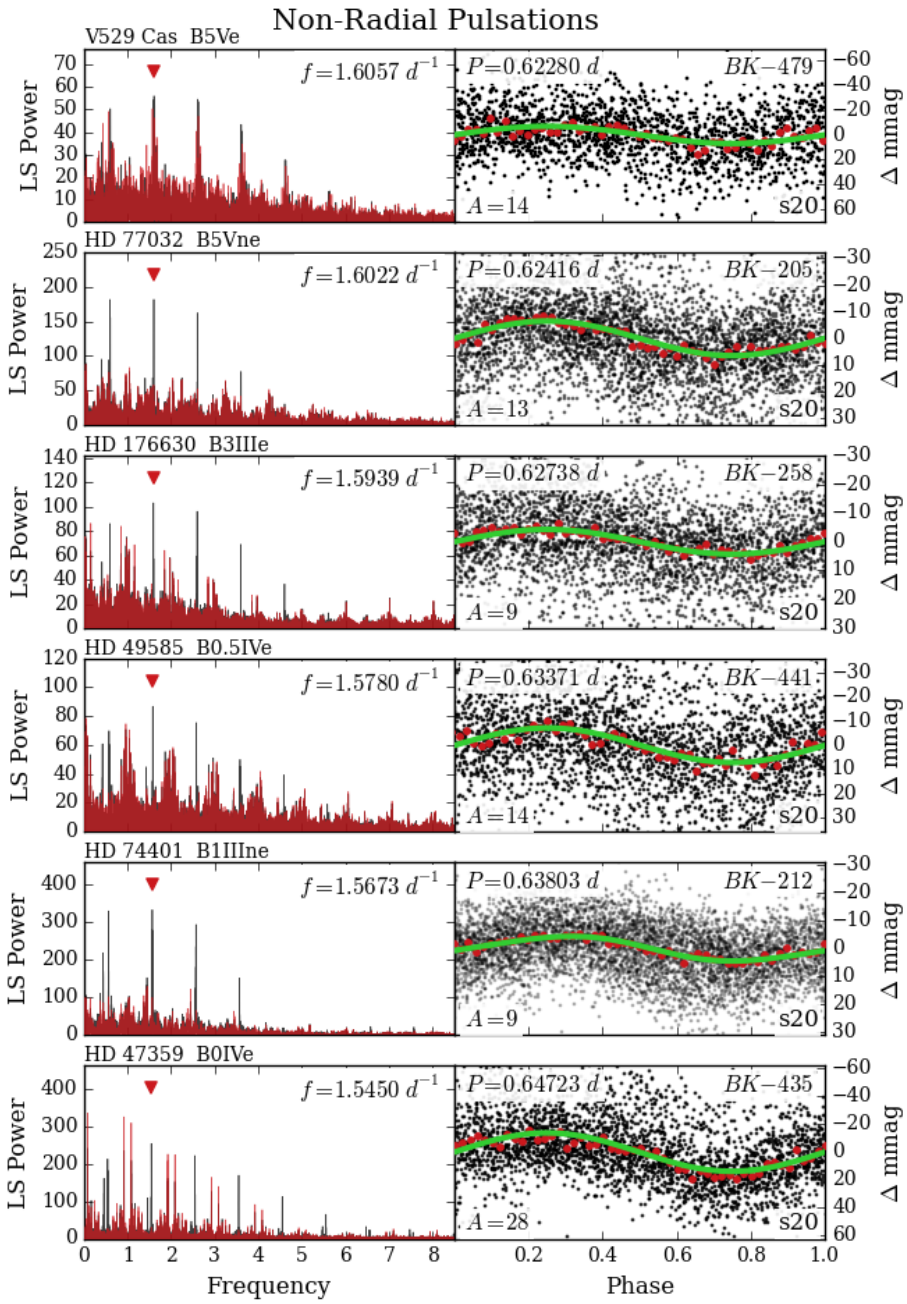

Non-Radial Pulsations
V529 Cas B5Ve
f=1.6057 d^-1
P=0.62280 d
BK−479
A=14
s20
HD 77032 B5Vne
f=1.6022 d^-1
P=0.62416 d
BK−205
A=13
s20
HD 176630 B3IIIe
f=1.5939 d^-1
P=0.62738 d
BK−258
A=9
s20
HD 49585 B0.5IVe
f=1.5780 d^-1
P=0.63371 d
BK−441
A=14
s20
HD 74401 B1IIIne
f=1.5673 d^-1
P=0.63803 d
BK−212
A=9
s20
HD 47359 B0IVe
f=1.5450 d^-1
P=0.64723 d
BK−435
A=28
s20
LS Power
Δ mmag
Frequency
Phase

Figure 3.10: L

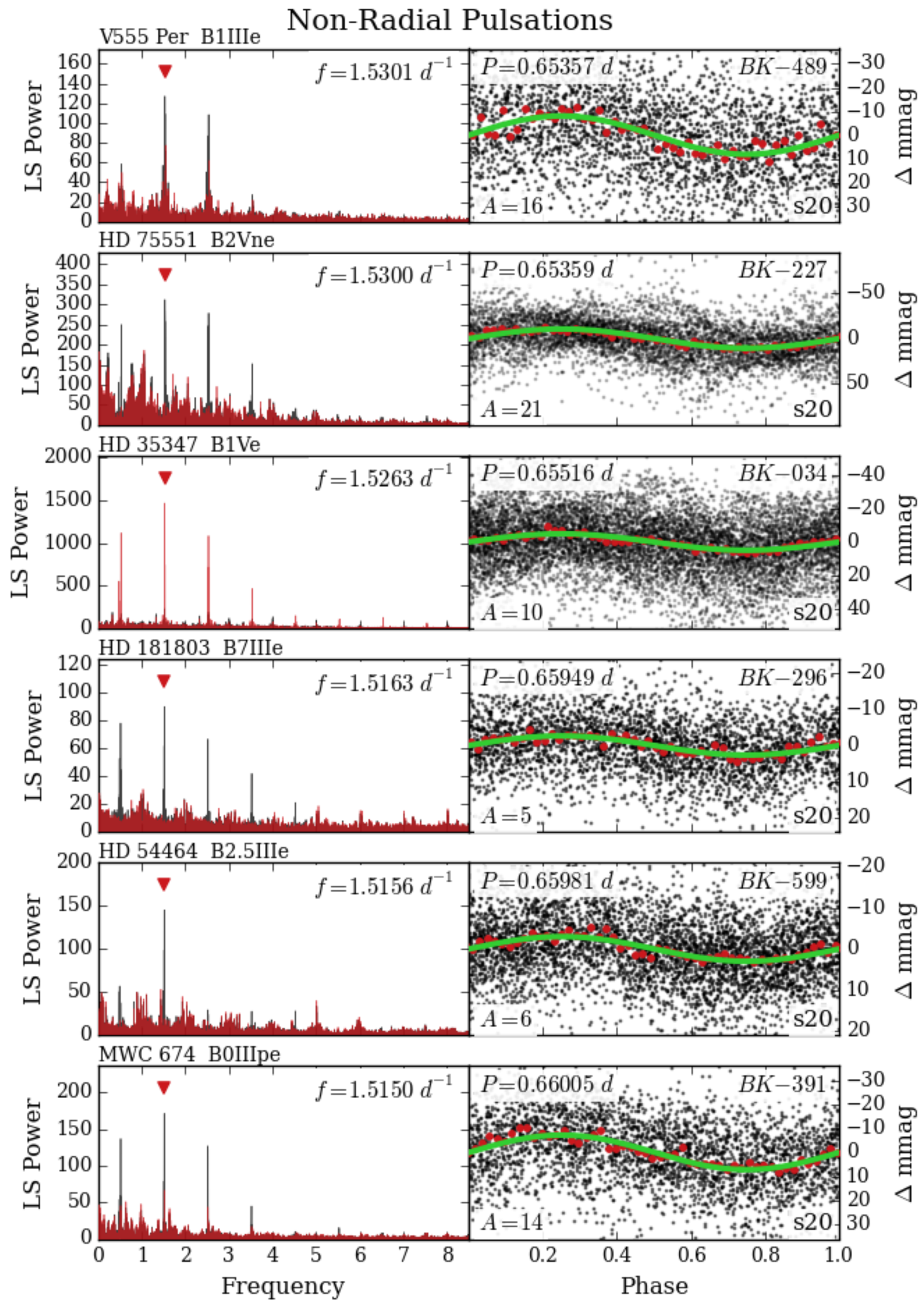

Non-Radial Pulsations
V555 Per B1IIIe
HD 75551 B2Vne
HD 35347 B1Ve
HD 181803 B7IIIe
HD 54464 B2.5IIIe
MWC 674 B0IIIpe
LS Power
Frequency
Phase
Δ mmag
f=1.5301 d^-1
P=0.65357 d
BK−489
A=16
f=1.5300 d^-1
P=0.65359 d
BK−227
A=21
f=1.5263 d^-1
P=0.65516 d
BK−034
A=10
f=1.5163 d^-1
P=0.65949 d
BK−296
A=5
f=1.5156 d^-1
P=0.65981 d
BK−599
A=6
f=1.5150 d^-1
P=0.66005 d
BK−391
A=14
s20

Figure 3.10: M

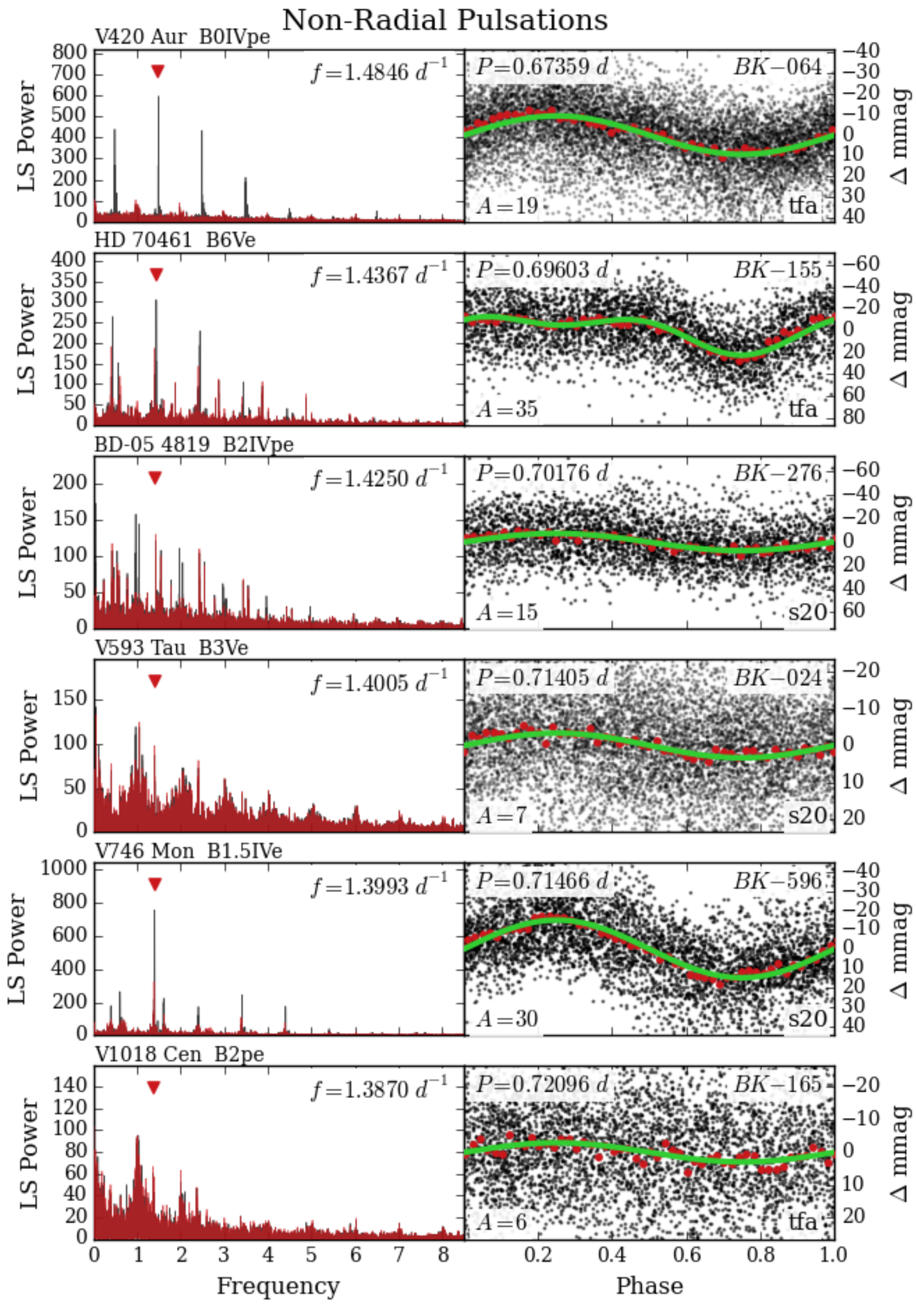
Non-Radial Pulsations
V420 Aur B0IVpe
f=1.4846 d^-1
P=0.67359 d
BK-064
A=19
tfa
HD 70461 B6Ve
f=1.4367 d^-1
P=0.69603 d
BK-155
A=35
tfa
BD-05 4819 B2IVpe
f=1.4250 d^-1
P=0.70176 d
BK-276
A=15
s20
V593 Tau B3Ve
f=1.4005 d^-1
P=0.71405 d
BK-024
A=7
s20
V746 Mon B1.5IVe
f=1.3993 d^-1
P=0.71466 d
BK-596
A=30
s20
V1018 Cen B2pe
f=1.3870 d^-1
P=0.72096 d
BK-165
A=6
tfa
LS Power
Δ mmag
Frequency
Phase

Figure 3.10: N

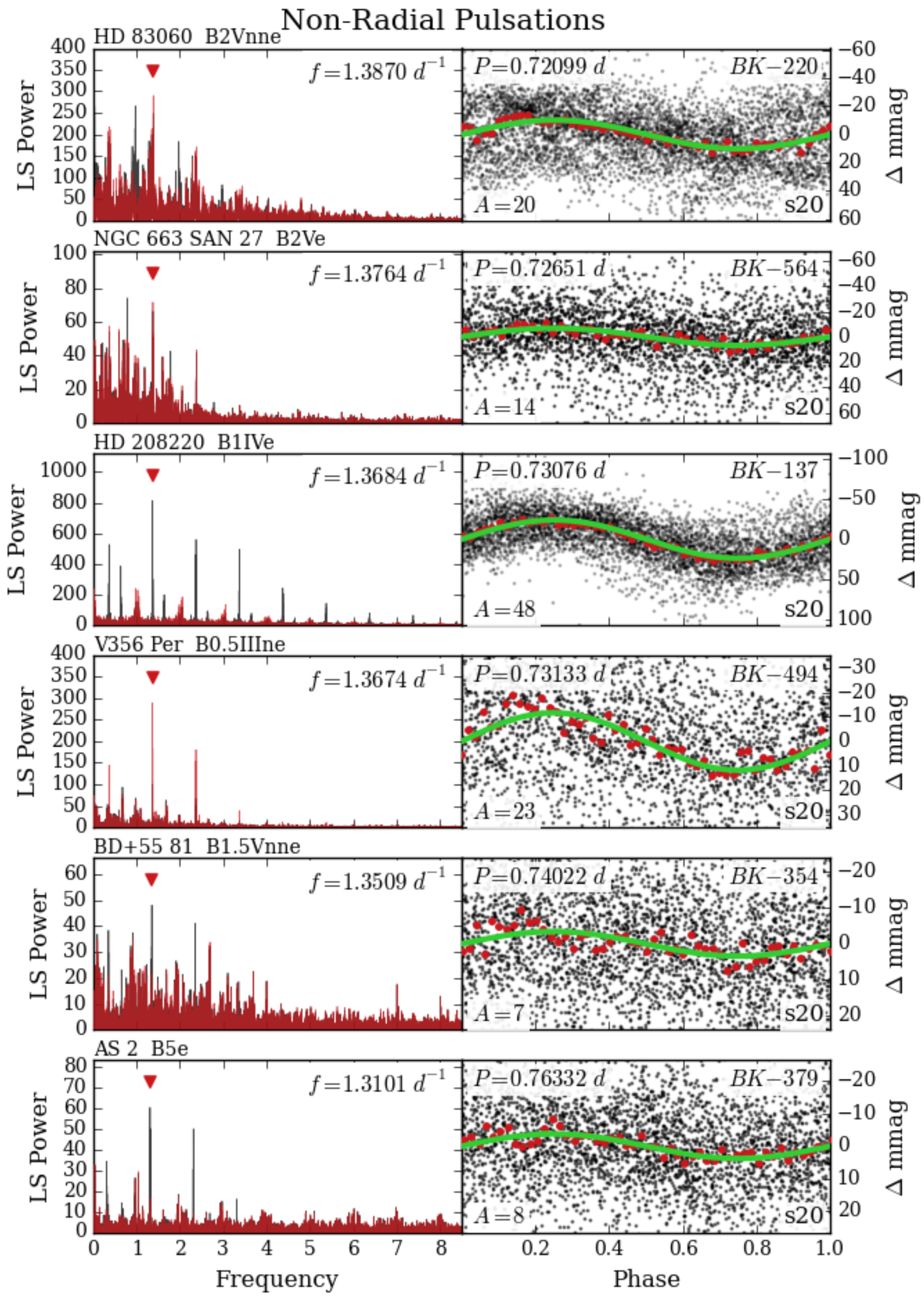

Non-Radial Pulsations
HD 83060 B2Vnne
f=1.3870 d^-1
P=0.72099 d
BK−220
A=20
s20
NGC 663 SAN 27 B2Ve
f=1.3764 d^-1
P=0.72651 d
BK−564
A=14
s20
HD 208220 B1IVe
f=1.3684 d^-1
P=0.73076 d
BK−137
A=48
s20
V356 Per B0.5IIIne
f=1.3674 d^-1
P=0.73133 d
BK−494
A=23
s20
BD+55 81 B1.5Vnne
f=1.3509 d^-1
P=0.74022 d
BK−354
A=7
s20
AS 2 B5e
f=1.3101 d^-1
P=0.76332 d
BK−379
A=8
s20
LS Power
Δ mmag
Frequency
Phase

Figure 3.10: O

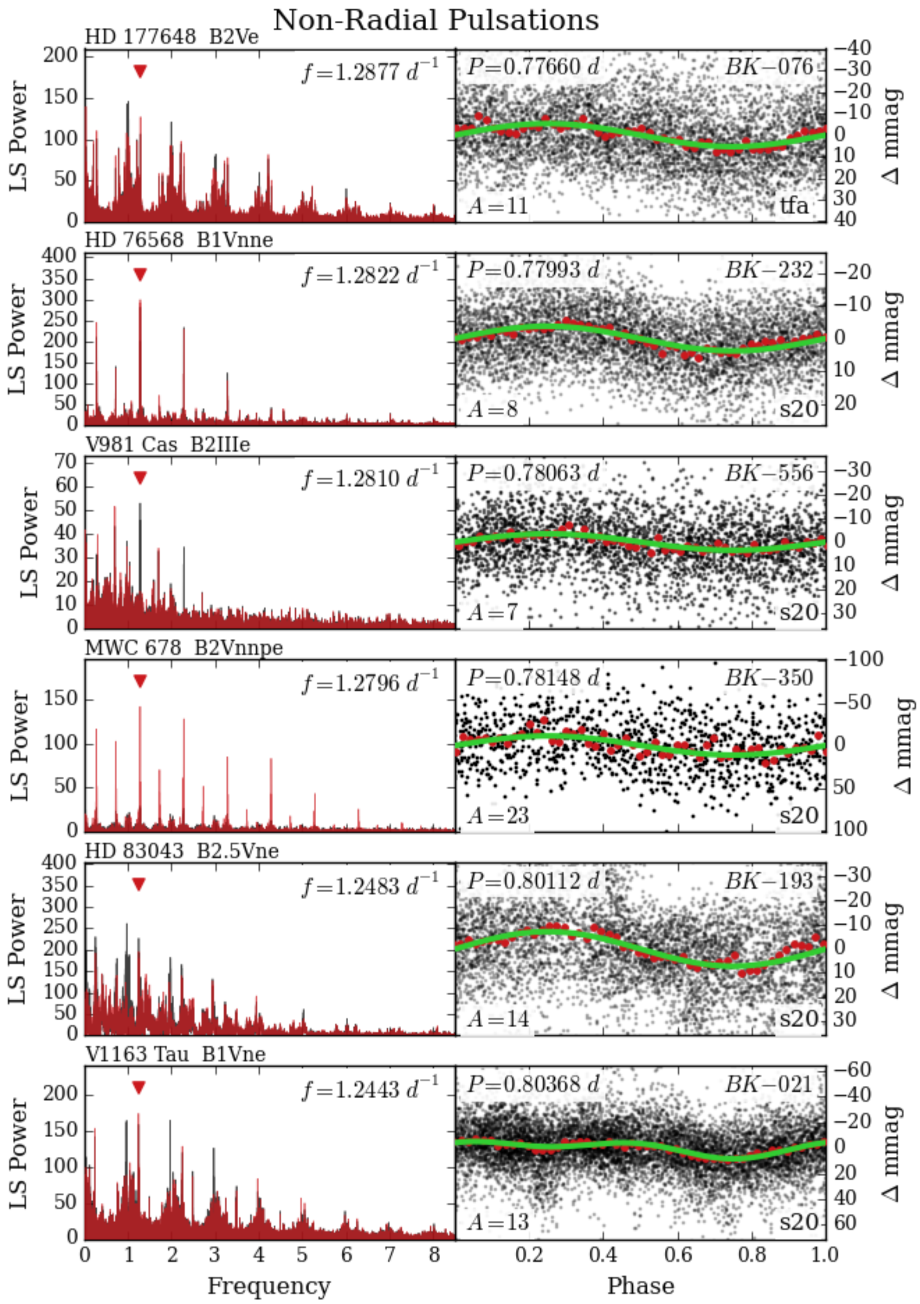

Non-Radial Pulsations
HD 177648 B2Ve
f=1.2877 d^-1
P=0.77660 d
BK−076
A=11
tfa
HD 76568 B1Vnne
f=1.2822 d^-1
P=0.77993 d
BK−232
A=8
s20
V981 Cas B2IIIe
f=1.2810 d^-1
P=0.78063 d
BK−556
A=7
s20
MWC 678 B2Vnnpe
f=1.2796 d^-1
P=0.78148 d
BK−350
A=23
s20
HD 83043 B2.5Vne
f=1.2483 d^-1
P=0.80112 d
BK−193
A=14
s20
V1163 Tau B1Vne
f=1.2443 d^-1
P=0.80368 d
BK−021
A=13
s20
LS Power
Δ mmag
Frequency
Phase

Figure 3.10: P

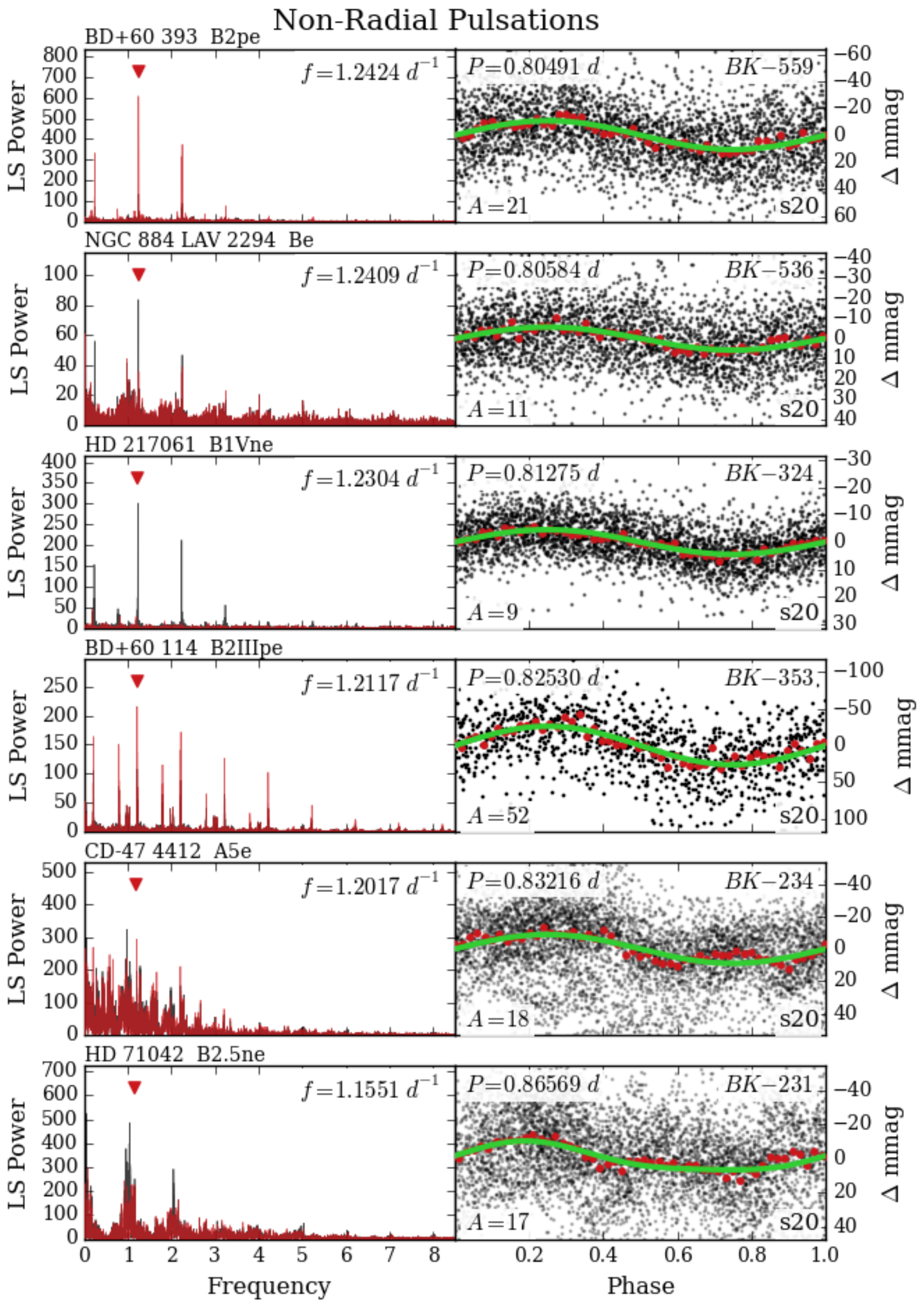

Non-Radial Pulsations
BD+60 393 B2pe
$f=1.2424\ d^{-1}$
$P=0.80491\ d$
$BK-559$
$A=21$
s20
NGC 884 LAV 2294 Be
$f=1.2409\ d^{-1}$
$P=0.80584\ d$
$BK-536$
$A=11$
s20
HD 217061 B1Vne
$f=1.2304\ d^{-1}$
$P=0.81275\ d$
$BK-324$
$A=9$
s20
BD+60 114 B2IIIpe
$f=1.2117\ d^{-1}$
$P=0.82530\ d$
$BK-353$
$A=52$
s20
CD-47 4412 A5e
$f=1.2017\ d^{-1}$
$P=0.83216\ d$
$BK-234$
$A=18$
s20
HD 71042 B2.5ne
$f=1.1551\ d^{-1}$
$P=0.86569\ d$
$BK-231$
$A=17$
s20
LS Power
Δ mmag
Frequency
Phase

Figure 3.10: Q

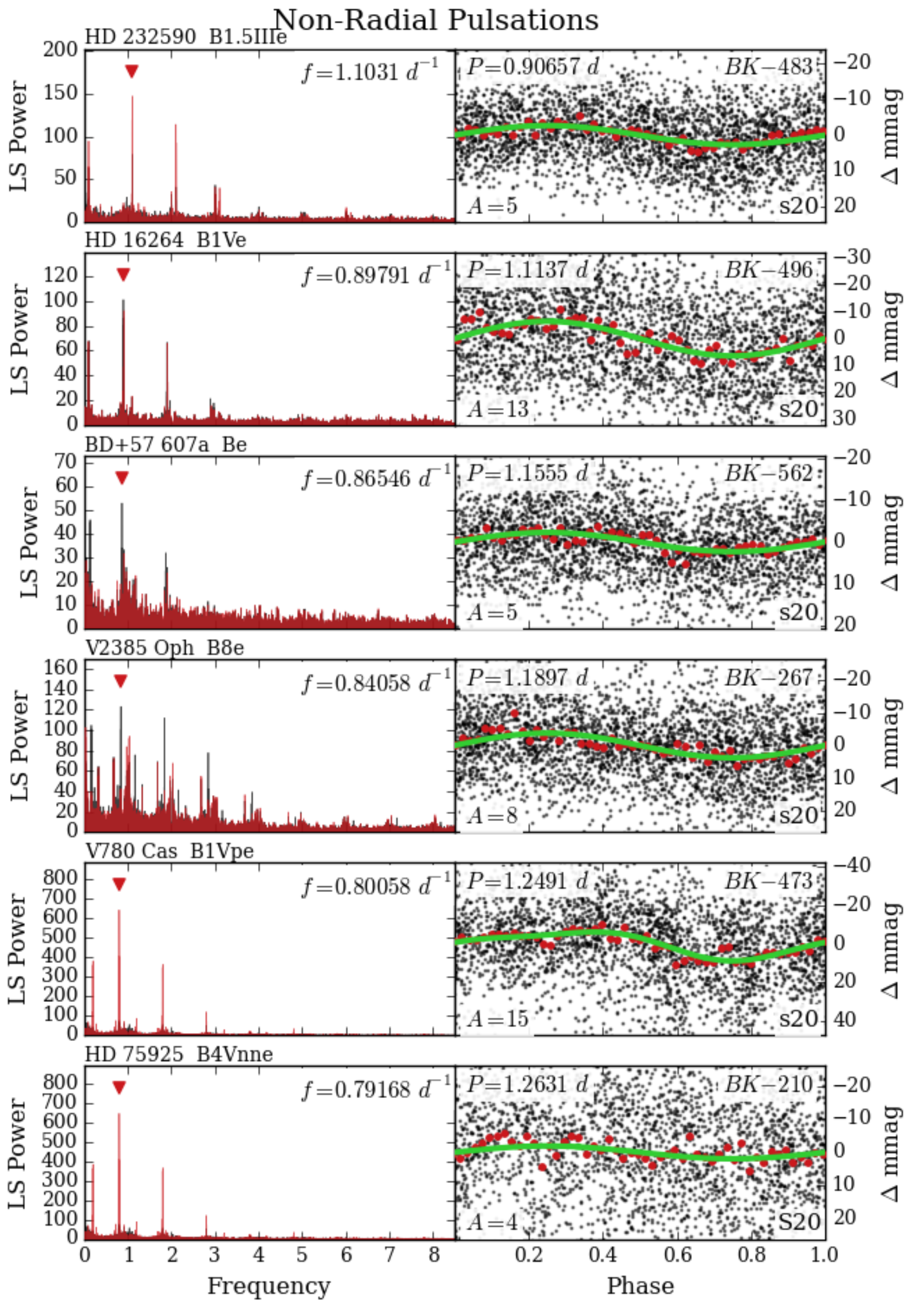

Non-Radial Pulsations
HD 232590 B1.5IIIe
f=1.1031 d^-1
P=0.90657 d
BK−483
A=5
s20
HD 16264 B1Ve
f=0.89791 d^-1
P=1.1137 d
BK−496
A=13
s20
BD+57 607a Be
f=0.86546 d^-1
P=1.1555 d
BK−562
A=5
s20
V2385 Oph B8e
f=0.84058 d^-1
P=1.1897 d
BK−267
A=8
s20
V780 Cas B1Vpe
f=0.80058 d^-1
P=1.2491 d
BK−473
A=15
s20
HD 75925 B4Vnne
f=0.79168 d^-1
P=1.2631 d
BK−210
A=4
S20
LS Power
Δ mmag
Frequency
Phase

Figure 3.10: R

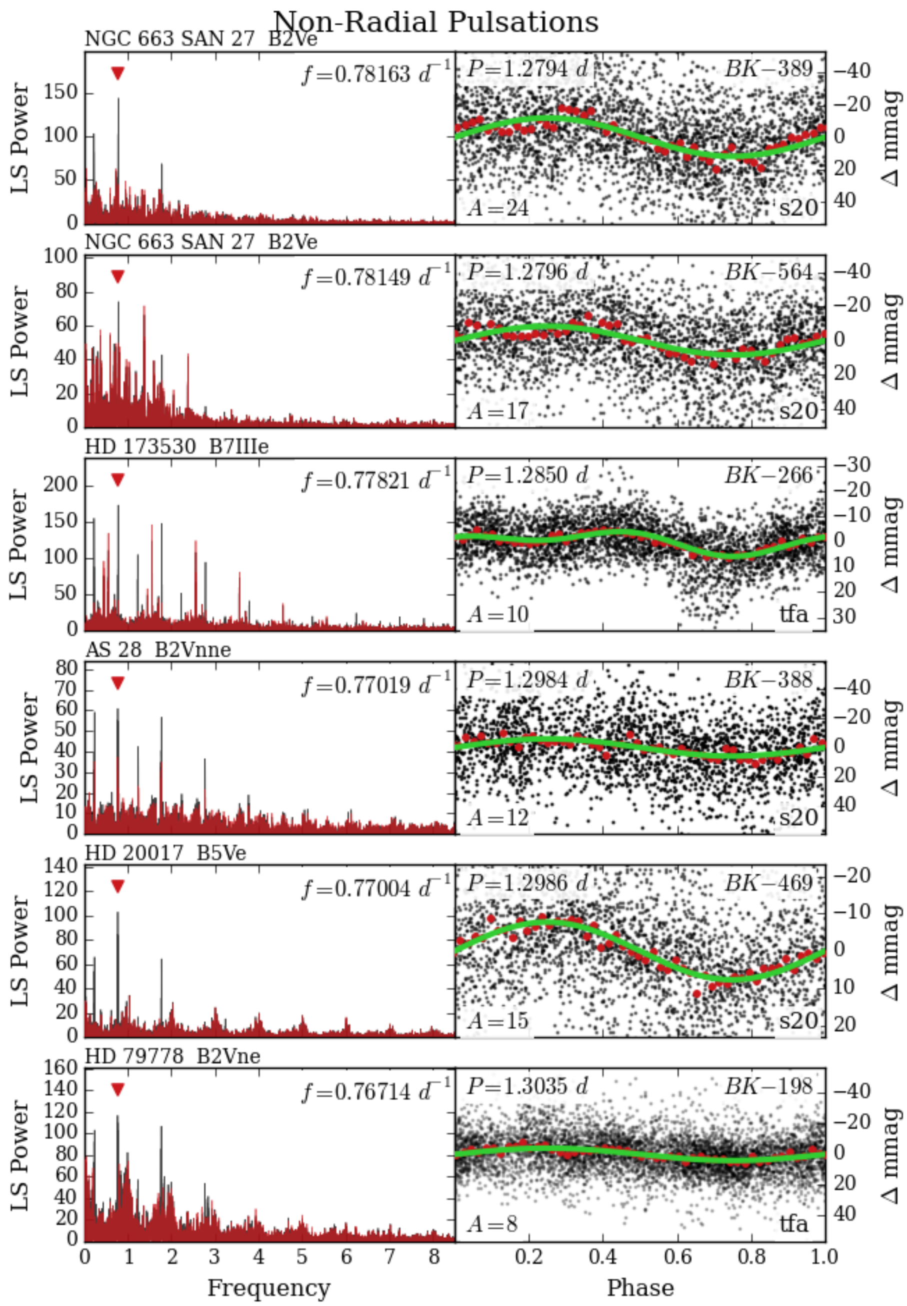
Non-Radial Pulsations
NGC 663 SAN 27 B2Ve
f=0.78163 d⁻¹
P=1.2794 d
BK−389
A=24
s20
NGC 663 SAN 27 B2Ve
f=0.78149 d⁻¹
P=1.2796 d
BK−564
A=17
s20
HD 173530 B7IIIe
f=0.77821 d⁻¹
P=1.2850 d
BK−266
A=10
tfa
AS 28 B2Vnne
f=0.77019 d⁻¹
P=1.2984 d
BK−388
A=12
s20
HD 20017 B5Ve
f=0.77004 d⁻¹
P=1.2986 d
BK−469
A=15
s20
HD 79778 B2Vne
f=0.76714 d⁻¹
P=1.3035 d
BK−198
A=8
tfa
LS Power
Δ mmag
Frequency
Phase

Figure 3.10: S

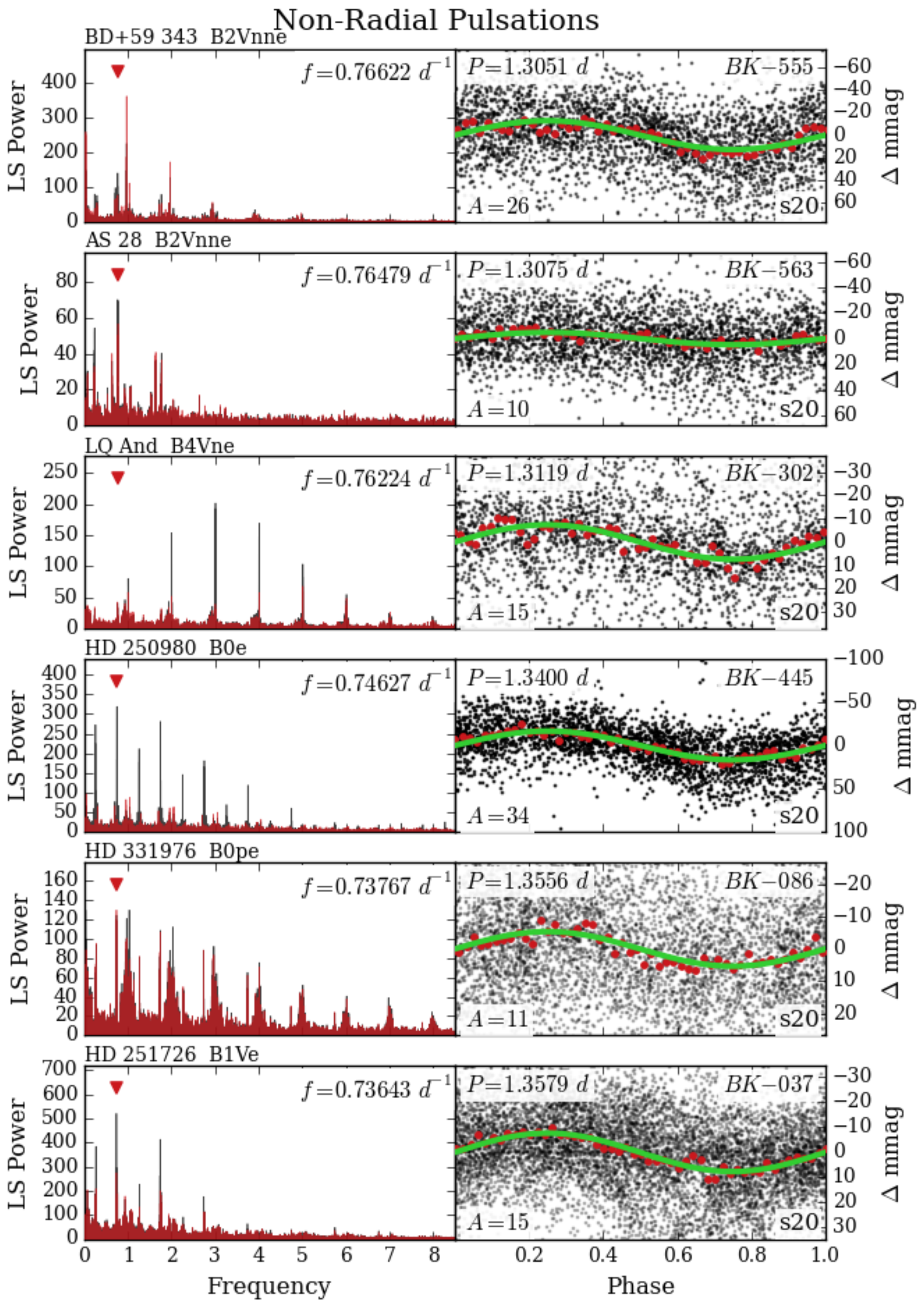
Non-Radial Pulsations
BD+59 343 B2Vnne
f=0.76622 d⁻¹
P=1.3051 d
BK−555
A=26
s20
AS 28 B2Vnne
f=0.76479 d⁻¹
P=1.3075 d
BK−563
A=10
s20
LQ And B4Vne
f=0.76224 d⁻¹
P=1.3119 d
BK−302
A=15
s20
HD 250980 B0e
f=0.74627 d⁻¹
P=1.3400 d
BK−445
A=34
s20
HD 331976 B0pe
f=0.73767 d⁻¹
P=1.3556 d
BK−086
A=11
s20
HD 251726 B1Ve
f=0.73643 d⁻¹
P=1.3579 d
BK−037
A=15
s20
LS Power
Δ mmag
Frequency
Phase

Figure 3.10: T

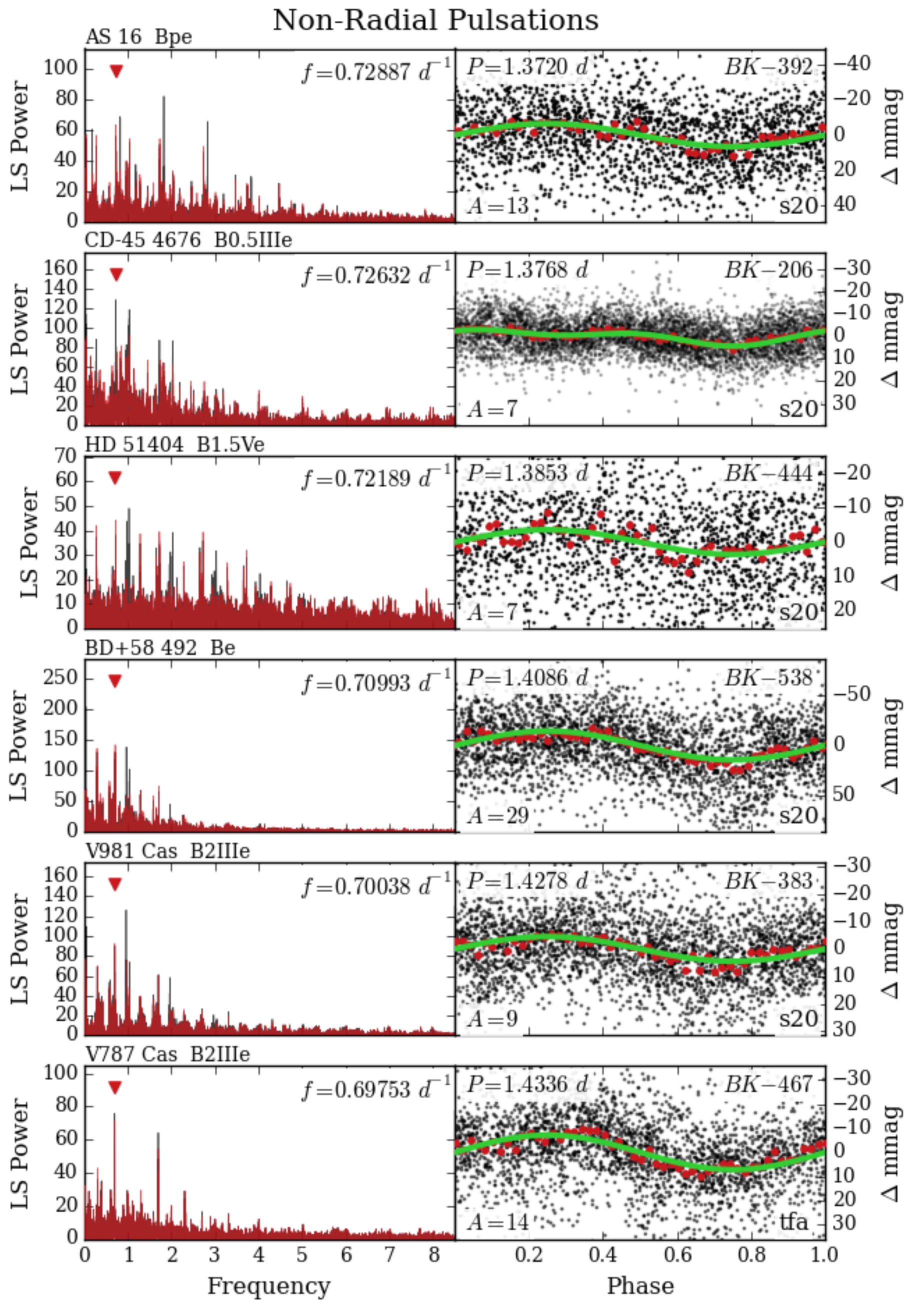
Non-Radial Pulsations
AS 16 Bpe
f=0.72887 d^-1
P=1.3720 d
BK-392
A=13
s20
CD-45 4676 B0.5IIIe
f=0.72632 d^-1
P=1.3768 d
BK-206
A=7
s20
HD 51404 B1.5Ve
f=0.72189 d^-1
P=1.3853 d
BK-444
A=7
s20
BD+58 492 Be
f=0.70993 d^-1
P=1.4086 d
BK-538
A=29
s20
V981 Cas B2IIIe
f=0.70038 d^-1
P=1.4278 d
BK-383
A=9
s20
V787 Cas B2IIIe
f=0.69753 d^-1
P=1.4336 d
BK-467
A=14
tfa
LS Power
Δ mmag
Frequency
Phase

Figure 3.10: U

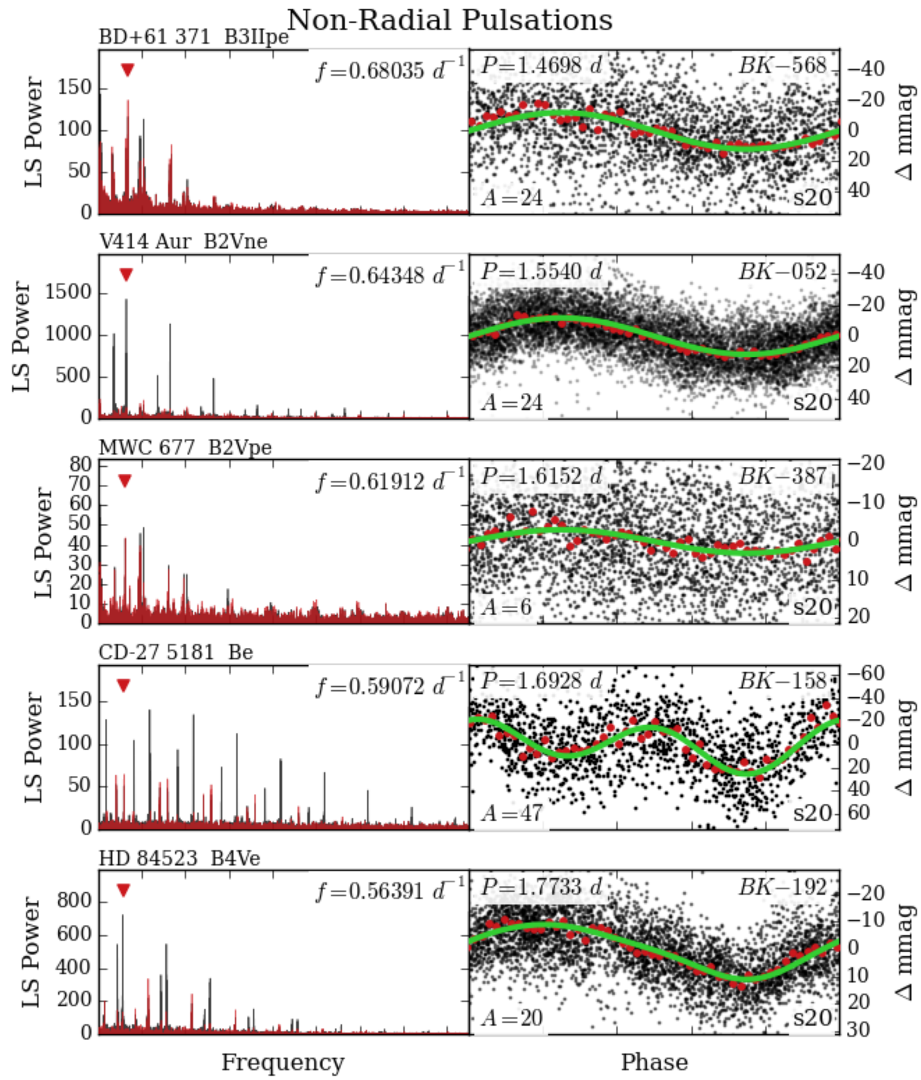

Non-Radial Pulsations
BD+61 371 B3IIpe
V414 Aur B2Vne
MWC 677 B2Vpe
CD-27 5181 Be
HD 84523 B4Ve
LS Power
Δ mmag
f=0.68035 d^-1
P=1.4698 d
BK−568
A=24
f=0.64348 d^-1
P=1.5540 d
BK−052
A=24
f=0.61912 d^-1
P=1.6152 d
BK−387
A=6
f=0.59072 d^-1
P=1.6928 d
BK−158
A=47
f=0.56391 d^-1
P=1.7733 d
BK−192
A=20
s20
Frequency
Phase

Figure 3.10: V

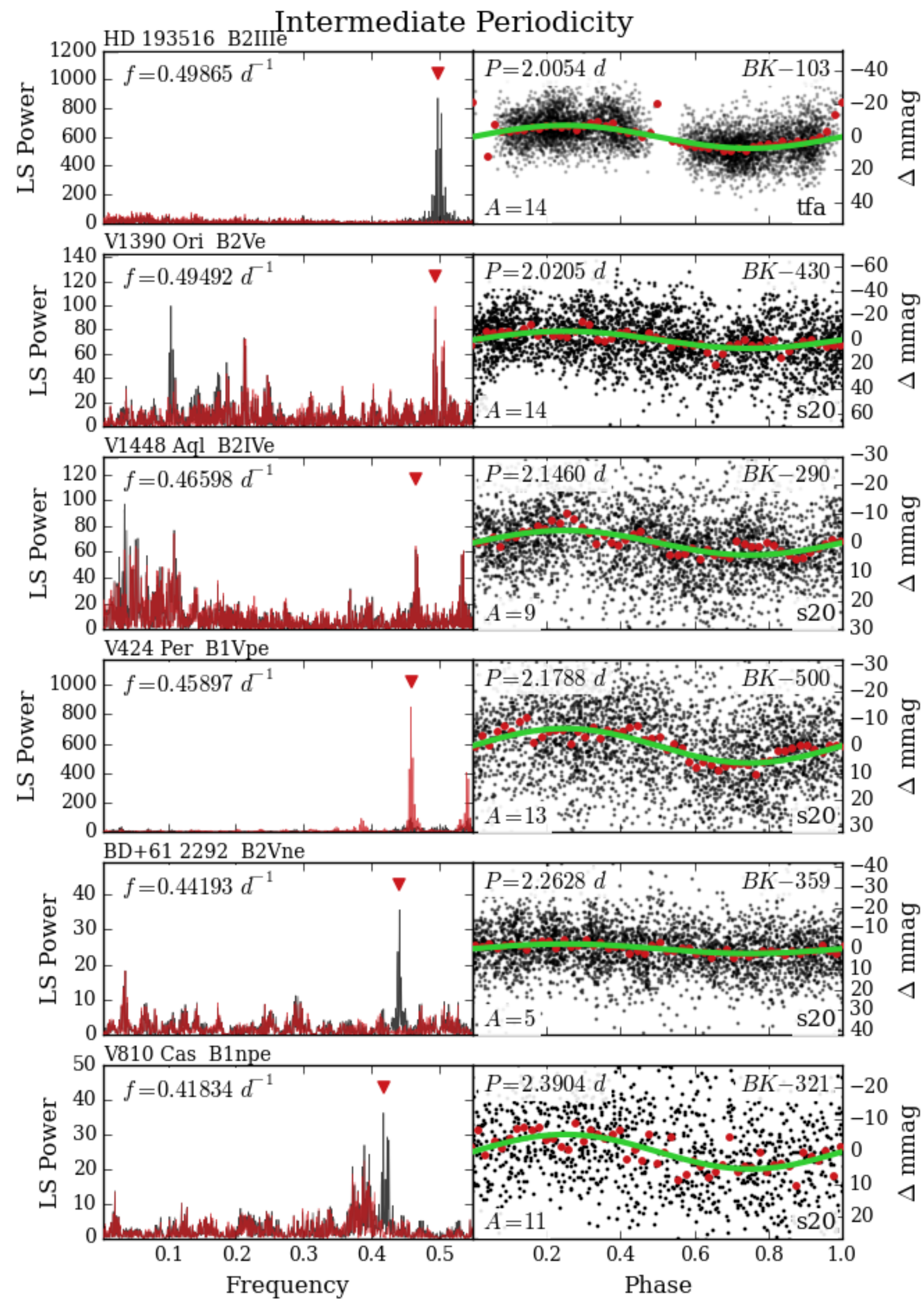

Figure 3.11: Same as Figure 3.10, but for intermediate periods >2 days.

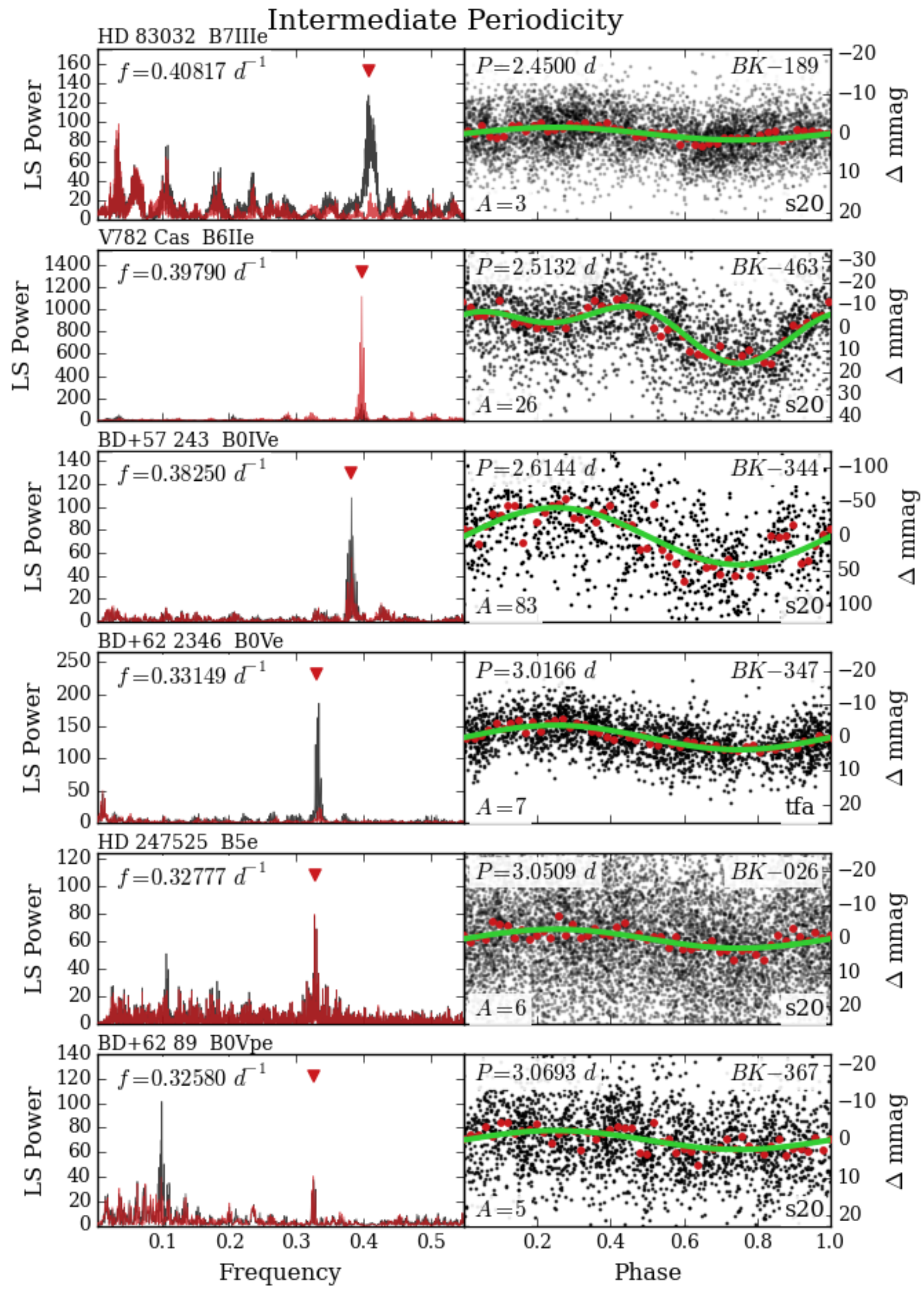

Intermediate Periodicity
HD 83032 B7IIIe
f=0.40817 d^-1
P=2.4500 d
BK−189
A=3
s20
V782 Cas B6IIe
f=0.39790 d^-1
P=2.5132 d
BK−463
A=26
s20
BD+57 243 B0IVe
f=0.38250 d^-1
P=2.6144 d
BK−344
A=83
s20
BD+62 2346 B0Ve
f=0.33149 d^-1
P=3.0166 d
BK−347
A=7
tfa
HD 247525 B5e
f=0.32777 d^-1
P=3.0509 d
BK−026
A=6
s20
BD+62 89 B0Vpe
f=0.32580 d^-1
P=3.0693 d
BK−367
A=5
s20
LS Power
Δ mmag
Frequency
Phase

Figure 3.11: B

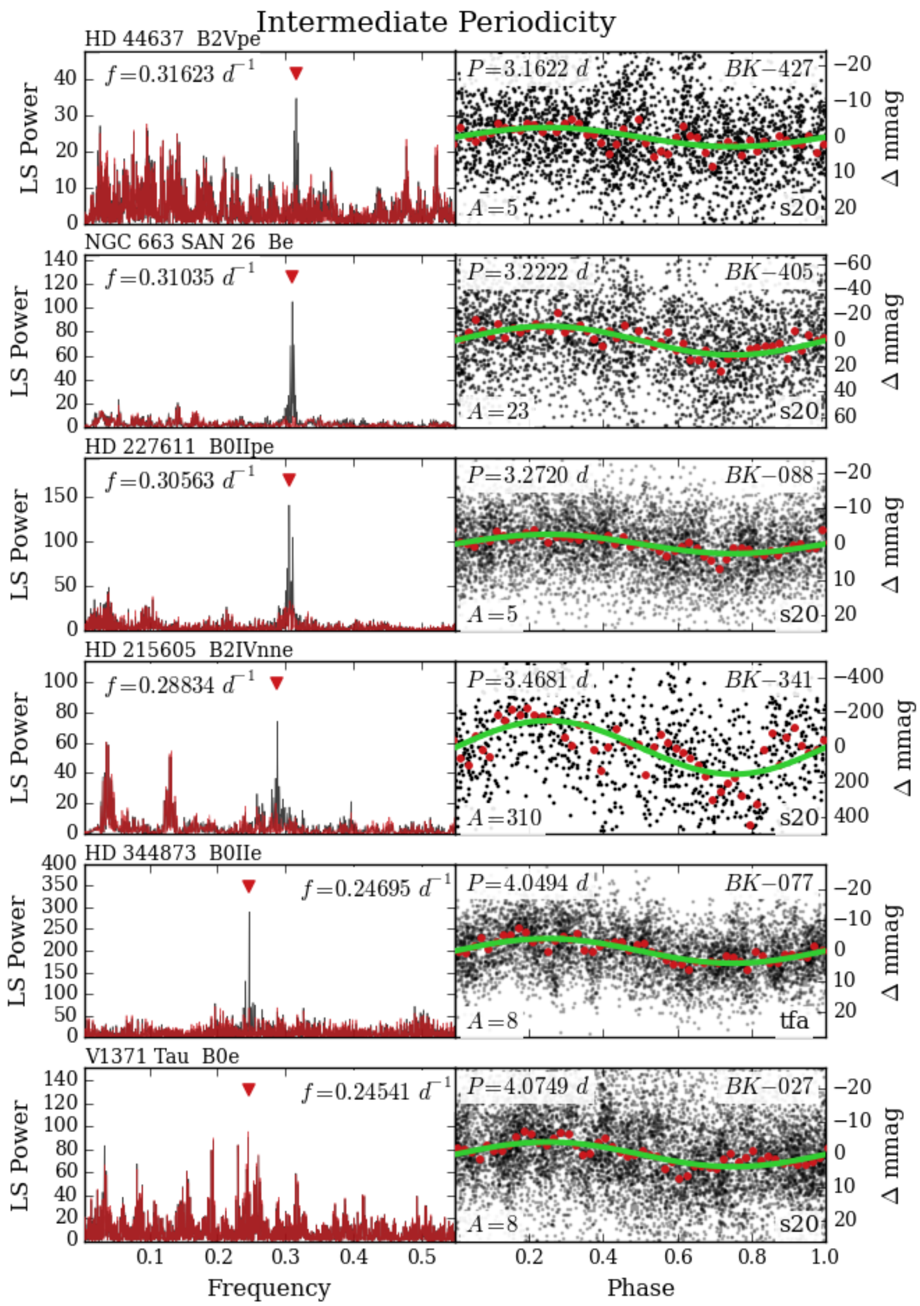
Intermediate Periodicity
HD 44637 B2Vpe
f=0.31623 d^-1
P=3.1622 d
BK−427
A=5
s20
NGC 663 SAN 26 Be
f=0.31035 d^-1
P=3.2222 d
BK−405
A=23
s20
HD 227611 B0IIpe
f=0.30563 d^-1
P=3.2720 d
BK−088
A=5
s20
HD 215605 B2IVnne
f=0.28834 d^-1
P=3.4681 d
BK−341
A=310
s20
HD 344873 B0IIe
f=0.24695 d^-1
P=4.0494 d
BK−077
A=8
tfa
V1371 Tau B0e
f=0.24541 d^-1
P=4.0749 d
BK−027
A=8
s20
LS Power
Δ mmag
Frequency
Phase

Figure 3.11: C

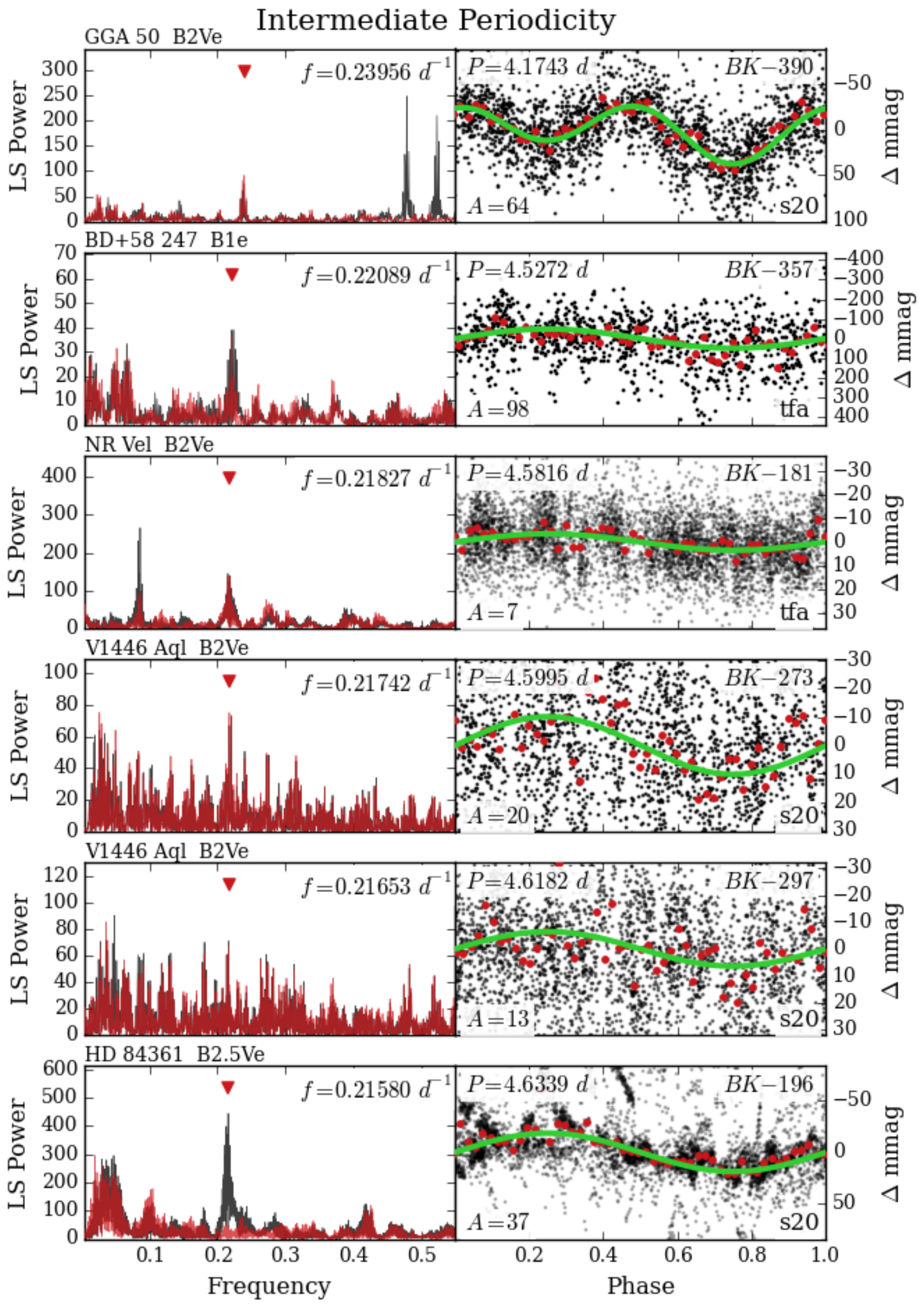

Intermediate Periodicity
GGA 50 B2Ve
BD+58 247 B1e
NR Vel B2Ve
V1446 Aql B2Ve
V1446 Aql B2Ve
HD 84361 B2.5Ve
LS Power
Δ mmag
Frequency
Phase

Figure 3.11: D

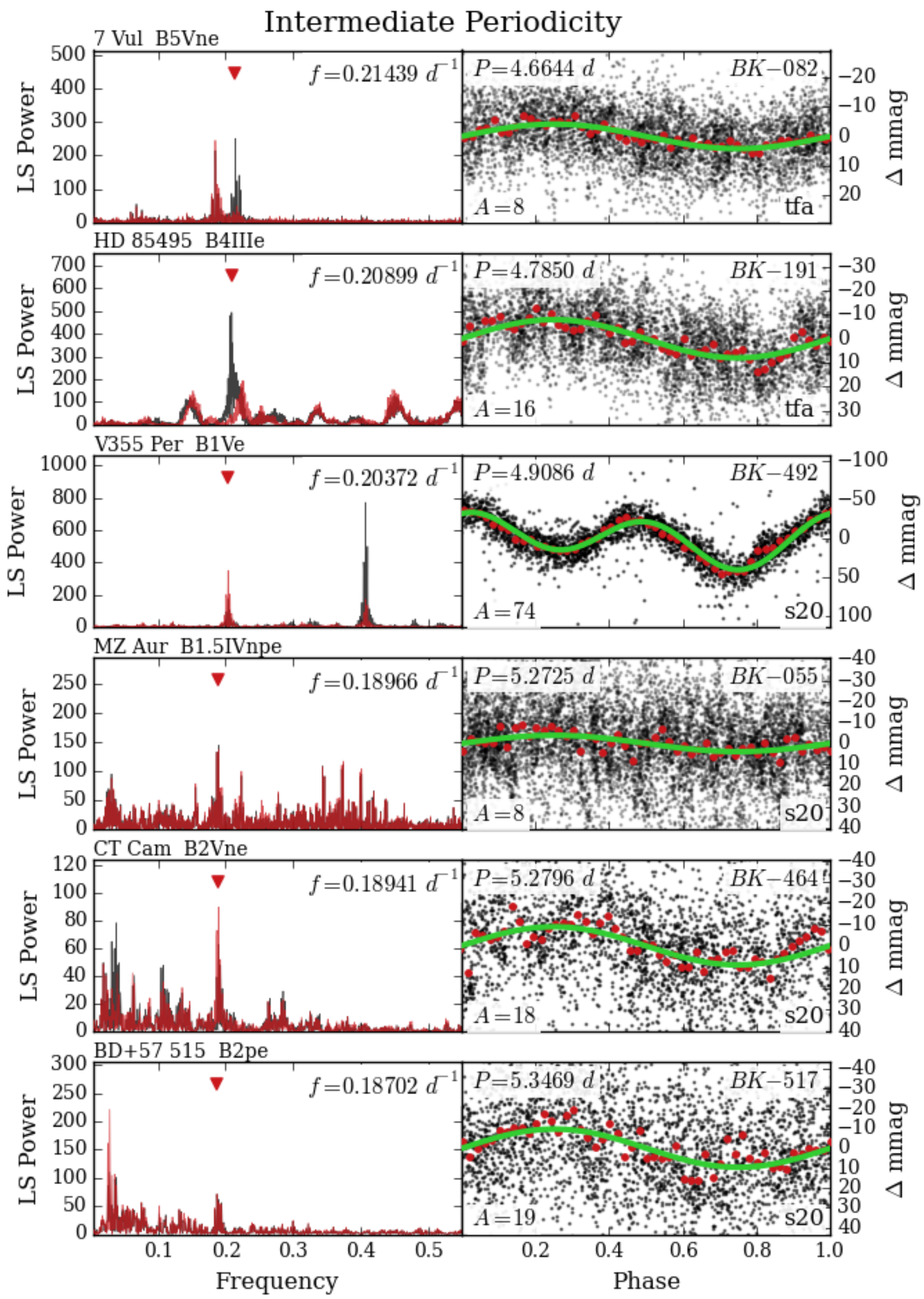
Intermediate Periodicity
7 Vul B5Vne
f=0.21439 d^-1
P=4.6644 d
BK−082
A=8
tfa
HD 85495 B4IIIe
f=0.20899 d^-1
P=4.7850 d
BK−191
A=16
tfa
V355 Per B1Ve
f=0.20372 d^-1
P=4.9086 d
BK−492
A=74
s20
MZ Aur B1.5IVnpe
f=0.18966 d^-1
P=5.2725 d
BK−055
A=8
s20
CT Cam B2Vne
f=0.18941 d^-1
P=5.2796 d
BK−464
A=18
s20
BD+57 515 B2pe
f=0.18702 d^-1
P=5.3469 d
BK−517
A=19
s20
LS Power
Δ mmag
Frequency
Phase

Figure 3.11: E

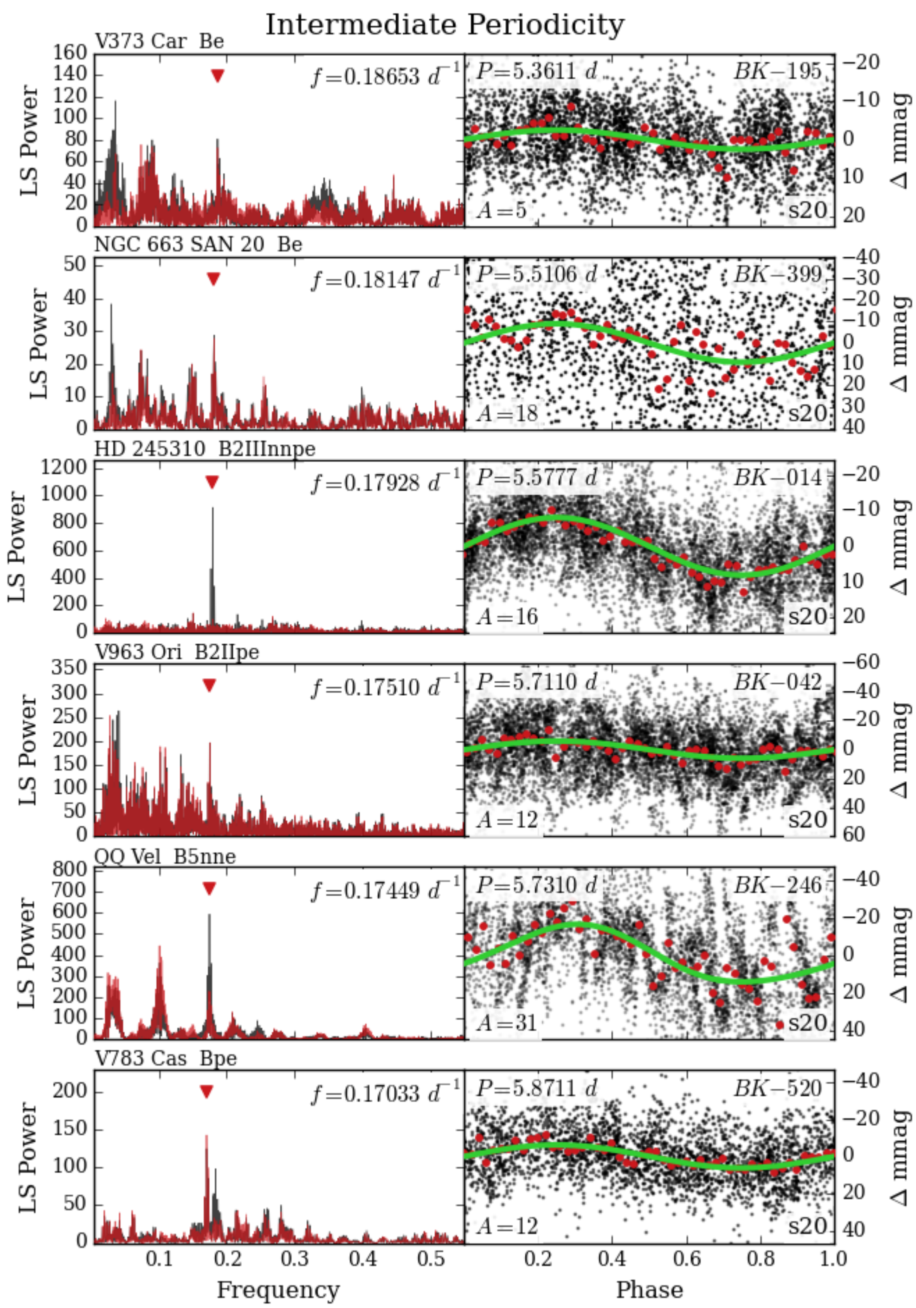

Intermediate Periodicity
V373 Car Be
f=0.18653 d^-1
P=5.3611 d
BK−195
A=5
s20
NGC 663 SAN 20 Be
f=0.18147 d^-1
P=5.5106 d
BK−399
A=18
s20
HD 245310 B2IIInnpe
f=0.17928 d^-1
P=5.5777 d
BK−014
A=16
s20
V963 Ori B2IIpe
f=0.17510 d^-1
P=5.7110 d
BK−042
A=12
s20
QQ Vel B5nne
f=0.17449 d^-1
P=5.7310 d
BK−246
A=31
s20
V783 Cas Bpe
f=0.17033 d^-1
P=5.8711 d
BK−520
A=12
s20
LS Power
Δ mmag
Frequency
Phase

Figure 3.11: F

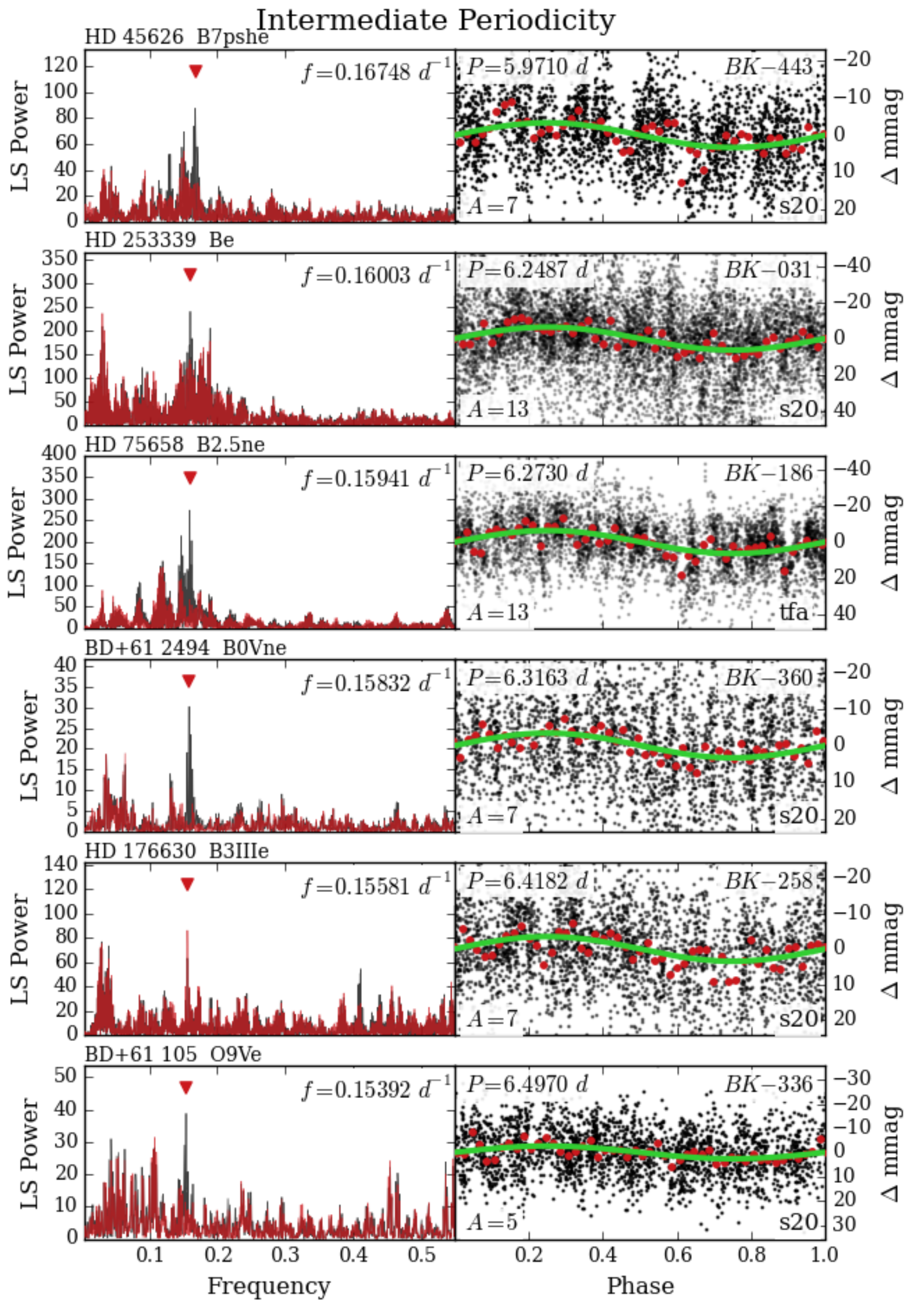
Intermediate Periodicity
HD 45626 B7pshe
f=0.16748 d^-1
P=5.9710 d
BK−443
A=7
s20
HD 253339 Be
f=0.16003 d^-1
P=6.2487 d
BK−031
A=13
s20
HD 75658 B2.5ne
f=0.15941 d^-1
P=6.2730 d
BK−186
A=13
tfa
BD+61 2494 B0Vne
f=0.15832 d^-1
P=6.3163 d
BK−360
A=7
s20
HD 176630 B3IIIe
f=0.15581 d^-1
P=6.4182 d
BK−258
A=7
s20
BD+61 105 O9Ve
f=0.15392 d^-1
P=6.4970 d
BK−336
A=5
s20
LS Power
Δ mmag
Frequency
Phase

Figure 3.11: G

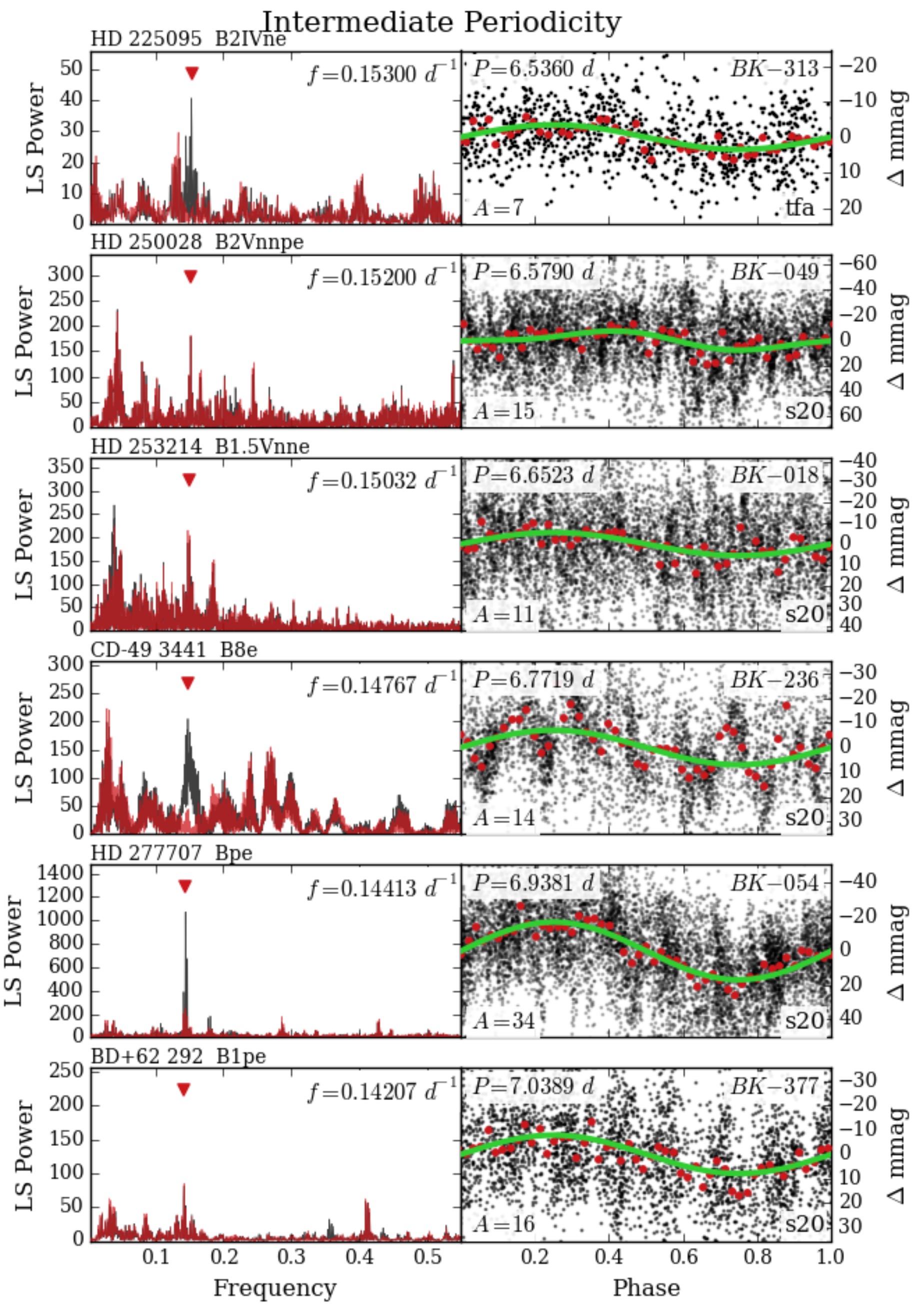

Intermediate Periodicity
HD 225095 B2IVne
f=0.15300 d⁻¹
P=6.5360 d
BK−313
A=7
tfa
HD 250028 B2Vnnpe
f=0.15200 d⁻¹
P=6.5790 d
BK−049
A=15
s20
HD 253214 B1.5Vnne
f=0.15032 d⁻¹
P=6.6523 d
BK−018
A=11
s20
CD-49 3441 B8e
f=0.14767 d⁻¹
P=6.7719 d
BK−236
A=14
s20
HD 277707 Bpe
f=0.14413 d⁻¹
P=6.9381 d
BK−054
A=34
s20
BD+62 292 B1pe
f=0.14207 d⁻¹
P=7.0389 d
BK−377
A=16
s20
LS Power
Δ mmag
Frequency
Phase

Figure 3.11: H

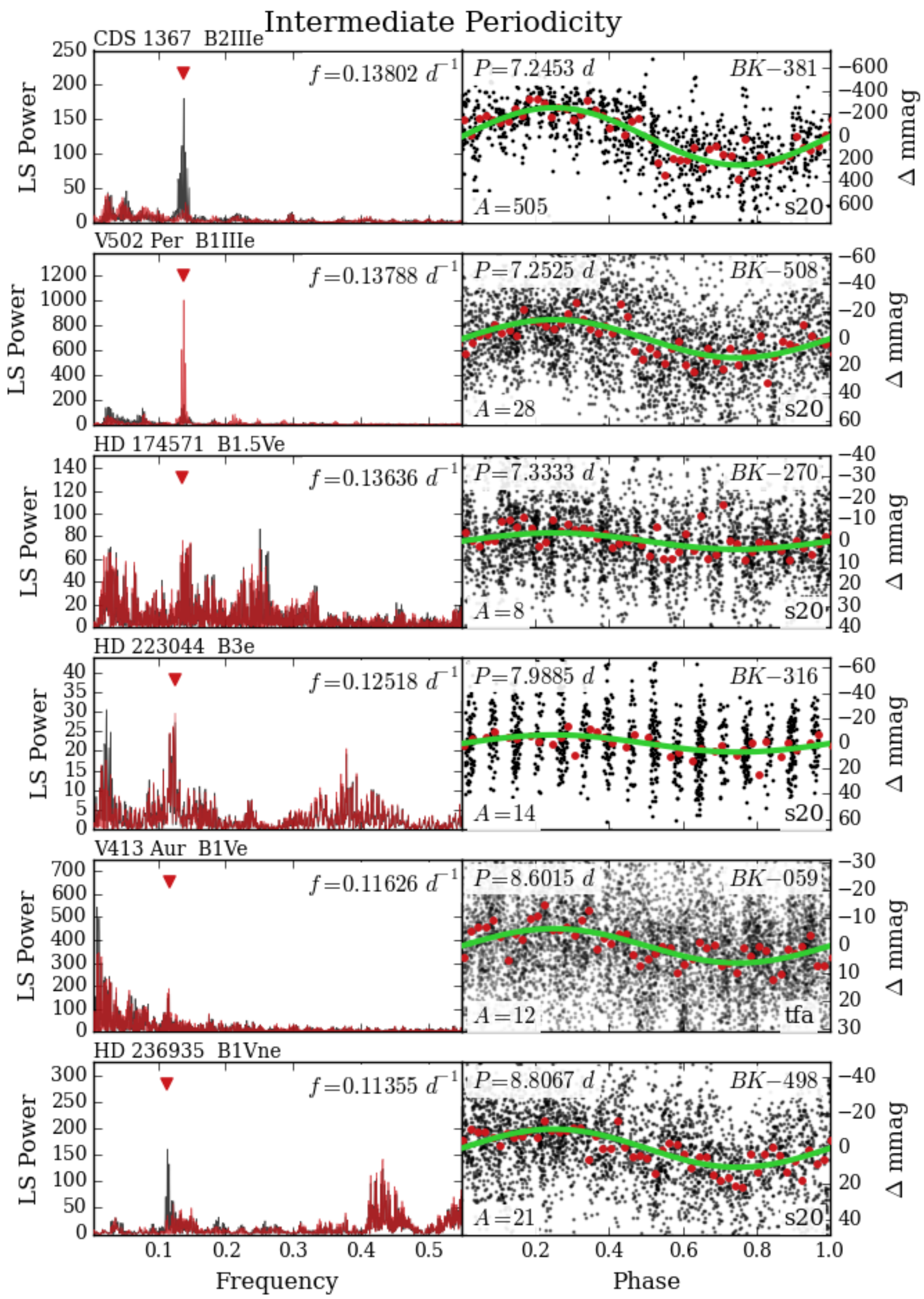

Intermediate Periodicity
CDS 1367 B2IIIe
f=0.13802 d^-1
P=7.2453 d
BK−381
A=505
s20
V502 Per B1IIIe
f=0.13788 d^-1
P=7.2525 d
BK−508
A=28
s20
HD 174571 B1.5Ve
f=0.13636 d^-1
P=7.3333 d
BK−270
A=8
s20
HD 223044 B3e
f=0.12518 d^-1
P=7.9885 d
BK−316
A=14
s20
V413 Aur B1Ve
f=0.11626 d^-1
P=8.6015 d
BK−059
A=12
tfa
HD 236935 B1Vne
f=0.11355 d^-1
P=8.8067 d
BK−498
A=21
s20
LS Power
Δ mmag
Frequency
Phase

Figure 3.11: I

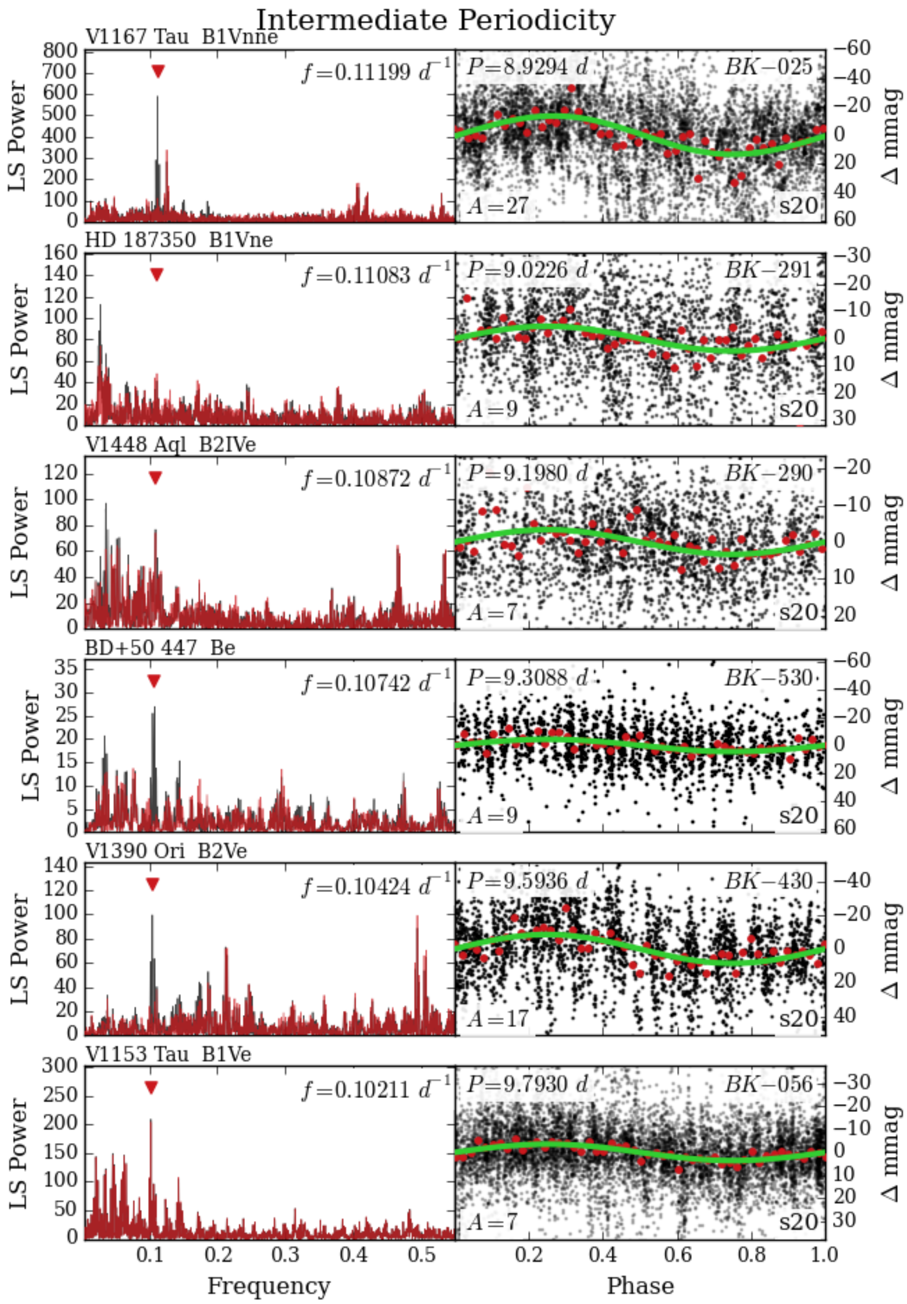
Intermediate Periodicity
V1167 Tau B1Vnne
f=0.11199 d^-1
P=8.9294 d
BK−025
A=27
s20
HD 187350 B1Vne
f=0.11083 d^-1
P=9.0226 d
BK−291
A=9
s20
V1448 Aql B2IVe
f=0.10872 d^-1
P=9.1980 d
BK−290
A=7
s20
BD+50 447 Be
f=0.10742 d^-1
P=9.3088 d
BK−530
A=9
s20
V1390 Ori B2Ve
f=0.10424 d^-1
P=9.5936 d
BK−430
A=17
s20
V1153 Tau B1Ve
f=0.10211 d^-1
P=9.7930 d
BK−056
A=7
s20
LS Power
Δ mmag
Frequency
Phase

Figure 3.11: J

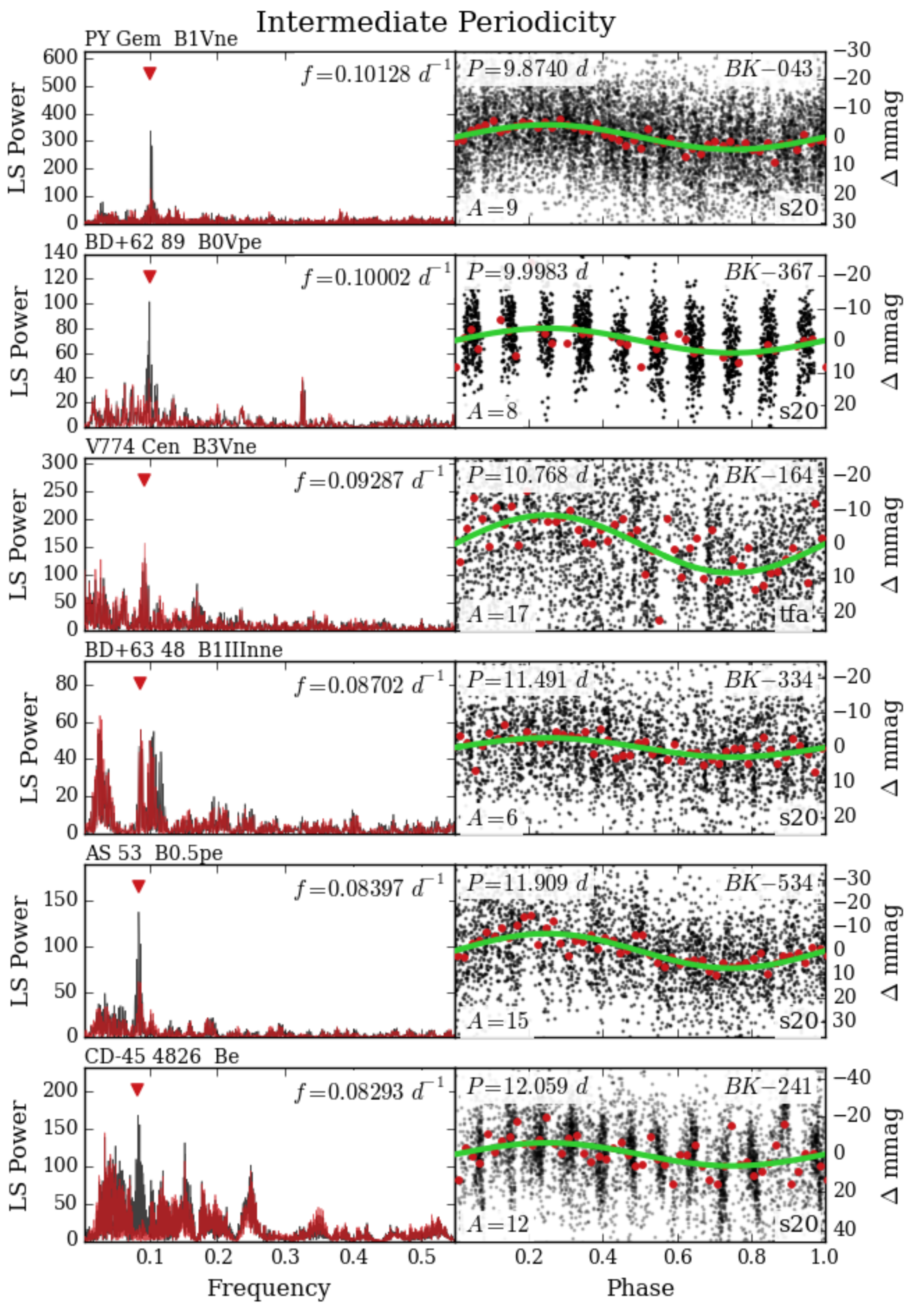
Intermediate Periodicity
PY Gem B1Vne
$f=0.10128\ d^{-1}$
$P=9.8740\ d$
BK−043
$A=9$
s20
BD+62 89 B0Vpe
$f=0.10002\ d^{-1}$
$P=9.9983\ d$
BK−367
$A=8$
s20
V774 Cen B3Vne
$f=0.09287\ d^{-1}$
$P=10.768\ d$
BK−164
$A=17$
tfa
BD+63 48 B1IIInne
$f=0.08702\ d^{-1}$
$P=11.491\ d$
BK−334
$A=6$
s20
AS 53 B0.5pe
$f=0.08397\ d^{-1}$
$P=11.909\ d$
BK−534
$A=15$
s20
CD-45 4826 Be
$f=0.08293\ d^{-1}$
$P=12.059\ d$
BK−241
$A=12$
s20
LS Power
Δ mmag
Frequency
Phase

Figure 3.11: K

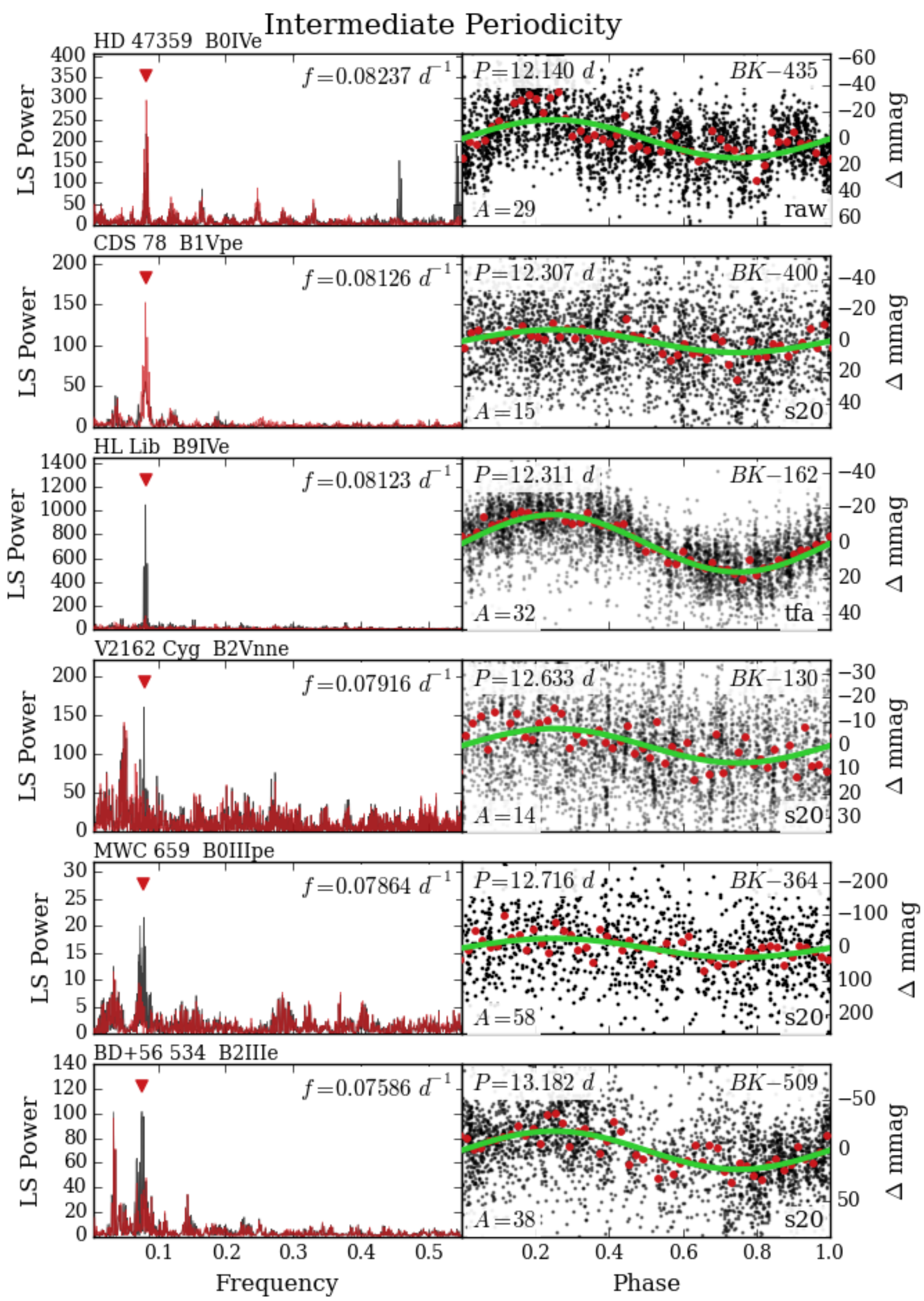
Intermediate Periodicity
HD 47359 B0IVe
f=0.08237 d^-1
P=12.140 d
BK−435
A=29
raw
CDS 78 B1Vpe
f=0.08126 d^-1
P=12.307 d
BK−400
A=15
s20
HL Lib B9IVe
f=0.08123 d^-1
P=12.311 d
BK−162
A=32
tfa
V2162 Cyg B2Vnne
f=0.07916 d^-1
P=12.633 d
BK−130
A=14
s20
MWC 659 B0IIIpe
f=0.07864 d^-1
P=12.716 d
BK−364
A=58
s20
BD+56 534 B2IIIe
f=0.07586 d^-1
P=13.182 d
BK−509
A=38
s20
LS Power
Δ mmag
Frequency
Phase

Figure 3.11: L

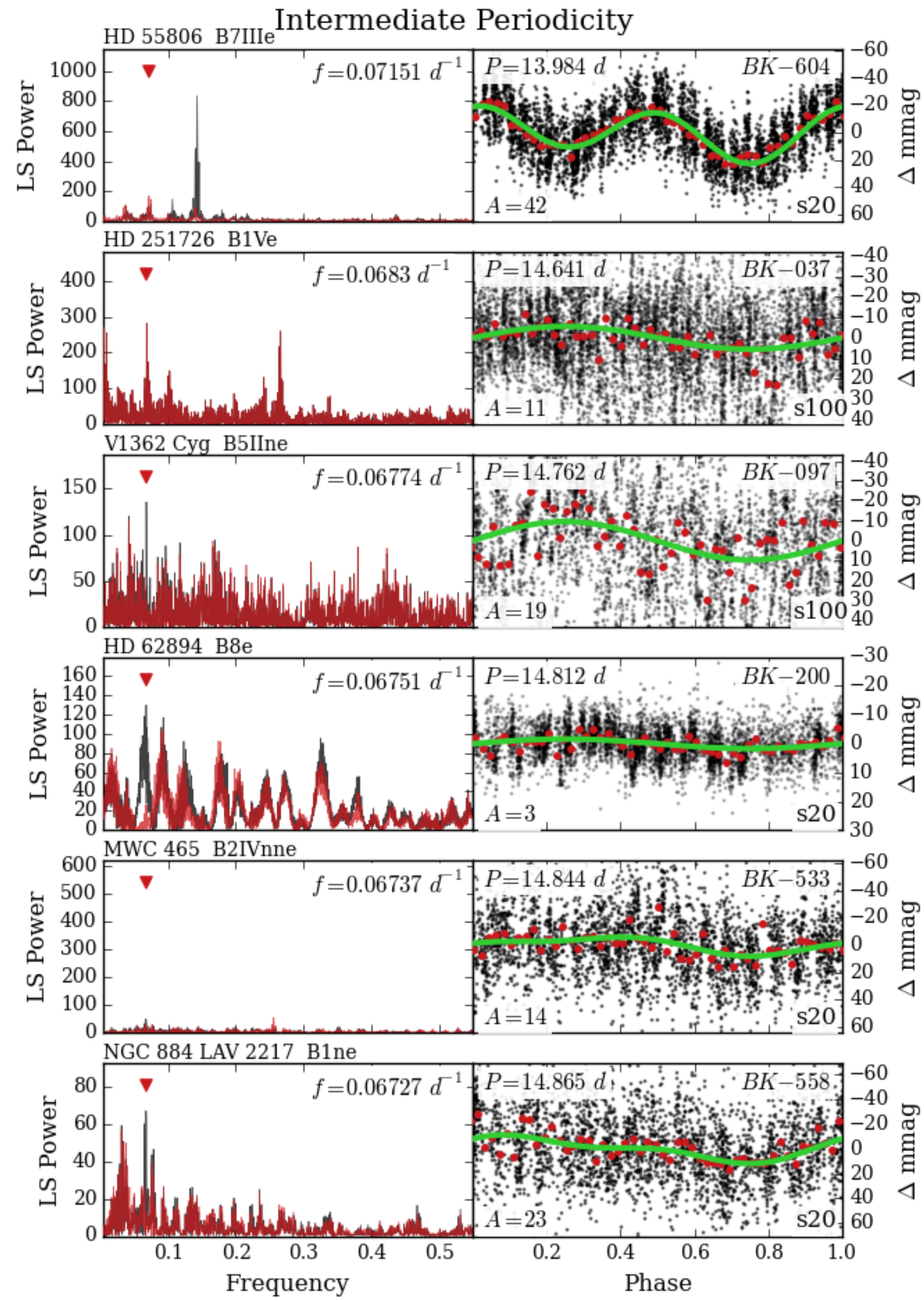

Intermediate Periodicity
HD 55806 B7IIIe
f=0.07151 d^-1
P=13.984 d
BK−604
A=42
s20
HD 251726 B1Ve
f=0.0683 d^-1
P=14.641 d
BK−037
A=11
s100
V1362 Cyg B5IIne
f=0.06774 d^-1
P=14.762 d
BK−097
A=19
s100
HD 62894 B8e
f=0.06751 d^-1
P=14.812 d
BK−200
A=3
s20
MWC 465 B2IVnne
f=0.06737 d^-1
P=14.844 d
BK−533
A=14
s20
NGC 884 LAV 2217 B1ne
f=0.06727 d^-1
P=14.865 d
BK−558
A=23
s20
LS Power
Δ mmag
Frequency
Phase

Figure 3.11: M

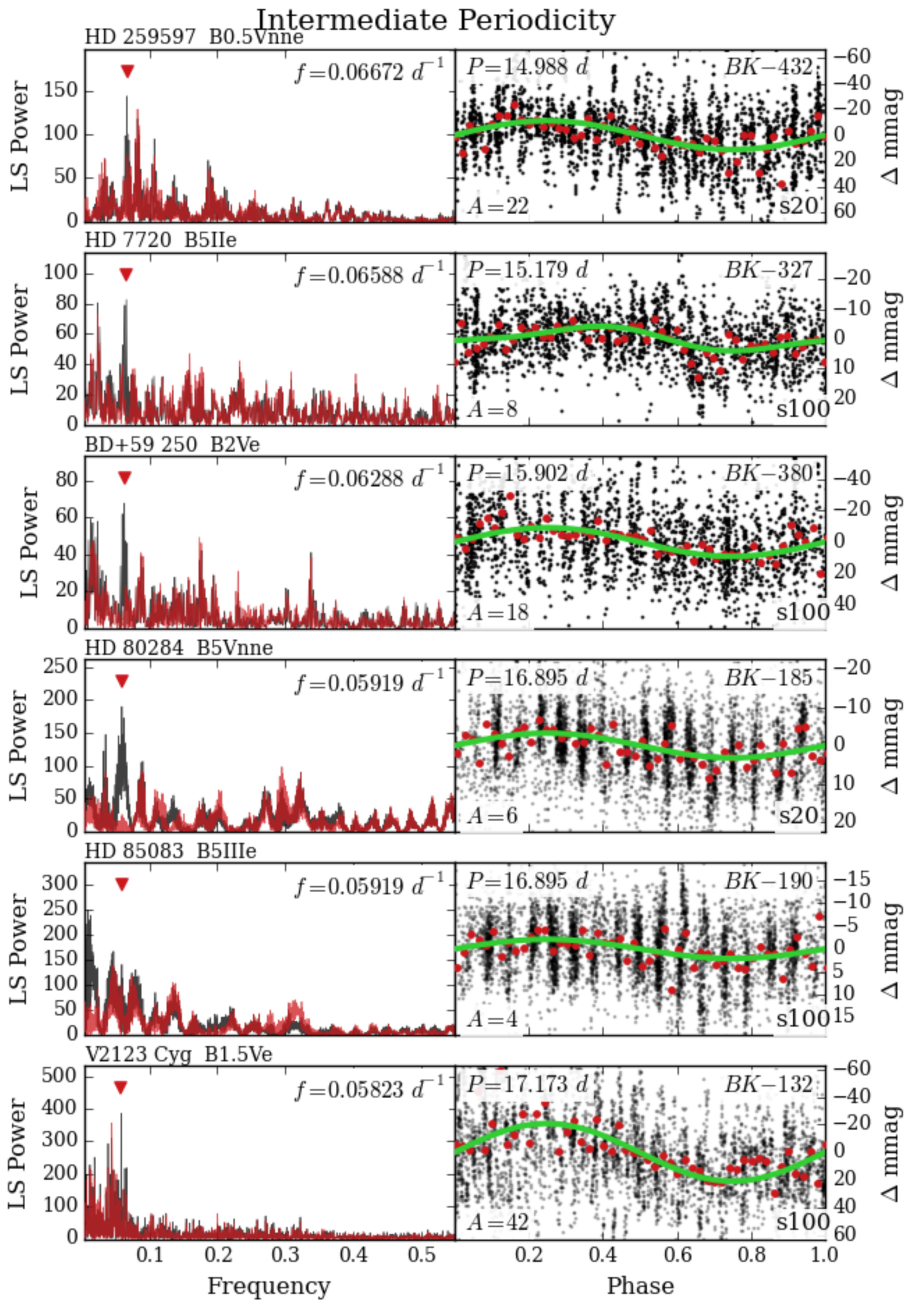
Intermediate Periodicity
HD 259597 B0.5Vnne
f=0.06672 d^-1
P=14.988 d
BK−432
A=22
s20
HD 7720 B5IIe
f=0.06588 d^-1
P=15.179 d
BK−327
A=8
s100
BD+59 250 B2Ve
f=0.06288 d^-1
P=15.902 d
BK−380
A=18
s100
HD 80284 B5Vnne
f=0.05919 d^-1
P=16.895 d
BK−185
A=6
s20
HD 85083 B5IIIe
f=0.05919 d^-1
P=16.895 d
BK−190
A=4
s100
V2123 Cyg B1.5Ve
f=0.05823 d^-1
P=17.173 d
BK−132
A=42
s100
LS Power
Δ mmag
Frequency
Phase

Figure 3.11: N

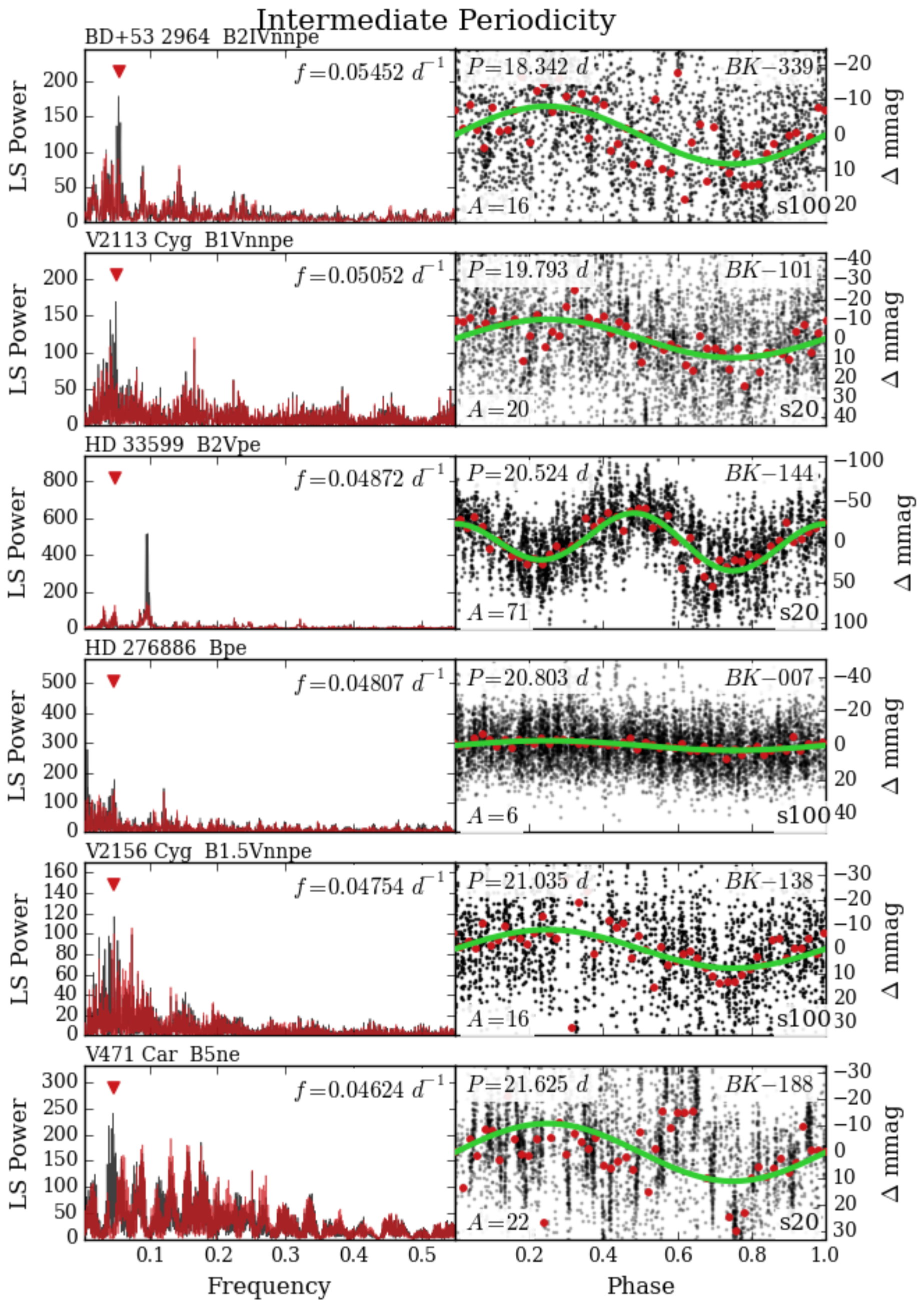

Intermediate Periodicity
BD+53 2964 B2IVnnpe
f=0.05452 d^-1
P=18.342 d
BK−339
A=16
s100
V2113 Cyg B1Vnnpe
f=0.05052 d^-1
P=19.793 d
BK−101
A=20
s20
HD 33599 B2Vpe
f=0.04872 d^-1
P=20.524 d
BK−144
A=71
s20
HD 276886 Bpe
f=0.04807 d^-1
P=20.803 d
BK−007
A=6
s100
V2156 Cyg B1.5Vnnpe
f=0.04754 d^-1
P=21.035 d
BK−138
A=16
s100
V471 Car B5ne
f=0.04624 d^-1
P=21.625 d
BK−188
A=22
s20
LS Power
Δ mmag
Frequency
Phase

Figure 3.11: O

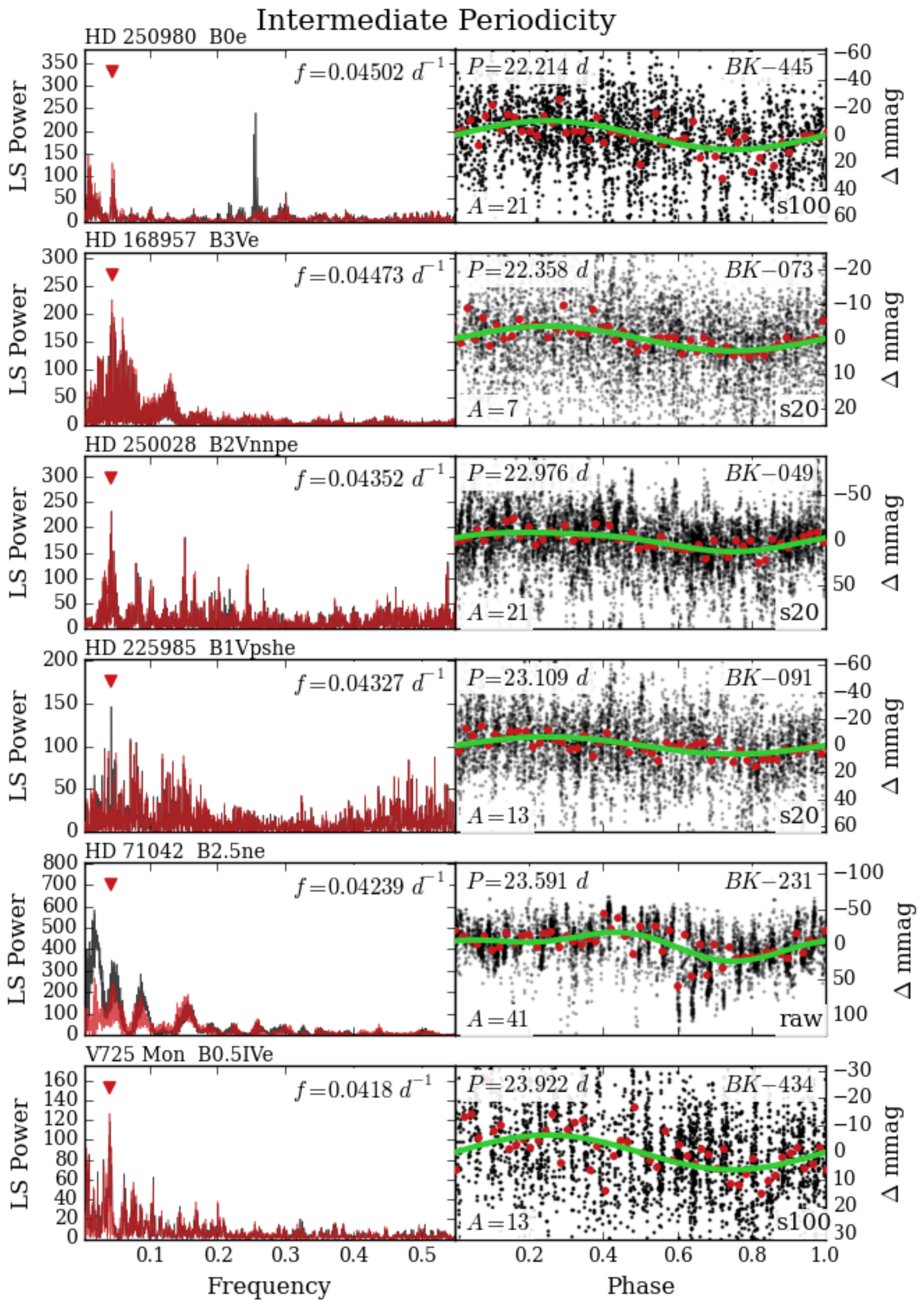
Intermediate Periodicity
HD 250980 B0e
f=0.04502 d^-1
P=22.214 d
BK-445
A=21
s100
HD 168957 B3Ve
f=0.04473 d^-1
P=22.358 d
BK-073
A=7
s20
HD 250028 B2Vnnpe
f=0.04352 d^-1
P=22.976 d
BK-049
A=21
s20
HD 225985 B1Vpshe
f=0.04327 d^-1
P=23.109 d
BK-091
A=13
s20
HD 71042 B2.5ne
f=0.04239 d^-1
P=23.591 d
BK-231
A=41
raw
V725 Mon B0.5IVe
f=0.0418 d^-1
P=23.922 d
BK-434
A=13
s100
LS Power
Δ mmag
Frequency
Phase

Figure 3.11: P

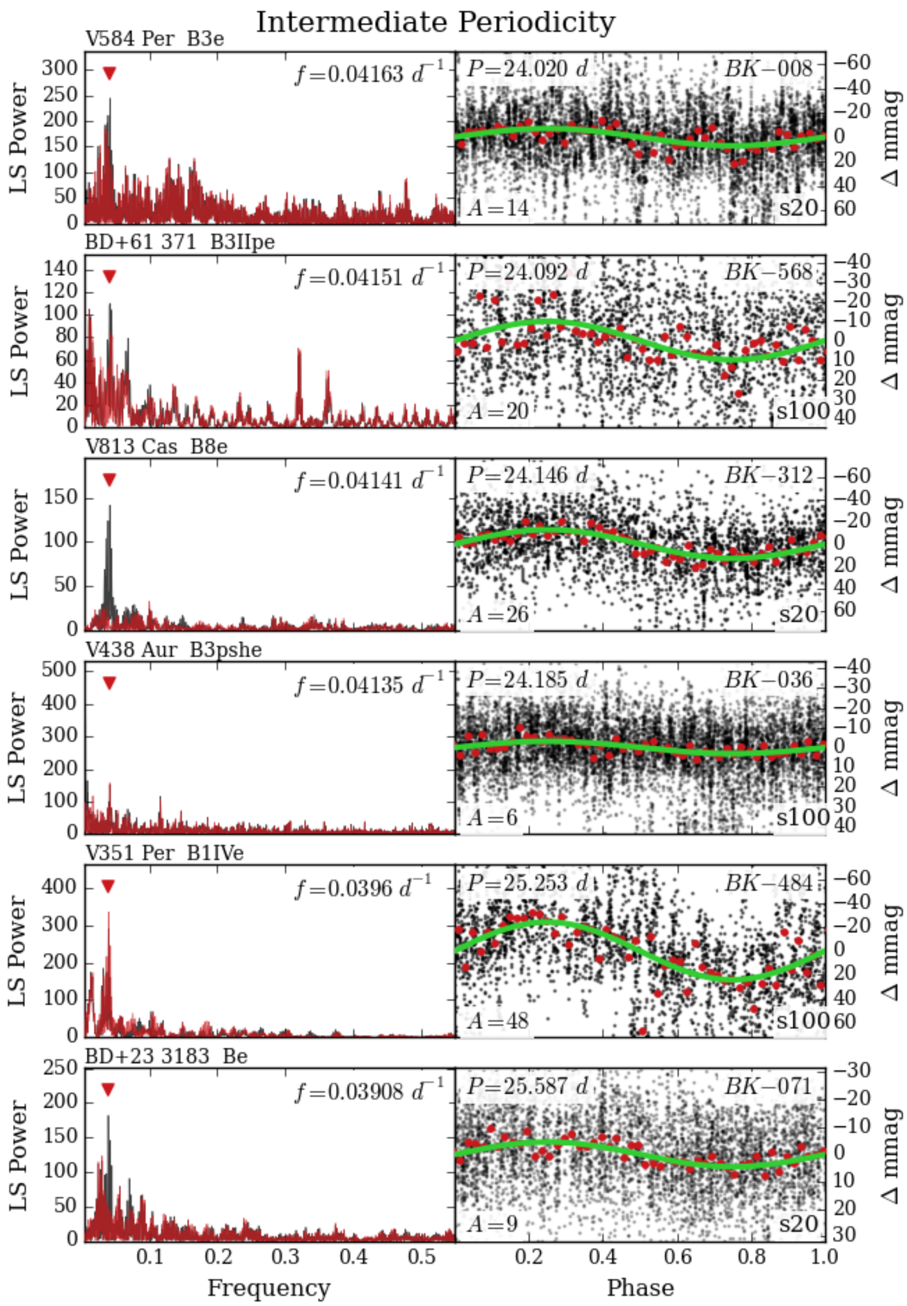

Intermediate Periodicity
V584 Per B3e
$f=0.04163\ d^{-1}$
$P=24.020\ d$
$BK-008$
$A=14$
s20
BD+61 371 B3IIpe
$f=0.04151\ d^{-1}$
$P=24.092\ d$
$BK-568$
$A=20$
s100
V813 Cas B8e
$f=0.04141\ d^{-1}$
$P=24.146\ d$
$BK-312$
$A=26$
s20
V438 Aur B3pshe
$f=0.04135\ d^{-1}$
$P=24.185\ d$
$BK-036$
$A=6$
s100
V351 Per B1IVe
$f=0.0396\ d^{-1}$
$P=25.253\ d$
$BK-484$
$A=48$
s100
BD+23 3183 Be
$f=0.03908\ d^{-1}$
$P=25.587\ d$
$BK-071$
$A=9$
s20
LS Power
Δ mmag
Frequency
Phase

Figure 3.11: Q

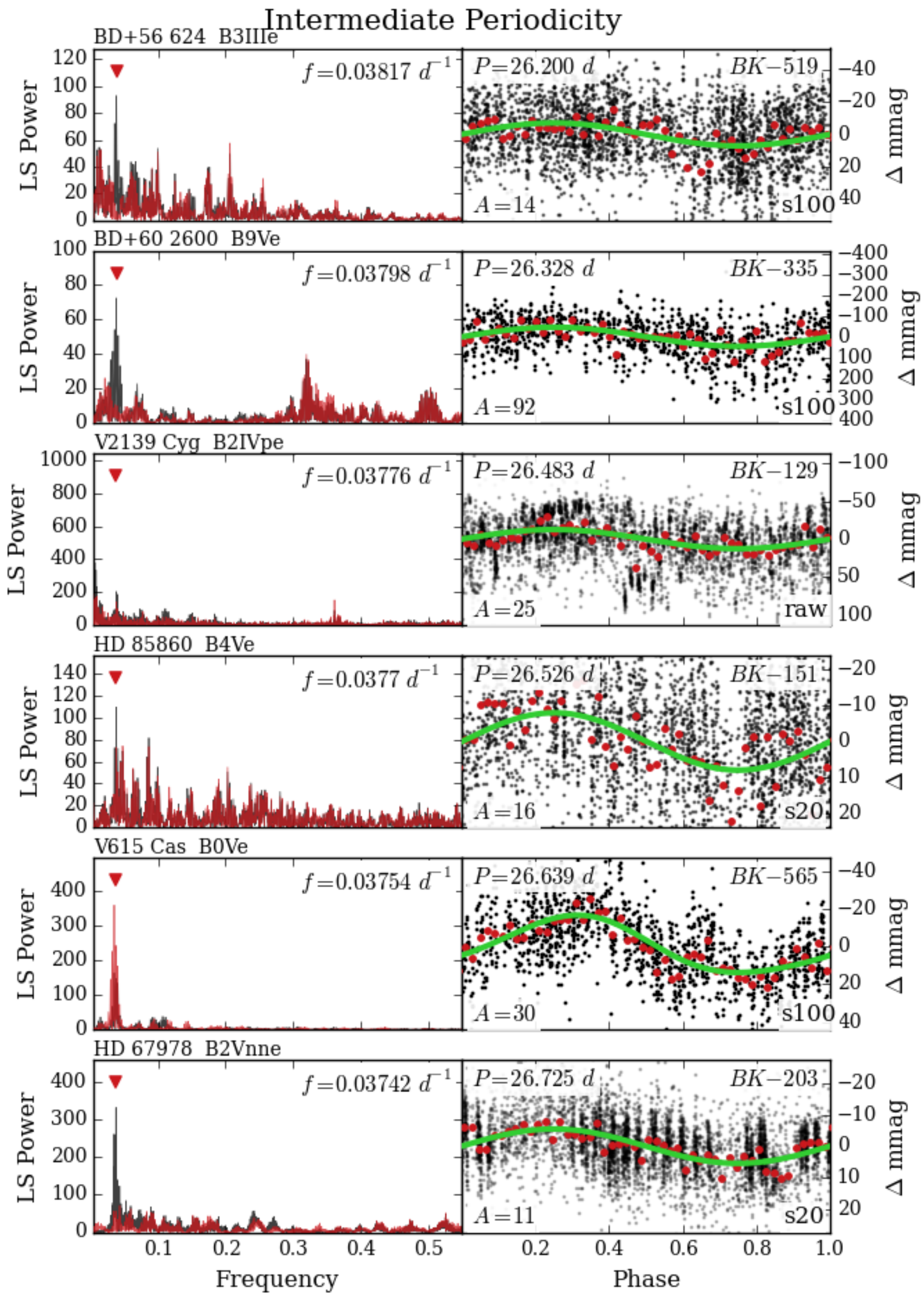

Intermediate Periodicity
BD+56 624 B3IIIe
$f=0.03817\ d^{-1}$
$P=26.200\ d$
$BK-519$
$A=14$
s100
BD+60 2600 B9Ve
$f=0.03798\ d^{-1}$
$P=26.328\ d$
$BK-335$
$A=92$
s100
V2139 Cyg B2IVpe
$f=0.03776\ d^{-1}$
$P=26.483\ d$
$BK-129$
$A=25$
raw
HD 85860 B4Ve
$f=0.0377\ d^{-1}$
$P=26.526\ d$
$BK-151$
$A=16$
s20
V615 Cas B0Ve
$f=0.03754\ d^{-1}$
$P=26.639\ d$
$BK-565$
$A=30$
s100
HD 67978 B2Vnne
$f=0.03742\ d^{-1}$
$P=26.725\ d$
$BK-203$
$A=11$
s20
LS Power
Δ mmag
Frequency
Phase

Figure 3.11: R

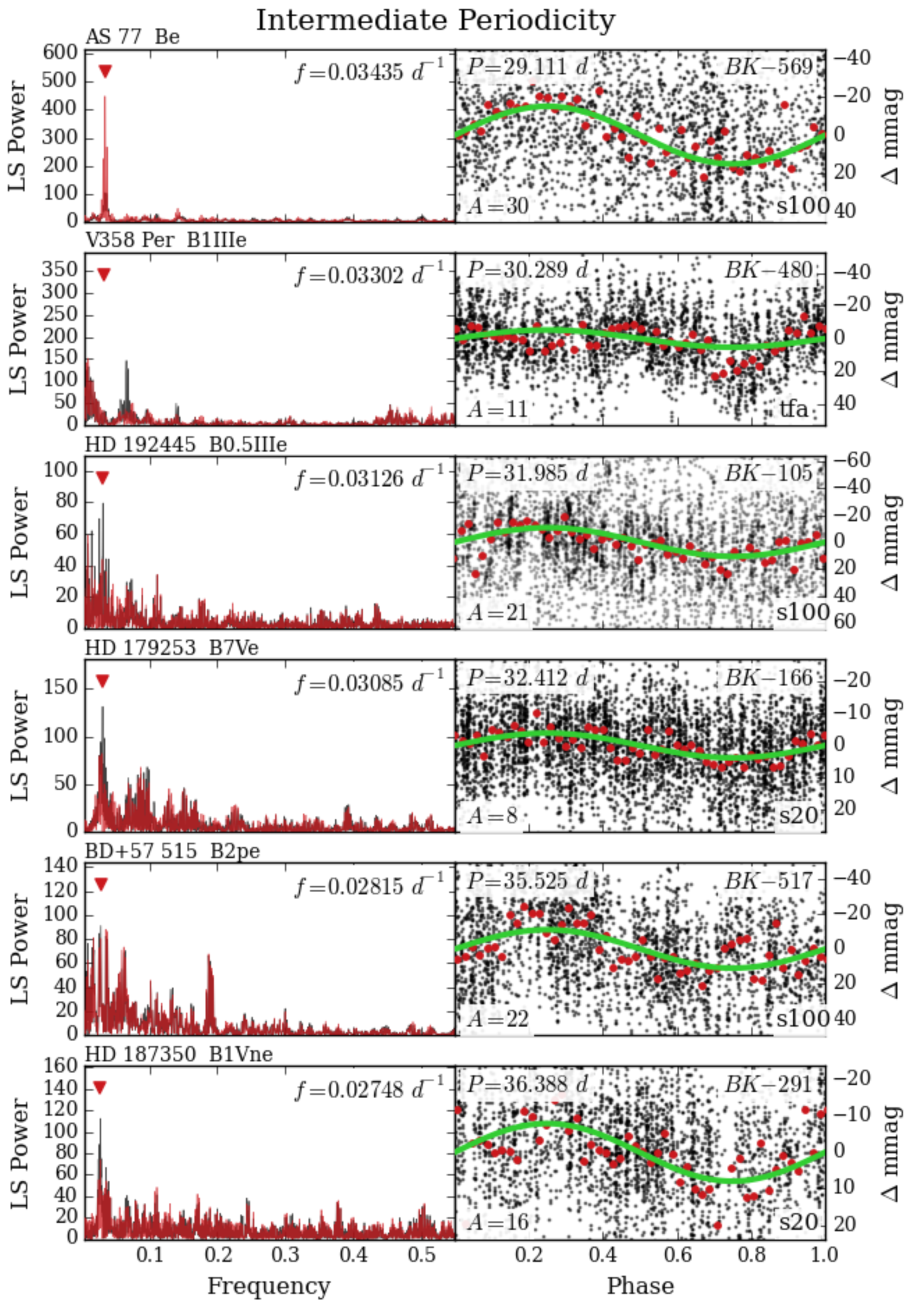

Intermediate Periodicity
AS 77 Be
f=0.03435 d^-1
P=29.111 d
BK-569
A=30
s100
V358 Per B1IIIe
f=0.03302 d^-1
P=30.289 d
BK-480
A=11
tfa
HD 192445 B0.5IIIe
f=0.03126 d^-1
P=31.985 d
BK-105
A=21
s100
HD 179253 B7Ve
f=0.03085 d^-1
P=32.412 d
BK-166
A=8
s20
BD+57 515 B2pe
f=0.02815 d^-1
P=35.525 d
BK-517
A=22
s100
HD 187350 B1Vne
f=0.02748 d^-1
P=36.388 d
BK-291
A=16
s20
LS Power
Δ mmag
Frequency
Phase

Figure 3.11: S

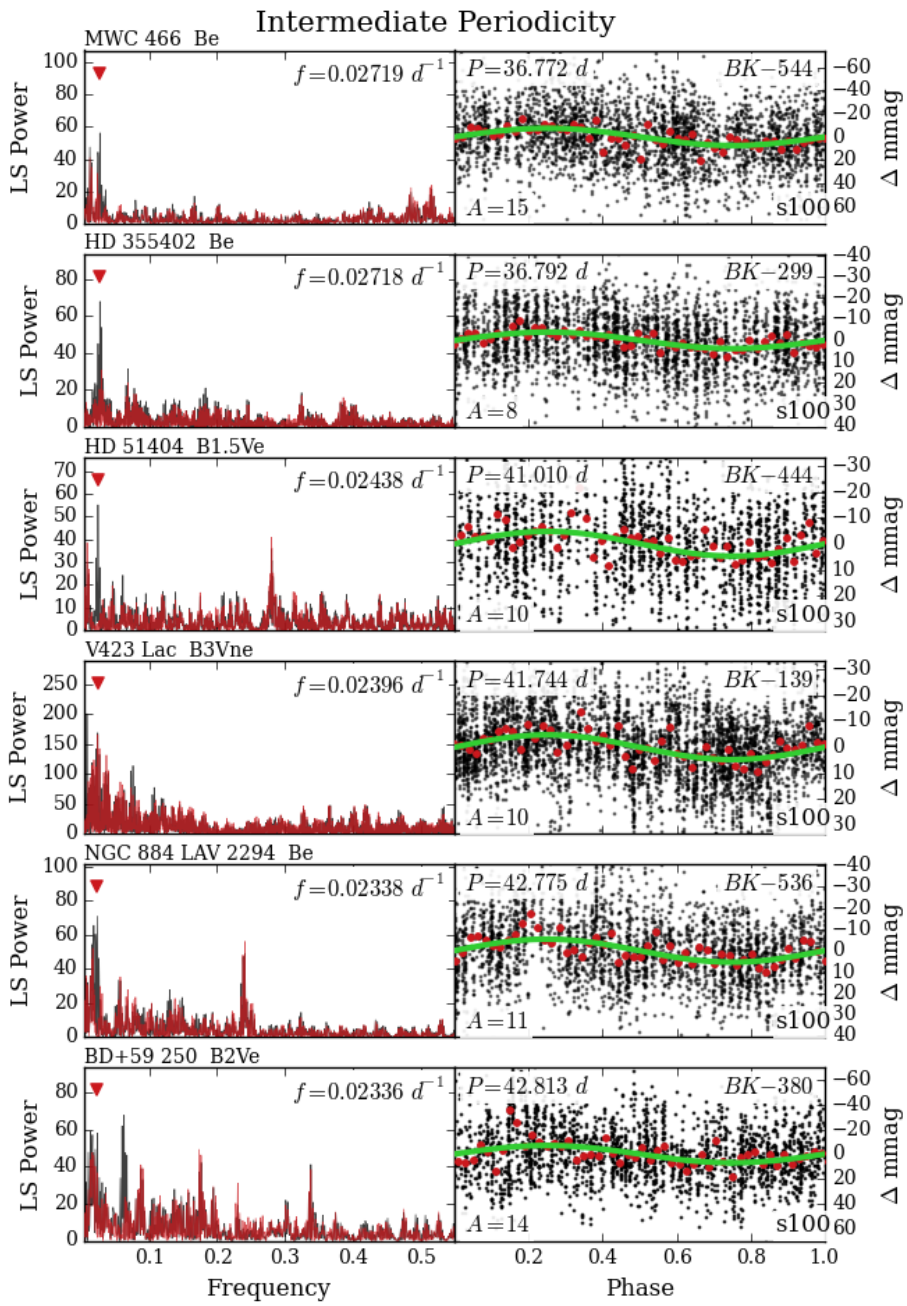

Intermediate Periodicity
MWC 466 Be
f=0.02719 d^-1
P=36.772 d
BK−544
A=15
s100
HD 355402 Be
f=0.02718 d^-1
P=36.792 d
BK−299
A=8
s100
HD 51404 B1.5Ve
f=0.02438 d^-1
P=41.010 d
BK−444
A=10
s100
V423 Lac B3Vne
f=0.02396 d^-1
P=41.744 d
BK−139
A=10
s100
NGC 884 LAV 2294 Be
f=0.02338 d^-1
P=42.775 d
BK−536
A=11
s100
BD+59 250 B2Ve
f=0.02336 d^-1
P=42.813 d
BK−380
A=14
s100
LS Power
Δ mmag
Frequency
Phase

Figure 3.11: T

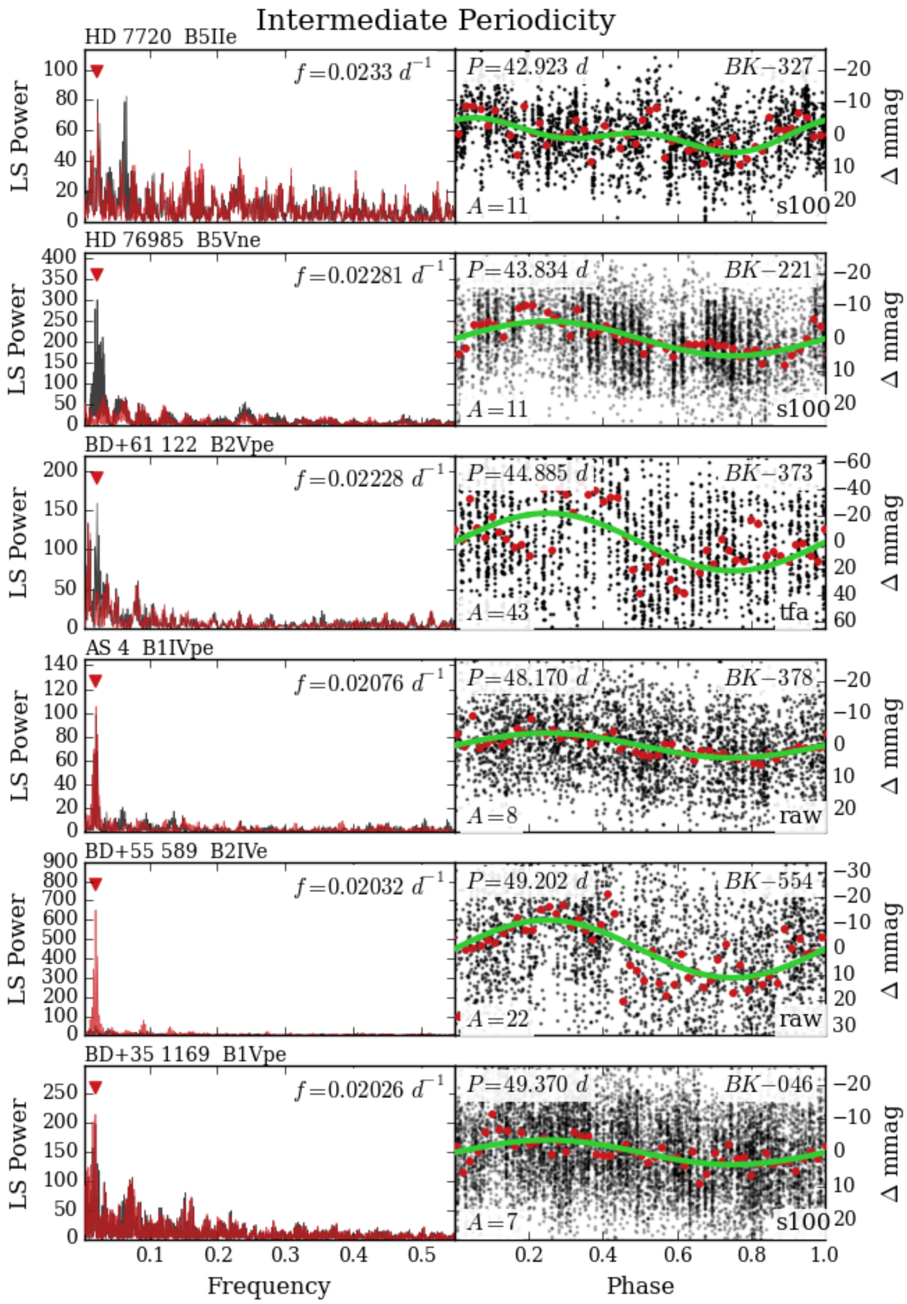
Intermediate Periodicity
HD 7720 B5IIe
f=0.0233 d^-1
P=42.923 d
BK−327
A=11
s100
HD 76985 B5Vne
f=0.02281 d^-1
P=43.834 d
BK−221
A=11
s100
BD+61 122 B2Vpe
f=0.02228 d^-1
P=44.885 d
BK−373
A=43
tfa
AS 4 B1IVpe
f=0.02076 d^-1
P=48.170 d
BK−378
A=8
raw
BD+55 589 B2IVe
f=0.02032 d^-1
P=49.202 d
BK−554
A=22
raw
BD+35 1169 B1Vpe
f=0.02026 d^-1
P=49.370 d
BK−046
A=7
s100
LS Power
Δ mmag
Frequency
Phase

Figure 3.11: U

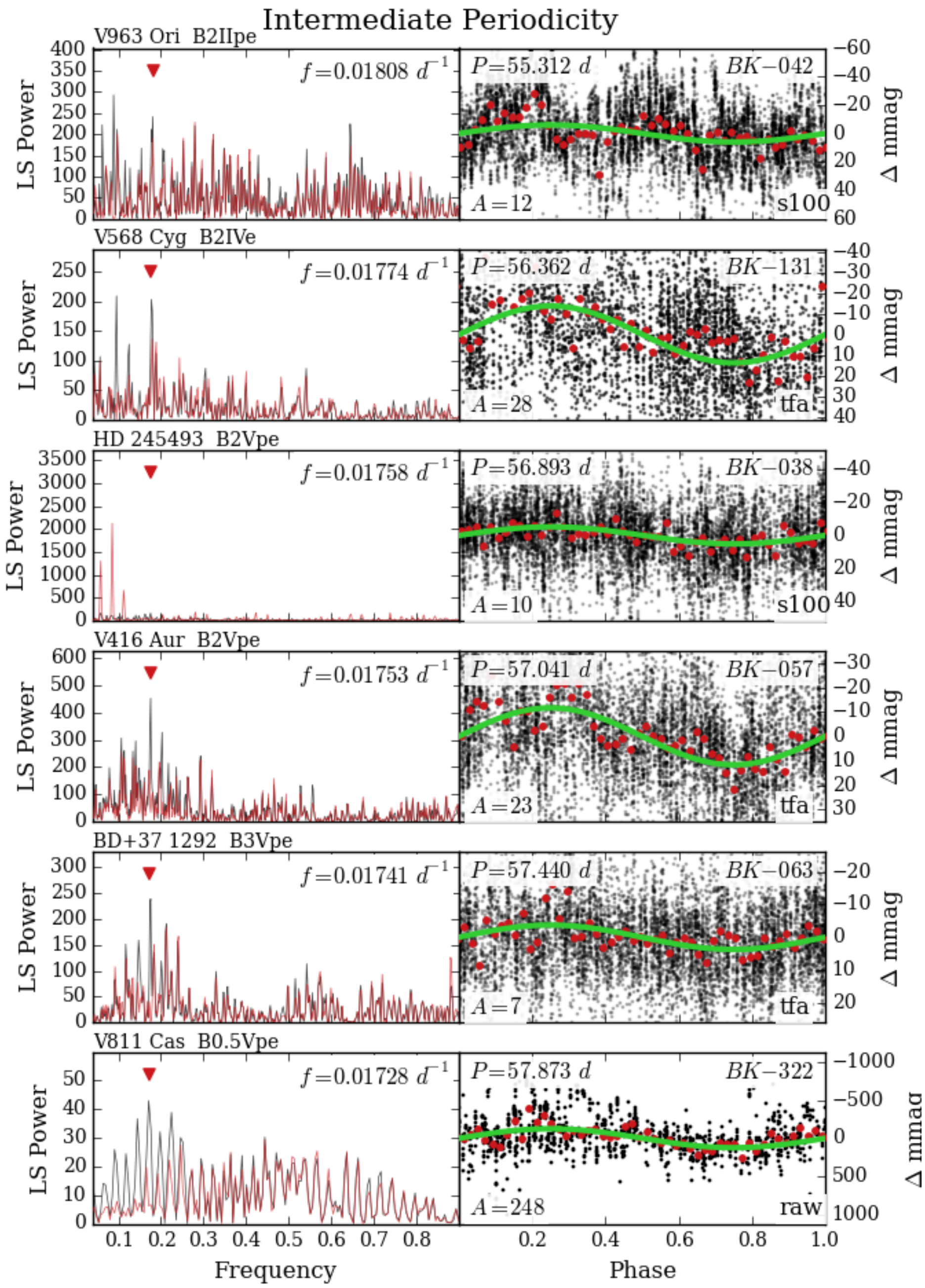

Intermediate Periodicity
V963 Ori B2IIpe
$f=0.01808\ d^{-1}$
$P=55.312\ d$
$BK-042$
$A=12$
s100
V568 Cyg B2IVe
$f=0.01774\ d^{-1}$
$P=56.362\ d$
$BK-131$
$A=28$
tfa
HD 245493 B2Vpe
$f=0.01758\ d^{-1}$
$P=56.893\ d$
$BK-038$
$A=10$
s100
V416 Aur B2Vpe
$f=0.01753\ d^{-1}$
$P=57.041\ d$
$BK-057$
$A=23$
tfa
BD+37 1292 B3Vpe
$f=0.01741\ d^{-1}$
$P=57.440\ d$
$BK-063$
$A=7$
tfa
V811 Cas B0.5Vpe
$f=0.01728\ d^{-1}$
$P=57.873\ d$
$BK-322$
$A=248$
raw
LS Power
Δ mmag
Frequency
Phase

Figure 3.11: V

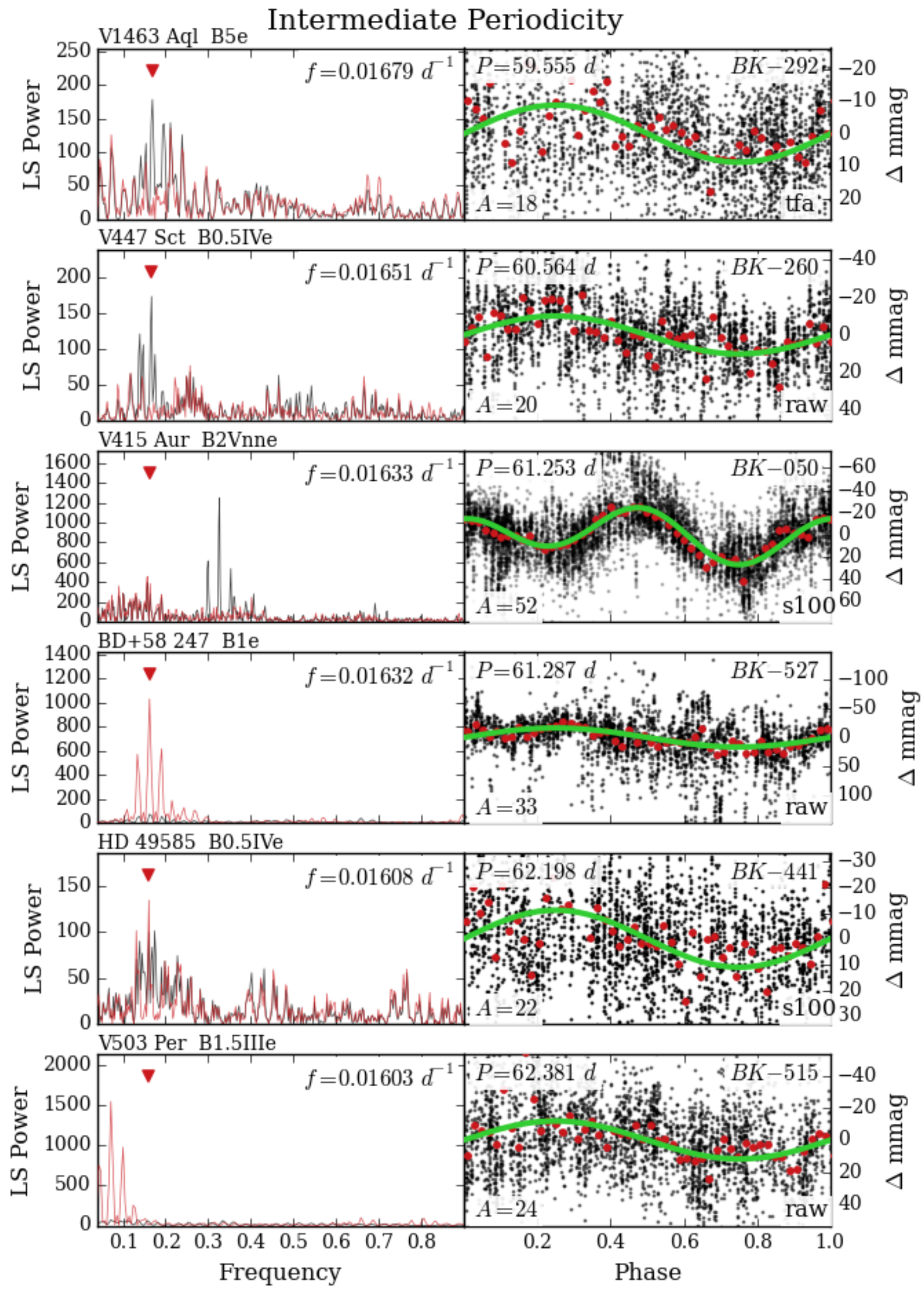

Intermediate Periodicity
V1463 Aql B5e
f=0.01679 d^-1
P=59.555 d
BK−292
A=18
tfa
V447 Sct B0.5IVe
f=0.01651 d^-1
P=60.564 d
BK−260
A=20
raw
V415 Aur B2Vnne
f=0.01633 d^-1
P=61.253 d
BK−050
A=52
s100
BD+58 247 B1e
f=0.01632 d^-1
P=61.287 d
BK−527
A=33
raw
HD 49585 B0.5IVe
f=0.01608 d^-1
P=62.198 d
BK−441
A=22
s100
V503 Per B1.5IIIe
f=0.01603 d^-1
P=62.381 d
BK−515
A=24
raw
LS Power
Δ mmag
Frequency
Phase

Figure 3.11: W

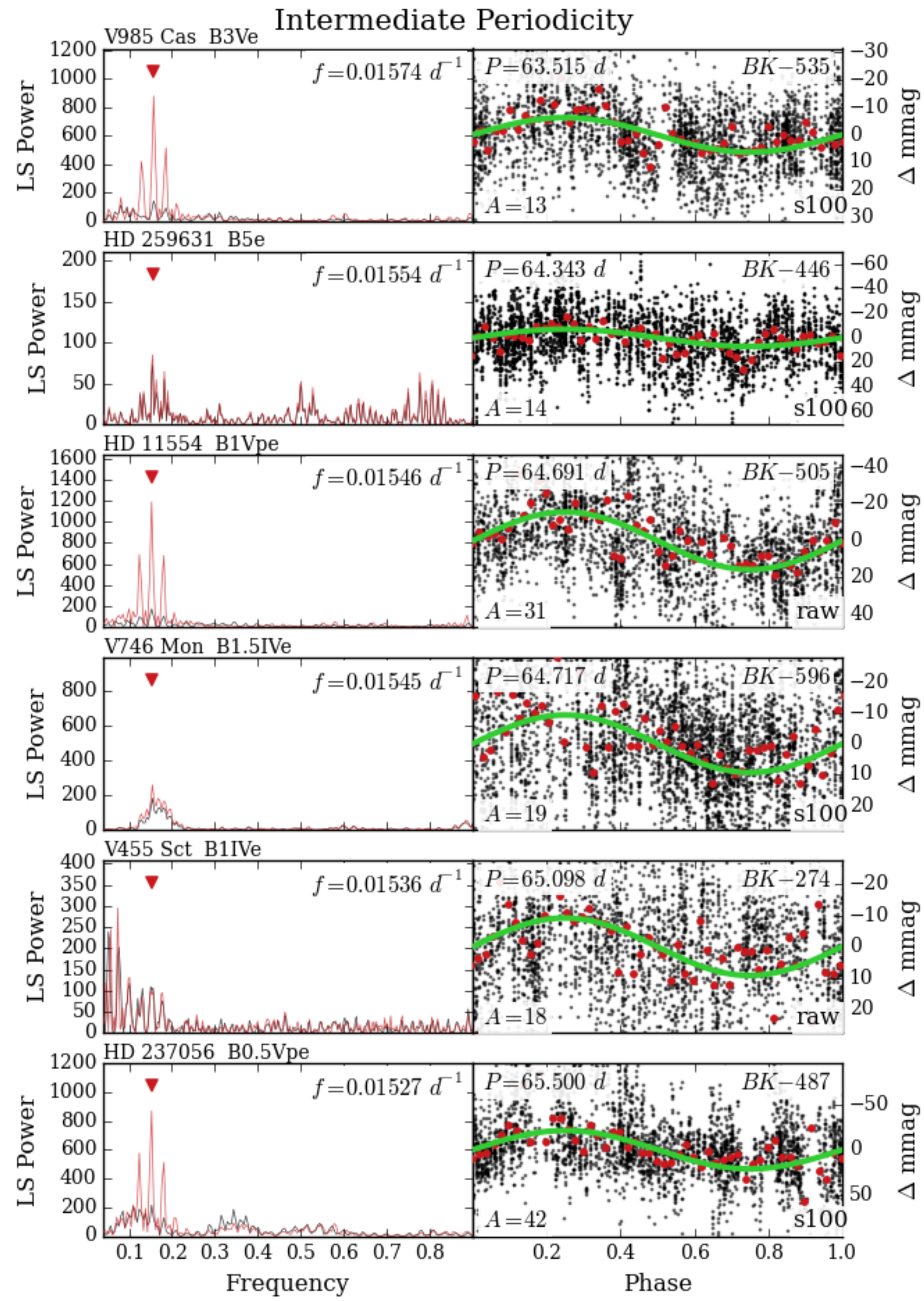
Intermediate Periodicity
V985 Cas B3Ve
f=0.01574 d^-1
P=63.515 d
BK−535
A=13
s100
HD 259631 B5e
f=0.01554 d^-1
P=64.343 d
BK−446
A=14
s100
HD 11554 B1Vpe
f=0.01546 d^-1
P=64.691 d
BK−505
A=31
raw
V746 Mon B1.5IVe
f=0.01545 d^-1
P=64.717 d
BK−596
A=19
s100
V455 Sct B1IVe
f=0.01536 d^-1
P=65.098 d
BK−274
A=18
raw
HD 237056 B0.5Vpe
f=0.01527 d^-1
P=65.500 d
BK−487
A=42
s100
LS Power
Δ mmag
Frequency
Phase

Figure 3.11: X

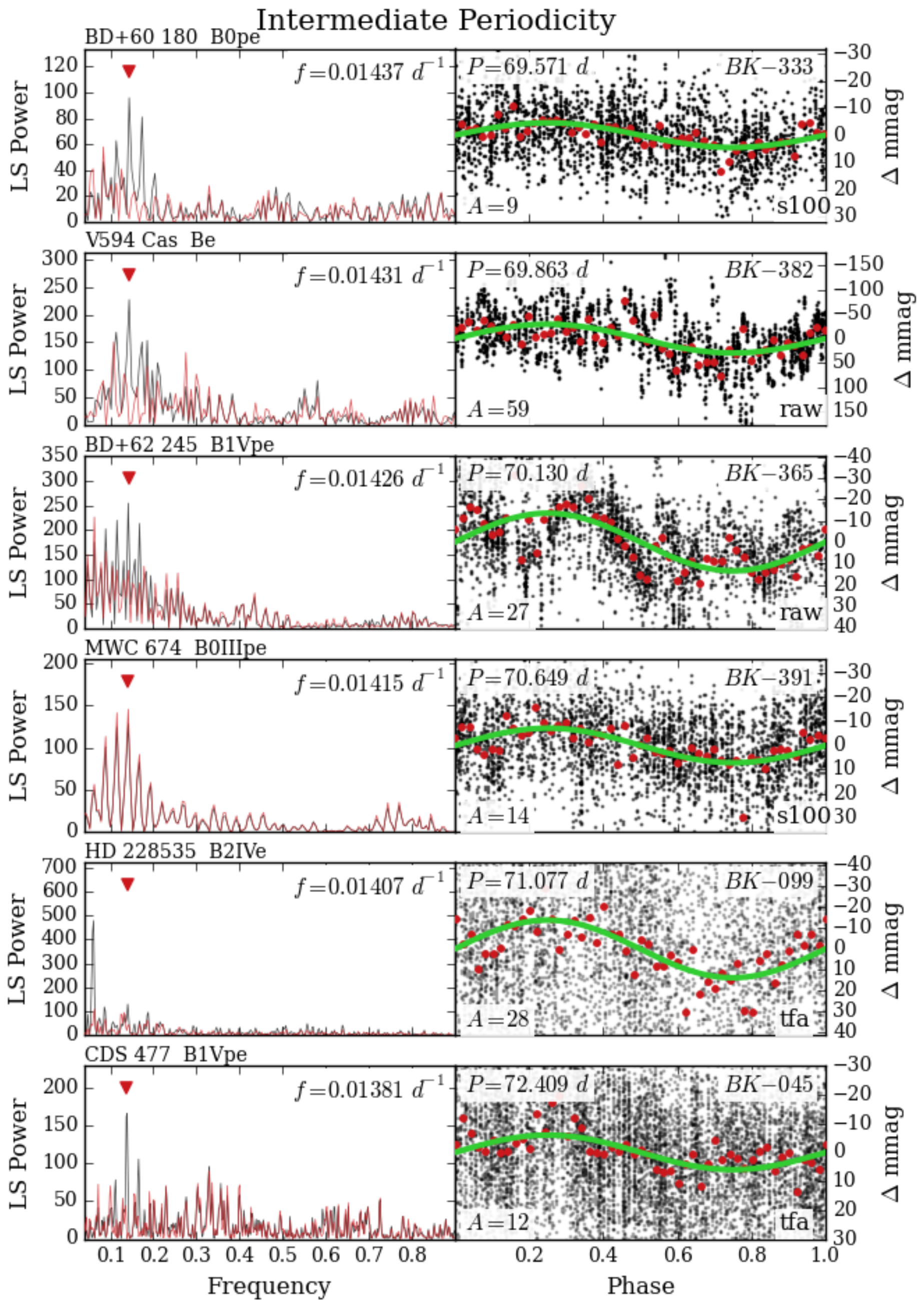
Intermediate Periodicity
BD+60 180 B0pe
f=0.01437 d^-1
P=69.571 d
BK-333
A=9
s100
V594 Cas Be
f=0.01431 d^-1
P=69.863 d
BK-382
A=59
raw
BD+62 245 B1Vpe
f=0.01426 d^-1
P=70.130 d
BK-365
A=27
raw
MWC 674 B0IIIpe
f=0.01415 d^-1
P=70.649 d
BK-391
A=14
s100
HD 228535 B2IVe
f=0.01407 d^-1
P=71.077 d
BK-099
A=28
tfa
CDS 477 B1Vpe
f=0.01381 d^-1
P=72.409 d
BK-045
A=12
tfa
LS Power
Δ mmag
Frequency
Phase

Figure 3.11: Y

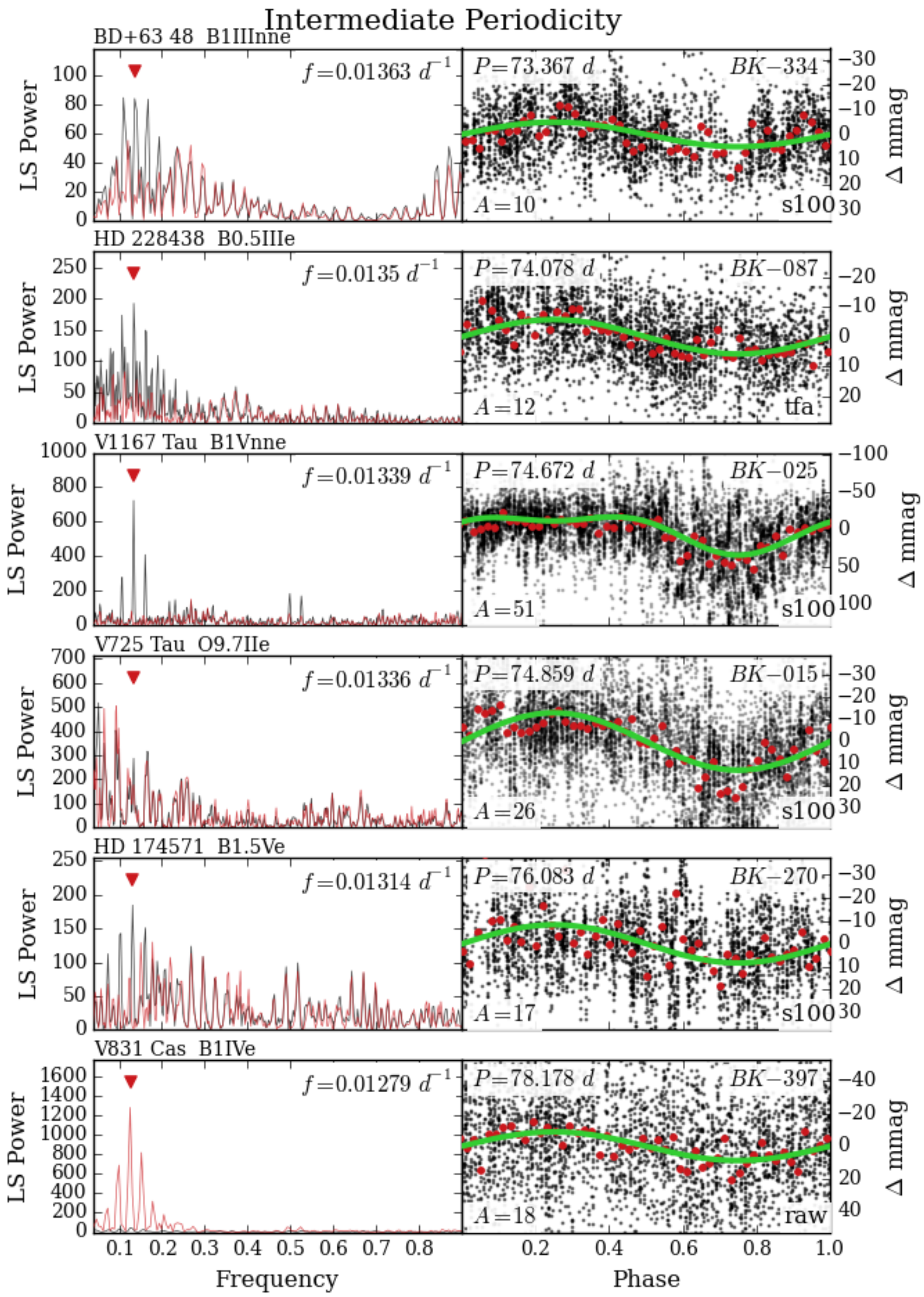

Intermediate Periodicity
BD+63 48 B1IIInne
$f=0.01363\ d^{-1}$
$P=73.367\ d$
$BK-334$
$A=10$
s100
HD 228438 B0.5IIIe
$f=0.0135\ d^{-1}$
$P=74.078\ d$
$BK-087$
$A=12$
tfa
V1167 Tau B1Vnne
$f=0.01339\ d^{-1}$
$P=74.672\ d$
$BK-025$
$A=51$
s100
V725 Tau O9.7IIe
$f=0.01336\ d^{-1}$
$P=74.859\ d$
$BK-015$
$A=26$
s100
HD 174571 B1.5Ve
$f=0.01314\ d^{-1}$
$P=76.083\ d$
$BK-270$
$A=17$
s100
V831 Cas B1IVe
$f=0.01279\ d^{-1}$
$P=78.178\ d$
$BK-397$
$A=18$
raw
LS Power
Δ mmag
Frequency
Phase

Figure 3.11: Z

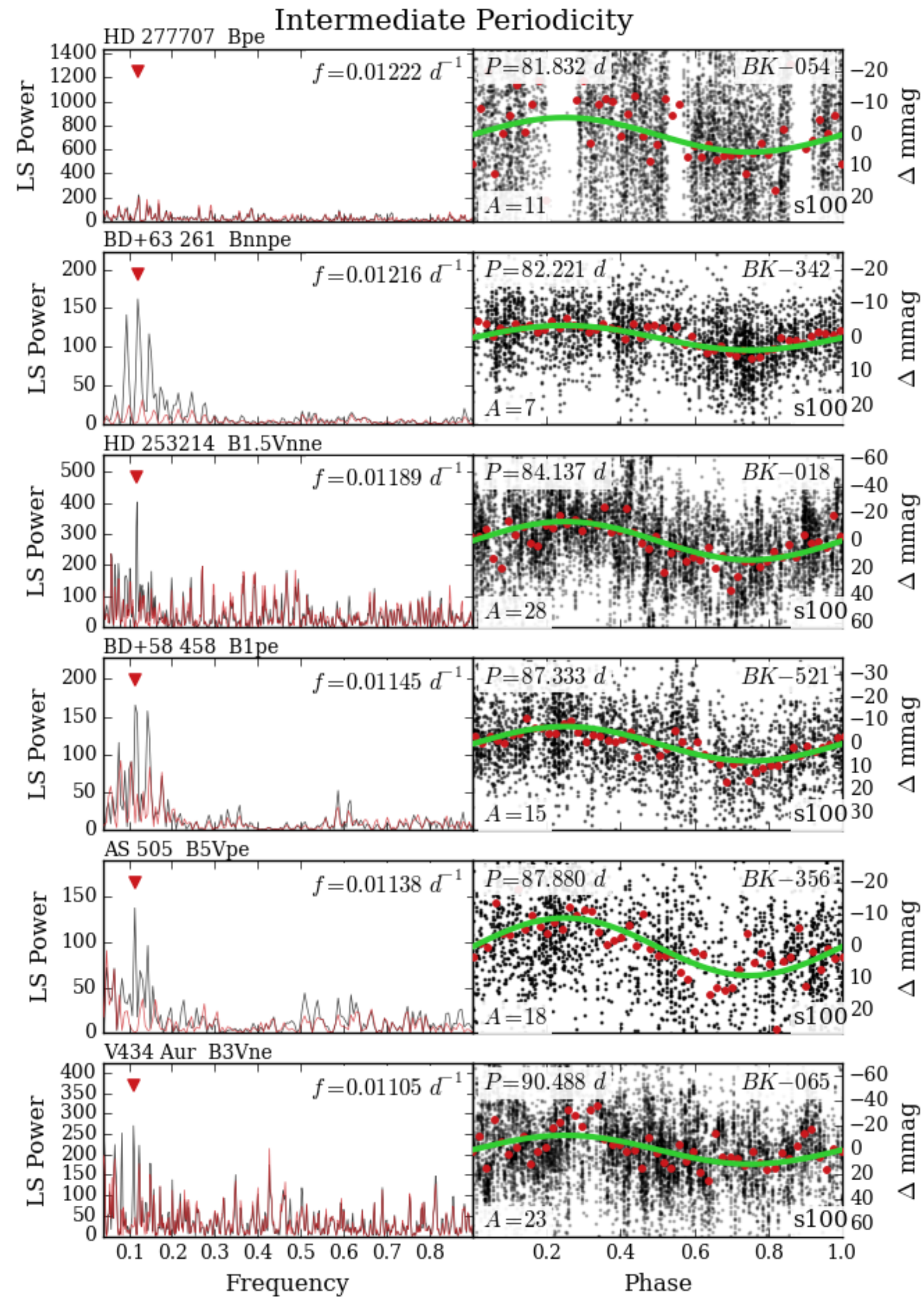

Figure 3.11: AA

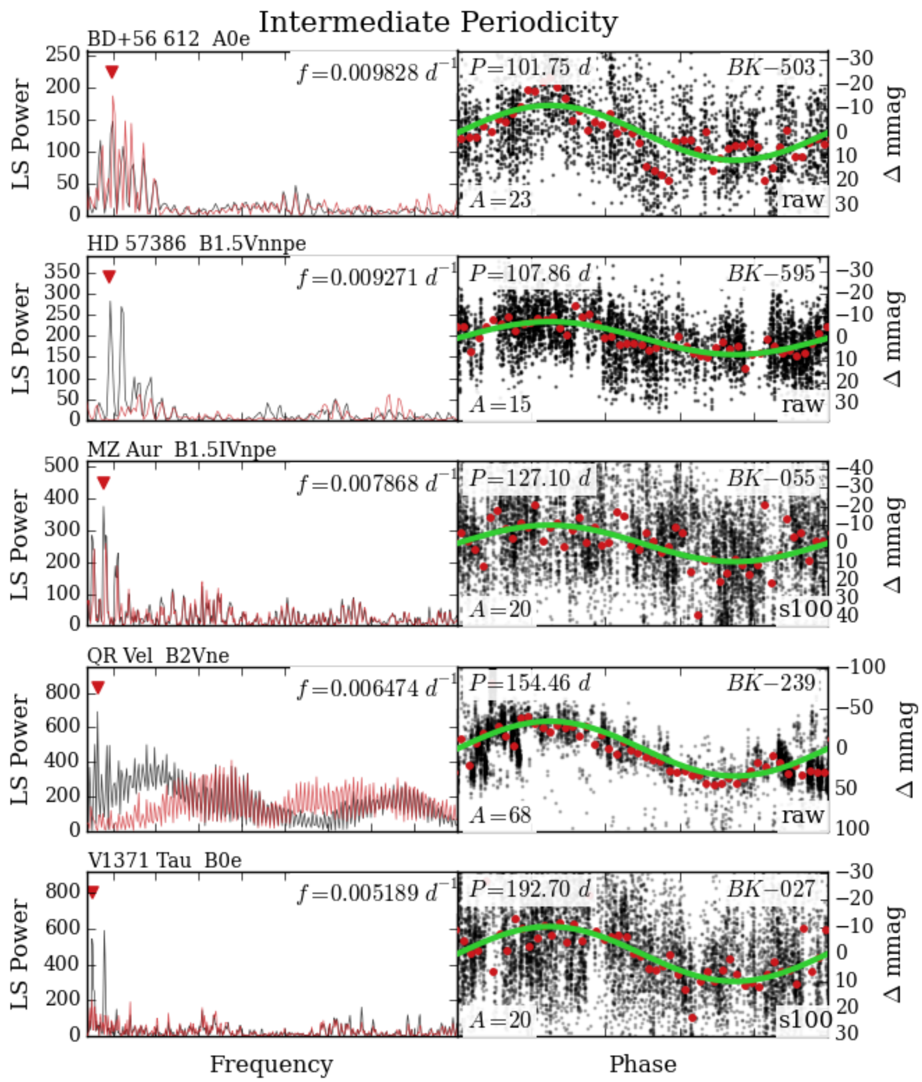

Figure 3.11: AB

Chapter 4

Outbursts

In order for a Be star disk to form, material must first be elevated from the stellar surface with sufficient velocity. Once material has been lifted from the stellar surface, the VDD model describes its evolution reasonably well. However, the mechanism for actually launching stellar material into orbit is not understood. Yet, we know that these star-to-disk mass transfer events do take place. Observational data reveal numerous instances of mass being ejected from the stellar surface, circularizing, and settling into a disk (*e.g.* Grundstrom et al. 2011; Rivinius et al. 1998). We refer to these episodes of mass transfer from star to disk as "outbursts." Recently ejected material orbits the star, circularizing and diffusing outward through viscous forces and orbital phase mixing. Simultaneously, a majority of the ejected mass falls back onto the star. This matter that falls back supplies the outflowing matter the required angular momentum that allows it to attain progressively wider orbits (Haubois et al. 2012a; Kroll and Hanuschik 1997). Line-driven ablation also potentially contributes to disk dissipation (Kee et al. 2016). Although outbursts are commonly seen in Be stars, their frequency, duration, and amplitude vary greatly from star to star, and a given Be star can show large variation in its outbursts over time. It is therefore necessary to amass a large number of observed outbursts for as many systems as possible, in order to better understand their systematic behavior and possible correlations with the underlying stellar properties.

Although outbursts are frequently observed, the engine driving them is not yet well understood. However, observational data give many hints. Be stars have the largest equatorial velocities of all stars on or near the MS, which acts to lower the effective gravity in the equatorial regions, making it easier for material to leave the surface of the star. Rapid rotation is certainly an important aspect of the mass-transfer mechanism, but is not the sole contributor. The average Be star rotates at about 80% of its critical break-up velocity, v_c. There is a narrow spread to this distribution, and it has been shown that the large majority of Be stars do not spin rapidly enough to reach their critical velocity (Rivinius et al. 2013, and references therein). Therefore, some additional mechanism(s) must be acting to eject mass. Since Be stars as a class are pulsators, and pulsations influence the kinematics at the stellar surface, the role of pulsation in the mass-transfer mechanism should be investigated. Except in the special case of very rapid rotation ($\gtrsim 0.95\ v_c$), single pulsation modes can not impart enough velocity to launch material into orbit. All Be stars that have been analyzed with high-cadence, space-based photometry are found to be multiperiodic. When such systems have multiple pulsation modes, these necessarily have beat frequencies that are governed by the frequency spacing between modes. The coupling of two or more pulsation modes with different frequencies can lead to constructive interference, where the resultant amplitude (which may be non-linear, having a higher amplitude than simply the sum of the contributing modes) is energetic enough to provide the velocity kick necessary to launch material into Keplerian orbit. Empirical evidence supports this idea in at least a few cases – μ Cen (Rivinius et al. 1998), StHα 166 (Rivinius et al. 2016), and η Cen (Baade et al. 2016c). Recent and future high-precision, space-based photometric missions (*e.g.* CoRoT, Kepler, K2, BRITE, TESS, and others) are opening the window to exploring these ideas in detail. We are also beginning to investigate this with KELT data (see the frequency analysis for ABE-A01 in Section 4.2).

4.1 Detecting Outbursts

Outbursts are a common feature in the light curves of Be stars, and are typically characterized by a monotonic increase in the brightness of the system (the 'rising phase,' where the disk grows), followed by a decay back towards baseline (the 'falling phase,' where the disk dissipates; Huat et al. 2009). In our terminology, these two distinct phases comprise a single outburst. In shell Be stars, this trend is reversed, and an outburst begins with a fading of the system, followed by a return towards baseline. This reversal is solely a consequence of inclination angle (Sigut and Patel 2013). Haubois et al. (2012a) predict V-band brightening of up to 0.4 mag ($i = 0^{\circ}$), and dimming of 0.2 mag ($i = 90^{\circ}$) when a previously disk-less star experiences an outburst, using the VDD model. At an inclination angle of $\sim 70^{\circ}$, there is effectively no net change in optical continuum flux during an outburst, as the disk absorbs approximately the same amount of flux that it emits along our line of sight (Haubois et al. 2012a). The material launched in an outburst will also contribute to spectral features, as will be shown directly in the next section.

Identifying aperiodic features, such as outbursts, requires careful visual examination of the light curve of each object. Use of a few variability statistics (*e.g.* Δm-Δt plots and peak-finding; Findeisen et al. 2015) was attempted, but the features seen are so disparate and varied that none of the statistical tests we applied were satisfactory, and a 'by-eye' analysis was deemed to be more reliable.

Light curves for all stars in both the BK and AK sample are inspected visually for the presence of outbursts, which are identified by their morphology. The number of discrete outburst events for each object is tallied, whenever tractable, and is used to calculate the rate at which outbursts occur for a given system (outbursts per year). We also measure the duration of the initial rising phase and the subsequent falling phase, as well as the photometric amplitude of the event for a subset of events in the AK sample, by a close visual inspection of the light curve. This can be done only for 'well-behaved' outbursts that are sufficiently sampled by KELT observations. It is sometimes unclear exactly when an outburst starts, reaches peak brightness, and ends. We account for this by including uncertainties, which again are measured visually. Figure 4.1 shows how a typical outburst appears in a KELT light curve. The duration of the rising and falling phases are shown, and the amplitude is clear. The error bars represent the uncertainty in the timing and amplitude. These uncertainties vary from event to event, but the average values are about 4 and 7 days for the duration of the rising and falling phases, respectively, and about 0.015 mag in amplitude.

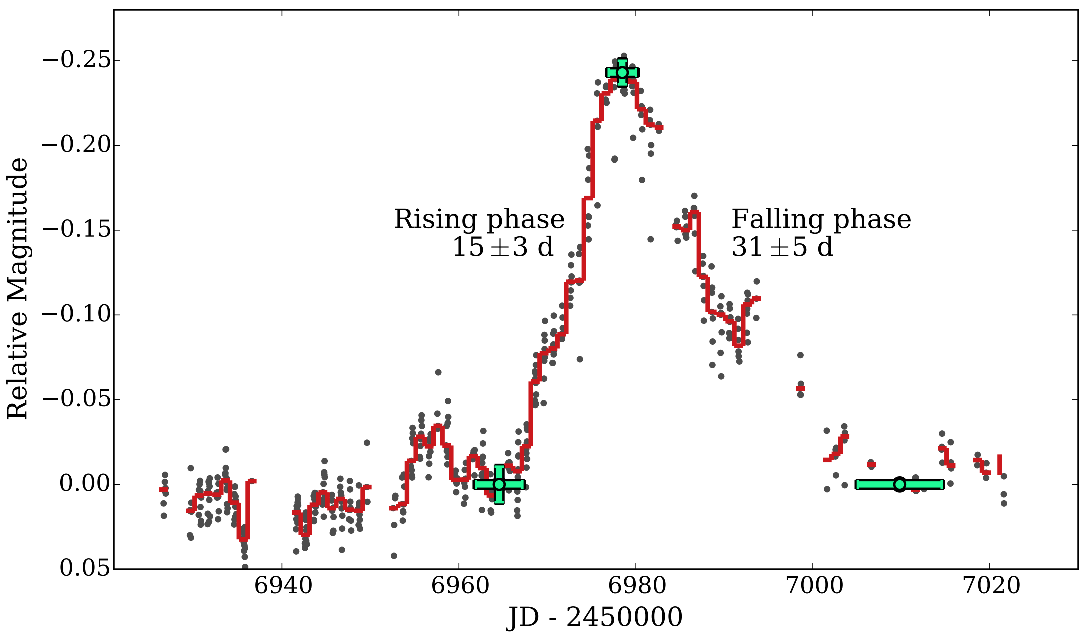

Figure 4.1: A typical outburst, as seen in photometry for the star ABE-105. The rising phase begins at JD=2456964 ± 3, and continues to rise up to a maximum brightness at JD=2456979 ± 2, fifteen days later. Then, the falling phase ensues, lasting 33 days until JD=2457010 ± 5. The system brightens by a maximum of 0.246 ± 0.013 magnitudes. The green points and error bars represent the adopted values and uncertainties in these measurements.

4.2 Illustrative examples of outbursts with simultaneous photometry and spectroscopy

There are four systems (ABE-098, -138, -A01, and -026) for which we provide a detailed analysis. For these stars, multiple APOGEE spectra are collected immediately before, during, or shortly after an outburst as seen in the KELT data, giving us snapshots of the circumstellar environment, with additional context provided by the light curves. Multiple archival spectra covering the Hα line are available from the BeSS database for ABE-138, -A01, and -026, giving us even more information about the changing circumstellar environment over a long observational baseline. Considering the different preferential formation loci of the various observables, a picture emerges of the disk both growing and dissipating from the inside outward, and a strong link is established between photometric outbursts and the injection of stellar material into the circumstellar environment.

ABE-098 (= BD+63 1955 = HD 219523)

ABE-098 has a spectral type of B5V (this work, from an ARCES spectrum). This is a system with two APOGEE spectra taken prior to the onset of a photometric outburst, and one spectrum taken just following the falling phase. Figure 4.2 shows the KELT light curve in the top panel, with a zoom-in on the region surrounding the outburst shown in the panel below. Downward pointing triangles indicate epochs of the three APOGEE spectra, and the corresponding Br11 lines are shown in the bottom panel. These spectra bracket the outburst nicely, giving us information about the circumstellar environment both before the rising phase and after the falling phase. The first spectrum has $W_{\rm Br11}$= 3.64 Å, and does not show obvious double-peaked emission at JD_0 = 2456195. There is a slight bump just to the violet side of the absorption core, which may be caused by noise, pulsation, or some circumstellar material, but there is no substantial Br11-emitting disk at this time. The next spectrum (JD_0 + 32 days) also shows no evidence of a disk. There is then a four day observing gap, followed by a photometric outburst. At the epoch of the third spectrum, JD_0 + 60 days, the Br11 line shows a very clear disk signature, with W_{Br11}= 2.10 Å (and Δv_p = 304 km s^{-1}). At this point, the brightness of the system in the KELT passband has relaxed back to baseline.

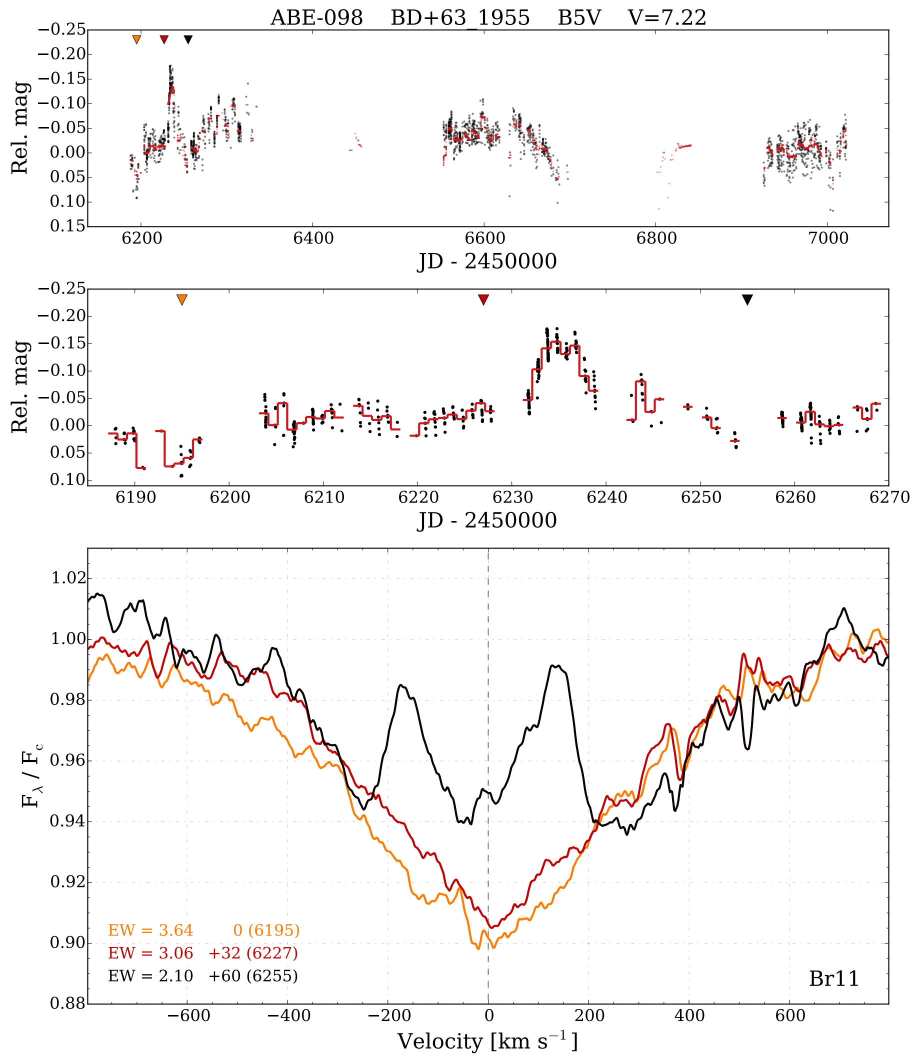

Figure 4.2: *Top:* full KELT light curve of ABE-098. *Middle:* zoom-in of an outburst. *Bottom:* APOGEE spectra, showing the Br11 line. Triangles in the upper two panels indicate epochs of APOGEE observations. We estimate a rising time of 6 days, a falling time of 129 days, and an amplitude of 0.14 mag for this outburst.

This sequence demonstrates that photometric outbursts correspond to the injection of stellar material into the circumstellar environment, some of which settles into a disk. It also provides evidence for the 'inside-out' clearing of Be star disks that is predicted by the VDD model. Since the brightness of the system in the KELT bandpass has returned to baseline (within observational errors) by the epoch of the final spectrum, there is no substantial inner disk at this time (otherwise there would be some photometric excess). Yet, the emission feature unambiguously shows the presence of a disk. Since the Br11 line probes the disk out to greater radii than does the KELT optical continuum photometry, the evidence for a disk in the Br11 line, and absence of a photometric excess in KELT data implies that the inner-most region of the disk is sparse, while some further out Br11-emitting material remains. The Br11 emission in the final spectrum shows a V/R ratio that is slightly less than unity, suggesting some asymmetry in the disk. This may indicate that the circumstellar material has not yet been thoroughly mixed.

Put simply, prior to the outburst there is no disk. During the rising phase, the inner disk grows. The falling phase shows the inner disk dissipating. During the falling phase, some amount of material has migrated radially outward, and is seen in the Br11 emission feature.

ABE-138 (= V1448 Aql = HD 180126)

Similar to the previous example, this Be star has multiple spectra in the vicinity of an outburst. Photometry shows an outburst with a short two-day rising phase, which is sampled by APOGEE spectra at the onset of the rising phase, and at peak brightness. These spectra give us a glimpse into the changes in the circumstellar environment that accompany the rising phase of this outburst.

Stellar parameters for ABE-138 are described by Frémat et al. (2006b), who found T_{eff} = 20,000 ± 1,500 K, log$g$ = 3.80 ± 0.10 (c.g.s), $v \sin i$ = 243 ± 20 km s^{-1}, an inclination angle between 39° - 60°, and a spectral type of B2 IV (nothing in our AO spectrum suggests that this estimate is inaccurate). The full KELT light curve is shown in the upper panel of Figure 4.3, with downward pointing triangles indicating the epochs of the four APOGEE observations, which occur in two groupings. Upward pointing triangles indicate epochs of Hα measurements from BeSS spectra. In the next panel, a portion of the light curve that includes the outburst near JD-2450000 = 6540 is shown. This baseline also includes four APOGEE, and three BeSS spectra. In the next row, the left (right) panel shows the Br11 lines from the first (second) grouping of APOGEE spectra, with the difference spectra plotted in the row below. The bottom panels show the Hα line from 13 BeSS spectra, spanning about 10 years, and with emission that varies in strength and sometimes disappears completely. Multiple outbursts are apparent in the light curve, and three of the four APOGEE spectra, and 8 out of the 13 BeSS spectra, show emission. This is a classical Be star at an intermediate inclination angle, with mass-loss episodes that are irregularly spaced and of varying amplitudes, and a disk that appears and disappears, and varies in strength.

The first group of APOGEE spectra (at JD_0 = 2456465, and JD_0 + 7 days) shows clear double-peaked Br11 emission, indicating the presence of a disk at these epochs. There is no obvious photometric excess at this time. It is possible that the Br11-emitting disk can be traced back to a recent outburst which may have occurred some time during the observing gap between JD-2450000 = 6440 – 6450. The photometry immediately after this gap shows a slight brightness enhancement before returning to baseline, possibly suggesting the tail end of an outburst. The majority of the change in W_{Br11} is likely due to continuum normalization issues (particularly on the red side of the line), but the decreasing emission in the line core, and the change in the V/R ratio (from V/R > 1 to V/R $\approx$ 1) is most likely real. The mean peak separation in these two measurements is 369 km s^{-1}.

The second grouping of spectra is valuable, as both are collected during the rising phase of an outburst. The first of these, taken at JD_0 + 72 days, shows only a very weak disk signature with W_{Br11}= 2.70 Å. Two days later, at the peak brightness of the outburst (JD_0 + 74 days), there is clearly emission, and W_{Br11}= 1.99 Å. Using the values for W_{Br11} and magnitude at the times of the final two spectra, we calculate $\Delta W_{Br11}/\Delta t$ = -0.36 Å d^{-1}, and $\Delta mag/\Delta t$ = -0.04 mag d^{-1}. It is possible that the strength of the Br11 emission in the final spectrum is somewhat suppressed due to line damping.

The circumstellar environment probed by the Br11 line is highly asymmetric at the epoch of the final APOGEE spectrum, with 84.3% (15.7%) of the enhancement between the final two APOGEE spectra originating from the violet (red) side. Rapid cyclic variations in the ratio of the strength of the violet and red peaks (V/R) are seen in other classical Be stars during outbursts (*e.g.* μ Cen; Rivinius et al. 1998), which can be explained if the outflow of material is not axisymmetric. So-called Štefl frequencies are sometimes detected during outburst events, and are interpreted as tracing large-scale gas-circularization (e.g. Baade et al. 2016b; Štefl et al. 2000). Through shearing and viscosity, anon-axisymmetric outflow will evolve towards a symmetric disk over time, according to the VDD model.

From the eight Hα measurements with well-defined emission peaks, we measure the peak separation and find the mean value for $\Delta v_p = 297$ km s^{-1}, with a standard deviation of 66 km s^{-1}. This is lower than the mean peak separation of the Br11 line, where $\Delta v_p = 369$ km s^{-1}. Relative to Br11, the smaller peak separation for Hα is likely caused by Hα-emitting material at larger radii, having a relatively slow orbital velocity. Non-coherent scattering broadening may also play a role if a portion of the disk is optically thick to the Hα line at the epoch of any BeSS observations.

One Hα spectrum is made bold in Figure 4.3. With an epoch of JD-2450000 = 6535, this spectrum is taken just four days prior to the third APOGEE spectrum. It is clear that a typical disk signature is seen in Hα at this epoch, but only a very weak (if any) disk signature exists in the Br11 line four days later. This is naturally explained by the VDD model, which predicts Be star disks both growing, and dissipating, from the inside outward. Between the 1st and 3rd APOGEE spectra, the 'inner' to 'mid' disk has dissipated (to the point of non-detection in KELT and APOGEE data), but the 'outer' disk remains largely intact, as evidenced by the three Hα double-lined emission profiles observed in this time span (at JD-2450000 = 6484, 6510, and 6534). The 'outer' disk also eventually dissipates, as there is no sign of Hα emission at JD-2450000 = 7617.

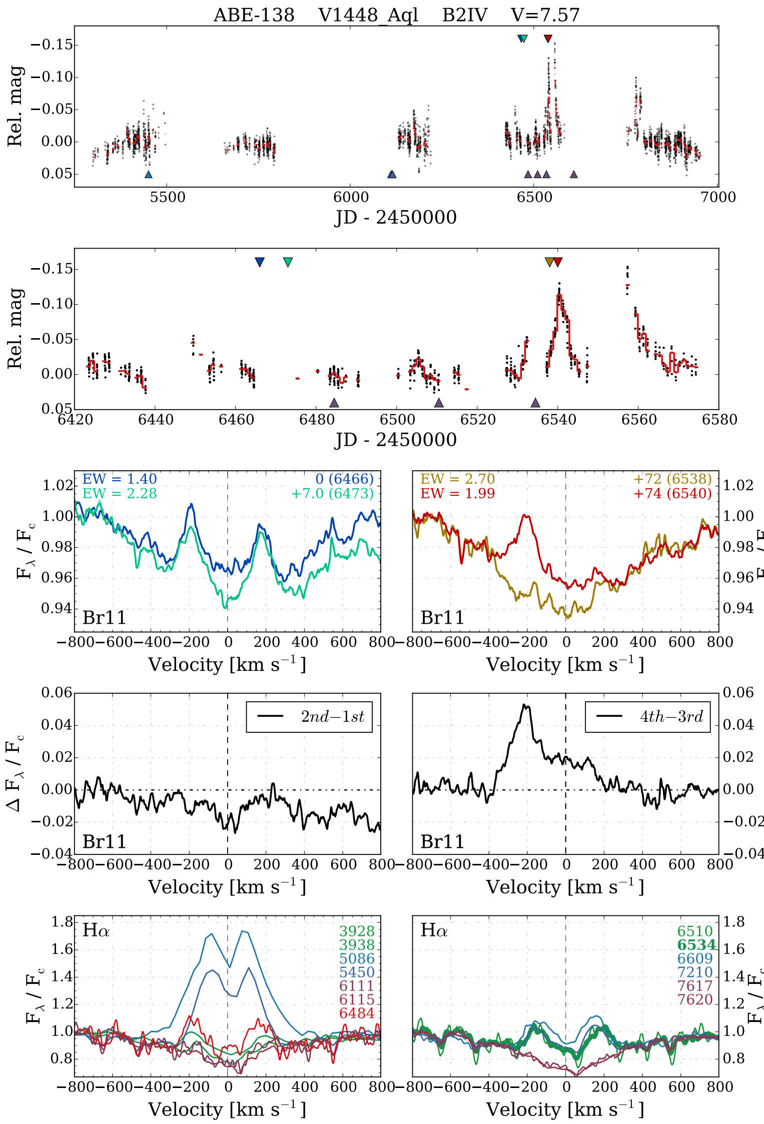

Figure 4.3: *1st row:* Raw KELT light curve of ABE-138. Colored downward pointing triangles correspond to epochs of APOGEE observations, and upward facing triangles indicate BeSS observations. *2nd row:* Zoom-in on the region above, highlighting the outburst near JD-2450000 = 6540. The red lines show the nightly median of the photometric data. *3rd row:* The Br11 line of the first (left) and second (right) groupings of APOGEE spectra. The Br11 EW is shown in the upper-left corner. The number of days since the first APOGEE spectrum is printed in the upper-right corner, with the JD-2450000 date in parenthesis. *4th row:* Difference spectra between the first (left) and the final (right) pairs of APOGEE spectra. *5th row:* Hα spectra from the BeSS database, with the JD-2450000 dates in the upper right.

ABE-A01 (= MWC 5 = BD+61 39)

Like the previous example of ABE-138, APOGEE observed ABE-A01 during the rising phase of an outburst. Morgan et al. (1953) assign this star a spectral type of B0.5IV (nothing in our AO spectrum suggests this is inaccurate). Figure 4.4 shows the full KELT light curve, a zoomed-in view of the outburst and the epochs of APOGEE observations, the Br11 line profile of the three APOGEE spectra and their differences, and 5 Hα spectra from the BeSS database. In all spectra, from both APOGEE and BeSS, we infer the presence of a disk, even when spectra are taken near photometric minimum (e.g. Hα at JD-2450000 = 6611 and 6997).

As the rising phase of the first outburst progresses and the system becomes brighter, there is a growing amount of emitting material, as evidenced by the increasingly negative values for the Br11 line EW ($W_{\rm Br11}$= -3.61, -5.13, and -6.37 Å, in chronological order). The central depression partially fills in, and the line profile edge becomes less sharp. The bulk of the increasing emission arises in the wings of the line profile. The growing emission wings can be attributed primarily to electron scattering. As the density in the inner disk rises, an increase in electron scattering of line photons causes the emission wings to grow, an effect that becomes stronger as the amount of circumstellar material (and free electrons) increases. The rising brightness in the light curve likewise indicates a growing inner disk.

A decrease in peak separation (Δv_p = 128, 130, and 108 km s^{-1}, in chronological order) is seen in the final Br11 line. This may be explained in part by the outer edge of the Br11-emitting disk moving out to larger radii, where material is orbiting at lower velocities. Also, as the disk builds up and becomes more dense, an increase in the optical thickness in the Br11 line may act to decrease the peak separation through non-coherent scattering of line photons.

Because the strength of the Br11 line is measured relative to the local continuum flux, an increase in the continuum level will serve to suppress the apparent strength of line emission. Because of this, it is likely that the Br11 line is increasing in absolute strength more dramatically than it is increasing in its strength relative to the continuum flux (which is what is plotted in Figure 4.4). Regardless of this effect, the increase in the emission wings still indicates a growing inner disk.

By taking the difference between spectra (lower left panel of Figure 4.4), we can more clearly see how the Br11 emission line profile is changing. Beyond highlighting the growth of the wings, the difference spectra allow us to compare the contributions from the red and violet halves of the line profile. Considering the difference between the 2nd and 1st spectra, 57.7% of the enhancement in W_{Br11} comes from the violet half of the line, and 42.3% from the red half. In the difference between the 3rd and 1st spectra, 46.3% of the W_{Br11} enhancement comes from the violet half of the line, and 53.7% from the red half. Between the 3rd and 2nd spectra, 32.0% of the W_{Br11} enhancement comes from the violet half, and 68.0% from the red half. Asymmetry in the changes of the Br11 line implies asymmetries in the disk as it grows during this rising phase.

By analyzing the three APOGEE spectra taken during the rising phase of a single outburst in ABE-A01, we see an increase in the amount of emitting material, especially at relatively high velocities, and we note that the Br11 line does not grow symmetrically. High-velocity material is being injected into the inner circumstellar environment in a seemingly asymmetric (in space, and/or velocity) fashion.

There are six discrete high-amplitude outbursts in the KELT light curve (see the top panel of Figure 4.4), but not all of these are sampled fully. The beginning of the rising phase is missing for the first, third, and fifth outbursts, and the final outburst is observed only during part of the initial rising phase. There is also other variability interspersed, with shorter timescales and lower amplitudes. These six major outbursts occur with some regularity, although they are not strictly periodic, varying somewhat in their amplitude and morphology. Their similarities in shape and timing are apparent when the light curve is phased to a period of 91.23 days, as shown in Figure 4.5.

Prompted by the interesting show of repeating outbursts, the photometric data for ABE-A01 were subjected to a frequency analysis, in order to search for signals with periods shorter than three days. This upper limit on the periodic signals of interest was chosen based on the typical pulsational periods of Be stars, and the timescales associated with Be star rotation and Keplerian orbits in the region of the circumstellar environment in which KELT photometry is sensitive to (Rivinius et al. 2013). This process requires first removing the high-amplitude variability on longer timescales (including the six major outbursts), which dominate the light curve. In the same manner employed in Rivinius et al. (2016), a Fourier-based high-pass filter was applied to the photometry, iteratively identifying and removing low-frequency sinusoidal signals. This process results in a detrended light curve with all long-term trends removed, suitable for recovering signals with periods less than three days. The entire detrended light curve was analyzed for periodic signals with a generalized LSP analysis.

The results of this analysis are shown in Figure 4.6. The top panel shows the LSP (black curve) out to a frequency of 10 d^{-1}. Higher frequencies were probed as well (up to 500 d^{-1}), but the periodogram is featureless beyond 10 d^{-1}. A single strong signal is detected at $f_1 = 0.53073$ d^{-1}. The other obvious peaks are aliases of this signal, caused mostly by the observing pattern of KELT (daily, monthly, and yearly aliases). The red curve shows the periodogram after pre-whitening against f_1. The middle panel shows the periodogram in the immediate vicinity of f_1 (left), and the light curve phased to the corresponding period (right). The bottom panel highlights the pre-whitened periodogram, in the same frequency range as the above plot, and identifies the top peak (of the pre-whitened periodogram) in this region.

Six separate and unique portions of the light curve, corresponding to the six major individual outbursts, were analyzed in this manner as well. This was done mainly to study f_1 over time. In each portion of the light curve, f_1 is recovered at the same frequency (to within ∼0.2%). This signal remains coherent (*i.e.* experiences no shift in phase) throughout the observational baseline, and does not appear to significantly vary in amplitude. The photometric signal does not appear to be double- or triple-waved when phased to two or three times the recovered period.

All of the observed features of f_1 are consistent with stellar pulsation. The frequency is within the range where pulsation in Be stars is expected, and is similar to the pulsations of the class of slowly pulsating B stars, of which Be stars have been conjectured to be a rapidly-rotating and more complicated sub-class (Aerts et al. 2006; Kurtz et al. 2015). The photometric amplitude is high (20.1 mmag), but not unusually so (Balona 1995), especially since pulsation amplitudes tend to be larger in early-type Be stars (Rivinius et al. 2013), which is the case with ABE-A01 (B0.5IVe). The fact that this signal persists throughout the entire observational baseline and remains coherent in phase is also consistent with pulsation.

So-called Štefl frequencies are sometimes detected in the light curves of Be stars. These signals are caused by asymmetries in the circumstellar material orbiting the star, which can modulate the net observed flux (and also line profiles; Štefl et al. 1998, 2000). The period of Štefl frequencies is determined by the orbital period close to the star, and can be of a similar timescale as the periodic signal recovered in ABE-A01. However, there are a number of reasons to doubt this as the cause for f_1. Štefl frequencies are found only in conjunction with pulsational signals of similar, but slightly higher, frequencies (*e.g.* Baade et al. 2016b; Štefl et al. 1998). There is only one significant frequency in the light curve of ABE-A01. Štefl frequencies are so far detected in photometry only for Be stars that have high inclination angles, since a photometric signal manifests only when the density enhancements are projected against the stellar disk (*e.g.* Baade et al. 2016b). ABE-A01 is at a low inclination angle. The fact that the signal is coherent (in phase and amplitude) over the entire observational baseline is an argument against the signal being a Štefl frequency, which are typically transient on timescales much longer than the orbital period in the inner regions of the disk, although exceptions are possible (*e.g.* η Cen Rivinius et al. 2003). We therefore attribute f_1 to pulsation.

It has been proposed that combinations of multiple pulsation modes can interact to control the 'clock' that dictates the time-variable mass-loss rates of Be stars (Kee et al. 2014; Rivinius et al. 1998). Such 'combination frequencies' are the preferred explanation for the low-frequency variability seen in the Be star η Cen (Baade et al. 2016b). Kurtz et al. (2015) argue that nonlinear mode coupling can give rise to combination frequencies in Be stars that have higher amplitudes than the parent frequencies. In this framework, the difference between two pulsation modes can be referred to as the 'difference frequency' ($\Delta f = |f_1 - f_2|$, where f_1 and f_2 are the frequencies of two pulsation modes). This Δf then describes the approximate frequency of the outbursts themselves.

We apply this idea to ABE-A01. Because the outbursts are approximately evenly spaced, we can measure their period (91.23 days) and therefore the frequency with which they occur (0.01096 d^{-1}), which we suppose is the difference frequency. We then have $\Delta f = 0.01096\ \mathrm{d}^{-1}$, and $f_1 = 0.53073\ d^{-1}$. We are motivated to search for a second pulsation mode, which should occur with a frequency $f_2 = f_1 \pm \Delta f$. The two solutions for f_2 are 0.51977 d^{-1} and 0.54169 d^{-1}. The bottom panel in Figure 4.6 shows our attempt to search for the signature of a second pulsation mode, f_2. This panel shows the pre-whitened periodogram, with the position of f_1 indicated by a vertical dashed line, and our predictions for possible expected values of f_2 marked by vertical dotted lines. After pre-whitening against f_1, there are no peaks with substantial power. However, there is a weak peak near one of the frequencies expected for f_2 (see the bottom panel in Figure 4.6). While it is possible that this signal is astrophysical and represents a pulsation mode in the star, this can neither be confirmed, nor ruled out, with the available data. It should be noted that ABE-A01 is viewed at a low inclination angle, which can cause certain non-radial pulsation modes to have a very low photometric amplitude, due to azimuthal averaging. The lack of additional strong peaks (besides f_1) in the periodogram computed from the KELT light curve therefore does not imply that the star oscillates in only one mode.

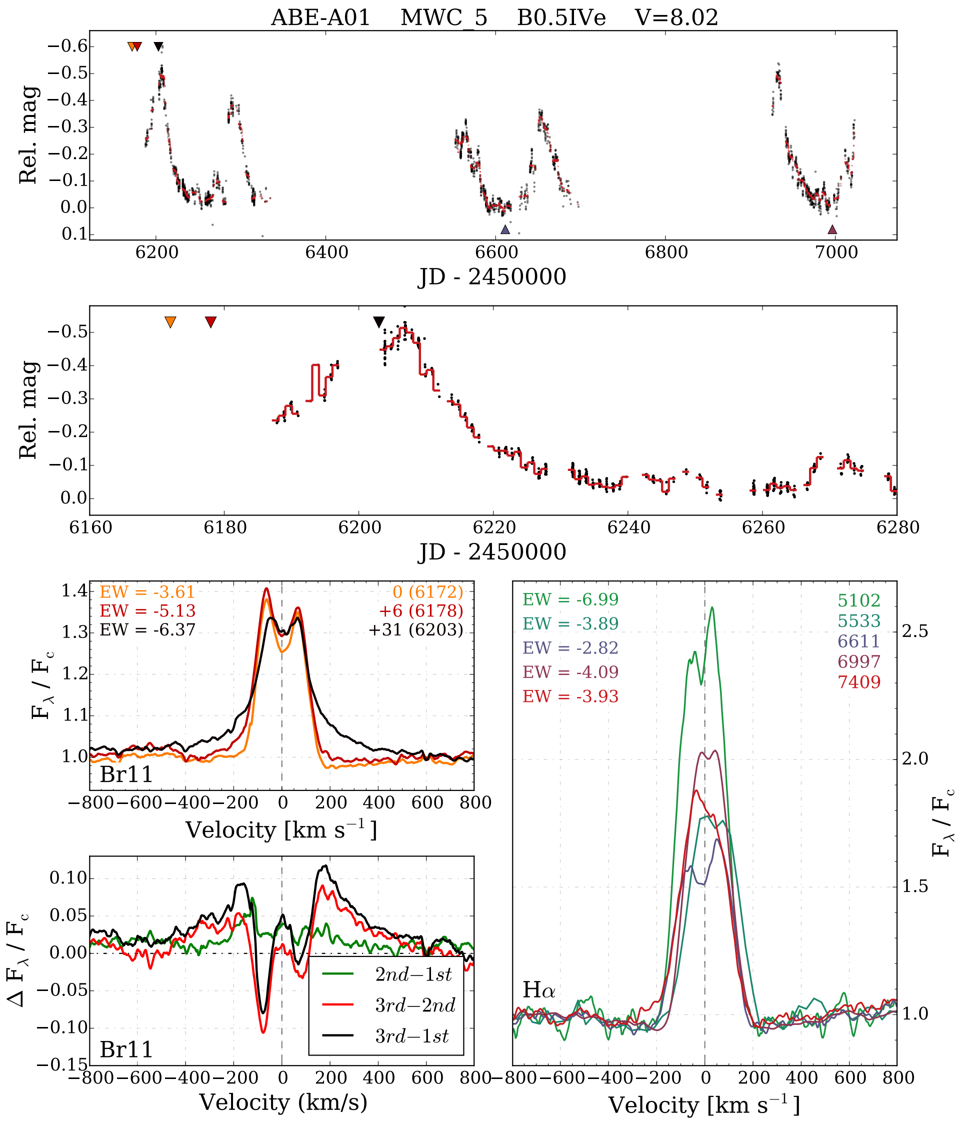

Figure 4.4: *Top:* Raw KELT light curve for ABE-A01, with downward (upward) pointing triangles indicating epochs of APOGEE (BeSS) observations. *Middle:* zoomed-in view of the first outburst. *Bottom:* The left two panels show the Br11 line of the three APOGEE spectra, with colors corresponding to the epoch of observation and the colored triangle markers in the light curve plots (upper), and the differences between these (lower). The right panel shows the Hα line from five BeSS spectra.

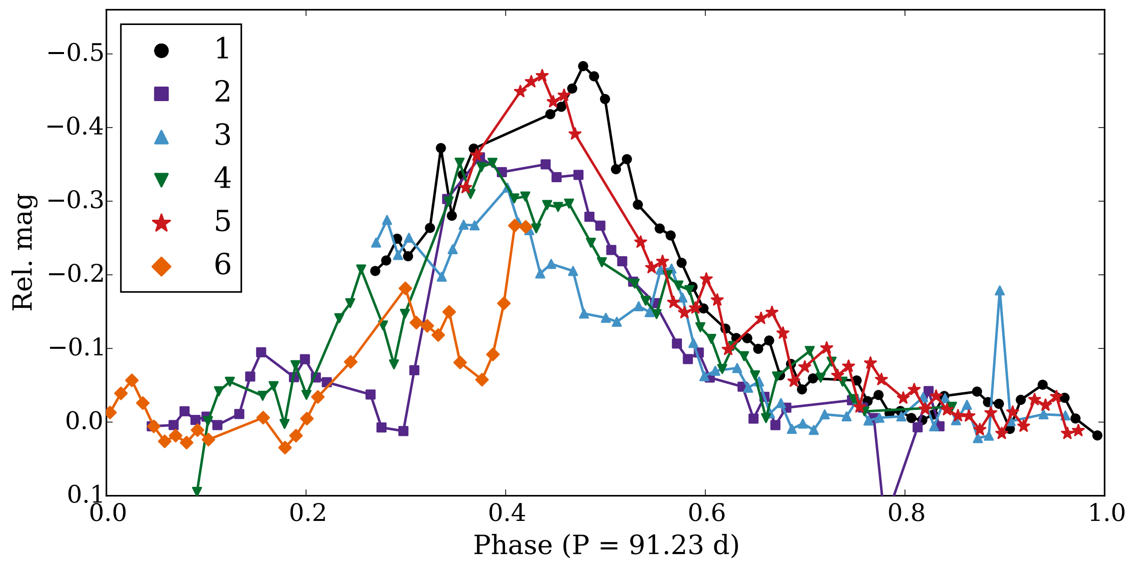

Figure 4.5: Light curve for ABE-A01 phased to a period of 91.23 days, showing that the outbursts occur with some regularity. Markers indicate the nightly median magnitude after outlier removal. The different colors and markers correspond to the six individual outbursts seen in the raw light curve in Figure 4.4.

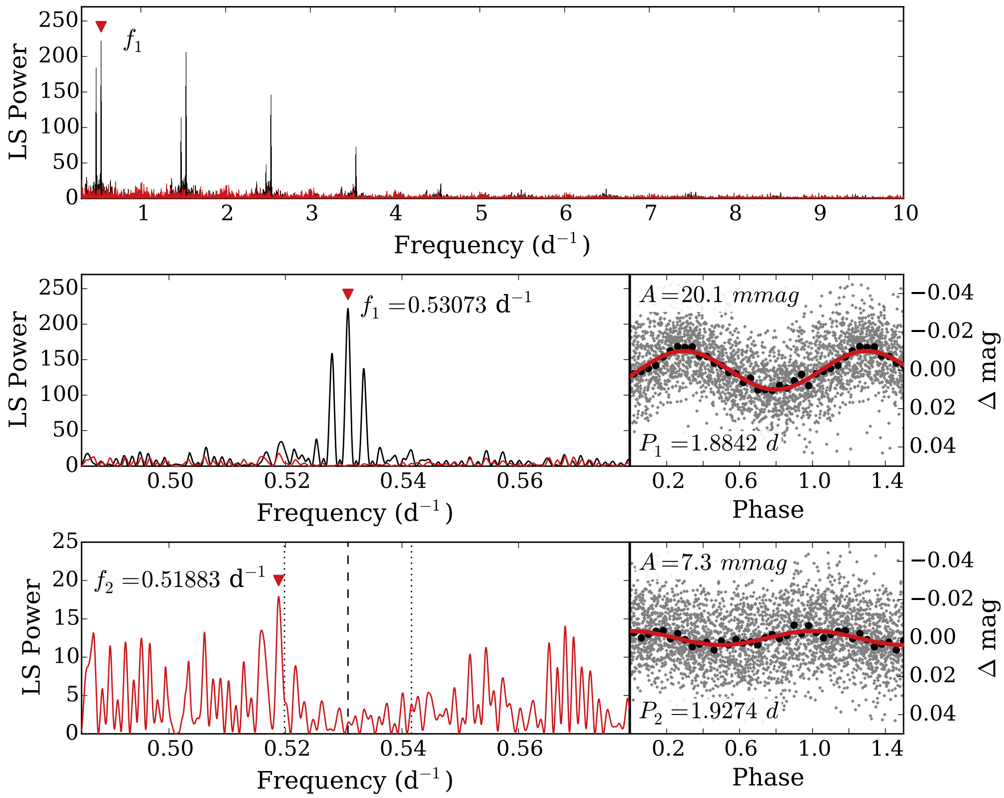

Figure 4.6: Frequency analysis for ABE-A01, after removal of low-frequency variability. In each LS periodogram (top, and left two panels), the black curve shows the periodogram, and the red curve shows the periodogram after pre-whitening against the top peak (f_1). *Top:* LS periodogram between 0.3 – 10 d^{-1}. *Middle:* Zoomed-in view of the top peak (left), and the light curve phased to this period (right). The gray '+' signs show the KELT data, larger black circles show the data median-binned (with 25 bins in phase), and the red curve is a sinusoidal fit to the median-binned data. *Bottom:* Zoomed-in view of the periodogram in the vicinity of f_1 after pre-whitening against f_1 (the position of which is shown as a vertical dashed line). The two dotted lines show the positions where we might expect to see another peak, if in fact the outbursts in this system are modulated by a delta frequency. The photometry is then phased to the strongest peak that exists in the vicinity of these two predicted frequencies. It is unclear if this peak is caused by genuine astrophysical variability, or is just a spurious peak caused by noise in the data and/or the sampling rates of KELT.

ABE-026 (= V438 Aur = HD 38708)

Among all the stars in this sample, ABE-026 has perhaps the most dramatic outburst. Viewed nearly edge-on, this is an excellent example of a shell star, where the growth of a disk causes the system to appear fainter, and also results in deep shell absorption in the hydrogen lines. Figure 4.7 shows the KELT light curve, 12 APOGEE spectra taken over 382 days, and 10 Hα spectra from BeSS, with a baseline of nearly 3000 days. The first four years of KELT data show little variability, and the first BeSS spectrum (at JD-2450000 = 4890) shows a broad absorption line with no evidence of emission or shell absorption. At the very end of the fourth season in the KELT light curve (approximately JD-2450000 = 5280), the system begins to rapidly dim, indicating the onset of an outburst. A spectrum from BeSS was serendipitously taken during this rising phase[1] at JD-2450000 = 5273, showing a deep absorption core and broad emission wings, with a large peak separation, indicative of a high-density inner disk and a small Hα-emitting region, both facts consistent with a forming disk. As the long falling phase of this outburst ensues, the brightness of the system relaxes towards baseline, and the Hα line continues to evolve. The emission wings evolve towards a smaller peak separation, suggesting that the size of the Hα-emitting region continues to grow outwards. Although an increasing optical depth can also cause Δv_p to shrink, we do not expect this to be a major contributing factor since the disk is dissipating (becoming more diffuse), and not building up. The final season of KELT data shows the system back at its baseline brightness. A weak disk in Hα is present at JD-2450000 = 7327, but has disappeared by JD-2450000 = 7411. The disk has completed its life cycle in these observational modes, persisting for between 2047 – 2131 days.

It is likely that in addition to the major disk build-up phase near JD-3450000 = 5280, some relatively minor outbursts take place before the disk has completely dissipated in photometry and in Hα. There is enhanced light curve activity near JD-2450000 = 5500 – 5700, and 6700, perhaps signifying further mass loss. The

[1] Although the system is dimming, we still refer to this as the rising phase of the outburst, since the disk is growing.

enhancement in the high-velocity wings of Hα at JD-2450000 = 7088 points to the addition of some new disk material between JD-2450000 = 6997 – 7088.

ABE-026 was visited 12 times by APOGEE over a 382 days span during the falling phase of the outburst. The Br11 line of each spectrum shows a deep, narrow, absorption core, with roughly symmetric emission wings. The difference between the final and the initial spectrum is shown in the lower-left panel of Figure 4.7. The absorption core becomes deeper, and the emission wings enhanced, as the falling phase of the outburst progresses. There is an obvious increase in the optical continuum flux during this spectroscopic sequence, and it is possible that the NIR continuum flux in the vicinity of the Br11 line is likewise changing. Therefore, variability in the Br11 line profile relative to the local continuum should be treated with caution.

Part of the reason this outburst has such a long falling time in its light curve is that we are not simply seeing some effect of the inner disk, which is generally the case for non-shell Be stars. Rather, we are mainly seeing the effect of stellar continuum photons being absorbed and scattered out of our line of sight by the intervening gas. So, even after the inner disk has dissipated, we still see a flux decrement because the outer disk continues to partially obscure the star.

After the disk life cycle shown in Figure 4.7, this system experiences another episode of disk growth and dissipation. Although we have no photometric data covering this second cycle at present, the KELT survey is ongoing, and further data reduction will likely reveal at least some of this event. Hα measurements from BeSS show the system evolving from a diskless state at JD-2450000 = 7411, to having a shell profile with emission wings at JD-2450000 = 7648. A third spectrum (ARCES; JD-2450000 = 7795) shows no disk signature in Hα. This sequence of three spectra spans 384 days, which is the maximum lifespan of the disk in this episode. This is much shorter than the $\sim$2100 day lifespan of the disk created by the first outburst.

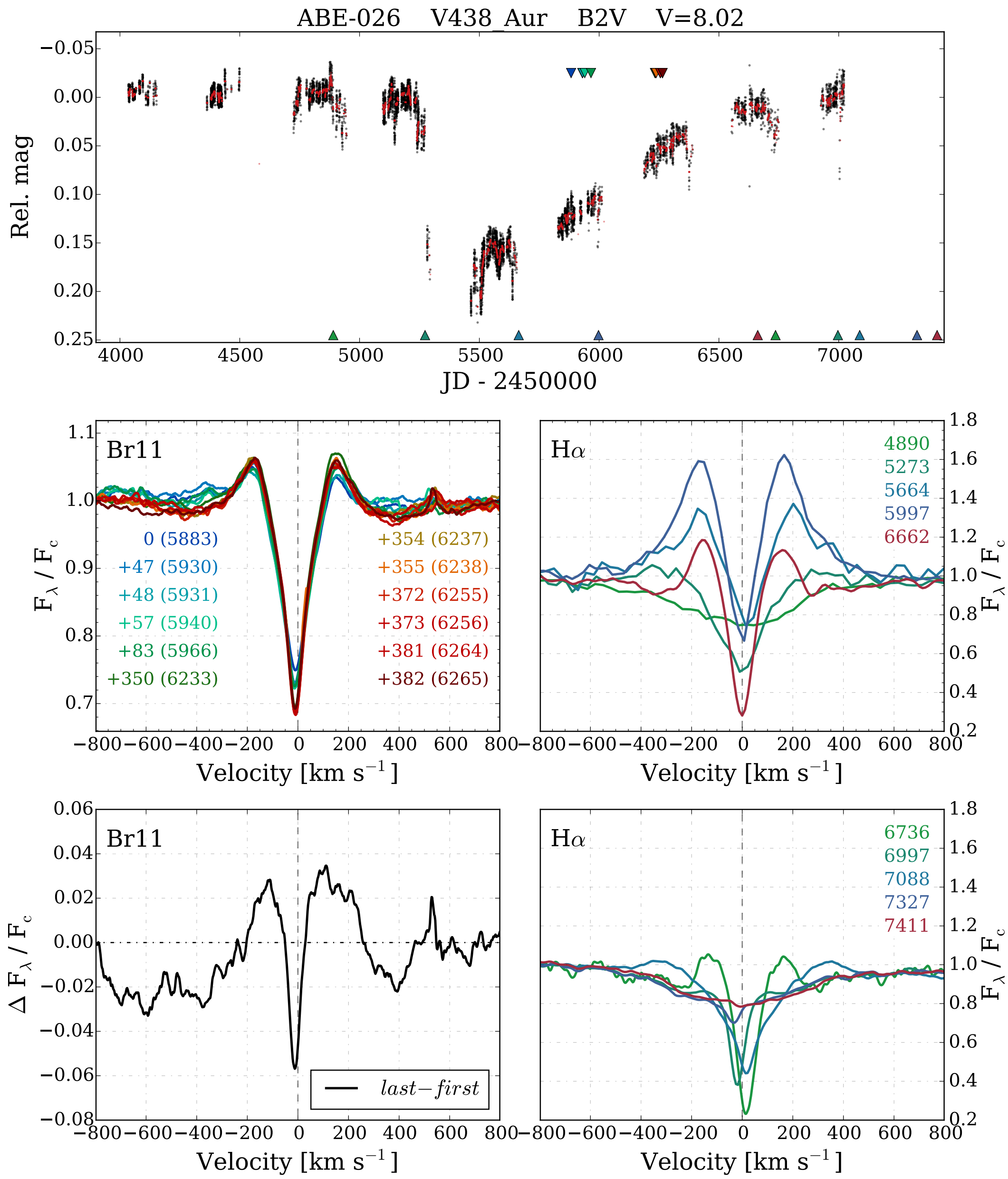

Figure 4.7: *Top:* KELT light curve for ABE-026, with downward (upward) pointing triangles indicating epochs of APOGEE (BeSS) spectra. *Middle-left:* Br11 line of 12 APOGEE spectra. *Middle- and bottom-right:* BeSS spectra, centered on Hα. *Bottom-left:* difference between the final and initial APOGEE spectra. Spectroscopic epochs are indicated in the same manner as in Figure 4.3.

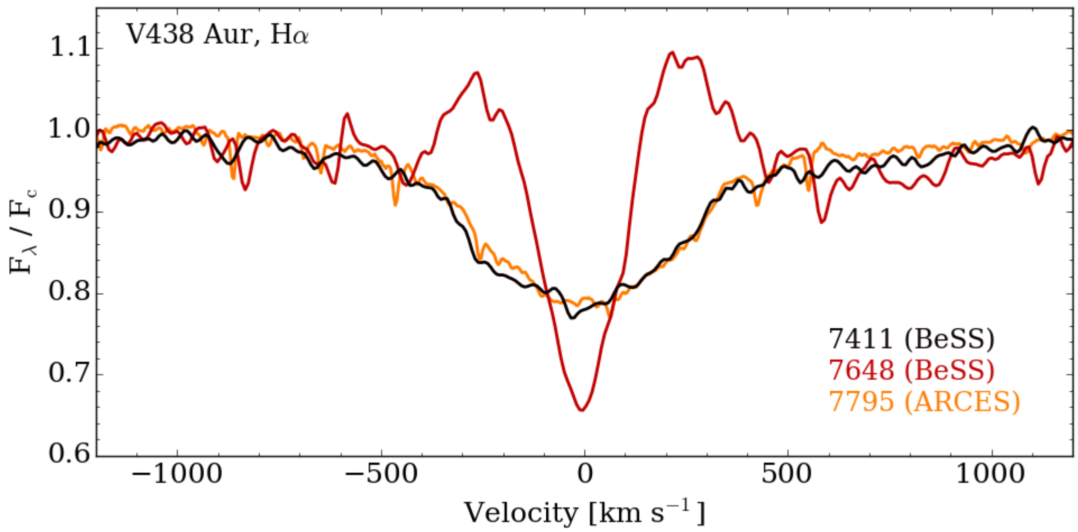

Figure 4.8: Spectra showing a new disk life cycle for ABE-026.

4.3 Further outburst diversity

The previous section demonstrated that photometric outbursts positively correspond to disk creation (or building, if a disk is present) events, that such events occur over a wide range of timescales, that disks are built and dissipate from the inside-outwards, and that material is, at least sometimes, asymmetrically distributed during the these events. This section further highlights the diversity in the outbursts of Be stars, as seen in their light curves.

BK-075 = HD 345122

Figure 4.9 shows the KELT light curve for BK-075 (HD 345122, upper panel). The first outburst, beginning near JD - 245000 = 5130) is enlarged in the middle panel of the same figure, and exhibits a characteristic quick rise and slow decay indicative of a typical, isolated outburst. The larger (both in amplitude and duration) outburst that follows (near JD - 2450000 = 5690) is actually comprised of at least two discrete events which build on each other before the system starts decaying back to baseline. The rise of this double-outburst is displayed in the lower panel of Figure 4.9, where it is clear that this is more complex than the prior outburst. We identify four outbursts in HD 345122, for an outburst rate of 1.7 outbursts/year.

BK-059 = HD 33152 = V413 Aur

An even more convoluted example is shown in Figure 4.10 for BK-059 (HD 33152). This system shows numerous outbursts that are irregularly spaced and of varying amplitude and duration, coincident with slower brightness variation on timescales of years. The net brightening of the system leading up to approximately JD - 2450000 = 6000 can be explained by a growing circumstellar disk that accumulates material following each outburst event, and is replenished (by outbursts) faster than it is dissipating. As the outbursts become less frequent and/or weaker (or rather, the time-averaged mass-loss rate decreases), the disk dissipates faster than it is being replenished, and the system begins to return to its baseline brightness. Many BeSS spectra for this object show a single-peaked Hα line in emission, indicating that this system is oriented nearly pole-on. The lower panel of Figure 4.10 shows a more detailed view of a single season of KELT data for this object, with individual outbursts marked with arrows. We identify 37 outbursts in HD 33152, for an outburst rate of 8.8 outbursts/year.

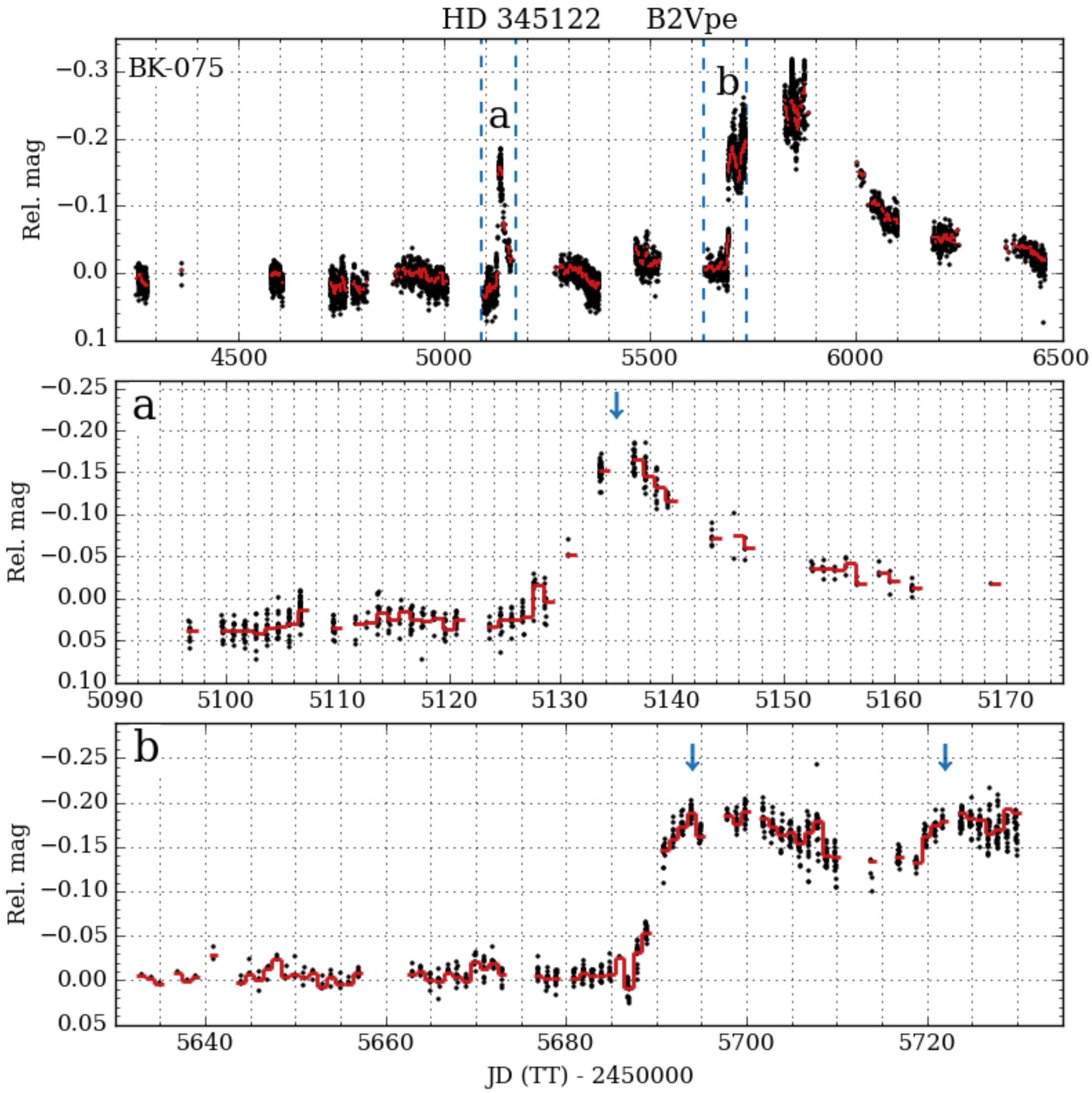

Figure 4.9: *Top:* Raw KELT light curve for BK-075 (HD 345122; B2Vpe). A relatively short outburst occurs near JD_{TT} = 2455100 (outburst 'a'), followed by a quick return back to baseline. Around 560 days later there is another outburst (outburst 'b') that is larger in amplitude and much longer in duration. *Middle:* A more detailed look at the region marked by the two vertical dashed lines bracketing outburst 'a' in the upper panel. This highlights the features of the first outburst, with an arrow indicating the time of maximum brightness. *Bottom:* A zoom-in on the rising phase of outburst 'b', showing more complexity than outburst 'a', with arrows marking the two distinct brightening events that are separated by about 28 days. The red line shows the data median-binned with a bin size of one day in both lower panels.

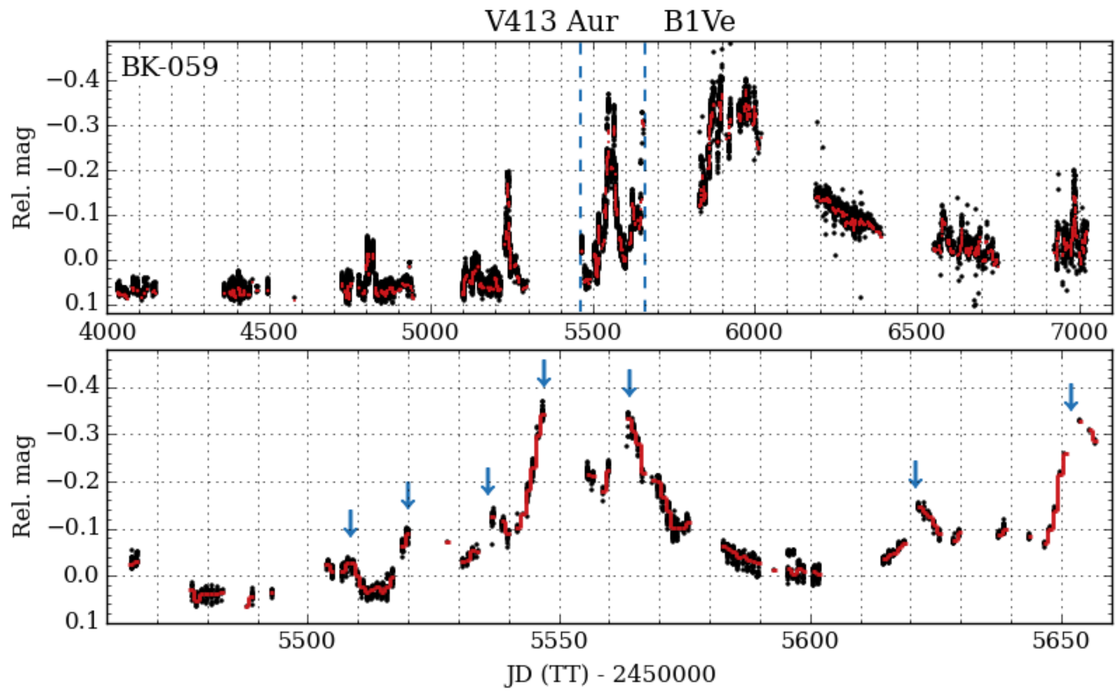

Figure 4.10: *Top:* Raw KELT light curve for BK-059 (HD 33152; B1Ve), a Be star with many irregularly spaced outbursts of varying amplitude and duration, together with longer term variability. *Bottom:* A more detailed look at the region marked by the two vertical dashed lines in the upper panel, with arrows indicating discrete outburst events. The red line in the lower panel shows the data median binned with a bin size of one day.

4.4 Semi-regular outbursts

While analyzing the light curves of these stars, we find some systems that have outbursts that occur at a somewhat regular rate. In essentially all of these cases, the outbursts are not strictly periodic. Instead, there are sometimes variations in the timing, amplitude, and shape of the outbursts. Cycles may be skipped, and additional outbursts sometimes occur, apparently at random. There are also cases where outbursts are roughly periodic within a certain segment of the light curve, but are not regular throughout the entire baseline of observation. We refer to such systems as "semi-regular outburst" (SRO) variables. This is a loosely defined category which primarily serves to identify systems that are particularly worthy of continued investigation. Objects categorized as SRO variables were identified when searching for periodic signals. For these systems, their somewhat regularly occurring outbursts impart a significant peak in the generated LSP. The individual outbursts are then roughly aligned when the photometric data is phased to the recovered period. Phased light curves for SRO variables are distinct from other types of periodic variability, as they do not closely resemble sinusoids, but rather adopt the shape of a ‘typical’ outburst.

Broadly speaking, there are two explanations invoked to explain SRO. The first is that there is some internal mechanism responsible for modulating the outburst behavior, such as the coupling of two or more NRP modes with different frequencies (Baade et al. 2016a,c). This internal mechanism may be stable, or it may turn on and off over time. SRO have been observed in the Be stars λ Eri and μ Cen (Mennickent et al. 1998; Rivinius et al. 1998). In both of these, no evidence for binarity could be found, and it is presumed that outbursts are triggered when the coupled difference frequency is of maximal amplitude. The second possibility for explaining SRO involves a Be star in an eccentric binary system. At periastron passage, the non-Be star component of the binary may exert enough of a gravitational influence to trigger an outburst in the Be star. The Be star δ Sco is known to be in a highly eccentric binary system with an orbital period of $\sim$10.6 years. Miroshnichenko et al. (2001) analyzed spectra during the system's periastron passage in 2000, and suggest a hypothesis in which the NRPs in the Be star component are amplified at periastron, triggering an increase in the mass loss rate. This system seems somewhat more complicated though, since spectroscopic data show that the disk began to form slightly before periastron (Miroshnichenko et al. 2013). However, the important conclusion that the mass loss rate is enhanced near periastron remains intact. The example of δ Sco supports the notion that although the binary orbit is strictly periodic, the outburst behavior can be more complicated. Be stars in eccentric binary systems can still have coupled difference frequencies from NRP modes, which may not be commensurate with the orbital period. The amplitude of the difference frequency at periastron will then be different from orbit to orbit, which may influence the strength and timing of an outburst, or dictate whether or not an outburst is triggered. On the other hand, the case of enhanced mass-loss near periastron for δ Sco may simply be a coincidence.

The star BK-184 (HD 81654) is an example of a system with SRO and a very high duty cycle, and is shown in Figure 4.11. Including the commissioning data (not shown in Figure 4.11), we identify 21 outbursts, and an outburst rate of 13.4 outbursts/year. It is clear from the raw light curve (upper panel) that the outbursts are not purely periodic, and also have varying amplitudes. However, when the light curve is phased to a period of 39.22 days (bottom panel), many of the outbursts are roughly aligned and binning the data traces what could be considered an 'average' outburst for this star. Lefèvre et al. (2009) use Hipparcos photometry to study variability among OB stars in a study that includes HD 81654. The authors list this star as having a variable type of 'GCAS?' (indicating the variability is irregular and the variability type cannot be easily classified), a period of 40.036 days, and an amplitude of 0.228 mag. The Hipparcos mission operated between 1990 and 1993, and the KELT data shown here was collected between 2012 - 2014. The fact that virtually the same period (to within 2%) is found in data taken $\sim$20 years apart indicates that the regularity of these outbursts is stable over decades. If this star is not part of a binary system and is in fact modulated by internal mechanisms (similar to λ Eri and μ Cen), then this points towards the "internal clock" being remarkably stable despite the obvious variability seen in the KELT light curve. Because the KELT light curve shows persistent activity with virtually no quiescent periods (i.e. the outbursts are the dominant features in the light curve), high-frequency low-amplitude signals attributed to pulsation were not recovered. Future work aims to rectify this situation, as it would be interesting to see if there are pulsational modes with a difference in frequency consistent with the observed frequency of outbursts. If, on the other hand, HD 81654 is a binary system, then it could prove to be an interesting case to study the role of binary interactions in triggering outbursts. Either way, this star is a good candidate for a more detailed investigation regarding the mechanism(s) responsible for the regularity of its outbursts. The single available BeSS spectrum for this object clearly shows Hα in emission.

There are five systems in the AK sample that show repeating outbursts. These are shown in Figure 4.12, where the left column displays the full KELT light curve, and the right column plots the data phased to the period that best describes the timing of the outbursts. Although these events repeat, they are not strictly periodic. Instead, there are sometimes variations in the timing, amplitude, and shape of the outbursts. Cycles may be skipped, and additional outbursts sometimes occur, apparently at random. Among the 145 Be stars in the BK sample with three or more outbursts, we find that 35 (24%) of these have outbursts occurring with enough regularity to be considered SRO variables. Objects categorized as SRO variables were identified when searching for periodic signals. For these systems, their somewhat regularly occurring outbursts impart a significant peak in the generated LSP. The individual outbursts are then roughly aligned when the photometric data is phased to the recovered period. Phased light curves for SRO variables are distinct from other types of periodic variability, as they do not closely resemble sinusoids, but rather adopt the shape of a 'typical' outburst. Both ABE-A01 and -A03 (from the AK sample) were identified as having repeating outbursts in the BK sample. The previously discussed systems BK-184 (= HD 81654), and ABE-A01 (= MWC 5 = BD+61 39; see Section 4.2) are among the more well-defined examples of SRO variables. All such systems from the BK sample are shown in Figure 4.12. Future work is planned to analyze the stellar properties and photometric behavior of all systems having repeating outbursts for which we have sufficient data, with a focus on links between pulsation and outbursts. However, a detailed analysis of these systems is beyond the scope of this work.

BK-184 (= HD 81654), and the previously discussed ABE-A01 (= MWC 5 = BD+61 39; see Section 4.2) are among the more well-defined examples of SRO systems. All such systems from the BK sample are shown in Figure 4.12.

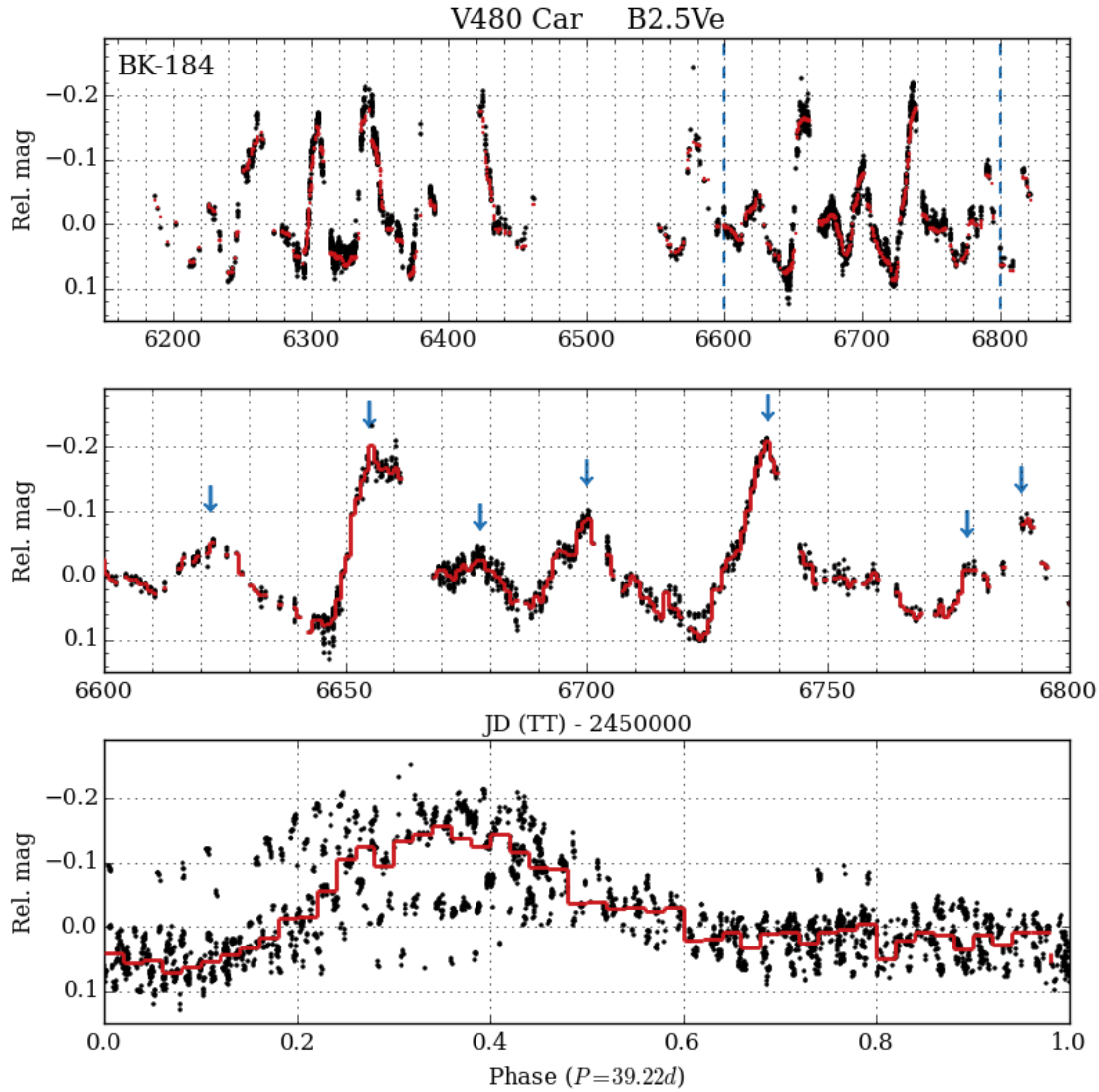

Figure 4.11: *Top:* Raw KELT light curve for BK-184 (HD 81654; B2.5Ve), a Be star with outbursts occurring semi-regularly every ∼40 days. *Middle:* A more detailed look at the region marked by the two vertical dashed lines in the upper panel. *Bottom:* The light curve is phased to a period of 39.22 days, highlighting the semi-regular nature of the outbursts. The outbursts do not align perfectly, but there is some degree of coherence in their occurrence. The red line in the middle panel shows the data median binned with a bin size of one day, while the lower panel uses a bin size of 0.02 in phase.

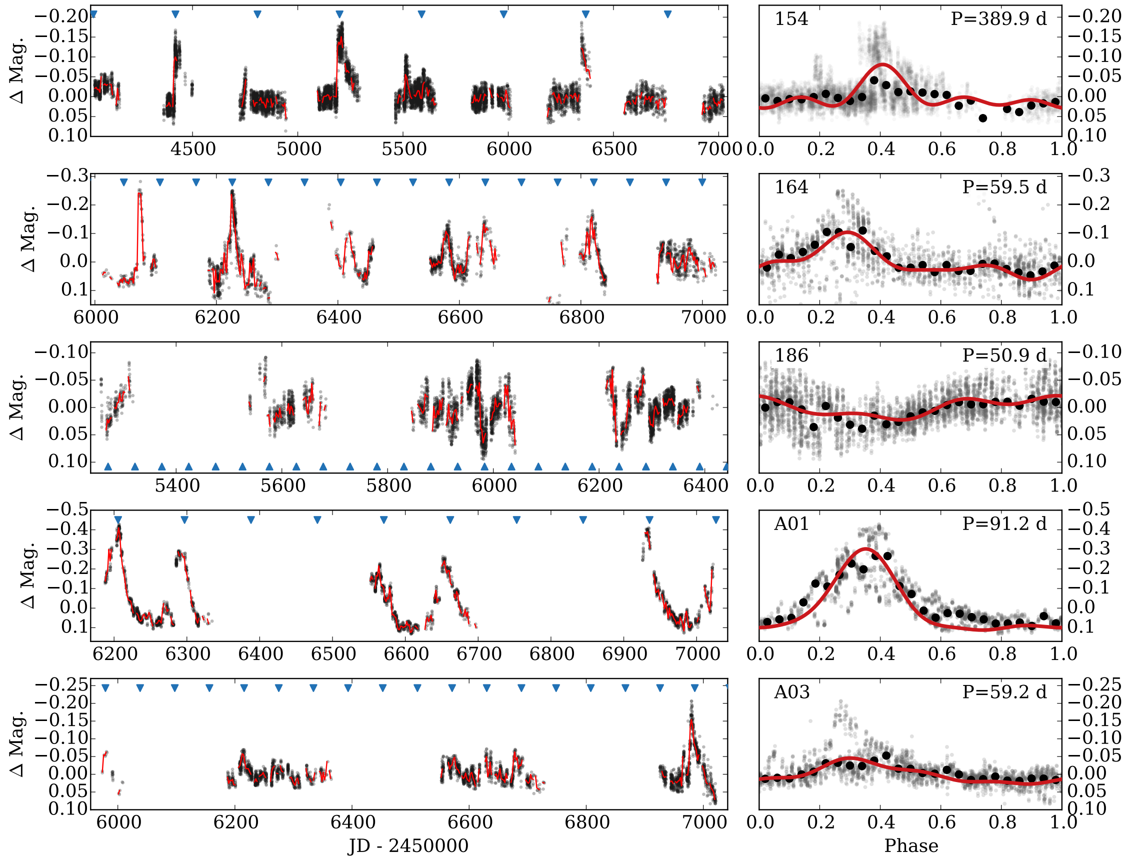

Figure 4.12: Plots for the five systems that show regularly repeating outbursts in the AK sample. *Left:* Raw light curve (black) with binned data in red. *Right:* Light curve phased to the period that best describes the pattern of outbursts in the raw data. The larger black circles show the data median-binned with 25 bins in phase, and the red curve is a 3-term Fourier fit, to guide the eye. The downward-pointing triangles in the plots of the raw light curves correspond to the ephemerides of the outbursts (*i.e.* if these outbursts were strictly periodic, each triangle would mark the peak of an event). ABE-186 (middle row) is a shell star (Chojnowski et al. 2015), where outbursts cause a dimming. For this reason, the triangles point upwards.

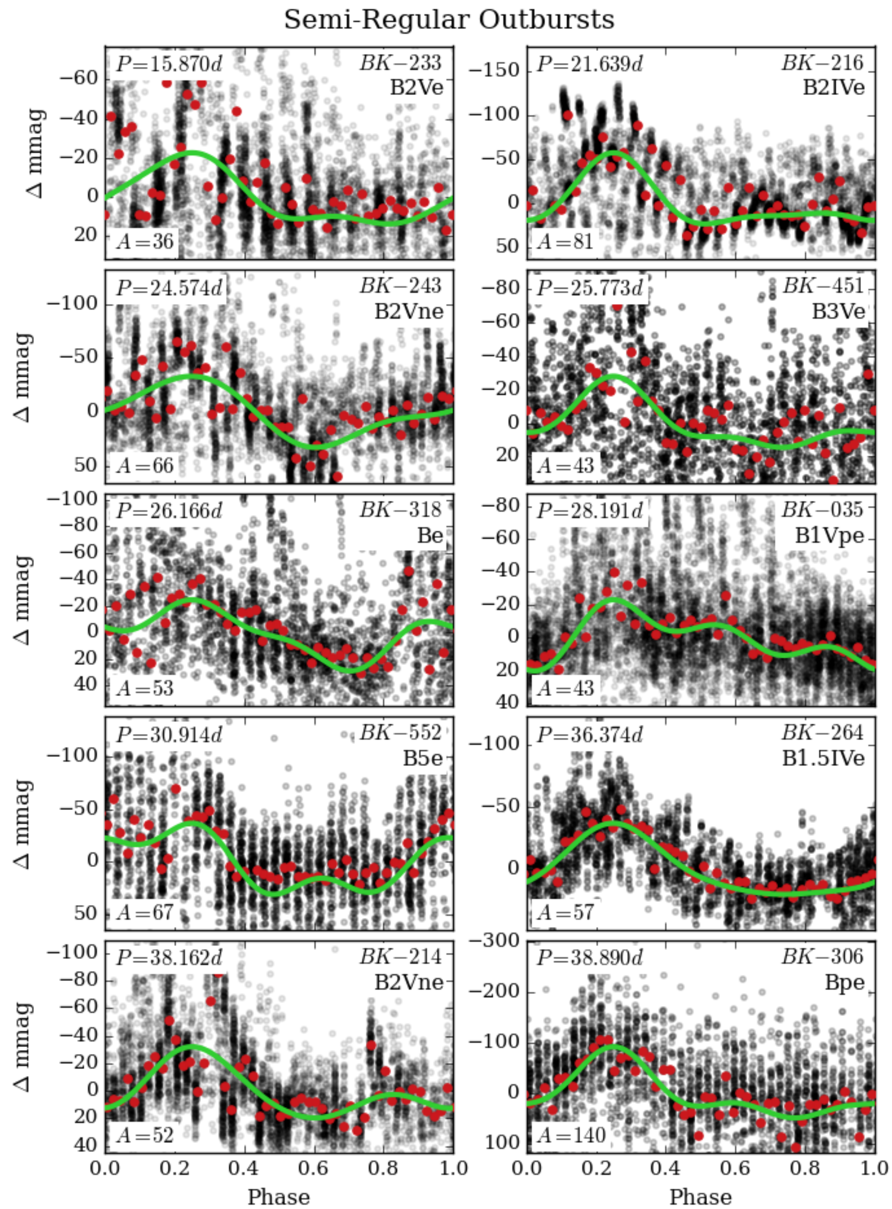

Figure 4.12: Phased KELT light curves for all objects from the BK sample exhibiting SRO, displayed in order of increasing period. Red points show the data median-binned with a bin size of 0.02 in phase. The solid green line shows a fit to the data using a combination of three sinusoids, to guide the eye. In each sub-plot, The object identifier and spectral type are printed in the title, the period in the upper left corner, the BeSS-KELT number in the upper right corner, and the $max - min$ amplitude of the fit, in mmag, is shown in the bottom left corner.

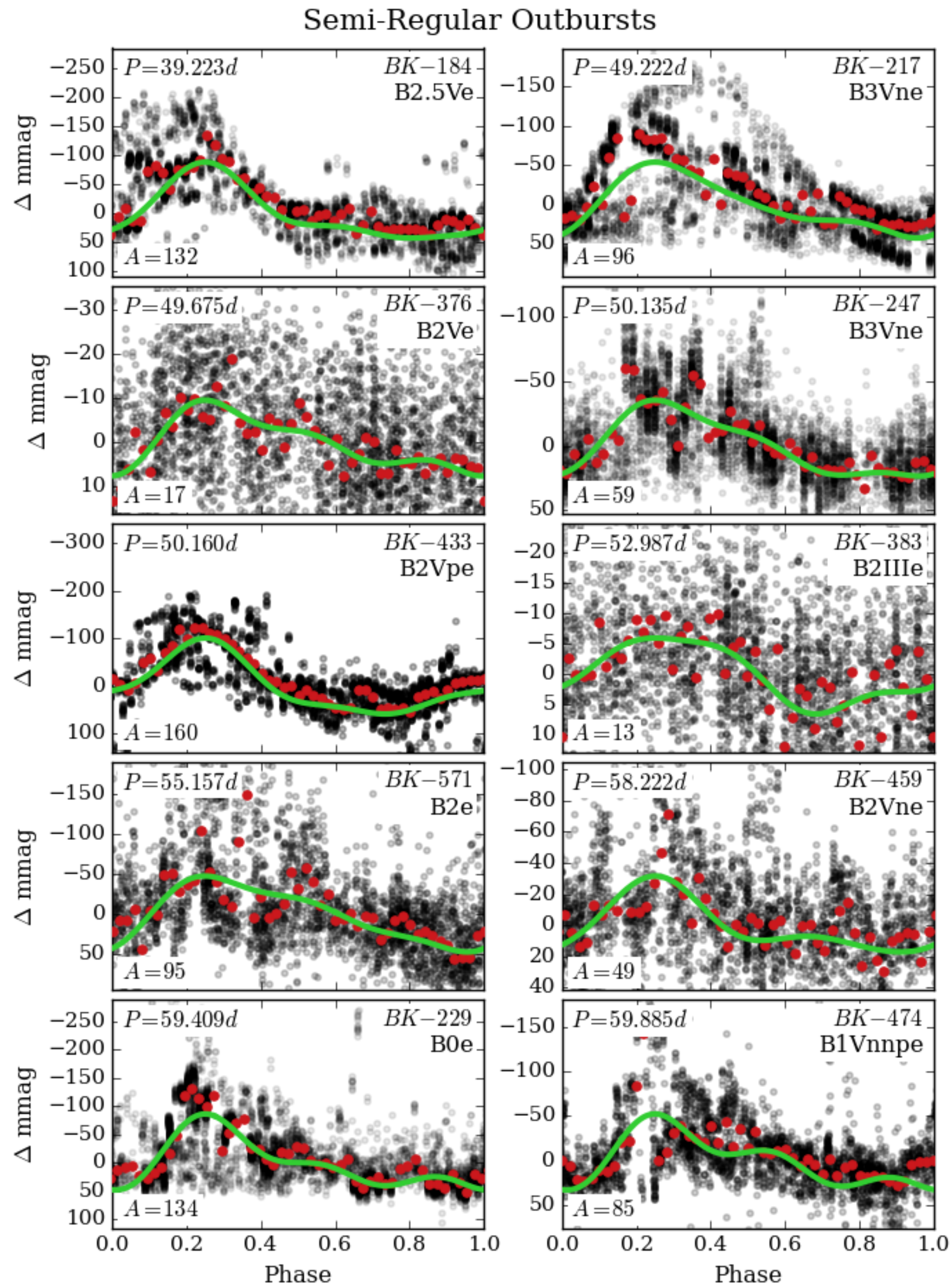

Semi-Regular Outbursts
P=39.223d
BK−184
B2.5Ve
A=132
P=49.222d
BK−217
B3Vne
A=96
P=49.675d
BK−376
B2Ve
A=17
P=50.135d
BK−247
B3Vne
A=59
P=50.160d
BK−433
B2Vpe
A=160
P=52.987d
BK−383
B2IIIe
A=13
P=55.157d
BK−571
B2e
A=95
P=58.222d
BK−459
B2Vne
A=49
P=59.409d
BK−229
B0e
A=134
P=59.885d
BK−474
B1Vnnpe
A=85
Δ mmag
Phase

Figure 4.12: B

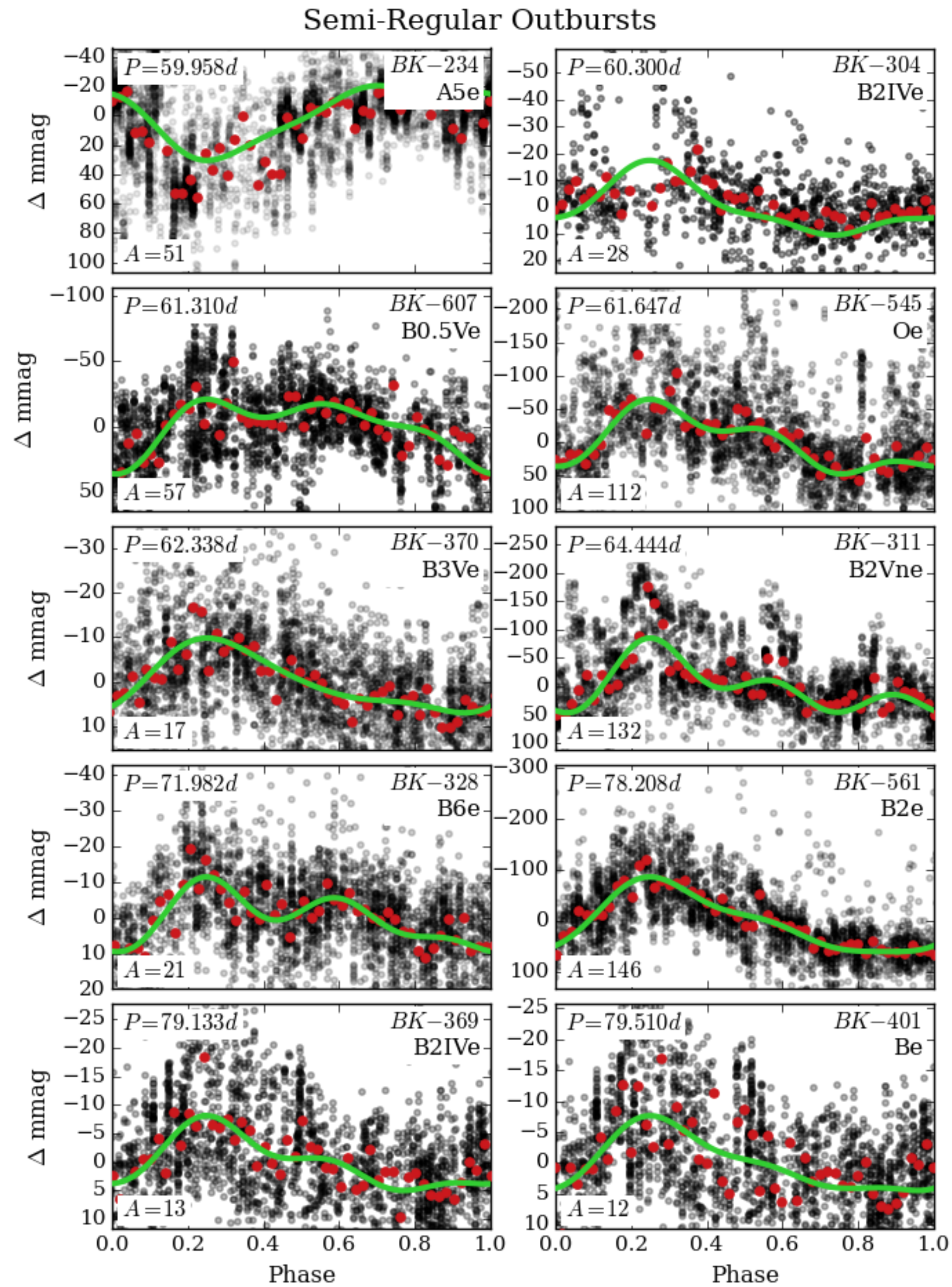

Semi-Regular Outbursts
P=59.958d
BK−234
A5e
A=51
P=60.300d
BK−304
B2IVe
A=28
P=61.310d
BK−607
B0.5Ve
A=57
P=61.647d
BK−545
Oe
A=112
P=62.338d
BK−370
B3Ve
A=17
P=64.444d
BK−311
B2Vne
A=132
P=71.982d
BK−328
B6e
A=21
P=78.208d
BK−561
B2e
A=146
P=79.133d
BK−369
B2IVe
A=13
P=79.510d
BK−401
Be
A=12
Δ mmag
Phase

Figure 4.12: C

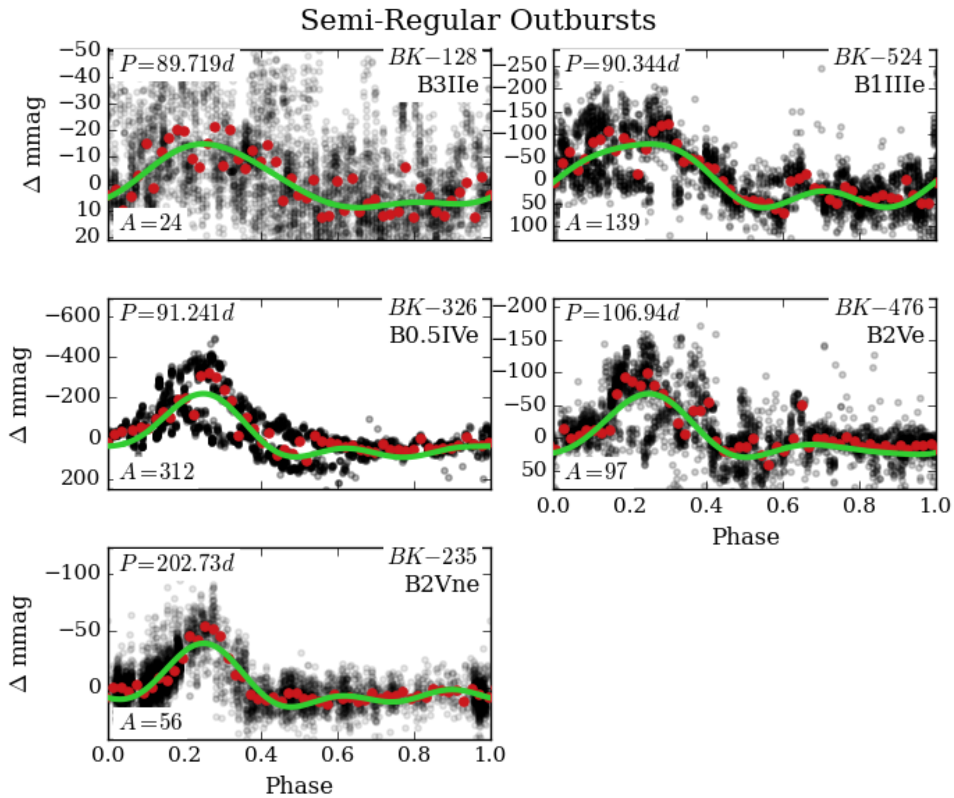
Semi-Regular Outbursts
P=89.719d
BK−128
B3IIe
A=24
P=90.344d
BK−524
B1IIIe
A=139
P=91.241d
BK−326
B0.5IVe
A=312
P=106.94d
BK−476
B2Ve
A=97
P=202.73d
BK−235
B2Vne
A=56
Δ mmag
Phase

Figure 4.12: D

4.5 Outburst Statistics

In order to count the number of outbursts seen in the KELT light curve for a given star, each season of observation was visually inspected for outburst signatures, and the number of outbursts tallied. Many situations arise that make counting the number of outbursts convoluted. For example, a star may brighten suddenly and begin to decay back to baseline, but then suddenly brighten again shortly after the first brightening. This example would count as two outbursts, even though the first outburst never fully decayed back to the pre-outburst brightness. The outburst rates for each star were calculated by adding up the length (in days) of each observing season, converting this number to years, and then dividing the number of outbursts by the total number of years observed. This method was chosen because the duration of a single outburst tends to be shorter than a single observing season. If instead the number of outbursts was divided by the full baseline of observation (including the $\sim$150 day gaps between seasons), then the outburst rates would be systematically underestimated for a majority of the stars. The few exceptions to this (i.e. cases where the chosen method overestimates outburst rates) are stars exhibiting very long outbursts lasting for multiple seasons. The outburst rates claimed for each star are an approximate lower limit, because the outbursts were judged by eye and are not mathematically defined, and outbursts with amplitudes below the detection threshold in a KELT light curve may be present. Future work will attempt to quantify outburst rates in a more rigorous way. Outbursts were tallied in this way for both the BK and AK samples.

The outburst rates (number of outbursts per year) were calculated for all stars where they could be reliably determined. In cases where the number of outbursts was ambiguous or otherwise uncertain, the star was not included in the final statistics. In total, there are 139 stars in the BK sample where the number of outbursts could be determined. The outburst rates for these are shown in Figure 4.13. It is apparent that there are a wide range of outburst rates in this sample, but it must be noted that neither the amplitude nor the duration of an outbursts is considered in this distribution. We find that 36% of the BK sample exhibits one or more outburst in its KELT light curve, with a higher occurrence rate (51%) seen in early-type stars compared to mid- (20%) and late- (5%) types. These fractions were calculated from the subset of the sample where it was unambiguous whether or not outbursts were present. There is a wide range in the number of detectable outbursts in the light curves of the stars in our sample, with some Be stars showing zero or one outburst, while others undergo several dozen outbursts throughout the observing baseline.

The same type of analysis was done for the AK sample. We detect one or more outburst in 28% of this sample (44/160). Outbursts are more commonly detected in early-type Be stars (57%; 31/54), compared to mid- (27%; 6/22) and late-types (8%; 5/61). The incidence rates according to spectral type are similar between the AK and BK samples, and are significantly higher in early-type stars. These results reflect the trend of earlier Be stars being more variable in general, while later-type systems tend to have more stable disks that last for longer times (*e.g.* Hubert and Floquet 1998; Rivinius et al. 2013). This may be because early-type Be stars are intrinsically more prone to mass loss episodes, or it could be that the observational signature of outbursts in Be stars of later spectral types is often too small to be detected with KELT. Evidence for the latter of these points is emerging, in that cooler Be stars create disks with surface densities that are too low to leave an obvious observational signature in visible continuum flux (Vieira et al. 2017). The observables used in this work are generally formed within the inner $\sim$20 R_* of the disk. The lack of any disk signature in optical photometry, or in the Br11 or Hα lines does not mean that no disk exists, as there may be material further out than the region in which a given observable is sensitive to. The outburst rates for the AK sample are shown in Figure 4.14.

There is a wide spread in the outburst rates across both samples, with many systems showing zero or a small number of outbursts, while others experience tens of outbursts throughout their observational baseline. The median and mean of this distribution for the AK sample is 1.9 and 3.3 outbursts year^{-1}, respectively. The median and mean of the distribution for the BK sample is 4.2 and 5.9 outbursts year^{-1}, respectively. When comparing these two samples, it is important to notice that the BK sample contains a higher fraction of early-type stars, which tend to be apparently more active than their cooler counterparts. For any given system, an outburst with a larger amplitude generally corresponds to a larger mass ejection episode. With this in mind, it is not necessarily the case that stars with high outburst rates have proportionally higher mass loss rates, since a single large outburst can eject more material than many small outbursts.

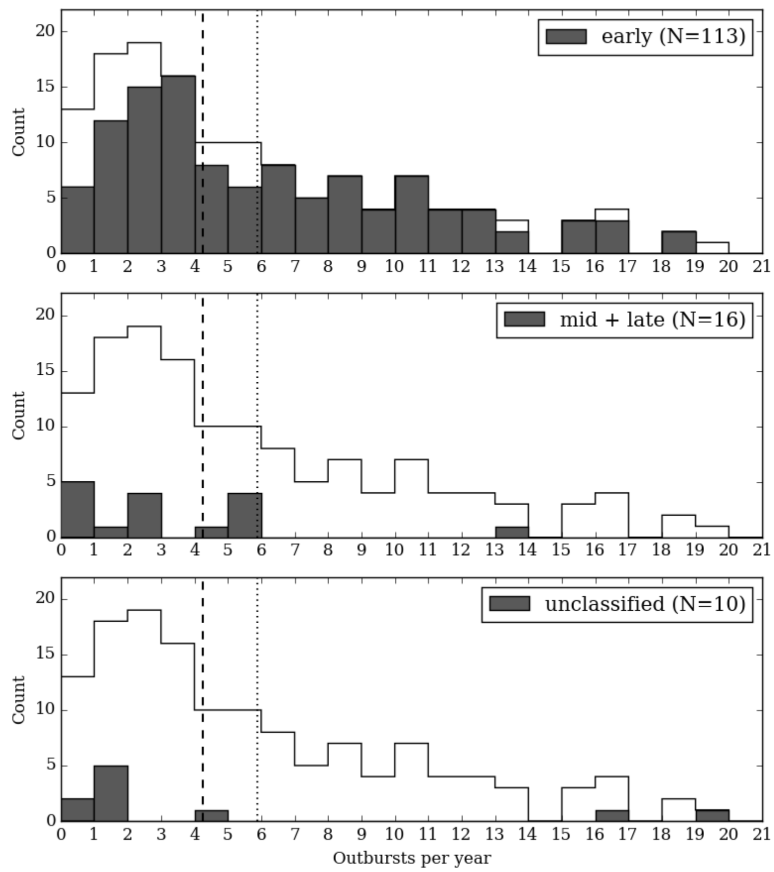

Figure 4.13: Distribution of outburst rates for early (*top*), mid + late (*middle*), and unclassified (*bottom*) spectral types, for the BK sample. These were calculated for all systems that show one or more outburst, so long as the number of outbursts is well defined. The solid line making up the envelope of the distribution in all three panels includes all stars, regardless of spectral type. The vertical dashed line denotes the median (4.2), and the vertical dotted line denotes the mean (5.9) of this distribution as a whole.

The distribution of outburst amplitudes, as measured in the KELT passband

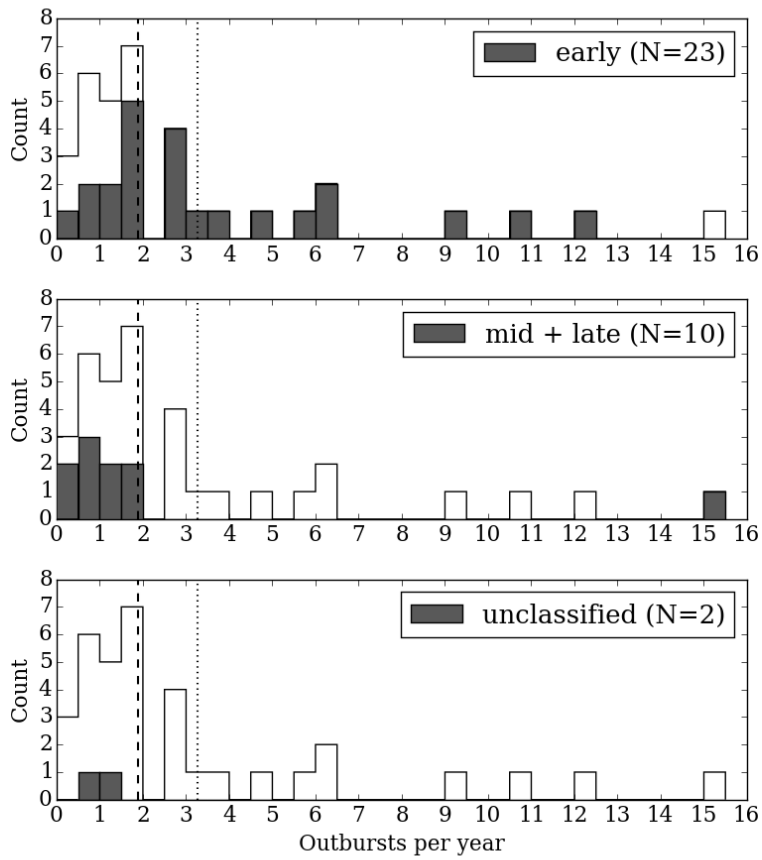

Figure 4.14: Same as Figure 4.13, but for the AK sample. The vertical dashed line denotes the median (1.9), and the vertical dotted line denotes the mean (3.3) of this distribution as a whole.

(approximately a broad R-band filter), is shown in Figure 4.15. This result should be viewed with caution, since the measured amplitude can be diluted by background sources for systems in crowded fields (although this is not a significant problem for the majority of these stars), and also depends on the Be star inclination angle. Half a magnitude is an approximate upper limit on the amplitude of Galactic Be star variability in the KELT passband.

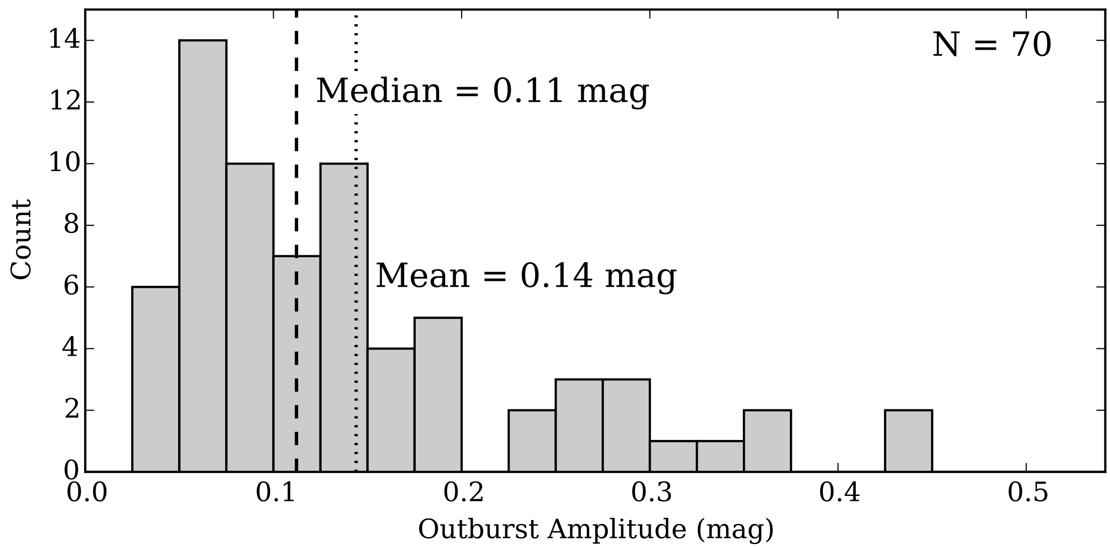

Figure 4.15: Histogram showing the amplitudes for 70 outbursts, for 24 unique stars in the AK sample (18 early, 4 mid, and 2 late). The outburst amplitude in the KELT passband depends strongly on the inclination angle of the system, which is not taken into account here.

4.5.1 Correlations between falling and rising times

Whenever possible, the photometric amplitude and duration of the rising and falling phases are measured for an outburst captured in KELT photometry. These three quantities can be measured only for outbursts that are reasonably well defined, and are thoroughly sampled in the light curve data, such as the example in Figure 4.1. There are 24 objects with such events (18 early-, 4 mid-, and 2 late-type), from which we measure 70 outbursts in total. Figure 4.16 shows the correlation between rising time and falling time for 70 well-behaved outbursts lasting 300 days or less. Although longer outbursts are seen in a few cases, they are relatively rare and have large uncertainties. Considering events shorter than 300 days allows us to focus on outbursts of roughly comparable magnitude. The dashed line has a slope of 1. The majority of points fall above this line, having longer falling, compared to rising, times, and those that do not are close (within measurement uncertainties). The median rising time is 8.3 days, and the median falling time is 16.0 days. The median of the ratios of falling time to rising time for this collection is ∼2. A best-fit line to each group has a slope of 1.97, 1.88, and 6.54 for early-, mid-, and late-type stars. This fit takes into account measurement uncertainties by assigning each point a weight proportional to one over the square of the error (in both the x- and y-directions). Although the sample size is too small to draw any definite conclusions, and there is significant scatter, these results suggest that, for a single event, relative to the rising time, the inner disk dissipates quickly for hotter stars (early- and mid-type), and more slowly for cooler late-type systems.

The observed trend of the rising time being shorter than dissipation time is a prediction of the VDD model. During disk build-up, the photometric variability is governed mainly by the timescales of matter redistribution over the inner disk, while during dissipation (*i.e.* when mass injection into the disk has significantly slowed or stopped), the inner disk is instead fed by matter re-accreting back from the entire disk, with naturally longer timescales. When an outburst occurs, the falling phase will proceed more slowly if there is a pre-existing disk. This 'mass reservoir effect' means that the dissipation timescales depend not only on the outburst being considered, but also on the previous history of mass injection into the disk (Ghoreyshi and Carciofi 2017). This effect is stronger when the disk is more massive. Lacking sufficient knowledge of the mass-injection history of the disks in this sample, we make no attempt to correct for this effect, and report the values measured from the photometric data with no regard to whether or not a disk already exists prior to the outburst.

Nevertheless, there are a few systems with spectroscopic data showing the lack of a pre-existing disk immediately before the time of outburst, meaning that there is essentially no mass reservoir effect acting in these cases. ABE-098 (B5V), as discussed in Section 4.2, has no Br11-emitting disk immediately before the outburst that occurs near JD-2450000 = 6230, which has a ratio of falling to rising time of about 2.7. ABE-154 and -162 both have a spectral type of B8, and each experience an outburst that is preceded by an APOGEE spectrum that shows no substantial Br11-emitting disk. So, for these events, we expect no interference from the mass reservoir effect. The outburst in ABE-162 has a ratio of falling to rising time of about 2.7. While the outburst that is bracketed by APOGEE spectra in ABE-154 is not fully sampled, the falling phase is many times (perhaps up to 10 times) longer than the rising phase. We have no knowledge of the status of the disk in the vicinity of the other outbursts in ABE-154, but they have similarly long falling, relative to rising, phases, and a similar baseline brightness. These two stars (ABE-154 and -162) are responsible for all 6 of the late-type outbursts depicted in Figure 4.16. Even though this sample size is small, and the scatter large, the relatively high slope of the fit to falling over rising time for late-type outbursts is likely not heavily influenced by the mass reservoir effect.

The aforementioned late-type systems stand in start contrast to the early-type systems that dominate Figure 4.16. The majority of early-type stars with measured outbursts have substantial disks at all observed epochs, particularly ABE-164 (B0Ve, 3 measured outbursts), -184 (B1Ve, 15 measured outbursts), -A01 (B0.5IVe, 5 measured outbursts), -A03 (B1Ve, 5 measured outbursts), and -A26 (B1 II/IIIe, 18 measured outbursts). Plots for these can be found in the Appendix (except for ABE-A01, discussed in Section 4.2). Together, these five systems contribute 46/56 of the measured outbursts for early-type systems. These systems exhibit some of the strongest spectroscopic disk signatures among the sample. Although the strength of these features varies over time, they never approach a disk-less state. All of the observed outbursts for these systems then occur while there is presumably already a substantial disk. Therefore, we expect the mass reservoir effect to 'interfere,' lengthening the time over which the photometric dissipation phase takes place. Without a pre-existing disk, it is reasonable to assume that a single typical outburst in an early-type star would have a smaller ratio of falling to rising time compared to the best-fit slope of 1.97 measured in this sample, seen in Figure 4.16.

ABE ID	Rise Time (d)	Fall Time (d)	Amp. (mag)	Rising Phase Begins (JD-2450000)	Time of Peak Brightness (JD-2450000)	Falling Phase Ends (JD-2450000)	Baseline Brightness (mag)	Peak Brightness (mag)
006	10	19	0.057	6157.9 ± 1	6167.6 ± 4	6186.9 ± 3	9.274 ± 0.005	9.217 ± 0.011
006	16	96	0.181	6510.4 ± 3	6526.4 ± 9	6622.0 ± 42	9.314 ± 0.006	9.133 ± 0.011
010	11	21	0.034	6958.4 ± 3	6969.3 ± 1	6990.0 ± 5	10.002 ± 0.002	9.968 ± 0.003
019	11	21	0.138	6936.6 ± 2	6947.2 ± 2	6968.5 ± 7	8.088 ± 0.011	7.950 ± 0.010
020	12	46	0.059	5682.3 ± 6	5694.3 ± 2	5739.9 ± 10	12.008 ± 0.008	11.950 ± 0.008
025	17	20	0.055	5114.1 ± 5	5130.9 ± 2	5150.6 ± 9	9.661 ± 0.005	9.607 ± 0.005
025	13	15	0.058	5228.8 ± 4	5241.8 ± 2	5256.6 ± 5	9.656 ± 0.005	9.598 ± 0.008
025	19	30	0.083	5523.8 ± 6	5543.3 ± 3	5573.7 ± 11	9.630 ± 0.005	9.546 ± 0.008
025	8	26	0.049	5833.6 ± 3	5841.4 ± 3	5867.4 ± 5	9.628 ± 0.003	9.579 ± 0.006
027	169	415	0.096	5483.9 ± 23	5653.3 ± 44	6068.0 ± 148	10.149 ± 0.008	10.053 ± 0.011
033	7	13	0.068	6188.9 ± 3	6196.2 ± 2	6209.7 ± 3	9.744 ± 0.006	9.677 ± 0.007
033	6	14	0.062	6211.3 ± 2	6217.1 ± 2	6231.2 ± 2	9.742 ± 0.004	9.680 ± 0.008
082	161	1281	0.317	5863.5 ± 199	6024.1 ± 172	7304.9 ± 192	11.075 ± 0.019	10.758 ± 0.051
098	6	14	0.137	6228.6 ± 1	6234.5 ± 1	6248.1 ± 3	7.588 ± 0.006	7.451 ± 0.017
098	6	8	0.048	6592.5 ± 1	6598.8 ± 2	6607.1 ± 2	7.569 ± 0.003	7.521 ± 0.003
105	15	31	0.235	6963.6 ± 3	6978.5 ± 2	7009.8 ± 5	9.407 ± 0.010	9.172 ± 0.007

138	5	6	0.101	6535.3 ± 2	6540.5 ± 1	6546.5 ± 2	8.588 ± 0.008	8.488 ± 0.008
138	5	16	0.096	6550.9 ± 4	6555.5 ± 3	6571.4 ± 4	8.592 ± 0.008	8.495 ± 0.012
154	9	150	0.143	4408.1 ± 4	4417.1 ± 5	4567.3 ± 43	10.896 ± 0.006	10.753 ± 0.010
154	18	42	0.068	4735.1 ± 4	4753.5 ± 9	4795.6 ± 17	10.898 ± 0.006	10.830 ± 0.011
154	22	130	0.148	5183.9 ± 5	5205.9 ± 10	5336.3 ± 45	10.873 ± 0.009	10.726 ± 0.017
154	6	34	0.083	5507.3 ± 2	5513.0 ± 2	5547.0 ± 6	10.885 ± 0.004	10.802 ± 0.010
154	14	110	0.140	6332.4 ± 5	6346.3 ± 7	6456.2 ± 58	10.883 ± 0.005	10.744 ± 0.013
160	91	419	0.204	6316.3 ± 48	6407.2 ± 44	6826.3 ± 123	8.249 ± 0.021	8.046 ± 0.026
162	34	74	0.162	6287.3 ± 13	6321.7 ± 6	6396.1 ± 26	10.162 ± 0.014	10.000 ± 0.010
164	8	15	0.289	6064.9 ± 2	6073.2 ± 2	6087.7 ± 5	7.480 ± 0.014	7.191 ± 0.017
164	22	40	0.341	6205.2 ± 3	6226.7 ± 2	6266.3 ± 15	7.463 ± 0.021	7.122 ± 0.020
164	13	13	0.125	6567.4 ± 2	6580.5 ± 2	6593.4 ± 2	7.431 ± 0.010	7.306 ± 0.010
165	64	310	0.098	6485.8 ± 46	6549.5 ± 37	6859.3 ± 48	8.532 ± 0.013	8.434 ± 0.021
176	124	265	0.046	5708.8 ± 69	5832.9 ± 37	6098.3 ± 88	9.566 ± 0.011	9.520 ± 0.016
184	13	32	0.116	4063.0 ± 3	4076.1 ± 6	4108.3 ± 10	10.119 ± 0.005	10.003 ± 0.023
184	6	6	0.066	4732.4 ± 3	4738.0 ± 2	4743.9 ± 3	10.098 ± 0.011	10.032 ± 0.010
184	5	7	0.065	4806.1 ± 1	4811.2 ± 2	4818.1 ± 4	10.116 ± 0.003	10.050 ± 0.010
184	12	32	0.152	4886.4 ± 4	4898.5 ± 6	4930.9 ± 6	10.135 ± 0.007	9.982 ± 0.033
184	7	10	0.092	5097.0 ± 2	5103.8 ± 1	5113.6 ± 3	10.083 ± 0.006	9.991 ± 0.012
184	3	7	0.050	5130.5 ± 1	5133.5 ± 1	5140.0 ± 2	10.096 ± 0.003	10.046 ± 0.011

184	8	29	0.256	5185.4 ± 2	5193.3 ± 2	5222.2 ± 7	10.084 ± 0.005	9.828 ± 0.018
184	3	8	0.056	5236.3 ± 1	5239.3 ± 2	5247.6 ± 3	10.073 ± 0.006	10.017 ± 0.009
184	9	10	0.095	5272.1 ± 2	5280.8 ± 3	5290.8 ± 2	10.058 ± 0.007	9.963 ± 0.018
184	4	30	0.157	5564.8 ± 2	5568.9 ± 2	5598.5 ± 5	9.982 ± 0.011	9.825 ± 0.013
184	7	13	0.108	5835.4 ± 1	5842.6 ± 2	5855.2 ± 3	10.058 ± 0.006	9.949 ± 0.008
184	10	19	0.101	5857.1 ± 2	5867.0 ± 1	5885.8 ± 8	10.062 ± 0.006	9.961 ± 0.009
184	7	13	0.149	6654.6 ± 3	6661.6 ± 2	6674.6 ± 4	10.101 ± 0.007	9.951 ± 0.010
184	10	10	0.134	6949.8 ± 2	6959.5 ± 1	6969.1 ± 3	10.120 ± 0.011	9.986 ± 0.010
184	10	22	0.234	6971.5 ± 3	6981.1 ± 1	7003.0 ± 9	10.076 ± 0.014	9.842 ± 0.011
A01	48	43	0.442	6159.1 ± 24	6206.8 ± 3	6249.4 ± 12	9.128 ± 0.029	8.687 ± 0.024
A01	6	9	0.079	6265.2 ± 2	6270.8 ± 3	6280.0 ± 3	9.163 ± 0.012	9.084 ± 0.019
A01	9	28	0.358	6280.8 ± 2	6289.9 ± 2	6318.0 ± 6	9.177 ± 0.013	8.819 ± 0.015
A01	16	38	0.301	6636.4 ± 3	6652.5 ± 3	6690.4 ± 8	9.161 ± 0.017	8.860 ± 0.011
A01	4	5	0.077	6982.5 ± 1	6986.5 ± 1	6991.7 ± 1	9.197 ± 0.005	9.120 ± 0.013
A02	19	81	0.046	6644.8 ± 8	6663.5 ± 3	6744.1 ± 42	8.378 ± 0.004	8.332 ± 0.003
A03	15	20	0.101	6200.0 ± 4	6215.1 ± 1	6235.6 ± 5	8.302 ± 0.009	8.201 ± 0.006
A03	4	11	0.085	6310.8 ± 3	6315.2 ± 3	6326.0 ± 4	8.313 ± 0.005	8.229 ± 0.013
A03	8	16	0.103	6672.4 ± 2	6680.0 ± 2	6696.0 ± 5	8.370 ± 0.005	8.267 ± 0.007
A03	5	3	0.071	6962.0 ± 1	6967.2 ± 1	6970.6 ± 2	8.391 ± 0.007	8.320 ± 0.007
A03	6	38	0.174	6973.7 ± 1	6980.0 ± 1	7018.0 ± 6	8.377 ± 0.009	8.203 ± 0.013
A16	8	48	0.178	5126.3 ± 2	5134.6 ± 3	5182.5 ± 17	10.582 ± 0.006	10.404 ± 0.012

A16	112	730	0.239	5682.4 ± 5	5794.2 ± 72	6524.0 ± 84	10.556 ± 0.005	10.317 ± 0.058
A20	4	25	0.067	5868.6 ± 3	5872.8 ± 3	5897.7 ± 9	8.053 ± 0.005	7.987 ± 0.010
A26	9	106	0.288	4066.4 ± 7	4075.5 ± 7	4181.3 ± 24	8.206 ± 0.016	7.918 ± 0.028
A26	18	14	0.184	4735.1 ± 3	4753.4 ± 3	4767.3 ± 10	8.304 ± 0.011	8.120 ± 0.013
A26	12	8	0.055	4798.0 ± 3	4810.2 ± 3	4818.1 ± 5	8.314 ± 0.005	8.259 ± 0.006
A26	7	13	0.268	4920.2 ± 4	4926.7 ± 5	4939.9 ± 5	8.348 ± 0.005	8.080 ± 0.019
A26	12	12	0.117	5186.7 ± 3	5198.7 ± 3	5210.9 ± 3	8.393 ± 0.005	8.275 ± 0.009
A26	8	9	0.091	5227.5 ± 4	5235.7 ± 2	5244.9 ± 4	8.398 ± 0.010	8.307 ± 0.010
A26	14	11	0.040	5496.2 ± 4	5509.7 ± 3	5520.8 ± 3	8.428 ± 0.005	8.389 ± 0.009
A26	7	9	0.041	5523.1 ± 3	5529.8 ± 4	5538.9 ± 3	8.425 ± 0.005	8.384 ± 0.007
A26	8	18	0.200	5560.4 ± 3	5568.4 ± 3	5586.4 ± 8	8.404 ± 0.006	8.204 ± 0.025
A26	9	8	0.136	5835.6 ± 2	5844.1 ± 1	5851.9 ± 4	8.373 ± 0.011	8.236 ± 0.018
A26	6	9	0.097	5867.4 ± 1	5873.3 ± 3	5882.3 ± 5	8.389 ± 0.009	8.292 ± 0.016
A26	5	10	0.059	5970.1 ± 1	5975.1 ± 2	5985.5 ± 3	8.419 ± 0.008	8.361 ± 0.018
A26	8	23	0.428	5988.8 ± 4	5996.8 ± 3	6019.5 ± 7	8.414 ± 0.016	7.986 ± 0.024
A26	6	13	0.146	6230.4 ± 2	6236.7 ± 3	6249.4 ± 4	8.357 ± 0.018	8.210 ± 0.021
A26	7	10	0.195	6261.0 ± 4	6268.2 ± 2	6277.8 ± 2	8.359 ± 0.009	8.164 ± 0.020
A26	10	20	0.363	6569.9 ± 2	6579.9 ± 2	6599.8 ± 4	8.396 ± 0.008	8.033 ± 0.018
A26	7	9	0.290	6656.1 ± 2	6663.3 ± 1	6672.7 ± 3	8.410 ± 0.019	8.120 ± 0.023
A26	11	21	0.261	6963.6 ± 2	6975.1 ± 2	6996.4 ± 3	8.239 ± 0.011	7.977 ± 0.017
A32	167	428	0.052	5337.7 ± 83	5504.6 ± 78	5932.7 ± 201	10.105 ± 0.006	10.053 ± 0.011

Table 4.1: Measurements and uncertainties for 70 outbursts from 24 unique systems. The magnitudes given in the final two columns are in the KELT passband, minus a constant value to make them approximately equal to the V-band magnitude.

4.6 Additional examples of outbursts with simultaneous spectroscopy

Here we highlight some interesting cases, where simultaneous photometry and spectroscopy reveal changes in the star + disk system. This selection shows diversity in light curve and emission-line variability, demonstrating episodes of disk growth and creation, inside-out disk clearing, and outwardly migrating disks.

Table 4.1 provides information for the 70 well-defined outbursts where the rising and falling times, and the photometric amplitudes are measured. Each of these are events where the brightness of the system increases first, then falls back to baseline. This is partly because systems with low to intermediate inclination angles ($i \lesssim 70°$) are more common than those with higher inclination angles, and also because outbursts that cause a net brightening tend to be better defined in the KELT data compared to their inverted counterparts. Table 4.1 includes the date of the beginning and end of each rising and falling phase, and the baseline and peak brightness associated with each outburst event (in the KELT passband). Table A.1 includes each object in this sample, reporting the ABE-ID, a common identifier, V-band magnitude, a spectral type, the corresponding reference, the T_{eff} class (early, mid, late, or unclassified), number of APOGEE visits, the KELT field, the first and last dates of KELT observations, and the number of detected outbursts. Spectral type references of "New" indicate that an object was discovered to be a Be star through inspection of APOGEE spectra, and is announced in Chojnowski et al. (2015). These systems do not have an available literature spectral type, nor has an optical spectrum been acquired with APO-ARCES or the AO long-slit spectrograph.

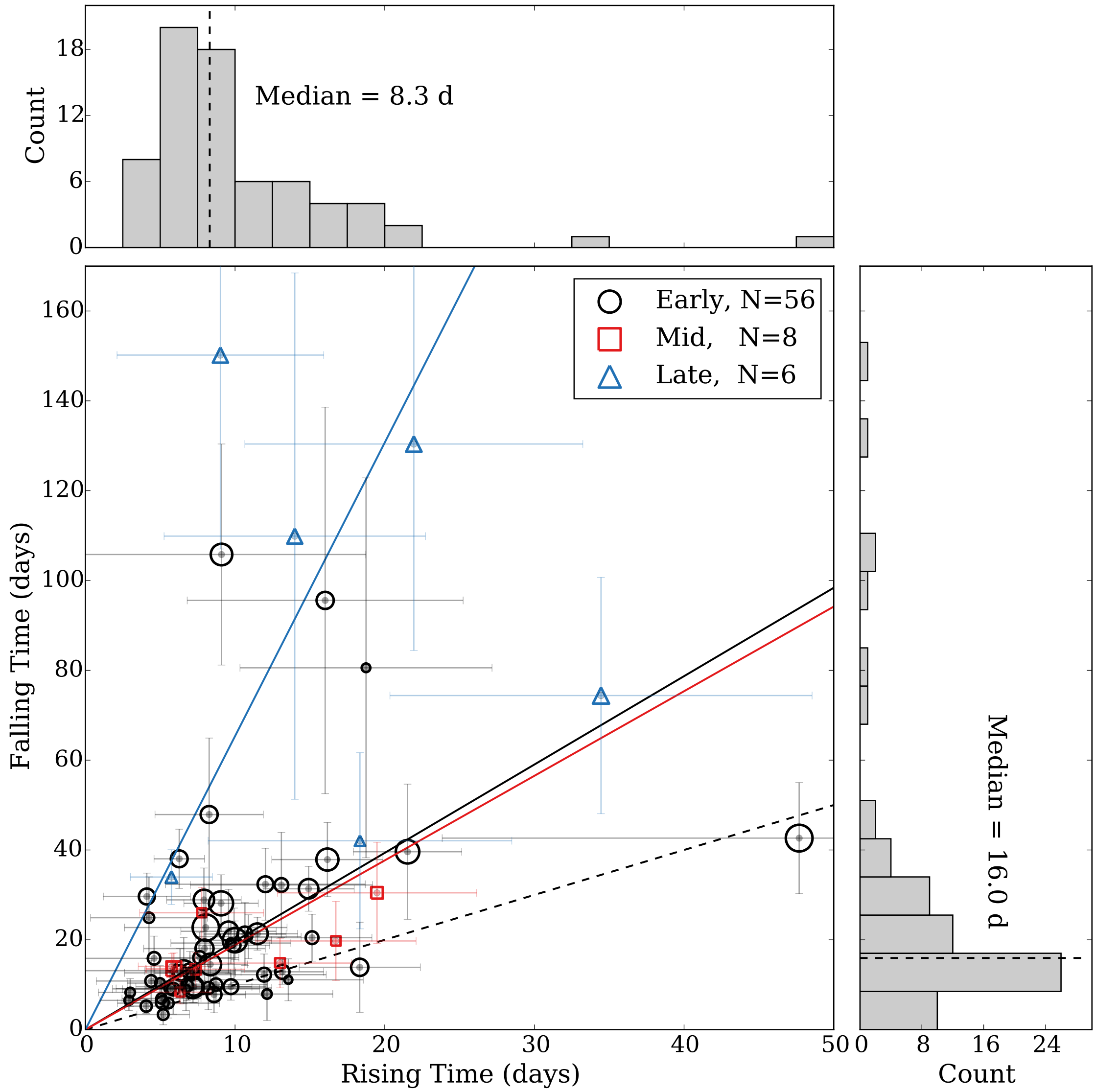

Figure 4.16: Each point represents the duration of the rising and falling times for 70 outbursts in 24 unique stars in the AK sample (18 early, 4 mid, and 2 late), with the marker size proportional to the photometric amplitude. The dashed line has a slope of 1. Circles, squares, and triangles correspond to earl-, mid-, and late-type stars, respectively. The black, red, and blue lines begin at the origin and are lines of best fit to the early-, mid-, and late-type groups. Their slopes are 1.97 (early), 1.88 (mid), and 6.54 (late). The top (right) panel shows a histogram of the rising (falling) times. Table 4.1 contains the information used to make this plot.

ABE-027

A photometric outburst occurs near JD - 2450000 = 5600, with an unusual morphology. A slow rising phase is followed by a much shorter falling phase, but the system beings to brighten again before the falling phase is complete. A gap in coverage prevents a better understanding of this event. In the season following the outburst, there is a very slight photometric excess, and Br11 shows a clear disk (Figure 4.17). A second grouping of APOGEE spectra, taken ∼300 days after the first group shows no sign of emission, and there is no longer any detectable photometric excess.

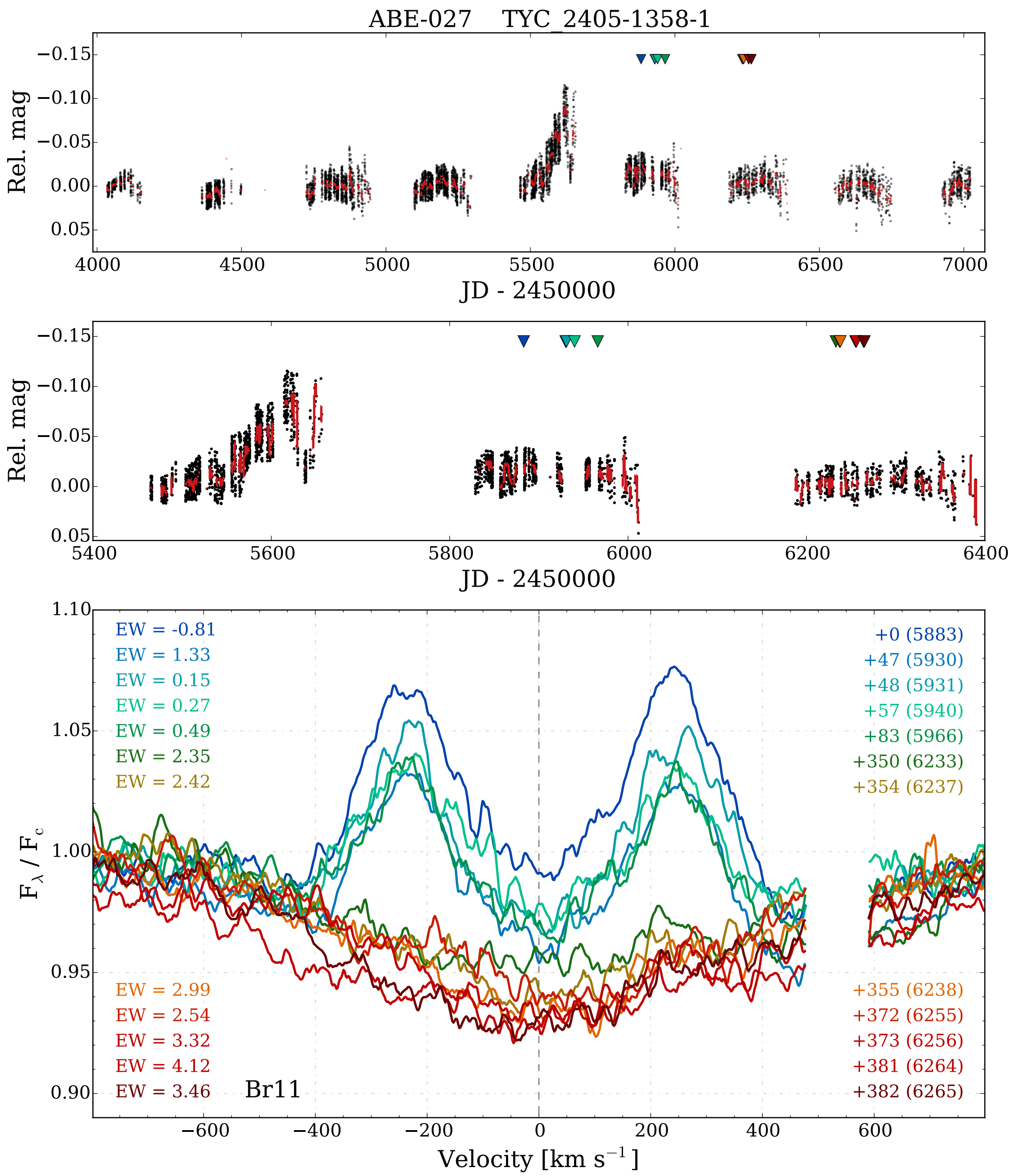

Figure 4.17: Light curve and spectra for the star ABE-027, in the same format as Figure 4.2.

ABE-082

The large photometric amplitude and long falling timescale apparent in the light curve of ABE-082 imply that a large amount of mass is ejected in this outburst, although the rising phase occurs during a gap in coverage (see Figure 4.18). The first grouping of three APOGEE spectra have an average W_{Br11}= -6.50 Å, and an average Br11 Δv_p = 273.2 km s^{-1}. The second grouping of six spectra, taken about a year later, shows much strong emission with an average W_{Br11}= -12.05 Å, and a lower peak separation, with the average Br11 Δv_p = 239.1 km s^{-1}. The diminished peak separation from the first to the second group of spectra indicates that the preferential formation radius has increased, and that the disk is dissipating. This is corroborated by the decreasing visible continuum flux in the KELT light curve. It is perhaps unexpected that the strength of the Br11 line appears to increase as the disk is dissipating. Because the strength of the emission line is measured here relative to the local continuum, the apparent increase in strength is best explained not by an absolute increase in the amount of Br11 line emission, but rather by a decrease in the strength of the local continuum. This example demonstrates the need for caution when interpreting relative line strengths for systems with significant continuum variability.

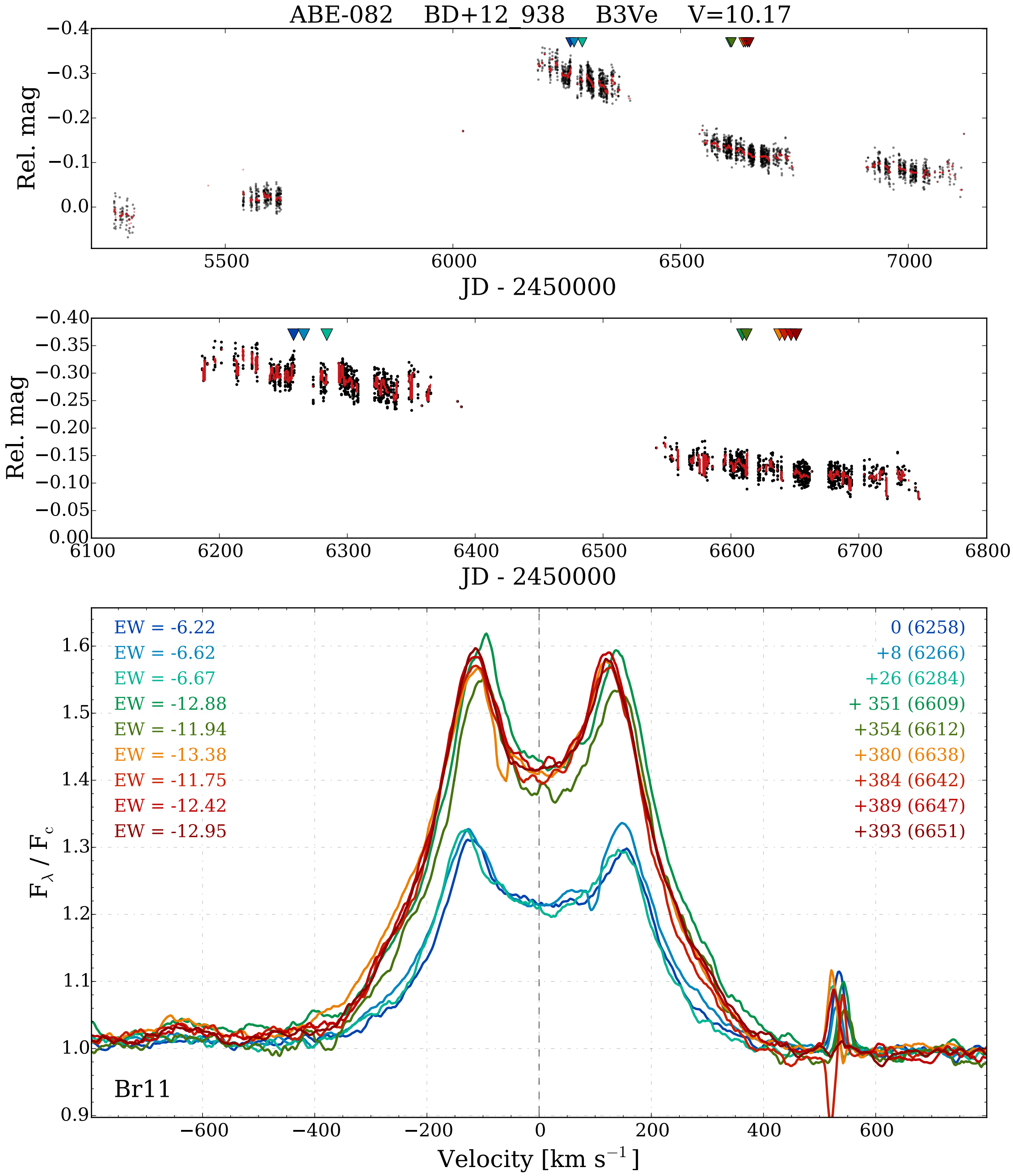

Figure 4.18: Light curve and spectra for the star ABE-082, in the same format as Figure 4.2.

ABE-154

This system has six detected photometric outbursts, one of which is bracketed by APOGEE spectra, as seen in Figure 4.19. Prior to the outburst there is no sign of a disk. The Br11 line ∼200 days after the outburst shows a clear disk signature, and there is no photometric excess. Although the coverage of the falling phase of this outburst is incomplete, it is clearly many times longer than the rising phase. This is the case with all observed outbursts in this late-type star.

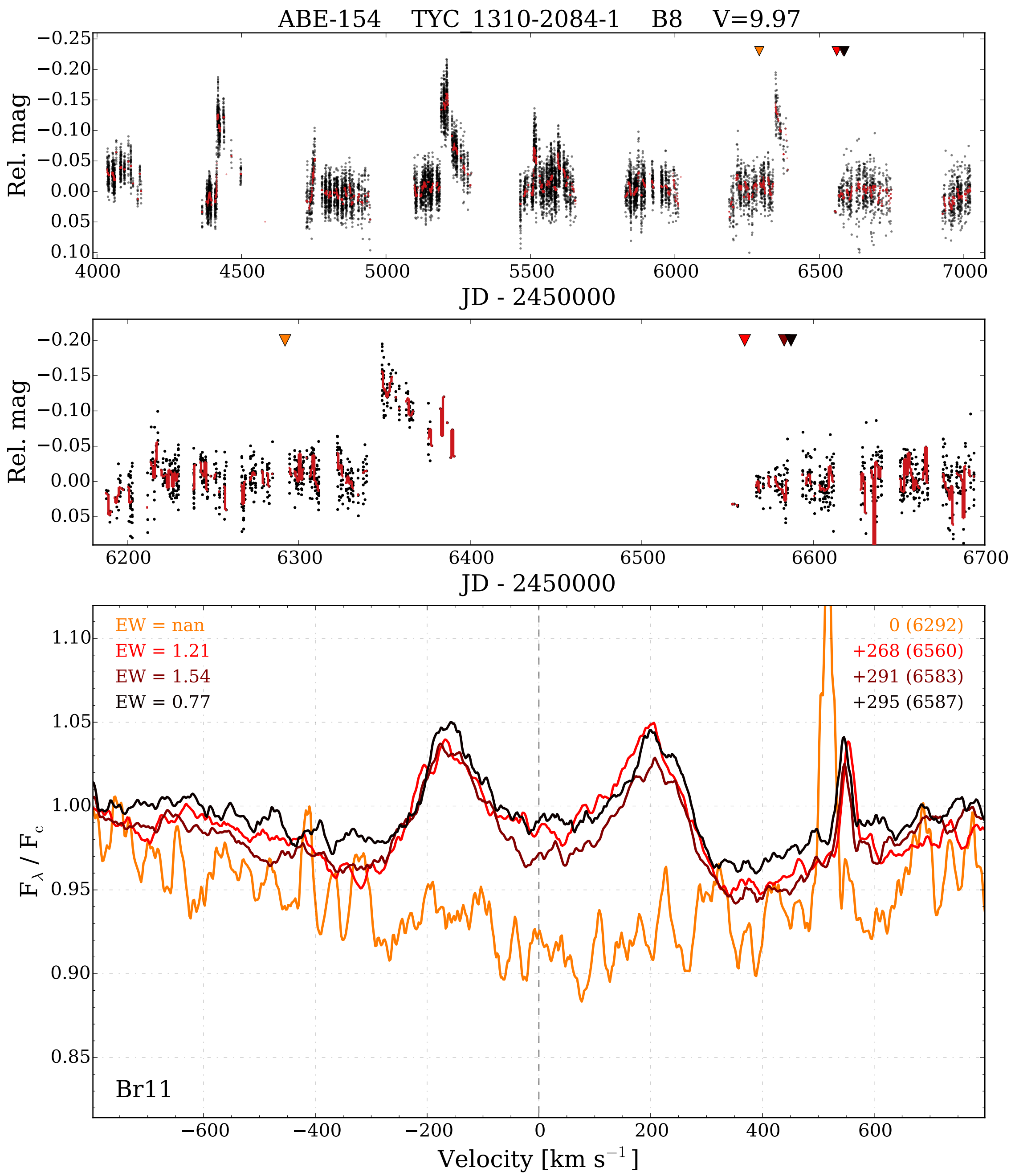

Figure 4.19: Light curve and spectra for the star ABE-154, in the same format as Figure 4.2.

ABE-160

This system has one large photometric outburst (reaching peak brightness near JD - 2450000 = 6400), as well as a few smaller ones (see Figure 4.20). Spectra taken during the falling phase of the major outburst show a clear disk signature. The emission strength relative to the local continuum decreases slightly during the 27 day APOGEE baseline.

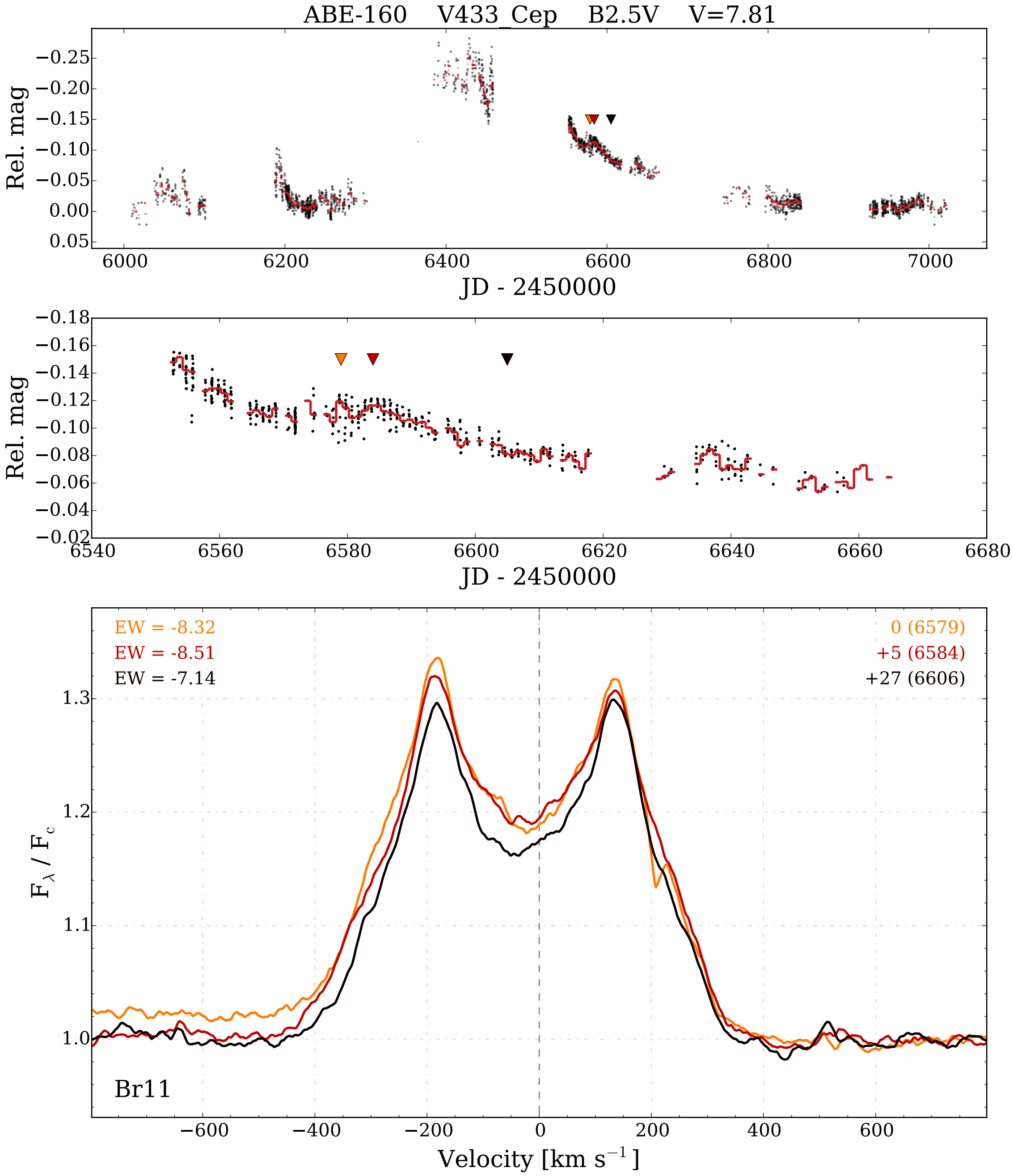

Figure 4.20: Light curve and spectra for the star ABE-160, in the same format as Figure 4.2.

ABE-162

Similar to ABE-154, there is a clear outburst in photometry seen in this late-type star. A spectrum taken prior to the outburst shows no sign of a disk in Br11, while spectra taken after the outburst do indicate the presence of a disk, even after the system has returned to its baseline brightness (see Figure 4.21).

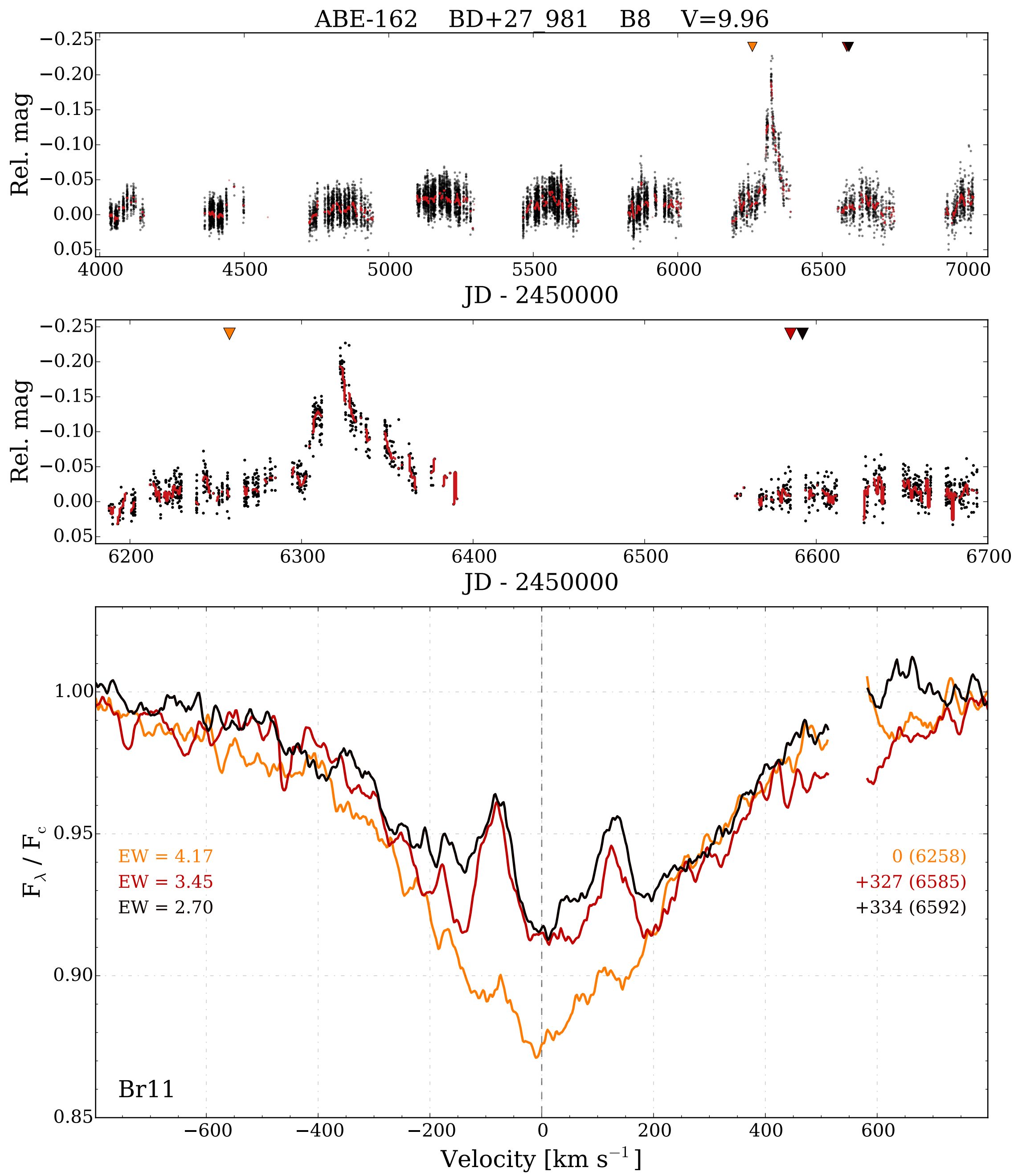

Figure 4.21: Light curve and spectra for the star ABE-162, in the same format as Figure 4.2.

ABE-164

This early-type system is very active in photometry, spending virtually no time in a photometrically quiescent state. Fifteen Hα measurements from BeSS span 5563 days, and all show the presence of a disk, which varies significantly in strength. The Hα EW spans an order of magnitude, ranging between -1.24 – -23.53. The line strength reaches to over four times the continuum level. Three Br11 measurements all show a strong disk signature (see Figure 4.22).

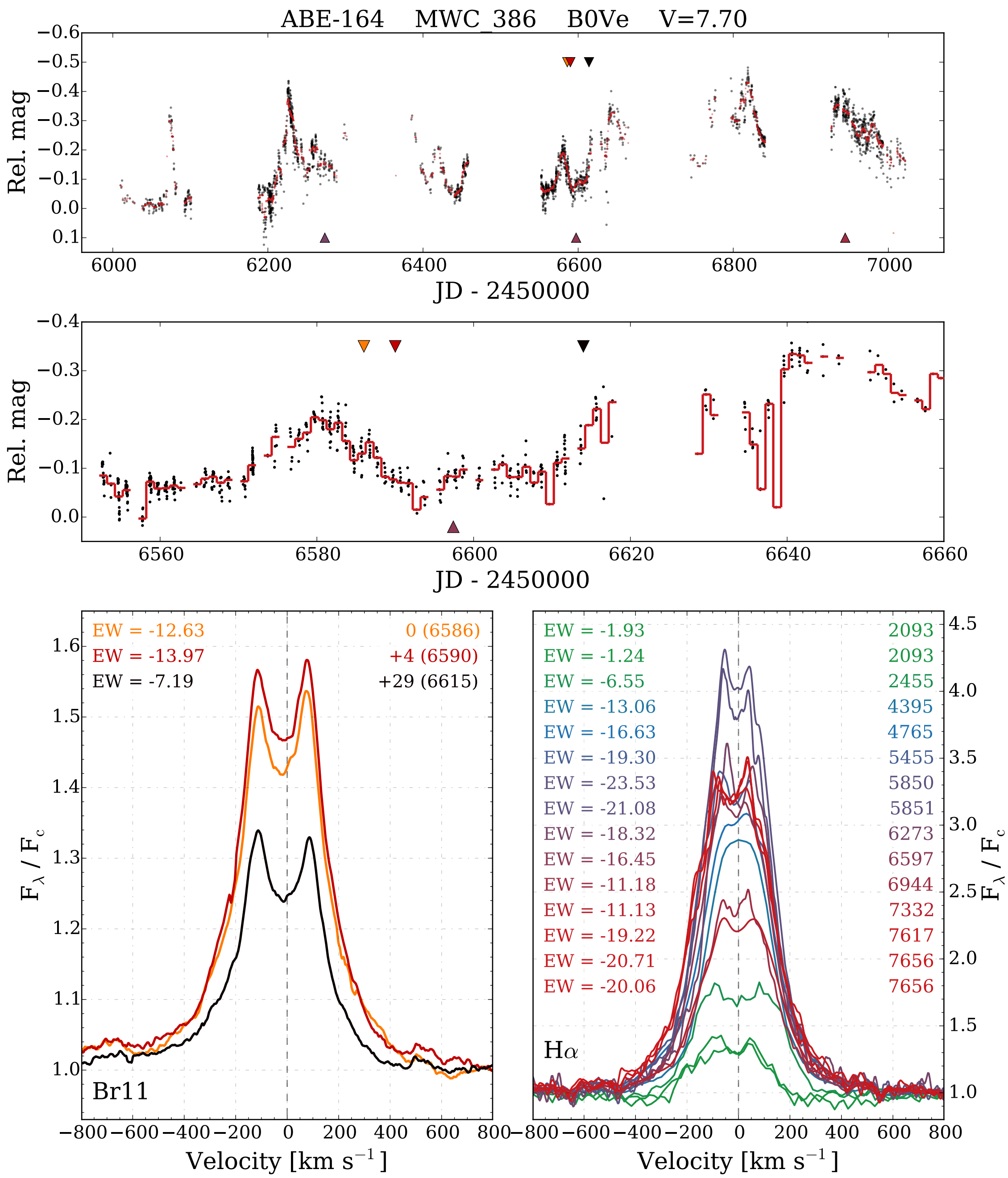

Figure 4.22: Light curve and spectra for the star ABE-164, in the same format as Figure 4.3.

ABE-167

Four BeSS spectra from between JD-2450000 = 2658 – 6024 show no sign of a disk. There begins to be some activity in the KELT light curve near JD-245000 = 6250, with sparse photometric coverage prior to this point. As the system becomes slightly brighter, the Br11 line shows variability, indicating activity in the circumstellar environment. By JD-2450000 = 6715, the brightness is markedly above baseline, and Hα is clearly in emission. This system appears to grow a disk from many closely-spaced low-amplitude mass-loss events, rather than a singular well-defined event (see Figure 4.23). The BeSS spectrum taken at JD-2450000 = 6682 is of low resolution, but does indicate the presence of emitting material. The final two BeSS spectra show clear double-peaked Hα emission. A significant change in the V/R ratio is apparent between the second-last BeSS spectrum (JD-2450000 = 6715) having V/R $\approx$ 1, and the final BeSS spectrum (JD-2450000 = 6718) showing clear asymmetry, with V/R $>$ 1. With just three days between these two spectra, the rapid change in the V/R ratio likely has its origins in an asymmetrical inner disk that is still in the process of circularizing. This hypothesis is supported by the relatively high photometric state near these epochs (implying a relatively dense inner disk), as well as the high level of photometric activity (implying active episodes of mass loss).

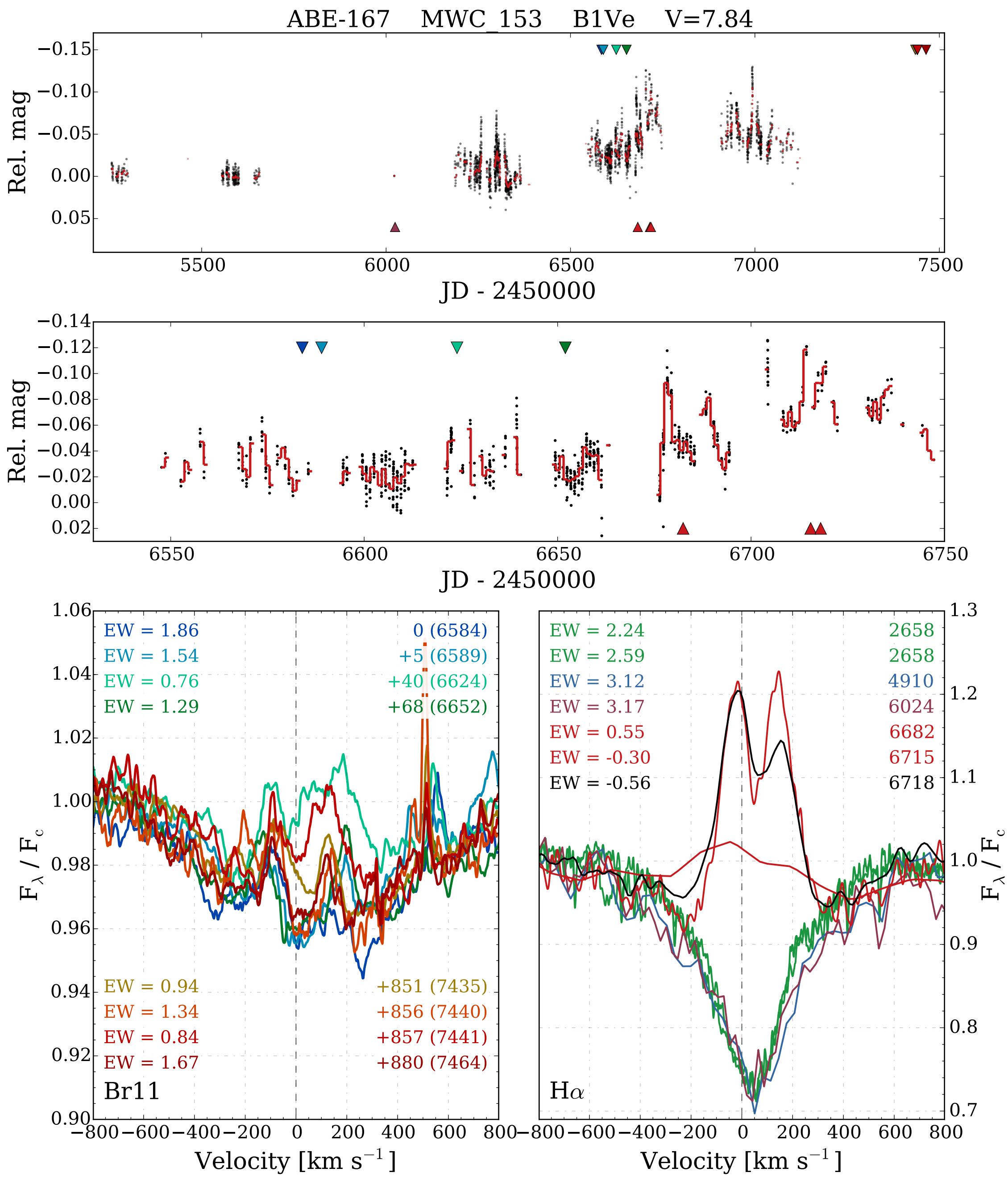

Figure 4.23: Light curve and spectra for the star ABE-167, in the same format as Figure 4.3.

ABE-176

There are two groupings of APOGEE spectra, both with simultaneous photometry. During the first grouping, the double-peaked emission increases in strength, seemingly associated with increased photometric activity. The disk has subsequently dissipated by the beginning of the second grouping, as the next four spectra (at JD_0 +295, +349, +351, and +352 days) show no disk. The final two spectra are preceded by a photometric outburst, and clearly show the presence of a disk (see Figure 4.24).

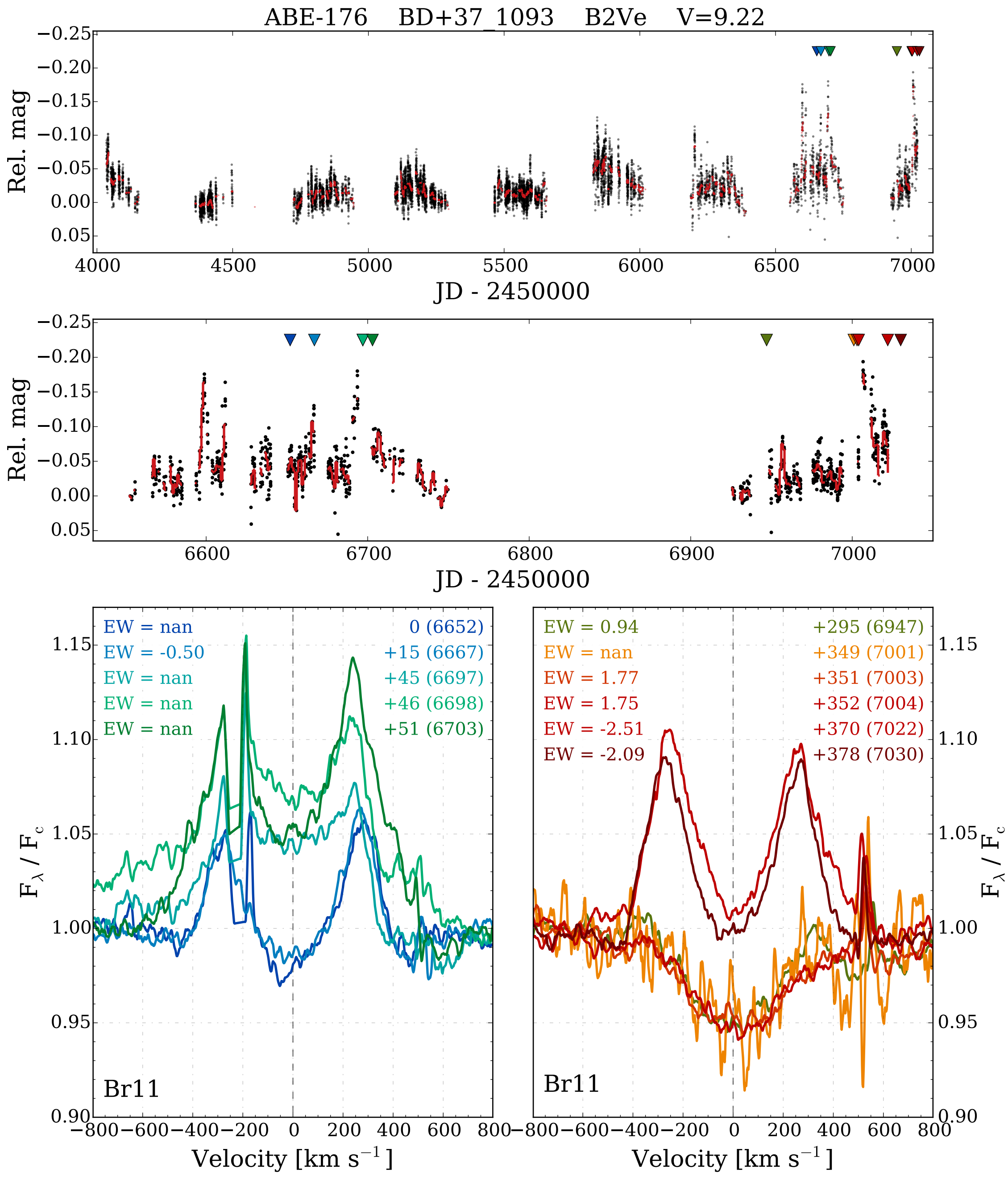

Figure 4.24: Light curve and spectra for the star ABE-176, in the same format as Figure 4.2. The feature at the violet peak of the emission lines plotted in the bottom-left panel is a detector artifact, and is not astrophysical.

ABE-184

This system is highly active in photometry, and is often in an outbursting state. A clear disk is present in all spectroscopic epochs, varying in strength. There is appreciable RV variation, which is especially apparent in the first three spectra (see Figure 4.25). One of the most RV-variable objects in the APOGEE Be star sample, this is identified as a possible binary in Chojnowski et al. (2017).

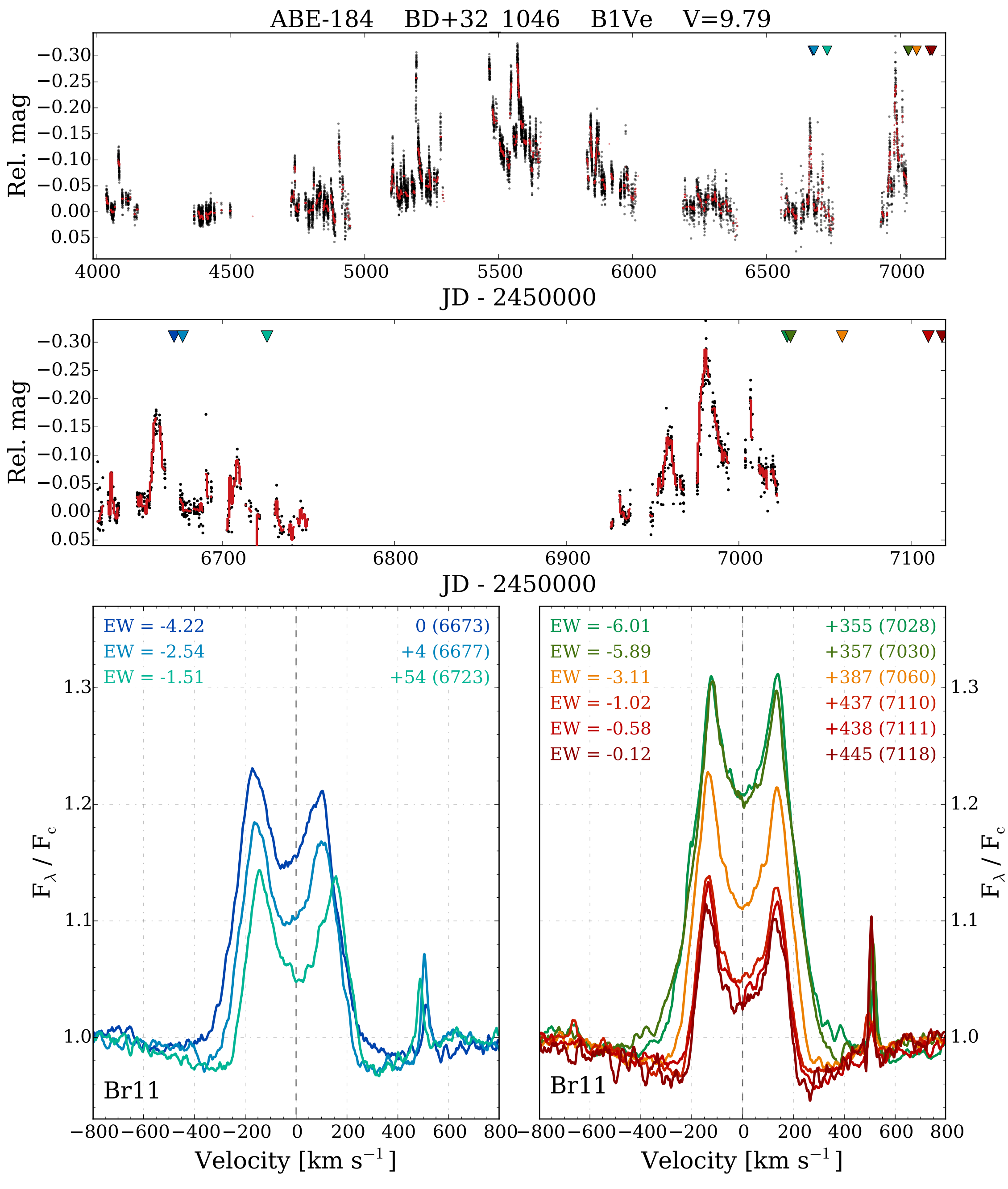

Figure 4.25: Light curve and spectra for the star ABE-184, in the same format as Figure 4.3.

ABE-187

The light curve of this system lacks well-defined outbursts, but there is stochastic variability that persists through the entire observational baseline. All 10 APOGEE spectra show a clear disk, as does the single low-resolution spectrum from BeSS. The Br11 line is variable, but within a well-defined 'envelope'. The lack of variability in the Br11 envelope implies that no significant changes in the inner disk occur. A strong C I 16895 feature is present in all APOGEE spectra. The very large peak separation, relative to the Br11 line, indicates that it is formed in the circumstellar environment close to the star. This seems to suggest that there is not a large gap between the star and disk, possibly indicating that the disk is fed nearly continuously (see Figure 4.26).

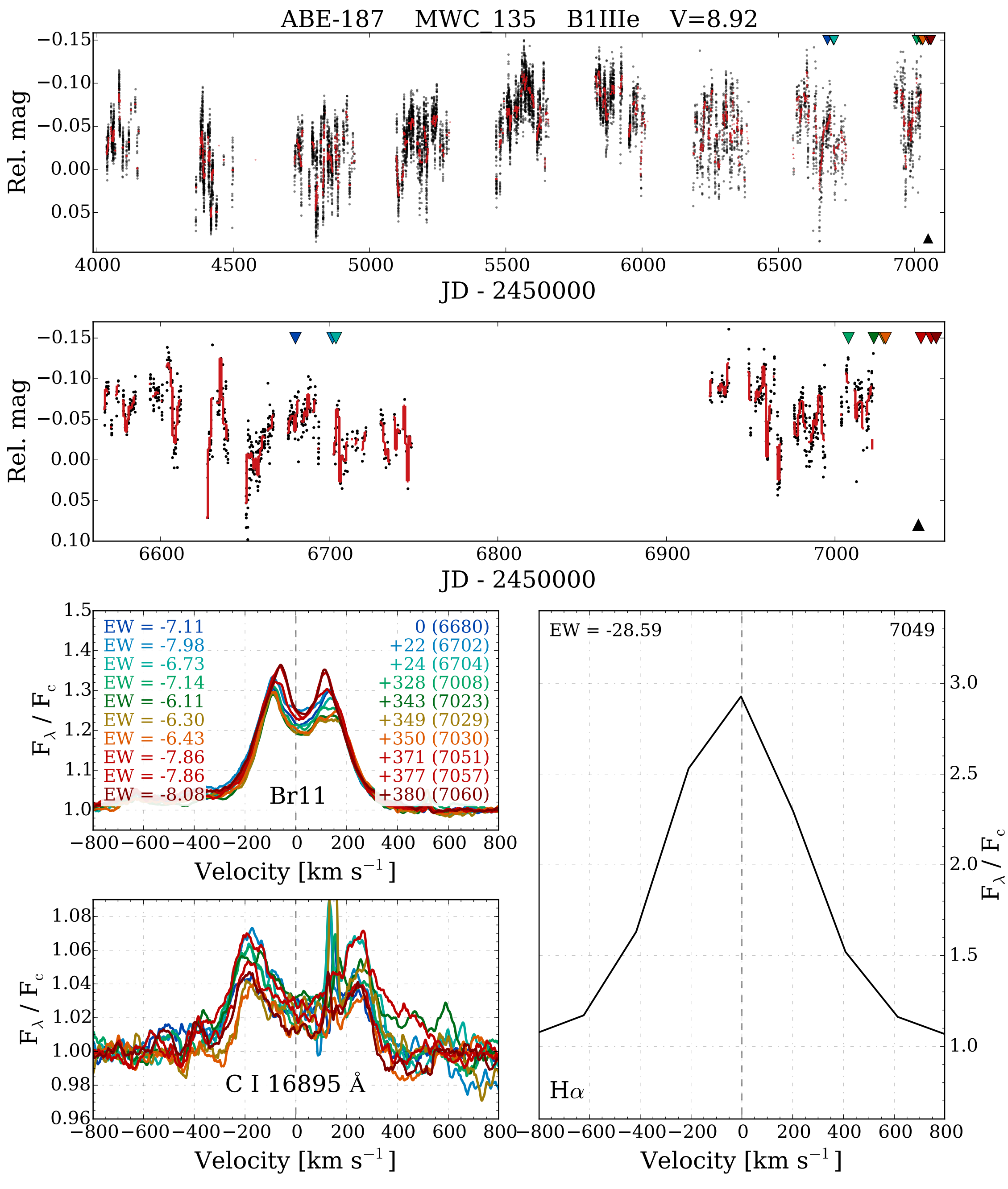

Figure 4.26: Light curve and spectra for the star ABE-187, in the same format as Figure 4.3.

ABE-A03

This system has remarkably strong and persistent single-peaked Hα emission (see Figure 4.27). The Br11 line is also strong, with an interesting profile showing a strong violet enhancement at all epochs. The line changes little over the 58 day APOGEE baseline, despite the presence of an outburst about 15 days prior to the final spectrum. The light curve shows gradual dimming over the three KELT seasons, with many outbursts interspersed.

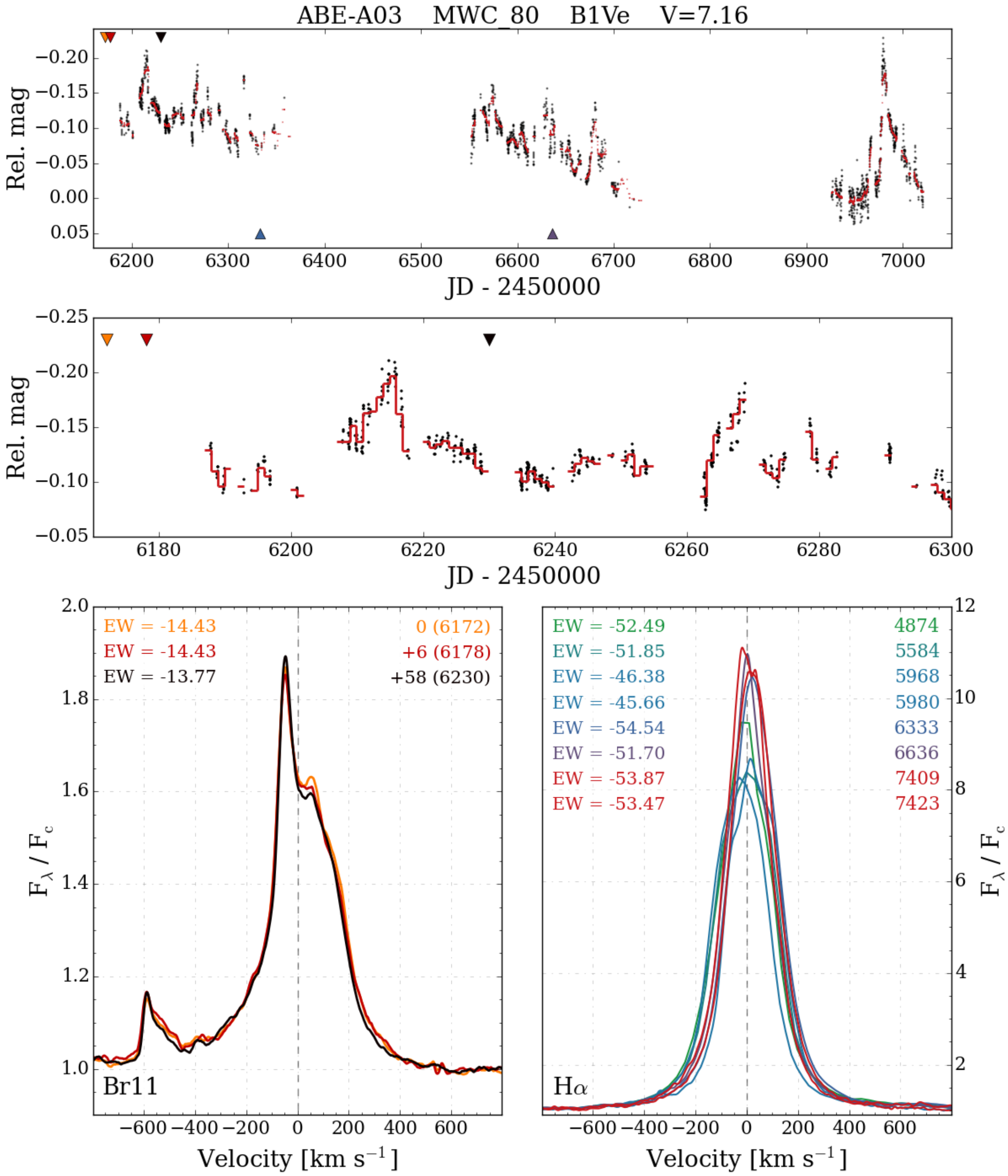

Figure 4.27: Light curve and spectra for the star ABE-A03, in the same format as Figure 4.3.

ABE-A26

A high level of activity is obvious in the light curve of this system (see Figure 4.28). Many high-amplitude outbursts occur in rapid succession. This is viewed at a very low inclination angle, as all spectra show single-peaked emission profiles. The disk is remarkably strong compared to other systems in this sample, with the Br11 emission peak reaching to nearly four times the continuum, and Hα reaching a peak around ten times the continuum level.

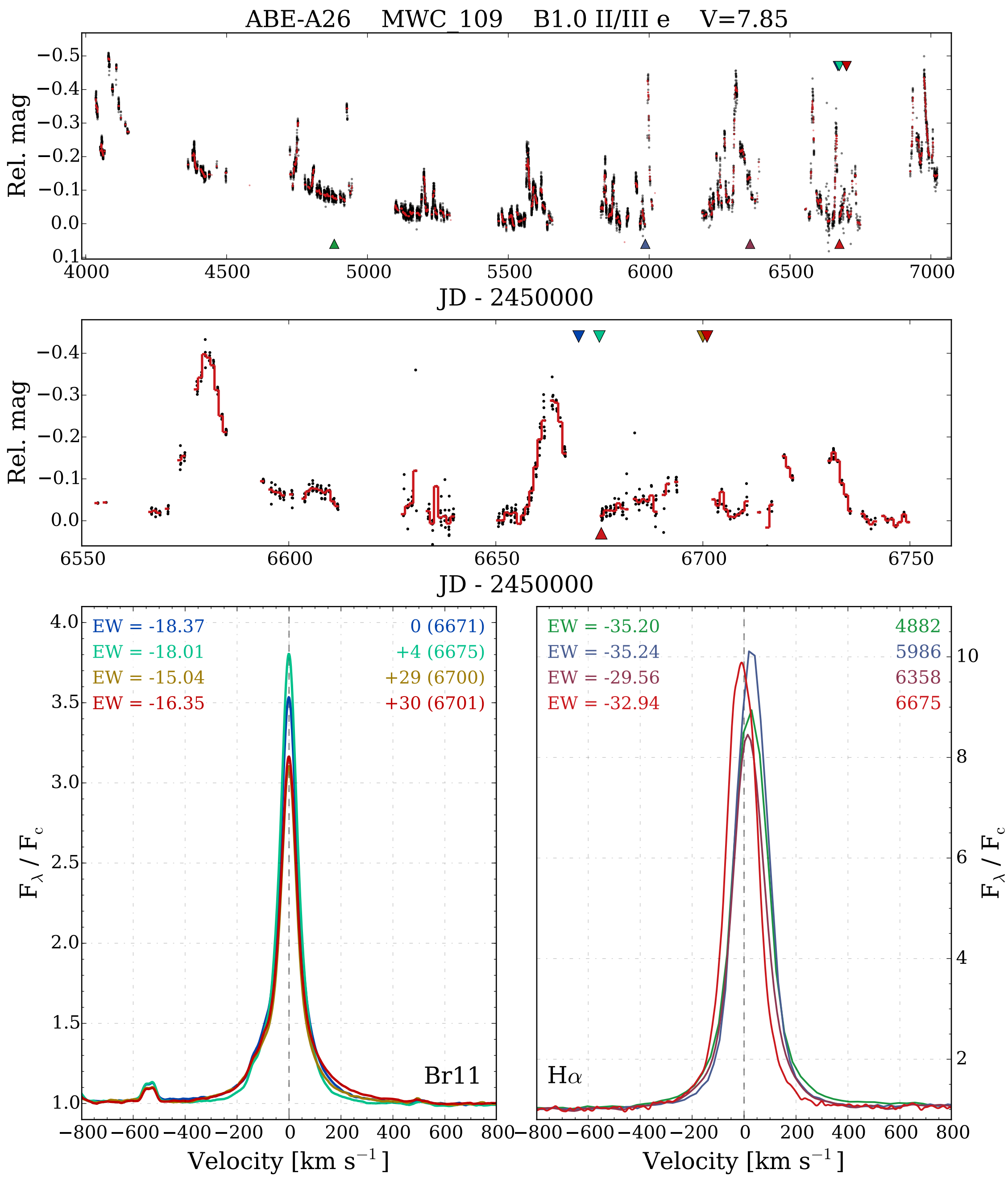

Figure 4.28: Light curve and spectra for the star ABE-A26, in the same format as Figure 4.3.

4.7 Additional outbursts

Here are shown light curves for all systems in the BK sample that experience at least one outburst (Figure 4.29).

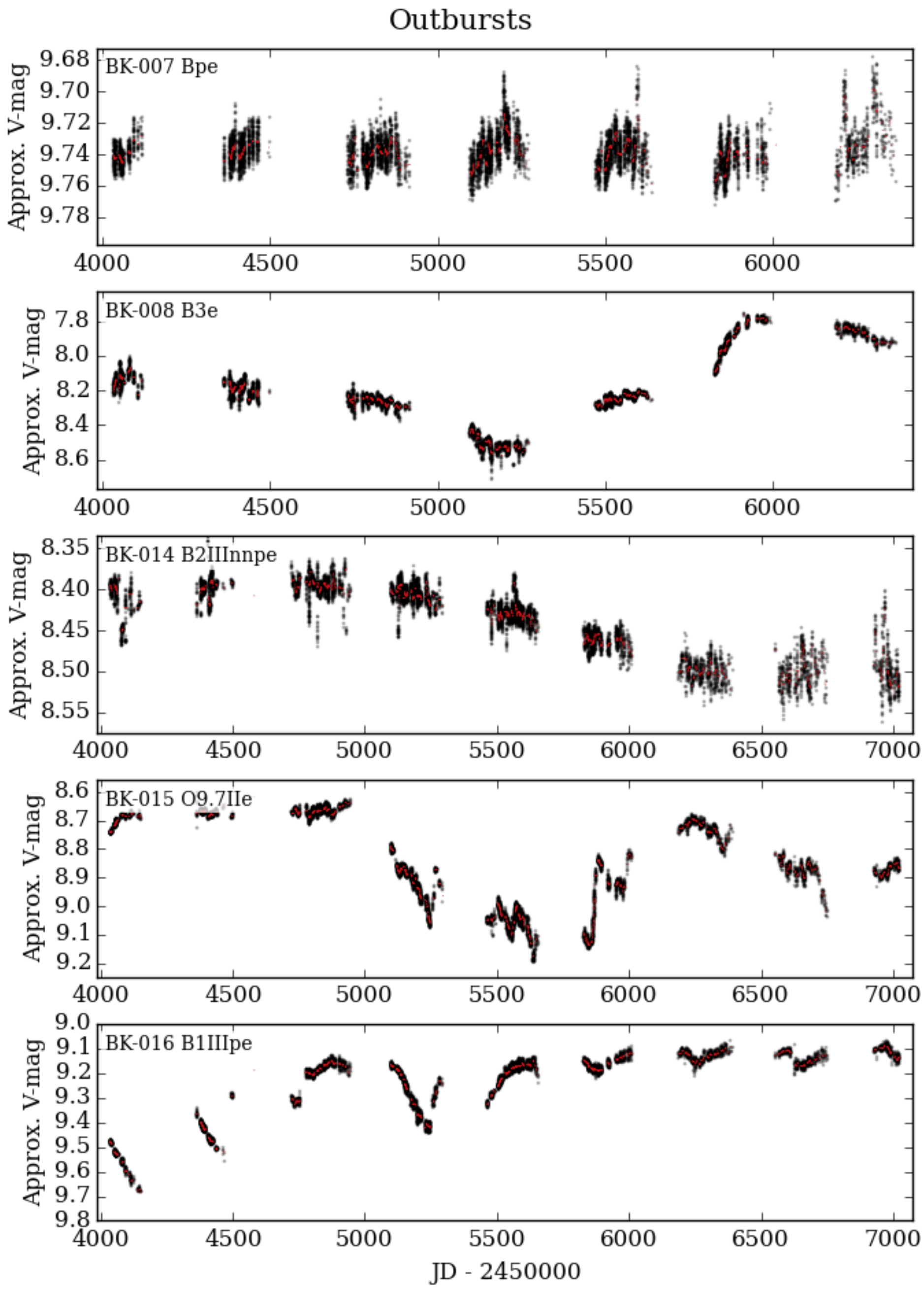

Figure 4.29: Light curves of systems with at least one outburst from the BK sample.

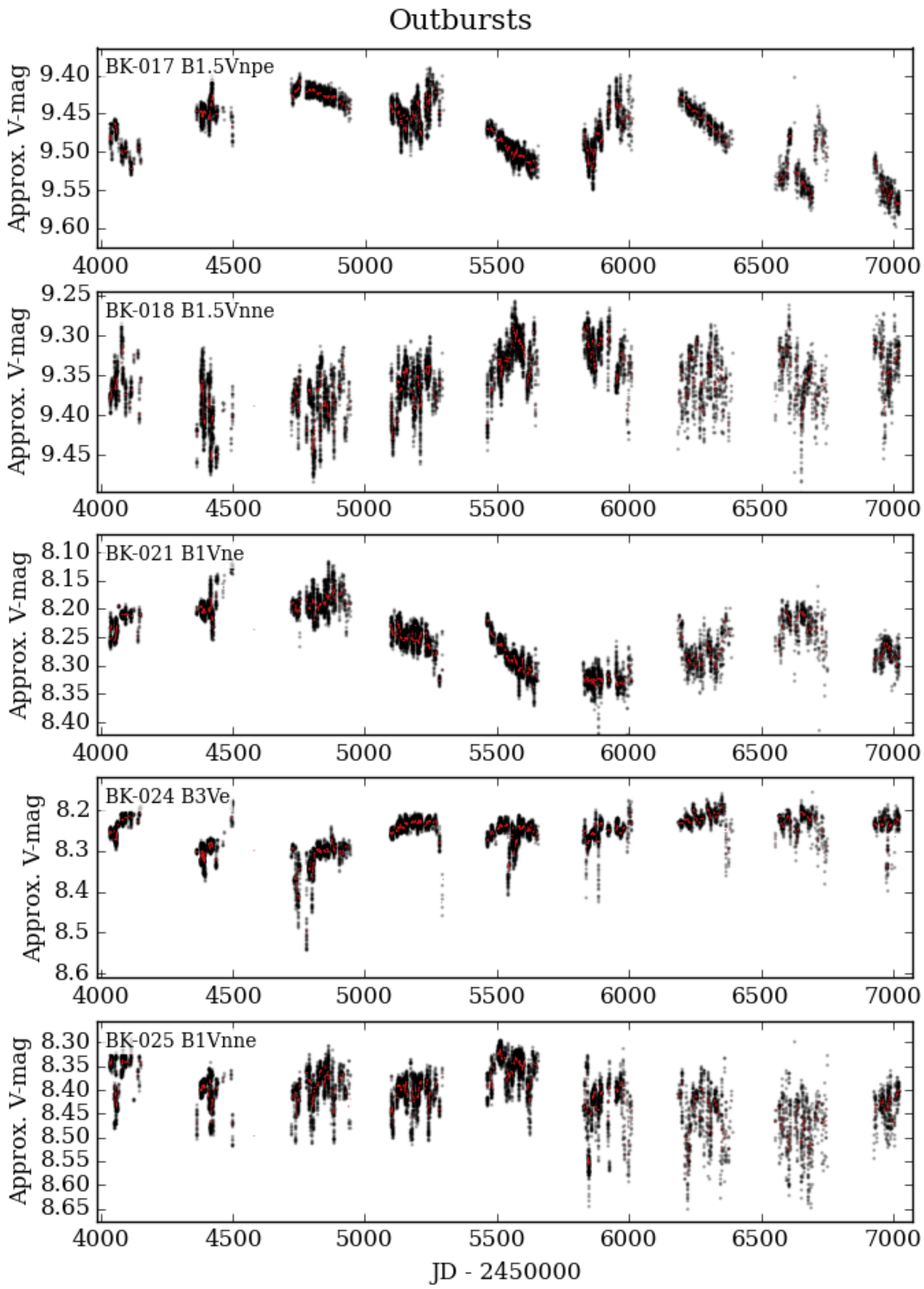

Outbursts
BK-017 B1.5Vnpe
BK-018 B1.5Vnne
BK-021 B1Vne
BK-024 B3Ve
BK-025 B1Vnne
Approx. V-mag
JD - 2450000

Figure 4.29: B

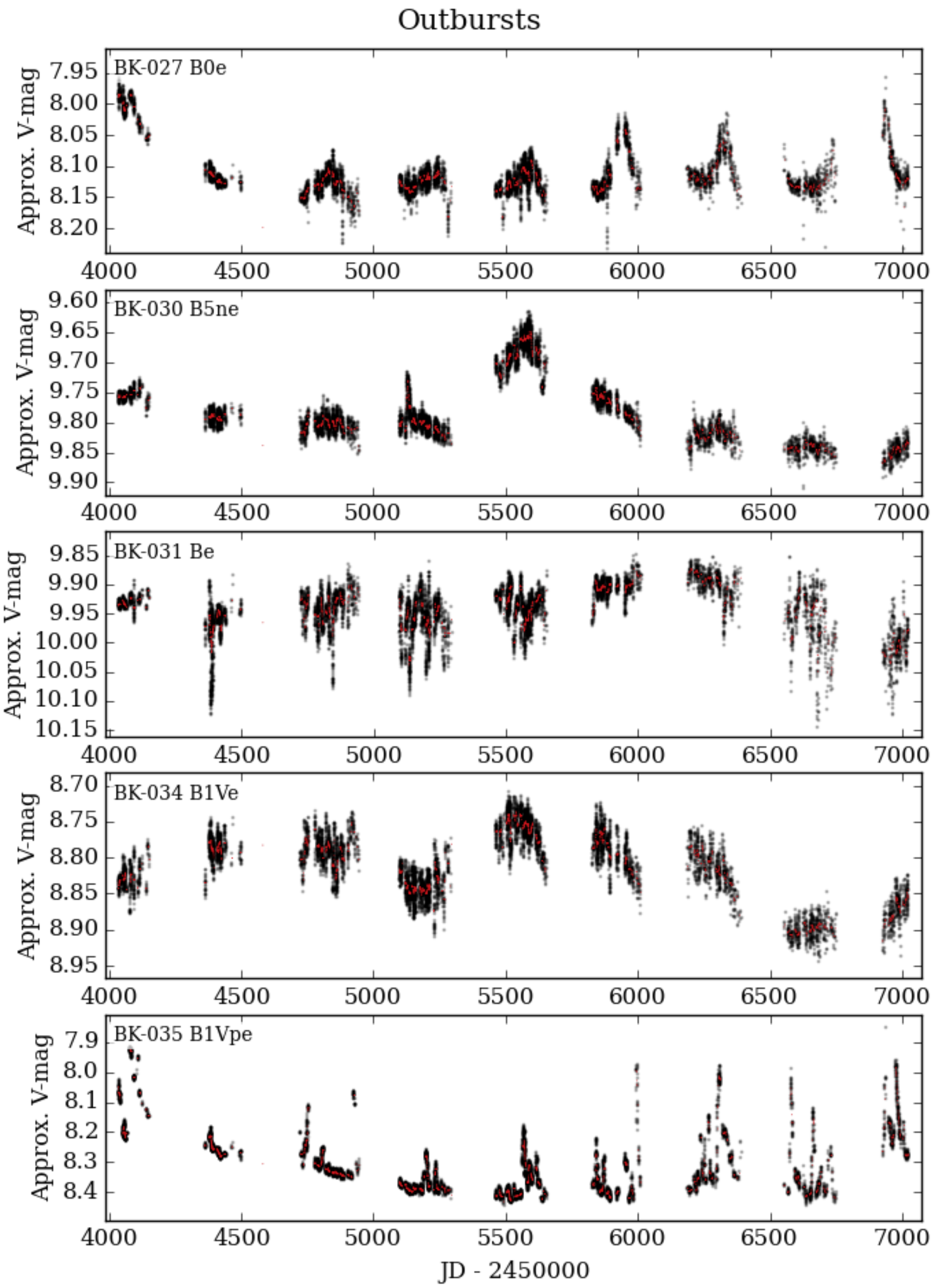

Outbursts
BK-027 B0e
BK-030 B5ne
BK-031 Be
BK-034 B1Ve
BK-035 B1Vpe
Approx. V-mag
JD - 2450000

Figure 4.29: C

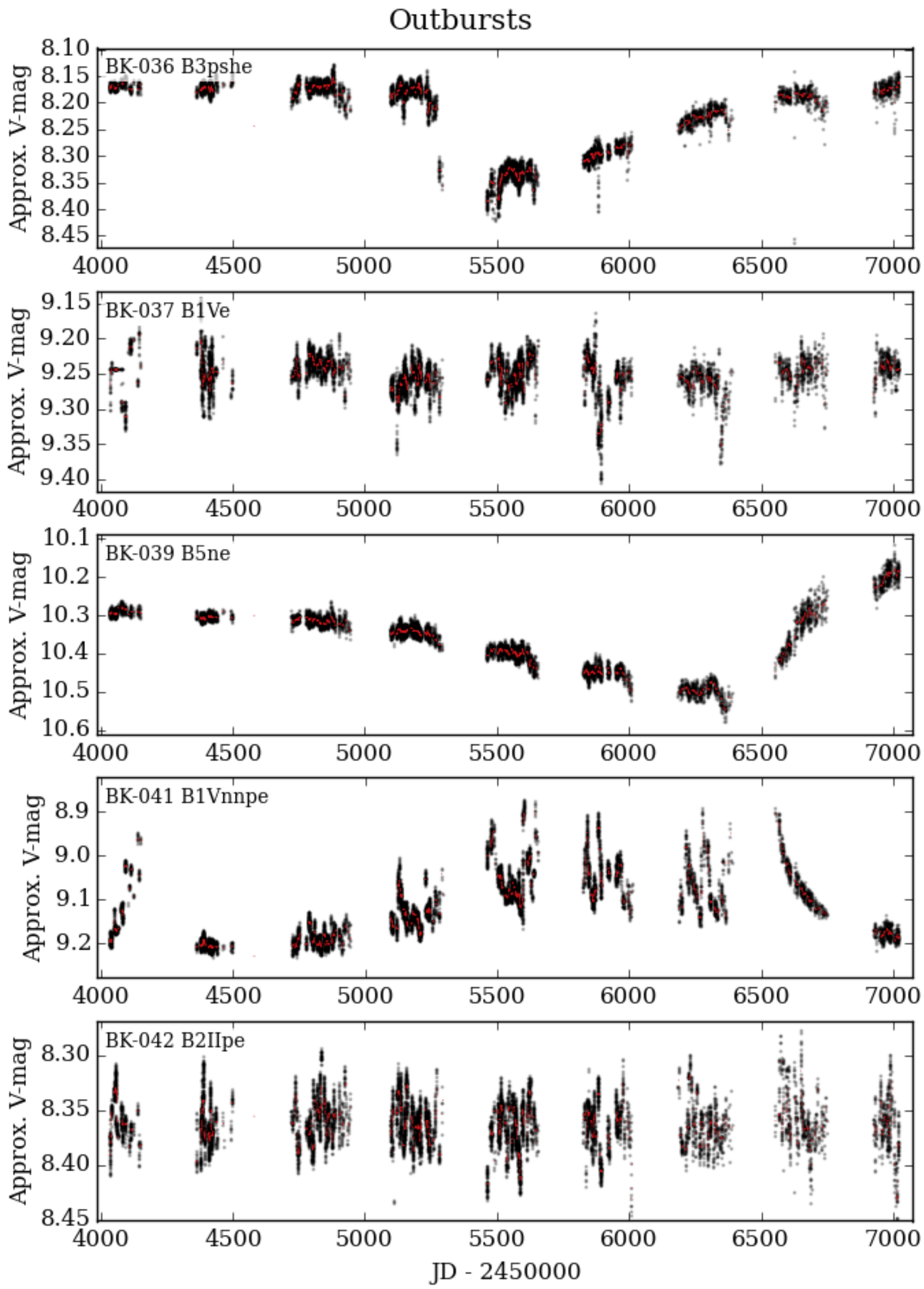
Outbursts
BK-036 B3pshe
BK-037 B1Ve
BK-039 B5ne
BK-041 B1Vnnpe
BK-042 B2IIpe
Approx. V-mag
JD - 2450000

Figure 4.29: D

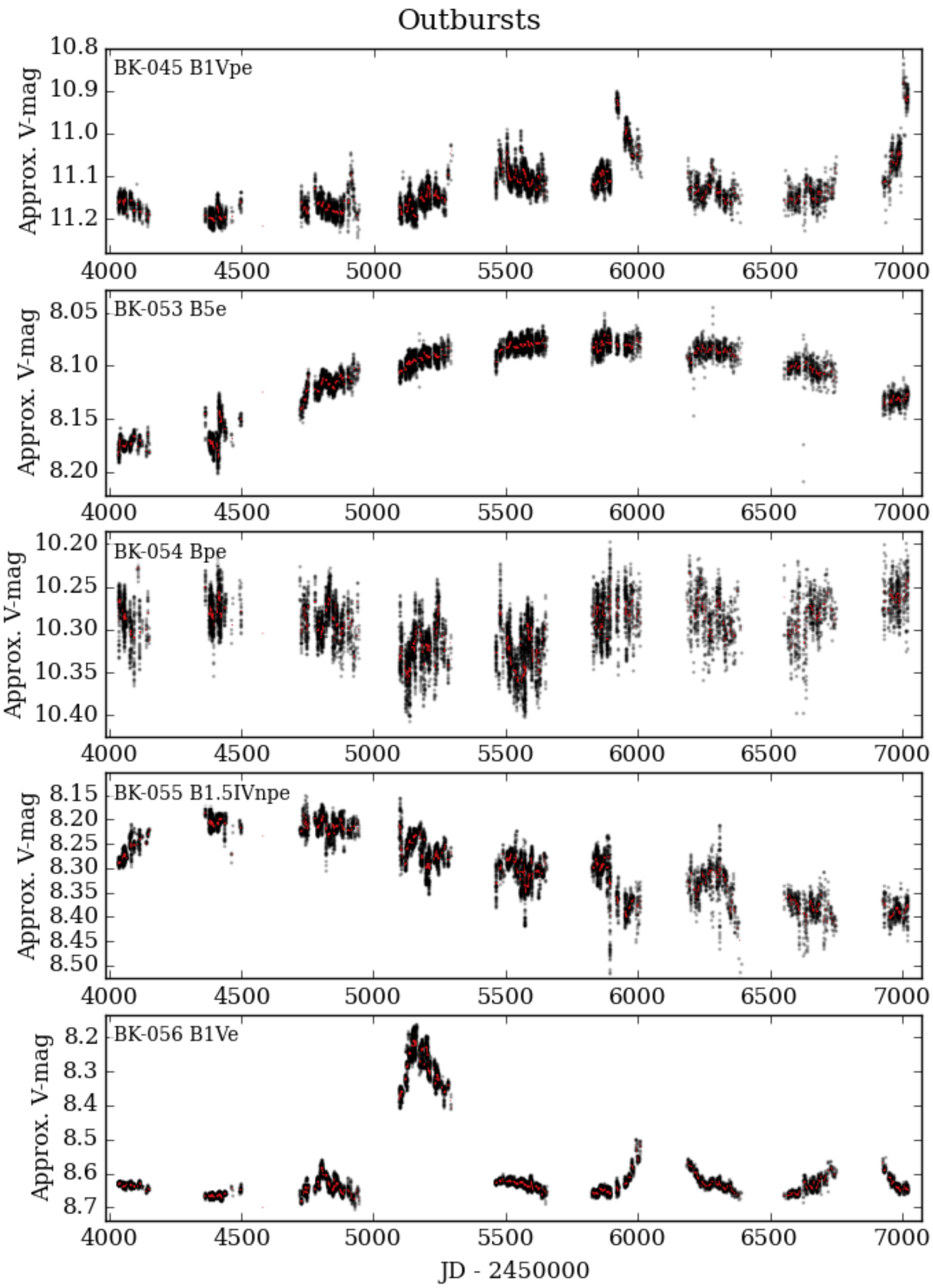
Outbursts
BK-045 B1Vpe
BK-053 B5e
BK-054 Bpe
BK-055 B1.5IVnpe
BK-056 B1Ve
Approx. V-mag
JD - 2450000
4000
4500
5000
5500
6000
6500
7000

Figure 4.29: E

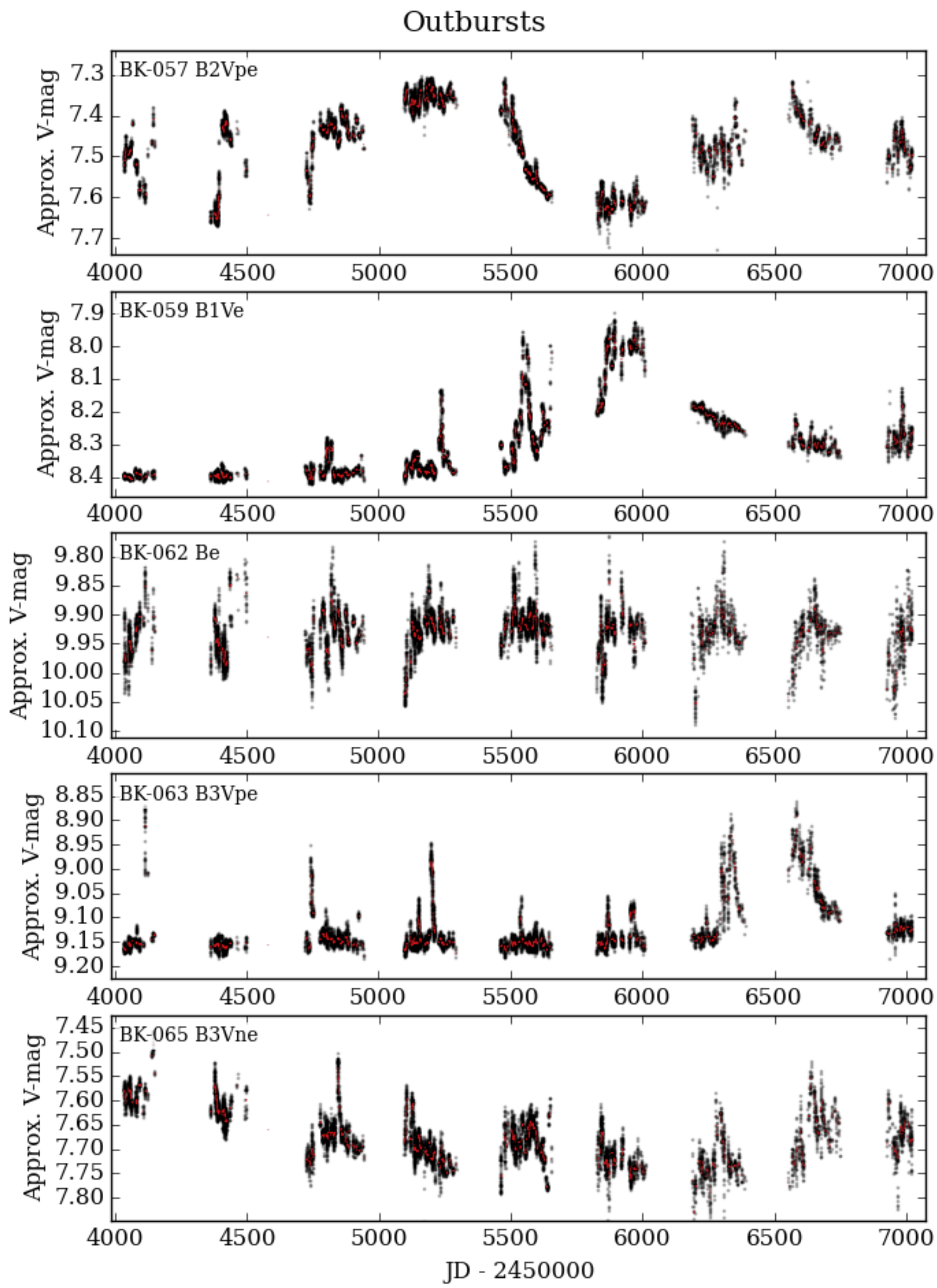
Outbursts
BK-057 B2Vpe
BK-059 B1Ve
BK-062 Be
BK-063 B3Vpe
BK-065 B3Vne
Approx. V-mag
JD - 2450000

Figure 4.29: F

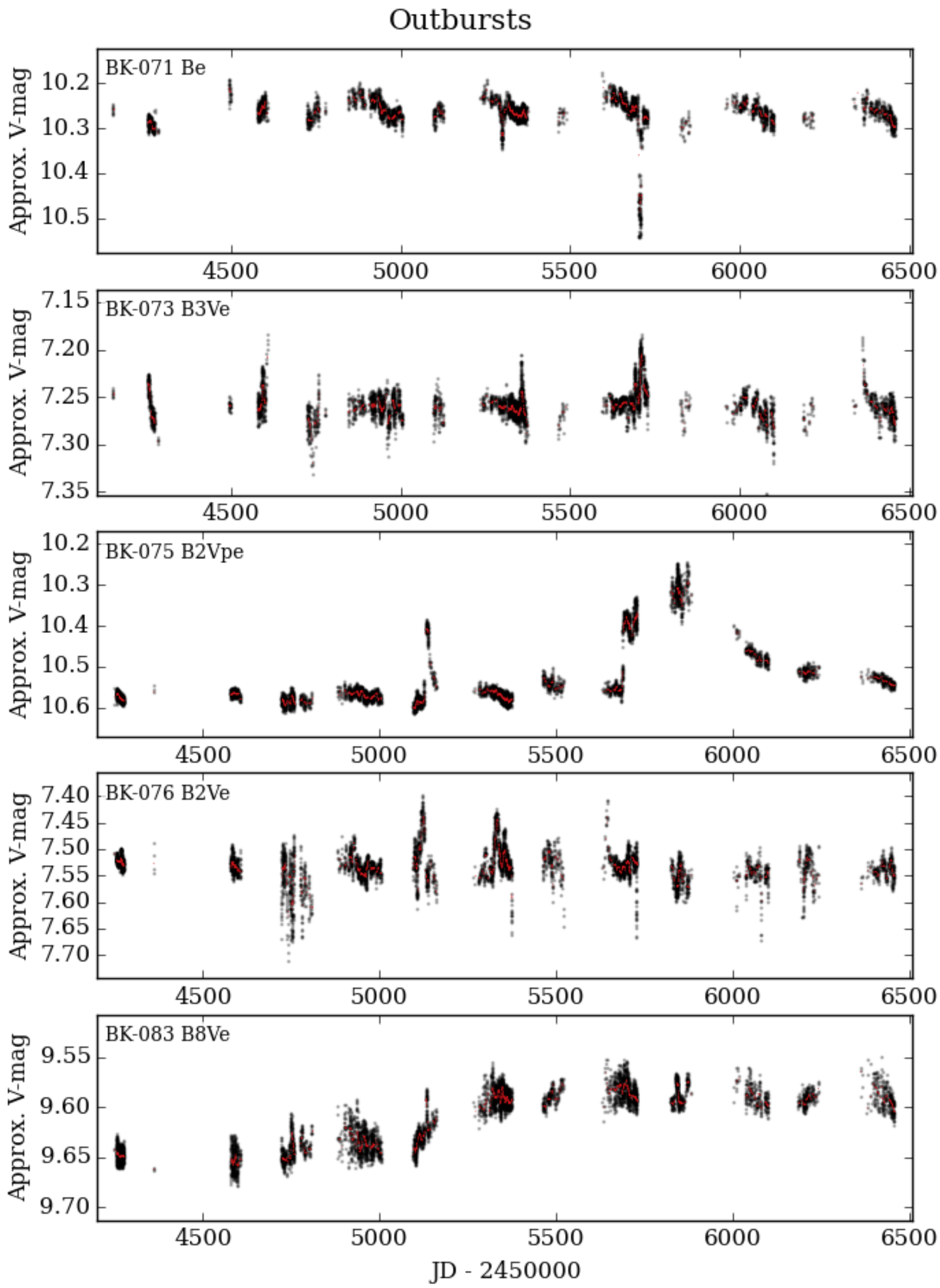
Outbursts
BK-071 Be
Approx. V-mag
BK-073 B3Ve
Approx. V-mag
BK-075 B2Vpe
Approx. V-mag
BK-076 B2Ve
Approx. V-mag
BK-083 B8Ve
Approx. V-mag
JD - 2450000

Figure 4.29: G

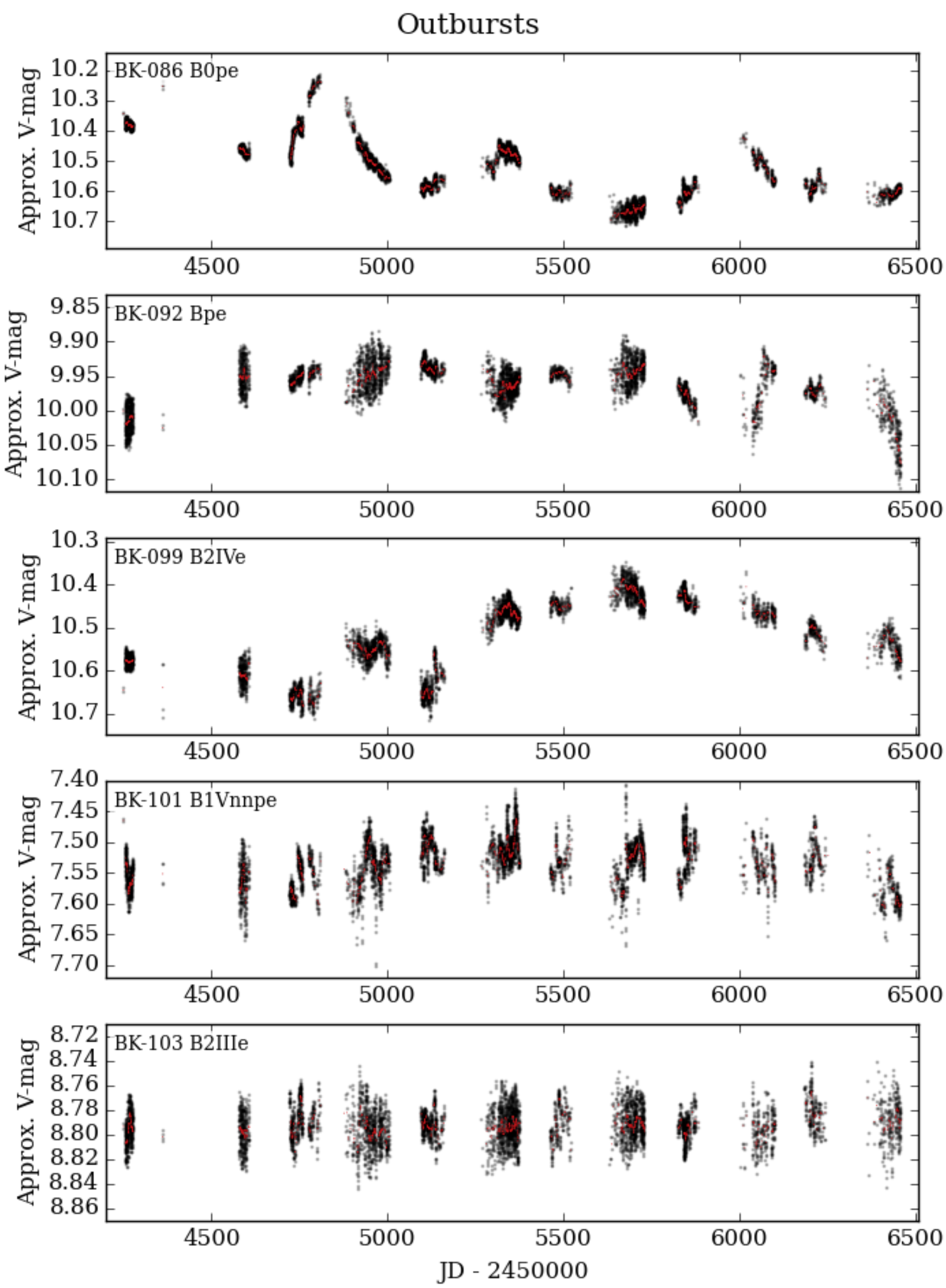

Outbursts
BK-086 B0pe
BK-092 Bpe
BK-099 B2IVe
BK-101 B1Vnnpe
BK-103 B2IIIe
Approx. V-mag
JD - 2450000

Figure 4.29: H

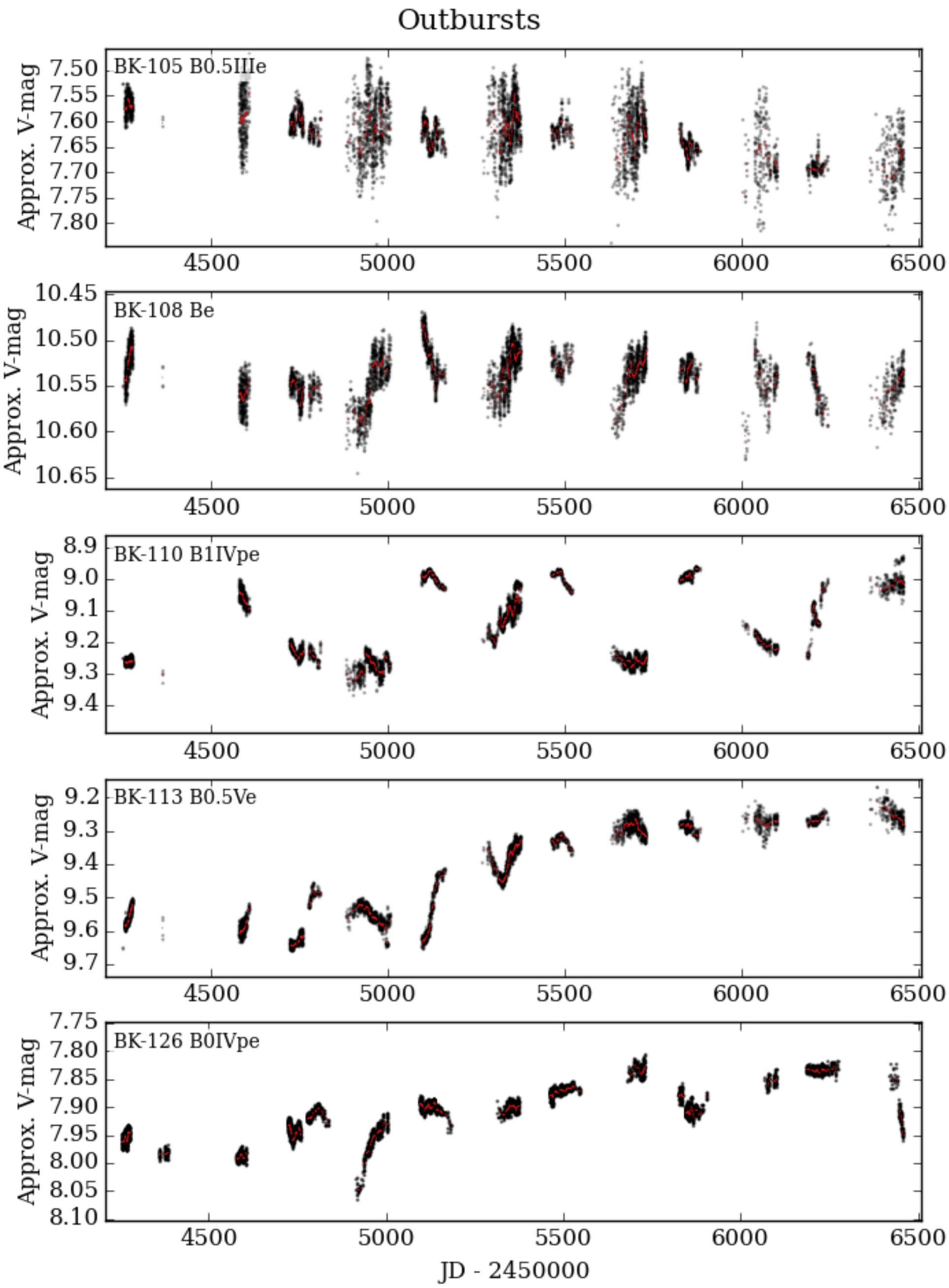
Outbursts
BK-105 B0.5IIIe
BK-108 Be
BK-110 B1IVpe
BK-113 B0.5Ve
BK-126 B0IVpe
Approx. V-mag
JD - 2450000

Figure 4.29: I

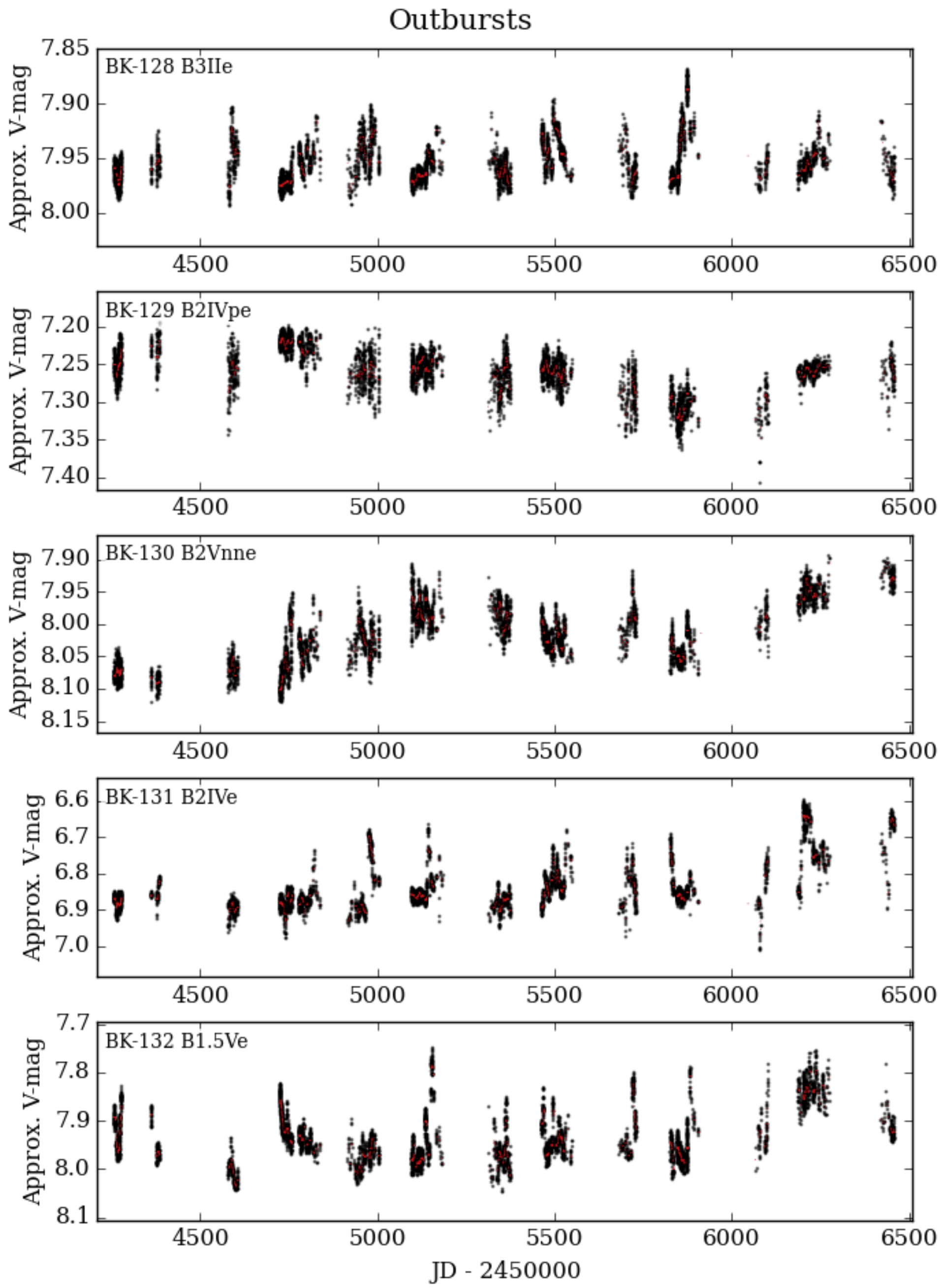

Outbursts
BK-128 B3IIe
BK-129 B2IVpe
BK-130 B2Vnne
BK-131 B2IVe
BK-132 B1.5Ve
Approx. V-mag
JD - 2450000

Figure 4.29: J

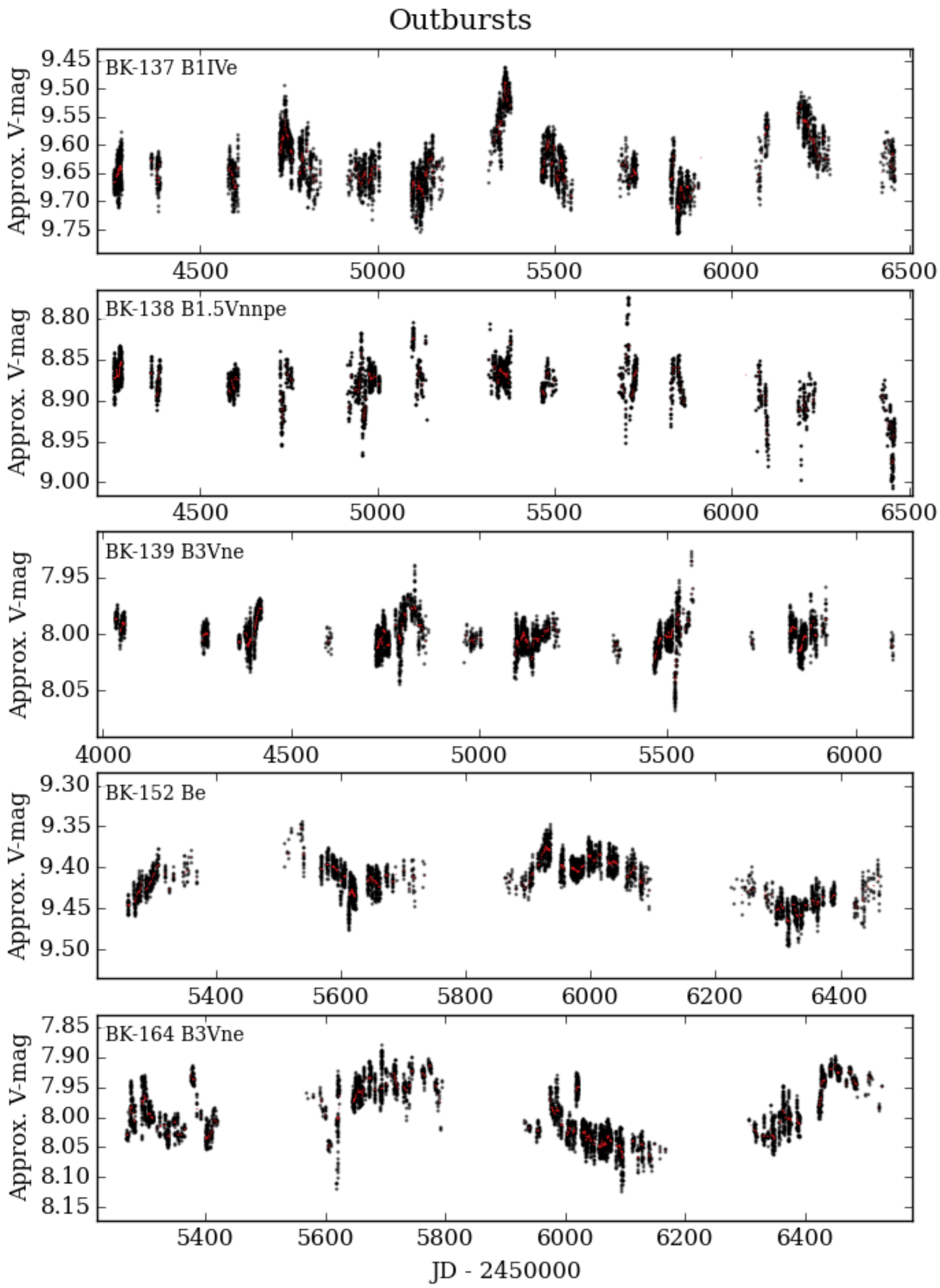
Outbursts
BK-137 B1IVe
BK-138 B1.5Vnnpe
BK-139 B3Vne
BK-152 Be
BK-164 B3Vne
Approx. V-mag
JD - 2450000

Figure 4.29: K

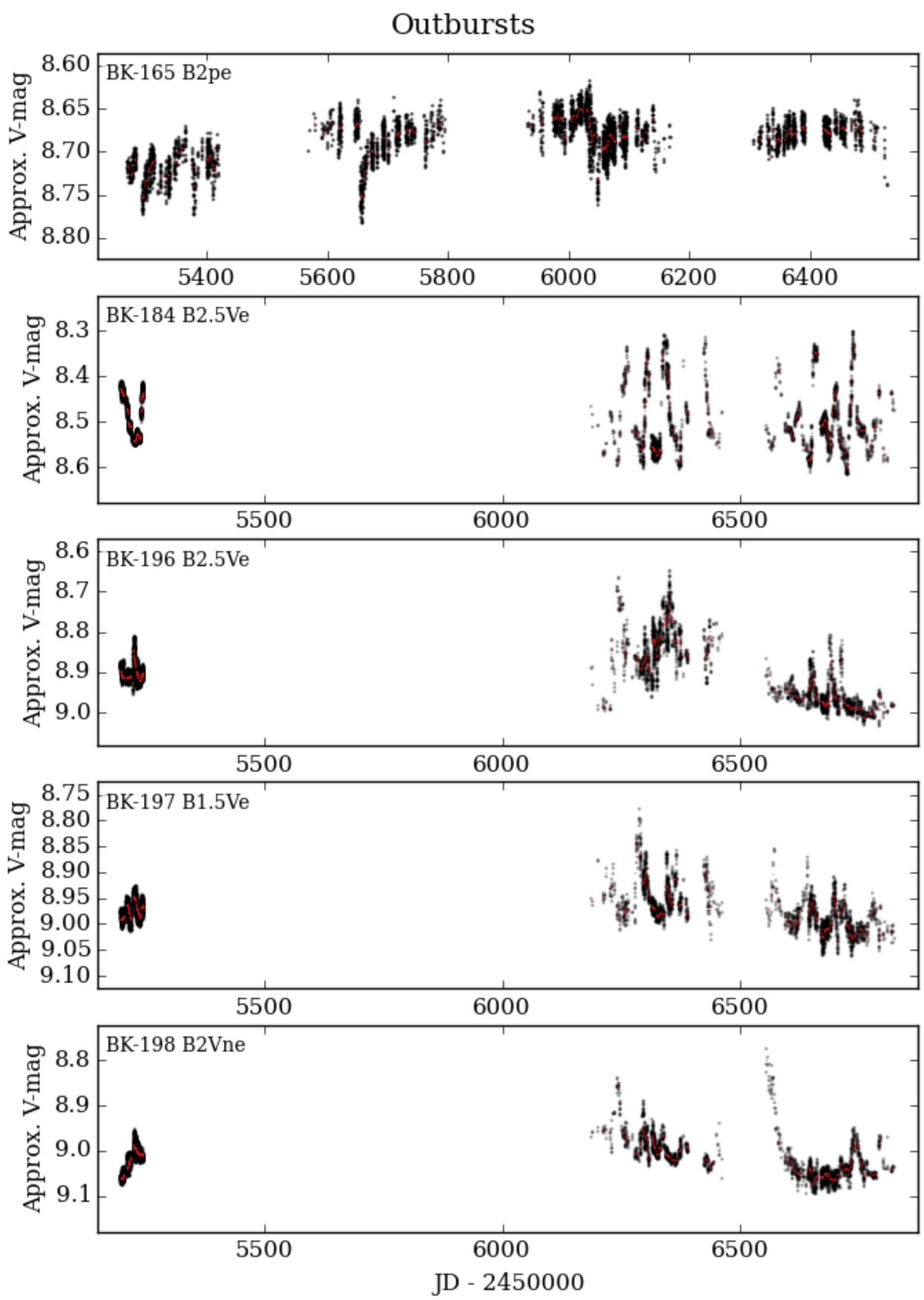

Outbursts
BK-165 B2pe
BK-184 B2.5Ve
BK-196 B2.5Ve
BK-197 B1.5Ve
BK-198 B2Vne
Approx. V-mag
JD - 2450000

Figure 4.29: L

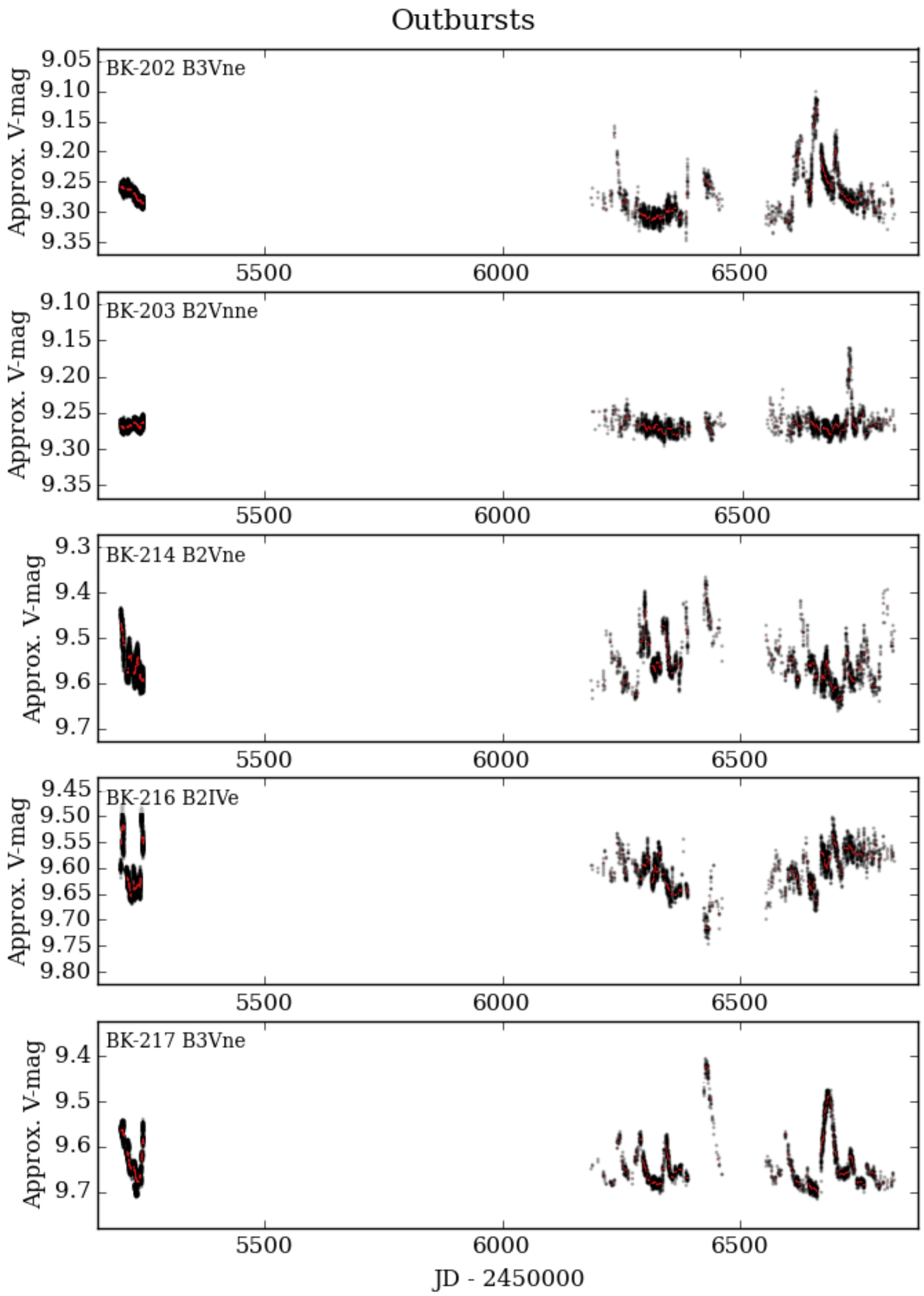
Outbursts
BK-202 B3Vne
BK-203 B2Vnne
BK-214 B2Vne
BK-216 B2IVe
BK-217 B3Vne
Approx. V-mag
JD - 2450000

Figure 4.29: M

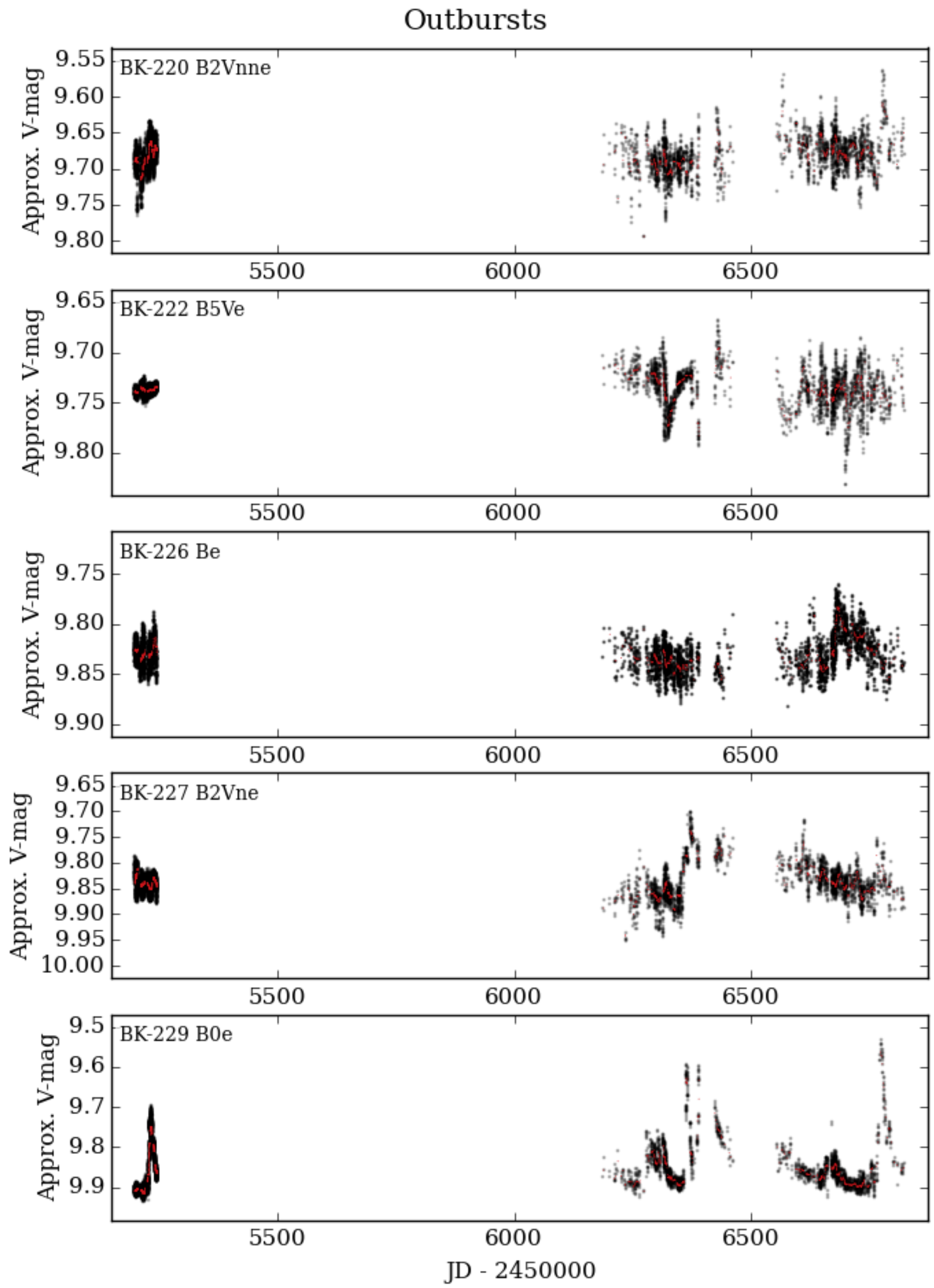
Outbursts
BK-220 B2Vnne
BK-222 B5Ve
BK-226 Be
BK-227 B2Vne
BK-229 B0e
Approx. V-mag
JD - 2450000
5500
6000
6500

Figure 4.29: N

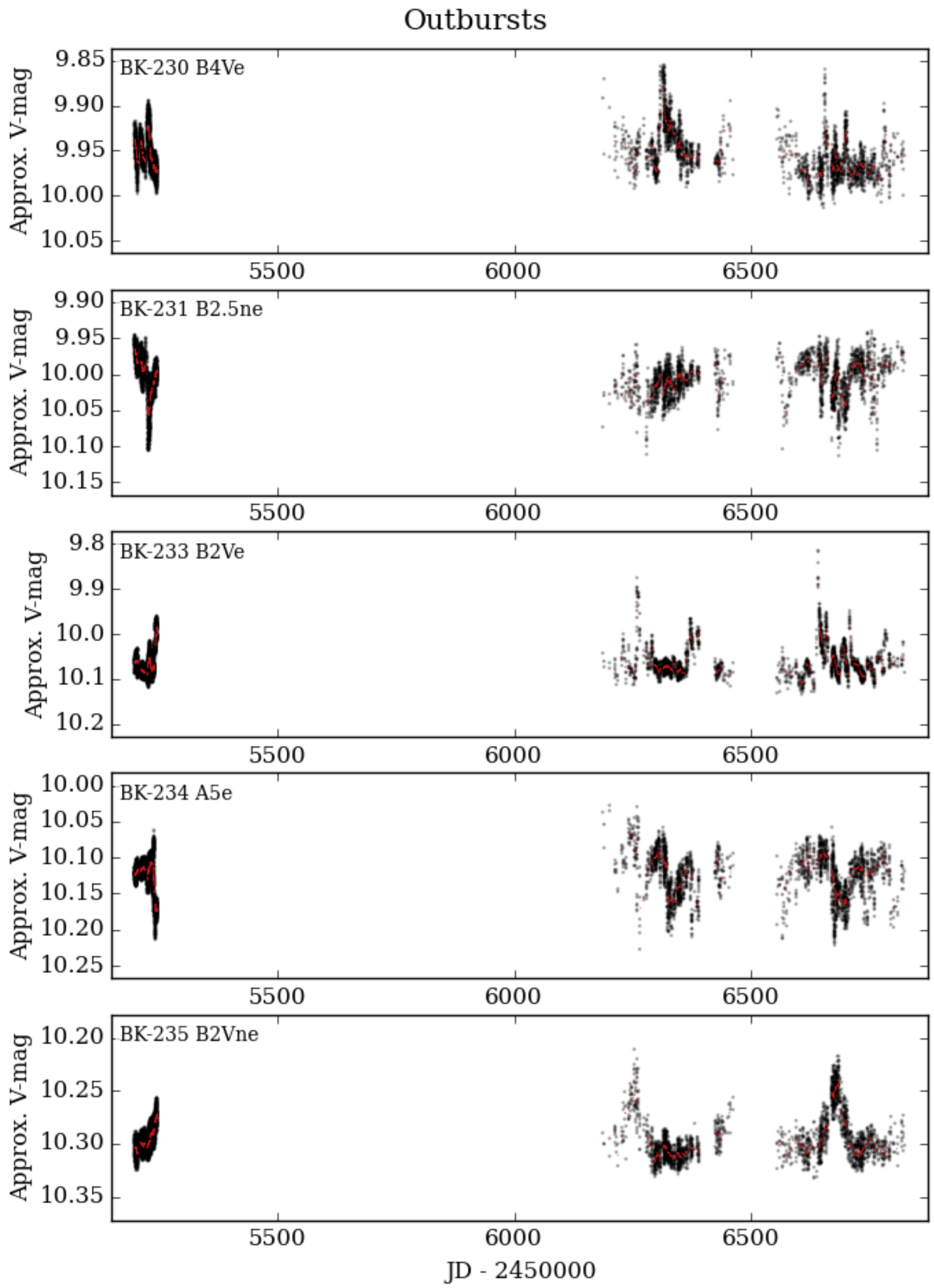
Outbursts
BK-230 B4Ve
BK-231 B2.5ne
BK-233 B2Ve
BK-234 A5e
BK-235 B2Vne
Approx. V-mag
JD - 2450000
5500
6000
6500

Figure 4.29: O

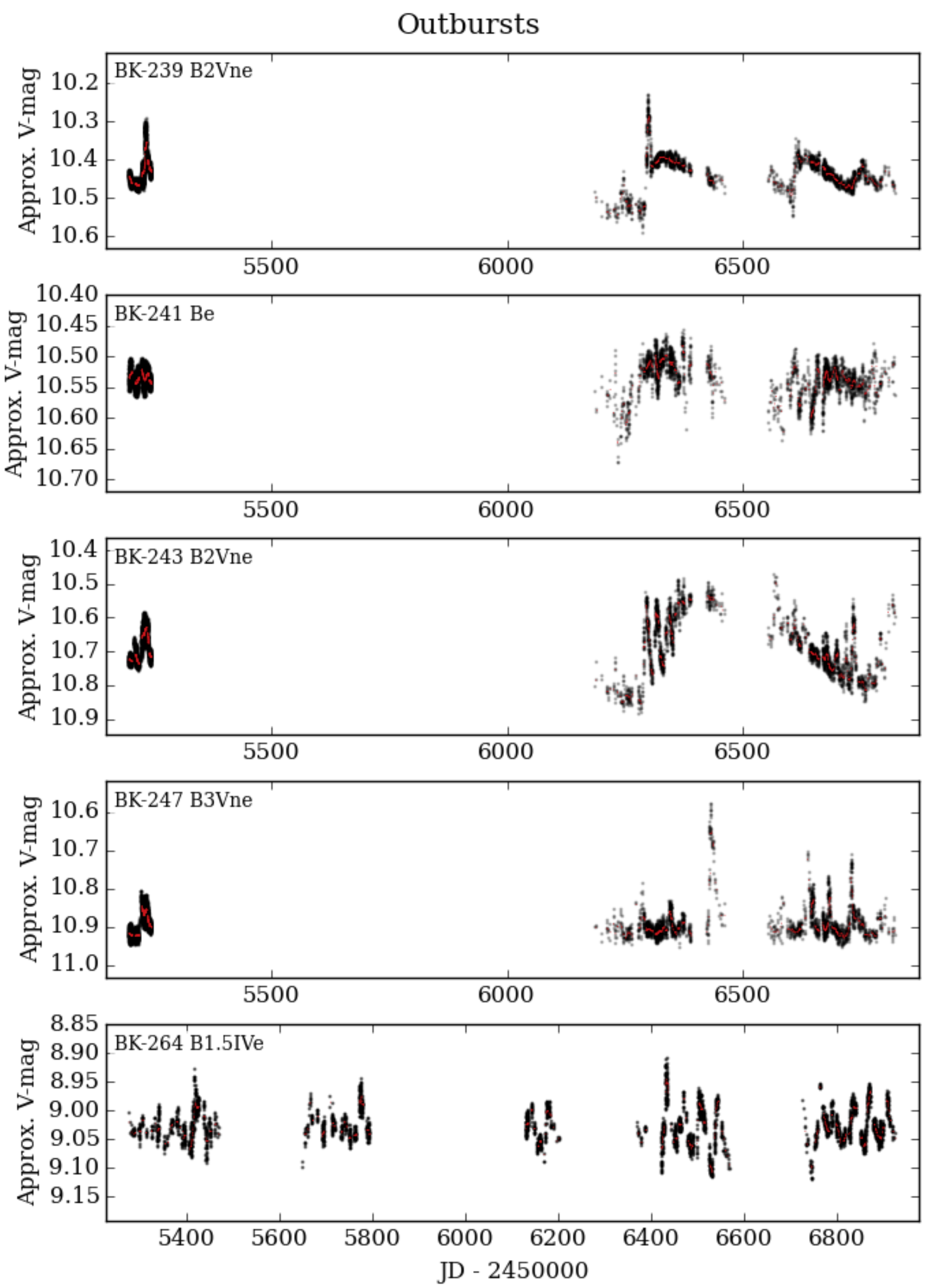

Outbursts
BK-239 B2Vne
BK-241 Be
BK-243 B2Vne
BK-247 B3Vne
BK-264 B1.5IVe
Approx. V-mag
JD - 2450000

Figure 4.29: P

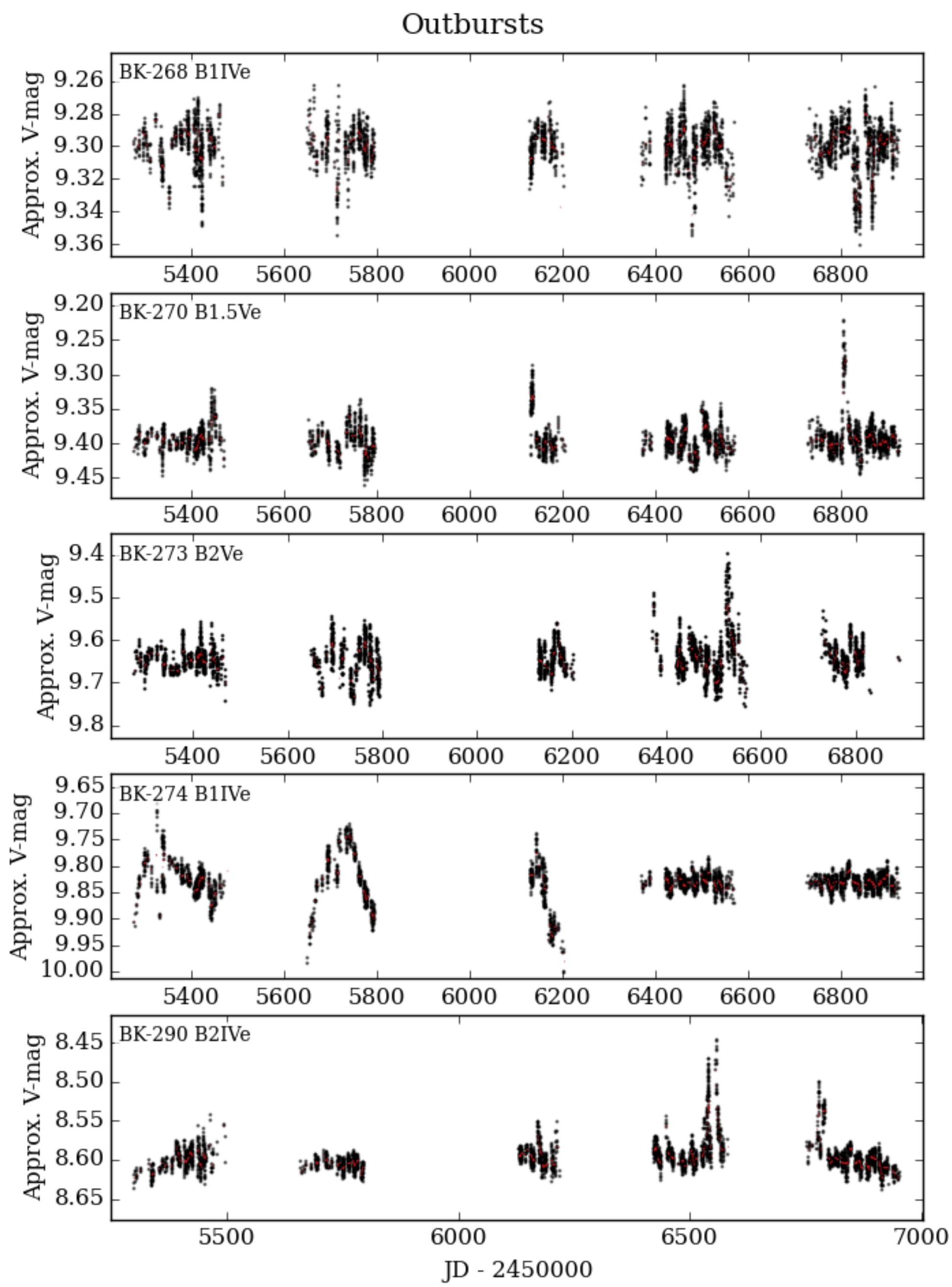

Outbursts
BK-268 B1IVe
BK-270 B1.5Ve
BK-273 B2Ve
BK-274 B1IVe
BK-290 B2IVe
Approx. V-mag
JD - 2450000

Figure 4.29: Q

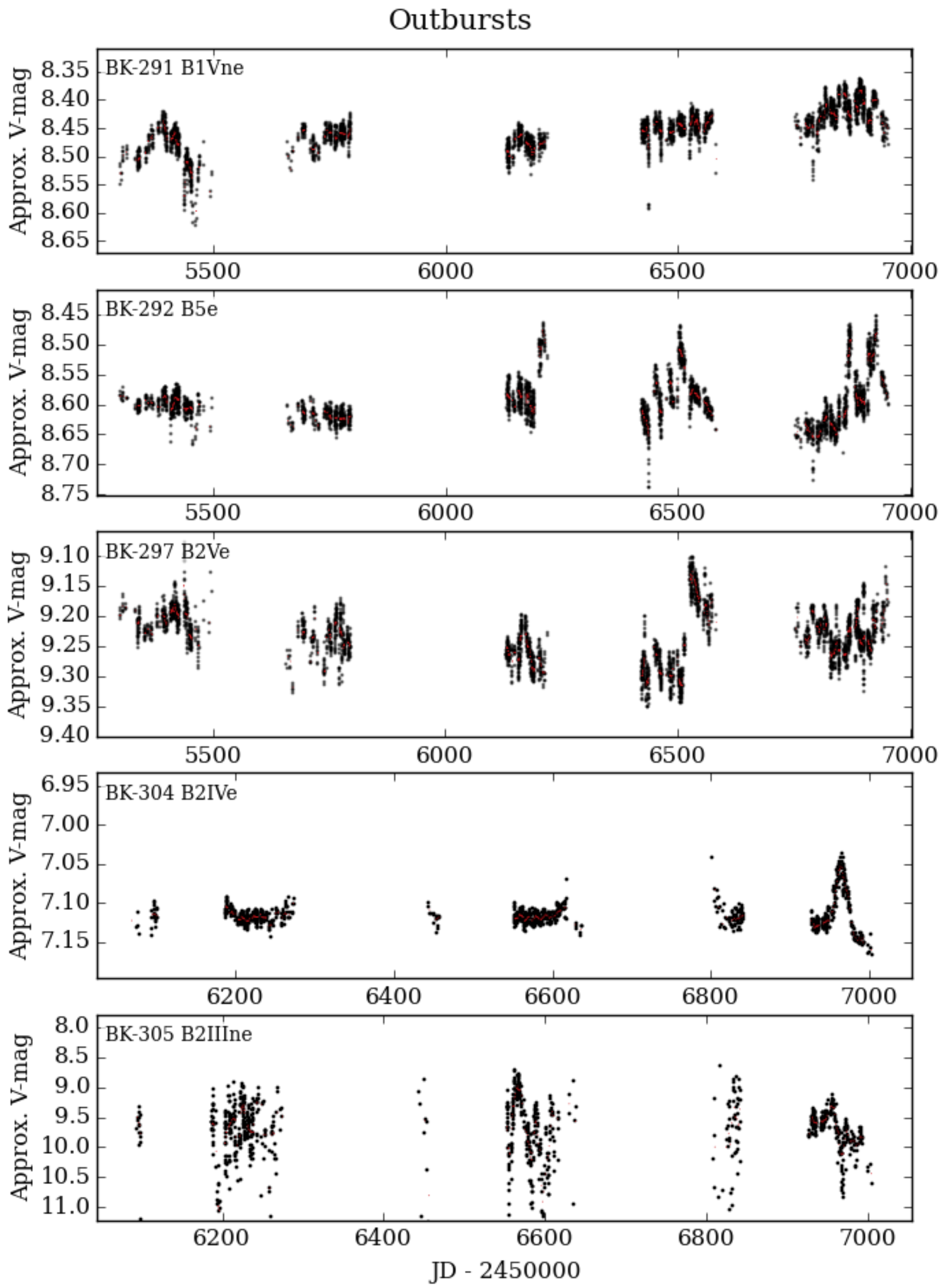
Outbursts
BK-291 B1Vne
BK-292 B5e
BK-297 B2Ve
BK-304 B2IVe
BK-305 B2IIIne
Approx. V-mag
JD - 2450000

Figure 4.29: R

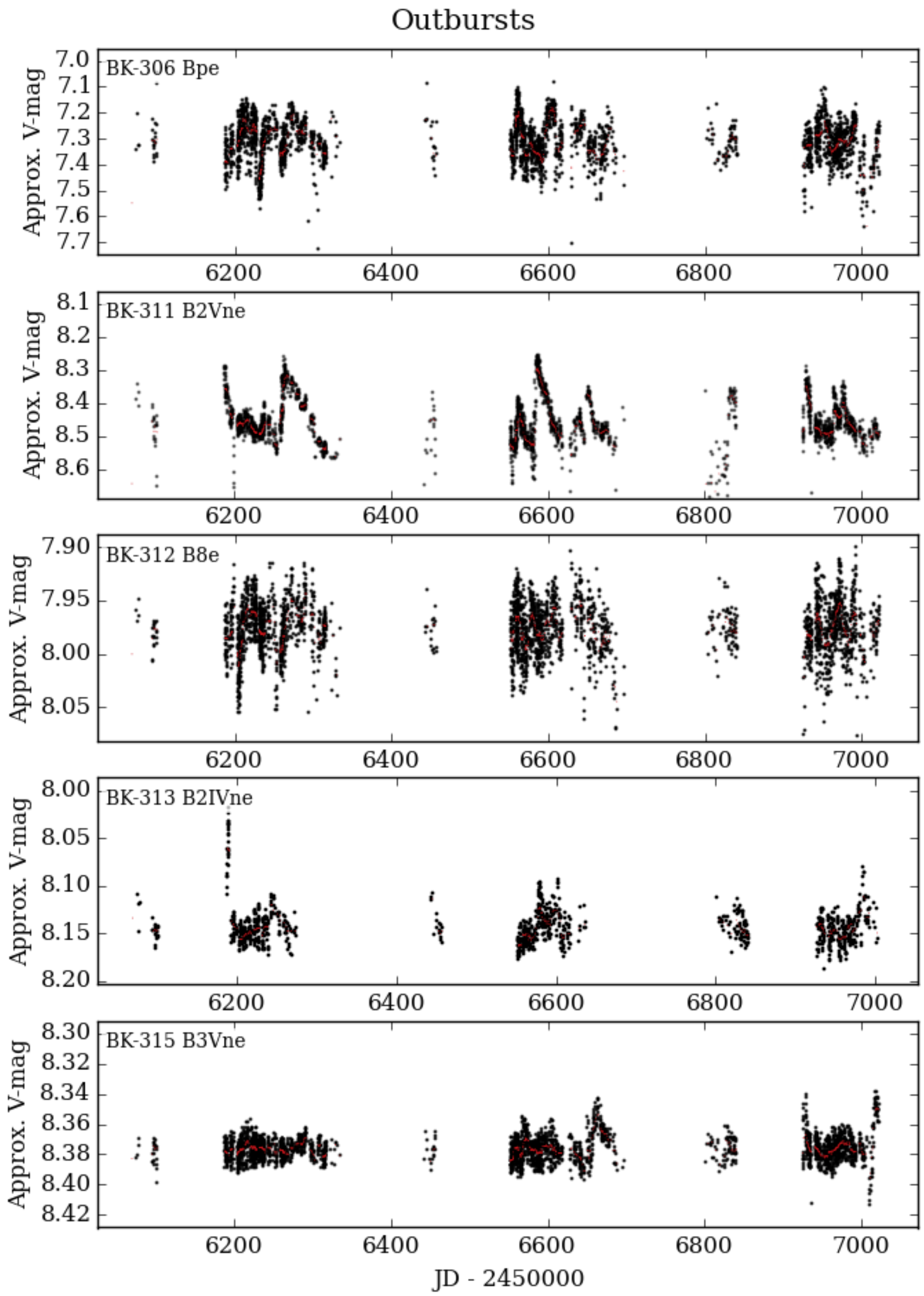
Outbursts
BK-306 Bpe
BK-311 B2Vne
BK-312 B8e
BK-313 B2IVne
BK-315 B3Vne
Approx. V-mag
JD - 2450000

Figure 4.29: S

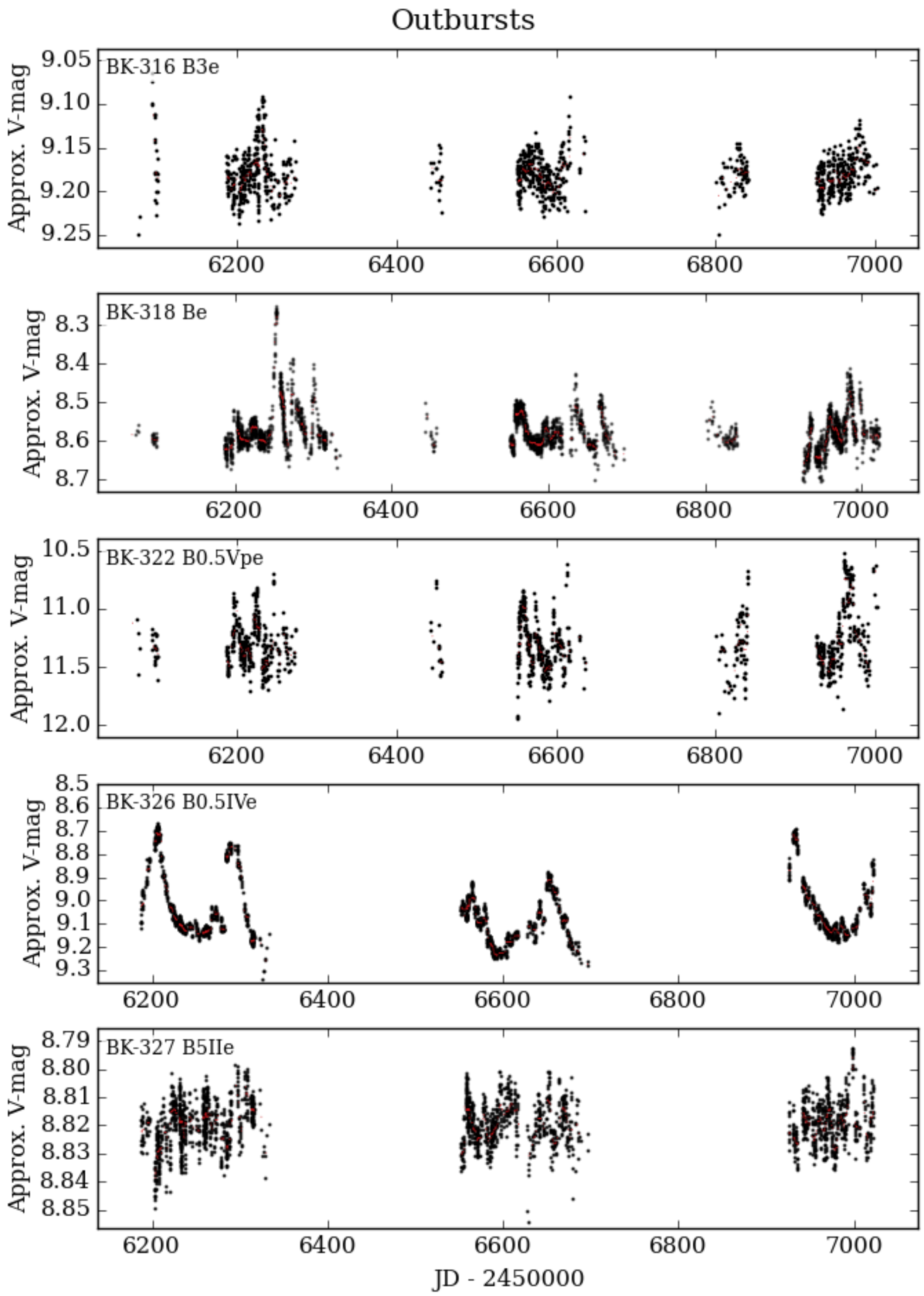
Outbursts
BK-316 B3e
BK-318 Be
BK-322 B0.5Vpe
BK-326 B0.5IVe
BK-327 B5IIe
Approx. V-mag
JD - 2450000

Figure 4.29: T

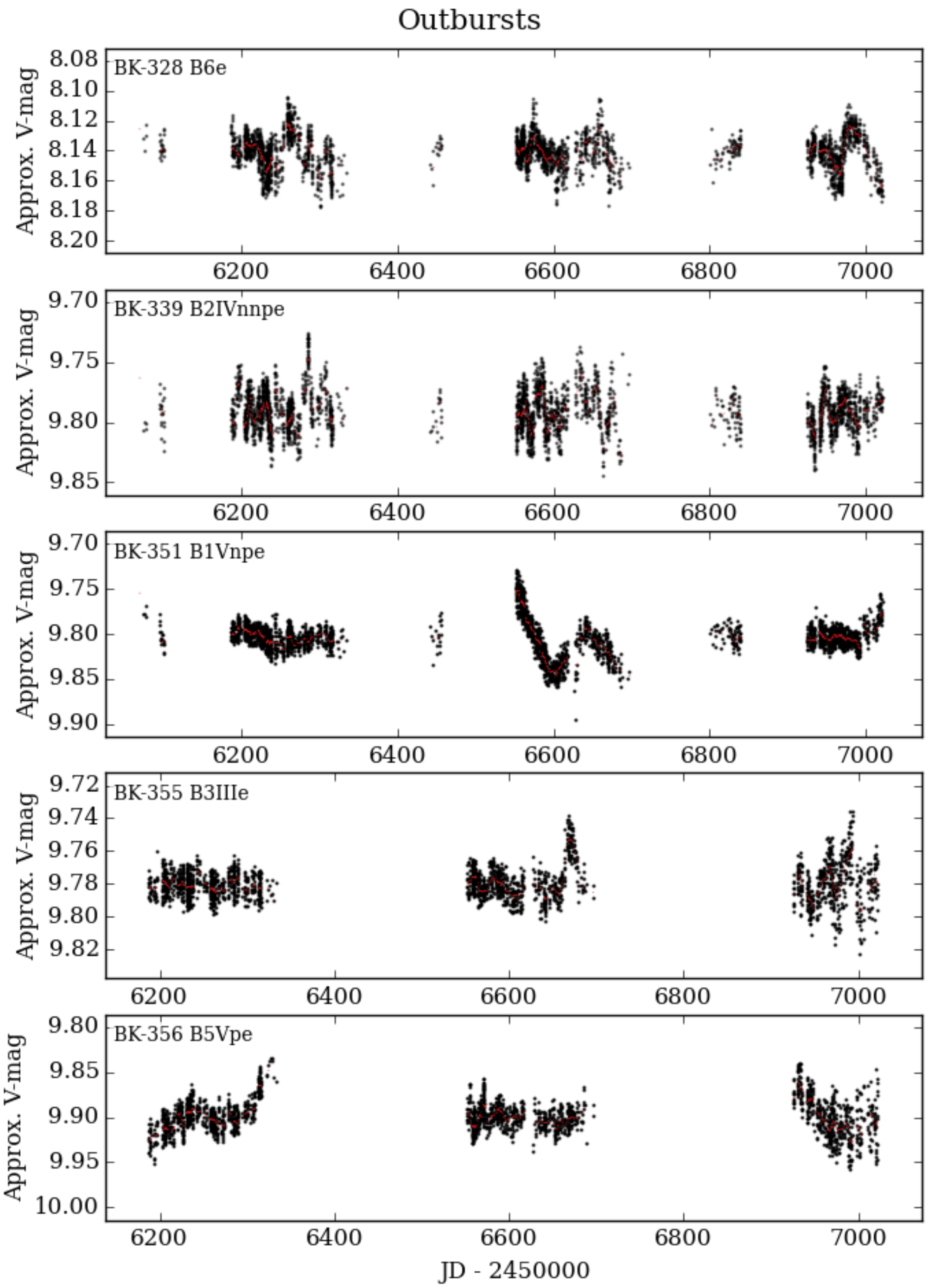

Outbursts
BK-328 B6e
BK-339 B2IVnnpe
BK-351 B1Vnpe
BK-355 B3IIIe
BK-356 B5Vpe
Approx. V-mag
JD - 2450000

Figure 4.29: U

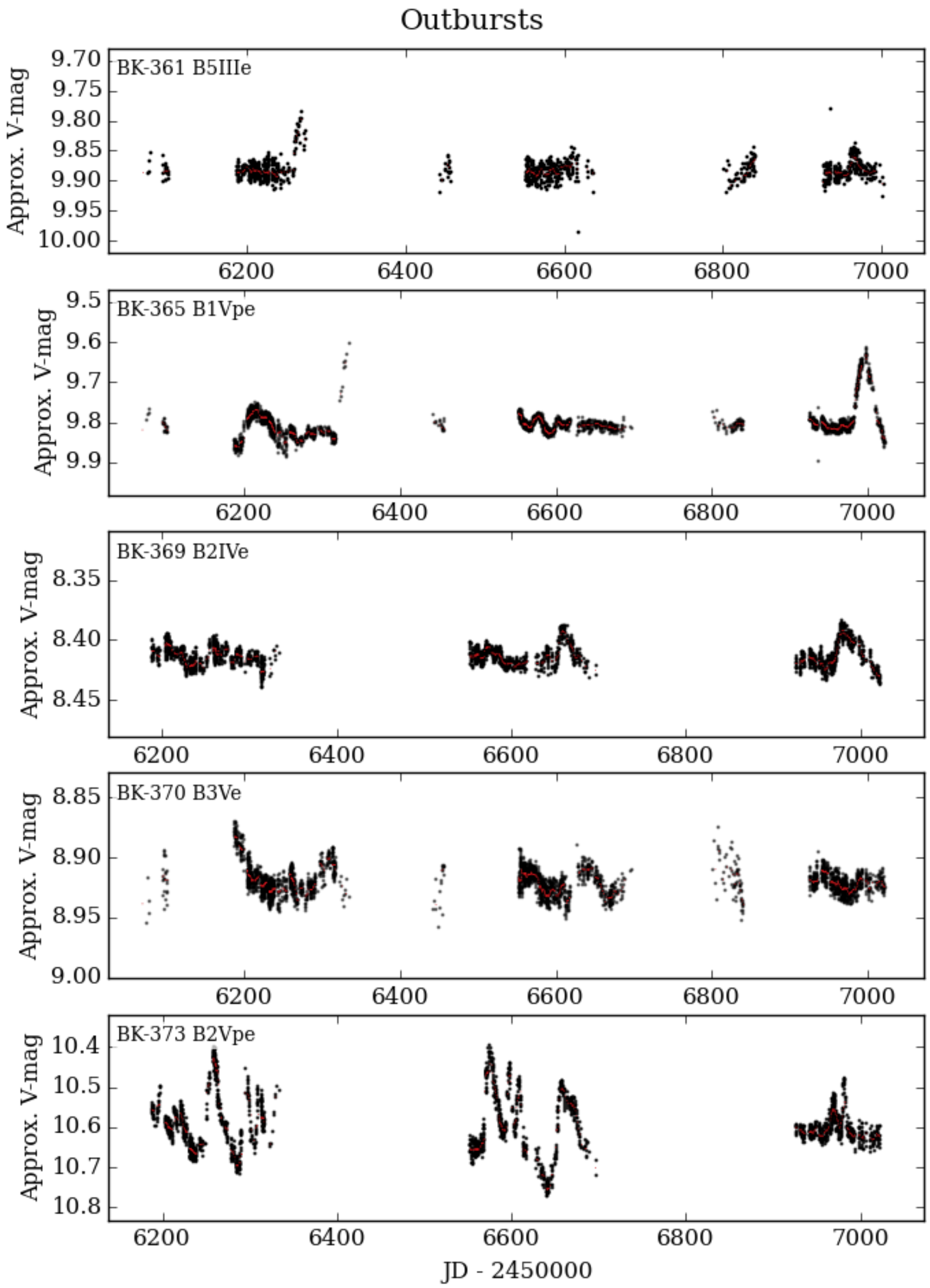

Outbursts
BK-361 B5IIIe
BK-365 B1Vpe
BK-369 B2IVe
BK-370 B3Ve
BK-373 B2Vpe
Approx. V-mag
JD - 2450000

Figure 4.29: V

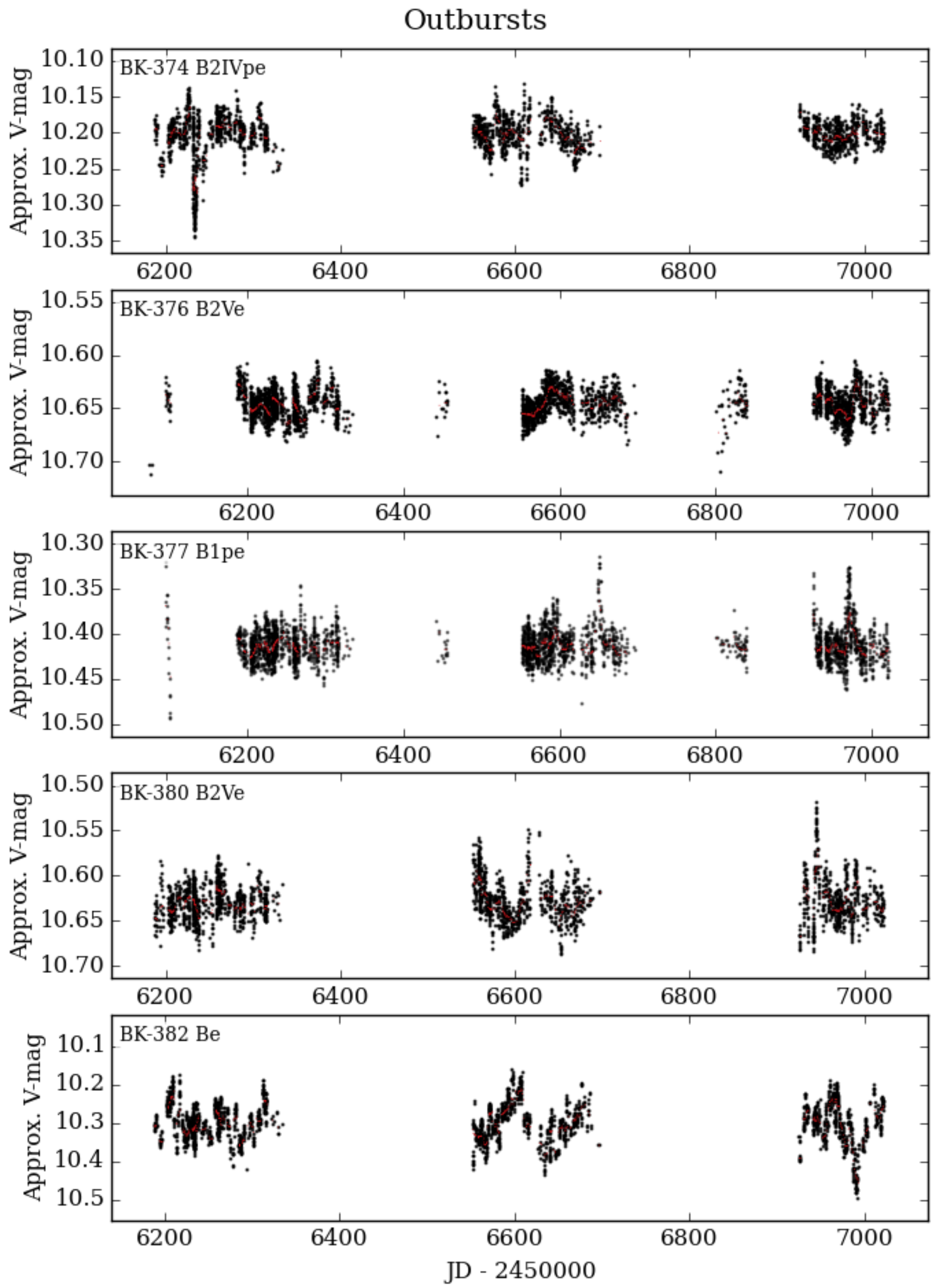
Outbursts
BK-374 B2IVpe
BK-376 B2Ve
BK-377 B1pe
BK-380 B2Ve
BK-382 Be
Approx. V-mag
JD - 2450000

Figure 4.29: W

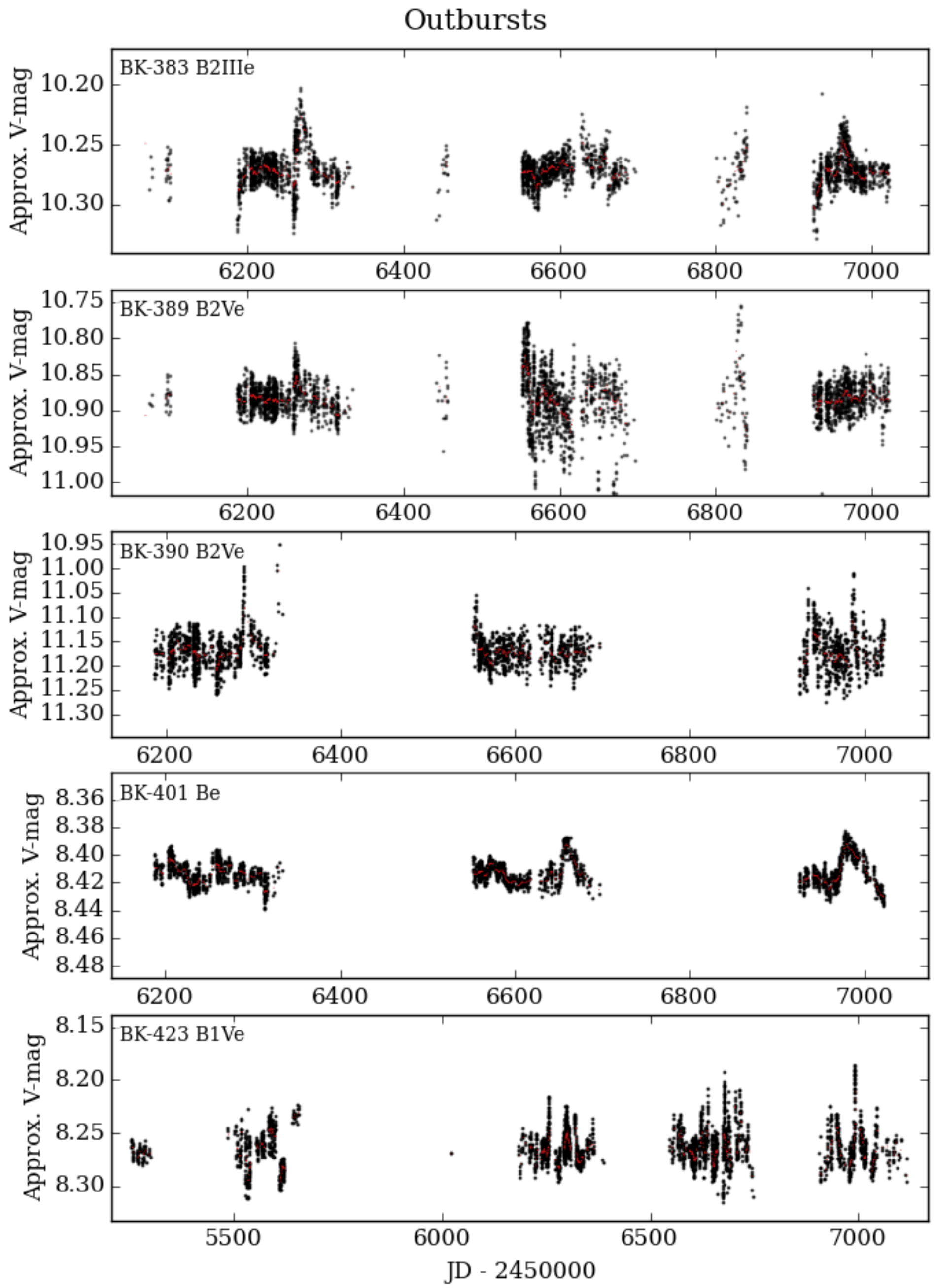
Outbursts
BK-383 B2IIIe
BK-389 B2Ve
BK-390 B2Ve
BK-401 Be
BK-423 B1Ve
Approx. V-mag
JD - 2450000

Figure 4.29: X

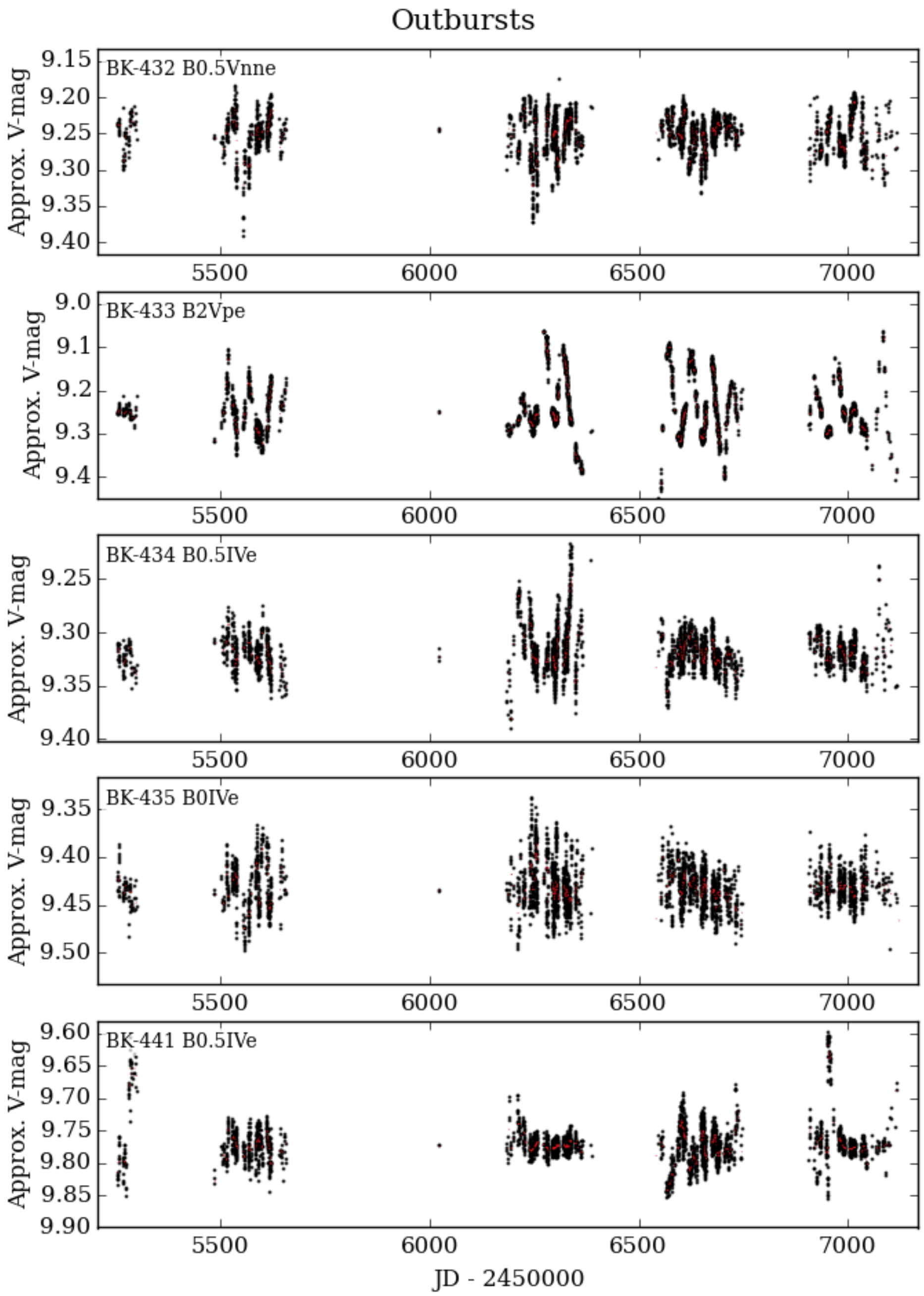

Outbursts
BK-432 B0.5Vnne
BK-433 B2Vpe
BK-434 B0.5IVe
BK-435 B0IVe
BK-441 B0.5IVe
Approx. V-mag
JD - 2450000

Figure 4.29: Y

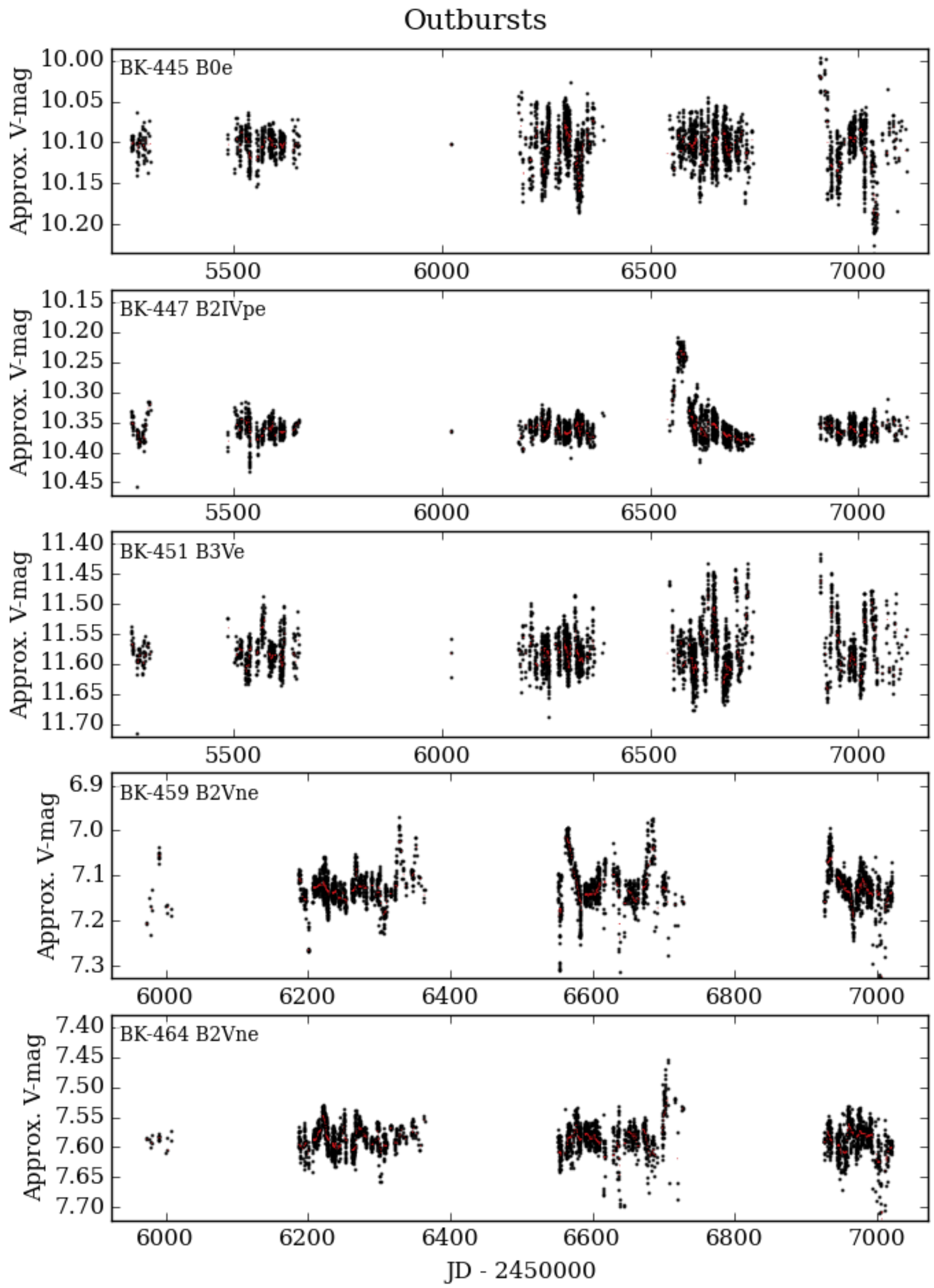
Outbursts
BK-445 B0e
BK-447 B2IVpe
BK-451 B3Ve
BK-459 B2Vne
BK-464 B2Vne
Approx. V-mag
JD - 2450000

Figure 4.29: Z

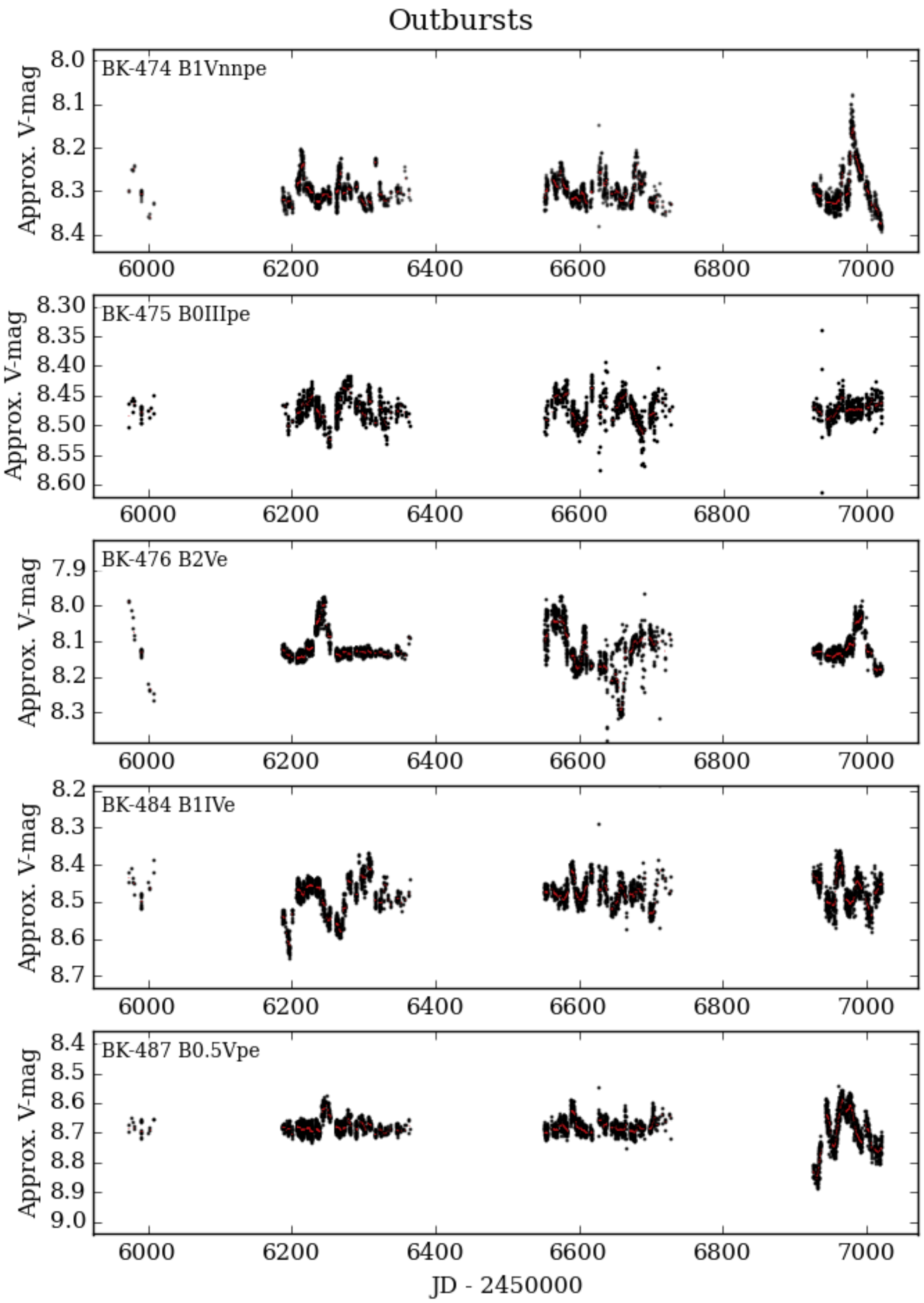

Figure 4.29: AA

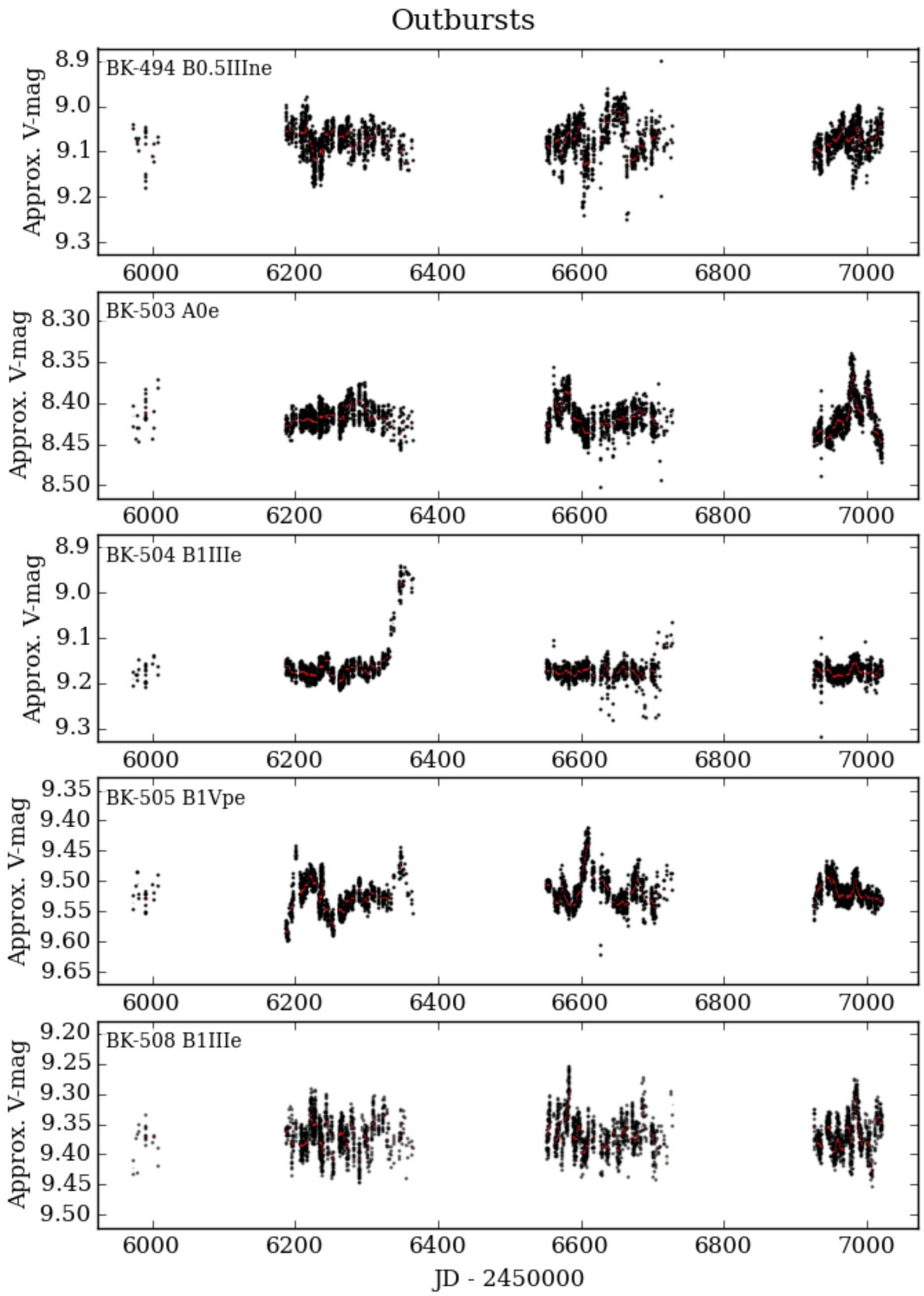

Figure 4.29: AB

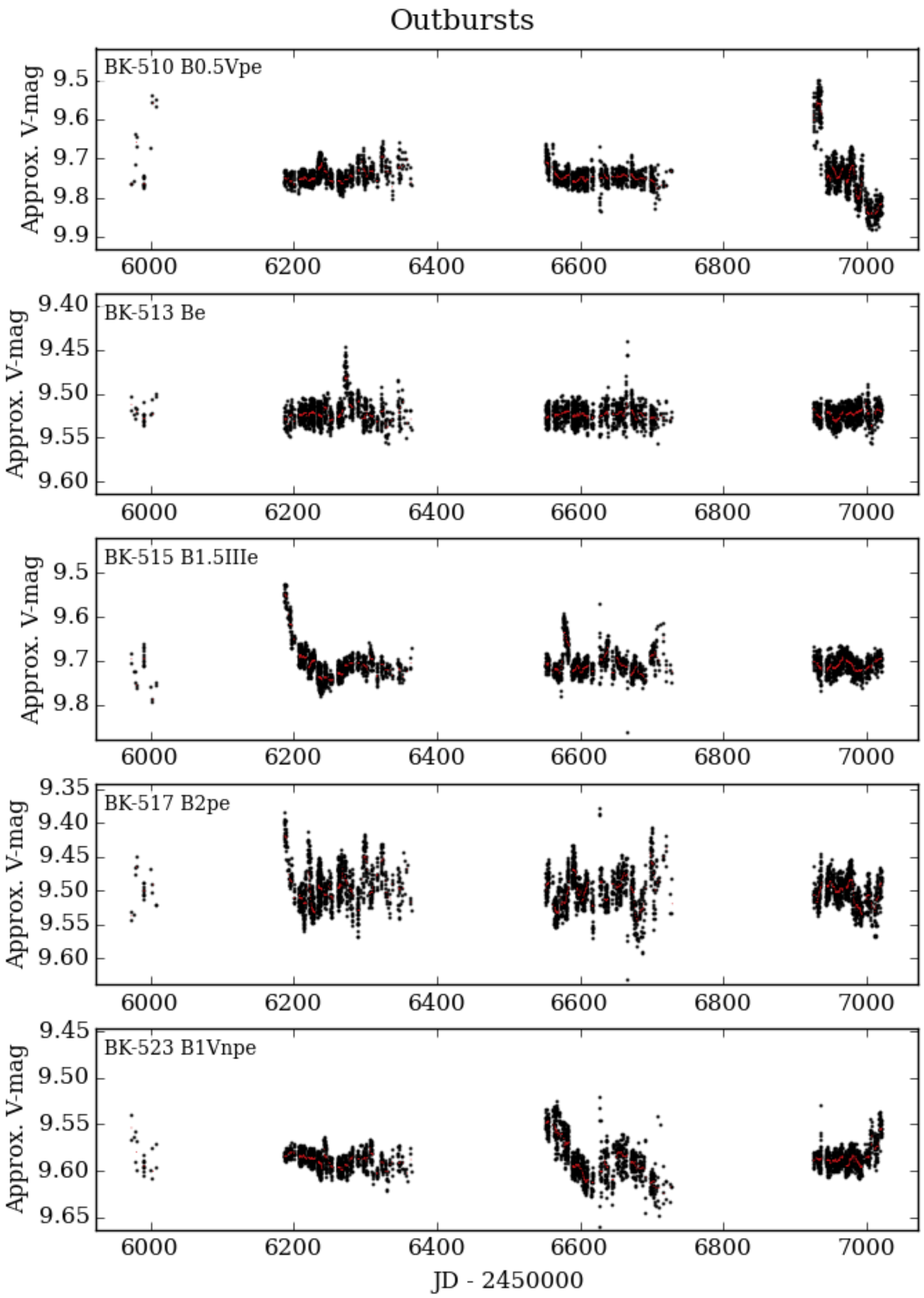

Figure 4.29: AC

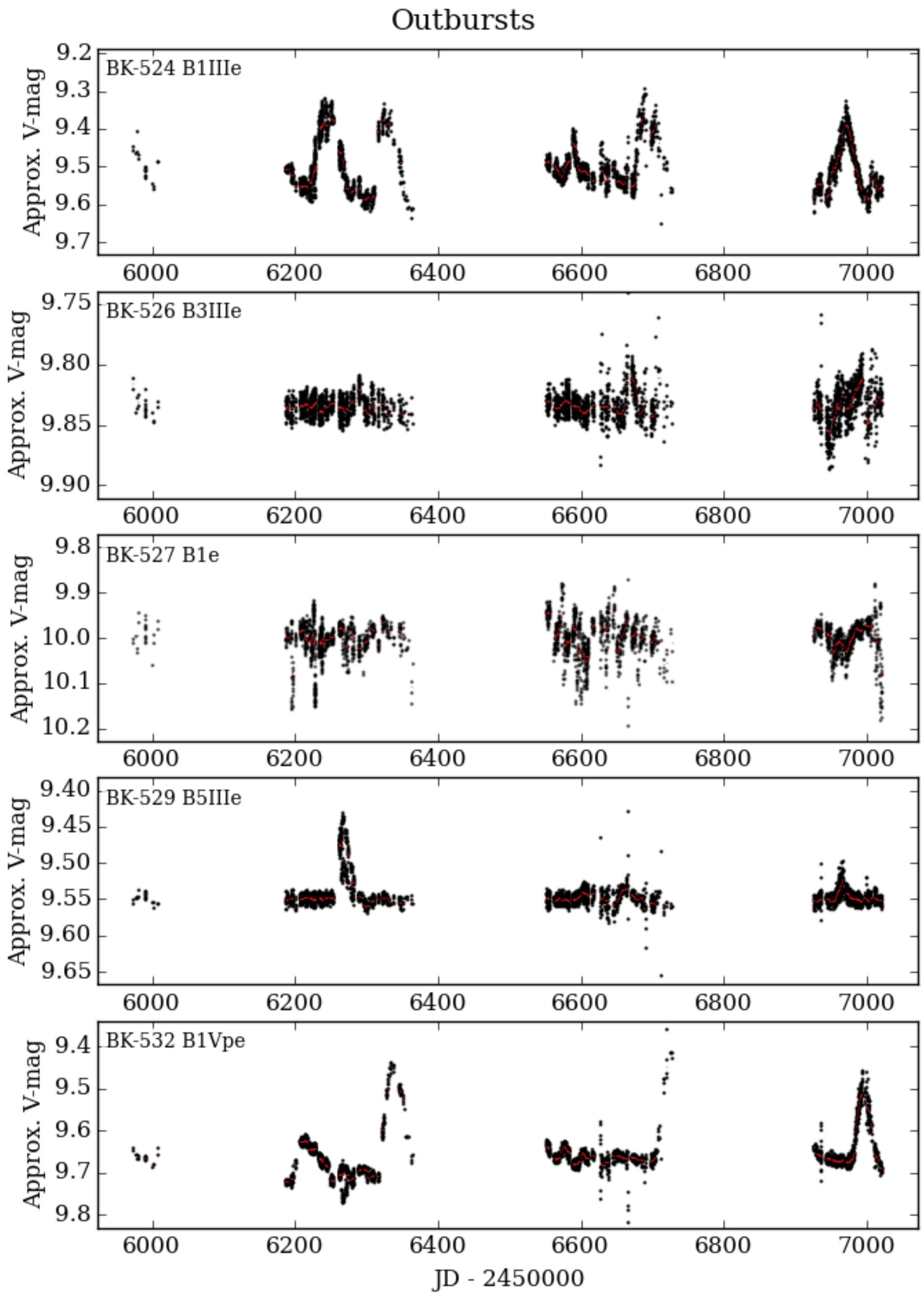

Figure 4.29: AD

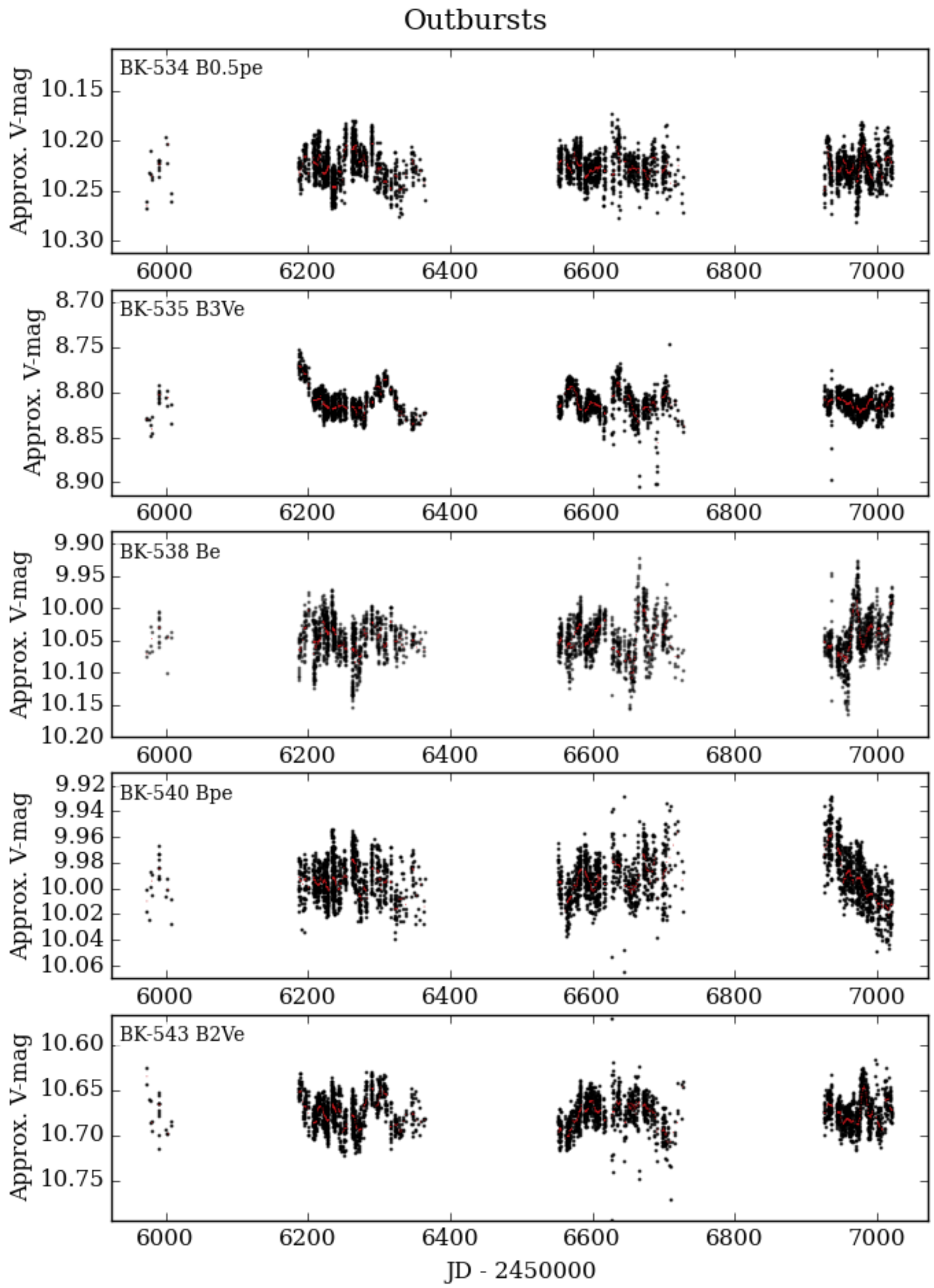

Figure 4.29: AE

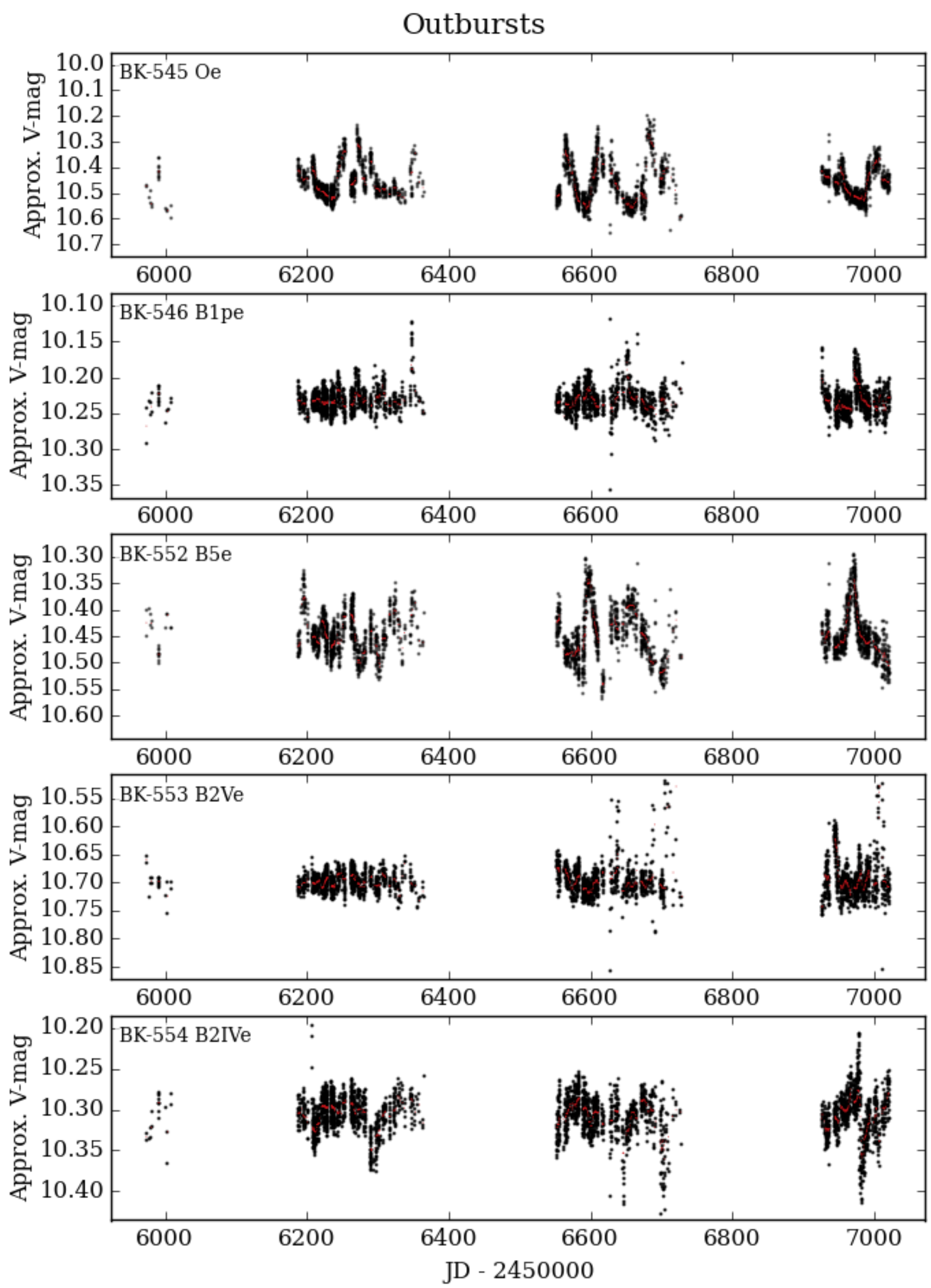

Figure 4.29: AF

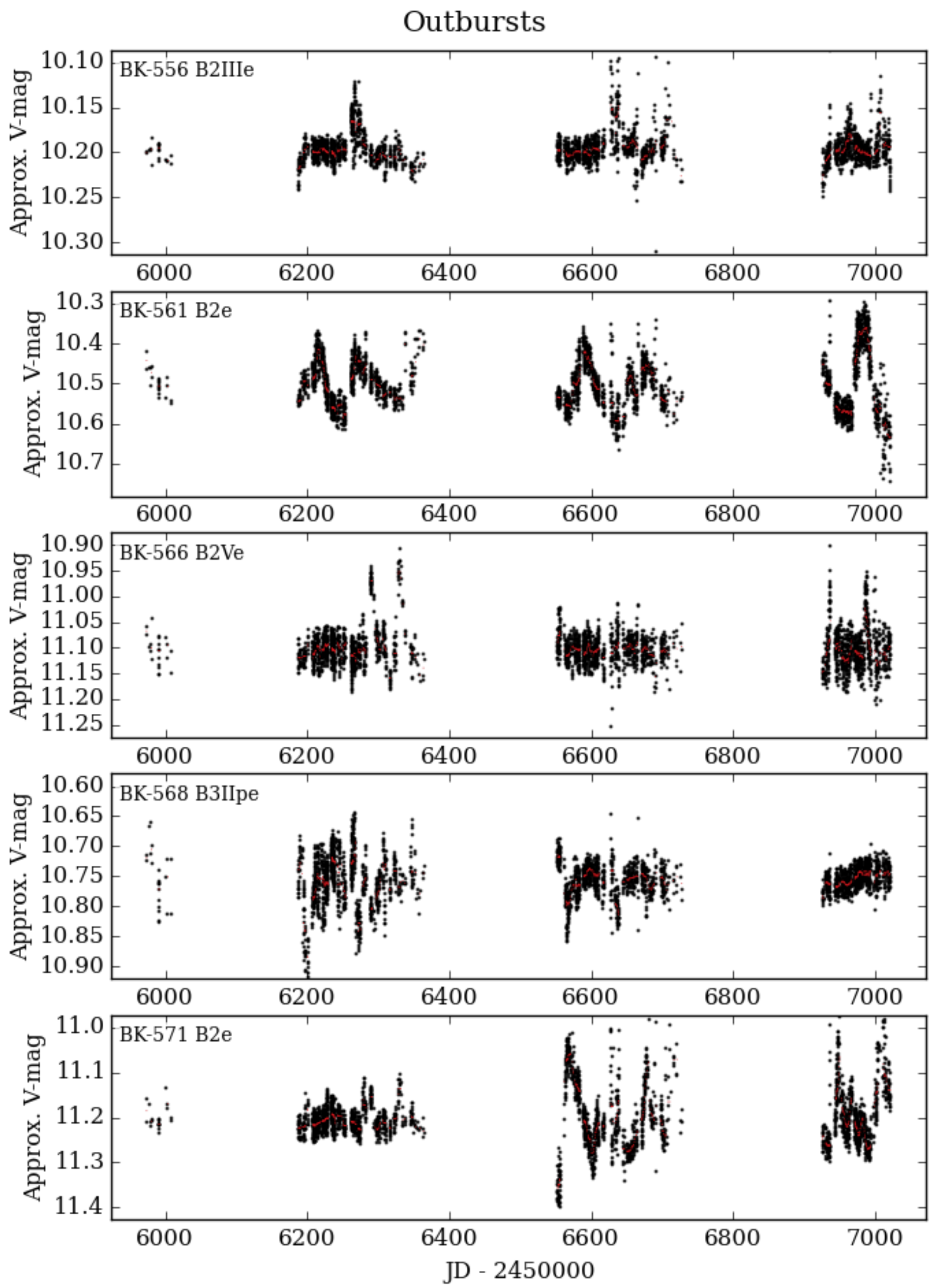

Figure 4.29: AG

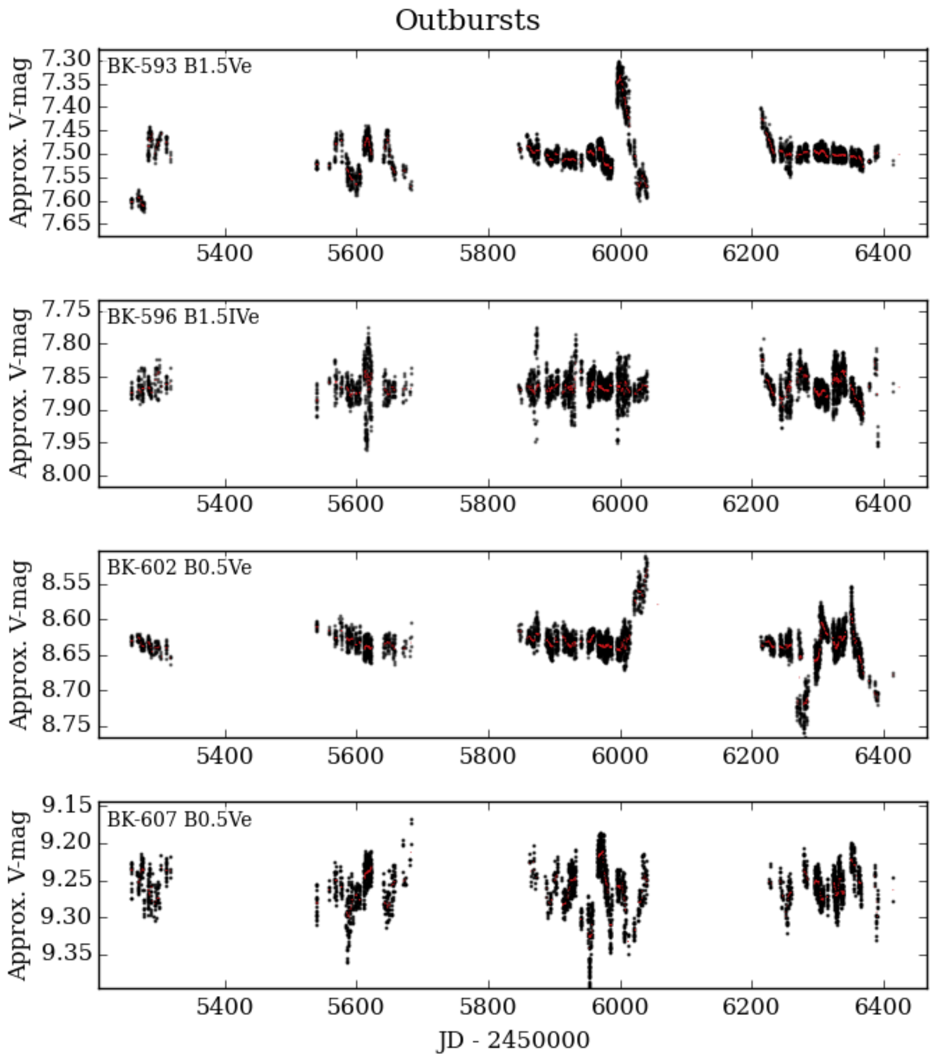

Figure 4.29: AH

Chapter 5

Long-Term Variation

Be star systems are known to be variable over long timescales of many years or decades. Variation on these timescales originates in the disk. Be stars sometimes transition from having a disk, to losing all observational evidence of a disk. This does not mean that such a system ceases to be a Be star, but is simply in a disk-less state. For such a system, at some point the "Be phenomenon" may turn back on, and the star will once more have a disk. Be stars that retain a disk for long times often find their disk varying in strength over years, presumably as the mass-loss rate of the star changes (McSwain et al. 2008; McSwain et al. 2009). Even systems that maintain a near-constant Hα EW (and therefore an approximately constant disk mass) sometimes show long-term variation in line morphology, particularly in the ratio of the violet to red emission peaks (V/R ratio). Such V/R variations are sometimes cyclic, with timescales on the order of 10 years. These cycles are generally attributed to one-armed spiral density waves (m=1 oscillation modes) in the disk (Okazaki 1991; Papaloizou et al. 1992).

The long baseline of KELT light curves allows for the detection of long-term variability (LTV) on the order of years. Variability at these timescales is generally attributed to changes in the circumstellar disk including growth, dissipation, and/or density oscillations (Haubois et al. 2012a). This behavior is well-known in spectroscopy, but is not as well studied photometrically. The raw KELT light curves for all stars in the BK sample were visually inspected for signs of LTV. Some systems remain photometrically stable for years, then begin to gradually dim or brighten at a rate of a few hundredths of a magnitude per year. Some systems seem to oscillate around an average brightness, while others show gradual variability interspersed with outbursts of relatively high amplitude. We classify all such stars as belonging to the LTV category, so long as we have a photometric baseline of at least four years.

From the 217 light curves in the BK sample that have a long enough baseline (4+ years) to detect LTV, we find that 80, or 37%, of systems belong to this category. Splitting this by spectral sub-types, LTV is detected in 45% of early-type, 29% of mid-type, and 13% of late-type stars. An example of oscillatory LTV is shown in Figure 5.1, for the star BK-052 (HD 33232). The upper panel shows that the light curve exhibits a slow oscillation in brightness, the timescale of which is comparable to cyclic V/R variation seen in some Be star disks (Štefl et al. 2009).

BK-052 also has spectroscopic measurements in BeSS, which are taken over a baseline of about six years. These spectra show variability in the V/R ratio of the Hα line (lower panel of Figure 5.1) at a timescale similar to that of the photometric variability. These contemporaneous observations support the idea that the same mechanism (global density oscillations in the circumstellar disk) can be responsible for the long term variability seen in both the V/R ratio in the emission line profile and the coherent gradual changes in brightness of the system. While the Hα line varies in its V/R ratio, the overall strength of Hα emission is relatively constant, indicating that the disk as a whole is neither growing nor dissipating in a significant manner over the $\sim$6 years of spectroscopic observation. Be star disks do dissipate over time, so in order for the disk surrounding this star to exist in a quasi-steady state for six years there must occasionally be mass transferred to the disk. However, no outbursts are detected in the KELT light curve for this star. We suspect that this system does experience mass loss events, but with amplitudes below the detection threshold of the KELT light curve. Or, perhaps this system sheds mass in a more continuous fashion. Merrill (1952) analyze spectra for this system, tracing the emission profile of the Hβ line (among others) between 1943 - 1952. They find a similar oscillatory trend where the relative strength of the V and R peaks varies, which is consistent with the idea of a density wave moving around the disk.

The line profile of BK-052 indicates that this system is viewed at a high inclination angle, because the central depression reaches down to approximately the continuum level. It is therefore likely that the star is partially obscured by the disk. While KELT data is generally sensitive to only the inner disk, the situation becomes more complicated for systems viewed nearly edge-on. Disk material, even at large distances from the star, will scatter and absorb continuum photons. Because of this, changes in the column density of the disk along our line of sight will potentially modulate the observed brightness. It is therefore unclear what exactly is the cause of the changing brightness. We know that there is a global density wave in the disk, as revealed by the slow changes in the V/R ratio of the Hα line, but it is not clear how the inner regions of the disk behave.

Haubois et al. (2012b) examine long-term photometric variability in the Be star 48 Lib, claiming correlations between its color and magnitude, and the long-term V/R variation. The authors comment that there is no indication the variability is caused by changes in the mass injection rate, but attribute the photometric variability to an azimuthal structure in the disk (one-armed density wave; Okazaki 1991). They also note that the Hα equivalent width and emission height were constant. Mennickent et al. (1994) also monitor 48 Lib over a long baseline of $\sim$8 years, and observe long-term trends in both brightness and the V/R ratio. The authors note that there is a possible relation between intermediate brightness levels corresponding to extrema of V/R. Put another way, maximum and minimum brightness seems to occur when V/R is near unity. The same authors note the opposite trend in another Be star (V1294 Aql), where brightness extrema correspond to V/R extrema. The case for HD 33232 appears different than both of these. The first photometric minimum roughly corresponds to a V/R maximum, and when V/R is near unity the system is near a photometric maximum. Some combination of spiral-shaped density waves and different disk densities and inclination angles may be a reasonable explanation for the differing phase delays between photometric and V/R extrema in the three aforementioned systems.

In the previous chapter we have seen many instances where a Be star initially has no substantial disk, and then forms a disk through mass-loss episodes. Alternatively, a Be star may support a somewhat stable disk for years, followed by a quiescent period where stellar mass-loss is significantly diminished. Figure 5.2 shows such a case, where the brightness is nearly constant for the first 4 seasons of KELT observations. A spectrum from BeSS is available, taken during the fourth season of the light curve. Although this spectrum is of low resolution, it clearly shows Hα in emission. This suggests that the flux from this system during the first 4 seasons can be attributed to the combined light from the star and a disk that is not substantially varying in its inner regions. For a disk to appear steady for about four years in optical photometry, it must be fed at a nearly constant rate via stellar mass loss. Then, between the fourth and fifth season of KELT data, the mass loss from the star slows down or stops, and we see the brightness of the system slowly decay over the next many years. This decay in brightness traces the slow dissipation of the inner disk. Three spectra from BeSS taken at different stages of this dissipation phase all show a strong disk in Hα, indicating that there is still a significant amount of emitting material at larger radii (compared to the region probed by the light curve).

BK-053 is another system that shows long-term variability in its brightness (see Figure 5.3). There are five spectra available from BeSS, which span five years and cover most of the photometric baseline. All spectra show a substantial disk in Hα. The single-peaked line profile indicates that we are viewing this system at a low inclination angle (near pole-on). Keeping in mind that a strong disk is known to exist over nearly the entire observational baseline, the slow changes in brightness are best explained by a near-continuous, but variable mass-loss rate from the star. As the brightness is increasing in the first $\sim$half of the light curve, the inner disk is growing. As the mass-loss rate from the star eventually begins to decrease, so too does the brightness of the system diminish.

Additional examples of systems from the BK sample showing LTV are shown in Figure 5.4. Some of these systems also have clear outbursts, while others do not. This seems to suggest that, in addition to the discrete disk-building events denoted by outbursts, sometimes some Be stars build discs through a more continuous process that slowly varies in strength over time.

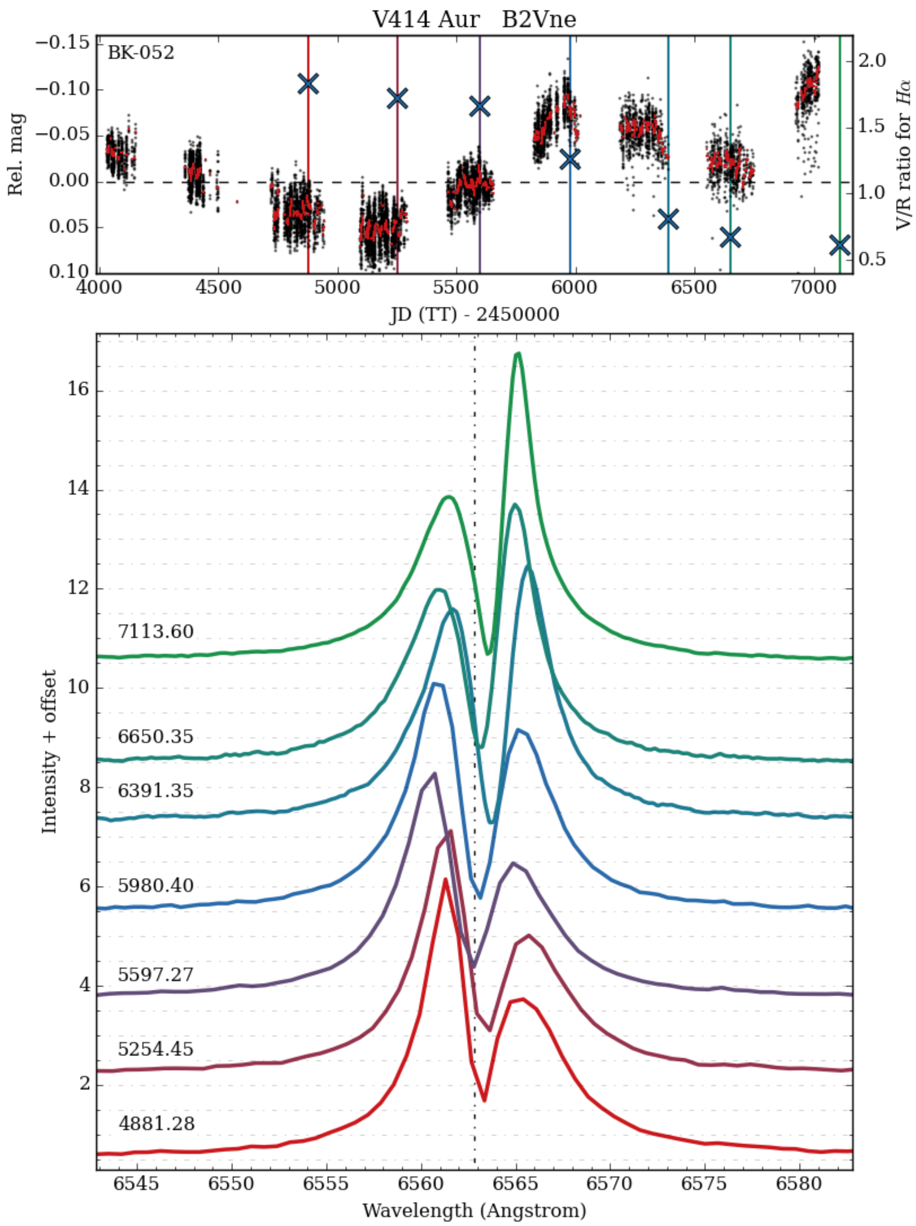

Figure 5.1: *Top:* Raw KELT light curve for BK-052 (HD 33232 = V414 Aur; B2Vne). The seven colored vertical lines correspond to dates of spectroscopic observations, and the blue X's show how the V/R ratio in the Hα emission peaks is changing over time, as determined from the existing BeSS spectra for this target. *Bottom:* Hα line profiles gathered from BeSS, increasing in time from bottom to top, show a gradual shifting in the V/R ratio over the $\sim$6 years of spectroscopic observation.

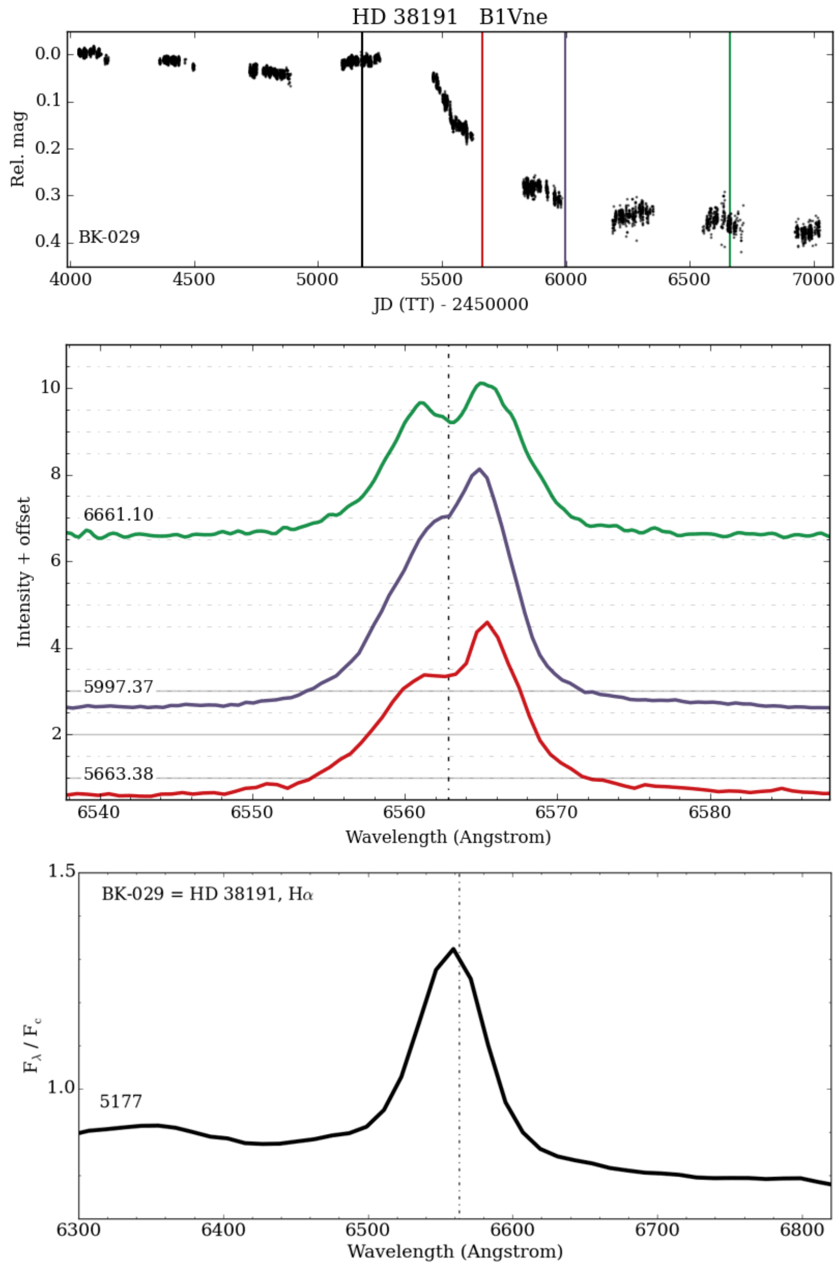

Figure 5.2: Raw KELT light curve for BK-029 (HD 38191; B1ne; *top*), with colored vertical lines denoting epochs of BeSS spectra, shown in the lower panels. The bottom panel shows the earliest available line profile, taken near the end of the photometrically stable phase. The remaining three are taken at various stages of the inner disk dissipation phase. The earliest spectrum is of very low resolution, and is plotted over a large range in wavelength compared to the latter three measurements.

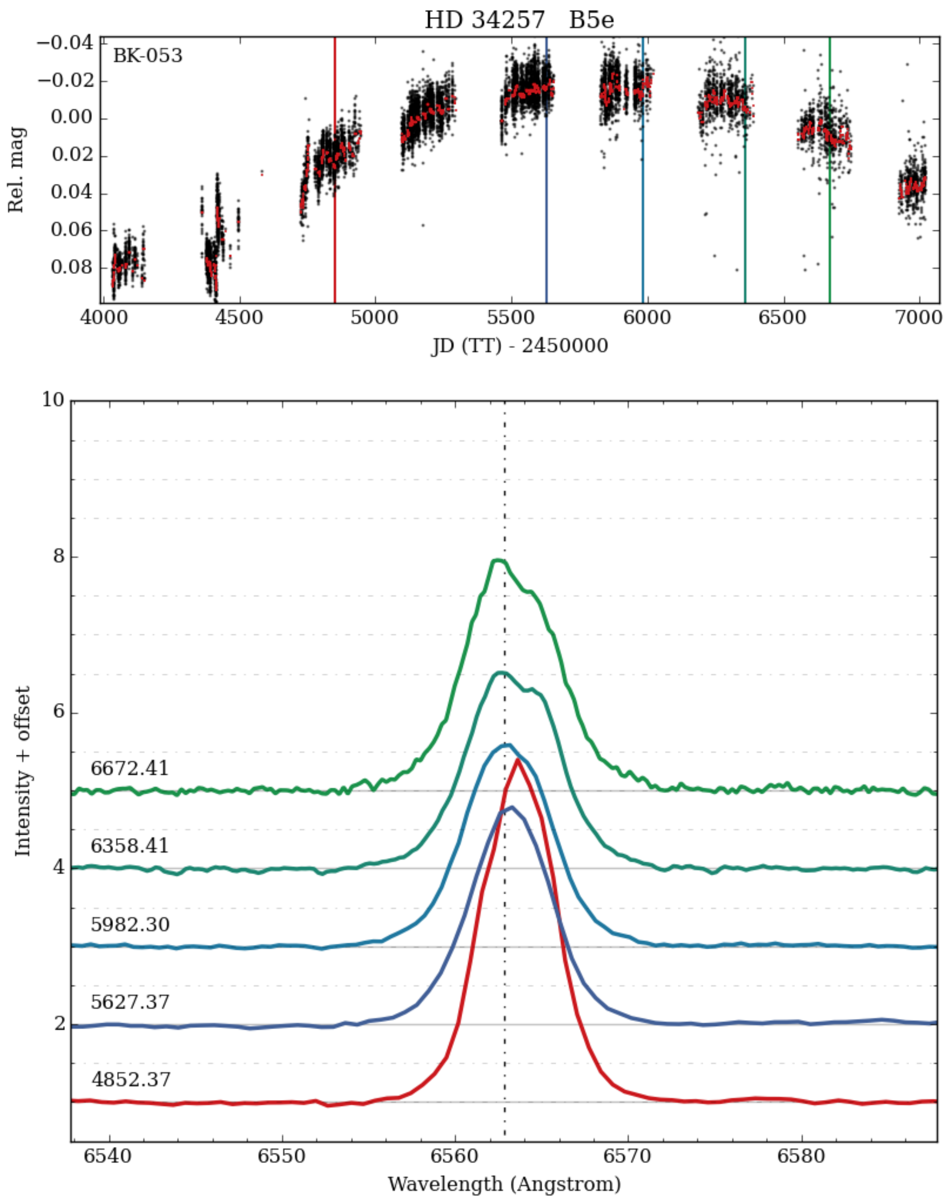

Figure 5.3: Raw KELT light curve for BK-053 (HD 34257; B5e; *top*). The five colored vertical lines correspond to dates of spectroscopic observations. The bottom panel shows the Hα lines of the available BeSS spectra.

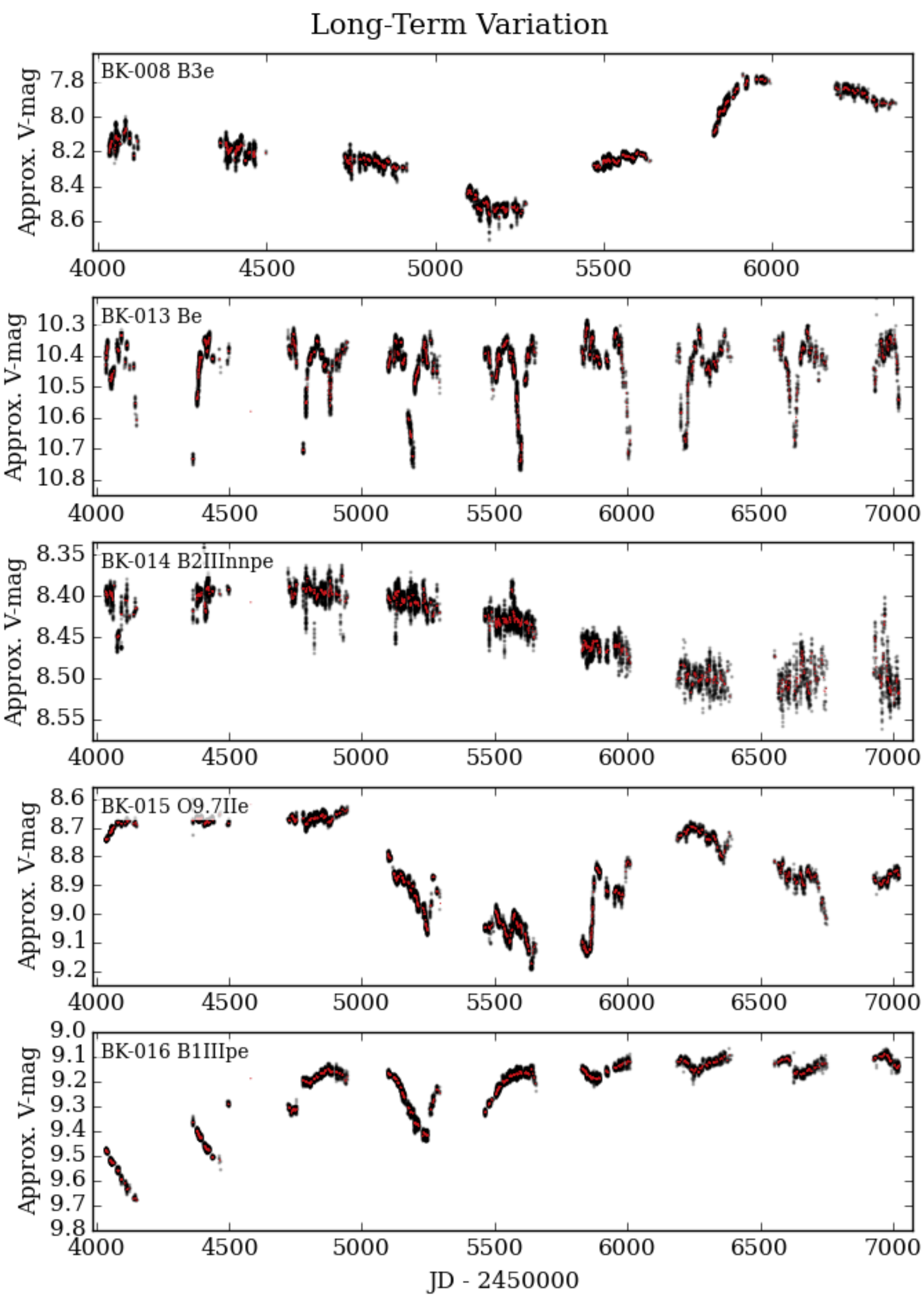

Figure 5.4: Light curves of systems showing photometric LTV in the BK sample.

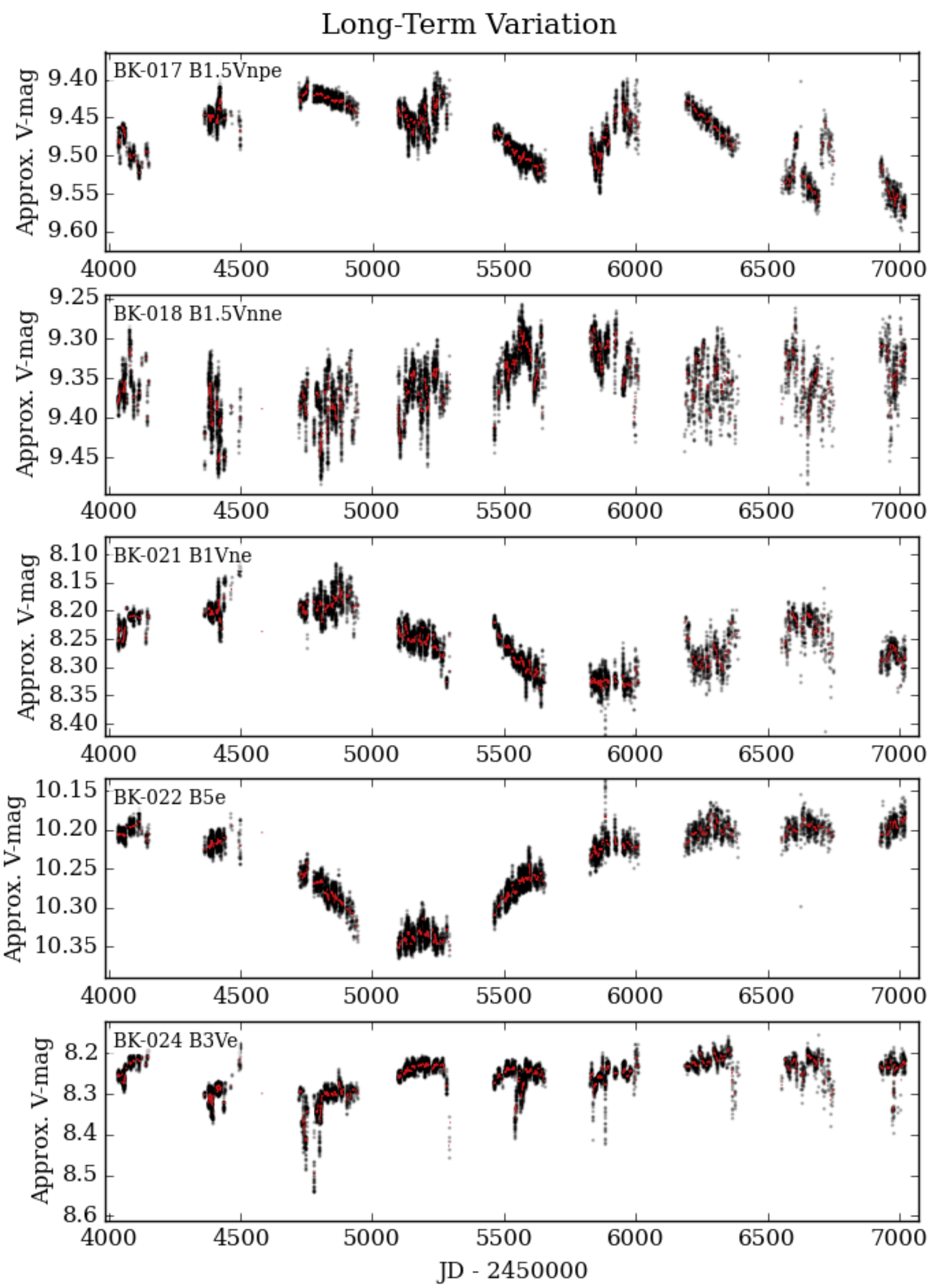

Long-Term Variation
BK-017 B1.5Vnpe
BK-018 B1.5Vnne
BK-021 B1Vne
BK-022 B5e
BK-024 B3Ve
Approx. V-mag
JD - 2450000

Figure 5.4: B

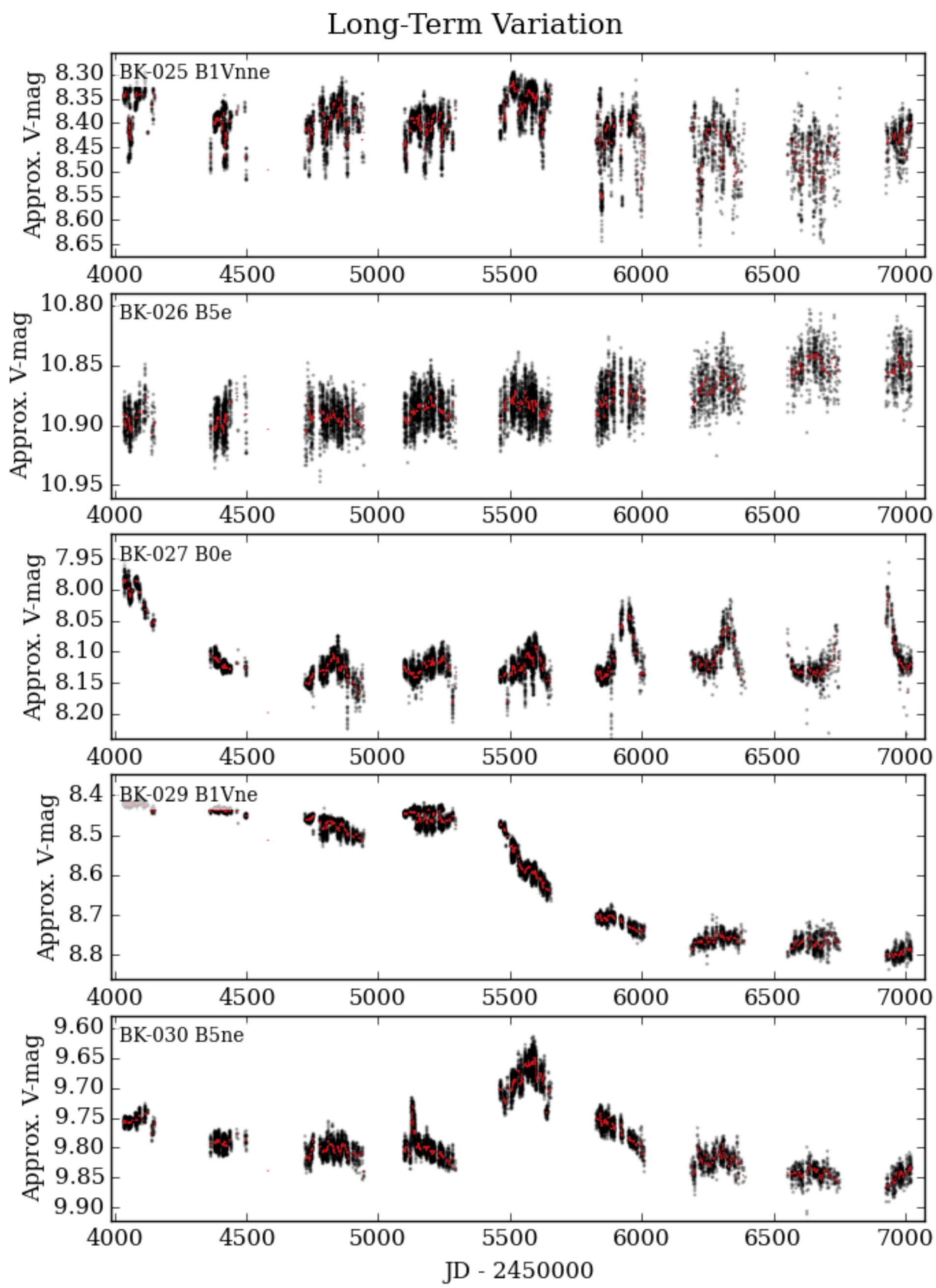
Long-Term Variation
BK-025 B1Vnne
BK-026 B5e
BK-027 B0e
BK-029 B1Vne
BK-030 B5ne
Approx. V-mag
JD - 2450000

Figure 5.4: C

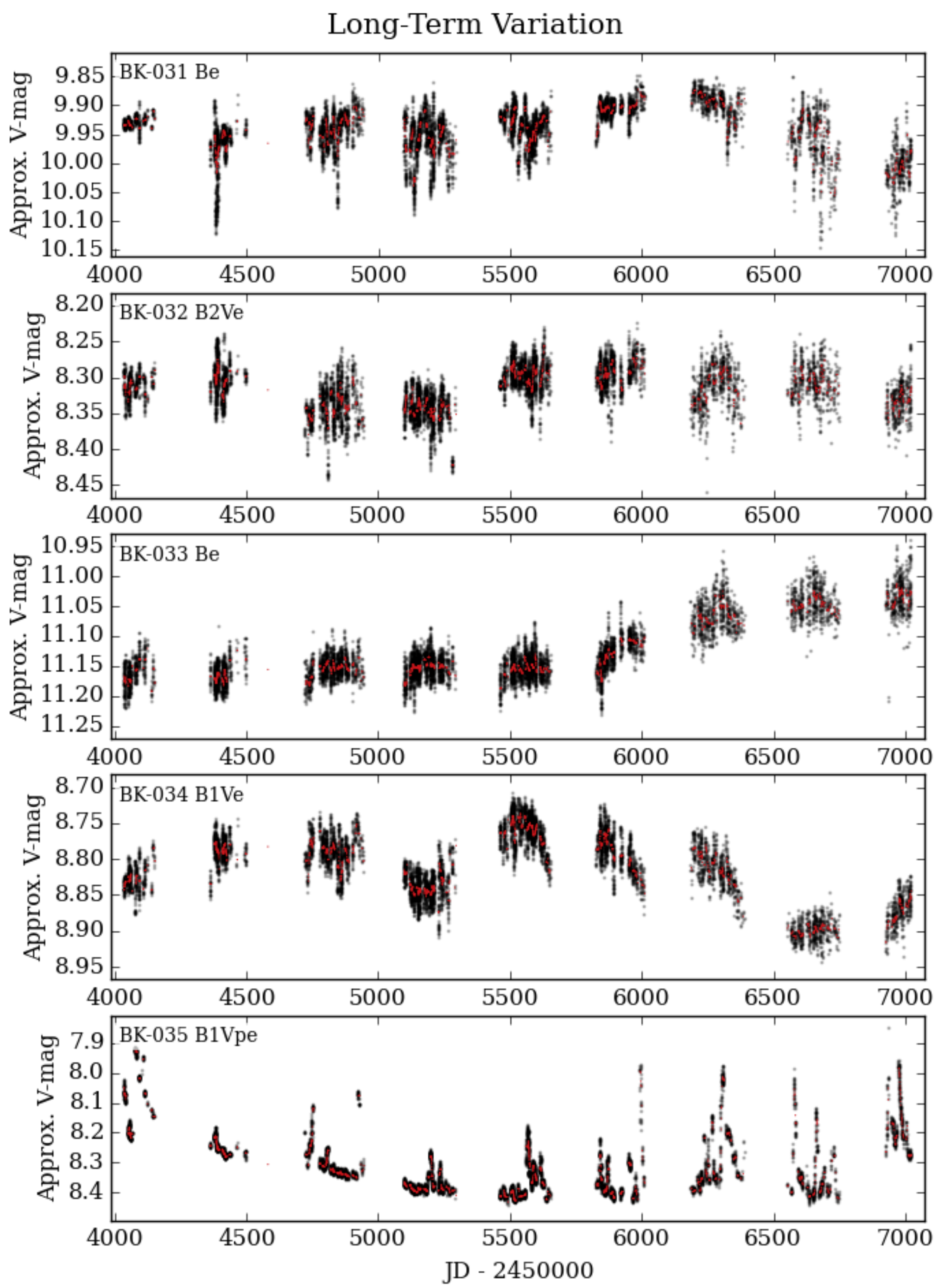
Long-Term Variation
BK-031 Be
BK-032 B2Ve
BK-033 Be
BK-034 B1Ve
BK-035 B1Vpe
Approx. V-mag
JD - 2450000

Figure 5.4: D

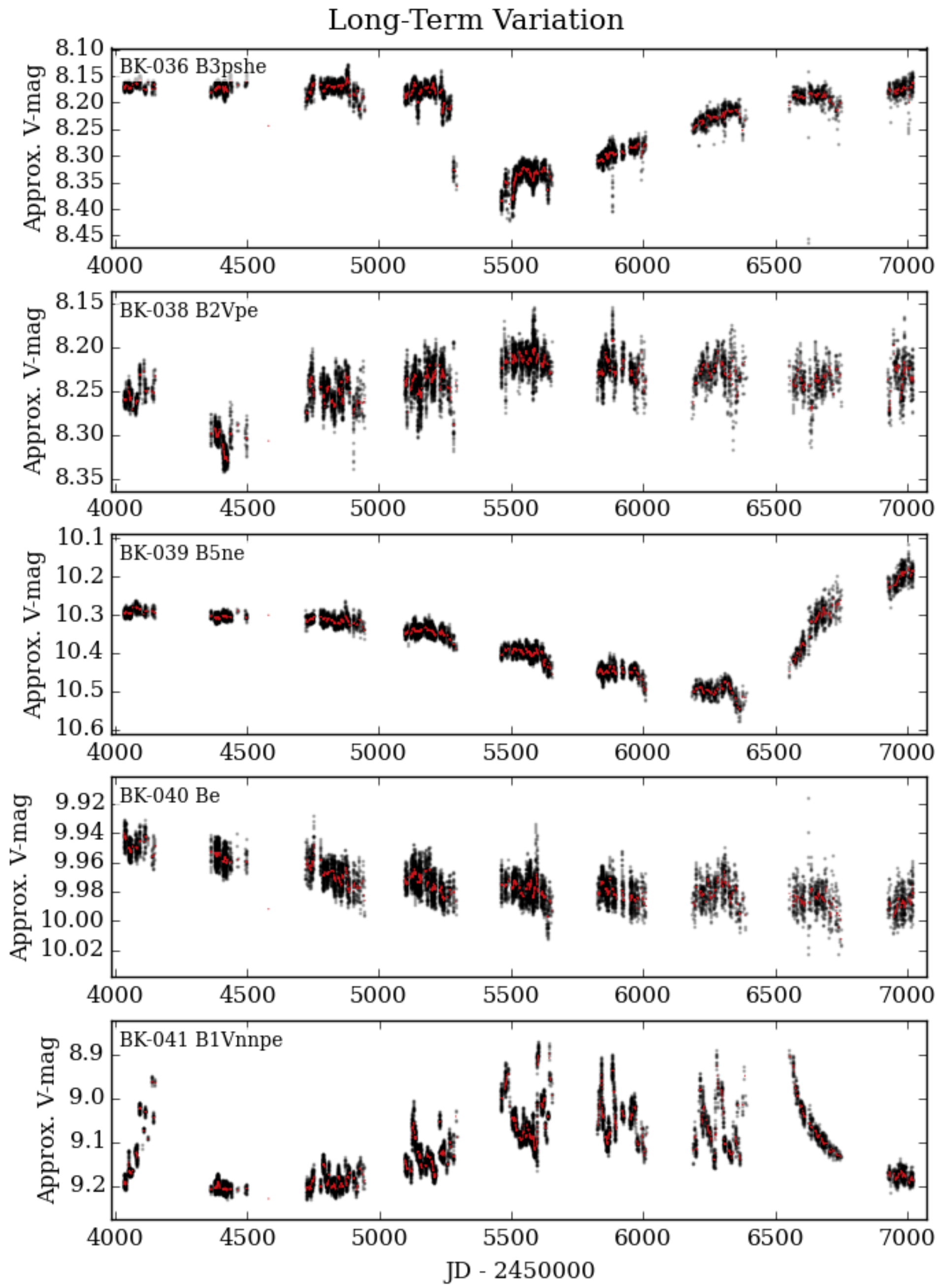

Long-Term Variation
BK-036 B3pshe
BK-038 B2Vpe
BK-039 B5ne
BK-040 Be
BK-041 B1Vnnpe
Approx. V-mag
JD - 2450000

Figure 5.4: E

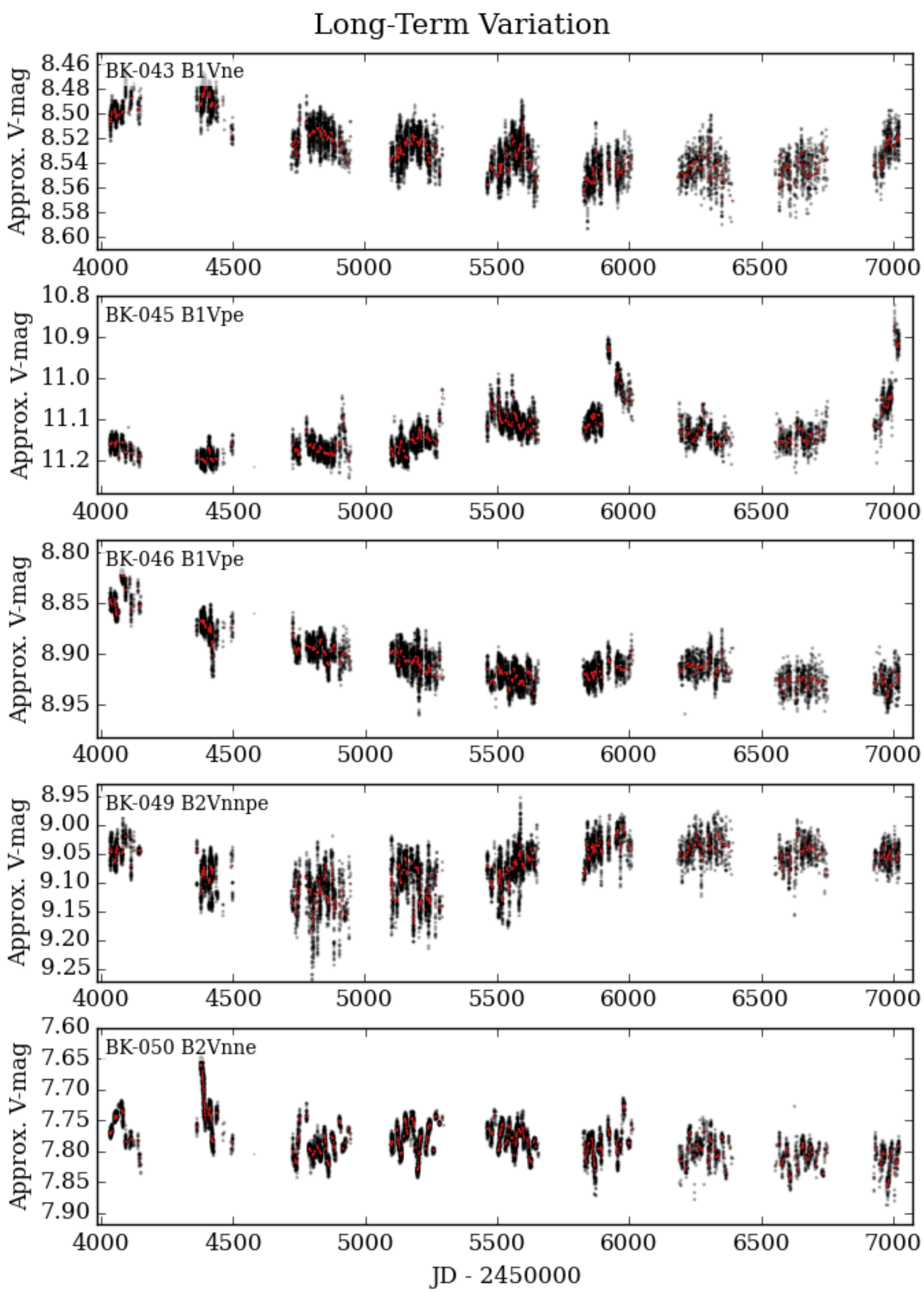

Long-Term Variation
BK-043 B1Vne
BK-045 B1Vpe
BK-046 B1Vpe
BK-049 B2Vnnpe
BK-050 B2Vnne
Approx. V-mag
JD - 2450000

Figure 5.4: F

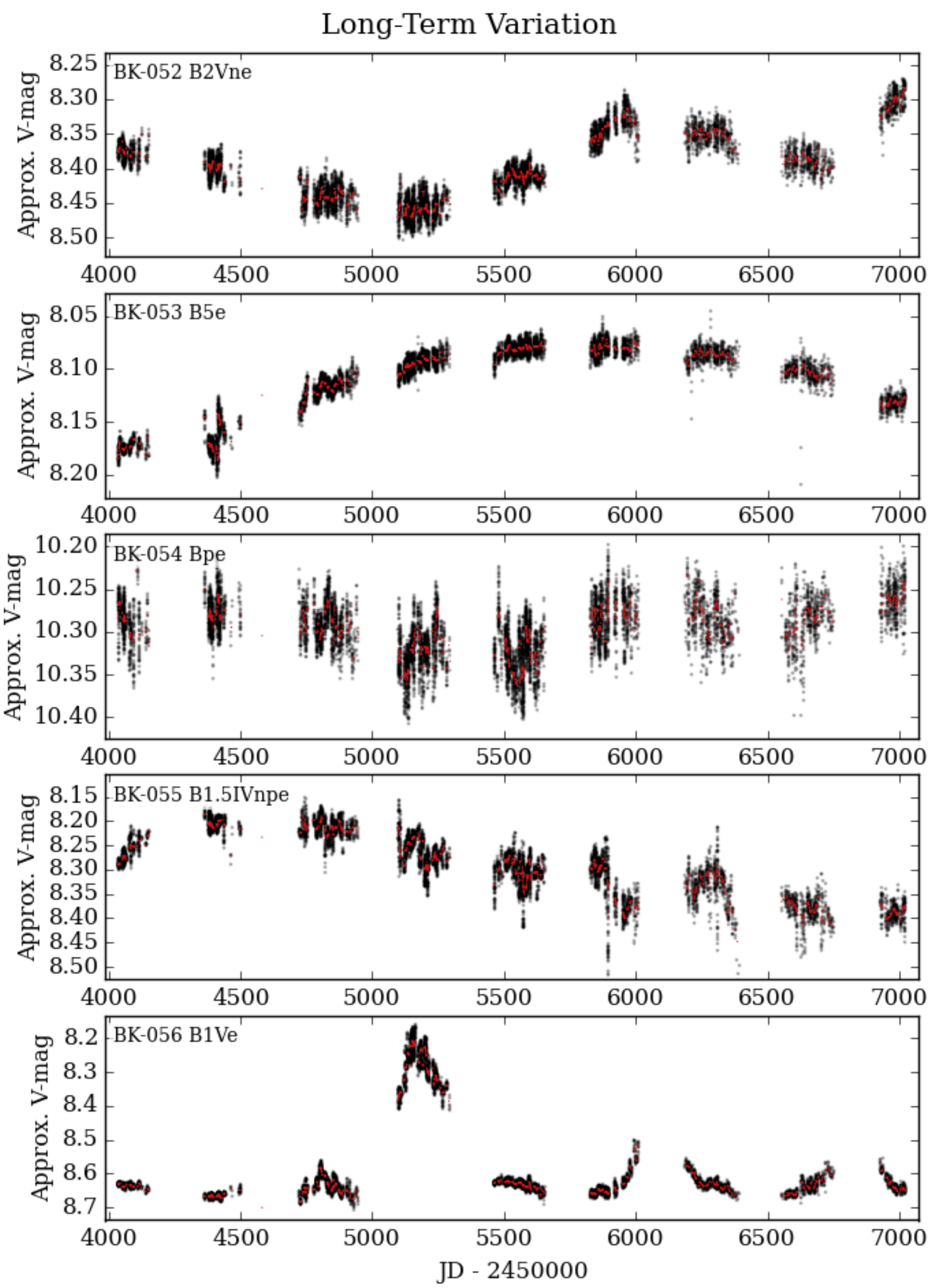
Long-Term Variation
BK-052 B2Vne
BK-053 B5e
BK-054 Bpe
BK-055 B1.5IVnpe
BK-056 B1Ve
Approx. V-mag
JD - 2450000

Figure 5.4: G

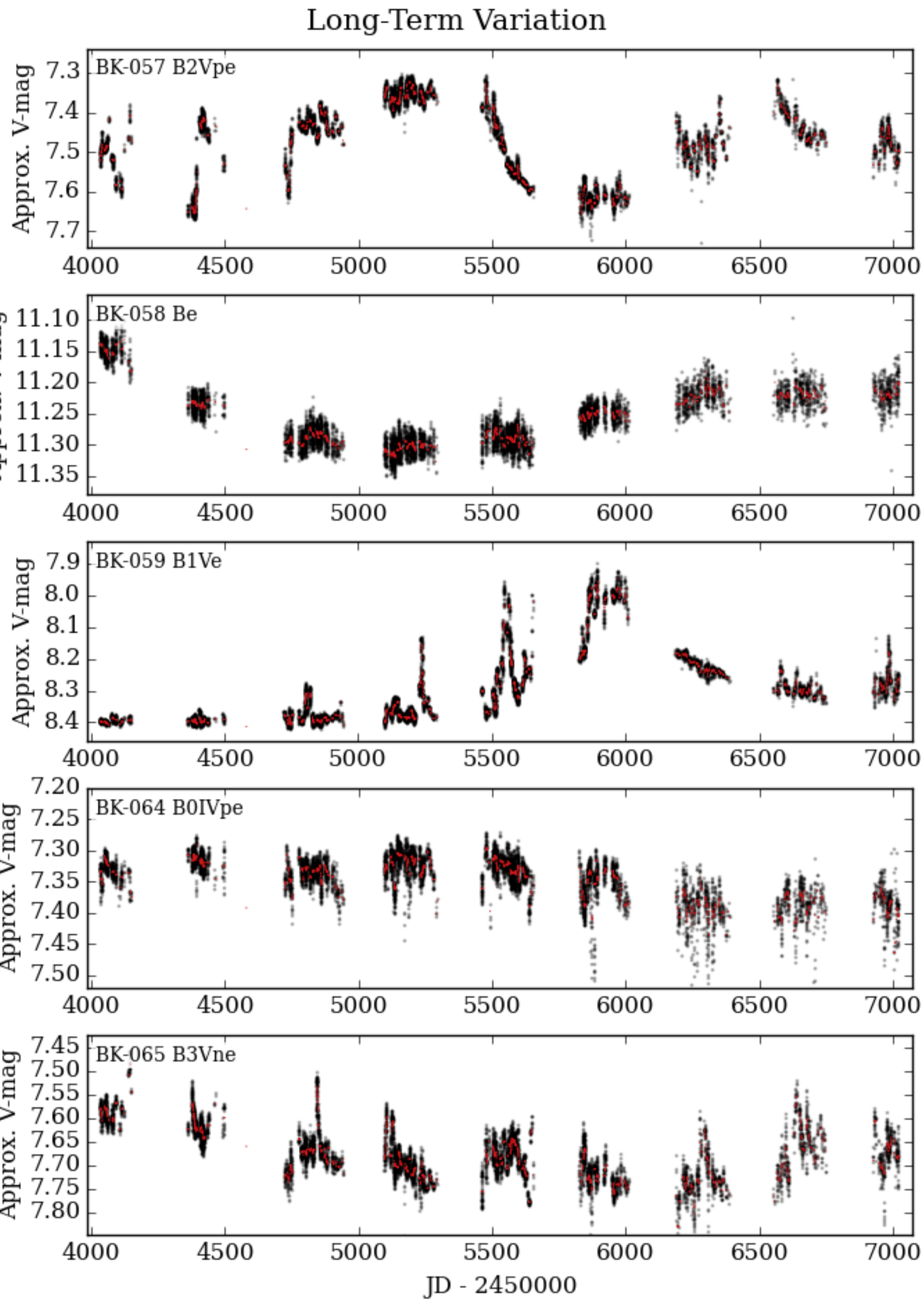

Long-Term Variation
BK-057 B2Vpe
BK-058 Be
BK-059 B1Ve
BK-064 B0IVpe
BK-065 B3Vne
Approx. V-mag
JD - 2450000

Figure 5.4: H

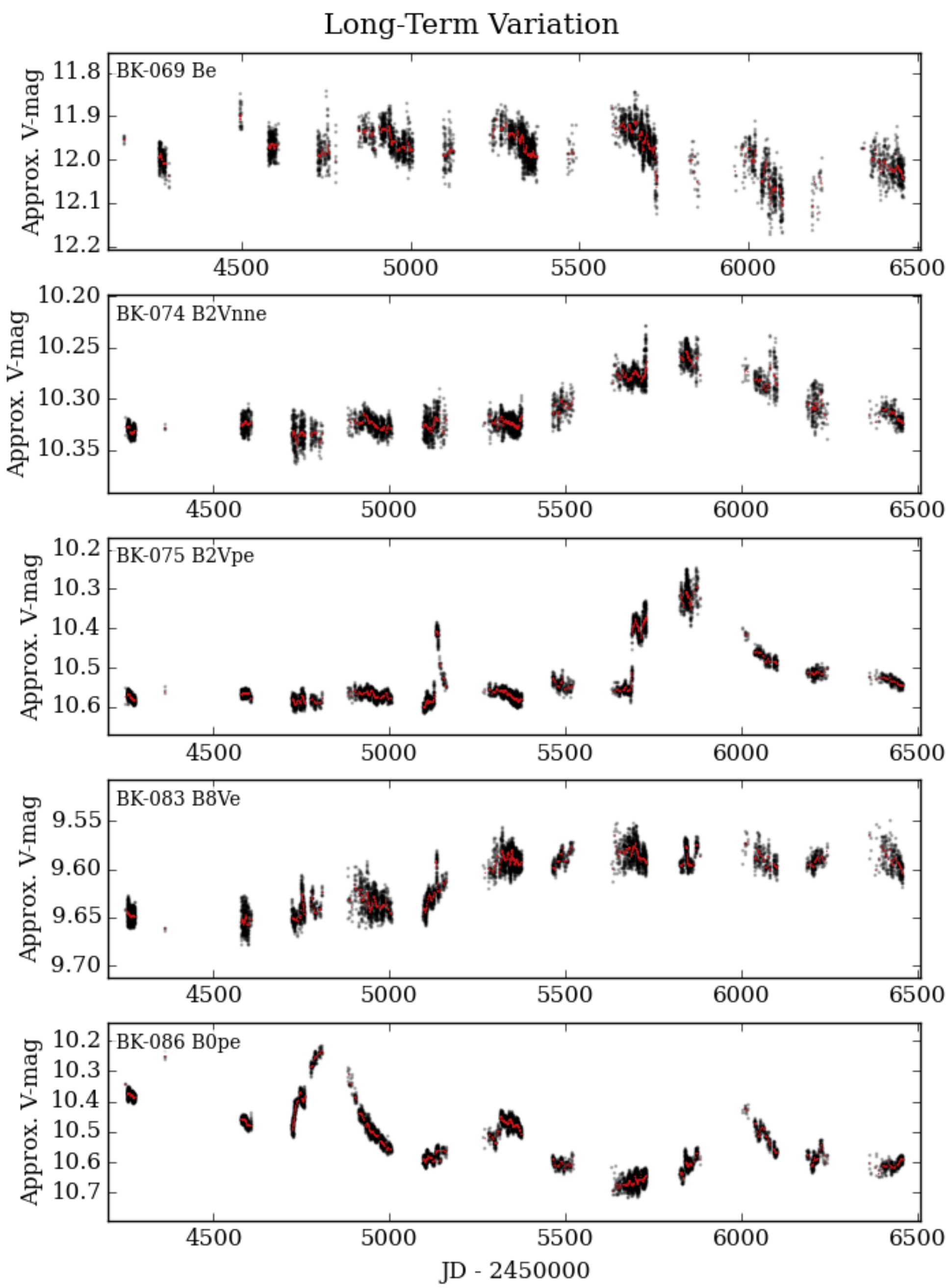

Long-Term Variation
BK-069 Be
BK-074 B2Vnne
BK-075 B2Vpe
BK-083 B8Ve
BK-086 B0pe
Approx. V-mag
JD - 2450000

Figure 5.4: I

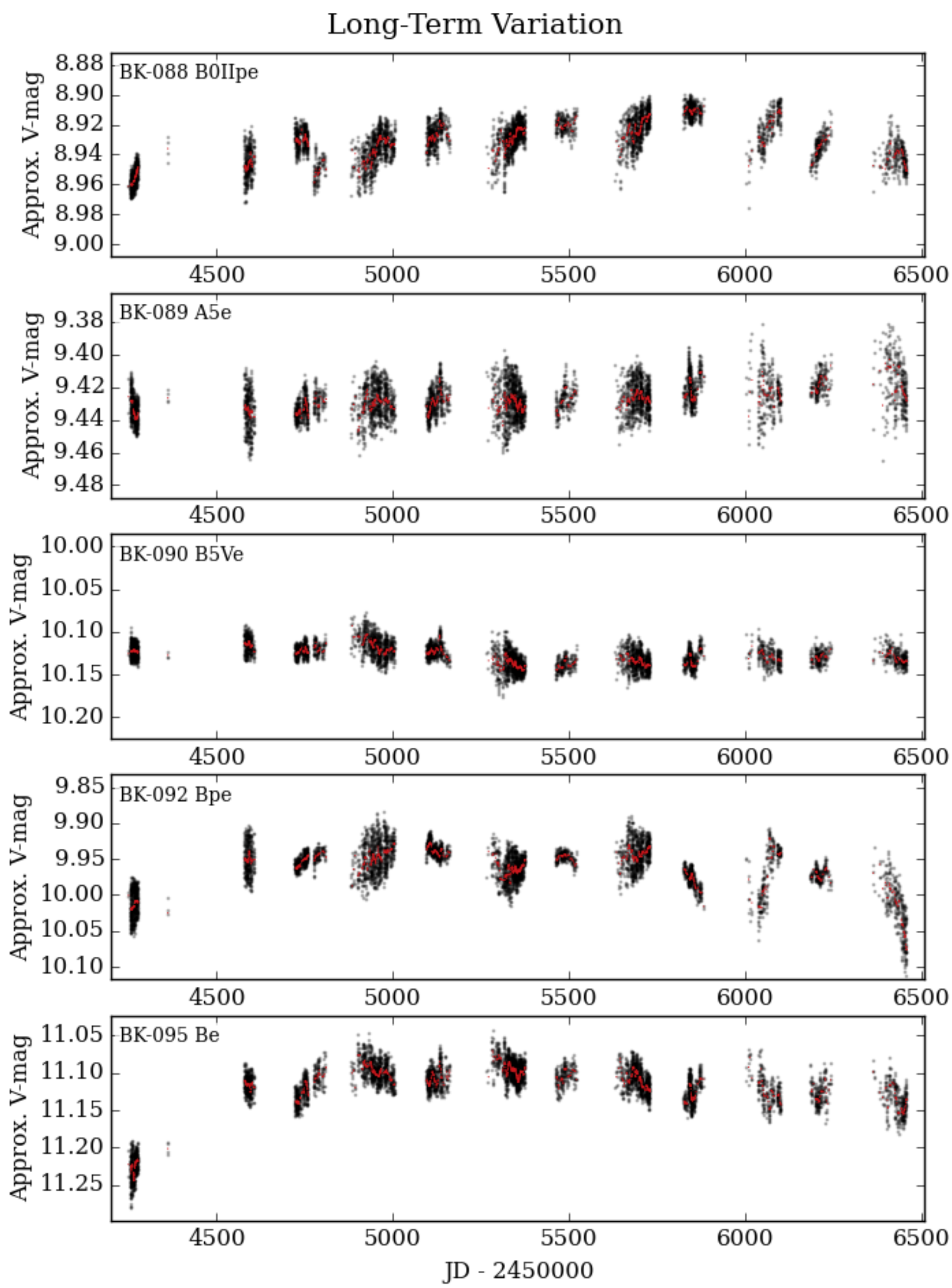
Long-Term Variation
BK-088 B0IIpe
BK-089 A5e
BK-090 B5Ve
BK-092 Bpe
BK-095 Be
Approx. V-mag
JD - 2450000
4500
5000
5500
6000
6500

Figure 5.4: J

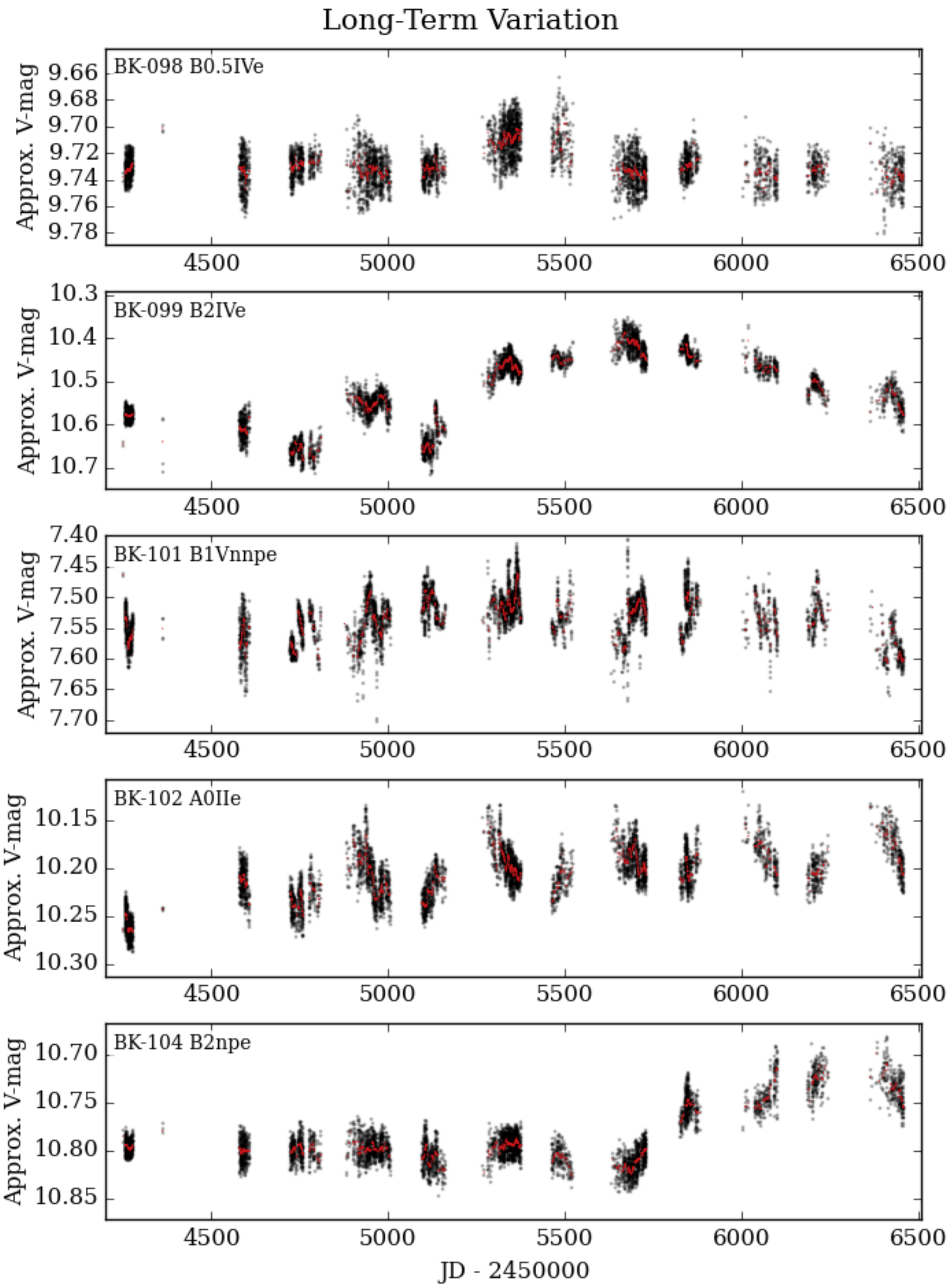

Long-Term Variation
BK-098 B0.5IVe
BK-099 B2IVe
BK-101 B1Vnnpe
BK-102 A0IIe
BK-104 B2npe
Approx. V-mag
JD - 2450000

Figure 5.4: K

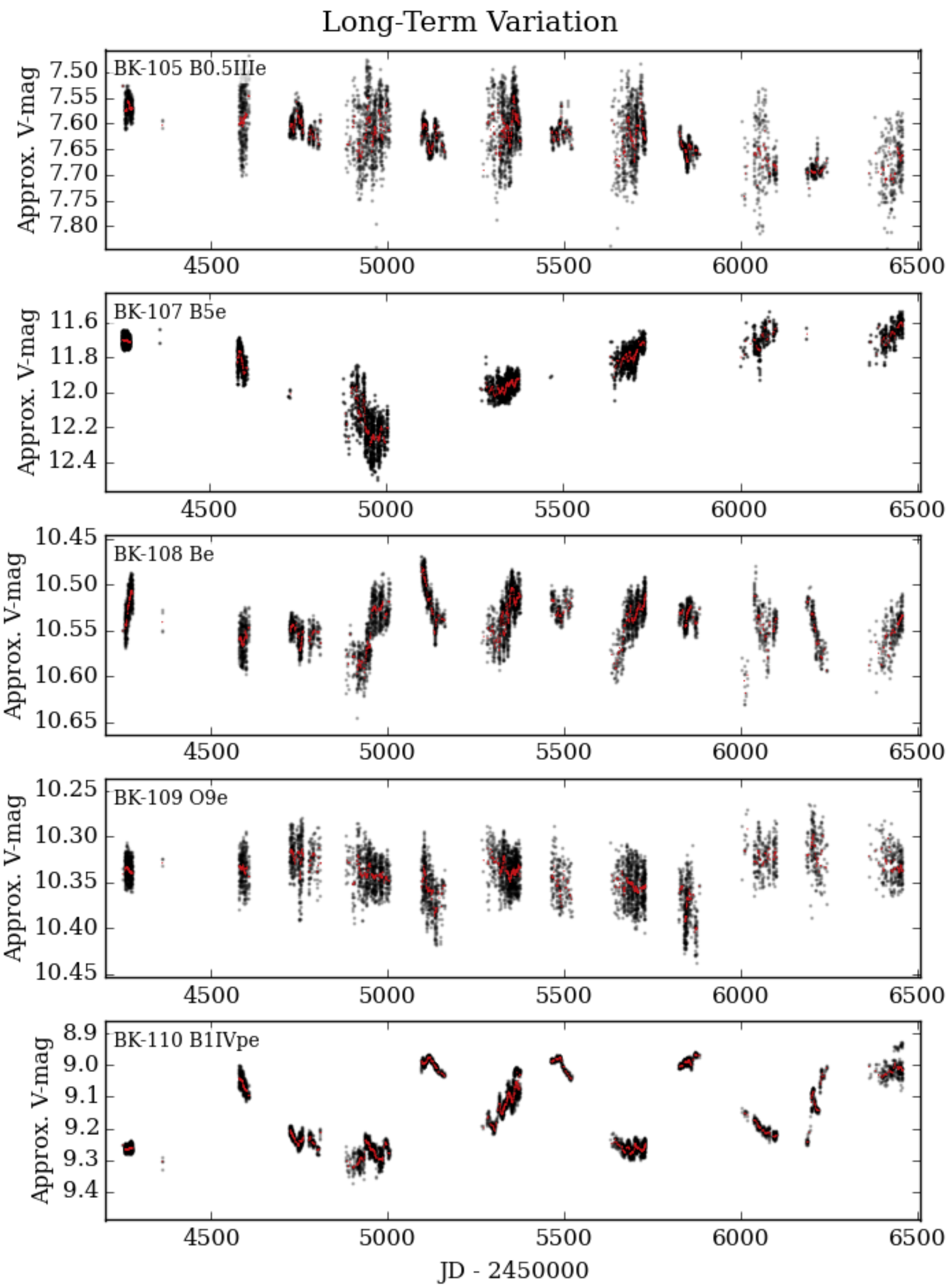
Long-Term Variation
BK-105 B0.5IIIe
BK-107 B5e
BK-108 Be
BK-109 O9e
BK-110 B1IVpe
Approx. V-mag
JD - 2450000

Figure 5.4: L

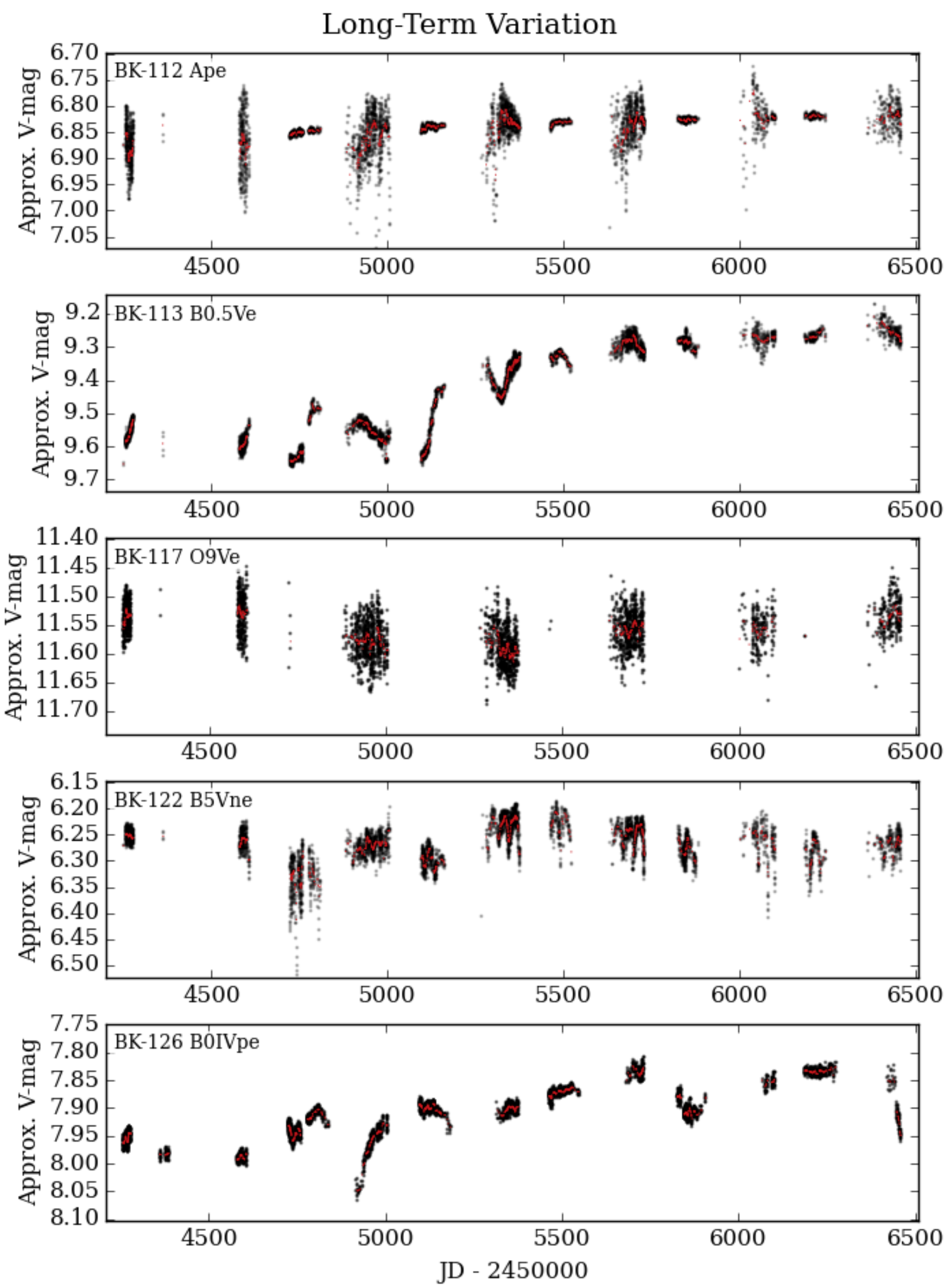
Long-Term Variation
BK-112 Ape
BK-113 B0.5Ve
BK-117 O9Ve
BK-122 B5Vne
BK-126 B0IVpe
Approx. V-mag
JD - 2450000

Figure 5.4: M

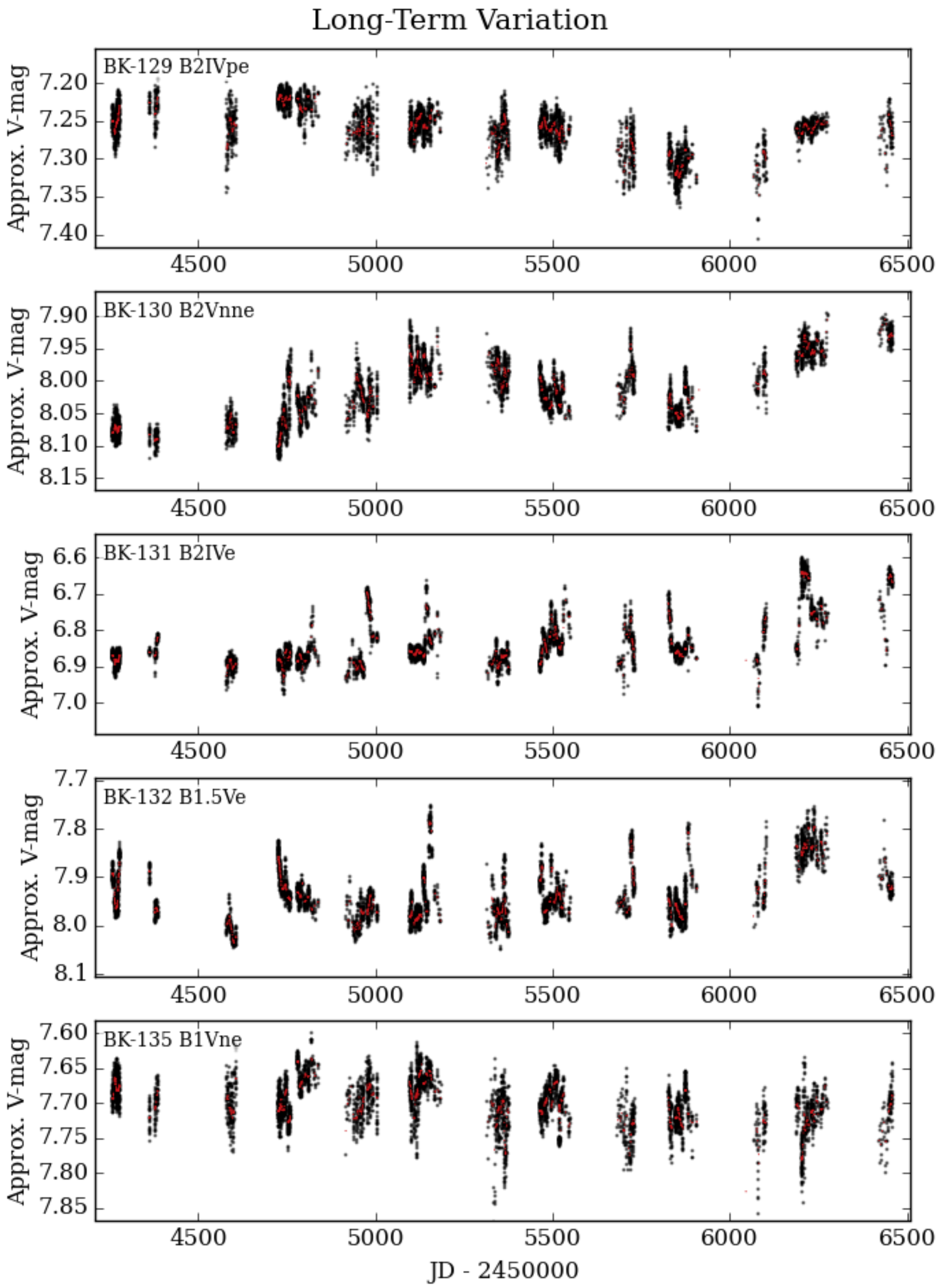

Long-Term Variation
BK-129 B2IVpe
BK-130 B2Vnne
BK-131 B2IVe
BK-132 B1.5Ve
BK-135 B1Vne
Approx. V-mag
JD - 2450000

Figure 5.4: N

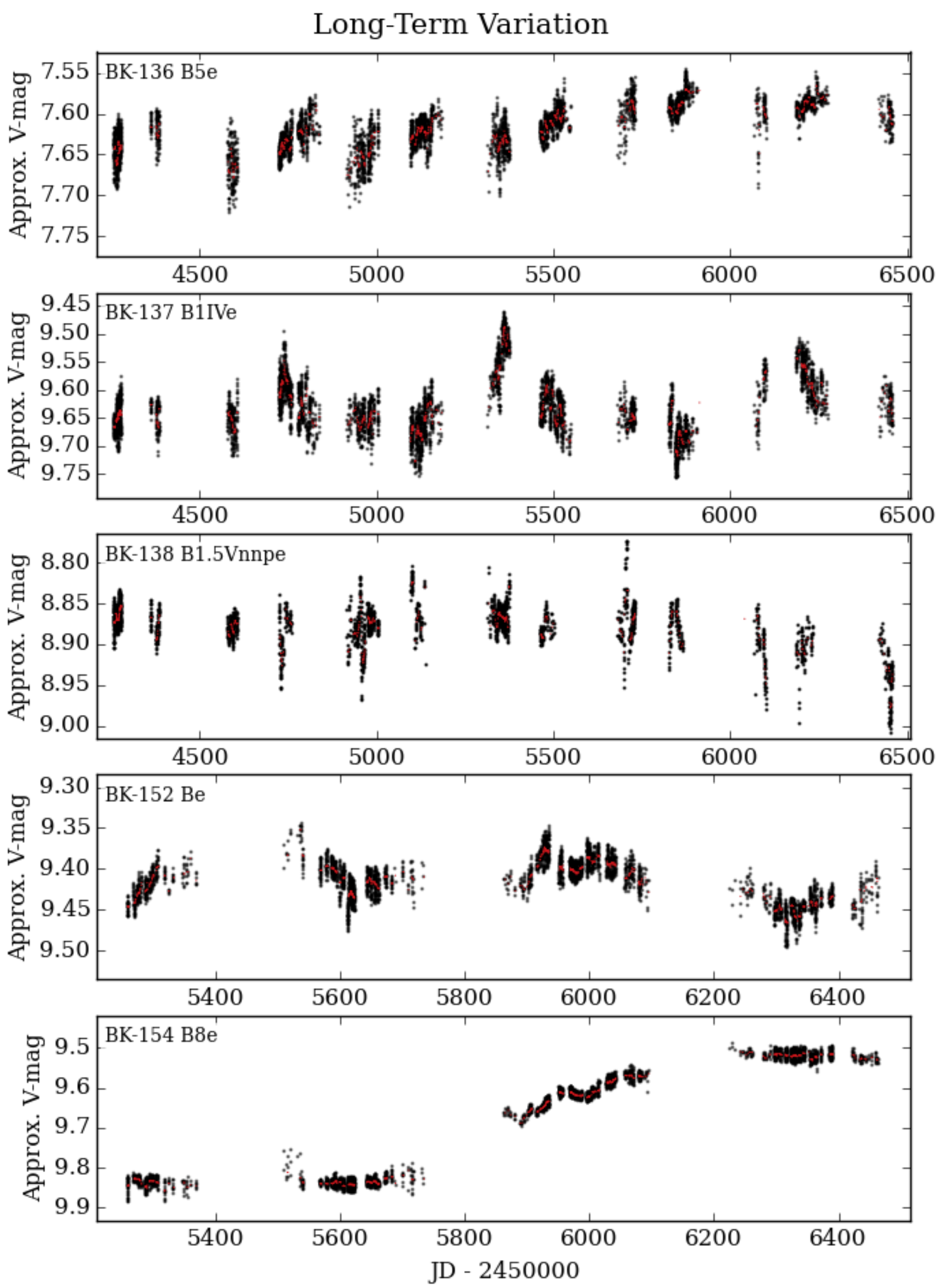
Long-Term Variation
BK-136 B5e
BK-137 B1IVe
BK-138 B1.5Vnnpe
BK-152 Be
BK-154 B8e
Approx. V-mag
JD - 2450000

Figure 5.4: O

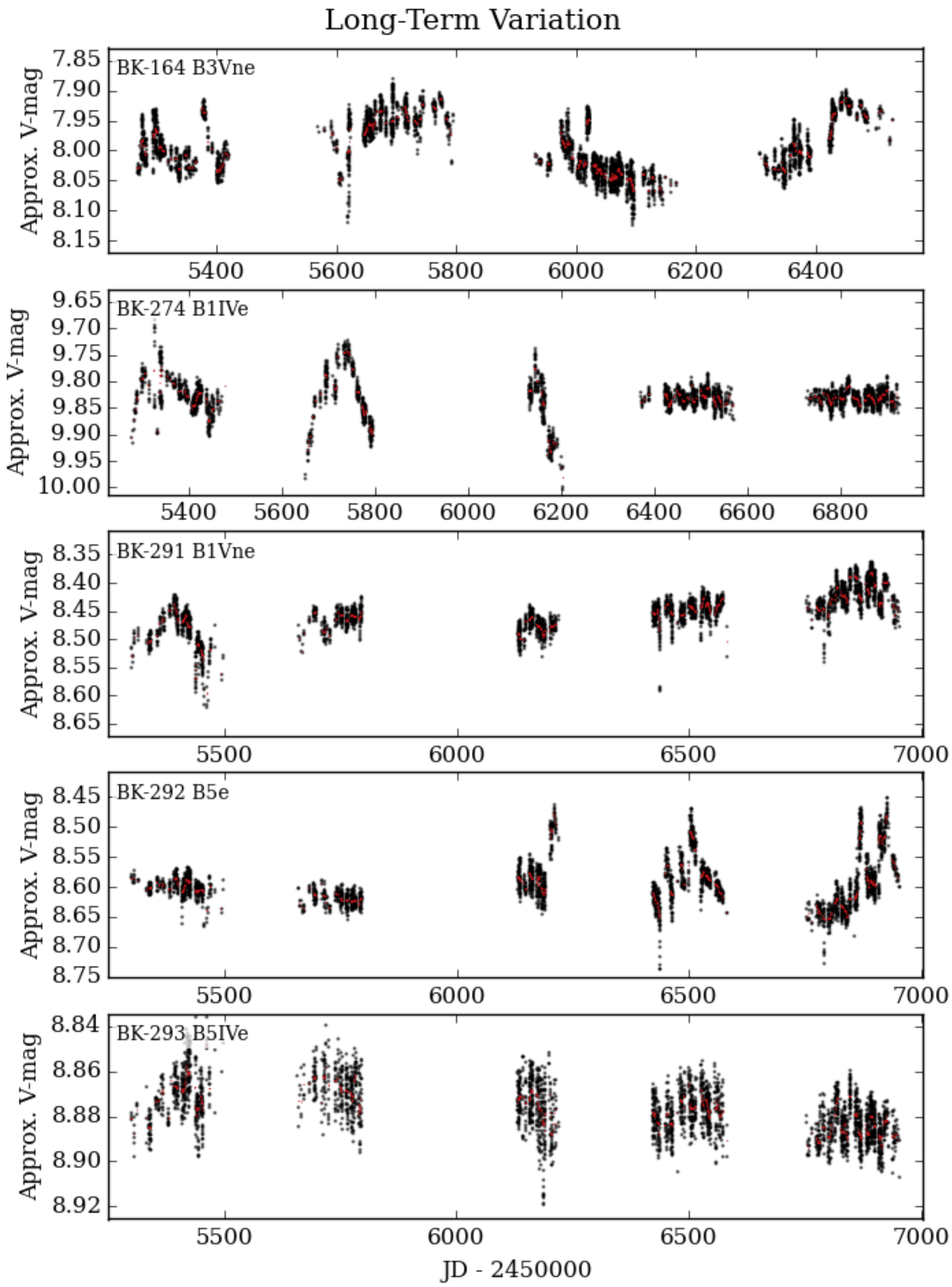
Long-Term Variation
BK-164 B3Vne
BK-274 B1IVe
BK-291 B1Vne
BK-292 B5e
BK-293 B5IVe
Approx. V-mag
JD - 2450000

Figure 5.4: P

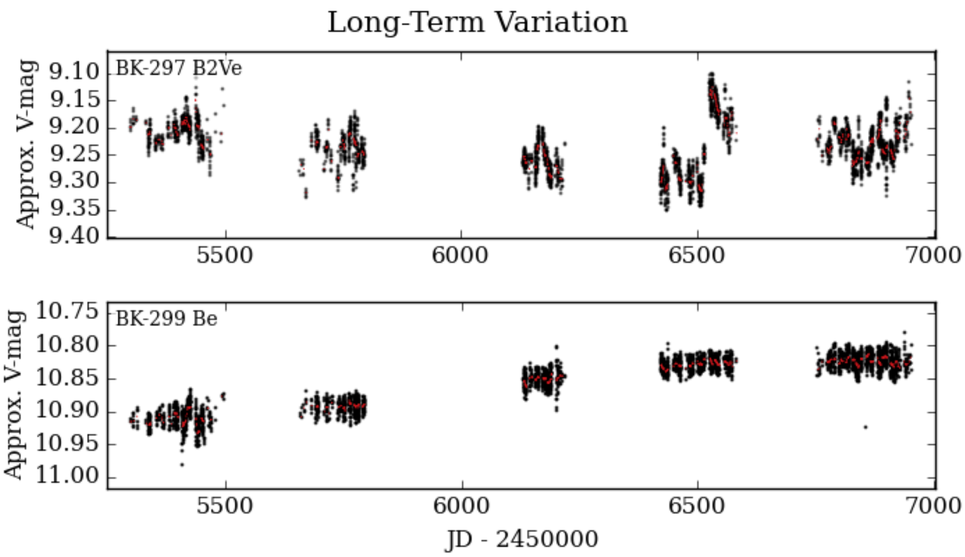

Long-Term Variation
BK-297 B2Ve
Approx. V-mag
9.10
9.15
9.20
9.25
9.30
9.35
9.40
5500
6000
6500
7000
BK-299 Be
Approx. V-mag
10.75
10.80
10.85
10.90
10.95
11.00
5500
6000
6500
7000
JD - 2450000

Figure 5.4: Q

Chapter 6

Related Work

Although the focus of this work is on classical Be stars, there are other taxonomically similar objects that are worth discussion. The systems highlighted in this section are generally massive (O- and B-type) stars, and have some commonalities with Be stars, such as emission features arising from hot circumstellar material, or pulsation. The same types of data and analysis methods can be used to learn about these non-Be star systems. However, interpreting the data requires some caution, since there are important physical distinctions between these related objects and classical Be stars.

6.1 Massive Magnetic Stars

Magnetic fields are ubiquitous among low- and intermediate-mass stars, such as our Sun, which have convective envelopes and thus allow a dynamo to generate and sustain a magnetic field. Until recently, magnetic fields were though to be rare among high-mass stars, which lack a large convective envelope. The Magnetism in Massive Stars (MiMeS) survey has challenged this paradigm, showing that strong magnetic fields exist in about 7% of high-mass stars (Wade et al. 2014a). A specific class of rapidly-rotating, massive stars with strong magnetic fields are known as σ Ori E analogs, after the prototype of this class. These stars share many similarities with classical Be stars, in that they are hot, massive, on or near the main sequence, rapidly rotating, and have strong hydrogen emission lines attributed to hot circumstellar gas. The key difference lies in that σ Ori E analogs have strong magnetic fields that trap circumstellar material and force it to co-rotate with the star, resulting in extremely large peak separations between the violet and red side of the emission line (recall that linear velocity increases with radius for rigidly rotating bodies, as is the case here), while the material around Be stars (which, as a rule, do not have strong magnetic fields; Wade et al. 2014b) orbits according to Kepler's laws, with orbital velocity decreasing with radius. Stars with magnetic fields spin down over time, because the stellar magnetic field interacts with circumstellar material, ultimately exerting a torque on the star that slows its rotation over time. The rapidly rotating and highly magnetic σ Ori E analogs are an interesting class of objects that can be used to test theories of the role of magnetism in stellar evolution, and the origin of these strong, largely dipolar, magnetic fields.

Two new σ Ori E analogs, HD 345439 and HD 23478, were recently discovered through analysis of APOGEE spectra, which show extremely large peak separations in its double-peaked hydrogen emission features (Eikenberry et al. 2014). One of these stars, HD 345439, also happens to be observed by KELT. Through a careful LS analysis, I recovered a strong signal at P = 0.77013 days in the KELT light curve, and found virtually the same signal in two other light curves of this source (SWASP and ASAS photometry). These results are published in Wisniewski et al. (2015), and are shown here in Figure 6.1. Unlike signals with similar timescales in Be stars, which are best explained by pulsation, the preferred explanation for this signal in HD 345439 is that this is the rotation period of the star. The brightness of the system is modulated by the rotation period, as regions of confined, hot, circumstellar plasma and hot spots on the stellar surface rotate into and out of view. The morphology of the light curve when phased to this period shows departures from a pure sinusoid, which is seen in other similar systems (*e.g.* σ Ori E; Hesser et al. 1977; Oksala et al. 2015).

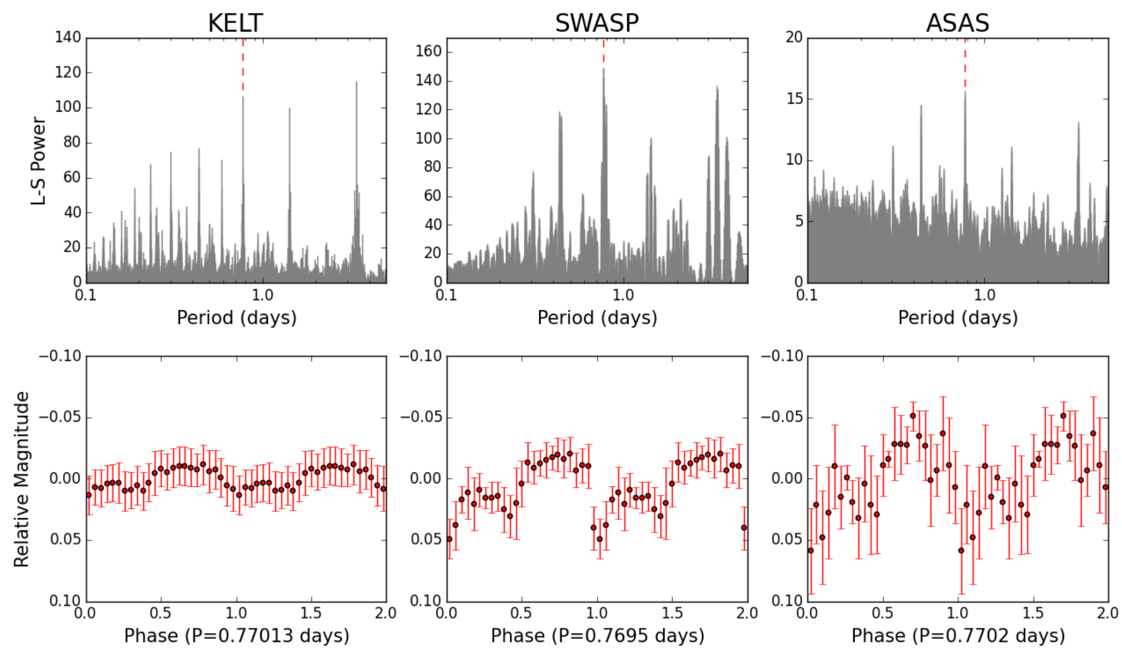

Figure 6.1: *Top:* LS periodograms, and *Bottom:* phase-folded median-binned light curve data from KELT, SWASP, and ASAS (from left to right) for the rapidly rotating, massive, magnetic star HD 345439.

6.2 Hot Pulsating Stars: β Cephei

The period-finding techniques discussed in Section 3 are being used to discover massive pulsating stars and to identify their pulsation period(s). This effort is discovering new hot pulsators, increasing the number of known objects of this class by a substantial amount. These stars will be monitored with the next-generation NASA Transiting Exoplanet Survey Satellite (TESS) mission (Ricker et al. 2014), which will provide extremely high precision photometry. The resulting TESS light curves will then be used to extract multiple pulsation modes, allowing the stellar interiors to be modeled via asteroseismology. The relatively modern technique of asteroseismology requires extremely high precision light curves, and connects theories of interior stellar structure and pulsation to observational data. This is currently the best way to learn about the otherwise inaccessible interior structure of stars.

6.2.1 *Introduction to β Cephei stars*

The first aspect of this project involves searching for stars of the β Cephei class, by performing a frequency search on KELT light curves of known hot stars. β Cephei stars are massive nonsupergiant variable stars with spectral type O or B with light, radial velocity, and/or line profile variations caused by low-order pressure and gravity mode pulsations (Stankov and Handler 2005). They tend to be early B-type stars (roughly spanning spectral types B0 – B2.5) with masses between 8 –17 $M_{\odot}$. They are characterized by their high-frequency pulsations (with typical periods between 2 – 7 hours) driven by the κ mechanism (Dziembowski et al. 1993; Moskalik and Dziembowski 1992; Stankov and Handler 2005).

Despite recent advances, there remain some uncertainties in regards to the evolution and structure of massive stars. β Cephei stars are amenable to detailed studies, and can help to alleviate some of these uncertainties. Currently, the role of rotation, internal angular momentum distribution and transport, and internal mixing are not satisfactorily understood in the context of stellar evolution. Mixing of material into the hydrogen-burning stellar core ("convective overshooting") considerably affects the main sequence lifetime of massive stars (*e.g.* Mowlavi and Forestini 1994), and cause surface abundances to change. Rotation influences this process, but the details remain poorly constrained (*e.g.* Maeder 1987). Differential rotation is sometimes measured in massive stars, but there remain significant uncertainties regarding the coupling between the stellar core and envelope, and the degree to which angular momentum is transported from the core outward (Aerts et al. 2017).

The pulsational properties of β Cephei stars make them particularly well-suited for detailed asteroseismologic studies. They tend to oscillate in several non-radial modes, and sometimes have both p- and g-mode pulsations (Jerzykiewicz 1978; Stankov and Handler 2005; Sterken and Jerzykiewicz 1993). Because the frequency of each oscillation mode is determined by the physical conditions in the region in which it propagates, measuring these frequencies (and knowing their geometries on the stellar surface and the interior) translates to constraints on the physical conditions in the stellar interior. Seismic modelling of a small number of β Cephei stars has led to significant progress. Quantitative estimates of the core overshooting parameter have been measured for the β Cephei star HD 129929 (Aerts et al. 2003), which is also found to undergo non-rigid internal rotation (Dupret et al. 2004). A similar analysis has been done for β CMa (Mazumdar et al. 2006), δ Ceti (Aerts et al. 2006), 12 Lac (Handler et al. 2006), V 2052 Oph (Handler et al. 2012), and a few others. Asteroseismology can also be used measure stellar mass, radius, surface rotation rate, and the evolutionary stage.

The technique of asteroseismology relies on having a long enough time baseline and a high enough cadence and precision to identify the periodic signals of as many pulsation modes as possible. Space-based time-series photometry provides excellent data for these purposes. Although current and past space observatories have been successfully used for asteroseismology, only a small number of the high-mass β Cephei type stars have been observed, and subsequently modeled, to date in this capacity (*e.g.* HD 180642 with CoRoT, Aerts et al. (2011); δ Ceti with MOST, Aerts et al. (2006)) – there have been no sufficiently comprehensive asteroseismologic studies of this class of star. The upcoming NASA TESS mission is an all-sky photometric survey with a precision similar to that of the Kepler mission, and will open a new window into our understanding of β Cephei stars, and therefore the interior structure of high-mass stars in general. While the primary science goal of the TESS mission is to discover transiting exoplanets, TESS light curves will be leveraged for a host of ancillary science efforts. Among these is the use of TESS data for an asteroseismic study of a large sample of β Cephei stars. To this end, we are mining ground-based time-series photometric data to identify as many β Cephei stars as possible, to then be targeted by TESS for the purpose of asteroseismology. The TESS light curves of these stars will allow for detailed modeling of an unprecedented number of massive stars across a wide range of parameter space, and will result in important constraints on theories regarding stellar structure and evolution.

The goal of this work is the identification of new and candidate β Cephei stars.

We begin with a star catalog which contains all stars brighter than 12th magnitude, and includes information helpful in locating the star in the H-R diagram (Balona 2015, private communications). All stars with literature spectral types of O and B, plus stars without a spectral classification, but with an effective temperature from photometry that is consistent with being an O- or B-type star were selected. The result is a total of 16682 stars with spectral types between O4 – B7, and 15494 stars with spectral types of B8 or B9. These lists were then cross-matched to the KELT catalog, resulting in 5840 matches with spectral type O4 – B7 (the "early sample"), and 10563 matches of B8 and B9 stars (the "late sample").

6.2.2 Analysis

For each of the 5840 stars in the early sample, and the 10563 stars in the late sample, a Fourier periodogram was computed in the range of 0 – 15 d^{-1}, and in a few cases 0 – 20 d^{-1}. Each periodogram with a strong peak in the range of known β Cephei star pulsation frequencies ($f \gtrsim 4$ d^{-1}) was visually inspected, as were the light curves phased to twice the recovered period. On the basis of these plots, and in doubtful cases based on additional frequency analyses, all stars that had either untrustworthy data, showed no variability, binary or rotational light curves, and those whose periodograms could be explained solely by reduction imperfections (residual differential color extinction) were rejected. Those that were not rejected were scrutinized again, and obviously non-pulsators were removed. The remainder are classified into β Cephei stars and candidate β Cephei stars. This analysis was done by Gerald Handler, a collaborator on this project.

Systems classified as β Cephei stars show periodic variability at multiple frequencies (suggesting they are multi-mode pulsators) in the range appropriate for β Cephei stars (between 4 – 14 d^{-1}). The group of candidates contains stars with primary periods somewhat longer than β Cephei stars (sometimes with multiple significant frequencies), and stars where only one frequency is detected. This group likely contains genuine β Cephei stars, but is contaminated by other types of variable systems. One reason a true β Cephei star may be classified as a candidate is if the photometric amplitudes of its pulsations are low, and only a single frequency is detected, with others falling below the detection threshold.

Other types of variable objects are found near β Cephei stars in the HR diagram. Slowly pulsating B (SPB) stars tend to have spectral types between approximately B2 – B9, and pulsate in relatively lower frequency g-modes compared to β Cephei stars (De Cat 2002). There are also 'hybrid' pulsators, oscillating in low-frequency g-modes and high-frequency p-modes simultaneously (De Cat et al. 2007; Handler 2009; Pigulski and Pojmański 2008). Classical Be stars span the entire spectral range of B-type stars (even extending into the O and A types), and are also pulsators, often in multiple modes. They are very rapidly rotating as a class, on average rotating at about 80% of their critical velocity, and occasionally eject matter to form a circumstellar disk (Rivinius et al. 2013). The rapid rotation of classical Be stars can complicate the observed frequency spectrum (*e.g.* Kurtz et al. 2015), as can variability in the circumstellar environment (Rivinius et al. 2016; Štefl et al. 1998). Although care was taken to select β Cephei stars based on their dominant frequency and the periodogram features, it is possible that some stars identified as such are imposters, being either hybrid, SPB, or classical Be stars. Nevertheless, all stars classified as β Cephei in this work have observational signatures consistent with their designation. The group of candidates is likely a mix of β Cephei , SPB, and Be stars, and binaries and rotational variables.

6.2.3 Results

We classify 106 stars as β Cephei stars, and an additional 131 as candidates. These are listed in Tables 6.1 and 6.2, respectively, sorted by increasing primary frequency. In addition to an identifier, the primary frequency and its photometric amplitude, coordinates, the V-band magnitude, and the spectral type are listed. The next column indicates if the star is previously known to belong to the β Cephei class (showing the appropriate reference), followed by a column that indicates if the star is a known cluster member. Remarks are listed next, which are especially useful if the target has close visual companions (which is important input for TESS target selection). Twenty of these 106 β Cephei stars were previously known as such; the rest are new discoveries. This is an $\approx$ 40% increase in the number of β Cephei stars known in the Galaxy. The amplitudes listed in Tables 6.1 and 6.2 should be viewed as lower limits, since light from neighboring sources can blend with the target star, acting to dilute the signal. This dilution is strongest in crowded fields. The sky positions (in Galactic coordinates) of the β Cephei and candidate stars identified in this work are shown in Figure 6.2.

In Figure 6.3 we show how the primary detected frequency and its photometric amplitude are distributed, according to spectral type. The β Cephei stars show no obvious correlation between their primary frequency distribution and spectral type, while for the candidates, the primary frequency is highest at a spectral type of B2. The overall median primary frequency is lower for the candidates than for the β Cephei stars. This is expected, since the stars identified as β Cephei pulsators in our analysis must have primary frequencies greater than 4 d^{-1} , while the candidates are not subject to this restriction. The β Cephei amplitudes span a wide range (up to over 40 mmag) between B0 – B3, and then diminish in stars classified as B3.5 and later. Candidates likewise show a wide range of amplitudes between B0 – B1.5, but amplitudes become consistently lower, and the distributions tighter, at B2 and later. Figure 6.4 shows histograms of the frequency, amplitude, and V-mag brightness for β Cephei and candidate stars.

6.2.4 Conclusion

Through a periodicity analysis of light curves for O- and B-type stars from the KELT survey, we identify 106 β Cephei pulsators, of which 86 are new discoveries. This is an $\approx$40% increase in the number of β Cephei stars known in the Galaxy. We identify a further 131 stars as β Cephei candidates, a group that likely contains a mix of genuine β Cephei stars, plus other O- and B-type variables. These new discoveries will be targeted by the TESS mission. The high-quality TESS light curves will then be used to perform asteroseismic studies on this population, revealing valuable information about their interior structure. This information can be leveraged to

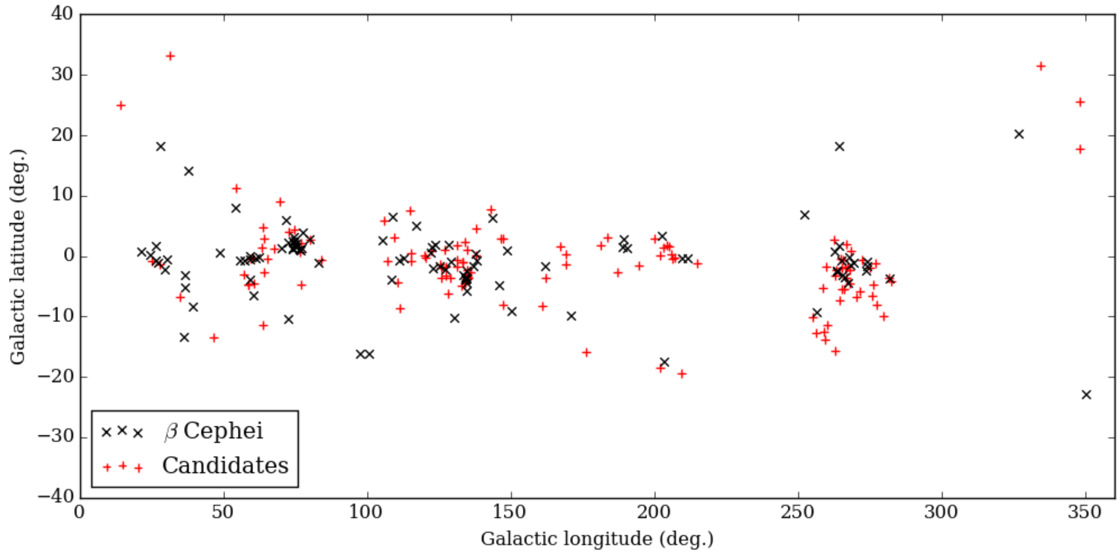

Figure 6.2: Distribution of β Cephei and candidate stars according to their Galactic latitude and longitude.

arrive at important constraints on the structure and evolution of massive stars.

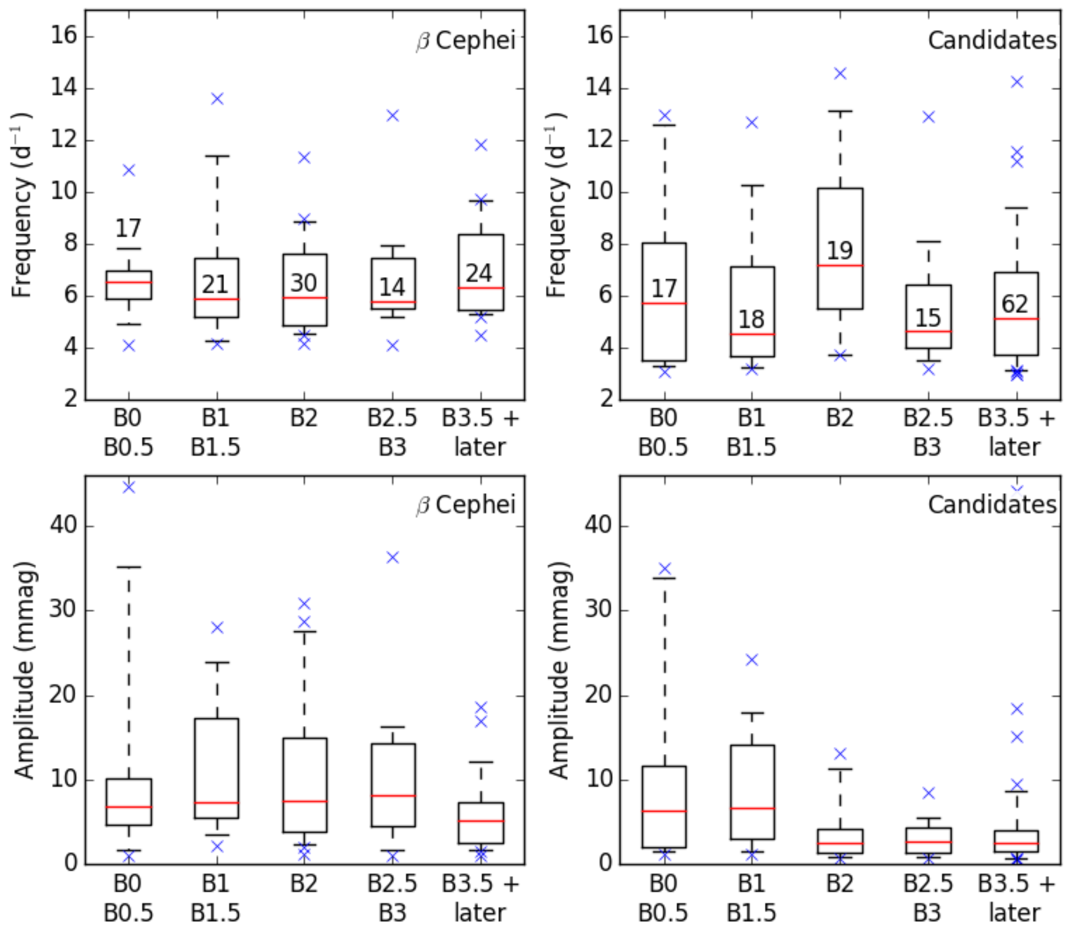

Figure 6.3: Boxplot showing the frequency (top row) and the amplitude (bottom row) distributions for the β Cephei stars (left column) and the candidates (right column). These are split into bins according to their spectral types, as reported in the literature. The numbers in the boxes in the top row indicate the number of objects in that bin. The corresponding bins in the lower row contain the same number of stars. The middle red line in each box is the median, the top and bottom of the boxes mark the 25th and 75th percentile, and the lower and upper whiskers denote the 5th and 95th percentile. Outliers are shown as blue x's.

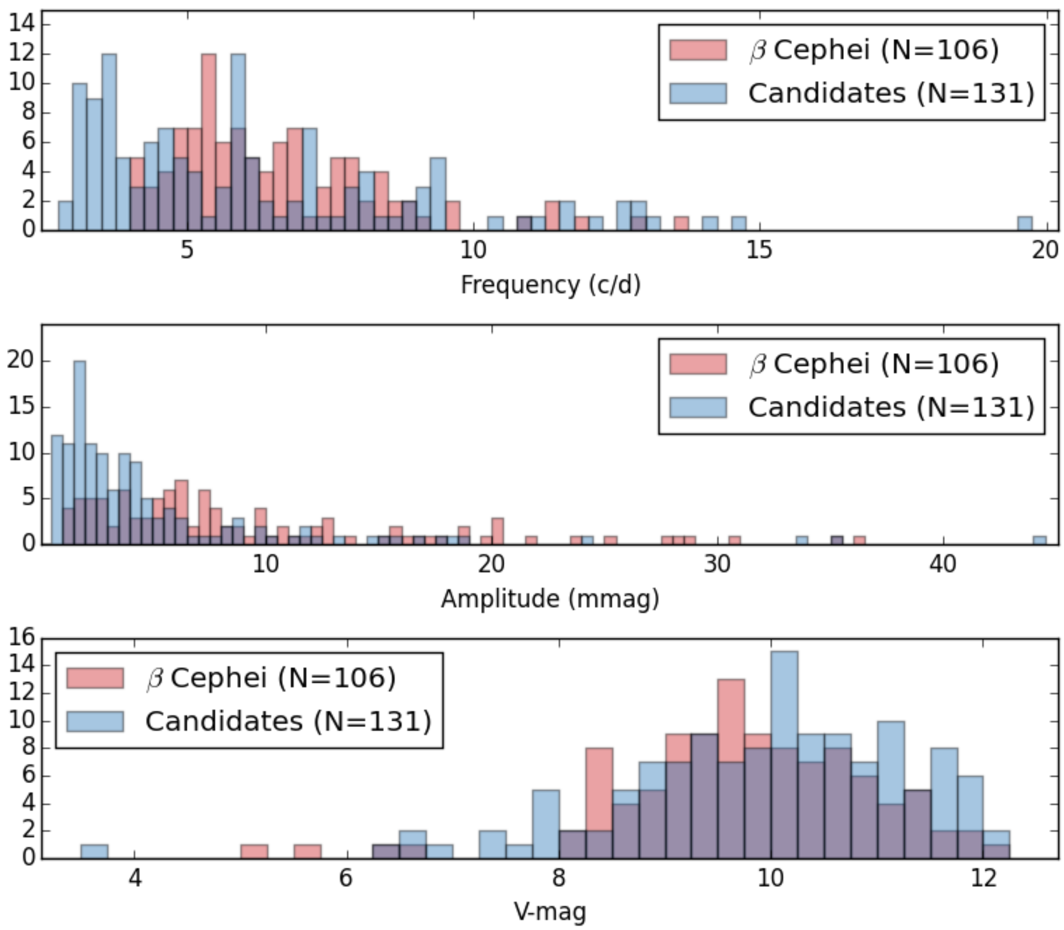

Figure 6.4: Distribution of the primary frequency (top) and the corresponding amplitude (middle) recovered, and the V-band magnitude (bottom) for the β Cephei and candidate stars.

Common ID	Freq. (d^{-1})	Amp. (mmag)	RA (2000)	Dec (2000)	V (mag)	Spectral Type	known?
V757 Per	4.0769	7.9	02 18 23.05	+57 00 36.7	8.43	B0.5III	
ALS 7546	4.1204	16.3	02 55 36.68	+59 24 40.1	10.52	B3III	
V665 Per	4.1275	20.4	02 18 48.02	+57 17 07.9	9.38	B2V	SH05
BD+55 2899	4.1698	20.4	23 07 08.78	+56 00 21.1	10.29	B1IIIp	
HD 350202	4.2299	9.5	19 38 41.60	+20 07 46.8	10.30	B1.5III	
HD 194205	4.4455	11.5	20 23 01.50	+39 20 40.5	9.08	B2III	
HD 190336	4.4571	21.7	20 03 18.68	+33 26 59.7	8.62	B0.7II-III	JSH09
HD 282433	4.4838	5.2	04 45 28.76	+30 16 54.4	9.52	B5	
HD 231124	4.5432	30.9	19 18 52.34	+14 19 41.0	11.10	B2III	
HD 73568	4.5453	3.9	08 37 19.48	−45 12 26.0	8.36	B2III/IV	PP08
HD 14357	4.6030	2.5	02 21 10.44	+56 51 56.4	8.52	B2II/III	
HD 13338	4.6360	6.3	02 12 19.17	+57 56 27.1	9.17	B1III	
BD+64 1677	4.7785	2.8	22 31 13.58	+65 27 58.5	9.00	B2III-IV	
HD 228461	4.7912	8.5	20 14 06.42	+38 14 38.4	9.56	B2II	
ALS 6426	4.8242	10.7	00 59 49.44	+64 39 37.4	10.99	B2III	
HD 14014	4.8970	6.3	02 18 00.02	+56 13 57.3	8.86	B0.5V	
KP Per	4.9558	15.5	03 32 38.98	+44 51 20.7	6.41	B2IV	SH05
BW Vul	4.9741	27.6	20 54 22.40	+28 31 19.2	6.54	B2III	SH05
ALS 12866	4.9919	44.6	23 17 13.70	+60 00 27.9	10.90	B0.5V	
HD 344775	5.1399	7.4	19 43 09.76	+23 26 15.7	10.36	B1III	

TYC 4032-1819-1	5.1536	5.6	01 46 35.59	+61 13 39.2	11.74	B1Ve	SH05?
CD-48 4390	5.1564	4.9	09 04 23.69	−48 46 25.1	11.32	B4/6	
HD 171305	5.1586	8.3	18 34 15.85	−04 48 48.8	8.72	B3III	PP08
12 Lac	5.1789	7.6	22 41 28.65	+40 13 31.6	5.22	B2III	SH05
ALS 6331	5.2183	4.5	00 45 35.06	+63 21 07.4	10.55	B0.5V	
HD 74339	5.2201	25.1	08 41 32.97	−48 01 30.7	9.38	B2III	PP08
V1143 Cas	5.2636	19.8	01 43 35.58	+64 02 06.8	10.86	B1	HM11
CD-46 4432	5.2911	5.8	08 40 30.48	−47 12 35.2	10.00	B5	
HD 232489	5.3769	7.5	01 39 12.85	+51 49 19.1	9.26	B5	
TYC 3324-92-1	5.3848	7.1	03 26 04.74	+50 49 46.6	11.33	B7	
TYC 4031-1770-1	5.3948	3.8	01 28 21.97	+60 14 43.9	10.94	B5	
ALS 9955	5.4431	23.9	18 45 34.43	−05 21 59.0	11.02	B1.5II	
CD-49 3738	5.4451	7.2	08 41 38.55	−49 35 52.9	9.69	B3	
IL Vel	5.4598	28.7	09 17 31.15	−52 50 19.5	9.16	B2III	SH05
HD 77769	5.4681	3.9	09 02 48.21	−46 57 48.9	9.37	B3IV	PP08
HD 75290	5.4869	1.9	08 47 33.74	−42 29 07.0	8.09	B3/5V	
HD 180642	5.4869	28.0	19 17 14.80	+01 03 33.9	8.29	B1.5II	SH05
HD 186610	5.4999	15.4	19 45 27.32	−03 09 06.6	9.70	B3n	PP08
HD 62894	5.5254	1.0	07 44 15.56	−43 01 04.2	9.60	B7/9e	
ALS 7146	5.5486	6.2	02 23 14.38	+58 09 49.5	10.56	B1V	
HD 76967	5.5781	5.2	08 57 54.00	−43 09 12.7	9.07	B3/5V	
HD 48553	5.5980	9.8	06 44 09.94	+02 23 29.6	9.08	B3	PP08

GSC 05124-02524	5.6387	36.3	18 35 53.63	−07 09 53.6	11.91	B3	
HD 232874	5.7400	5.6	04 02 15.74	+53 45 11.8	8.92	B2III	
HD 225884	5.8220	3.0	19 48 15.12	+37 21 59.2	9.43	B5	
16 Lac	5.8503	4.4	22 56 23.63	+41 36 13.9	5.58	B2IV	SH05
HD 228690	5.8721	9.3	20 16 29.22	+37 55 21.2	9.29	B0.5V	
HD 173006	5.8779	35.1	18 43 26.26	−05 46 47.7	10.06	B0.5 IV	PP08
BD+54 490	5.8959	3.5	02 14 20.11	+55 03 33.6	9.53	B1V	
ALS 12345	5.9461	15.9	22 21 51.49	+60 17 09.7	10.43	B3V	
HD 228450	5.9532	4.7	20 13 59.02	+36 32 37.9	9.24	B0.5p	
ALS 10332	6.0443	12.9	19 33 11.45	+01 56 44.2	12.07	B2	
HD 228463	6.0847	17.3	20 14 03.30	+37 45 30.1	9.60	B1V	
V372 Sge	6.0859	17.5	20 09 39.59	+21 04 43.6	8.34	B0.5IIIe	H05
HD 298411	6.0909	5.4	09 26 27.12	−52 09 33.0	10.53	B2/5	
HD 30209	6.1933	12.2	04 47 30.26	+42 19 11.8	8.39	B1.5V	
BD+56 488	6.2736	5.3	02 18 13.52	+57 21 30.9	10.10	B	
HD 228101	6.2998	4.1	20 10 36.69	+37 27 30.6	8.49	B1IV	
BD+56 477	6.3488	6.1	02 17 04.49	+56 58 07.2	10.02	B	
BD+57 655	6.3730	6.5	02 53 28.41	+58 19 32.9	10.12	B2III	
HD 344842	6.5255	6.3	19 41 44.28	+21 29 03.5	9.78	B2III	
ALS 10035	6.5490	6.3	18 53 57.85	−03 48 49.0	11.40	B0.5III	
HD 344894	6.5681	9.5	19 45 48.21	+23 11 42.7	9.61	B2IIIn	
TYC 4030-800-1	6.6171	7.3	01 11 12.15	+61 06 06.2	11.96	B5	

ALS 10186	6.6275	6.9	19 10 27.87	+02 07 32.3	11.67	B0.5V	
CD-44 4596	6.6530	5.6	08 36 59.62	−45 17 23.1	9.30	B1III	
HD 339003	6.7997	12.7	19 51 02.86	+25 57 15.4	9.93	B0.5III	
HD 229085	6.8744	5.5	20 21 35.13	+38 36 47.8	9.80	B0V	
CD-47 4562	6.8803	8.6	08 58 23.73	−48 11 08.7	10.90	B5V	
BD+57 614	6.9250	2.4	02 42 19.47	+58 05 30.0	10.69	B2III	
BD+41 3736	6.9397	2.6	20 24 33.90	+42 14 15.5	10.55	B6	
V836 Cen	6.9661	8.2	14 46 25.76	−37 13 20.1	8.05	B3V	SH05
BD-02 4752	6.9779	7.0	18 49 25.06	−02 21 09.8	10.48	B0.5V	
HD 178987	7.1466	7.6	19 12 59.64	−47 09 39.5	9.83	B2II	PP08
BD+66 1651	7.2884	1.8	23 52 12.14	+67 10 07.5	9.97	B3e	
HD 166331	7.4476	12.6	18 09 50.41	+10 46 26.5	9.39	B1.5III	
HD 86248	7.4897	6.2	09 56 33.26	−31 26 31.0	9.56	B3II	PP08
HD 343642	7.5007	11.2	19 01 46.01	+22 34 17.8	10.42	B3	
HD 253021	7.5753	3.7	06 11 42.41	+21 37 58.7	10.16	B2	
HD 228699	7.5964	2.7	20 16 36.74	+37 41 12.8	9.46	B0.5III	
HD 160233	7.6411	4.1	17 38 40.64	+04 20 09.8	9.04	B2IV/V	
HD 81370	7.7088	10.1	09 23 17.73	−52 44 52.3	8.81	B0.5IVn	
CD-44 4876	7.7826	16.9	08 50 16.09	−45 23 02.5	10.94	B3/5	
HD 227977	7.8305	20.1	20 09 17.22	+37 30 07.9	9.68	B2III	
HD 86162	7.8416	1.0	09 54 47.75	−59 16 03.3	9.21	B01/IV	
ALS 14570	7.9203	1.1	00 49 11.38	+64 11 21.9	11.28	B3IV	

ALS 6392	7.9518	13.5	00 53 35.57	+60 47 08.7	10.32	B2IVnn
HD 345370	8.0541	18.8	19 56 58.66	+21 19 49.7	9.75	B2III
HD 228456	8.1827	5.5	20 14 02.31	+36 48 07.0	10.20	B2IV
HD 339039	8.2695	9.5	19 48 46.69	+24 48 21.0	9.69	B1.5V
HD 228365	8.2886	5.0	20 13 01.17	+41 01 42.1	9.97	B1V
HD 73918	8.2949	2.0	08 39 53.96	−30 29 59.9	9.70	B5III
TYC 2682-73-1	8.4179	3.8	20 05 57.78	+35 57 13.7	10.09	B1Vn
HD 18100	8.5480	1.6	02 53 40.81	−26 09 20.4	8.44	B5II/III
HD 290564	8.6575	12.2	05 32 08.73	+00 07 36.8	11.20	B5
HD 192003	8.8495	3.0	20 11 16.85	+38 13 48.0	8.85	B2IV
HD 227728	8.9711	1.2	20 06 49.54	+38 01 39.4	9.91	B2V
TYC 4280-2061-1	9.1495	18.7	23 29 03.17	+60 46 16.5	11.07	B6V
TYC 750-467-1	9.6644	2.3	06 44 16.00	+10 28 11.8	11.26	B6/9
TYC 3152-1307-1	9.6946	1.8	20 23 06.70	+38 49 15.6	10.62	B5
HD 49330	10.8591	1.7	06 47 57.27	+00 46 34.0	8.95	B0nnep
BD-09 4742	11.3216	2.1	18 28 20.13	−09 35 05.2	10.50	B2V
HD 199021	11.3847	2.2	20 52 53.21	+42 36 27.9	8.49	B1IV
BD+60 770	11.7894	10.8	04 00 49.57	+61 17 26.5	9.80	B5
HD 254346	12.9661	2.9	06 16 57.32	+22 11 42.0	9.74	B2/3III
HD 42896	13.5970	7.3	06 14 06.19	+20 10 10.9	8.62	B1Vnn

Table 6.1: Stars identified as β Cephei variables through light curve analysis. The final column indicates if a star is previously known to be a β Cephei variable by listing the appropriate reference. The majority of these are new discoveries. H05 : Handler (2005); HM11 : Handler and Meingast (2011); JSH09 : Jurcsik et al. (2009); PP08 : Pigulski and Pojmański (2008); S13 : Saesen et al. (2013); SH05 : Stankov and Handler (2005)

Common ID	Freq. (d^{-1})	Amp. (mmag)	RA (2000)	Dec (2000)	V (mag)	Spectral Type	known?
CD-45 4896	2.9677	4.7	09 08 50.23	−46 25 58.9	10.75	B7IV	
HD 72539	2.9852	1.6	08 31 22.31	−48 44 56.9	7.97	B5V	
ALS 6915	3.0730	7.1	02 06 08.56	+63 22 11.8	10.24	B0.5e	
CD-49 4294	3.0901	5.7	09 18 19.05	−50 18 46.9	11.24	B3/5	
CPD-55 2071	3.1218	1.6	09 18 11.17	−56 01 33.3	10.80	B7e	
HD 248434	3.1336	4.0	05 51 38.52	+21 32 28.1	10.68	B5ne	
CPD-52 1713	3.1628	1.8	08 51 15.55	−53 27 03.0	11.30	B7e	
HD 298610	3.1712	4.0	09 39 00.81	−54 03 45.3	9.83	B2/4	
BD+05 4404	3.1828	2.4	20 04 42.72	+05 33 19.6	10.47	B5	
V447 Cep	3.1845	18.0	22 10 59.56	+63 23 58.5	7.46	B1Vk	
HD 333172	3.2152	6.9	19 57 53.88	+28 19 51.2	10.35	B1II	
HD 279639	3.2317	4.0	04 18 03.37	+38 57 47.0	11.06	B7	
HD 261630	3.2593	2.6	06 39 49.73	+05 04 37.7	10.07	B5	
TYC 3151-109-1	3.2891	3.0	20 17 43.65	+39 20 36.2	11.02	B5V	
BD+61 2515	3.3052	11.6	23 45 43.89	+62 17 31.2	10.00	B0.5V	
ALS 6330	3.3131	2.5	00 45 17.23	+63 42 36.8	11.10	B1III	
ALS 7879	3.3264	10.4	04 05 03.97	+56 13 06.3	11.79	B0p	
HD 331621	3.3436	1.2	19 56 59.97	+31 17 16.0	9.98	B7	
HD 220300	3.3830	8.7	23 22 10.46	+56 20 53.6	7.93	B6IVne	

HD 62755	3.4328	0.8	07 43 23.09	−47 02 48.0	7.85	B5V
HD 74533	3.4462	1.2	08 42 28.52	−49 45 53.1	9.17	B5IV
HD 229171	3.5030	9.8	20 23 02.88	+38 27 20.8	9.38	B0.5IIIne
TYC 4033-2268-1	3.5118	4.6	02 15 28.61	+60 09 44.6	11.69	B3
ALS 7011	3.5118	5.7	02 15 24.53	+60 08 21.4	10.63	B0III
CD-56 2603	3.5513	3.6	09 05 41.99	−57 00 02.9	11.76	B1III/Ve
BD+41 3731	3.5563	2.8	20 24 15.72	+42 18 01.4	9.84	B2/3ne
V352 Per	3.6438	2.9	02 13 37.02	+56 34 14.3	9.31	B1III
HD 78206	3.6997	1.8	09 04 22.00	−59 09 24.9	8.84	B7/8V
CD-40 4269	3.7008	4.4	08 27 31.64	−41 24 48.4	10.35	B1/3
HD 59325	3.7152	3.9	07 26 56.07	−51 11 07.0	10.55	B7V
HD 261172	3.7193	11.3	06 38 31.56	+09 25 12.2	10.10	B2III
HD 249179	3.7216	2.8	05 55 55.05	+28 47 06.4	10.00	B5ne
HD 339483	3.7241	17.8	20 04 00.75	+26 16 16.8	8.98	B1IIIe
TYC 3315-1807-1	3.7614	44.1	03 21 39.63	+47 27 18.8	11.73	B7
HD 19635	3.8763	2.4	03 12 56.84	+63 11 12.4	8.94	B4
TYC 4804-1086-1	3.9139	18.5	06 50 31.54	−02 19 45.9	11.91	B5
BD+56 579	3.9560	1.5	02 22 19.23	+57 37 12.9	10.88	B7IVe
BD+57 579	3.9621	4.0	02 30 14.05	+57 40 30.3	10.09	B2III
BD+60 192	4.0051	9.5	01 14 30.29	+60 53 28.8	9.39	B5
HD 196035	4.0083	2.8	20 34 09.98	+20 59 06.7	6.47	B3IV
HD 76307	4.0110	4.9	08 53 28.33	−47 31 07.6	9.27	B2/3V

BD+62 258A	4.3293	8.3	01 30 06.14	+63 34 57.2	10.32	B1IV	
HD 78507	4.3680	0.9	09 05 39.03	−62 06 12.6	8.12	B6V	
ALS 8706	4.4060	4.6	06 06 28.15	+27 18 32.3	11.68	B1IIIe	
NGC 884 2579	4.4147	3.9	02 22 50.28	+57 08 50.7	11.91	B3e	S13
HD 86214	4.4426	12.4	09 54 58.43	−59 49 46.7	9.21	B1III	PP08
HD 29332	4.4491	1.5	04 39 04.89	+41 15 00.0	8.71	B3ne	
HD 74581	4.5450	15.1	08 42 47.92	−48 13 31.1	9.12	B6/8V	
BD+56 584	4.5816	3.8	02 22 29.86	+57 12 28.8	9.61	OB	S13
HD 280753	4.6168	1.4	05 18 05.96	+38 17 40.6	10.21	B3	
HD 29450	4.6172	0.7	04 39 13.54	+22 39 08.1	8.57	B7V	
KK Vel	4.6373	14.8	09 07 42.52	−44 37 56.8	6.78	B1.5II	SH05
HD 172367	4.6882	8.5	18 40 09.71	−07 15 02.0	9.54	B2III	
CD-44 4571	4.7460	1.5	08 35 52.40	−44 39 23.5	10.88	B5V	
HD 60794	4.7814	4.3	07 34 06.86	−46 38 37.7	8.73	B3/5IIIe	
ALS 10464	4.8883	11.8	19 44 21.08	+23 17 05.9	11.82	B0.5V	
BD+58 241	4.8896	1.6	01 27 54.88	+59 14 08.9	9.91	B1V	
TYC 4050-1949-1	4.9542	3.9	02 30 19.98	+63 00 23.4	11.21	B7V	
o Vel	4.9773	0.7	08 40 17.59	−52 55 18.8	3.63	B3/5V	
HD 350990	5.0251	3.4	19 58 49.85	+20 31 29.9	10.32	B7II/III	
BD+56 560	5.1899	4.4	02 21 32.75	+57 34 07.1	10.24	B2III	
HD 14645	5.2131	1.7	02 24 01.13	+58 19 25.9	9.43	B0IVnn	
HD 190088	5.2399	3.0	20 01 45.46	+38 44 06.9	7.86	B5	

HD 67980	5.4045	2.3	08 08 44.04	−42 37 07.6	10.53	B7II	
GSC 00155-00374	5.5399	8.0	06 38 13.40	+05 33 20.0	11.90	B7V	
HD 140543	5.6086	2.0	15 44 56.66	−21 48 53.9	8.88	B0.5IIIn	
BD+60 416	5.7340	1.6	02 01 44.21	+61 03 13.0	9.61	B0.5III	
HD 277933	5.7713	1.4	05 17 51.12	+40 23 27.0	10.14	B3	
CPD-45 2977	5.7728	2.3	08 45 10.44	−45 58 54.7	10.98	O9.5II	
HD 236939	5.7791	3.6	02 04 33.68	+56 33 00.6	10.19	B5	
V611 Per	5.8246	3.2	02 18 29.83	+57 09 03.1	9.35	B0.5I/V	SH05
BD+68 1373	5.8301	3.8	23 22 50.65	+69 00 34.7	9.14	B2III	
HD 260858	5.8902	1.2	06 37 46.71	+12 46 05.1	9.15	B6He	
HD 262595	5.9053	5.9	06 43 06.31	+07 36 03.8	11.19	B3/5	
HD 37115	5.9098	6.0	05 35 54.08	−05 37 42.3	7.40	B7Ve	
BD+55 334	5.9102	1.5	01 28 39.05	+56 21 04.3	10.41	B2e	
ALS 1302	5.9676	8.6	09 25 42.12	−53 14 19.5	11.73	B3	
HD 130195	5.9765	1.6	14 47 31.92	−24 12 05.2	10.66	B6II	
TYC 4269-482-1	5.9867	1.9	22 50 26.49	+62 42 03.0	10.78	B5/8V	
TYC 4031-1324-1	6.0165	3.5	01 27 04.47	+60 49 08.1	11.07	B5	
HD 69824	6.0635	3.6	08 16 38.69	−48 26 11.2	9.09	B4/6V	PP08
HD 261589	6.0890	5.0	06 39 44.90	+06 27 35.6	11.43	B7	
HD 258853	6.1398	2.5	06 31 14.87	+09 47 25.0	8.83	B3Vnn	
HD 72090	6.1756	1.6	08 28 52.24	−48 11 25.6	7.84	B6V	
HD 144941	6.3440	1.5	16 09 24.55	−27 13 38.2	10.02	B1/2II	

HD 59259	6.4427	1.5	07 27 03.03	−44 10 40.2	9.95	B7/8V
HD 33308	6.7355	0.9	05 11 07.96	+37 18 06.8	8.78	B3
HD 332408	6.7778	2.5	19 42 07.98	+28 59 45.6	8.94	B2IV
BD+56 537A	6.8061	2.3	02 19 39.13	+57 16 13.2	10.34	B2V
HD 190066	7.0184	15.6	20 02 22.10	+22 09 05.2	6.60	B1Iab
HD 59446	7.0191	0.8	07 27 42.78	−47 24 50.4	7.59	B6II/III
TYC 1624-299-1	7.0305	1.4	19 58 41.30	+20 31 48.6	12.04	B7IVnnp
HD 228290	7.1226	7.5	20 12 20.66	+38 00 07.6	9.47	B1II
CD-44 4484	7.1391	3.2	08 30 53.51	−44 58 33.2	9.76	B5
HD 61193	7.1893	0.7	07 36 14.33	−42 04 56.2	8.20	B2Vn
GSC 01314-00792	7.2264	5.4	06 12 02.90	+15 23 10.0	11.50	B5
HD 237204	7.3604	13.1	04 00 23.28	+56 54 05.7	9.18	B2III
BD+35 4258	7.5905	2.9	20 46 12.66	+35 32 25.6	9.46	B0.5Vn
BD+56 540	7.7903	3.2	02 19 42.66	+56 58 45.8	10.28	B5
CD-46 4639	7.9231	0.7	08 49 39.68	−46 50 53.2	10.05	B3He
HD 236664	7.9873	33.9	01 13 41.79	+59 05 57.4	10.05	B0.5V
TYC 8610-895-1	8.0080	4.3	09 53 23.95	−58 57 36.2	11.23	B5/7
BD+61 77	8.0205	1.2	00 26 23.21	+62 45 38.9	9.61	B1IV
ALS 13180	8.0279	35.0	23 47 51.68	+61 05 45.9	11.00	B0III
CD-45 4663	8.0717	5.5	08 52 29.74	−45 37 03.9	11.31	B1/4
BD+29 3644	8.3034	2.4	19 33 49.91	+29 29 56.3	11.27	B5
HD 338862	8.6542	4.0	19 46 18.34	+27 27 37.4	9.92	B2V

ALS 11602	8.7851	1.3	20 53 04.97	+43 37 13.2	11.21	B2Vn
TYC 2682-3173-1	8.9049	2.4	19 58 39.75	+37 00 23.3	11.72	B5
CD-47 4494	9.0207	0.6	08 54 20.85	−48 25 49.5	9.69	B5
TYC 746-578-1	9.0529	2.9	06 41 53.08	+08 24 17.7	11.68	B6/9
HD 35612	9.0839	0.8	05 26 06.00	+00 50 02.4	8.30	B7Vn
ALS 12613	9.2767	16.6	22 47 39.21	+58 09 32.6	10.66	B0.5V
V652 Her	9.3474	3.7	16 48 04.69	+13 15 42.4	10.51	B2He
BD+60 185	9.3790	1.5	01 13 05.69	+61 24 44.9	10.07	B7V
ALS 10538	9.3965	24.3	19 48 53.68	+19 58 07.0	11.33	B1V
HD 344880	9.4929	1.3	19 45 42.31	+23 59 04.0	9.34	B0.5IIInn
HD 174298	10.2571	5.3	18 48 55.63	+24 03 21.1	6.53	B1.5IV
BD+62 647	10.9253	2.3	04 05 34.01	+62 47 28.6	9.58	B2V
TYC 3683-1328-1	11.1849	4.5	01 39 47.92	+58 45 24.4	11.68	B5
HD 183535	11.5196	1.6	19 28 38.16	+36 46 45.1	8.64	B5
LS I +61 294	11.6465	1.3	02 33 43.00	+61 26 12.2	10.89	B2III
ALS 7541	12.2005	1.9	02 54 57.47	+59 15 57.6	10.71	B2II
HD 151654	12.5893	6.4	16 48 49.41	−03 36 39.4	8.60	B0.5V
ALS 9974	12.6760	6.4	18 47 15.69	−05 00 57.5	12.21	B1V
TYC 4032-93-1	12.9147	2.0	01 58 38.10	+60 05 55.7	10.68	B3
ALS 6216	12.9568	2.0	00 28 37.71	+62 29 17.7	10.20	B0.5V
CD-44 4871	13.1270	1.2	08 50 09.76	−44 37 22.5	10.44	B1/3
HD 221991	14.2427	0.8	23 36 32.16	+52 37 12.6	9.84	B5

HD 76554	14.5878	0.9	08 55 25.94	−41 04 43.9	8.33	B2Vne
HD 181124	19.7114	1.7	19 19 18.34	−01 22 50.4	9.62	B5

Table 6.2: Stars identified as candidate β Cephei variables through light curve analysis. The final column indicates if a star is previously known to be a β Cephei variable by listing the appropriate reference. H05 : Handler (2005); HM11 : Handler and Meingast (2011); JSH09 : Jurcsik et al. (2009); PP08 : Pigulski and Pojmański (2008); S13 : Saesen et al. (2013); SH05 : Stankov and Handler (2005)

6.3 Eclipsing Binaries

We identify 11 stars from the BK sample as eclipsing binaries (EBs). The orbital periods of these systems range from ~1 day to 206 days, and show a wide range of morphologies. Some of these systems have been studied extensively in the literature (e.g. BK-048 = HD 33357), while others are newly discovered EBs. A few of these systems are decidely not classical Be stars, despite being previously identified as such in the literature. Brief descriptions of these systems are given below, ordered by increasing orbital period. Plots of phased light curves for these systems are displayed in Figure 6.5.

BK-560 = AS 25 = ALS 6626 (P = 0.98521 d)

This is not listed in the literature as an EB, but is marked as being RV variable by McCuskey et al. (1974). This object is also listed in a catalog of stars with Hα emission (Kohoutek and Wehmeyer 1999). No BeSS spectra are available. Given the short orbital period derived from KELT photometry (P=0.98521 days), and the previously identified RV variability, this is not a classical Be star with a decretion disk, but is more likely to be a binary system where one of the two components is accreting mass from the other (an Algol system). It is this accretion disk that gives rise to the hydrogen emission.

BK-048 = HD 33357 = SX Aur (P = 1.2101 d):

This star is listed in BeSS as having spectral type B1Vne, although none of the contributed BeSS spectra for this object show Hα in emission. This has been known to be an EB since at least 1938 (Luyten 1938). This system was recently studied by Öztürk et al. (2014), who modeled the orbital and stellar parameters of the system. They conclude that the system is a rare example of a binary pair at the border between semi-detached and contact phases with the primary and secondary components having spectral types of B2V and B4V respectively. Furthermore, they determine that the orbital period is increasing at a rate of 0.0055 s/yr as a result of non-conservative mass transfer from the secondary to the primary component.

BK-047 = IU Aur = HD 35652 (P = 1.8115 d):

This star is listed in BeSS as having a spectral type of B3Vnne, although none of the contributed BeSS spectra for this object show Hα in emission. This system is a known β Lyrae type EB. Özdemir et al. (2003) analyze the timing of this system and find evidence for a third component orbiting the system on an eccentric orbit ($e = 0.62$) with a period of 293.3 days, noting that the third body is likely a binary pair itself.

BK-345 = BD+61 2408 = V808 Cas ($P = 2.5991$ d):
This star is listed in BeSS as having a spectral type B0IIIpe, and is classified as a B0.2IV star by Negueruela et al. (2004). The two contributed BeSS spectra do not show emission features, and it is unclear where this has been identified as an emission line star. Lefèvre et al. (2009) list this as a variable OB star based on Hipparcos photometry. More specifically, they classify V808 Cas as a SPB type star with a period of 1.300 days and an amplitude of 0.187 mag. This is half the period we find using KELT data, but we classify this system as an EB based on the morphology of the phased light curve, which shows two distinct eclipses with different depths. A literature search gives no indication of V808 Cas being a classical Be star, nor is this system known to be an EB.

BK-310 = CW Cep = HD 218066 ($P = 2.7291$ d):
This object is a known early-type double-lined EB with apsidial motion indicating a third companion (e.g. Wolf et al. 2006). Many BeSS spectra show clear emission, although it is unclear if the emission can be attributed to a decretion disk typical of a classical Be star.

BK-005 = RW Tau = HD 25487 ($P = 2.7688$ d):
Although listed as a Be star in BeSS, this system is not a classical Be star. Vesper and Honeycutt (1993) present evidence that this is a B8V + K0IV system, noting six different explanations for the Hα emission (their section 7), none of which is a 'normal' Be star decretion disk. The Hα line is modulated by the orbital period, and the most likely explanation is the presence of an accretion disk where mass is being transferred to the B-type component. When the hot B-type star is eclipsed by the cooler giant, the depth of the primary eclipse dips below KELT's faintness

threshold, but appears to be at least three magnitudes deep in the KELT passband.

BK-600 = RY Gem = HD 58713 ($P = 9.3014$ d):

This is a known EB of Algol type. BeSS spectra show that this is indeed an emission line star. Plavec and Dobias (1987) classify this as a moderately interacting Algol-type EB consisting of an A0V primary and a K0IV secondary, with clear evidence for circumstellar absorption and emission from circumstellar material around the primary component. The primary eclipse reaches a depth of around 1.5 mag in the KELT passband.

BK-009 = RW Per = HD 276247 ($P = 13.197$ d):

This is a known EB of Algol type, where the two components are a B9.6e IV-V and a K2 III-IV star (Wilson and Plavec 1988). Two BeSS spectra show emission with clear double-peaks.

BK-213 = HD 84511 ($P = 32.996$ d):

This star is included in the Jaschek and Egret (1982) catalog of Be stars, and the single BeSS spectrum shows Hα in emission. There is significant out of eclipse variability in the KELT light curve. Houk and Cowley (1975) find this to have shell-absorption lines, classifying HD 84511 as a Bp shell star. This was found to be an EB with a period of 32.99 days by Pojmanski (2003).

BK-175 = FY Vel = HD 72754 ($P = 33.745$ d):

Many BeSS spectra show an extremely strong, narrow, single-peaked Hα emission feature, but this is listed as a shell star in BeSS (B2IIpshe). This system is a known β Lyrae type EB (Thackeray et al. 1970).

BK-013 = MWC 800 ($P = 205.64$ d):

No BeSS spectra are available for this object. This is included in the Kohoutek and Wehmeyer (1999) catalog of Hα emission stars in the Northern Milky Way, which is where the B'e' designation comes from. Likely an interesting system, but is not a classical Be star judging by the morphology of the KELT light curve when phased to what we presume is the orbital period.

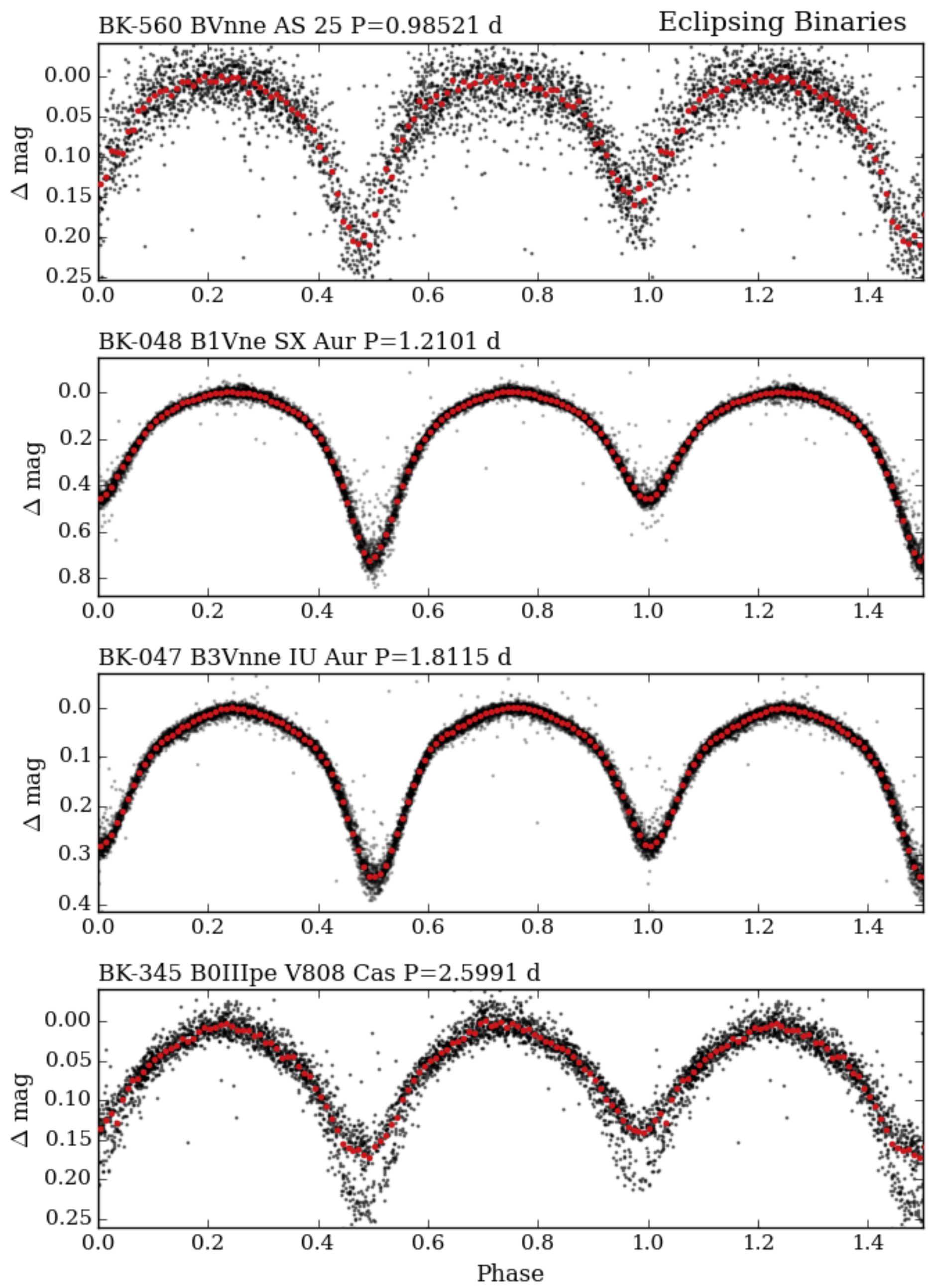

Figure 6.5: Phased KELT light curves for all objects identified as EBs from the BK sample, displayed in order of increasing period. Red points show the data median-binned with a bin size of 0.01 in phase. The object identifier, spectral type, BK number, and period are printed above each sub-plot.

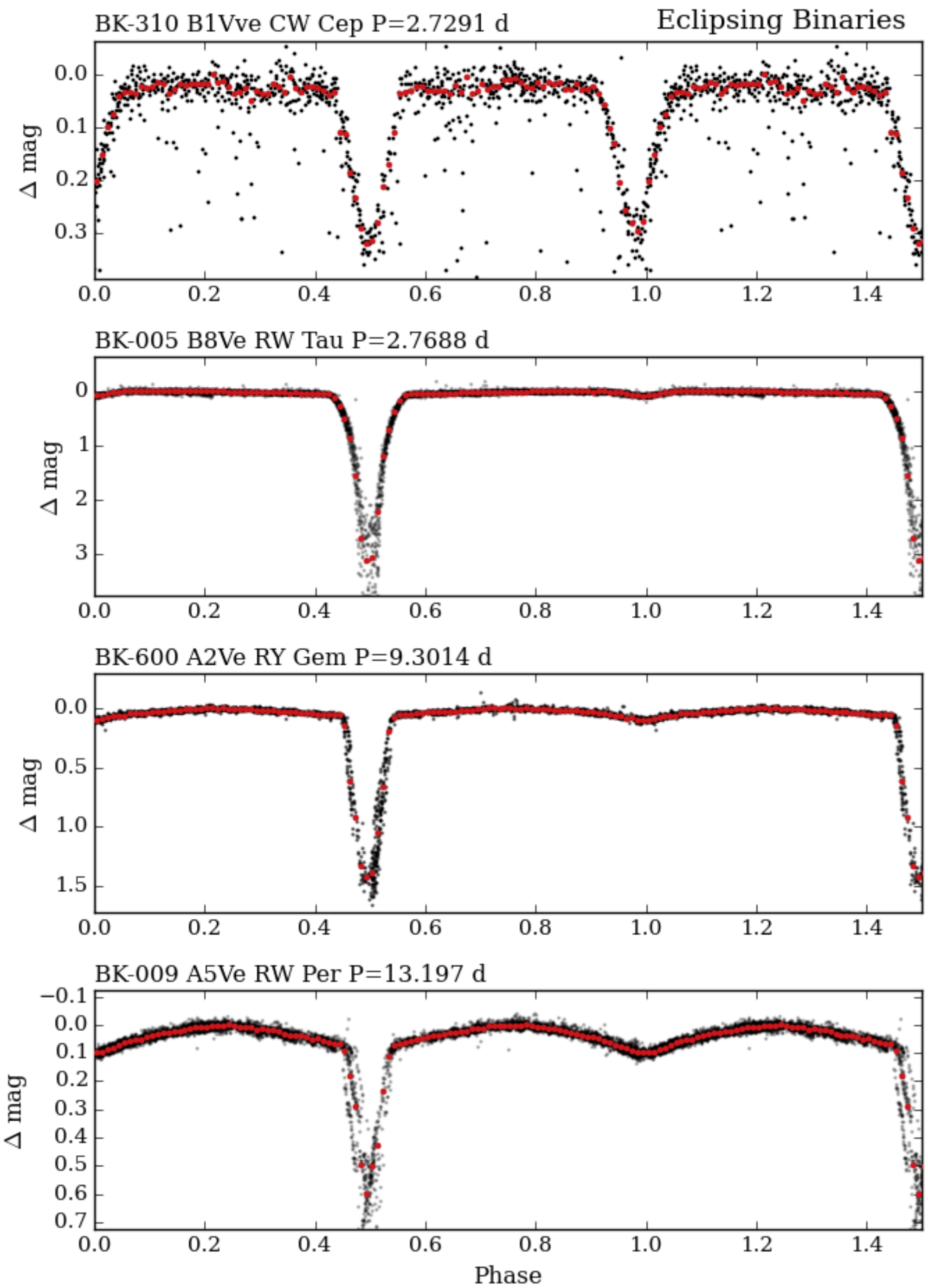
BK-310 B1Vve CW Cep P=2.7291 d
Eclipsing Binaries
BK-005 B8Ve RW Tau P=2.7688 d
BK-600 A2Ve RY Gem P=9.3014 d
BK-009 A5Ve RW Per P=13.197 d
Δ mag
Phase

Figure 6.5: B

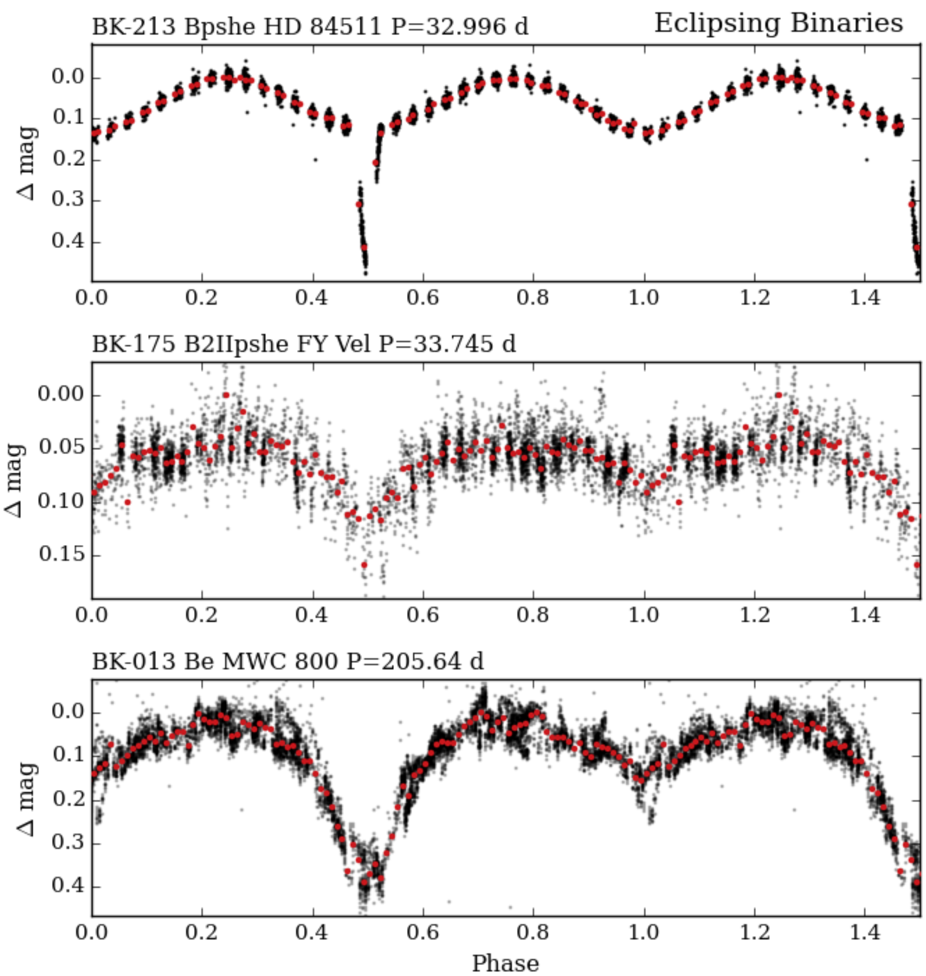
BK-213 Bpshe HD 84511 P=32.996 d
Eclipsing Binaries
Δ mag
0.0
0.1
0.2
0.3
0.4
0.0
0.2
0.4
0.6
0.8
1.0
1.2
1.4
BK-175 B2IIpshe FY Vel P=33.745 d
Δ mag
0.00
0.05
0.10
0.15
BK-013 Be MWC 800 P=205.64 d
Δ mag
Phase

Figure 6.5: C

Chapter 7

Conclusions and Future Work

7.1 Summary

The fractions of stars in the BK sample showing different types of variability are summarized in Table 7.1. There are many cases where a star exhibits both non-periodic (*e.g.* outbursts) and periodic variability (*e.g.* pulsations). These categories are not mutually exclusive.

From analyzing the KELT light curves of the BK sample of Be stars, we arrive at a few important conclusions. Consistent with other studies (*e.g.* Chojnowski et al. 2015; Cuypers et al. 1989; Gutiérrez-Soto et al. 2008), we find that Be stars are a highly variable class of objects, with a greater apparent degree of variability seen in earlier, compared to later, spectral types. About 1/4 of Be stars with three or more clear photometric outbursts have them occurring at semi-regular intervals. Intermediate periodicity between 2 and about 100 days is a common occurrence, and is seen in 38% of our sample. Systems showing periodic variability on timescales of tens of days or greater are good targets for further study, as some of these are likely to be binaries. By combining KELT data with BeSS spectra, we provide evidence that photometric outbursts correspond to disk creation or disk building events, and that global disk oscillations manifesting in V/R variability can also modulate the brightness of a Be star + disk system. It is clear that Be star variability can vary

Table 7.1: Variability fractions, according to variable type and spectral designation

Variable Type	*All*	*Early*	*Mid + Late*	*Unclassified*
OTB	36% (168/470)	51% (135/265)	12% (16/139)	26% (17/66)
SRO	24% (35/145)	24% (29/121)	25% (3/12)	25% (3/12)
LTV	37% (81/217)	45% (54/121)	21% (15/73)	52% (12/23)
NRP	24% (124/510)	28% (80/287)	21% (32/155)	18% (12/68)
IP	38% (194/510)	51% (145/287)	19% (30/155)	28% (19/68)
EB	2.2% (11/510)	1.7% (5/287)	1.9% (3/155)	4.4% (3/68)

Fraction of stars showing each type of variability in the BK sample, according to their spectral type. The category 'all' includes early-, mid-, and late-type stars, as well as those unclassified in BeSS. Variable types mean the following: "OTB" : one or more outburst, "SRO" : semi-regular outbursts, "LTV" : long-term variability on timescales of years, "NRP" : signals corresponding to stellar non-radial pulsations, with periods less than two days, "IP" : intermediate periodicity, on timescales longer than two, and up to about 100 days, "EB" : eclipsing binary. The fraction of systems with SRO is calculated from the subset of stars showing at least three outbursts, and EBs from all non-saturated objects. See Sections 4 and 5, for explanations of the subsets of the BK sample considered for these variability types.

dramatically from object to object, and even a wide range of behavior is sometimes seen in a single given system.

It has become clear that some systems listed as classical Be stars in BeSS have been mis-classified as such. Given the intrinsic variability of classical Be stars, they may or may not have a circumstellar disk (and the associated emission-line signals) at a given epoch, making it difficult to validate or invalidate their classification. However, there are some cases where there is substantial evidence against the 'classical Be star' designation. For example, KELT photometry reveals some systems that are short-period eclipsing binaries, where an accretion disk in a mass-transferring binary system is a more reasonable explanation for any observed emission-line signals. We therefore urge the reader to use caution when consulting the literature regarding the spectral classification of B-type emission line stars, as there are taxonomically different systems that can produce similar observables (see Porter and Rivinius (2003) for an overview of these).

We have analyzed optical light curves for 160 classical Be stars in the AK sample to study the disk creation process, and to monitor the evolution and demise of these disks once formed. These discrete episodes of disk creation leave a generally consistent imprint in a light curve, rising from baseline to a peak brightness, then falling back towards baseline on a relatively longer timescale. The frequency of occurrence, amplitude, and associated timescales can vary greatly, not only from one star to the next, but also for any given system. In most cases, outbursts occur with no discernible pattern. However, there are some systems that experience outbursts that repeat at a nearly regular rate, and with similar amplitudes. ABE-A01 is one such example, with four others shown in Figure 4.12. In this sample, we find 44 stars (28%) to have at least one outburst detected in their KELT light curve. On average, the duration of the falling phase is about twice that of the rising phase for early- and mid-type stars, and larger for late-type stars (see Figure 4.16). Amplitudes up to $\sim$0.5 mag (in a wide $\sim$R-band filter) are seen (Figure 4.15). A higher degree of photometric variability is seen in early-type stars, which are more likely to have at least one detectable outburst compared to their cooler counterparts (see Table 7.1).

KELT light curves are generally sensitive to only the inner-most region of Be star disks, giving us clues as to how the circumstellar environment closest to the star changes. By including time-series spectroscopy of the hydrogen Brackett series from the NIR APOGEE survey, and Hα spectra from the BeSS database, we have many 'snapshots' of the circumstellar environment. This allows us to unambiguously infer the presence of a disk, and also to measure its strength, projected velocity profile, and any asymmetries. By leveraging spectra taken during active outburst phases, we have shown that the circumstellar environment can be quite asymmetric during disk growth (ABE-138, -A01). The material settles into a more axisymmetric configuration over time, according to the predictions of the VDD model. Another advantage of combining optical photometry and the Br11 and Hα lines is that these observables probe different regions of the disk. Instances where these different observational modes are measured near-contemporaneously show evidence of the Be star disk both growing, and also dissipating, from the inside outward, in agreement with theoretical expectations.

The Be stars discussed in detail in the AK sample experience outbursts that occur over a wide range of timescales – days (*e.g.* ABE-138), weeks (*e.g.* ABE-098), months (*e.g.* ABE-A01), and years (*e.g.* ABE-026; and ABE-082, -160 in the Appendix for non-shell stars). Other works have similarly observed apparent outbursts over a large range in time. Analysis of Kepler data has shown aperiodic Be star variability with amplitudes below 10 mmag and timescales of days to weeks, which may indicate small-scale outbursts (Balona et al. 2015; Rivinius et al. 2016). On the other hand, some Be stars experience outbursts with timescales of many hundreds or thousands of days and greater. These longer outbursts can leave a qualitatively different light curve signature, where the rising phase is followed by a plateau in brightness. This plateau can persist for thousands of days, and even up to decades, so long as the disk-feeding mechanism remains active. In this scenario, the inner disk continues to be fed by mass ejected from the star, but at some point becomes saturated, and the addition of new material does not increase its brightness. These 'more complete' disk building events are modeled in Haubois et al. (2012a), and are observed in some Be stars (*e.g.* ω CMa; Ghoreyshi and Carciofi 2017). Be stars lose mass in episodes of vastly varying intensity and duration. With this in mind, the outbursts explored in detail in this work address only part of the story of Be star mass loss.

7.2 Future Work

There is still much that can be done with both currently available data, and further observations, beyond what has been discussed in this work. Light curve analysis has revealed numerous interesting systems that are deserving of closer scrutiny. The methods used to recover variability in this work are being refined, and larger sample sizes are being used to arrive at more robust statistics. New discoveries of previously unknown Be stars are being made, and light curves will be modeled to reveal more details about the dynamical processes involved with disk growth and dissipation. Of particular interest is analyzing the light curves of the SRO variables to look for evidence of difference frequencies that may be tied to the observed outburst events.

7.2.1 Discovering New Be Stars

Although Be stars as a population are diverse, there are often certain characteristic features imprinted in their optical light curves, such as outbursts and long-term variation. This provides a natural path for discovering new Be star candidates through light curve analysis. I have already begun this process with KELT data for Be stars in both hemispheres. First, I cross-matched a list of known O- and B-type stars in the Galaxy to the KELT catalog, finding 28045 matches. A subset of this sample includes classical Be stars, some of which leave a detectable characteristic photometric signature. These light curves are being analyzed to detect likely Be star candidates. Because these sources are bright, it is inexpensive to obtain low-resolution spectra and/or narrow-band imaging, which can confirm the Be star nature of those systems currently possessing a disk. This project has the potential to result in the discovery of hundreds of new Be stars. A preliminary analysis of these light curves finds about 200 'strong' candidates that are very likely Be stars, and another ~ 200 'weak' candidates that show variability suggestive of Be stars, but less convincing than the 'strong' sample. Some of these systems are already known Be stars, but most are not. Light curves for two examples of strong candidates are shown in Figures 7.1 and 7.2.

7.2.2 New Be Star Binaries

I am using KELT light curves of Be stars as a first step for discovering new binary systems. The brightness of binary systems comprised of a Be star and a companion may be modulated by the orbital period of this system, and can be detected in KELT data. Such signals are recovered through the methods described in Section 3. Over 200 systems analyzed in this work have photometric signals compatible with binarity. The next step is to obtain spectroscopic measurements of Hα for these sources, to look for hints of binarity in this emission line. Some of these already have spectra archived in the BeSS database. Others will require new measurements.

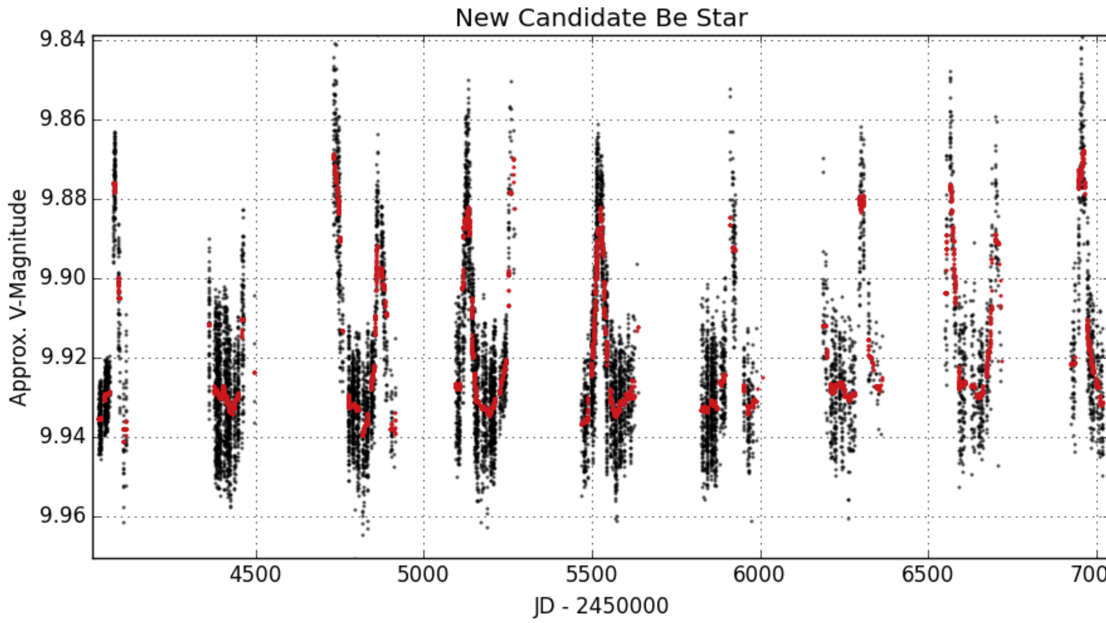

Figure 7.1: KELT light curve of a new candidate Be star, showing many similar outbursts that appear to repeat at a somewhat regular rate.

Because these sources are bright, a single low-resolution spectrum covering Hα can be obtained with relative ease. Systems showing hints of binarity in both photometry and Hα will then be viewed with high-resolution spectra to search for two sets of lines in the spectrum. Any systems showing two sets of lines will then become high priority targets, requiring additional high-resolution spectra over time, in order to trace out the RV orbits of both the Be star and its companion. Systems that show only one set of spectral lines can still be confirmed as binaries, by tracing the RV orbit of the Be star.

This program is already underway. The top $\sim$50 candidates were chosen based on analysis of KELT photometry and available spectroscopic data, as well as visibility and magnitude. Collaborators in the SDSS-III/APOGEE program are working to acquire and analyze the spectroscopic data needed to confirm these candidates as binaries.

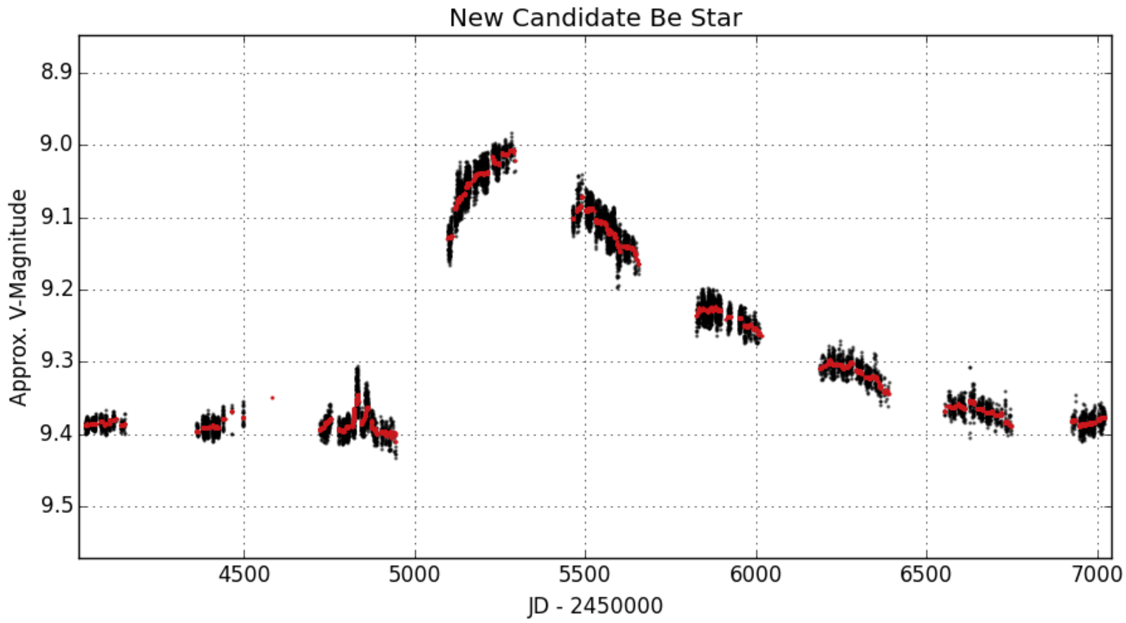

Figure 7.2: KELT light curve of a new candidate Be star showing a very prominent, high-amplitude outburst, followed by a years-long decay. This dramatic event is preceded by smaller scale outbursts.

7.2.3 Modeling of Galactic Be Stars

Another exciting avenue for further Be star science involves taking light curves as input for computer modelling. The observational signatures left in the light curves of Be stars during episodes of disk growth and dissipation can constrain details about the mass injection rate and the disk viscosity parameters. The life cycles of Be star disks are already being studied in the Large and Small Magellanic Clouds, thanks in part to multi-year OGLE light curves. In order to study the effects of metallicity on Be stars, their disks, and the transport of mass and angular momentum, a similar effort must be undertaken for Galactic Be stars. Although relatively bright, studying the population of Galactic Be stars is challenging because they are not concentrated on a small region of the sky, and they are at various distances and subject to different amounts of interstellar reddening. KELT monitors statistically significant numbers of Be stars across the whole sky, and Gaia parallaxes can be used for reliable distance estimates. Interstellar reddening can be dealt with in part through SED fitting. Identifying and modeling disk growth and dissipation with KELT light curves for Galactic Be stars will yield distributions of star and disk parameters, allowing for comparisons between the SMC, LMC, and Milky Way. This is thus an excellent opportunity to study the physics of disk build-up and dissipation, and to learn about the role of metallicity and stellar temperature in the Be phenomenon. Spectroscopic data will also be included in this work, providing more rigorous constraints. The proposed project will not only serve to better understand rapidly rotating massive stars and disk physics, but will contribute to our understanding of stellar evolution and how the life and fate of massive stars is influenced by their rotation and composition.

7.3 Conclusion

This work has revealed details about the variability of a large sample of Be stars. Through the use of high-cadence and long-baseline KELT light curves, we have measured stellar pulsation, signals possibly associated with binarity, and many episodes of disk growth, variability, and dissipation. Multiple spectra for hundreds of these systems, often simultaneous with the available photometry, reveal details about the changing circumstellar environment, and allows us to see how the brightness of a system and its spectral features change together.

In addition to the scientific results already presented, this work demonstrates the opportunities available to the stellar astrophysics community through the use of large datasets. The APOGEE and KELT surveys were both designed without consideration for Be stars. Yet, their data products are useful beyond the original survey goals. The Be star community, as well as other branches of astrophysics, will benefit immensely from the use of existing and future surveys.

Appendix A

Tables for AK and BK Samples

A.1 Table of Be stars in the AK sample

Table A.1 shows a table for the AK sample. The "Number of Outbursts" column shows the number of outbursts detected in the KELT light curve for a given system, or "?" if the system seems to have outbursts, but the exact number is not clear.

ABE ID	STAR NAME	NOMAD V mag.	Spectral Type	Spectral Type Reference	T_{eff} Class	APOGEE visits	KELT field	Number of Outbursts
003	HR 7757	6.55	B7Ve	ARCES + AO	late	11	N11	0
004	MWC 344	6.73	B0IIIe	ARCES	early	4	N11	0
005	Hen 3-1876	9.70	OB	1	unclassified	7	N11	0
006	MWC 615	8.08	B2Ve	2	early	3	S14	3
007	BD-05 4897	9.24	B8II/III	3	late	3	S14	0
009	TYC 3586-282-1	9.19	B8	4	late	15	N24	0
010	BD+50 3188	9.31	B3IIIe	ARCES	early	3	N24	3
011	TYC 3583-670-1	9.70	B3Ve	ARCES	early	3	N24	0
012	WISE J205547.33+504028.8	10.77	...	New	unclassified	3	N24	0
013	EM* CDS 1038	10.43	B7Ve	ARCES	late	17	S13	0
014	V2163 Cyg	6.93	B5IVe	ARCES + AO	mid	20	N24	0
019	BD+56 3106	8.18	B1IIIe	ARCES	early	7	N16	2
020	SS 412	10.53	OB:e	5	unclassified	32	S13	2
023	BD+44 709s	10.55	OB	6	unclassified	14	N17	0
024	TYC 1846-17-1	9.60	A3	4	late	13	N04	0
025	BD+29 981	9.16	B4Ve	ARCES	mid	12	N04	8
026	V438 Aur	8.02	B2V	ARCES + AO	early	12	N04	3
027	TYC 2405-1358-1	9.82	B4V	ARCES	mid	12	N04	1
028	MWC 794	8.09	B8Ve	ARCES	late	13	N04	0
029	BD+34 1307	9.17	B7Ve	ARCES	late	13	N04	6

030	BD+34 1318	8.81	B8shell	ARCES	late	13	N04	0
032	SS 453	10.20	Be:	5	unclassified	3	N24	0
033	BD+55 2936	9.25	B4Ve	ARCES	mid	3	N16	17
034	MWC 1085	8.79	B3Ve	7	early	3	N16	0
037	BD+31 1154	9.21	B8	8	late	14	N04	0
038	BD+22 3902	10.60	A3	9	late	20	N11	0
045	TYC 3692-1234-1	10.32	B7shell	ARCES	late	3	N17	0
046	V353 Per	9.06	B0III	ARCES	early	3	N17	0
047	BD+37 1271	7.31	B8Ve	ARCES	late	3	N04	0
048	BD+42 4162	8.92	B8shell	ARCES	late	13	N12	0
051	BD+21 3985	9.87	A0	9	late	3	N11	4
054	BD+22 825	6.52	B8Ve	ARCES + AO	late	12	N04	0
055	BD+04 1529	9.08	B8Ve	AO	late	15	J06	0
057	TYC 4056-415-1	9.29	B5Ve	AO	mid	3	N17	0
060	BD+38 1712	8.30	B8shell	ARCES + AO	late	3	N05	0
062	TYC 4060-96-1	8.40	...	New	unclassified	3	N17	0
063	TYC 158-270-1	9.42	B8III	10	late	15	S05	0
064	TYC 5126-2325-1	10.73	...	New	unclassified	3	S13	0
065	BD-06 4858	9.36	B9IV	3	late	3	S13	0
066	TYC 5121-940-1	10.30	...	New	unclassified	3	S13	3
067	HR 1047	5.90	B8Ve	ARCES + AO	late	8	N17	0
070	BD-09 4724	9.55	A0IV	4	late	2	S13	0

073	BD+54 2887	9.54	A0	11	late	3	N16	1
074	BD+38 3568	8.82	B8V	AO	late	18	N11	0
077	WISE J044231.14+383046.9	10.45	...	New	unclassified	6	N03	0
078	TYC 3975-1585-1	10.10	B8	12	late	3	N24	0
080	BD+44 3475	9.45	...	New	unclassified	3	N24	0
081	BD+57 21	7.52	B9V	AO	late	3	N16	0
082	BD+12 938	10.17	B3Ve	ARCES	early	9	S05	1
083	BD+13 976	9.99	A0	13	late	9	S05	0
084	MWC 683	8.98	B8Ve	ARCES	late	3	N16	0
085	NGC 457 198	8.85	B1.5Vpsh	AO	early	4	N16	0
086	TYC 3683-1262-1	9.84	B5Ve	ARCES	mid	4	N17	?
088	MWC 10	6.84	B8Ve	ARCES	late	3	N16	0
089	TYC 4029-428-1	9.60	...	New	unclassified	3	N16	0
090	BD+66 64	8.59	B9	4	late	3	N16	0
094	MWC 671	8.85	B7Ve	ARCES	late	3	N16	0
095	BD+08 1343	8.91	A2	8	late	3	S05	0
096	BD+08 1366	8.51	B5Ve	ARCES	mid	3	S05	0
097	MWC 488	8.50	B6Ve	ARCES	mid	3	N04	0
098	BD+63 1955	7.22	B5V	ARCES + AO	mid	3	N16	1
099	BD+27 991	8.60	B6Vne:	14	mid	3	N04	0
102	TYC 2400-1784-1	10.40	...	New	unclassified	3	N04	0
105	BD+50 3189	8.65	B0II	ARCES	early	15	N24	6

107	TYC 3617-2074-1	10.11	...	New	unclassified	3	N24	0
108	BD+23 1295	8.63	...	New	unclassified	3	N04	0
109	BD+25 1244	9.73	A2	8	late	3	N04	0
111	AS 332	9.64	Be	15	unclassified	17	S13	0
113	BD+40 999	7.32	B8IV	AO	late	3	N03	0
128	HIP 91591	8.82	B8Ve	16	late	6	S13	0
129	GSC 05692-00540	10.45	B7	17	late	6	S13	0
130	GSC 05692-00399	10.51	B7	17	late	6	S13	0
131	BD-07 4647	9.64	B5	17	mid	6	S13	0
132	BD-07 4630	8.96	B9	17	late	6	S13	0
133	88 Her	6.91	B6IIInpsh	AO	mid	3	N23	0
134	WISE J182959.95-090837.6	10.76	...	New	unclassified	1	S13	0
138	V1448 Aql	7.57	B2IV	AO	early	4	S14	6
139	BD+10 3849	7.58	B9Vpsh	AO	late	4	S14	0
140	HR 7807	6.23	B2Vne	AO	early	4	N11	0
141	BD+27 3970	9.00	B7Ve	ARCES	late	4	N12	0
144	BD+30 3853	7.12	B6Ve	ARCES + AO	mid	3	N11	0
146	BD+26 1082	7.13	B9IV	18	late	3	N04	0
147	BD+42 3425	8.48	B9Va	AO	late	2	N11	0
148	BD+21 4007	9.68	B8	9	late	3	N11	0
150	WISE J184125.48-053403.7	10.90	...	New	unclassified	3	S13	0
152	SS 120	10.73	B8e:	19	late	4	J06	0

154	TYC 1310-2084-1	9.97	B8	11	late	4	N04	6
155	TYC 3692-1671-1	10.61	B3Ve	ARCES	early	3	N17	0
156	BD+55 2992	8.34	A2	8	late	3	N16	0
158	AS 478	9.79	B6Ve	ARCES	mid	3	N24	0
159	MWC 1062	8.80	B5:e	20	mid	3	N24	0
160	V433 Cep	7.81	B2.5V	AO	early	3	N24	4
161	TYC 3968-1354-1	10.57	OB-	21	unclassified	3	N24	0
162	BD+27 981	9.96	B8	13	late	3	N04	1
163	BD+52 3293	8.10	A0	8	late	3	N16	0
164	MWC 386	7.70	B0Ve	ARCES + AO	early	3	N24	10
165	MWC 1059	8.68	B2Ve	ARCES + AO	early	3	N24	10
166	TYC 4812-2496-1	9.97	...	New	unclassified	3	S05	0
167	MWC 153	7.84	B1Ve	2	early	4	S05	4
168	V747 Mon	8.22	B3IIIe	ARCES	early	4	J06	0
169	BD+22 1147	8.00	B9	8	late	6	N04	0
170	HR 2116	6.40	B8VSB2	ARCES	late	6	N04	0
171	TYC 1326-1188-1	10.26	A2	13	late	6	N04	0
173	TYC 1283-1360-1	10.62	...	New	unclassified	3	S05	0
176	BD+37 1093	9.22	B2Ve	ARCES	early	11	N04	?
177	BD+38 1116	9.65	B2.5Vne	AO	early	11	N04	0
179	EM* RJHA 51	10.56	B5Ib	22	mid	2	S05	0
180	EM* RJHA 40	10.61	B3Ib	22	early	2	S05	0

182	TYC 2934-118-1	10.24	B7Ve	ARCES	late	8	N04	0
184	BD+32 1046	9.79	B1Ve	ARCES	early	9	N04	25
185	BD+24 1043	7.56	B8Ve	ARCES	late	3	N04	0
186	BD+01 1699	9.67	B2II	ARCES	early	3	J06	7
187	MWC 135	8.92	B1IIIe	ARCES	early	10	N04	?
188	MWC 795	10.44	B8Ve	ARCES	late	10	N04	0
196	VES 860	10.84	B8	23	late	9	N04	0
204	WISE J185142.47+134817.6	10.70	...	New	unclassified	1	S13	0
205	BD+03 3861	7.88	B8	24	late	3	S13	0
A01	MWC 5	8.02	B0.5IVe	AO	early	3	N16	13
A02	MWC 6	7.52	B3:Vne	25	early	3	N16	3
A03	MWC 80	7.16	B1Ve	ARCES + AO	early	3	N17	13
A04	MWC 494	7.95	B0Ve	ARCES	early	3	N04	?
A05	MWC 125	8.38	B0Ve	ARCES	early	3	N04	0
A07	MWC 799	7.47	B1IV:p?	26	early	3	N04	0
A09	MWC 149	7.78	B1Vnne	27	early	3	S05	?
A11	MWC 828	7.88	B0.5Ve	2	early	3	J06	5
A12	MWC 541	8.04	B1.5IVe	2	early	3	J06	4
A15	MWC 549	8.70	B1Venp	ARCES + AO	early	3	J06	0
A16	AS 367	8.96	B3Ve	28	early	3	N11	4
A17	MWC 998	8.19	B6Ve	AO	mid	3	N11	0
A18	MWC 362	8.02	B5V	AO	mid	7	N24	0

A19	MWC 640	7.21	B1IIIe	ARCES	early	3	N12	0
A20	MWC 370	7.64	B1.5Vnpe	AO	early	3	N12	?
A21	MWC 649	8.70	B3e	29	early	3	N24	0
A22	AS 483	9.63	B1.5V:nne:	26	early	3	N24	0
A24	MWC 752	7.53	B8Ve	ARCES	late	5	N04	0
A25	MWC 753	9.58	B6Ve	ARCES	mid	5	N04	0
A26	MWC 109	7.85	B1.0II/IIIe	ARCES + AO	early	4	N04	40
A27	EM* CDS 496	8.67	OB	30	unclassified	4	N04	0
A28	MWC 786	8.08	B2:V:nep	31	early	3	N04	?
A29	MWC 127	7.58	B3Ve	ARCES	early	3	N04	6
A30	MWC 128	7.36	B2:Vnne	25	early	3	N04	?
A31	MWC 129	7.69	B2Ve	ARCES	early	3	N04	?
A32	IGR J06074+2205	10.19	B0.5Ve	32	early	3	N04	3
A34	AS 118	7.64	B1IIIe	ARCES	early	3	N04	8
Q01	MWC 1016	7.09	B0.2III	AO	early	4	N11	0
Q02	Hen 3-1880	9.39	B8	19	late	4	N11	0
Q03	BD+36 4032	7.57	O8.5III	33	early	4	N11	0
Q05	BD+00 1516	9.32	B9	34	late	7	S05	0
Q07	VES 95	10.53	B7IIIn	35	late	3	N11	0
Q08	BD+21 4017	9.48	B0	36	early	3	N11	0
Q09	MWC 1120	7.47	O6.5nfp	37	early	3	N16	0
Q11	MWC 670	9.52	B9	20	late	13	N16	0

Q13	EM* CDS 144	10.50	B	21	unclassified	4	N17	0
Q14	EM* CDS 427	10.15	B8	9	late	3	N03	0
Q15	MWC 475	8.25	B3V	AO	early	3	N03	0
Q16	EM* CDS 468	8.97	B1V	AO	early	9	N04	0
Q17	SS 20	7.75	B5III	AO	mid	7	N03	2
Q18	AS 128	9.61	B5	34	mid	12	S05	0
Q20	EM* CDS 487	6.63	O7.5(f)II	AO	early	5	N04	0
Q23	EM* CDS 1299	10.24	OB-e:	30	unclassified	3	N24	0

Table A.1: Table showing the internal ABE-ID number, a common identifier, V-band magnitude, spectral type, source of spectral type, classification based on spectral type, number of APOGEE observations, KELT field, and number of outbursts detected in the KELT light curve. **References.** (1) Nassau and Harris (1952); (2) Frémat et al. (2006a); (3) Houk and Swift (1999); (4) Skiff (2013); (5) Stephenson and Sanduleak (1977a); (6) Reed (2003); (7) MacConnell (1968); (8) Ochsenbein (1980); (9) Nesterov et al. (1995); (10) Voroshilov et al. (1985); (11) Kharchenko (2001); (12) Alknis (1958); (13) Fabricius et al. (2002); (14) Clausen and Jensen (1979); (15) Bopp (1988); (16) Grillo et al. (1992); (17) Roslund (1963); (18) Grenier et al. (1999); (19) Stephenson and Sanduleak (1977b); (20) Merrill and Burwell (1949); (21) Hardorp et al. (1959); (22) Sebastian et al. (2012); (23) McCuskey (1959); (24) Uzpen et al. (2008); (25) Guetter (1968); (26) Morgan et al. (1955); (27) Turner (1976); (28) Radoslavova (1989); (29) Merrill et al. (1942); (30) Wackerling (1970); (31) Christy (1977); (32) Reig et al. (2010); (33) Negueruela (2004); (34) Cannon and Mayall (1949); (35) Turner (1993); (36) Popper (1950); (37) Walborn et al. (2010).

A.2 Table of Be stars in the BK sample

Table A.2 shows a table for the BK sample. The recovered periods are in units of days. The "Variability Type(s)" listed in the final column are as follows. "ObV": Outburst Variation - outbursts are present in the raw light curve; "SRO": Semi-Regular Outbursts - outbursts occur with some regularity; "LTV": Long Term Variation - long term variability in the raw light curve; "NRP": Non-Radial Pulsator candidate - shows periodic variability at timescales of less than 2 days; "IP": Intermediate Periodicity - shows periodic variability at timescales greater than 2 days; "EB": Eclipsing Binary; "DW(S/I)": Double Wave - indicates double-waved modulation at (S)hort or (I)ntermediate periods; "SAT": Saturated - saturation issues in the KELT photometry make analysis of this star intractable at the present time. Variable types followed by "?" indicate some uncertainty in the ascribed characteristic.

BK ID	STAR NAME	NOMAD V mag.	Spectral Type	KELT Field	Recovered Period(s)	Variability Type(s)
000	BD+34 113	9.90	B2IIIe	N01	...	none
001	HD 224544	6.52	B6IVe	N01	...	SAT
002	HD 30123	8.61	B8e	N03	...	none
003	HD 276738	9.70	B7Ve	N03	...	SAT
004	HD 29373	8.50	B6Ve	N03	...	none
005	RW Tau	8.08	B8Ve	N03	2.76877	EB,IP
006	HD 21650	7.33	B6e	N03	...	none
007	HD 276886	9.51	Bpe	N03	20.80286	IP,ObV
008	V584 Per	8.02	B3e	N03	24.01979	IP,LTV,ObV
009	RW Per	9.72	A5Ve	N03	13.19694	EB,IP
010	HD 19993	8.26	A7.5IIe	N03	...	none
011	HD 29866	6.10	B8IVne	N03	...	SAT
012	HD 18552	6.12	B8Vne	N03	...	SAT
013	EM* MWC 800	11.13	Be	N04	205.99	EB,IP,LTV
014	HD 245310	8.96	B2IIInnpe	N04	5.57772	IP,LTV,ObV
015	V725 Tau	9.19	O9.7IIe	N04	74.85888	IP,LTV,ObV
016	HD 244894	10.13	B1IIIpe	N04	...	LTV,ObV
017	HD 250163	9.77	B1.5Vnpe	N04	...	LTV,ObV
018	HD 253214	9.54	B1.5Vnne	N04	84.13716,6.652270	IP,LTV,ObV
019	HD 37352	7.69	B8e	N04	...	none

020	HD 43703	8.65	B1IVpe	N04	...	none
021	V1163 Tau	8.41	B1Vne	N04	0.80368	DWS,LTV,NRP,ObV
022	HD 248390	9.93	B5e	N04	...	LTV,ObV?
023	HD 246878	9.37	B0.5Vpe	N04	...	none
024	V593 Tau	8.13	B3Ve	N04	0.71405	LTV,NRP,ObV
025	V1167 Tau	8.48	B1Vnne	N04	8.92936,74.671730	IP,LTV,ObV
026	HD 247525	10.79	B5e	N04	3.05094	IP,LTV
027	V1371 Tau	8.16	B0e	N04	4.07486,192.701250	IP,LTV,ObV
028	V1162 Tau	8.96	B5ne	N04	...	none
029	HD 38191	8.60	B1Vne	N04	...	LTV
030	HD 249179	10.00	B5ne	N04	32.82274	LTV,ObV
031	HD 253339	10.41	Be	N04	6.24868	IP,LTV,ObV
032	HD 39478	8.25	B2Ve	N04	0.54780	LTV,NRP
033	HD 253215	10.76	Be	N04	...	LTV
034	HD 35347	8.93	B1Ve	N04	0.65516	LTV,NRP,ObV
035	HD 35345	8.43	B1Vpe	N04	28.19131	IP,LTV,ObV,SRO
036	V438 Aur	8.05	B3pshe	N04	24.18518	IP,LTV,ObV
037	HD 251726	9.34	B1Ve	N04	1.35791,14.640840	IP,NRP,ObV
038	HD 245493	8.44	B2Vpe	N04	0.54252,56.892750	IP,LTV,NRP,ObV?
039	HD 241570	10.29	B5ne	N04	...	LTV,ObV
040	HD 280999	9.93	Be	N04	...	LTV
041	HD 249695	9.16	B1Vnnpe	N04	...	LTV,ObV

042	V963 Ori	8.49	B2IIpe	N04	55.31239,5.711030	IP,ObV
043	PY Gem	8.46	B1Vne	N04	0.14205,9.873950	IP,LTV,NRP
044	HD 42529	8.23	B9e	N04	...	none
045	EM* CDS 477	11.10	B1Vpe	N04	72.408576	IP,LTV,ObV
046	BD+35 1169	9.35	B1Vpe	N04	49.36974	IP,LTV,ObV?
047	IU Aur	8.39	B3Vnne	N04	1.8114741	EB
048	SX Aur	8.55	B1Vne	N04	1.2100827	EB
049	HD 250028	9.14	B2Vnnpe	N04	0.56028,22.975920,6.579010	IP,LTV,NRP,ObV?
050	V415 Aur	7.82	B2Vnne	N04	61.2531236	DWI,IP,LTV,ObV?
051	HD 250854	11.60	B5e	N04	...	none
052	V414 Aur	8.24	B2Vne	N04	1.55404	LTV,NRP
053	HD 34257	8.10	B5e	N04	56.35602	IP,LTV,ObV
054	HD 277707	10.41	Bpe	N04	6.93814,81.832040	IP,LTV,ObV
055	MZ Aur	8.16	B1.5IVnpe	N04	0.36334,5.272500,127.100820	IP,LTV,NRP,ObV
056	V1153 Tau	8.36	B1Ve	N04	9.79301	IP,LTV,ObV
057	V416 Aur	7.38	B2Vpe	N04	57.04087	IP,LTV,ObV
058	[KW97] 26-56	11.51	Be	N04	...	LTV
059	V413 Aur	8.13	B1Ve	N04	8.60150	IP,LTV,ObV
060	HD 250289	8.23	B2IIIe	N04	...	none
061	HBHA 2215-15	11.70	Be	N04	...	none
062	HD 246537	9.48	Be	N04	...	ObV
063	BD+37 1292	9.23	B3Vpe	N04	57.43979	IP,ObV

064	V420 Aur	7.45	B0IVpe	N04	0.67359	LTV,NRP,ObV?
065	V434 Aur	7.25	B3Vne	N04	90.48757	IP,LTV,ObV
066	V731 Tau	6.23	B2.5Ve	N04	...	SAT
067	V1165 Tau	6.82	B1Vpe	N04	...	SAT
068	HD 32188	6.12	A2IIIshe	N04	...	SAT
069	EM* StHA 143	12.02	Be	N10	...	LTV
070	HD 162428	7.10	A0e	N10	...	SAT
071	BD+23 3183	10.01	Be	N10	25.58702	IP,ObV
072	V974 Her	6.43	B8Vne	N10	...	SAT?
073	HD 168957	6.98	B3Ve	N10	22.35759	IP,ObV
074	HD 344800	10.06	B2Vnne	N11	...	LTV,ObV?
075	HD 345122	9.80	B2Vpe	N11	...	LTV,ObV
076	HD 177648	7.23	B2Ve	N11	0.77660	NRP,ObV
077	HD 344873	8.81	B0IIe	N11	4.04944	IP
078	HD 339483	8.98	B1IIIe	N11	0.26852	NRP
079	HD 333226	10.26	B1Ve	N11	...	none
080	HD 333452	9.49	B0IIInpe	N11	...	none
081	HD 344313	9.45	B2Vpe	N11	...	none
082	7 Vul	6.33	B5Vne	N11	4.66436	IP
083	V2103 Cyg	9.13	B8Ve	N11	...	LTV,ObV
084	HD 190150	8.29	B9e	N11	0.42766	NRP
085	V396 Vul	7.76	B2Vnne	N11	0.40983	NRP

086	HD 331976	9.94	B0pe	N11	1.35562	LTV,NRP,ObV
087	HD 228438	8.37	B0.5IIIe	N11	74.07762	IP
088	HD 227611	8.80	B0IIpe	N11	3.27197	IP,LTV
089	HD 191378	8.99	A5e	N11	...	LTV
090	Cl* NGC 6871 BP 2	11.98	B5Ve	N11	...	LTV
091	HD 225985	9.16	B1Vpshe	N11	23.10936	IP,LTV?,ObV?
092	HD 228256	10.02	Bpe	N11	...	LTV,ObV
093	V372 Sge	8.34	B0.5IIIe	N11	0.16431	NRP
094	BD+41 3731	9.84	B3ne	N11	...	none
095	EM* AS 368	10.82	Be	N11	...	LTV,ObV?
096	HD 189689	7.28	B9e	N11	...	SAT
097	V1362 Cyg	8.18	B5IIne	N11	14.76216	IP,ObV?
098	HD 228860	9.72	B0.5IVe	N11	...	LTV
099	HD 228535	10.43	B2IVe	N11	71.07708	IP,LTV,ObV
100	HD 345120	10.25	B5e	N11	...	LTV?
101	V2113 Cyg	7.16	B1Vnnpe	N11	19.79321	IP,LTV,ObV
102	BD+30 3526	9.89	A0IIe	N11	...	LTV,ObV?
103	HD 193516	8.60	B2IIIe	N11	2.00540	IP,ObV
104	V425 Cyg	10.60	B2npe	N11	...	LTV
105	HD 192445	7.23	B0.5IIIe	N11	31.98469	IP,LTV,ObV
106	HD 229171	9.38	B0.5IIIne	N11	0.28547	NRP
107	Cl* NGC 6913 SAND 151	12.57	B5e	N11	...	LTV

108	EM* MWC 622	12.00	Be	N11	...	LTV,ObV
109	BD+36 3956B	10.50	O9e	N11	0.15616	LTV,NRP
110	HD 228104	9.06	B1IVpe	N11	...	LTV,ObV
111	V532 Lyr	6.54	B4Ve	N11	...	SAT
112	HD 193182	6.55	Ape	N11	...	LTV
113	HD 228041	9.04	B0.5Ve	N11	...	LTV,ObV
114	HD 181409	6.57	B2IVe	N11	...	SAT
115	HD 190864	7.79	O7IIIe	N11	...	SAT
116	HD 344783	9.80	B0IVe	N11	...	none
117	EM* VES 195	11.98	O9Ve	N11	...	LTV
118	HD 228658	10.24	B0.5Ve	N11	...	none
119	11 Cyg	6.03	B8Vne	N11	...	SAT
120	V558 Lyr	6.29	B3Ve	N11	...	SAT
121	HD 174179	6.05	B3IVpe	N11	...	SAT
122	HD 171780	6.09	B5Vne	N11	...	LTV,SAT
123	EM* AS 396	10.89	B2.5IVe	N11	...	none
124	BD+40 4353	9.46	B2Ve	N12	...	none
125	BD+36 4145	8.96	O9Ve	N12	...	none
126	HD 195407	7.80	B0IVpe	N12	...	LTV,ObV
127	V2166 Cyg	8.16	B2Vne	N12	0.61520	NRP
128	HD 194779	7.80	B3IIe	N12	89.71926	IP,ObV,SRO
129	V2139 Cyg	7.16	B2IVpe	N12	0.60932,26.483400	IP,LTV,NRP,ObV

130	V2162 Cyg	7.63	B2Vnne	N12	12.63288	IP,LTV,ObV
131	V568 Cyg	6.67	B2IVe	N12	56.36210	IP,LTV,ObV
132	V2123 Cyg	7.82	B1.5Ve	N12	17.17283	IP,LTV,ObV
133	HD 199218	6.70	B8Vnne	N12	...	none
134	HD 197038	8.18	B7e	N12	...	none
135	V2153 Cyg	7.52	B1Vne	N12	3.65775	LTV
136	HD 205060	7.22	B5e	N12	0.59862	LTV,NRP
137	HD 208220	9.45	B1IVe	N12	0.73076	LTV,NRP,ObV
138	V2156 Cyg	8.91	B1.5Vnnpe	N12	21.03466	IP,LTV,ObV
139	V423 Lac	7.97	B3Vne	N13	41.74408	IP,ObV
140	V378 And	6.55	B3Vpe	N13	...	ObV?
141	8 Lac B	6.48	B2Ve	N13	...	SAT
142	BG Phe	10.18	B5e	S18	...	none
143	HD 19818	9.06	B9.5Vne	S19	...	none
144	HD 33599	8.97	B2Vpe	S20	20.52402	DWI,IP
145	HD 53048	7.92	B6Vne	S21	...	none
146	HD 33453	8.03	B8Vne	S21	0.30506	NRP
147	HD 43789	8.55	B6.5Ve	S21	...	none
148	HD 81753	6.10	B6Ve	S22	...	SAT
149	HD 84567	6.44	B0.5IIIne	S22	...	SAT
150	HD 71072	6.89	B4IIIe	S22	...	none
151	HD 85860	7.17	B4Ve	S22	26.52577	IP

152	CD-29 6963	9.25	Be	S22	0.61017	LTV,NRP,ObV
153	HD 70234	8.83	B9IIIe	S22	0.43832	NRP
154	HD 72043	8.83	B8e	S22	...	LTV,ObV?
155	HD 70461	8.99	B6Ve	S22	0.69603	DWS,NRP
156	HD 75740	9.50	A0IIIe	S22	...	none
157	HD 78482	9.54	B8Ve	S22	...	none
158	CD-27 5181	10.90	Be	S22	1.69284	DWS,NRP
159	OY Hya	6.21	B5Ve	S23	...	SAT
160	HD 89884	7.13	B5IIIe	S23	4.74956	SAT
161	HD 102383	9.18	B6Vne	S24	0.61042	NRP
162	HL Lib	6.96	B9IVe	S25	12.31067	IP
163	V958 Cen	7.12	B5Ve	S25	...	none
164	V774 Cen	7.61	B3Vne	S25	10.76797	IP,LTV,ObV
165	V1018 Cen	7.93	B2pe	S25	0.72096	NRP,ObV
166	HD 179253	9.78	B7Ve	S27	32.41217	IP
167	HD 169999	10.52	B8Vne	S27	0.44626	NRP
168	HD 68423	6.31	B6Ve	S34	...	SAT
169	IU Vel	6.05	B2.5Vne	S34	0.61692	NRP
170	HD 75081	6.21	B9Ve	S34	...	SAT
171	HD 72014	6.58	B1.5Vnne	S34	...	SAT
172	HD 87543	6.20	B7IVne	S34	...	SAT
173	HD 69404	6.43	B2Vnne	S34	0.44902	NRP

174	HD 69168	6.48	B2Ve	S34	...	SAT
175	FY Vel	6.90	B2IIpshe	S34	33.75389	DWI,EB,IP
176	HD 65663	6.74	B8Ve	S34	9.83990	SAT
177	HD 65930	6.84	B2IIIe	S34	...	SAT
178	HD 76838	7.31	B2IVe	S34	3.85243	DWI,EB,IP
179	HD 63988	7.08	B8Ve	S34	...	none
180	HD 80459	7.39	B6Vne	S34	0.52344	NRP
181	NR Vel	7.67	B2Ve	S34	4.58157	IP
182	HD 79206	7.73	B3.5Vne	S34	0.35408	NRP
183	HD 64831	7.83	B8Vne	S34	...	none
184	V480 Car	7.88	B2.5Ve	S34	39.22309	IP,ObV,SRO
185	HD 80284	8.89	B5Vnne	S34	16.89453	IP
186	HD 75658	8.12	B2.5ne	S34	6.27296	IP,ObV?
187	OU Vel	8.04	B2Vne	S34	...	none
188	V471 Car	8.06	B5ne	S34	21.62499	IP,ObV?
189	HD 83032	7.97	B7IIIe	S34	2.44996	IP
190	HD 85083	8.27	B5IIIe	S34	16.89453	IP
191	HD 85495	7.94	B4IIIe	S34	4.78500	IP
192	HD 84523	7.97	B4Ve	S34	1.77334	NRP
193	HD 83043	8.52	B2.5Vne	S34	0.80112	NRP
194	HD 59197	8.10	B6Ve	S34	...	none
195	V373 Car	8.98	Be	S34	5.36108	IP

196	HD 84361	8.43	B2.5Ve	S34	4.63393	IP,ObV
197	HD 69026	8.44	B1.5Ve	S34	70.66992	IP,ObV,SRO?
198	HD 79778	8.31	B2Vne	S34	1.30355	NRP,ObV
199	HD 77147	8.45	B8Ve	S34	...	none
200	HD 62894	9.60	B8e	S34	14.81164	IP
201	HD 64716	8.44	B6Ve	S34	...	none
202	HD 71823	8.82	B3Vne	S34	...	ObV
203	HD 67978	8.75	B2Vnne	S34	26.72540	IP,ObV
204	HD 60794	8.73	B4IIIe	S34	0.20926,0.422750	NRP
205	HD 77032	8.68	B5Vne	S34	0.62416	NRP
206	CD-45 4676	9.09	B0.5IIIe	S34	1.37680	DWS,NRP
207	HD 67985	8.89	B8Vne	S34	...	none
208	HD 74559A	10.30	B9Ve	S34	...	none
209	HD 74559B	10.30	B9Ve	S34	...	none
210	HD 75925	8.95	B4Vnne	S34	0.40745,1.263140	NRP
211	HD 80156	8.72	B8.5IVe	S34	0.36740	NRP
212	HD 74401	9.21	B1IIIne	S34	0.63803	NRP
213	HD 84511	8.86	Bpshe	S34	33.032069	EB
214	HD 75661	9.02	B2Vne	S34	38.16176	IP,ObV,SRO
215	HD 74867	8.71	B7IVe	S34	...	none
216	CD-44 4392	9.25	B2IVe	S34	21.63942	IP,ObV,SRO
217	OR Vel	9.01	B3Vne	S34	49.22229	IP,ObV,SRO

218	HD 78328	9.20	B9.5IIIe	S34	...	none
219	HD 63453	9.16	B9Vne	S34	...	none
220	HD 83060	9.10	B2Vnne	S34	0.72099	NRP,ObV
221	HD 76985	9.05	B5Vne	S34	43.83445	IP
222	HD 79811	9.32	B5Ve	S34	0.58583	NRP,ObV
223	HD 87366	9.42	B9IIIe	S34	...	none
224	HD 86272	9.43	B5Vne	S34	0.40547,0.370590	NRP
225	HD 72126	9.31	B2nne	S34	0.32870	NRP
226	CD-46 4821	9.08	Be	S34	0.43371,0.206350	NRP,ObV
227	HD 75551	9.24	B2Vne	S34	0.65359	NRP,ObV
228	HD 84777	9.24	B8Vne	S34	...	none
229	HD 298298	9.16	B0e	S34	59.40933	IP,ObV,SRO
230	HD 81354	9.35	B4Ve	S34	0.38442,20.400940	IP,NRP,ObV
231	HD 71042	9.44	B2.5ne	S34	0.86569,23.590900	IP,NRP,ObV
232	HD 76568	9.45	B1Vnne	S34	0.77993	NRP
233	HD 83597	9.07	B2Ve	S34	15.8696146	IP,ObV,SRO
234	CD-47 4412	9.59	A5e	S34	59.95840,0.832160	IP,NRP,ObV,SRO
235	GW Vel	8.97	B2Vne	S34	202.73433	IP,ObV,SRO
236	CD-49 3441	10.34	B8e	S34	6.77192	IP
237	HD 86119	9.66	B8.5IVe	S34	...	none
238	HD 60669	9.76	B8IIIe	S34	...	none
239	QR Vel	10.10	B2Vne	S34	154.46425	IP,ObV

240	HD 57551	9.87	B8IIIe	S34	...	none
241	CD-45 4826	10.16	Be	S34	12.05855	IP,ObV
242	HD 70064	10.09	B5Ve	S34	...	none
243	CD-45 4394	10.27	B2Vne	S34	24.57386	IP,ObV,SRO
244	HD 69651	10.16	B9Vne	S34	...	none
245	HD 86689	10.10	A3ne	S34	...	none
246	QQ Vel	9.77	B5nne	S34	5.73101	IP,ObV?
247	HD 298377	10.25	B3Vne	S34	50.13523	IP,ObV,SRO
248	HD 298339	10.54	B2Vne	S34	...	none
249	CD-46 4657	10.28	A1IIe	S34	...	none
250	HD 174512	8.56	Be	S13	...	SAT
251	V986 Oph	6.15	B0IIIne	S13	...	SAT
252	NW Ser	6.15	B2.5IIIe	S13	...	SAT
253	HD 166917	6.70	B8IIIe	S13	...	SAT
254	HD 174105	6.93	B8e	S13	...	SAT
255	HD 173371	6.88	B7IVe	S13	...	SAT
256	HD 179343	6.95	B8IIIe	S13	...	SAT
257	V448 Sct	7.38	B1.5IVe	S13	...	SAT
258	HD 176630	7.65	B3IIIe	S13	0.62738,6.418250	IP,NRP
259	HD 171219	7.65	B5IIIe	S13	...	SAT
260	V447 Sct	7.88	B0.5IVe	S13	60.56355	IP
261	QT Ser	7.73	B5e	S13	...	SAT

262	HD 170009	8.00	B9IIIe	S13	...	SAT
263	V2315 Oph	8.33	B9e	S13	...	none
264	V457 Sct	8.70	B1.5IVe	S13	36.37432	IP,ObV,SRO
265	HD 166256	8.62	B9e	S13	0.35001	NRP
266	HD 173530	8.82	B7IIIe	S13	1.28500	DWS,NRP
267	V2385 Oph	8.84	B8e	S13	1.18966	NRP
268	HD 230579	9.10	B1IVe	S13	...	ObV
269	V1437 Aql	8.98	B5IVe	S13	...	none
270	HD 174571	8.89	B1.5Ve	S13	0.57376,7.333300,76.082960	IP,NRP,ObV
271	HD 173817	8.63	B6IVe	S13	...	none
272	V1443 Aql	8.93	B3Ve	S13	...	none
273	V1446 Aql	9.12	B2Ve	S13	0.50553,4.599470	IP,NRP,ObV
274	V455 Sct	9.29	B1IVe	S13	65.09772	IP,LTV,ObV
275	EM* AS 315	11.30	Be	S13	...	none
276	BD-05 4819	10.60	B2IVpe	S13	0.70176	NRP
277	BD-05 4823	10.48	Be	S13	0.52943	NRP
278	HBHA 703-05	11.17	B5IIe	S13	...	none
279	EM* AS 341	11.00	Be	S13	...	none
280	HD 161306	8.30	B0ne	S13	...	none
281	V923 Aql	6.09	B6she	S14	...	SAT
282	HD 194244	6.14	B9IIIe	S14	...	SAT
283	HD 196712	6.22	B7IIIne	S14	...	SAT

284	V1339 Aql	6.48	B2.5IVe	S14	...	SAT
285	V1466 Aql	6.50	B7VA5Ve	S14	...	SAT
286	HD 179343	6.95	B8IIIe	S14	...	SAT
287	V1294 Aql	6.98	B0Ve	S14	...	SAT
288	HD 184767	7.15	A0IIIe	S14	...	SAT
289	LZ Del	7.47	B9e	S14	...	SAT
290	V1448 Aql	7.99	B2IVe	S14	2.14600,9.198010	IP,ObV
291	HD 187350	8.14	B1Vne	S14	36.38773,9.022570	IP,LTV,ObV
292	V1463 Aql	8.15	B5e	S14	59.55546	IP,LTV,ObV
293	HD 181308	8.66	B5IVe	S14	...	LTV
294	HD 181231	8.69	B5IVe	S14	...	none
295	HD 181709	8.77	B6IIIe	S14	...	none
296	HD 181803	9.03	B7IIIe	S14	0.65949	NRP
297	V1446 Aql	9.12	B2Ve	S14	4.61825	IP,LTV,ObV
298	HD 181367	9.34	B6IVe	S14	...	none
299	HD 355402	10.87	Be	S14	36.79204	IP,LTV
300	HBHA 703-05	11.17	B5IIe	S14	...	none
301	HD 216057	6.13	B5Vne	N16	...	SAT
302	LQ And	6.54	B4Vne	N16	1.31192	NRP
303	KY And	6.76	B3IVe	N16	...	none
304	V442 And	6.82	B2IVe	N16	60.29997	IP,ObV,SRO
305	V764 Cas	6.89	B2IIIne	N16	...	ObV

306	KX And	7.02	Bpe	N16	38.89025	IP,ObV,SRO
307	V742 Cas	7.08	B5IIe	N16	...	SAT
308	HD 6343	7.26	B8e	N16	...	none
309	V782 Cas	7.62	B6IIe	N16	...	none
310	CW Cep	7.67	B1Vve	N16	2.7291384	EB,IP
311	V818 Cas	7.74	B2Vne	N16	64.44378	IP,ObV,SRO
312	V813 Cas	7.93	B8e	N16	24.14602,0.295830	IP,NRP,ObV
313	HD 225095	7.95	B2IVne	N16	6.5360102	IP,ObV
314	V423 Lac	7.97	B3Vne	N16	...	none
315	HD 2789	8.36	B3Vne	N16	...	ObV
316	HD 223044	8.43	B3e	N16	7.98827	IP,ObV
317	HD 224905	8.47	B1Vne	N16	74.77196	IP
318	V817 Cas	8.50	Be	N16	26.16647	ObV,SRO
319	HD 216044	8.52	B0IIe	N16	...	none
320	BD+62 271	8.58	B8Ve	N16	...	none
321	V810 Cas	8.59	B1npe	N16	2.39041	IP
322	V811 Cas	8.62	B0.5Vpe	N16	57.87303	IP,ObV
323	HD 4931	8.72	B8Ve	N16	...	none
324	HD 217061	8.80	B1Vne	N16	0.81275	NRP
325	BD+62 285	8.85	B8Ve	N16	...	none
326	BD+61 39	8.85	B0.5IVe	N16	91.24125	IP,ObV,SRO
327	HD 7720	8.86	B5IIe	N16	15.17923,42.813200	IP,ObV

328	V978 Cas	8.92	B6e	N16	71.98248	IP,ObV,SRO
329	HD 223387	8.99	Bpe	N16	...	none
330	BD+62 287	9.07	B8Ve	N16	...	none
331	BD+61 2380	9.14	B9Ve	N16	...	none
332	V415 Lac	9.19	B1IVnnpe	N16	...	SAT
333	BD+60 180	9.25	B0pe	N16	0.29945,69.571460	IP,NRP
334	BD+63 48	9.26	B1IIInne	N16	73.36676,11.491180	IP
335	BD+60 2600	9.34	B9Ve	N16	26.32815,0.594180	IP,NRP
336	BD+61 105	9.34	O9Ve	N16	6.49695	IP
337	BD+59 246	9.43	Be	N16	...	none
338	HD 236689	9.47	B1.5Vpe	N16	18.69299	IP
339	BD+53 2964	9.47	B2IVnnpe	N16	18.34169	IP,ObV
340	BD+62 11	9.60	B5Ve	N16	27.82858	none
341	HD 215605	9.61	B2IVnne	N16	3.46809,0.533780	IP,NRP
342	BD+63 261	9.62	Bnnpe	N16	82.22137	IP
343	BD+61 2355	9.63	B7IVe	N16	...	none
344	BD+57 243	9.63	B0IVe	N16	2.61440	IP
345	V808 Cas	9.70	B0IIIpe	N16	2.59882	EB,IP
346	HD 224599	9.70	B0.5Vnnpe	N16	47.68620	SAT
347	BD+62 2346	9.73	B0Ve	N16	3.01665	IP,ObV?
348	BD+57 2678	9.81	B0.5Ve	N16	0.58161	NRP
349	BD+59 2829	9.86	B1Ve	N16	...	none

350	EM* MWC 678	9.89	B2Vnnpe	N16	0.78148,53.408540	IP?,NRP,ObV?
351	BD+62 300	9.92	B1Vnpe	N16	90.83504	ObV
352	BD+60 2405	9.93	B3Vnne	N16	0.58422	NRP
353	BD+60 114	9.94	B2IIIpe	N16	0.82530	NRP
354	BD+55 81	10.02	B1.5Vnne	N16	0.74022	NRP
355	V972 Cas	10.03	B3IIIe	N16	...	ObV
356	EM* AS 505	10.04	B5Vpe	N16	87.87973	IP,ObV
357	BD+58 247	10.04	B1e	N16	4.52724	IP,ObV?
358	BD+56 2811	10.04	Be	N16	...	none
359	BD+61 2292	10.04	B2Vne	N16	2.26279	IP
360	BD+61 2494	10.07	B0Vne	N16	6.31634	IP
361	BD+60 340	10.12	B5IIIe	N16	...	ObV
362	PS Cep	10.14	B6Vne	N16	0.60770	NRP
363	BD+62 2158	10.14	B9Ve	N16	...	none
364	EM* MWC 659	10.15	B0IIIpe	N16	12.71632	IP
365	BD+62 245	10.15	B1Vpe	N16	70.12999	IP,ObV
366	BD+65 1970	10.17	B5e	N16	...	none
367	BD+62 89	10.25	B0Vpe	N16	9.99829,3.069330	IP,ObV?
368	BD+56 251	10.29	Be	N16	7.92076	IP?
369	V977 Cas	10.30	B2IVe	N16	79.13341	IP,ObV,SRO
370	V985 Cas	10.31	B3Ve	N16	62.33777	IP,ObV,SRO
371	BD+60 2584	10.33	B1IVpe	N16	...	none

372	BD+56 259	10.37	Be	N16	...	none
373	BD+61 122	10.39	B2Vpe	N16	44.88481	IP,ObV
374	BD+62 1	10.46	B2IVpe	N16	0.30036	NRP,ObV
375	BD+58 277	10.48	Be	N16	...	none
376	BD+60 307	10.49	B2Ve	N16	49.67541	IP,ObV,SRO
377	BD+62 292	10.55	B1pe	N16	0.60750,7.038880	IP,NRP,ObV
378	EM* AS 4	10.58	B1IVpe	N16	48.17010	IP
379	EM* AS 2	10.58	B5e	N16	0.76332	NRP
380	BD+59 250	10.60	B2Ve	N16	15.90205,42.813200	IP,ObV
381	EM* CDS 1367	10.60	B2IIIe	N16	7.24534	IP
382	V594 Cas	10.64	Be	N16	69.86255	IP,ObV
383	V981 Cas	10.65	B2IIIe	N16	1.42780,52.987110	IP,NRP,ObV,SRO
384	BD+60 274	10.66	B3IIIe	N16	0.35019	NRP
385	EM* AS 3	10.67	Be	N16	...	none
386	EM* AS 25	10.70	BVnne	N16	...	none
387	EM* MWC 677	10.71	B2Vpe	N16	1.61519	NRP
388	EM* AS 28	10.76	B2Vnne	N16	1.29838	NRP
389	Cl* NGC 663 SAN 27	10.80	B2Ve	N16	1.27937	NRP,ObV
390	EM* GGA 50	10.81	B2Ve	N16	4.17429	DWI,EB,IP,ObV
391	EM* MWC 674	10.85	B0IIIpe	N16	0.66005,70.649470	IP,NRP,ObV?
392	EM* AS 16	10.90	Bpe	N16	0.54745,1.371990	NRP
393	BD+63 124	10.92	B1Ve	N16	...	none

394	BD+62 99	10.94	Be	N16	...	none
395	EM* VES 704	11.16	Be	N16	...	none
396	EM* MWC 685	11.28	Be	N16	...	SAT
397	V831 Cas	11.34	B1IVe	N16	78.17770	IP
398	EM* CDS 1464	11.38	B2Ve	N16	...	SAT
399	Cl* NGC 663 SAN 20	11.41	Be	N16	5.51061	IP
400	EM* CDS 78	11.42	B1Vpe	N16	12.30668	IP
401	V976 Cas	11.48	Be	N16	79.51024	IP,ObV,SRO
402	NGC 7654 930	11.60	Be	N16	0.38305	NRP
403	Cl* NGC 663 SAN 17	11.74	Be	N16	...	SAT
404	V986 Cas	12.20	B2.5Ve	N16	14.71889	none
405	Cl* NGC 663 SAN 26	12.42	Be	N16	3.22219	IP
406	HD 42477	6.04	A0Vnne	S05	...	SAT
407	HD 43285	6.05	B5IVe	S05	...	SAT
408	HD 45995	6.14	B2Vnne	S05	...	SAT
409	V715 Mon	6.15	B3IIIe	S05	...	SAT
410	HD 44783	6.24	B9IIIe	S05	...	SAT
411	V1369 Ori	6.52	B5Vpe	S05	...	SAT
412	V743 Mon	6.58	B7IIIe	S05	...	SAT
413	PZ Gem	6.64	O9pe	S05	...	SAT
414	AX Mon	6.74	B2IIIpshev	S05	...	SAT
415	V742 Mon	6.92	B2IIIe	S05	...	SAT

416	HD 47160	7.11	B8IVe	S05	...	SAT
417	HD 37115	7.16	B6Ve	S05	...	SAT
418	V1372 Ori	7.24	B2Vne	S05	...	SAT
419	HD 38856	7.25	B5Ve	S05	...	SAT
420	HD 37330	7.38	B6Ve	S05	...	SAT
421	HD 43264	7.51	B9IIIe	S05	...	SAT
422	V1374 Ori	7.51	B8e	S05	...	SAT
423	HD 49787	7.54	B1Ve	S05	...	ObV,SAT
424	HD 46484	7.65	B0.5IVe	S05	...	SAT
425	HD 43913	7.86	Be	S05	...	SAT
426	HD 42406	7.99	B4IVe	S05	...	SAT
427	HD 44637	8.00	B2Vpe	S05	3.16221	IP
428	HD 37149	8.02	B8Ve	S05	...	none
429	V728 Mon	8.05	B1.5IVe	S05	...	none
430	V1390 Ori	8.10	B2Ve	S05	9.59358,2.020520	IP
431	HD 50209	8.36	B8IVe	S05	...	none
432	HD 259597	8.59	B0.5Vnne	S05	14.98756	IP,ObV
433	V733 Mon	8.72	B2Vpe	S05	50.15997	IP,ObV,SRO
434	V725 Mon	8.87	B0.5IVe	S05	23.92245	IP,ObV
435	HD 47359	8.87	B0IVe	S05	12.14021,0.647230	IP,NRP,ObV
436	V739 Mon	8.95	B0.5IVe	S05	...	none
437	HD 45260	9.05	B8e	S05	...	none

438	HD 39557	9.07	B5IIIe	S05	...	none
439	HD 258782	9.09	B9IVe	S05	...	SAT
440	HD 259440	9.12	B0pe	S05	...	none
441	HD 49585	9.13	B0.5IVe	S05	62.19836,0.633710	IP,NRP,ObV
442	HD 253084	9.21	B5e	S05	...	none
443	HD 45626	9.25	B7pshe	S05	5.97104	IP
444	HD 51404	9.41	B1.5Ve	S05	41.00991,1.385260	IP,NRP
445	HD 250980	9.56	B0e	S05	1.34000,22.213700	IP,NRP,ObV
446	HD 259631	9.61	B5e	S05	0.35180,64.343130	IP,NRP,ObV?
447	HD 256577	9.77	B2IVpe	S05	...	ObV
448	HD 290662	9.98	A0Vpe	S05	...	none
449	HD 254647	10.01	Bpe	S05	...	none
450	Cl* NGC 2244 PS 26	11.41	B7Ve	S05	...	none
451	EM* GGA 399	12.46	B3Ve	S05	6.67063,25.772800	IP,ObV,SRO
452	Cl* NGC 2244 PS 543	12.81	B8Ve	S05	...	none
453	HD 23552	6.15	B8Vne	N17	...	SAT
454	HD 21455	6.23	B7Ve	N17	...	SAT
455	HD 21620	6.28	A0Vne	N17	...	SAT
456	V801 Cas	6.50	B1Ve	N17	...	SAT
457	HD 21641	6.77	B8.5Ve	N17	...	SAT
458	HD 23800	6.98	B1IVe	N17	...	SAT
459	V777 Cas	7.02	B2Vne	N17	58.22151	IP,ObV,SRO

460	HD 9709	7.07	B9e	N17	...	none
461	HD 17505	7.10	O6Ve	N17	...	SAT
462	HD 20134	7.47	B2.5IVe	N17	...	SAT
463	V782 Cas	7.62	B6IIe	N17	2.51317	DWI,EB?,IP
464	CT Cam	7.69	B2Vne	N17	5.27956	IP,ObV
465	HD 13867	7.71	B5Ve	N17	...	none
466	V549 Per	7.86	B2IVe	N17	0.39349	NRP
467	V787 Cas	7.90	B2IIIe	N17	1.43364	NRP
468	HD 13669	7.90	B3IVe	N17	0.51945,0.600740	NRP
469	HD 20017	7.91	B5Ve	N17	1.29863	NRP
470	HD 232552	7.94	B0pe	N17	...	none
471	HD 15963	8.03	A1IIe	N17	...	none
472	HD 23982	8.08	B3e	N17	...	none
473	V780 Cas	8.11	B1Vpe	N17	1.24910	NRP
474	DE Cam	8.18	B1Vnnpe	N17	59.88529	IP,ObV,SRO
475	V473 Per	8.26	B0IIIpe	N17	43.45410	IP,ObV,SRO?
476	CR Cam	8.31	B2Ve	N17	106.93802	IP,ObV,SRO
477	HD 20899	8.40	B9e	N17	...	none
478	HD 18877	8.40	B7IIIe	N17	...	none
479	V529 Cas	8.49	B5Ve	N17	0.62280	NRP
480	V358 Per	8.50	B1IIIe	N17	30.28880	DWI,EB,IP,ObV?
481	BD+62 271	8.58	B8Ve	N17	...	none

482	HD 12856	8.60	B0pe	N17	...	ObV?
483	HD 232590	8.62	B1.5IIIe	N17	0.90657	NRP
484	V351 Per	8.64	B1IVe	N17	25.25283	IP,ObV
485	HD 13561	8.85	B8e	N17	...	none
486	BD+62 285	8.85	B8Ve	N17	...	none
487	HD 237056	8.90	B0.5Vpe	N17	65.49953	IP,ObV
488	HD 237091	8.91	B1Vnnpe	N17	...	none
489	V555 Per	9.00	B1IIIe	N17	0.65357	NRP
490	BD+62 287	9.07	B8Ve	N17	...	none
491	BD+56 511	9.11	B3IIIe	N17	...	none
492	V355 Per	9.14	B1Ve	N17	4.90863	DWI,IP
493	HD 13429	9.19	B3Ve	N17	0.41406	NRP
494	V356 Per	9.20	B0.5IIIne	N17	63.51470,0.731330	IP,NRP,ObV,SRO?
495	HD 237060	9.20	B9Ve	N17	...	none
496	HD 16264	9.26	B1Ve	N17	1.11370	NRP
497	HD 13900	9.33	B1IVe	N17	...	none
498	HD 236935	9.36	B1Vne	N17	8.80666	IP
499	HD 14162	9.37	Be	N17	...	SAT
500	V424 Per	9.39	B1Vpe	N17	2.17878	IP
501	HD 237118	9.42	B6Ve	N17	...	none
502	BD+59 246	9.43	Be	N17	...	none
503	BD+56 612	9.43	A0e	N17	101.74685	IP,ObV

504	V506 Per	9.45	B1IIIe	N17	...	ObV
505	HD 11554	9.47	B1Vpe	N17	64.69090	IP,ObV
506	HD 237134	9.49	B5Ve	N17	0.20922	NRP
507	BD+56 579	9.50	B7IVe	N17	...	none
508	V502 Per	9.57	B1IIIe	N17	7.25254	IP,ObV
509	BD+56 534	9.58	B2IIIe	N17	13.18230	IP
510	V361 Per	9.58	B0.5Vpe	N17	...	ObV
511	HD 236940	9.59	B2e	N17	...	none
512	NGC 884 2079	9.61	Be	N17	...	none
513	BD+58 610	9.61	Be	N17	0.55297	NRP,ObV
514	BD+63 261	9.62	Bnnpe	N17	...	none
515	V503 Per	9.65	B1.5IIIe	N17	62.38051	IP,ObV
516	BD+56 573	9.66	B2IIIe	N17	...	none
517	BD+57 515	9.76	B2pe	N17	35.52517,5.346900	IP,ObV
518	BD+56 493	9.77	B1Vpe	N17	...	none
519	BD+56 624	9.78	B3IIIe	N17	26.19981	IP
520	V783 Cas	9.82	Bpe	N17	5.87111	IP
521	BD+58 458	9.86	B1pe	N17	87.33271	IP
522	V507 Per	9.86	B2Ve	N17	...	SAT
523	BD+62 300	9.92	B1Vnpe	N17	...	ObV
524	V504 Per	9.96	B1IIIe	N17	90.34419	IP,ObV,SRO
525	BD+56 509	10.01	B1e	N17	...	none

526	V972 Cas	10.03	B3IIIe	N17	...	ObV
527	BD+58 247	10.04	B1e	N17	61.28661	IP,ObV
528	BD+56 489	10.07	B5e	N17	...	ObV?
529	BD+60 340	10.12	B5IIIe	N17	...	ObV
530	BD+50 447	10.12	Be	N17	9.30883	IP
531	EM* MWC 433	10.14	B1Vpe	N17	...	none
532	BD+62 245	10.15	B1Vpe	N17	...	ObV
533	EM* MWC 465	10.19	B2IVnne	N17	0.57252,14.844090	IP,NRP
534	EM* AS 53	10.24	B0.5pe	N17	11.90901,0.325410	IP,NRP,ObV
535	V985 Cas	10.31	B3Ve	N17	63.51470	IP,ObV
536	Cl* NGC 884 LAV 2294	10.36	Be	N17	0.80584,42.775210	IP,NRP
537	BD+56 259	10.37	Be	N17	...	none
538	BD+58 492	10.45	Be	N17	1.40859	NRP,ObV
539	BD+60 368	10.46	B1IIIe	N17	...	none
540	EM* GGA 148	10.47	Bpe	N17	...	ObV
541	BD+59 497	10.47	B0Ve	N17	...	none
542	BD+58 277	10.48	Be	N17	...	none
543	BD+60 307	10.49	B2Ve	N17	...	ObV
544	EM* MWC 466	10.50	Be	N17	36.77167	IP
545	Cl* NGC 884 LAV 2425	10.54	Oe	N17	61.64662	IP,ObV,SRO
546	BD+62 292	10.55	B1pe	N17	0.60753	NRP,ObV
547	BD+50 395	10.55	Be	N17	...	none

548	BD+55 521	10.56	B6e	N17	...	none
549	BD+59 334	10.58	B0Ve	N17	...	none
550	EM* MWC 715	10.58	Be	N17	...	none
551	Cl* NGC 884 LAV 2224	10.59	B2IIIe	N17	...	none
552	BD+56 727	10.60	B5e	N17	30.91423	IP,ObV,SRO
553	BD+59 250	10.60	B2Ve	N17	...	ObV
554	BD+55 589	10.60	B2IVe	N17	49.20153	IP,ObV
555	BD+59 343	10.61	B2Vnne	N17	1.30510	NRP,ObV?
556	V981 Cas	10.65	B2IIIe	N17	0.78063	NRP,ObV
557	BD+60 274	10.66	B3IIIe	N17	...	none
558	Cl* NGC 884 LAV 2217	10.67	B1ne	N17	14.86514	IP
559	BD+60 393	10.70	B2pe	N17	0.80491	NRP
560	EM* AS 25	10.70	BVnne	N17	0.98523	EB
561	EM* MWC 448	10.72	B2e	N17	78.20840	IP,ObV,SRO
562	BD+57 607a	10.73	Be	N17	1.15545	NRP
563	EM* AS 28	10.76	B2Vnne	N17	1.30754	NRP
564	Cl* NGC 663 SAN 27	10.80	B2Ve	N17	1.27960,0.726510	NRP
565	V615 Cas	10.80	B0Ve	N17	26.63923	IP
566	EM* GGA 50	10.81	B2Ve	N17	...	ObV
567	EM* MWC 50	10.87	O9Ve	N17	...	none
568	BD+61 371	10.96	B3IIpe	N17	1.46984,24.091780	IP,NRP,ObV
569	EM* AS 77	11.15	Be	N17	29.11090	IP,ObV?

570	EM* VES 704	11.16	Be	N17	0.58141	NRP
571	NGC 869 1438	11.29	B2e	N17	55.15750	IP,ObV,SRO
572	V831 Cas	11.34	B1IVe	N17	3.21964	IP
573	Cl* NGC 663 SAN 20	11.41	Be	N17	0.46361	NRP
574	Cl* NGC 663 SAN 17	11.74	Be	N17	0.24092	NRP
575	EM* VES 728	11.85	Oe	N17	...	none
576	V986 Cas	12.20	B2.5Ve	N17	...	none
577	NGC 884 2600	12.37	Be	N17	...	SAT
578	Cl* NGC 663 SAN 26	12.42	Be	N17	...	none
579	V975 Cas	12.71	Be	N17	...	none
580	HD 50820	6.27	B3IVe	J06	...	SAT
581	HD 57682	6.40	O9Ve	J06	...	SAT
582	OT Gem	6.45	B2Ve	J06	...	SAT
583	HD 70340	6.50	A2Vnnpe	J06	...	SAT
584	V695 Mon	6.51	B2.5Ve	J06	...	SAT
585	HD 53416	7.05	B8e	J06	...	SAT
586	HD 62367	7.13	B9e	J06	...	SAT
587	V749 Mon	7.20	B4IVe	J06	...	SAT
588	HD 50581	7.52	A0IVe	J06	...	SAT
589	HD 51506	7.69	B2.5IVe	J06	...	none
590	HD 53667	7.76	B0IIIe	J06	...	SAT
591	BT CMi	7.77	B2Vne	J06	...	SAT

592	V763 Mon	7.83	B5e	J06	...	SAT
593	V744 Mon	7.85	B1.5Ve	J06	...	ObV
594	HD 64109	7.99	B8e	J06	...	none
595	HD 57386	8.00	B1.5Vnnpe	J06	107.86087	IP,ObV?
596	V746 Mon	8.06	B1.5IVe	J06	0.71466,64.716520	IP,NRP,ObV
597	HD 51452	8.08	B0IVe	J06	...	none
598	HD 54858	8.19	A0IIe	J06	0.27477	NRP
599	HD 54464	8.40	B2.5IIIe	J06	0.65981	NRP
600	RY Gem	8.68	A2Ve	J06	9.30226	EB
601	HD 50696	8.87	B1.5IIIe	J06	0.47067	NRP
602	HD 50891	8.88	B0.5Ve	J06	...	ObV
603	HD 55606	9.04	B0.5Ve	J06	0.39308	NRP
604	HD 55806	9.15	B7IIIe	J06	13.98436	DWI,IP
605	V647 Mon	9.33	B1Vne	J06	...	none
606	HD 53032	9.36	A2e	J06	0.57412	NRP,ObV?
607	HD 56670	9.66	B0.5Ve	J06	61.31039	IP,ObV,SRO
608	BD-06 1895	9.93	Be	J06	...	none
609	HD 266894	10.66	Be	J06	...	none

Table A.2: Table showing the internal BK number, a common identifier, V-band magnitude, spectral type, KELT field, up to three periods detected in the KELT data, and variability notes.

Bibliography

C. Aerts, A. Thoul, J. Daszyńska, R. Scuflaire, C. Waelkens, M. A. Dupret, E. Niemczura, and A. Noels. Asteroseismology of HD 129929: Core Overshooting and Nonrigid Rotation. *Science*, 300:1926–1928, June 2003. doi: 10.1126/science.1084993.

C. Aerts, S. V. Marchenko, J. M. Matthews, R. Kuschnig, D. B. Guenther, A. F. J. Moffat, S. M. Rucinski, D. Sasselov, G. A. H. Walker, and W. W. Weiss. δ Ceti Is Not Monoperiodic: Seismic Modeling of a β Cephei Star from MOST Space-based Photometry. , 642:470–477, May 2006. doi: 10.1086/500800.

C. Aerts, M. Briquet, P. Degroote, A. Thoul, and T. van Hoolst. Seismic modelling of the β Cephei star HD 180642 (V1449 Aquilae). , 534:A98, Oct. 2011. doi: 10.1051/0004-6361/201117629.

C. Aerts, T. Van Reeth, and A. Tkachenko. The interior angular momentum of core hydrogen burning stars from gravity-mode oscillations. *ArXiv e-prints*, Sept. 2017.

S. Alam, F. D. Albareti, C. Allende Prieto, F. Anders, S. F. Anderson, T. Anderton, B. H. Andrews, E. Armengaud, É. Aubourg, S. Bailey, and et al. The Eleventh and Twelfth Data Releases of the Sloan Digital Sky Survey: Final Data from SDSS-III. , 219:12, July 2015. doi: 10.1088/0067-0049/219/1/12.

A. Alknis. Determination of size, color indices, and spectral classes of stars in an area centered on R.A.=21h24m, Dec=+58.5deg. *Trudy Astrofiz. Lab. Riga*, 7: 33–97, 1958.

D. Baade, T. Rivinius, A. Pigulski, A. Carciofi, G. Handler, R. Kuschnig, C. Martayan, A. Mehner, A. F. J. Moffat, H. Pablo, A. Popowicz, S. M. Rucinski, G. A. Wade, W. W. Weiss, and K. Zwintz. Pulsations and outbursts in Be stars: Small differences - big impacts. *ArXiv e-prints*, Nov. 2016a.

D. Baade, T. Rivinius, A. Pigulski, A. C. Carciofi, C. Martayan, A. F. J. Moffat, G. A. Wade, W. W. Weiss, J. Grunhut, G. Handler, R. Kuschnig, A. Mehner, H. Pablo, A. Popowicz, S. Rucinski, and G. Whittaker. Short-term variability and mass loss in Be stars. I. BRITE satellite photometry of η and μ Centauri. , 588:A56, Apr. 2016b. doi: 10.1051/0004-6361/201528026.

D. Baade, T. Rivinius, A. Pigulski, A. C. Carciofi, C. Martayan, A. F. J. Moffat, G. A. Wade, W. W. Weiss, J. Grunhut, G. Handler, R. Kuschnig, A. Mehner, H. Pablo, A. Popowicz, S. Rucinski, and G. Whittaker. Short-term variability and mass loss in Be stars. I. BRITE satellite photometry of η and μ Centauri. , 588:A56, Apr. 2016c. doi: 10.1051/0004-6361/201528026.

D. Baade, T. Rivinius, A. Pigulski, D. Panoglou, A. Carciofi, G. Handler, R. Kuschnig, C. Martayan, A. Mehner, A. F. J. Moffat, H. Pablo, A. Popowicz, S. M. Rucinski, G. A. Wade, W. W. Weiss, and K. Zwintz. BRITEning up the Be Phenomenon. *ArXiv e-prints*, Aug. 2017.

L. A. Balona. Tests of the Pulsation and Starspot Models for the Periodic Be-Stars. , 277:1547, Dec. 1995. doi: 10.1093/mnras/277.4.1547.

L. A. Balona, A. S. Baran, J. Daszyńska-Daszkiewicz, and P. De Cat. Analysis of Kepler B stars: rotational modulation and Maia variables. , 451:1445–1459, Aug. 2015. doi: 10.1093/mnras/stv1017.

B. W. Bopp. Spectroscopy of unusual emission-line stars. , 95:1543–1546, May 1988. doi: 10.1086/114750.

H. Bozic, P. Harmanec, J. Horn, P. Koubsky, G. Scholz, D. McDavid, A.-M. Hubert, and H. Hubert. Toward a consistent model of the B0.5IVe + sdO binary Persei. , 304:235, Dec. 1995.

A. J. Cannon and M. W. Mayall. The Henry Draper extension. II . *Annals of Harvard College Observatory*, 112:1–295, 1949.

A. C. Carciofi. The circumstellar discs of Be stars. In C. Neiner, G. Wade, G. Meynet, and G. Peters, editors, *Active OB Stars: Structure, Evolution, Mass Loss, and Critical Limits*, volume 272 of *IAU Symposium*, pages 325–336, July 2011. doi: 10.1017/S1743921311010738.

A. C. Carciofi, J. E. Bjorkman, S. A. Otero, A. T. Okazaki, S. Štefl, T. Rivinius, D. Baade, and X. Haubois. The First Determination of the Viscosity Parameter in the Circumstellar Disk of a Be Star. , 744:L15, Jan. 2012. doi: 10.1088/2041-8205/744/1/L15.

S. D. Chojnowski, D. G. Whelan, J. P. Wisniewski, S. R. Majewski, M. Hall, M. Shetrone, R. Beaton, A. Burton, G. Damke, S. Eikenberry, S. Hasselquist, J. A. Holtzman, S. Mészáros, D. Nidever, D. P. Schneider, J. Wilson, G. Zasowski, D. Bizyaev, H. Brewington, J. Brinkmann, G. Ebelke, P. M. Frinchaboy, K. Kinemuchi, E. Malanushenko, V. Malanushenko, M. Marchante, D. Oravetz, K. Pan, and A. Simmons. High-Resolution H-Band Spectroscopy of Be Stars With SDSS-III/Apogee: I. New Be Stars, Line Identifications, and Line Profiles. , 149: 7, Jan. 2015. doi: 10.1088/0004-6256/149/1/7.

S. D. Chojnowski, J. P. Wisniewski, D. G. Whelan, J. Labadie-Bartz, M. Borges Fernandes, C.-C. Lin, S. R. Majewski, G. S. Stringfellow, R. E. Mennickent, A. Roman-Lopes, B. Tang, F. R. Hearty, J. A. Holtzman, J. Pepper, and G. Zasowski. High-resolution H-band Spectroscopy of Be Stars with SDSS-III/APOGEE. II. Line Profile and Radial Velocity Variability. , 153:174, Apr. 2017. doi: 10.3847/1538-3881/aa64ce.

J. W. Christy. The radial velocities of early-type stars within six degrees of the galactic anticenter direction. , 217:127–133, Oct. 1977. doi: 10.1086/155561.

J. V. Clausen and K. S. Jensen. Classification Based on 102/A/mm Objective Prism

Spectra. In M. F. McCarthy, A. G. D. Philip, and G. V. Coyne, editors, *IAU Colloq. 47: Spectral Classification of the Future*, volume 9 of *Ricerche Astronomiche*, page 479, 1979.

J. Cuypers, L. A. Balona, and F. Marang. Intensive photometry of southern Be variables. I - Winter objects. , 81:151–186, Dec. 1989.

P. De Cat. An Observational Overview of Pulsations in β Cep Stars and Slowly Pulsating B Stars (invited paper). In C. Aerts, T. R. Bedding, and J. Christensen-Dalsgaard, editors, *IAU Colloq. 185: Radial and Nonradial Pulsationsn as Probes of Stellar Physics*, volume 259 of *Astronomical Society of the Pacific Conference Series*, page 196, 2002.

P. De Cat, M. Briquet, C. Aerts, K. Goossens, S. Saesen, J. Cuypers, K. Yakut, R. Scuflaire, M.-A. Dupret, K. Uytterhoeven, H. van Winckel, G. Raskin, G. Davignon, L. Le Guillou, R. van Malderen, M. Reyniers, B. Acke, W. De Meester, J. Vanautgaerden, B. Vandenbussche, T. Verhoelst, C. Waelkens, P. Deroo, K. Reyniers, M. Ausseloos, E. Broeders, J. Daszyńska-Daszkiewicz, J. Debosscher, S. De Ruyter, K. Lefever, G. Decin, K. Kolenberg, A. Mazumdar, C. van Kerckhoven, J. De Ridder, R. Drummond, C. Barban, E. Vanhollebeke, T. Maas, and L. Decin. Long term photometric monitoring with the Mercator telescope. Frequencies and mode identification of variable O-B stars. , 463:243–249, Feb. 2007. doi: 10.1051/0004-6361:20066202.

M.-A. Dupret, A. Thoul, R. Scuflaire, J. Daszyńska-Daszkiewicz, C. Aerts, P.-O. Bourge, C. Waelkens, and A. Noels. Asteroseismology of the β Cep star HD 129929. II. Seismic constraints on core overshooting, internal rotation and stellar parameters. , 415:251–257, Feb. 2004. doi: 10.1051/0004-6361:20034143.

W. A. Dziembowski, P. Moskalik, and A. A. Pamyatnykh. The Opacity Mechanism in B-Type Stars - Part Two - Excitation of High-Order G-Modes in Main Sequence Stars. , 265:588, Dec. 1993. doi: 10.1093/mnras/265.3.588.

S. S. Eikenberry, S. D. Chojnowski, J. Wisniewski, S. R. Majewski, M. Shetrone, D. G. Whelan, D. Bizyaev, H. J. Borish, J. R. A. Davenport, G. Ebelke, D. Feuillet, P. M. Frinchaboy, A. Garner, F. Hearty, J. Holtzman, Z.-Y. Li, S. Mészáros, D. L. Nidever, D. P. Schneider, M. Skrutskie, J. C. Wilson, and G. Zasowski. Discovery of Two Rare Rigidly Rotating Magnetosphere Stars in the APOGEE Survey. , 784:L30, Apr. 2014. doi: 10.1088/2041-8205/784/2/L30.

M. Emilio, L. Andrade, E. Janot-Pacheco, A. Baglin, J. Gutiérrez-Soto, J. C. Suárez, B. de Batz, P. Diago, J. Fabregat, M. Floquet, Y. Frémat, A. L. Huat, A. M. Hubert, F. Espinosa Lara, B. Leroy, C. Martayan, C. Neiner, T. Semaan, and J. Suso. Photometric variability of the Be star CoRoT-ID 102761769. , 522:A43, Nov. 2010. doi: 10.1051/0004-6361/201014081.

C. Fabricius, V. V. Makarov, J. Knude, and G. L. Wycoff. Henry Draper catalogue identifications for Tycho-2 stars. , 386:709–710, May 2002. doi: 10.1051/0004-6361:20020249.

K. Findeisen, A. M. Cody, and L. Hillenbrand. Simulated Performance of Timescale Metrics for Aperiodic Light Curves. , 798:89, Jan. 2015. doi: 10.1088/0004-637X/798/2/89.

Y. Frémat, C. Neiner, A.-M. Hubert, M. Floquet, J. Zorec, E. Janot-Pacheco, and J. Renan de Medeiros. Fundamental parameters of Be stars located in the seismology fields of COROT. , 451:1053–1063, June 2006a. doi: 10.1051/0004-6361:20053305.

Y. Frémat, C. Neiner, A.-M. Hubert, M. Floquet, J. Zorec, E. Janot-Pacheco, and J. Renan de Medeiros. Fundamental parameters of Be stars located in the seismology fields of COROT. , 451:1053–1063, June 2006b. doi: 10.1051/0004-6361:20053305.

M. R. Ghoreyshi and A. C. Carciofi. Analysis of the V-Band Light Curve of the Be Star ω CMa with the Viscous Decretion Disk Model. In A. Miroshnichenko, S. Zharikov, D. Korčáková, and M. Wolf, editors, *The B[e] Phenomenon: Forty*

Years of Studies, volume 508 of *Astronomical Society of the Pacific Conference Series*, page 323, Feb. 2017.

R. O. Gray and C. Corbally, J. *Stellar Spectral Classification*. 2009.

S. Grenier, M.-O. Baylac, L. Rolland, R. Burnage, F. Arenou, D. Briot, F. Delmas, M. Duflot, V. Genty, A. E. Gómez, J.-L. Halbwachs, M. Marouard, E. Oblak, and A. Sellier. Radial velocities. Measurements of 2800 B2-F5 stars for HIPPARCOS. , 137:451–456, June 1999. doi: 10.1051/aas:1999489.

F. Grillo, S. Sciortino, G. Micela, G. S. Vaiana, and F. R. Harnden, Jr. An Einstein Observatory SAO-based catalog of B-type stars. , 81:795–863, Aug. 1992. doi: 10.1086/191705.

E. D. Grundstrom, M. V. McSwain, C. Aragona, T. S. Boyajian, A. N. Marsh, and R. M. Roettenbacher. Observations of Be Disk Building: Optical Spectra of NW Serpentis (HD 168797) over 35 days. *Bulletin de la Societe Royale des Sciences de Liege*, 80:371–375, Jan. 2011.

H. H. Guetter. Spectral Classifications of 239 Early-Type Stars. , 80:197, Apr. 1968. doi: 10.1086/128611.

J. Gutiérrez-Soto, J. Fabregat, J. Suso, M. Lanzara, R. Garrido, A.-M. Hubert, and M. Floquet. A photometric study of Be stars located in the seismology fields of COROT. , 476:927–933, Dec. 2007. doi: 10.1051/0004-6361:20078252.

J. Gutiérrez-Soto, C. Neiner, A.-M. Hubert, M. Floquet, A.-L. Huat, P. D. Diago, J. Fabregat, B. Leroy, B. De Batz, L. Andrade, M. Emilio, W. Facanha, Y. Fremat, E. Janot-Pacheco, C. Martayan, and J. Suso. First results on the Be stars observed with the CoRoT satellite. *Communications in Asteroseismology*, 157:70–74, Dec. 2008.

G. Handler. Five New beta Cephei Stars Revealed in ASAS Photometry. *Information Bulletin on Variable Stars*, 5667, Dec. 2005.

G. Handler. Confirmation of simultaneous p and g mode excitation in HD 8801 and γ Peg from time-resolved multicolour photometry of six candidate 'hybrid' pulsators. , 398:1339–1351, Sept. 2009. doi: 10.1111/j.1365-2966.2009.15005.x.

G. Handler and S. Meingast. New β Cephei stars in the young open cluster NGC 637. , 533:A70, Sept. 2011. doi: 10.1051/0004-6361/201116874.

G. Handler, M. Jerzykiewicz, E. Rodríguez, K. Uytterhoeven, P. J. Amado, T. N. Dorokhova, N. I. Dorokhov, E. Poretti, J.-P. Sareyan, L. Parrao, D. Lorenz, D. Zsuffa, R. Drummond, J. Daszyńska-Daszkiewicz, T. Verhoelst, J. De Ridder, B. Acke, P.-O. Bourge, A. I. Movchan, R. Garrido, M. Paparó, T. Sahin, V. Antoci, S. N. Udovichenko, K. Csorba, R. Crowe, B. Berkey, S. Stewart, D. Terry, D. E. Mkrtichian, and C. Aerts. Asteroseismology of the β Cephei star 12 (DD) Lacertae: photometric observations, pulsational frequency analysis and mode identification. , 365:327–338, Jan. 2006. doi: 10.1111/j.1365-2966.2005.09728.x.

G. Handler, R. R. Shobbrook, K. Uytterhoeven, M. Briquet, C. Neiner, T. Tshenye, B. Ngwato, H. van Winckel, E. Guggenberger, G. Raskin, E. Rodríguez, A. Mazumdar, C. Barban, D. Lorenz, B. Vandenbussche, T. Şahin, R. Medupe, and C. Aerts. A multisite photometric study of two unusual β Cep stars: the magnetic V2052 Oph and the massive rapid rotator V986 Oph. , 424:2380–2391, Aug. 2012. doi: 10.1111/j.1365-2966.2012.21414.x.

J. Hardorp, K. Rohlfs, A. Slettebak, and J. Stock. Luminous stars in the Northern Milky Way. Part I. *Hamburger Sternw. Warner & Swasey Obs.*, 1959.

J. Hartman. VARTOOLS: Light Curve Analysis Program. Astrophysics Source Code Library, Aug. 2012.

X. Haubois, A. C. Carciofi, T. Rivinius, A. T. Okazaki, and J. E. Bjorkman. Dynamical Evolution of Viscous Disks around Be Stars. I. Photometry. , 756:156, Sept. 2012a. doi: 10.1088/0004-637X/756/2/156.

X. Haubois, A. C. Carciofi, T. Rivinius, A. T. Okazaki, and J. E. Bjorkman. Dynamical Study of Be Viscous Decretion Disks: Photometric Predictions. In A. C.

Carciofi and T. Rivinius, editors, *Circumstellar Dynamics at High Resolution*, volume 464 of *Astronomical Society of the Pacific Conference Series*, page 133, Dec. 2012b.

J. E. Hesser, P. P. Ugarte, and H. Moreno. On the period and luminosity stability of sigma Orionis E. , 216:L31–L33, Aug. 1977. doi: 10.1086/182503.

N. Houk and A. P. Cowley. *University of Michigan Catalogue of two-dimensional spectral types for the HD stars. Volume I. Declinations -90_ to -53_0.* 1975.

N. Houk and C. Swift. Michigan catalogue of two-dimensional spectral types for the HD Stars, Vol. 5. In *Michigan Spectral Survey, Ann Arbor, Dep. Astron., Univ. Michigan, Vol. 5, p. 0 (1999)*, volume 5, page 0, 1999.

A.-L. Huat, A.-M. Hubert, M. Floquet, C. Neiner, H. Saio, C. Lovekin, and F. Baudin. Correlation Between a Light Outburst and Pulsations in a CoRoT Be Star: HD 49330. In J. A. Guzik and P. A. Bradley, editors, *American Institute of Physics Conference Series*, volume 1170 of *American Institute of Physics Conference Series*, pages 382–384, Sept. 2009. doi: 10.1063/1.3246520.

A. M. Hubert and M. Floquet. Investigation of the variability of bright Be stars using HIPPARCOS photometry. , 335:565–572, July 1998.

W. Hummel. Line formation in Be star envelopes. 1: Inhomogeneous density distributions. , 289:458–468, Sept. 1994.

W. Hummel and J. Dachs. Non-coherent scattering in vertically extended Be star disks - Winebottle-type emission-line profiles. , 262:L17–L20, Sept. 1992.

J. B. Hutchings and R. O. Redman. HD 173219. A periodic Be star. , 163:219–227, 1973. doi: 10.1093/mnras/163.2.219.

M. Jaschek and D. Egret. A Catalogue of Be-Stars. In M. Jaschek and H.-G. Groth, editors, *Be Stars*, volume 98 of *IAU Symposium*, page 261, Apr. 1982.

M. Jerzykiewicz. Nonradial oscillations of the Beta Cephei star 12 Lacertae. , 28: 465–496, 1978.

C. E. Jones, P. A. Wiegert, C. Tycner, G. W. Henry, R. P. Cyr, R. J. Halonen, and M. W. Muterspaugh. Using Photometry to Probe the Circumstellar Environment of δ Scorpii. , 145:142, May 2013. doi: 10.1088/0004-6256/145/5/142.

J. Jurcsik, A. Sodor, and G. Hajdu. HD 190336 a new beta Cep star. *Information Bulletin on Variable Stars*, 5881, Mar. 2009.

S. D. Kawaler, M. D. Reed, A. C. Quint, R. H. Østensen, R. Silvotti, A. S. Baran, S. Charpinet, S. Bloemen, D. W. Kurtz, J. Telting, G. Handler, H. Kjeldsen, J. Christensen-Dalsgaard, W. J. Borucki, and D. G. Koch. First Kepler results on compact pulsators - II. KIC 010139564, a new pulsating subdwarf B (V361 Hya) star with an additional low-frequency mode. , 409:1487–1495, Dec. 2010. doi: 10.1111/j.1365-2966.2010.17528.x.

N. Kee, S. Owocki, R. Townsend, and H.-R. Müller. Pulsational Mass Ejection in Be Star Disks. *ArXiv e-prints*, Dec. 2014.

N. D. Kee, S. Owocki, and J. O. Sundqvist. Line-driven ablation of circumstellar discs - I. Optically thin decretion discs of classical Oe/Be stars. , 458:2323–2335, May 2016. doi: 10.1093/mnras/stw471.

N. V. Kharchenko. All-sky compiled catalogue of 2.5 million stars. *Kinematika i Fizika Nebesnykh Tel*, 17:409–423, Oct. 2001.

R. Klement, Carciofi, A. C., Rivinius, T., Matthews, L. D., Vieira, R. G., Ignace, R., Bjorkman, J. E., Mota, B. C., Faes, D. M., Bratcher, A. D., Cur, M., and tefl, S. Revealing the structure of the outer disks of be stars. *AA*, 601:A74, 2017. doi: 10.1051/0004-6361/201629932. URL `https://doi.org/10.1051/0004-6361/201629932`.

L. Kohoutek and R. Wehmeyer. Catalogue of H-alpha emission stars in the Northern Milky Way. , 134:255–256, Jan. 1999. doi: 10.1051/aas:1999101.

G. Kovács, G. Bakos, and R. W. Noyes. A trend filtering algorithm for wide-field variability surveys. , 356:557–567, Jan. 2005. doi: 10.1111/j.1365-2966.2004.08479.x.

P. Kroll and R. W. Hanuschik. Dynamics of Self-Accreting Disks in Be Stars. In D. T. Wickramasinghe, G. V. Bicknell, and L. Ferrario, editors, *IAU Colloq. 163: Accretion Phenomena and Related Outflows*, volume 121 of *Astronomical Society of the Pacific Conference Series*, page 494, 1997.

D. W. Kurtz, H. Shibahashi, S. J. Murphy, T. R. Bedding, and D. M. Bowman. A unifying explanation of complex frequency spectra of γ Dor, SPB and Be stars: combination frequencies and highly non-sinusoidal light curves. , 450:3015–3029, July 2015. doi: 10.1093/mnras/stv868.

J. Labadie-Bartz, S. D. Chojnowski, D. G. Whelan, J. Pepper, M. V. McSwain, M. Borges Fernandes, J. P. Wisniewski, G. S. Stringfellow, R. J. Siverd, A. L. Glazier, S. G. Anderson, A. J. Caravello, K. G. Stassun, M. B. Lund, D. J. Stevens, J. E. Rodriguez, D. J. James, and R. B. Kuhn. Outbursts and Disk Variability in Be Stars. *ArXiv e-prints*, Aug. 2017a.

J. Labadie-Bartz, J. Pepper, M. V. McSwain, J. E. Bjorkman, K. S. Bjorkman, M. B. Lund, J. E. Rodriguez, K. G. Stassun, D. J. Stevens, D. J. James, R. B. Kuhn, R. J. Siverd, and T. G. Beatty. Photometric Variability of the Be Star Population. , 153:252, June 2017b. doi: 10.3847/1538-3881/aa6396.

U. Lee, Y. Osaki, and H. Saio. Viscous excretion discs around Be stars. , 250: 432–437, May 1991. doi: 10.1093/mnras/250.2.432.

L. Lefèvre, S. V. Marchenko, A. F. J. Moffat, and A. Acker. A systematic study of variability among OB-stars based on HIPPARCOS photometry. , 507:1141–1201, Nov. 2009. doi: 10.1051/0004-6361/200912304.

W. J. Luyten. On the ellipticity of close binaries. , 98:459, Apr. 1938. doi: 10.1093/mnras/98.6.459.

D. J. MacConnell. A Study of the Cepheus IV Association. , 16:275, Oct. 1968. doi: 10.1086/190175.

A. Maeder. Evidences for a bifurcation in massive star evolution. The ON-blue stragglers. , 178:159–169, May 1987.

S. R. Majewski, R. P. Schiavon, P. M. Frinchaboy, C. Allende Prieto, R. Barkhouser, D. Bizyaev, B. Blank, S. Brunner, A. Burton, R. Carrera, S. D. Chojnowski, K. Cunha, C. Epstein, G. Fitzgerald, A. E. Garcia Perez, F. R. Hearty, C. Henderson, J. A. Holtzman, J. A. Johnson, C. R. Lam, J. E. Lawler, P. Maseman, S. Meszaros, M. Nelson, D. Coung Nguyen, D. L. Nidever, M. Pinsonneault, M. Shetrone, S. Smee, V. V. Smith, T. Stolberg, M. F. Skrutskie, E. Walker, J. C. Wilson, G. Zasowski, F. Anders, S. Basu, S. Beland, M. R. Blanton, J. Bovy, J. R. Brownstein, J. Carlberg, W. Chaplin, C. Chiappini, D. J. Eisenstein, Y. Elsworth, D. Feuillet, S. W. Fleming, J. Galbraith-Frew, R. A. Garcia, D. Anibal Garcia-Hernandez, B. A. Gillespie, L. Girardi, J. E. Gunn, S. Hasselquist, M. R. Hayden, S. Hekker, I. Ivans, K. Kinemuchi, M. Klaene, S. Mahadevan, S. Mathur, B. Mosser, D. Muna, J. A. Munn, R. C. Nichol, R. W. O'Connell, A. C. Robin, H. Rocha-Pinto, M. Schultheis, A. M. Serenelli, N. Shane, V. Silva Aguirre, J. S. Sobeck, B. Thompson, N. W. Troup, D. H. Weinberg, and O. Zamora. The Apache Point Observatory Galactic Evolution Experiment (APOGEE). *ArXiv e-prints*, Sept. 2015.

C. Martayan, A. M. Hubert, M. Floquet, J. Fabregat, Y. Frémat, C. Neiner, P. Stee, and J. Zorec. A study of the B and Be star population in the field of the LMC open cluster NGC 2004 with VLT-FLAMES. , 445:931–937, Jan. 2006. doi: 10.1051/0004-6361:20052760.

R. G. Martin, J. E. Pringle, C. A. Tout, and S. H. Lubow. Tidal warping and precession of Be star decretion discs. , 416:2827–2839, Oct. 2011. doi: 10.1111/j.1365-2966.2011.19231.x.

A. Mazumdar, M. Briquet, M. Desmet, and C. Aerts. An asteroseismic study of the β Cephei star β Canis Majoris. , 459:589–596, Nov. 2006. doi: 10.1051/0004-6361:20064980.

S. W. McCuskey. Stellar Spectra in Milky way Regions. VII. a Region in Aurigga. , 4:1, Jan. 1959. doi: 10.1086/190042.

S. W. McCuskey, P. Pesch, and G. A. Snyder. The space distribution and radial velocities of some early-type stars in the Perseus spiral arm. , 79:597, May 1974. doi: 10.1086/111581.

M. V. McSwain, W. Huang, D. R. Gies, E. D. Grundstrom, and R. H. D. Townsend. The B and Be Star Population of NGC 3766. , 672:590-603, Jan. 2008. doi: 10.1086/523934.

M. V. McSwain, W. Huang, and D. R. Gies. Variability of Be Stars in Southern Open Clusters. , 700:1216–1232, Aug. 2009. doi: 10.1088/0004-637X/700/2/1216.

R. E. Mennickent, N. Vogt, and C. Sterken. Long-term photometry of Be stars. I. Fading events and variations on time scales of years. , 108, Nov. 1994.

R. E. Mennickent, C. Sterken, and N. Vogt. Long-term photometry of Be stars. III. Evidence for periodic outbursts of lambda ERI and photometric activity in HR2142. , 330:631–640, Feb. 1998.

P. W. Merrill. Oscillations in the Shell Star HD 33232. , 116:516, Nov. 1952. doi: 10.1086/145643.

P. W. Merrill and C. G. Burwell. Second Supplement to the Mount Wilson Catalogue and Bibliography of Stars of Classes B and a whose Spectra have Bright Hydrogen Lines. , 110:387, Nov. 1949. doi: 10.1086/145215.

P. W. Merrill, C. G. Burwell, and W. C. Miller. Discovery and Observations of Stars of Class Be. Third Paper. , 96:15, July 1942. doi: 10.1086/144428.

A. S. Miroshnichenko, J. Fabregat, K. S. Bjorkman, D. C. Knauth, N. D. Morrison, A. E. Tarasov, P. Reig, I. Negueruela, and P. Blay. Spectroscopic observations of the δ Scorpii binary during its recent periastron passage. , 377:485–495, Oct. 2001. doi: 10.1051/0004-6361:20010911.

A. S. Miroshnichenko, A. V. Pasechnik, N. Manset, A. C. Carciofi, T. Rivinius, S. Štefl, V. V. Gvaramadze, J. Ribeiro, A. Fernando, T. Garrel, J. H. Knapen, C. Buil, B. Heathcote, E. Pollmann, B. Mauclaire, O. Thizy, J. Martin, S. V. Zharikov, A. T. Okazaki, T. L. Gandet, T. Eversberg, and N. Reinecke. The 2011 Periastron Passage of the Be Binary δ Scorpii. , 766:119, Apr. 2013. doi: 10.1088/0004-637X/766/2/119.

M. Moe and R. Di Stefano. Mind your Ps and Qs: the Interrelation between Period (P) and Mass-ratio (Q) Distributions of Binary Stars. *ArXiv e-prints*, June 2016.

W. W. Morgan and P. C. Keenan. Spectral Classification. , 11:29, 1973. doi: 10.1146/annurev.aa.11.090173.000333.

W. W. Morgan, A. E. Whitford, and A. D. Code. Studies in Galactic Structure. I. a Preliminary Determination of the Space Distribution of the Blue Giants. , 118: 318, Sept. 1953. doi: 10.1086/145754.

W. W. Morgan, A. D. Code, and A. E. Whitford. Studies in Galactic STRUCTURE.II.LUMINOSITY Classification for 1270 Blue Giant Stars. , 2:41, July 1955. doi: 10.1086/190016.

P. Moskalik and W. A. Dziembowski. New opacities and the origin of the Beta Cephei pulsation. , 256:L5–L8, Mar. 1992.

N. Mowlavi and M. Forestini. Semi-convection and overshooting in intermediate mass and massive stars. , 282:843–857, Feb. 1994.

J. J. Nassau and D. Harris, III. OB Stars in the P Cygni Region. , 115:459, May 1952. doi: 10.1086/145559.

I. Negueruela. A search for luminous Be stars. *Astronomische Nachrichten*, 325: 380–392, June 2004. doi: 10.1002/asna.200310245.

I. Negueruela, I. A. Steele, and G. Bernabeu. On the class of Oe stars. *Astronomische Nachrichten*, 325:749–760, Dec. 2004. doi: 10.1002/asna.200310258.

C. Neiner, A.-M. Hubert, and C. Catala. The Identification of New Be Stars in GAUDI. , 156:237–243, Feb. 2005. doi: 10.1086/426670.

C. Neiner, B. de Batz, F. Cochard, M. Floquet, A. Mekkas, and V. Desnoux. The Be Star Spectra (BeSS) Database. , 142:149, Nov. 2011. doi: 10.1088/0004-6256/142/5/149.

V. V. Nesterov, A. V. Kuzmin, N. T. Ashimbaeva, A. A. Volchkov, S. Röser, and U. Bastian. The Henry Draper Extension Charts: A catalogue of accurate positions, proper motions, magnitudes and spectral types of 86933 stars. , 110, Apr. 1995.

F. Ochsenbein. The SAO Catalogue with Astrophysical Data. *Bulletin d'Information du Centre de Donnees Stellaires*, 19:74, July 1980.

A. T. Okazaki. Long-term V/R variations of Be stars due to global one-armed oscillations of equatorial disks. , 43:75–94, Feb. 1991.

M. E. Oksala, O. Kochukhov, J. Krtička, R. H. D. Townsend, G. A. Wade, M. Prvák, Z. Mikulášek, J. Silvester, and S. P. Owocki. Revisiting the rigidly rotating magnetosphere model for σ Ori E - II. Magnetic Doppler imaging, arbitrary field RRM, and light variability. , 451:2015–2029, Aug. 2015. doi: 10.1093/mnras/stv1086.

R. Østensen, U. Heber, R. Silvotti, J.-E. Solheim, S. Dreizler, and H. Edelmann. Four new subdwarf B pulsators. , 378:466–476, Nov. 2001a. doi: 10.1051/0004-6361:20011218.

R. Østensen, J.-E. Solheim, U. Heber, R. Silvotti, S. Dreizler, and H. Edelmann. Detection of pulsations in three subdwarf B stars. , 368:175–182, Mar. 2001b. doi: 10.1051/0004-6361:20000488.

R. D. Oudmaijer and A. M. Parr. The binary fraction and mass ratio of Be and B stars: a comparative Very Large Telescope/NACO study. , 405:2439–2446, July 2010. doi: 10.1111/j.1365-2966.2010.16609.x.

S. Özdemir, P. Mayer, H. Drechsel, O. Demircan, and H. Ak. Refinement of third body parameters and new photometric results for the early-type multiple system IU Aurigae. , 403:675–681, May 2003. doi: 10.1051/0004-6361:20030392.

O. Öztürk, F. Soydugan, and C. Çiçek. SX Aurigae: A close binary at the early stage of contact phase. , 30:100–104, July 2014. doi: 10.1016/j.newast.2014.01.005.

D. Panoglou, A. C. Carciofi, R. G. Vieira, I. H. Cyr, C. E. Jones, A. T. Okazaki, and T. Rivinius. Be discs in binary systems - I. Coplanar orbits. , 461:2616–2629, Sept. 2016. doi: 10.1093/mnras/stw1508.

J. C. Papaloizou, G. J. Savonije, and H. F. Henrichs. On the long-term periodicities in Be stars. , 265:L45–L48, Nov. 1992.

J. Pepper, R. W. Pogge, D. L. DePoy, J. L. Marshall, K. Z. Stanek, A. M. Stutz, S. Poindexter, R. Siverd, T. P. O'Brien, M. Trueblood, and P. Trueblood. The Kilodegree Extremely Little Telescope (KELT): A Small Robotic Telescope for Large-Area Synoptic Surveys. , 119:923–935, Aug. 2007. doi: 10.1086/521836.

J. Pepper, R. B. Kuhn, R. Siverd, D. James, and K. Stassun. The KELT-South Telescope. , 124:230–241, Mar. 2012. doi: 10.1086/665044.

T. M. D. Pereira and I. P. Lopes. Amplitude variations in the sdBV star ¡AS-TROBJ¿PG 1605+072¡/ASTROBJ¿: Another beating time scale? , 426:213–217, Oct. 2004. doi: 10.1051/0004-6361:20041181.

A. Pigulski and G. Pojmański. β Cephei stars in the ASAS-3 data. II. 103 new β Cephei stars and a discussion of low-frequency modes. , 477:917–929, Jan. 2008. doi: 10.1051/0004-6361:20078581.

M. J. Plavec and J. J. Dobias. The moderately interacting Algol-type eclipsing binary RY Geminorum. , 93:440–450, Feb. 1987. doi: 10.1086/114329.

G. Pojmanski. The All Sky Automated Survey. The Catalog of Variable Stars. II. 6ˆh-12ˆh Quarter of the Southern Hemisphere. , 53:341–369, Dec. 2003.

D. M. Popper. Studies of Faint B-Type Stars. , 111:495, May 1950. doi: 10.1086/145292.

J. M. Porter and T. Rivinius. Classical Be Stars. , 115:1153–1170, Oct. 2003. doi: 10.1086/378307.

W. H. Press, S. A. Teukolsky, W. T. Vetterling, and B. P. Flannery. *Numerical recipes in C. The art of scientific computing*. 1992.

T. Radoslavova. Surface distribution of the luminous and early-type emission stars in the OB Vulpecula associations. *Astronomische Nachrichten*, 310:223–226, 1989. doi: 10.1002/asna.2113100313.

B. C. Reed. Catalog of Galactic OB Stars. , 125:2531–2533, May 2003. doi: 10.1086/374771.

M. D. Reed, S. D. Kawaler, R. H. Østensen, S. Bloemen, A. Baran, J. H. Telting, R. Silvotti, S. Charpinet, A. C. Quint, G. Handler, R. L. Gilliland, W. J. Borucki, D. G. Koch, H. Kjeldsen, and J. Christensen-Dalsgaard. First Kepler results on compact pulsators - III. Subdwarf B stars with V1093 Her and hybrid (DW Lyn) type pulsations. , 409:1496–1508, Dec. 2010. doi: 10.1111/j.1365-2966.2010.17423.x.

P. Reig, A. Zezas, and L. Gkouvelis. The optical counterpart to IGR J06074+2205: a Be/X-ray binary showing disc loss and V/R variability. , 522:A107, Nov. 2010. doi: 10.1051/0004-6361/201014788.

G. R. Ricker, J. N. Winn, R. Vanderspek, D. W. Latham, G. Á. Bakos, J. L. Bean, Z. K. Berta-Thompson, T. M. Brown, L. Buchhave, N. R. Butler, R. P. Butler, W. J. Chaplin, D. Charbonneau, J. Christensen-Dalsgaard, M. Clampin, D. Deming, J. Doty, N. De Lee, C. Dressing, E. W. Dunham, M. Endl, F. Fressin, J. Ge, T. Henning, M. J. Holman, A. W. Howard, S. Ida, J. Jenkins, G. Jernigan, J. A.

Johnson, L. Kaltenegger, N. Kawai, H. Kjeldsen, G. Laughlin, A. M. Levine, D. Lin, J. J. Lissauer, P. MacQueen, G. Marcy, P. R. McCullough, T. D. Morton, N. Narita, M. Paegert, E. Palle, F. Pepe, J. Pepper, A. Quirrenbach, S. A. Rinehart, D. Sasselov, B. Sato, S. Seager, A. Sozzetti, K. G. Stassun, P. Sullivan, A. Szentgyorgyi, G. Torres, S. Udry, and J. Villasenor. Transiting Exoplanet Survey Satellite (TESS). In *Space Telescopes and Instrumentation 2014: Optical, Infrared, and Millimeter Wave*, volume 9143 of , page 914320, Aug. 2014. doi: 10.1117/12.2063489.

T. Rivinius, D. Baade, S. Stefl, O. Stahl, B. Wolf, and A. Kaufer. Stellar and circumstellar activity of the Be star MU Centauri. I. Line emission outbursts. , 333:125–140, May 1998.

T. Rivinius, D. Baade, S. Štefl, R. H. D. Townsend, O. Stahl, B. Wolf, and A. Kaufer. Stellar and circumstellar activity of the Be star mu Centauri. III. Multiline non-radial pulsation modeling. , 369:1058–1077, Apr. 2001. doi: 10.1051/0004-6361:20010185.

T. Rivinius, D. Baade, and S. Štefl. Non-radially pulsating Be stars. , 411:229–247, Nov. 2003. doi: 10.1051/0004-6361:20031285.

T. Rivinius, A. C. Carciofi, and C. Martayan. Classical Be stars. Rapidly rotating B stars with viscous Keplerian decretion disks. , 21:69, Oct. 2013. doi: 10.1007/s00159-013-0069-0.

T. Rivinius, D. Baade, and A. C. Carciofi. Short-term variability and mass loss in Be stars. II. Physical taxonomy of photometric variability observed by the Kepler spacecraft. , 593:A106, Sept. 2016. doi: 10.1051/0004-6361/201628411.

C. Roslund. A survey of O and B stars in a region of Scutum. *Arkiv for Astronomi*, 3:97–120, 1963.

S. Saesen, M. Briquet, C. Aerts, A. Miglio, and F. Carrier. Pulsating B-type Stars in the Open Cluster NGC 884: Frequencies, Mode Identification, and Asteroseismology. , 146:102, Oct. 2013. doi: 10.1088/0004-6256/146/4/102.

H. Saio, C. Cameron, R. Kuschnig, G. A. H. Walker, J. M. Matthews, J. F. Rowe, U. Lee, D. Huber, W. W. Weiss, D. B. Guenther, A. F. J. Moffat, S. M. Rucinski, and D. Sasselov. MOST Detects g-Modes in the Late-Type Be Star β Canis Minoris (B8 Ve). , 654:544–550, Jan. 2007. doi: 10.1086/509315.

D. Sebastian, E. W. Guenther, V. Schaffenroth, D. Gandolfi, S. Geier, U. Heber, M. Deleuil, and C. Moutou. Multi-object spectroscopy of stars in the CoRoT fields. I. Early-type stars in the CoRoT-fields IRa01, LRa01, LRa02. , 541:A34, May 2012. doi: 10.1051/0004-6361/201118032.

N. I. Shakura and R. A. Sunyaev. Black holes in binary systems. Observational appearance. , 24:337–355, 1973.

T. A. A. Sigut and P. Patel. The Correlation between Hα Emission and Visual Magnitude during Long-term Variations in Classical Be Stars. , 765:41, Mar. 2013. doi: 10.1088/0004-637X/765/1/41.

B. A. Skiff. VizieR Online Data Catalog: General Catalogue of Stellar Spectral Classifications. *VizieR Online Data Catalog*, 1, 2013.

A. Slettebak, G. W. Collins, II, and R. Truax. Physical properties of Be star envelopes from Balmer and Fe II emission lines. , 81:335–376, July 1992. doi: 10.1086/191696.

A. Stankov and G. Handler. Catalog of Galactic β Cephei Stars. , 158:193–216, June 2005. doi: 10.1086/429408.

C. B. Stephenson and N. Sanduleak. New H-alpha emission stars in the Milky Way. , 33:459–469, Apr. 1977a. doi: 10.1086/190437.

C. B. Stephenson and N. Sanduleak. New position determinations, and other data, for 1280 known Hα-emission stars in the milky way. *Publications of the Warner & Swasey Observatory*, 2:4, 1977b.

C. Sterken and M. Jerzykiewicz. Beta Cephei stars from a photometric point of view. , 62:95–171, 1993.

C. Sterken, N. Vogt, and R. Mennickent. Evidence for ellipsoidal variations of the Be star binary HD 50123. , 291:473–480, Nov. 1994.

C. Sterken, N. Vogt, and R. E. Mennickent. Long-term photometry of Be stars. II. Periodic variations on time scales of days to months. , 311:579–586, July 1996.

A. D. Thackeray, J. B. Alexander, and P. W. Hill. HD 72754 - a New Be Variable Star of Beta Lyrae Type. *Information Bulletin on Variable Stars*, 483, Nov. 1970.

R. H. D. Townsend. Asymptotic expressions for the angular dependence of low-frequency pulsation modes in rotating stars. , 340:1020–1030, Apr. 2003. doi: 10.1046/j.1365-8711.2003.06379.x.

R. H. D. Townsend, S. P. Owocki, and I. D. Howarth. Be-star rotation: how close to critical? , 350:189–195, May 2004. doi: 10.1111/j.1365-2966.2004.07627.x.

D. G. Turner. The value of R in Monoceros. , 210:65–75, Nov. 1976. doi: 10.1086/154803.

D. G. Turner. A detailed study of the sparce open cluster Roslund 3 - A case for circumstellar extinction. , 97:755–767, Feb. 1993.

B. Uzpen, H. A. Kobulnicky, D. R. Semler, T. Bensby, and C. Thom. A GLIMPSE into the Nature of Galactic Mid-IR Excesses. , 685:1157-1182, Oct. 2008. doi: 10.1086/591119.

S. Štefl, D. Baade, T. Rivinius, O. Stahl, B. Wolf, and A. Kaufer. Circumstellar Quasi-periods Accompanying Stellar Periods of Be Stars. In P. A. Bradley and J. A. Guzik, editors, *A Half Century of Stellar Pulsation Interpretation*, volume 135 of *Astronomical Society of the Pacific Conference Series*, page 348, 1998.

S. Štefl, A. Budovičová, D. Baade, A. Kaufer, T. Rivinius, O. Stahl, and B. Wolf. Tracing the Transient Periods in the Be Star 28 ω CMa. In M. A. Smith, H. F. Henrichs, and J. Fabregat, editors, *IAU Colloq. 175: The Be Phenomenon in Early-Type Stars*, volume 214 of *Astronomical Society of the Pacific Conference Series*, page 240, 2000.

S. Štefl, T. Rivinius, A. C. Carciofi, J.-B. Le Bouquin, D. Baade, K. S. Bjorkman, E. Hesselbach, C. A. Hummel, A. T. Okazaki, E. Pollmann, F. Rantakyrö, and J. P. Wisniewski. Cyclic variability of the circumstellar disk of the Be star ζ Tauri. I. Long-term monitoring observations. , 504:929–944, Sept. 2009. doi: 10.1051/0004-6361/200811573.

F. van Leeuwen. The HIPPARCOS Mission. , 81:201–409, Aug. 1997. doi: 10.1023/A:1005081918325.

J. T. VanderPlas. Understanding the Lomb-Scargle Periodogram. *ArXiv e-prints*, Mar. 2017.

D. N. Vesper and R. K. Honeycutt. Full-orbit H-alpha emission in RW Tauri. , 105: 731–747, July 1993. doi: 10.1086/133224.

R. G. Vieira, A. C. Carciofi, J. E. Bjorkman, T. Rivinius, D. Baade, and L. R. Rímulo. The life cycles of Be viscous decretion discs: time-dependent modelling of infrared continuum observations. , 464:3071–3089, Jan. 2017. doi: 10.1093/mnras/stw2542.

V. I. Voroshilov, N. G. Guseva, N. B. Kalandadze, L. N. Kolesnik, V. I. Kuznetsov, M. D. Metreveli, and A. N. Shapovalov. *Catalog of BV magnitudes and spectral classes of 6000 stars*. 1985.

L. R. Wackerling. A catalogue of early-type stars whose spectra have shown emission lines. , 73:153, 1970.

G. A. Wade, J. Grunhut, E. Alecian, C. Neiner, M. Aurière, D. A. Bohlender, A. David-Uraz, C. Folsom, H. F. Henrichs, O. Kochukhov, S. Mathis, S. Owocki, V. Petit, and Petit. The magnetic characteristics of Galactic OB stars from the MiMeS survey of magnetism in massive stars. In P. Petit, M. Jardine, and H. C. Spruit, editors, *Magnetic Fields throughout Stellar Evolution*, volume 302 of *IAU Symposium*, pages 265–269, Aug. 2014a. doi: 10.1017/S1743921314002233.

G. A. Wade, V. Petit, J. Grunhut, and C. Neiner. Magnetic fields of Be stars: preliminary results from a hybrid analysis of the MiMeS sample. *ArXiv e-prints*, Nov. 2014b.

N. R. Walborn and E. L. Fitzpatrick. Contemporary optical spectral classification of the OB stars - A digital atlas. , 102:379–411, Apr. 1990. doi: 10.1086/132646.

N. R. Walborn, I. D. Howarth, C. J. Evans, P. A. Crowther, A. F. J. Moffat, N. St-Louis, C. Fariña, G. L. Bosch, N. I. Morrell, R. H. Barbá, and J. T. van Loon. The Onfp Class in the Magellanic Clouds. , 139:1283–1294, Mar. 2010. doi: 10.1088/0004-6256/139/3/1283.

G. A. H. Walker, R. Kuschnig, J. M. Matthews, C. Cameron, H. Saio, U. Lee, E. Kambe, S. Masuda, D. B. Guenther, A. F. J. Moffat, S. M. Rucinski, D. Sasselov, and W. W. Weiss. MOST Detects g-Modes in the Be Star HD 163868. , 635:L77–L80, Dec. 2005a. doi: 10.1086/499362.

G. A. H. Walker, R. Kuschnig, J. M. Matthews, P. Reegen, T. Kallinger, E. Kambe, H. Saio, P. Harmanec, D. B. Guenther, A. F. J. Moffat, S. M. Rucinski, D. Sasselov, W. W. Weiss, D. A. Bohlender, H. Božić, O. Hashimoto, P. Koubský, R. Mann, D. Ruždjak, P. Škoda, M. Šlechta, D. Sudar, M. Wolf, and S. Yang. Pulsations of the Oe Star ζ Ophiuchi from MOST Satellite Photometry and Ground-based Spectroscopy. , 623:L145–L148, Apr. 2005b. doi: 10.1086/430254.

S.-i. Wang, R. H. Hildebrand, L. M. Hobbs, S. J. Heimsath, G. Kelderhouse, R. F. Loewenstein, S. Lucero, C. M. Rockosi, D. Sandford, J. L. Sundwall, J. A. Thorburn, and D. G. York. ARCES: an echelle spectrograph for the Astrophysical Research Consortium (ARC) 3.5m telescope. In M. Iye and A. F. M. Moorwood, editors, *Instrument Design and Performance for Optical/Infrared Ground-based Telescopes*, volume 4841 of , pages 1145–1156, Mar. 2003. doi: 10.1117/12.461447.

D. G. Whelan and R. D. Baker. HD 46487 is Now a Classical Be Star. , 45:60–68, May 2017.

R. E. Wilson and M. J. Plavec. RW Persei and the disk hypothesis. , 95:1828–1836, June 1988. doi: 10.1086/114779.

J. P. Wisniewski, S. D. Chojnowski, J. R. A. Davenport, J. Bartz, J. Pepper, D. G. Whelan, S. S. Eikenberry, J. R. Lomax, S. R. Majewski, N. D. Richardson, and M. Skrutskie. Characterizing the Rigidly Rotating Magnetosphere Stars HD 345439 and HD 23478. , 811:L26, Oct. 2015. doi: 10.1088/2041-8205/811/2/L26.

M. Wolf, H. Kučáková, M. Kolasa, P. Štastný, Z. Bozkurt, P. Harmanec, M. Zejda, L. Brát, and K. Hornoch. Apsidal motion in eccentric eclipsing binaries: CW Cephei, V478 Cygni, AG Persei, and IQ Persei. , 456:1077–1083, Sept. 2006. doi: 10.1051/0004-6361:20065327.

M. Zechmeister and M. Kürster. The generalised Lomb-Scargle periodogram. A new formalism for the floating-mean and Keplerian periodograms. , 496:577–584, Mar. 2009. doi: 10.1051/0004-6361:200811296.

Curriculum Vitae

Jonathan Labadie-Bartz

Education

Ph.D. Physics, Lehigh University, 2018

M.S. Physics, Lehigh University, 2014

B.S. Physics, Clarion University, 2011

Publications

Labadie-Bartz, Jonathan & 13 co-authors, 2017, "*Photometric Variability of the Be Star Population*", The Astronomical Journal, Volume 153, Issue 6, article id. 252, 21 pp

Labadie-Bartz, Jonathan & 17 co-authors, 2017, "*Outbursts and Disk Variability in Be Stars*", Accepted for publication in the Astronomical Journal, 23 pp, eprint arXiv:1708.02594

Chojnowski, S. Drew, Wisniewski, John P., Whelan, David G., Labadie-Bartz, Jonathan & 11 co-authors, 2017, "*High-Resolution, H-Band Spectroscopy of Be Stars with SDSS-III/APOGEE: II. Line Profile and Radial Velocity Variability*", The Astronomical Journal, Volume 153, Issue 4, article id. 174, 22 pp

Gaudi, Scott B. & 59 co-authors, 2017, "*A giant planet undergoing extreme-ultraviolet irradiation by its hot massive-star host*", Nature, Volume 546, Issue 7659, pp. 514 - 518

Lund, Michael B. & 48 co-authors, 2017, "*KELT-20b: A giant planet with a period of P 3.5 days transiting the V 7.6 early A star HD 185603*", The Astronomical Journal, Volume 154, Issue 5, article id. 194, 16 pp

McLeod, Kim K. & 56 co-authors, 2017, "*KELT-18b: Puffy Planet, Hot Host, Probably Perturbed*", The Astronomical Journal, Volume 153, Issue 6, article id. 263, 15 pp

Pepper, Joshua & 37 co-authors, 2017, "*KELT-11b: A Highly Inflated Sub-Saturn Exoplanet Transiting the V=8 Subgiant HD 93396*", The Astronomical Journal, Volume 153, Issue 5, article id. 215, 15 pp

Oberst, Thomas E. & 48 co-authors, 2017, "*KELT-16b: A highly irradiated, ultra-short period hot Jupiter nearing tidal disruption*", The Astronomical Journal, Volume 153, Issue 3, article id. 97, 18 pp

Stevens, Daniel J. & 49 co-authors, 2017, "*KELT-12b: A P5 Day, Highly Inflated Hot Jupiter Transiting a Mildly Evolved Hot Star*", The Astronomical Journal, Volume 153, Issue 4, article id. 178, 15 pp

Lubin, Jack, & 28 co-authors, 2017, "*A Bright Short Period M-M Eclipsing Binary from the KELT Survey: Magnetic Activity and the Mass-Radius Relationship for M-Dwarfs*", The Astrophysical Journal, Volume 844, Issue 2, article id. 134, 12 pp

Temple, L. Y. & 48 co-authors, 2017, "*WASP-167b/KELT-13b: joint discovery of a hot Jupiter transiting a rapidly rotating F1V star*", Monthly Notices of the Royal Astronomical Society, Volume 471, Issue 3, pp. 2743 - 2752

Zhou, George & 48 co-authors, 2016, "*KELT-17b: A hot-Jupiter transiting an A-star in a misaligned orbit detected with Doppler tomography*", The Astronomical Journal, Volume 152, Issue 5, article id. 136, 15 pp

Rodriguez, Joseph E. & 31 co-authors, 2016, "*KELT-14b and KELT-15b: An Independent Discovery of WASP-122b and a New Hot Jupiter*", The Astronomical Journal, Volume 151, Issue 6, article id. 138, 16 pp

Wisniewski, J. P., Chojnowski, S.D., Davenport, J.R.A., Labadie-Bartz, Jonathan & 7 co-authors, 2015, "*Characterizing the Rigidly Rotating Magnetosphere Stars*

HD 345439 and HD 23478", The Astrophysical Journal Letters, Volume 811, Issue 2, article id. L26, 7 pp

Siverd, Robert J. & 47 co-authors, 2017, "*KELT-19Ab: A P 4.6 Day Hot Jupiter Transiting a Likely Am Star with a Distant Stellar Companion*", Submitted to AAS Journals, 16 pp, eprint arXiv:1709.07010